THE UNIVERSITY *of* EDINBURGH

This thesis has been submitted in fulfilment of the requirements for a postgraduate degree (e. g. PhD, MPhil, DClinPsychol) at the University of Edinburgh. Please note the following terms and conditions of use:

- This work is protected by copyright and other intellectual property rights, which are retained by the thesis author, unless otherwise stated.
- A copy can be downloaded for personal non-commercial research or study, without prior permission or charge.
- This thesis cannot be reproduced or quoted extensively from without first obtaining permission in writing from the author.
- The content must not be changed in any way or sold commercially in any format or medium without the formal permission of the author.
- When referring to this work, full bibliographic details including the author, title, awarding institution and date of the thesis must be given.

Mocean Energy's *Blue Star* wave energy converter for off-grid applications – development via small-scale physical model testing

ANDREA CAIO

A thesis submitted in partial fulfilment of the requirements for the award of an Engineering Doctorate (EngD)

Supervised by:

Dr J. Cameron McNatt, Dr Thomas Davey, Prof Lars Johanning, Dr Laibing Jia

The University of Edinburgh

November 2022

IDCORE

This thesis is submitted in partial fulfilment of the requirements for the award of an Engineering Doctorate, jointly awarded by the University of Edinburgh, the University of Exeter, and the University of Strathclyde.

The work presented has been conducted under the industrial supervision of Mocean Energy Ltd. as a project within the Industrial Doctoral Centre for Offshore Renewable Energy (IDCORE).

THE UNIVERSITY of EDINBURGH

UNIVERSITY OF EXETER

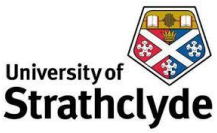

SCOTTISH ASSOCIATION for MARINE SCIENCE

Declaration

I declare that this thesis was composed by myself, that the work contained herein is my own except where explicitly stated otherwise in the text, and that this work has not been submitted for any other degree or professional qualification except as specified.

Parts of this work have been published in [ISOPE 2019 Conference, Chapter 5] and [EWTEC 2021 conference, Chapter 6].

The experimental work is entirely my own but has interfaced with other activities, particularly numerical, carried out by colleagues within the host company. Any contributions or complementary analysis from colleagues, such as simulations, diagrams or calibrations, are clearly indicated and acknowledged in the text.

Andrea Caio

This thesis is dedicated to whoever
will choose to read it.

Abstract

Ocean waves represent a promising source of renewable energy. This can be harnessed via wave energy converters (WECs) – machines that convert the energy carried by ocean waves into useful power, such as electricity. Although wave energy potential is significant, the industry lags other renewable technologies in maturity, as well as public and private confidence.

The present research adopts a “small-mid-grid” development approach, in accordance with the sponsoring company Mocean Energy, which is formally articulated as a framework within this research. Fundamentally, this approach aims to streamline commercial returns and technical learning by targeting applications that require relatively small WECs – producing 10s of kilowatts – to power local, off-grid, offshore assets. Such markets can be beachheads for larger-sized machines that ultimately feed national grids.

An analogous ‘reduced scale’ paradigm can be applied to physical model testing, a key part of a WEC’s development. Can a developer accelerate the learning process by iterating designs with a relatively small physical model, while still capturing sufficient device characteristics to gather the *type* and *quality* of data needed to validate and advance performance? This question is investigated from three perspectives: (i) what data is required from physical model tests, in order to validate the chosen quantities of interest (QOIs) linked to device performance (i.e. metrics); (ii) how the collection of this data can be accelerated and economised; and (iii) whether the quality of the gathered data is sufficient to unlock performance insights and provide confidence in WEC development outcomes and process success.

To address these areas, two 1:20 scale physical models of Mocean’s off-grid WEC, *Blue Star*, have been designed, built, and tested as part of this research. By doing so in the context of Mocean’s wider design optimisation activities, several outcomes are drawn, among which:

- Performance and experimental requirements cannot typically be linked to numerical models via single quantitative metrics. Multiple QOIs can be measured, including those linked to power capture, but ideally beyond it, in order to represent other performance areas, such as reliability. Device

optimisation criteria may alter numerical inputs based on the target market, but largely does not affect validation process in the tank, where power matrix validation remains central.

- A key output is the development of a new folding physical model, which incorporates a representative power-take-off (PTO) at the target scale, expanding its capability and relevance to tracked performance metrics. A bench-testing method is applied and developed to account for frictional PTO losses, with static friction measuring 6.8% of the design torque limit. Considered metrics are shown to broadly improve compared to a previous *Blue Star* geometry iteration, though experimental comparison is limited by the lack of PTO in the former.
- A relatively low-cost and easily accessible wave tank – the Edinburgh Curved Tank – is used to reduce overall testing expense and timelines. Using the Curved Tank facilitates test execution, but introduces limitations on the power matrix coverage in combination with the smallest practical scale of the model itself, thus limiting validation scope.
- Testing methodologies mandated in standards are blended with more novel techniques, including artificially assembled polychromatic seas (in part emerging from academic literature), and applied to the *Blue Star* WEC. Their successful implementation suggests possible improvements to formal testing guidance, particularly at early development stages. For example, performance insights and comparative assessment of different device configurations can be facilitated by faster identification of optimal PTO damping, and measurement of RAO responses and characteristic max-to-mean indicators, among others.
- A high-level uncertainty analysis is carried out to assess confidence in relevant measured metrics and behaviour. This suggests that accuracy levels (e.g. reflection coefficients) from the Curved Tank are comparable to a larger tank such as FloWave. Errors are instead dominated by the physical model embodiment, in particular its PTO and associated hinge friction, as well as the hydrodynamic influence of stiff power and feedback motor cables.
- An attempt to quantify scaling effects is made via an additional 1:40 scale model, revealing associated difficulties in assigning discrepancies to specific hydrodynamic versus other factors. Recommendations are given to better account for and isolate these in future campaigns, e.g. via free decay tests. Though formal guidance on scaling effects assessment is scarce, it is an important step in providing confidence to the overall performance evaluation and validation efforts.

This research demonstrates the challenges in identifying the optimal trade-off between physical model scale, costs, and quality of results. Its applicability to different sizes of full-scale WECs bears relevance to wave energy's evolving market, where many developers are shifting towards offering a range of WECs with different power capabilities targeting a range of applications.

Lay Summary

Ocean waves are a promising source of renewable energy. Machines called wave energy converters (WECs) can be used to convert this into electricity. Global wave energy potential is large, but the industry is currently less developed than other renewables.

Mocean Energy – this EngD's sponsoring company – is developing a relatively small WEC (*Blue Star*) that generates power for local, offshore, subsea equipment. Starting from relatively small machines, the gathered data and experience is used to guide the development of mid-sized, and ultimately large-sized WECs. This *stepped* approach of learning-by-doing can be applied both technically and commercially, and is formalised and followed in this research.

The technical perspective involves testing reduced scale versions of WECs, known as physical models. These are tested in wave tanks, where conditions similar to the real sea can be reproduced in a controlled environment to measure their responses. The research investigates what kind of data is most useful at early development stages. It also explores whether small physical models can be used to collect this data and with what levels of uncertainty. The suggestion is that the process can occur more quickly and with less expense than with larger sized prototypes. If the data is 'good (i.e. relevant and accurate) enough', it should enable design progression with sufficient confidence.

In this research, two successive physical models (20 times smaller than the real Blue Star) have been designed, built, and tested in the Edinburgh University Curved Tank. Notably, a power-take-off (PTO) system, which mimics the mechanical-to-electrical conversion stage, is also included. Benefits include the use of cheaper tanks and models, which can be practically used for different types of tests. This means they are quicker to evaluate and iterate, and therefore can be better integrated in the wider development process. The main challenges are the sources of experimental error, some of which arise from the PTO. Some uncertainties can be quantified and accounted for, while others are difficult to measure in isolation, lowering confidence in the results. Some challenges, such

as identifying and measuring indicators of WEC performance beyond power, are not tied to the scale of model but to early-stage development more broadly.

Outcomes relate to both the process of development and the WEC itself. The technical work has complemented the optimisation of Blue Star, which represents an attractive solution offering for its intended customers. Commercially, the ‘stepped’ approach has been positively received by industry partners, potential customers, and other stakeholders. It has also enabled Mocean to ‘reinvest’ lessons learned in the development of its next, larger WEC. Results point to the positive impact of this ‘stepped’ commercial roadmap and to its parallels with iterative physical testing. They also highlight where testing guidance and standards could be updated, since other wave energy developers are pursuing similar development pathways.

Acknowledgements

Many people deserve much credit for this piece of research, both for its undertaking and for it reaching this stage of completion.

The first thank you goes to my lead supervisor, Dr Tom Davey, for his unfailing support, both technical and pastoral, and for all his guidance through the rollercoaster of this doctorate. Thanks also to my other supervisors Prof Lars Johanning and Dr Laibing Jia for the insights they offered, and to Dr Grégory Payne, who I was fortunate enough to have as a supervisor for the first year only, though long enough to set me off on the right track.

Secondly, I am deeply grateful to Dr Cameron McNatt and Dr Chris Retzler for taking me on at Mocean. It was a privilege to be the first person joining their mission back in 2018, as it remains to this day, while the company continues to grow and flourish. I would like to thank Cameron for his industrial supervision, his encouragement, and for creating a unique company atmosphere where effort and wellbeing are balanced in good measure. Chris, for being a fountain of knowledge, and for his precious advice in the physical modelling and tank testing phases of this research.

Also at Mocean, a sincere thank you goes to Dr Gabriel Scarlett and Dr Alfred Cotten for all the numerical modelling work that interlinked with this research effort, both before, during, and after physical testing. I am grateful to Gabriel for running many, many, optimisations and for his dark dry humour that kept us moving forward even when things did not go to plan. And to Alfred for being a constant sounding board for discussion and answering every possible question on wave theory and numerical modelling with composure and great clarity.

A special thank you is reserved for Yan (“Mooch”) Gunawardena – the man who can fix anything – for his help in getting the Curved Tank up and running, particularly tinkering with tired wavemakers and drive belts. I am also deeply grateful to the rest of his family – Cinthia, Luca and Nina – for hosting me during busy lab testing months towards the end of my practical work, offering food, warmth, care, and entertainment. You have been a second family and a home away from home.

My gratitude extends to everyone else at Mocean, for making the work environment so special. I deeply care about you all and am honoured to be on your same team.

Prof Tom Bruce played a key role in facilitating the resuscitation of the Curved Tank at the University of Edinburgh. None of the testing would have occurred without his coordination efforts, in conjunction with Tom Davey, and notable others such as Morris Dixon of Edinburgh Designs, who troubleshot the tank driver program, helped to fix paddle #11, and sourced a replacement wavemaker belt.

A significant portion of the team at FloWave TT also deserves a dedicated mention. Roman Gabl helped with the Qualisys camera set-ups. Laura-Beth Jordan helped with load cell and other sensor set-ups, and Martyn Lennon who machined many of the parts used in the physical models – including a complex Aluminium tube with internal features and 36 tapped M3 holes – loaded 3D printed parts, tolerated last minute design changes, and was always at hand to help. I am grateful for his patience and perennial good will.

At the University of Edinburgh, Iain Gold and Angus Spray provided invaluable assistance in wiring up the model PTO and somehow managing to squeeze motor and cables in an ambitiously tight space within the nacelle of the active powered physical model. Thank you for your dedication and for your wizardry. Charlie Westerling of Sequentec provided the other nacelle “piece” in setting up the controller of the motor drive and assisting with its calibration, providing practical advice and general troubleshooting. Thank you for hosting me at your office in Queensferry for a few days.

I’d like to thank Prof Stephen Salter, for his motivating correspondence, his pertinent advice, and significant insights he shared in relation to reduced scale testing, and motivating correspondence. It was an honour to – in some minute way – contribute to the legacy he started.

Francesco Marsich and Leticia Diaz (“Fra e Leti”) for being great teachers, and helping me to overcome the customary ‘existential hiccup’ during the doctorate, wade through the doubts and uncertainties, and enabling me to see it through.

I reserve the deepest thank you to my family, especially my parents, for their presence and their sacrifices. Thank you for coping with my time “off grid”. My sister Cecilia has never stopped showing me the way. I thank her and Jason for literally introducing new life into our collective existence with the arrival of Matteo. My grandmothers Emilia and Olga, whose thoughts always follow me, and my now passed grandfathers Mario and Severino, who perhaps wondered from above what I was up to in a wave tank.

Abdu, for being a brother and a source of joy, wisdom, and an example.

Rebecca, for filling every crevice and canyon of my life since the start of this effort, and (both intentionally and unintentionally) teaching me hard lessons that I hope to never unlearn.

Last but not least, those human beings I am lucky enough to call friends, including: “i dottorandi” Livio e Marcella, Fefé, Julian, Alex, Aidan, Ad, AST, Tiago, Roderik, Gérard, Baylor & Sam, George, Lotte, Ésterelle, Kate & Andy, Fareid & Pete, Laura & Jóse, Matt, Sam and the rest of the Cambridge crew, and many others. Whether hosting, sharing time and space, teasing, motivating, consoling, laughing, inspiring, you have done all this and more.

I also thank Diana and Branoc of the 2017 IDCORE cohort with whom I shared the first year of this EngD journey, lectures, tutorials, joint projects, trips, onerous assignments and funny moments.

Numerous individuals have been named, while others may have unintentionally been omitted. If you, as the reader, are wondering whether you might be among this work’s contributors, it likely means you are, and I thank you for it.

Contents

Abstract vii
Lay Summary ix
Acknowledgements xi
Chapter 1. Introduction 3
1.1 Introduction to ocean wave energy 3
1.1.1 Challenges 4
1.2 Introduction to Mocean Energy 9
1.2.1 Technology introduction 11
1.2.2 Introduction to IDCORE industrial doctorate (EngD) 14
1.3 Contextual motivations 15
1.3.1 Mocean aims & development principles 16
1.3.2 IDCORE project aims & objectives 17
1.4 Locating activities & contributions within Mocean 20
1.5 Research timeline 23
1.6 Guide to the reader 25
1.6.1 Thesis flow chart 25
1.6.2 Chapter summaries 26
1.7 Research outputs 29
Chapter 2. Commercial literature review 33
2.1 Key industrial challenges 33
2.1.1 Technology development priorities 33
2.1.1.1 The link to physical modelling 38
2.1.2 Measuring performance 42
2.1.3 Linking metrics and performance 44
2.2 Early-stage metrics 45
2.2.1 Nature of metrics 46
2.2.1.1 The LCOE trap 49
2.2.4 Metrics integration within the design process 53
2.3 Markets for wave energy applications 56
2.3.1 Emerging markets 57
2.3.2 Physical modelling implications 61
Chapter 3. Physical Model Testing 65
3.1 Role and purpose 65
3.1.2 Historical pathway 68

3.2 Standards & Guidance 70
3.2.1 Limitations 77
3.3 Quantities of Interest 78
3.3.1 Inclusion of power-take-off 80
3.3.2 Hybrid testing 84
3.4 Tank testing 89
3.4.1 The Curved Tank 91
3.4.2 Reducing tank time 93
3.5 Scaling 96
3.6 Uncertainties 101
3.7 Another 'trilemma' 107
Chapter 4. Underpinnings of WEC development 113
4.1 Theoretical underpinnings 113
4.1.1 Hydrodynamics of ocean waves 113
4.1.2 Linear wave theory 114
4.1.2.1 Potential flow theory 116
4.1.2.2. Reality checks 117
4.1.2.3 Wave definitions 118
4.1.3 Links to Mocean's numerical model 120
4.1.3.1 Power absorption 120
4.1.4 Scaling 122
4.1.4.1 Froude similarity 124
4.2 Geometry optimisation 125
4.2.1 Guiding the optimisation 127
4.2.1.1 Fitness function 128
4.2.1.2 Numerical representation of PTO 129
4.3 Progress to date 129
4.3.1 Geometry evolution 130
4.3.2 Review of prior physical testing campaigns 131
4.3.3 Gaps and pointers 133
4.3.3.1 Build 134
4.3.3.2 Validation 135
4.3.3.1 Performance 136
4.3.3.4 Uncertainty 137
Chapter 5. The Wave Energy Paradox 139
5.1 Definition of the wave energy paradox 139

5.1.1 Real life examples 142
5.2 Tackling the wave energy paradox 146
5.2.1 Markets 146
5.2.1.1 Chosen market(s)? 148
5.2.2 Size & scale 150
5.2.2.1 Chosen size and scale? 151
5.2.3 Metrics 151
5.2.3.1 Dimensionality 152
5.2.3.2 Integration 155
5.2.3.3 Alignment 157
5.2.3.4 Chosen metrics? 158
Chapter 6. Blue Star – baseline 163
6.1 Background 163
6.1.1 Commercial context 164
6.1.2 Numerical inputs and constraints 167
6.2 Model design and build 168
6.2.1 Choice of scale 168
6.2.2 Build methodology and materials 169
6.2.2.1 Model dimensions 170
6.3 Detailed design 172
6.3.1 Dimensional reference table 172
6.3.2 Trimming and buoyancy 173
6.3.2.1 Trimming calculations 173
6.3.2.2 Trimming analysis in CAD 174
6.3.3 Waterproofing 175
6.4 Instrumentation 176
6.4.1 Rotary sensor 176
6.4.2 Qualisys targets 178
6.5 Tank characterisation 178
6.6 Test plan 179
6.6.1 Tank set-up 179
6.6.2 Sea states 180
6.6.3 Mooring system 182
6.6.4 Measurement set-up 182
6.7 Experimental results 183
6.7.1 Reflection analysis 184

6.7.2 Power producing degree of freedom response 184
6.7.3 All degree of freedom responses 187
Chapter 7. Model PTO 191
7.1 Performance requirements 191
7.2 Design 192
7.2.1 Choice of PTO damper 192
7.2.2 Minimising friction 196
7.2.3 Inclusion in existing physical model and modularity 197
7.3 Build 198
7.3.1 Nacelle 198
7.4 Proposed approach 201
7.4.1 Calibration aim 204
7.4.1.1 Static calibration 204
7.4.5 Controller 205
7.5 Dynamic calibration 208
7.5.1 Lever arm driving period 208
7.5.2 Identifying max gain 209
7.5.3 Zero gain 210
7.5.3.1 Static friction 211
7.5.3.2 Dynamic friction 212
7.5.3.3 Variations with mean period 214
7.5.4 Example calibration 215
7.5.5 PTO damping per unit gain 217
7.5.6 Torque constant 217
7.5.7 Spring coefficient per unit gain 218
7.5.8 Coarse calibration sweep with filtering 219
7.5.10 Calibration variables summary 221
7.6 Optimal Dpto value 221
7.7 Additional considerations 222
7.7.1 Computational errors 222
7.7.2 Repeatability 223
7.7.3 Water tightness 223
7.7.4 Controller 224
7.8 Characterisation conclusion & next steps 225
7.9 Chapter conclusions 225
Chapter 8. Blue Star – folding 227

8.1 Novel elements compared to baseline tests 227
8.2 Commercial model context 230
8.3 Numerical inputs, constraints, and outputs 232
8.3.1 Moonpooling effects 232
8.3.2 Hydrodynamic scaling 233
8.4 Testing campaign aims 234
8.4.1 Design Statement 236
8.4.1.1 What are the appropriate device parameters? 236
8.4.1.2 What is the suitable geometric scale? 236
8.5 Physical model build 237
8.5.1 20th scale model 237
8.5.1.1 Power take off 239
8.5.2 40th scale model 240
8.6 Test set-up 243
8.6.1 Mooring system 243
8.6.2 Equipment/sensors 243
8.6.3 Tank capabilities 244
8.7 Test plan 245
8.7.1 Ir0 seas 248
8.7.1.1 Proposed IR0 seas 249
8.7.2 Power matrix coverage 250
8.8 Empty basin results 255
8.9 Physical model results 256
8.9.1 Recap 256
8.9.2 Signal checks 257
8.9.3 Regular wave RAOs 259
8.9.3.1 Flex RAOs 259
8.9.3 Optimal PTO damping 263
8.9.4 Flex RAO comparisons 269
8.9.4.1 PTO gain effect on RAOs 269
8.9.4.2 Mooring effects on RAOs 269
8.9.5 Power capture 270
8.9.5.1 Power checks 273
8.9.7 Hull Gap and No Gap 277
8.9.8 Irregular waves 279
8.9.9 40th scale flex responses 282

8.10 Uncertainty analysis 286
8.10.1 Trimming error effects 288
8.10.2 Adjusting Morison's damping 288
8.10.3 Effects of friction 289
8.10.4 Irregular waves 290
8.10.5 Ir0 seas 291
8.11 Decay tests 293
8.11.1 Natural period as computed numerically 296
8.12 Ir0 sea responses 298
8.12.1 RAOs from Ir0 seas 298
8.12.2 Comparing moorings and gap effects via Ir0 302
Chapter 9. Discussion 307
9.1 Metrics application 307
9.1.1 Device comparison via metrics 309
9.1.2 Device evolution 314
9.1.2.1 Impact via experimental data 315
9.1.2.2 Impact via numerical optimisation data 316
9.1.3 Comparing different devices 317
9.1.4 Effect of markets on metrics (and process) 319
9.2 Integrating physical model testing 320
9.2.1 Relative merits of small-scale 324
9.2.1.1 Reacting to available technology 325
9.2.1.2 Tank related aspects 326
9.2.1.3 Model costs 328
9.2.2 Addressing numerical modelling limitations 329
9.2.3 Mitigating physical modelling limitations 330
9.2.3.1 Uncertainty 332
9.3 Impact of Wave Energy Paradox approach 333
9.3.1 Streamlining design and tracking progress 336
9.3.2 The Blue Star WEC 338
9.4 Test methods 341
9.4.1 Application of the Ir0 method 341
9.4.2 Experimental scaling investigation 344
9.5 Future work recommendations 347
9.5.1 Improving the physical modelling process 348
9.5.2 Improving WEC performance 350

Chapter 10. Conclusion....353
10.1 Research recap....353
10.2 Outcomes relating to the sector....354
10.2.1 Metrics....354
10.2.2 Method....357
10.2.3 Uncertainty....361
10.3 Outcomes relating to commercialisation pathway....366
10.3.1 The Blue Star WEC....366
10.3.2 The development process....367
Appendix A – Chapter 1....373
A.1 Origin of ocean waves....373
A.2 Curved Tank Letter of Support....374
A.3 Publications....376
Appendix B – Chapter 2....407
B.1 Use-case for oil & gas applications....407
B.2 Mocean's design process....408
Appendix C – Chapter 3....409
C.1 Initial mind-map....409
C.2 Design process....410
C.3 Summary of QOIs and types of physical model testing....411
Appendix D – Chapter 4....415
D.1 Key equations....415
D.2 Theory mind-map....418
D.3 Wave characterisation....423
D.4 Limitations....425
D.5 Drag coefficients....426
D.6 Numerical optimisation....427
D.6.1 Fitness function....427
D.6.2 Optimisation parameters....429
D.6.3 Numerical modelling of PTO....429
D.7 Previous testing programmes....430
D.7.1 Wave Energy Scotland NWEC1....430
D.7.2 Wave Energy Scotland NWEC2....432
Appendix E – Chapter 5....435
E.1 System block diagram....435
E.2 Dimensionality of metrics....436

Appendix F 437
F.1 Model build 437
F.1.1 Wave channel fins 437
F.1.2 Permitted angular flex range 438
F.1.3 Concept sketches 438
F.2 Flange clamping forces 441
F.2.1 PTO damper inclusion 443
F.3 Model trimming 444
F.3.1 Ballasting 444
F.3.2 Trimming images 445
F.4 Curved Tank operational envelope 447
F.4.1 Steepness Limit 447
F.4.2 Stroke Limit 448
F.4.3 Operating Envelope 450
F.5 Tank snapshot 454
F.6 Measured wave signals 455
F.6.1 Amplitude spectra from Rotary Sensor data 455
F.6.2 Cropped time series from Rotary Sensor data 456
F.6.3 Amplitude spectra from Qualisys analysis 457
F.6.4 Cropped time series from Qualisys analysis 458
F.6.5 Amplitude sweep spectra from Rotary Sensor data 459
F.6.6 Cropped time series from amplitude sweep Rotary Sensor data 460
Appendix G 461
G.1 Calibration set-up 461
G.1.1 Equations 461
G.1.2 Set-up 462
G.1.3 Torque sensor 463
G.2 Calibration 464
G.2.1 Static calibration 464
G.2.2 Dynamic calibration 470
G.2.3 Calibration sweep data 475
G.2.3.1 Initial 475
G.2.3.2 Calibration Repeats to check calibration parameter effects 477
G.3 Motor comparison 481
G.4 Additional supporting images 485
G.4.1 Nacelle build 485

G.4.2 Weighing the nacelle 486
Appendix H 489
H.1 BST-folding optimisation output 489
H.2 Guidance and applicability of IEC TS 62600-103 Standards 491
H.2.1 Stage 1 criteria 491
H.2.2 Stage 2 criteria 492
H.2.3 Additional notes on scaling 493
H.2.4 Reporting 495
H.3 Model build 496
H.3.1 20th scale model 496
H.3.2 40th scale model 497
H.4 Mooring set up 499
H.5 Prescribed seas 501
H.6 Proposed seas 502
H.6.1 Focused waves 502
H.6.2 40th scale waves 502
H.6.3 Tuning of the PTO 503
H.6.3.1 PTO damping 503
H.6.3.2 Torque limit 504
H.6.3.3 Thermal limits 506
H.6.3.4 Comparing power in short-crested seas 506
H.7 Moonpooling effects 506
H.8 Signal checks 508
H.8.1 Regular waves 512
H.9 Optimal PTO damping 515
H.10 Capture Width 517
H.11 Power capture checks 518
H.12 Gap vs No Gap 523
H.13 Effect of torque limit on power capture 524
H.13 40th scale model 531
Appendix I – Chapter 9 535
I.1 Metrics plots 535
I.2 Survival tests Plymouth 536
I.2.1 Lazy ‘S’ mooring 537
Appendix J – Blue Star – baseline seas calibration 541
J.1 Reflection analysis 541

J.1.1 Suryanto method 541
J.1.2 Comparison with raw WG signals 544
J.1.3 Comparison with WaveLab analysis 545
J.1.4 Quantification of reflection error 549
J.2 Rotary Sensor Calibration 550
Appendix K – Irregular seas 553
K.1 Flex RAOs 553
Appendix L – Ir0 seas calibration 557
L.1 Initial set up 557
L.2 Proposed IR0 seas 558
L.3 Demand seas 563
L.3.1 Summary tables 565
L.3.1.1 Qualitative observations of 'open tank' Ir0 seas 570
L.4 Empty basin calibration runs 571
L.4.1 IROa (steepness seas) 571
L.4.2 IRObb (envelope seas) 572
L.4.3 IROc (energy seas) 574
L.5 Segmenting of individual Ir0 seas 577
Appendix M – Mass properties 583
M.1 20th scale 584
M.2 40th scale 585
Appendix N – Trimming 587
N.1 Trimming analysis 587
N.1.1 20th model 587
N.1.1.1 20th model without hull gap 591
N.1.2 40th model 593
N.1.2.1 40th model without hull gap 594
N.2 Trimming images 596
Appendix O – Uncertainties 599
O.1 Effects of MWL and trim line 599
O.2 Morison's damping 602
O.3 Friction effects 603
O.4 Irregular waves 604
O.5 Seed number effects 605
Bibliography 609

Part 0:
Context, Aims & Objectives

This initial part – composed of a single chapter – provides relevant background to the whole thesis. It outlines wave energy as a sector, as well as to the company that hosted this research effort - Mocean Energy – introduced alongside its core technology. This part also presented Mocean Energy's development objectives, relating these to EngD research objectives and the associated research questions. Finally, it summarises the content and structure of this thesis, and its associated publications.

"As the wave energy industry is still at a prototype stage, technology development and commercial forecasts are still overwhelmingly dependent on predictions from research tools such as: small scale experimental wave tank tests, numerical simulations and analytical models." (O'Boyle *et al.*, 2015)

- Louise O'Boyle, Jos van 't Hoff, Kenneth Doherty, 2015

Chapter 1. Introduction

This chapter provides the initial context to this industrial doctorate (EngD) research. It situates it within the wider context of ocean wave energy, and relates it to Mocean Energy's (host company) drivers and motivations as a relatively young and fast-growing wave energy developer. The aim is also to clarify the author's role and contributions as part of Mocean Energy. Specific research motivations are linked to Mocean Energy's objectives, from which research questions are extracted. These are provided with this project's scope, as an EngD within the Industrial Doctorate Centre in Offshore Renewable Energy (IDCORE). A guide to the reader, including chapter summaries, is provided at the end of the chapter along with a list of research outputs.

1.1 Introduction to ocean wave energy

According to the Intergovernmental Panel on Climate Change (IPCC), 70-85% of global electricity demand should be supplied by renewable technologies by the year 2050 (IPCC, 2018). As the global energy mix shifts towards renewables, ocean wave energy (henceforth just "wave energy") is considered a largely untapped, yet highly promising resource[1]. Indeed, ocean waves can be considered a renovating 'spring' of energy, ultimately arising from the sun's localised heating of the Earth's surface. The Earth's geographical features, inclination, and rotation, contribute to the generation of temperature gradients and thus air pressure changes; the genesis of winds. Winds, in turn, pass over the Earth's oceans, pushing the water surface over extended distances. The greater the distance over which the wind can blow without obstacles, the greater what is known as 'fetch' (see illustration in Appendix A). For example, in Europe's case, the longest waves arrive from the West Atlantic supported by prevailing westerly winds. The resulting dynamic changes in water elevation are what is ultimately referred to as 'ocean waves'. It is not unreasonable, then, to

[1] A resource, that is, in the early etymological sense of the word – *resource* (French) "a source, a spring", *resurgere* (Latin) "rise again" – contrarily to its more common modern-day interpretation as an exploitable raw material linked to a country's wealth and material supplies (*Resource*, no date).

consider waves a concentrated form of wind power, and/or an indirect form of solar energy. In fact, ocean waves are often presented as the most energy dense form of renewable energy. Even tides, with their tidal stream currents, can be thought of as a very large, long wave, continuously travelling around the world at approximately 450 mph (~724 kph) (Bascom, 1959), with crests and troughs corresponding to ebb and neap cycles.

When appraising renewables, wave energy has been – and often continues to be – considered in competition with wind and solar. This despite the fact that these energy forms are actually inextricable from one another and can be naturally considered as complementary, rather than competing alternatives (CorPower Ocean, 2022). Wave energy is also advocated as having a greater level of resource predictability compared to solar or wind (Falcão, 2010). On the other hand, the inherent technical challenges and the start-stop historical development have resulted in a low level of industry maturity and associated public and investor confidence. The idea of using ocean waves to generate electricity may seem novel given such relatively low levels of maturity, but actually leans on a surprisingly long history of design and development; one could reasonably state that “modern” wave energy conversion technology started in the 1970s at the University of Edinburgh (Salter, 1974). Machines that convert ocean wave energy into electrical energy – or other forms of useful energy – are commonly referred to as wave energy converters (WECs).

1.1.1 Challenges

As noted by (Magagna and Uihlein, 2015), there is evermore a “clear need for the sector to identify ways to facilitate technology development and deployment”.

From a technical standpoint, WECs (particularly those that are floating and further from shore) face the challenge of needing to maintain their position at sea (i.e. “station-keep”) while also moving in response to – and being as sensitive as possible to – wave excitation. This in some ways contrasts ships and platforms requirements, which are designed to be either insensitive or stationary with respect to waves (Clément *et al.*, 2002). Reliability of moving parts in an offshore environment is also not straightforward, not least due to saline corrosion and the rapid build-up of biofouling – i.e. accumulation of marine

organisms such as algae and small animals – on submerged structures. Naturally, the servicing of WECs becomes more arduous the further they are from shore.

Another recurring challenge is WEC survival due to the highly energetic marine environment. Salter pointed out that, "to complain of the dangerously high waves at a good wave site is like complaining of the high temperatures in the flame of a thermal plant" (Salter, 2005). However, the challenge is more nuanced, since the largest waves are rare but must still be designed for, while most of the revenues and energy yield for a wave energy converter arise from the smaller, more frequently occurring, waves. This issue does not present itself for solar and tidal stream energy conversion – where maximum irradiance and flow speed correspond to maximum energy generation. Wind turbines have a cut-in and cut-off wind speed, between which the turbine is permitted to spin and generate electricity. Above the cut-off speed, the turbine can be effectively isolated by pitching of the blades into the wind direction (aerodynamic braking) and in rare cases by mechanical and/or electrical braking. Although challenging, this is easier to implement above the water line and with wind speed as the single input variable as opposed to both height and wavelength for wave energy.

'Extreme events' at sea can be spectacularly severe. For example, abnormally high waves referred to as 'rogue' or 'freak' waves[2] are unique to the ocean environment. Several have been recorded, the largest of which was a 17.6m high wave in the coastal waters off Vancouver Island, Canada (Gemmrich and Cicon, 2022). To continue the analogy, this would be akin to a thermal plant occasionally erupting like a volcano, although analogously extreme events – e.g. earthquakes – do happen on land as well. Other notable rogue waves have been measured, studied, and named, including the "Draupner" (1995, North Sea), "Killard" (2014, West coast of Ireland), and "Andrea" waves, the latter detected in the year 2007 in the North Sea.

[2] Not to be confused with tidal waves – originating from seismic shocks.

Even in the absence of extreme waves, WECs can be subject to significant forces. Salter somewhat countered this perspective noting that, "for low-freeboard[3] devices the stresses in large waves rise at slightly less than the first power of wave height, while the available power rises with the square" (Salter, 2005). Thus, economic viability should theoretically rise with increasing wave height. The presence of buoyancy to counter the force of gravity also distributes loading, rendering loading conditions more benign. However, an additional and significant challenge arises due to wave irregularity. At any given point, the shape of the sea and the waves that characterise it are non-deterministically produced. Among other parameters, waves vary in length, height, period, direction, and time, making it difficult to optimise WEC efficiency over such a broad range of conditions. There is no obvious design point in contrast to wind turbines, which begin to convert wind energy within a specific wind speed interval and continue to do so at a specified rated speed. For WECs, there can be significant ratios in average-to-peak loading conditions; an important contributor to failure. Large variability in available power creates challenges for the power-take-off (PTO) dimensioning and design. Furthermore, the coupling of irregular, slow motion that requires large forces and slow velocities in a reciprocating manner increases the technical challenge. This is partly because most established generators have been designed for high-speed, mono-directional rotation.

Returning to the issue of maturity, industry standards and best practices are very much in flux and have not yet crystallised. In 2019, W. Sheng wrote that “no well-accepted standards to assess and standardise the diversified wave energy technologies” existed (Sheng, 2019). Part of the challenge is the fact that the transformation of energy is different across different WEC systems, of which multiple ‘families’ exist – e.g. point absorbers, attenuators, oscillating water columns (OWCs), and more (Zhang, 2022). While some tend to compare wave with wind, expecting that wave energy will ultimately converge towards one

[3] Freeboard is defined as the overall height minus the draft, which is the submerged section of the height.

common technology embodiment – such as the horizontal-axis 3-blade wind turbines – the author's opinion is that this is unlikely to be the case in the wave sector. Wave energy is perhaps better compared with hydro-electric technology, where different turbines are employed: Kaplan, Francis, Pelton, cross-flow, and many others. This is likely to be the case for wave energy power-take-off (PTO) systems. Given the current – and likely future – diversity within the wave energy sector, it is not surprising that one of the recurring themes in wave energy has been confusion, particularly from the perspective of investors, who are left wrestling with the question: *"Which WEC (out of the many more of less developed concepts) is the best?"*

Linked to maturity is the theme of cooperation within the industry. At a 2020 panel discussion during the Ocean Energy Europe (OEE) conference, Francisco Garcia Lorenzo (CEO of Wedge Global and coordinator of the SEA TITAN project) stated: "We have been paying for more than 10 years for several patents all over the world from the patent corporation treaty. They are expensive and we are not making money from any of them now. We need to change our approach and need to think of freedom to operate (FTO) instead of intellectual property (IP) for protection."[4]

Several commercialisation barriers have been mentioned to this point, such as a harsh operating environment and low technology maturity. Others exist and persist: high capital costs (and thus onerous investment); a somewhat opaque policy landscape; complex spatial planning; consenting restrictions; and grid availability. These have all contributed to the sector failing to meet the once anticipated progress. However, there may be *additional contributing factors* related to the optimality of the design process and the way this links back to device performance measurement, as well as the specific performance objectives that are chosen. Broadly speaking, this research project focuses on these 'additional factors', examining the design process from the perspective of a WEC developer, Mocean Energy. The proposed analysis considers 'device-specific' elements that centre on *development* as opposed to broader 'industry-

[4] Personal communication, cited with permission from Francisco Garcia Lorenzo.

specific' elements associated with *deployment*, though it will be seen that these are not so extricable from one another. The scope is limited to factors that have a directly quantifiable impact on techno-economic performance, without considering those outside of developer control – such as political will, public support, consenting constraints, country resources and financial incentives – though they will too, of course, ultimately affect commercialisation outcomes.

Despite the historical "doom and gloom", examples exist of operational grid-connected and off-grid WECs. Most notably, the power plant in Mutriku (Basque Country) has been producing grid-connected electricity since its operational debut in 2011 (Torre-Enciso *et al.*, 2009) and has supplied over 2.1GWh of energy to the grid since (Ocean Energy Systems, 2021). More recently, the Guangzhou Institute of Energy Conversion (GIEC) developed and deployed the Sea Eagle 500kW rated WEC, which had accumulated 18 months of successful operation as of December 2020 and remains operational today. More promising examples of emerging wave technology can be found in (Ocean Energy Systems, 2021).

Figure 1 - The Mutriku wave power plant is an enclosed set of OWCs attached to a breakwater in the Basque Country (Otaola *et al.*, 2019).

Figure 2 - The floating Sea Eagle WEC, powering a semisubmersible open-sea aquaculture platform (OES, 2019).

Winding back to its genesis in the 1970s, the wave energy industry has been characterised by a series of highs and lows. Spurred on by the oil crisis of the 60s, wave energy research was kicked off with great resolve and conviction in the UK in the 70s, only to be left trailing in the wake of nuclear energy in the 80s and 90s. From the 00s it began to re-emerge, and at the onset of the 2010s it

enjoyed a new peak level of public confidence, with two flagship companies from Scotland (Pelamis Wave Power and Aquamarine) leading the charge in the UK and globally. Unfortunately, both folded following setbacks in the deployment of very large prototype WECs, in 2014 and 2015 respectively. A confidence vacuum ensued as investors and other stakeholders lost interest (OCEANERA-NET, 2017); the focus shifted to other forms of renewable energy, such as wind and solar. However, we are now in the course of a cautious 'rebirth' of wave energy occurring in Scotland and elsewhere – at least from the viewpoint of industry players. This is occurring within a wider drive for offshore renewable energy, evidenced in the policy domain through initiatives at European and country-level, such as the EU Offshore Renewable Energy Strategy published in 2020 (European Commission, 2020), Spain's Offshore Wind and Marine Energy Roadmap in 2021 (PLOCAN, 2021), and Italy's Recovery & Resilience Plan[5], also in 2021, that includes a EUR 700m pot dedicated to innovative renewable energy technology, among which wave energy is specifically mentioned (Governo Italiano. Presidenza del Consiglio dei Ministri, 2021). More details on wave energy's history, its potential to supply useful energy in different markets, and associated development assessment approaches, will be provided in Chapters 2-3. The following section highlights Mocean Energy's genesis and the author's role and contribution in the company over the last 3-4 years.

1.2 Introduction to Mocean Energy

Mocean Energy Ltd (or just "Mocean") – the company hosting this EngD research – designs and develops WECs, from concept to transfer-to-manufacture. Mocean was founded in 2015 by Dr Cameron McNatt and Dr Chris Retzler, both PhD's from the University of Edinburgh, where they initially met. Dr McNatt started out developing naval architecture software, which he then applied in the realm of hydrodynamic modelling and numerical simulations. Dr Retzler was the co-founder and Principal Scientist at Pelamis Wave Power, with extensive physical modelling and tank testing expertise. In September 2008,

[5] Piano Nazionale di Ripresa e Resilienza (PNRR).

three Pelamis devices deployed off the northern coast of Portugal became the first grid-connected wave farm in the world (OES, 2008). However, following Pelamis' closure, they met at the University of Edinburgh, joined forces, and utilised their complementary backgrounds to set up Mocean. The company's founding was based on Dr Retzler's experiential insights and Dr McNatt's emergent work on computerised WEC geometry generation and hydrodynamic performance optimisation. In other words, a numerical optimisation routine able to optimise a WEC's shape in order to maximise a particular indicator (or metric) of performance. The resulting geometry could then be validated and refined via tank testing, engineering considerations and practical experience (more in Part II and Part III).

Crucially, Mocean's genesis almost exactly overlapped with the creation of Wave Energy Scotland (WES) in 2014. WES, a Scottish public body, was started by the Scottish Government with the explicit role of 'picking up the pieces' of past, commercially unsuccessful, wave energy projects and to try to breathe new life into the industry. A distinctive feature of WES has been its focus on competitive pre-commercial procurement (PCP) programmes to drive innovation in the sector. Mocean's successful involvement in successive phases of one such programme - the Novel Wave Energy Converter (NWEC) innovation stream - has allowed the company to competitively access around £4.4m in funding thus far. One of the distinctive features of this PCP is its focus on 'phased' innovation and the use of specific metrics to assess technology performance and potential. This concept (further explored in Chapter 5), has now been adopted at European level through the EuropeWave PCP programme, of which WES is a leading player.

A final, important note is a consideration about the end-use of wave energy – i.e. its *target market*. Traditionally, wave energy has aimed to develop grid-connected WECs able to power national electricity grids. This end-use involves large individual or multiple (i.e. farms of) devices typically able to deliver 100s of kilo-watts (kW) to mega-watts (MW) of power and of very large physical size. For example, the second iteration of the Pelamis WEC, the *P2*, was 180m long, 4m wide, and weighed 1,350 tonnes (EMEC, no date); the Aquamarine *Oyster 800*

WEC was 26m wide and 13m tall. Such devices are also described as ‘utility-scale’, in practice a synonym of ‘grid-connected’ when describing a WEC.

In this context, the WES programme was conceived as a structured route towards grid-connected WECs. As part of NWEC Stage 3, Mocean built and tested what was originally conceived as a ½-scale prototype of a 100kW-rated[6], grid-connected WEC. This prototype was successfully tested in open water at the European Marine Energy Centre (EMEC) in the Orkney Isles, Scotland, in the latter half of 2021. Due to specific commercial considerations and opportunities, the prototype has been re-conceived as a full-scale 10kW-rated WEC for off-grid applications. This shift in commercialisation tracks – or this double-track – has been an important piece of context to the present research. Among other things, it implies a change of stakeholder priorities and associated product requirements. These, in turn, can affect the WEC’s development pathway both in terms of design process and performance assessment. Such implications are explored in Chapter 2, and their implementation is approached in Chapter 5, with specific activities stemming off and being pursued in Part III (Chapters 6-8).

1.2.1 Technology introduction

Once more, it is helpful to anchor to a wave pioneer such as Stephen Salter’s insights on WEC technology. Salter highlighted the importance of “design[ing] devices which can either hide from extremes or yield in a controlled way to loads greater than those associated with the economic power limit” (Salter, 2005). One motivation is the lack of investment returns in resisting rare extreme loads, because that energy lies outside any economical limit. In other words, the

[6] WEC nominal power ratings can often be misleading, since a universally accepted definition is not available. For wave energy, power rating is more nebulous than for wind energy, where it corresponds to a fairly well defined operating point (approximately constant power within particular wind speed boundaries). For Oscillating Water Column (OWC) type WECs, rated power is a bit more straightforward to define and analogous to wind as power is being converted by pumping air or liquid through a turbine. For most WECs, though, the operating point is more difficult to define as operation is distributed over a range of sea states with differing wave heights and periods; and thus highly site specific. IEA-OES Annex II (2004) gives the following indication: "For preliminary analyses and comparability of results the rated power is defined as the average absorbed power in a sea state of Hs = 5 metres." (Nielsen, 2003). This presents its own problems, because it does not specify period, and because Hs = 5m may be outside the operating range.

suggestion is to seek to maximise yield by expanding the range of frequency sensitivity of the device, making the ability to convert energy from the largest waves as redundant as possible in terms of overall energy yield contribution. In such a way, the design can focus on the reduction of sensitivity to the very high peak forces at the extremes, without the need to resist them in order to convert their energy. This was certainly one of the guiding principles for Mocean's core technology concept, as outlined in the continuation of this section.

Figure 3 - Mocean's Blue X prototype in action at Scapa Flow, EMEC. [Courtesy of Mocean Energy]

Mocean has been developing a range of WECs based on a common set of fundamental features and design/operation principles. The central concept is a floating hinged-raft with a semi-submerged prime mover[7] structure embodying unique geometrical features. These include asymmetric hulls and sloped sections referred to as "wave channels" at the front and rear of the WEC, which project into the wave flow (Figure 5). Fundamental power absorption and

[7] *Prime mover* refers to the part of a WEC's structure that is directly interacting with its surrounding fluid (i.e. waves). It is sometimes also referred to as *captor*.

survival characteristics are briefly outlined below, and address Salter's previously explored suggestions.

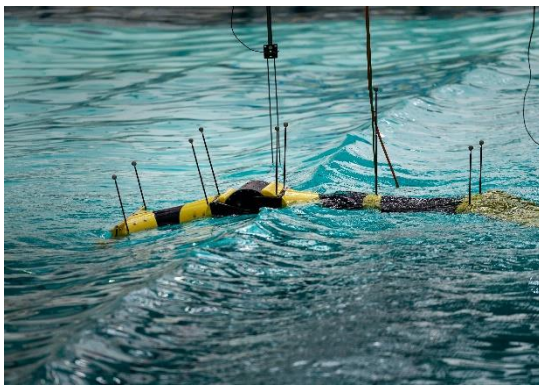

Figure 4 - A Blue X scaled physical model excited by waves travelling right to left.

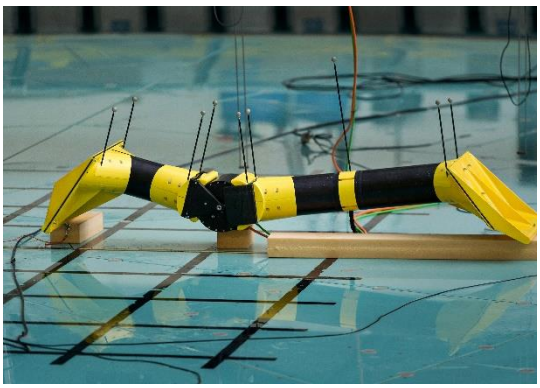

Figure 5 – The same Blue X scaled physical model on the tank floor at the FloWave tank testing facility.

POWER ABSORPTION

- When excited by waves, the induced relative motion of the hulls is converted into electrical power by an electro-magnetic generator located at the hinge, parallel to the wave crests (as seen in Figure 4).
- The implemented geometry innovations have the combined effect of broadening the frequency response of the WEC, rendering it sensitive to wavelengths that far exceed its total length and increasing overall capture yield.
- Wave channels affect energy absorption by increasing the *added mass* of the WEC. This relates to hydrodynamic loading, and more specifically the reactance component of the device's radiation impedance (i.e. the effect of the moving WEC on its surrounding fluid). Added mass is associated with energy storage behaviour and is proportional to the prime mover's acceleration (explored further in Chapter 4 & mind-map in Appendix D).
- Although there is a single power-capturing degree of freedom (DoF), power absorption increases via the cross-coupling of various modes of motion enabled by WEC asymmetry.
- As the WEC gets longer, it can absorb longer waves and theoretically increase its AEP, but at the expense of a higher torque limit.

SURVIVABILITY

- The survival strategy involves disconnecting the PTO, allowing the hulls to rotate freely about the hinge, and enabling large enough rotations such that no end-stops are required to limit the pitching range of motion.
- The survival strategy is crucially enabled by the WEC's natural load shedding mechanism: the device dives under steep incident waves, limiting power absorption in more extreme sea conditions (Yemm *et al.*, 2012) and avoiding wave slamming, see Figure 4. This behaviour is akin to that of a surfer 'duck-diving' under waves when swimming out from shore.
- The WEC is self-referencing. It reacts against itself, not relying on taut attachments to moorings or structures fixed at the seabed. This, generally speaking, lowers mooring loads, and makes the WEC deployable in a wider range of depths.

1.2.2 Introduction to IDCORE industrial doctorate (EngD)

For clarity and scope definition purposes, a brief overview of the EngD programme is provided and key differences with respect to a PhD are highlighted. According to the 2017-18 IDCORE handbook (University of Edinburgh, 2017):

"The EngD degree is equivalent in academic standing to a conventional PhD, but is achieved through research which is much more industrially focused and which is designed to produce graduates who have a sound understanding of the business implications of industrial research activity."

"Research projects are identified by sponsoring companies and concern a topic related to business activities of the industrial sponsor."

In short, IDCORE EngD research projects are anchored to company priorities. Since these are not static, the research can be less topic-centric and more application-centric compared to a traditional PhD. The impact, novelty and innovation primarily aims to address company requirements, which can have wider industrial relevance but are not necessarily geared towards generalised solutions/conclusions, although they often indirectly contribute to these also.

1.3 Contextual motivations

Recently, the “start small, go big” philosophy has become a central theme for a growing number of wave energy players. In the commercial domain, it plays out as WEC developers targeting beachhead[8] markets that do not require large utility-scale sized machines. This is a strategy for alleviating commercialisation barriers, by accelerating deployment, learning, and intermediate returns – it is discussed further in Chapter 5. Mocean’s embodiment of this approach is a WEC called *Blue Star*, designed to generate 10kW average power in central North Sea wave climates. Its applications include markets such as: subsea oil and gas (O&G), residential autonomous subsea drones, sensors and monitoring, and carbon capture and storage (CCS) tiebacks. This has been a major driver for the present research, which has centred on the Blue Star WEC.

A parallel concept applies to the technical domain, particularly for physical modelling. Whatever the target market, a fundamental element of the design and development process involves testing physical models (i.e. dimensionally shrunk representations) of WECs in wave tanks: basins where ocean conditions can be physically reproduced. This is a key step as it allows a developer to visually observe device behaviour, build intuitive understanding based on empirical evidence, boost development confidence, validate numerical models, and capture effects that are difficult to model numerically or analytically. Available standards and guidelines point to increasing scales (or sizes) and complexity of models to be used as technology readiness level (i.e. device maturity) increases. However, in practice, this is not a linear evolution process, and often requires iteration.

Thus, the proposition is that the more one can advance the performance of the model (and WEC) at the earlier stages, the more time and money can ultimately be saved as a developer while moving through the development phases towards technical and commercial readiness. Further, the more sophisticated the small-scale model, the more can be learned about its overall performance, provided

[8] Also termed in literature as ‘alternative’, ‘intermediate’ or – somewhat misleadingly – ‘niche’ markets.

that this additional data is of sufficient quality. Thus, physical testing that is fast-turnaround and small-scale can potentially be a very valuable tool in advancing the design and performance of a WEC.

Mocean's unique context further motivates this streamlined approach in three specific ways:

- The numerical model underlying WEC optimisation routine *rapidly* produces geometries based on various inputs;
- a *shifting* commercial landscape means specific WEC requirements also shift (no longer a single application of grid-connected power);
- proximity – and facilitated access – to tank testing facilities (e.g. the Edinburgh University Curved Tank) reduces some of the economic and logistical barriers and offers greater opportunity for physical modelling *integration* in the wider development activities.

The above feeds into the research questions and objectives set out in Section 1.3.2.

1.3.1 Mocean aims & development principles

Mocean's primary aim as a wave energy developer is to:

> *Design, build, and sell a wave energy converter that can provide local off-grid power to equipment offshore (and ultimately scale up its technology to power national electricity grids).*

This vision is enabled by a series of more specific product and process principles:

1. A WEC that performs in the required way
    i. To deliver appropriate performance
    ii. To satisfy cost requirements
    iii. To meet other end-user/stakeholder requirements
2. A process that allows to start small and then scale to go big
    i. To accelerate learning, technical and commercial evidence
    ii. To access commercial returns and reduce reliance on grants and subsidies

   iii. To ensure continuity and flexibility (both technical and commercial)
3. A design methodology that enables principle (1), and can be applied to principle (2)
   i. To link back to Mocean's distinctive WEC optimisation routine – rapid iteration and validation of WEC designs
   ii. To enable Mocean's business model of IP licensing to go-to-market partners

1.3.2 IDCORE project aims & objectives

Thesis aims are anchored to the company (and industry) landscape outlined above. The core question being addressed here is:

To what extent can Mocean's Blue Star concept be developed by streamlining technical learning through iterative WEC designs with a relatively small physical model, while still capturing sufficient device characteristics to gather the type and quality of data needed to validate and advance performance?

Three perspectives are investigated to form the project aims:

1. Identify what data is required from physical model tests, in order to validate (the chosen qualities of interest that indicate) device performance (i.e. metrics);
2. Explore how the collection of such data can be accelerated and economised (from both a model and tank point of view); and
3. Establish whether the quality of the gathered data is appropriate to unlock performance insights and provide confidence in WEC performance and development progress/success.

By doing so in the context of Mocean's wider design optimisation activities, the following objectives can be set to address the project's aims:

1. Investigate the integration of physical modelling and experimental testing within the wider optimisation routine
   i. Review performance/fitness metrics suggested by literature, the wave sector industry, and those used by Mocean thus far
   ii. Explore the link between experimental and numerical models via metrics

   iii. Review how current standards and guidelines apply to an off-grid WEC like *Blue Star*
   iv. Suggest suitable metrics for use with small-scale models and point to associated model capabilities required to measure appropriate quantities of interest

2. Design, build, and test at least two small-scale physical models of successive iterations of Mocean's off-grid WEC, *Blue Star*
   i. Identify smallest viable model scale, taking into account capability (as opposed to uncertainty) limits of available tank-model combination, testing aims, and other scale-determining considerations
   ii. Expand model capabilities by designing and implementing a new modular nacelle with an active PTO model, and characterising PTO friction and damping behaviour
   iii. Critically review testing standards and guidelines with a focus on: small-scale, fast-turnaround, and 'performance before readiness'
   iv. Implement an adapted test methodology for testing in the University of Edinburgh (UoE) Curved Tank (CT), building on previous Mocean campaigns and emergent methods from literature, with the goal of enabling faster comparative and absolute assessments
3. Assess the suitability/effectiveness of the above process in obtaining appropriate typology of data of satisfactory quality to validate models and advance WEC development
   i. Compare numerically and experimentally obtained quantities of interest (/metrics) to undertake validation
   ii. Qualify – and to the extent possible quantify –experimental uncertainty during test campaigns to assess confidence in measured metrics, in particular:
      a. Measure PTO friction and tank reflections
      b. Consider practical differences between as-simulated and as-tested models, and associated effects

c. Compare Curved Tank data to data obtained at the University of Plymouth's COAST Lab and in relevant prior Mocean campaigns
d. Estimate scaling effects by testing different sized models at 1:20 and 1:40 Froude-scale in equivalent full-scale seas

iii. Discuss any limitations of smaller-scale models based on the above findings and make recommendations for future testing campaigns

1.4 Locating activities & contributions within Mocean

A simple diagram of Mocean's current company structure is given in Figure 6, to help locate the author's role in the wider company context. EngD activities have predominantly occurred as part of the Physical Modelling team within the Technology R&D group. The author's core contribution here has been the design, build, testing, data collection and analysis of two 20th scale physical models, known as *BST-baseline* (Model #1) and *BST-folding* (Model #2) as denoted in Figure 8. However, these activities have required inputs from – and fed outputs back to – several other company activities. Relevant links with the Numerical Modelling, Engineering, Commercial, and Programmes teams are outlined in Figure 7 and Table 1, where Mocean personnel contributions into this thesis are highlighted and acknowledged. They will also be outlined – wherever relevant – at the start of each subsequent chapter.

mocean energy

Company Structure

Groups	Business Management Managing Director				Technology R&D Technical Director		
	Management	**Operations**	**Commercial**	**Programmes**	**Engineering**	**Physical Modelling**	**Numerical Modelling**
Teams	Finance, Investment, Corporate, HR	Facilities, QHSE, IP, Resources, Admin	Customers, Partners, Market research, Strategy, Marketing	Project management, Applications, Funding bids, Budgeting	Product design, Mechanical, Electrical, Systems, Mooring, Offshore	Prototypes, Tank testing, Model design, Model build, Data collection, Data analysis	Optimisation, Software development, Performance modelling

Figure 6 - Mocean Energy company structure, simplified to show groups and the teams they are composed of. Individuals can work in multiple teams and occasionally multiple groups.

Figure 7 shows core research contributions (green colour), linked to complementary activities within the Technology R&D domain (orange), and associated input/output relationships with broader peripheral activities and outputs (blue). Activities classed as 'Linked' were not within the remit of the author, and were the sole responsibility of Mocean's numerical modelling team. Activities classed as 'Peripheral' were partly in the author's remit, but not central

to the research and consisted in either commercial interfacing elements of development (end-use requirements) or reporting as a result of particular grants being received by the company that required external reporting (company deliverables).

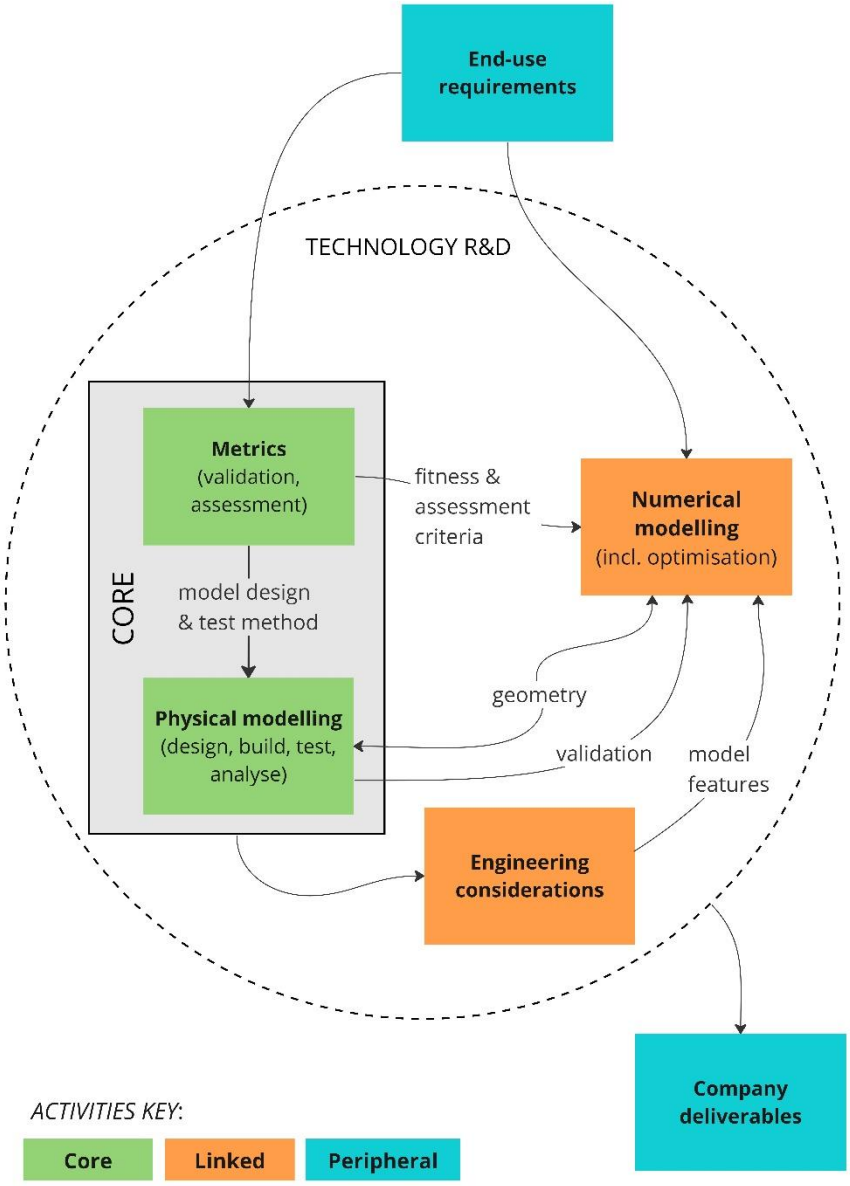

Figure 7 – Author's contribution to WEC development shown in the CORE box and coloured in green. Other linked activities within and outside of the technology R&D domain are also shown.

Table 1 lists specific Mocean personnel contributions that have fed into EngD activities and outputs. Note that some additional assistance was received from multiple non-Mocean personnel in various stages of the present research. This is accordingly noted in the Acknowledgements section.

Contributor	Team(s)	Input(s) to present research
Gabriel Scarlett	Numerical Modelling	• Set up and running of the numerical optimisation routine runs, including expansion of objectives and supporting algorithms • Numerical concept geometries, with associated performance parameters such as dimensions, mass, torque limit, and PTO damping • Spectral-domain based analysis to predict WEC power matrix and response RAOs
Alfred Cotten	Numerical Modelling	• Time-domain modelling for validation purposes • Insights relating to fundamental theoretical underpinnings • Additional numerical sensitivity studies
Chris Retzler	Physical Modelling, Engineering	• Prior Mocean physical testing campaigns • Associated advice in setting up physical testing, physical model design, and model building • Feedback on test plans developed
Cameron McNatt	Commercial, Numerical Modelling	• Original optimisation routine development and continuous refinement • Fitness function definition and metrics advice • Commercial development and engagement

Table 1 - Links with other Mocean personnel and associated contributions that have fed into the EngD.

1.5 Research timeline

This EngD, just as Mocean's activities, has taken place over the course of a rapidly evolving context, evident in the company's growth from 2 to 19 company personnel just over the course of the main EngD research phase. A timeline is provided to inform the reader regarding notable company and project specific milestones, as well as additional events that have impacted it (Figure 8).

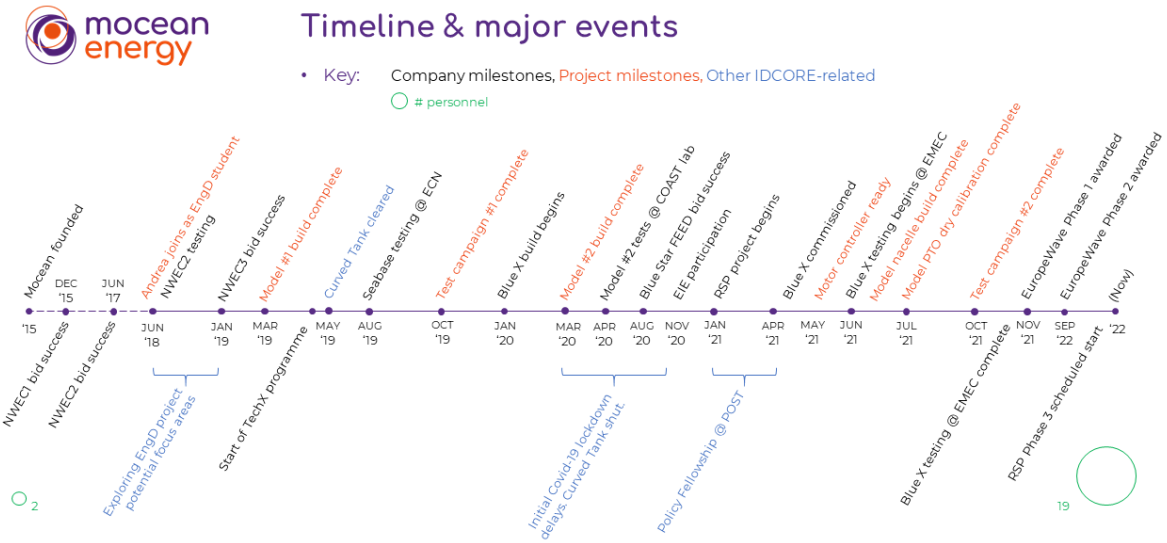

Figure 8 - Overall EngD activity timeline within the context of Mocean Energy activities and major milestones.

Upon joining Mocean in June 2018, the author was immediately involved in the testing of a 20th scale physical model for NWEC Stage 2, at the FloWave facility. The next 6 months at Mocean were characterised by the submission of NWEC2 deliverables and the submission of the NWEC Stage 3 application. The success of the latter had decisive effects on the author's ability to continue the doctorate with the company. The remit of the project was rather open during the initial 6 months. Taking a bigger picture approach, the author was attracted by the discussions around metrics and alternative (non-utility grid) markets, which were thereby explored. Following the successful WES NWEC Stage 3 submission, and the recruitment of a numerical modeller, a decision was taken to focus on physical modelling. Thus, two different physical models were designed, built, tested, and analysed – referred to as Model #1 and Model #2 in Figure 8, and

respectively as *Blue Star-baseline* and *Blue Star-folding* in the latter thesis chapters. Model #1 was a passive model of a very early geometry of Blue Star, tested when the numerical model was still relatively undeveloped. Model #2 was based on a more recent Blue Star geometry iteration. It built on the first round of testing and consisted in an active, more sophisticated, model that included a PTO and different mooring configurations. A passive version (without PTO) of Model #2 was also built, but tested externally.

Finally, two different events caused core EngD activities to be temporarily interrupted. The first – the onset of the Covid-19 pandemic and associated lockdowns in the UK – is discussed in a separate supporting statement. The second consisted in a 3-month policy fellowship at the Parliamentary Office of Science and Technology (POST), an internal research body of the UK Parliament. This took place as part of the UKRI Policy Internship Scheme, and the associated publication is publically accessible (Caio and Miller, 2021). During this 3-month period, EngD activities were paused, to be resumed in May 2021. A final point of note is made in relation to the prospect of the Curved Tank facility closure towards the end of 2019, independently of Covid-19 pandemic impacts. A copy of the letter of support sent to relevant personnel is included in Appendix A – happily, the facility remains open at the time of writing.

1.6 Guide to the reader

1.6.1 Thesis flow chart

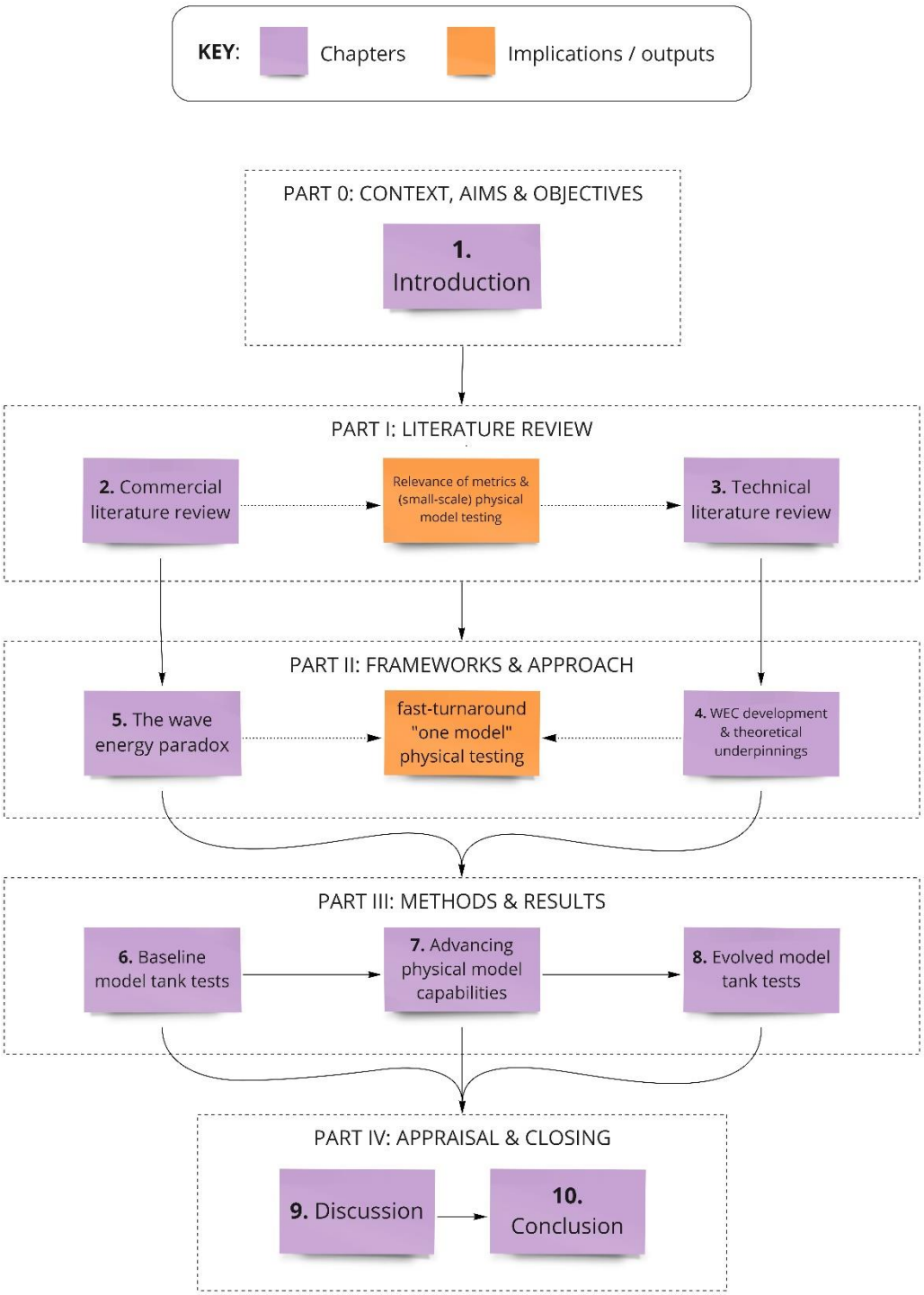

Figure 9 - Thesis flow chart (showing Parts and Chapters).

1.6.2 Chapter summaries

Chapter 1 has introduced ocean wave energy, Mocean Energy's position within the industry, and the broader sector context. From these, research questions and objectives have been formulated. The author's core research contributions and specific role have been pointed to and linked to other Mocean activities and personnel whose outputs have fed into the present research effort. An overall EngD timeline has also been outlined, including relevant highlights and milestones of the EngD and more widely for Mocean.

The remainder of the thesis spans a further nine chapters, arranged in four parts, covering: (I) commercial background and literature review; (II) WEC development and approach to physical modelling; (III) methods relating to physical model testing, addressing the main aims laid out in Section 1.3.2; and, lastly, an appraisal and closing part (IV), including a discussion of the results and presentation of conclusions. Individual chapter summaries follow below.

PART I: LITERATURE REVIEW

Chapter 2 is a commercially oriented literature review, focusing on performance definition and assessment as one of the key industrial challenges. It reviews technology development priorities, particularly at early development stages, and the associated links with physical modelling. Metrics are examined in terms of their nature and their potential integration within the overall design process. Markets for wave energy are introduced, with a focus on off-grid applications. The implications of moving from grid-connected to off-grid domains is also reviewed.

Chapter 3 is a technical literature review focusing on physical modelling, including its purpose, and the challenges and opportunities of shifting to smaller scale models. Attention is given to the inclusion of model PTOs and the accounting of experimental uncertainties. Testing and development standards and guidelines are reviewed, as well as tank testing methods focusing on the Edinburgh University Curved Tank in particular. The trade-off between cost, accuracy, and representability of physical models is also explored.

PART II: FRAMEWORKS & APPROACH

Chapter 4 outlines the fundamental features and linear wave theory underpinning Mocean's numerical model and optimisation routine that leads to specific WEC geometries and performance predictions. It also describes Froude scaling, an essential theoretical framework for reduced scale physical testing. Thus, the chapter begins to link numerical and experimental aspects of WEC development. Prior physical modelling campaigns carried out by Mocean are also summarised in terms of outputs and lessons learned, in order to inform core physical modelling activities of this thesis.

Chapter 5 proposes a framework – denoted *Wave Energy Paradox* – for device development and commercialisation. This is formulated on the basis of the examined literature and the commercial context. It informs the choice of WEC to be developed, and the approach to the particular activities that support iterative WEC development, specifically aiming to maximise learning and accelerating commercial returns. In the technical sphere, this framework bears relevance to an analogous accelerated learning pathway, that seeks to utilise physical modelling that is as far as permissible *small-scale* and *fast-turnaround*.

PART III: METHODS & RESULTS

Chapter 6 outlines the first round of physical model testing undertaken with an early model of the Blue Star WEC, referred to as *Blue Star-baseline*. This 1:20 scale model serves as an initial reference for future testing rounds. As well as the physical model itself, characterisation of the wave tank used for testing - Edinburgh University Curved Tank – is undertaken to identify an approximate operational envelope. Reflection coefficient and RAO analysis are presented based on passive (i.e. free) hinge model behaviour, without power extraction.

Chapter 7 describes the design, testing, and characterisation of a new physical model PTO, to expand small-scale physical model capabilities. A new, modular, nacelle that contains the PTO is built and dry bench-tested to characterise damping and torque performance, particularly in light of additional friction introduced by the need to isolate the powered nacelle from wet testing environments. The new nacelle is designed as part of a latter geometry of Blue Star, featuring the ability of the forward hull to fully fold within the aft hull.

Chapter 8 presents the second, and more in-depth, round of physical model tank testing with an updated geometry of the Blue Star WEC – i.e. *Blue Star-folding*. A 1:20 scale model is designed and built, with expanded model capabilities that include active damping and power take-off. A refined test methodology is also implemented. The model includes a moon-pool in the aft section, and is tested both with and without it. A refined sprung-taut mooring system that is depth agnostic is implemented and compared with the simple slack mooring previously utilised. A geometrically identical 1:40 scale passive model is also tested to provide initial estimation of hydrodynamic scaling effects. Results are presented focusing on motion and power RAO responses, and a preliminary uncertainty analysis is also outlined.

PART IV: APPRAISAL & CLOSING

Chapter 9 discusses physical model testing results from the previous Part and their implications, particularly in terms of enabling performance evaluation, device comparison, and the integration of physical modelling in the overall development process. Via the comparison of different elements of performance of the two tested Blue Star iterations, and their relation to tracking progress from a commercial as well as technical perspective, it discusses implications to the impact of the *Wave Energy Paradox* in development success. It also presents future work recommendations regarding improvement of physical modelling processes and Blue Star WEC performance.

Chapter 10 outlines the main conclusions and research contributions of the present work, relating these back to the research questions of Chapter 1. It contextualises findings relating to EngD goals in terms of metrics, method, and uncertainties. It also interlinks these with Mocean's objectives in terms of commercial impact of the Blue Star WEC and the pursued development pathway. The technical and commercial implications are extended to the wider wave energy sector where possible and relevant.

1.7 Research outputs

Core research outputs include:

- ISOPE 2019 conference paper
    - Title: Tackling the Wave Energy Paradox – Stepping Towards Commercial Deployment
    - URL: https://www.researchgate.net/publication/336403124_Tackling_the_Wave_Energy_Paradox_-_Stepping_towards_Commercial_Deployment
- EWTEC 2021 conference paper (x2)
    - Title: Preliminary hydrodynamic assessment of Mocean Energy's Blue Star WEC via fast-turnaround physical model testing
    - URL: https://www.researchgate.net/publication/354780820_Preliminary_hydrodynamic_assessment_of_Mocean_Energy's_Blue_Star_WEC_via_fast-turnaround_physical_model_testing
    - Title: Extreme responses of hinged raft type wave energy converter
    - URL: https://pearl.plymouth.ac.uk/bitstream/handle/10026.1/19705/EWTECpaper2021_4.pdf?sequence=1&isAllowed=y
- POSTnote publication (during Fellowship undertaken at the Parliamentary Office of Science & Technology, POST)
    - Title: Research briefing – Sustainable Cooling
    - URL: https://post.parliament.uk/research-briefings/post-pn-0642/
- Physical models (x2) and modular nacelle (x1)

The aforementioned publications can be found in Appendix A.

Part I:
Literature Review

Part I lays out the technical and commercial literature that underpins this EngD, building on the context of Chapter 1. Based on the project aims, relevant topics are thematically explored using industry and academic sources. First, in Chapter 2, relevant commercial considerations are extracted and linked to WEC technology development practices. These are reviewed with a particular eye to challenges faced by developers at early stages. Commercial considerations act as a bridge towards locating the role and potential of physical modelling in advancing WEC development and technology commercialisation. In Chapter 3, more specific challenges and opportunities for small-scale physical model testing are explored from a historical, technical, and practical perspective. Design efforts upstream and downstream of physical modelling are also touched on where appropriate. In highlighting knowledge gaps and opportunities for research contributions, company specific variables are also referred to.

"Measurement is not an alternative to judgement, measurement demands judgement" (Muller, 2018).

- Jerry Z. Muller, 2018

Chapter 2. Commercial literature review

Before reviewing the literature specific to physical model testing, a step back is taken to draw out some of the key challenges of wave energy development. This helps to locate the potential relevance, impacts, and role of physical modelling in WEC technology progress, particularly at earlier development stages and from a developer's point of view. Such challenges are numerous; this chapter focuses on identifying development priorities, defining and measuring performance, and the implications of different target markets on the development process itself.

2.1 Key industrial challenges

Industry or commercial challenges are varied and numerous (Villate *et al.*, 2020). Multiple papers, such as (Clément et al., 2002; Falcão, 2010), have reviewed the wave energy technology landscape, pointing to its breadth and lack of convergence as a primary obstacle to commercial progress (Drew, Plummer and Sahinkaya, 2009). The design space is still broad, which translates to challenges for stakeholders other than developers, such as investors and public bodies – who either struggle to choose "what horse to bet on" or doubt whether any horse is worth betting on at all. Other papers, such as (Magagna and Uihlein, 2015) and (Jin and Greaves, 2021), focus on the policy perspective, which is also vast and remains largely outside the scope of this chapter. Instead, the following sections pick out three elements that characterise the industry and relate to developers' efforts towards commercialising technology, namely: identifying development priorities, measuring performance (via e.g. metrics), and the choice of target markets.

2.1.1 Technology development priorities

For a developer, priority areas of development evolve as the WEC design progresses. Figure 10 shows six stages of development progress as listed by the recent OES Evaluation and Guidance Framework from 2021, which represents broad consensus within the industry (Hodges *et al.*, 2021). Figure 11 shows the stages as defined by one of the major marine energy standards (the International Electrotechnical Commission, IEC), with the first two OES stages effectively falling within Stage 1 of the IEC definition. Both definitions use

Technology Readiness Level (TRL)[9] as the indicator of 'progress', and a threshold for assessment, as further discussed in this chapter's continuation. Figure 11 also shows an increase in scale guide (i.e. growing size of physical models tested and assessed) as progress is made, and will be of particular relevance again in Chapter 3 and Chapter 5.

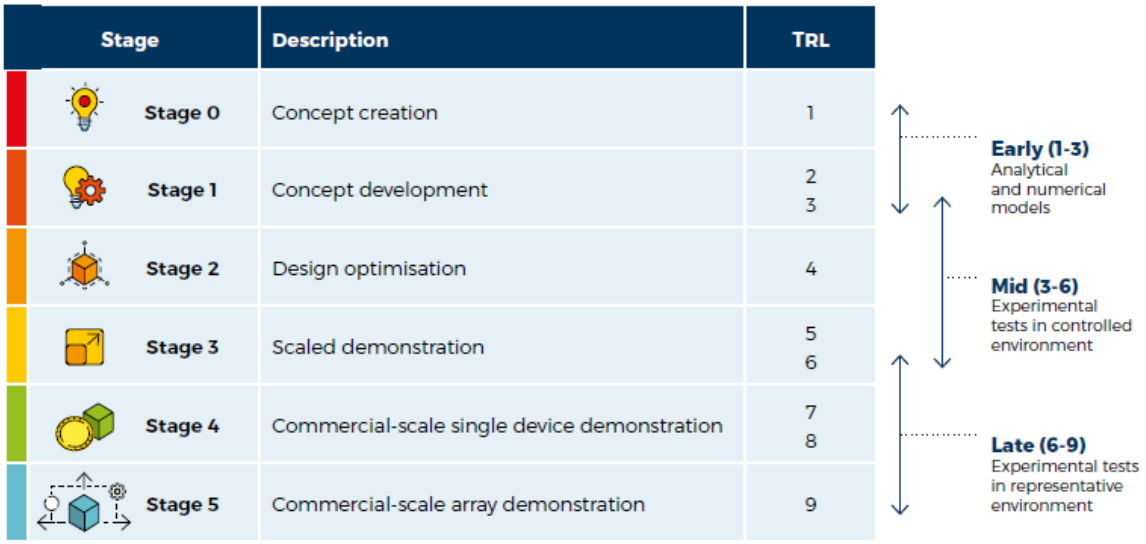

Figure 10 – Staged development progress according to IEA-OES (Hodges *et al.*, 2021).

[9] Originally conceptualised by the National Aeronautics and Space Administration (NASA). Now widely used in wave energy as well as many other industries, such as oil and gas. Originally, only 7 readiness levels were defined, but a 1-9 scale is now common and adopted throughout this thesis. Applying such a scale universally across technologies is not straightforward. Additional considerations can be found in (De Rose, Olivieri and Strazza, 2017), which attempts to homogenise TRLs across different technologies, though wave is not explicitly featured.

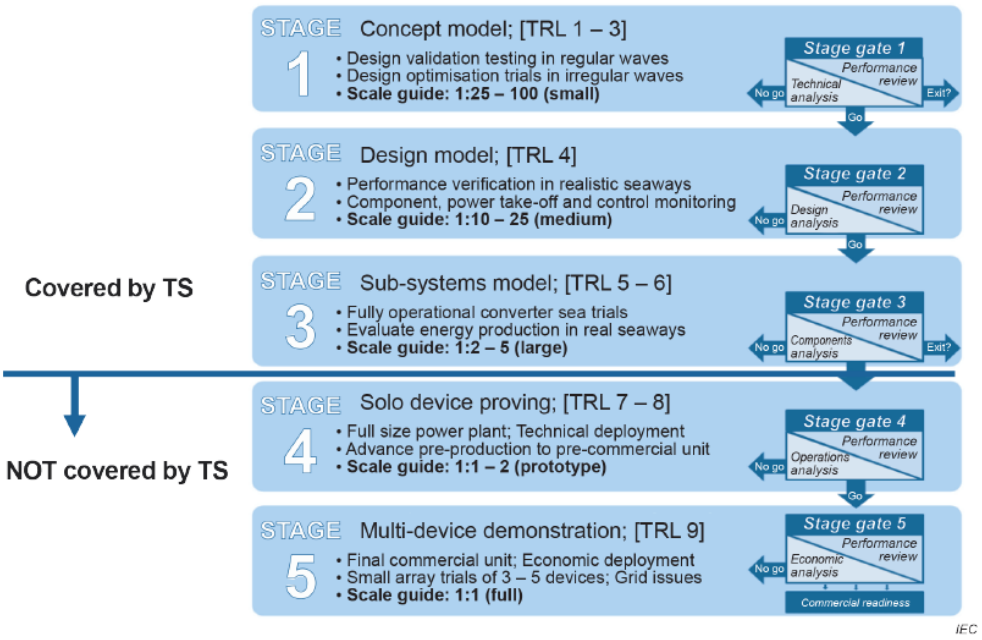

Figure 11 – Staged development approach as defined by IEC standards (IEC TS 62600-103, 2018).

The European Commission-funded MaRINET2 programme – one of the major collaborative research projects in ocean energy – released its Deliverable 2.8 Ocean Energy Technology Guidance Report in December 2021 (Judge *et al.*, 2021). In its introduction, it immediately presents several key challenges facing technology developers, specifically in relation to physical model testing.

> *"Physical testing is expensive and suitable test facilities are not available in every country. Furthermore, the guidance available for conducting physical testing is limited, and standardised processes for each stage of development have not yet been fully developed."*

Costs, guidance, and standards are picked out, and then linked to issues of broader technological advancement and investment:

> *"It is not always clear what technological advancement should be prioritised at each stage of development and where money is best spent."*

These obstacles are emblematic of the industry and common for developers, beginning to illustrate how difficulties associated with what appears as an exclusively technical aspect (physical testing) have very real repercussions on wider technology development, and, ultimately, on its commercialisation.

Technical aspects of physical model testing are reviewed in detail in Chapter 3, while commercial aspects are expanded on below.

When it comes to guidance on prioritising particular aspects for WEC technology development, Weber offers the paradigm of seeking *performance ahead of readiness,* as found in e.g. (Weber, 2012) and (Weber, Costello and Ringwood, 2013). The argument can be summarised as follows: *if a developer can initially focus on maximising WEC (techno-economic) performance, this will ultimately result in a reduction of development time, cost, and risk*. It is noted here that this directly speaks to one of this thesis' goals of implementing this philosophy in practice. Returning to Weber, the concept of Technology Performance Level (TPL) is introduced in order to illustrate the paradigm, complementing the more widely utilised TRL. In essence, TPL indicates – rather than measures – "how well a technology performs" in terms of economic viability, while TRL indicates "how ready a technology is" for commercialisation (Weber, 2012)[10,11]. The need to complement TRL is due to readiness alone "not representing a pathway to success" (Judge *et al.*, 2021).

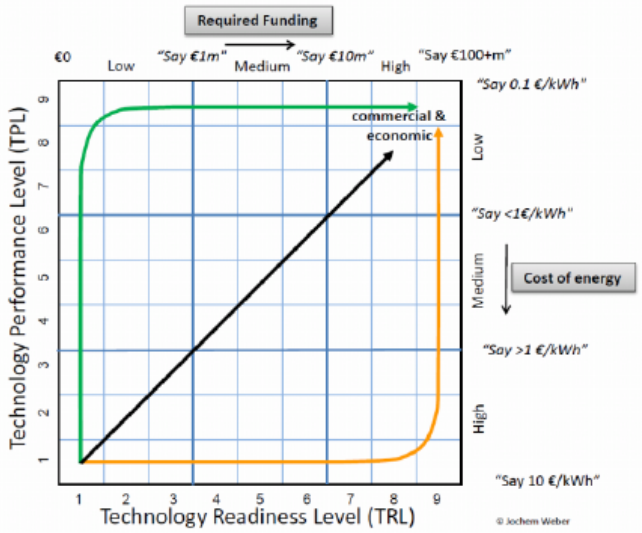

Figure 12 – Generic WEC technology development trajectories (Weber, 2012)
{Green: performance before readiness; Orange: readiness before performance}

[10] OES defines it as the 'commercial ability' of a technology (IEA-OES, 2015).

[11] An embedded assumption is that funders and investors will prioritise – or at least aim for – the highest possible performance and readiness. While in practice the human element is very important too, as well as the wider market and company context.

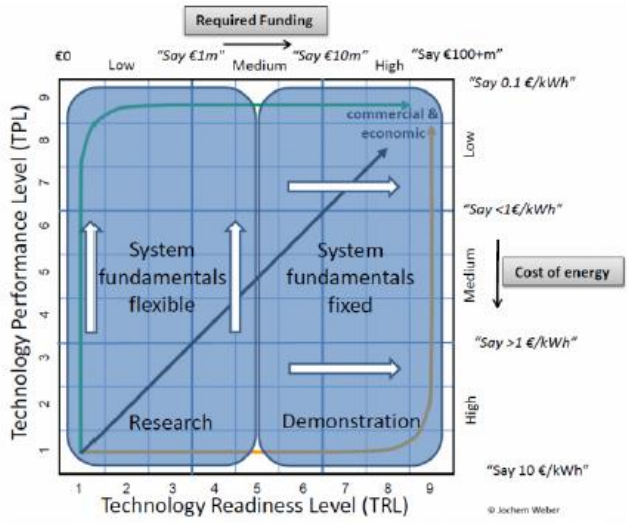

Figure 13 – Generic WEC technology development domains (Weber, 2012).

Weber's proposition is that developers should initially focus on raising TPL, before moving across the matrix to increase TRL (see green line in Figure 12). This assumes that increasing TRL is more time and funding-intensive than increasing TPL; when technology is at a higher TRL, any necessary re-designs required to significantly raise TPL will necessitate greater overall development time and costs. Similarly, Salter points out that "premature deployment of unreliable devices leads to painfully slow and expensive learning" (Salter, 2005) – however, note the difference between broad economic viability (i.e. TPL) and specific *reliability*, as pointed to by Salter. Instances of relatively late fundamental re-designs are not uncommon among wave energy developers.[12]

It may be, however, that although less funding is required to begin with, this may be more difficult to acquire if, for example, the company does not manage to build momentum and visibility via publicity and PR while moving through the TRLs. In addition, demonstration of sufficient time in the water (associated with high TRLs) is a crucial element for many encountered investors, and this may be preferable to marginal performance improvements. This "chicken and egg" scenario is formalised in Chapter 5 via a dedicated framework. Here we simply

[12] An example is Marine Power Systems, who have revolutionised their design relatively late on in TRL.

point out the difficulty in identifying *when* to switch focus from performance to radiness – i.e. what is 'good enough' from a performance point of view?

2.1.1.1 The link to physical modelling

In practice, the TPL-TRL matrix illustrates the push-pull relationship between readiness and performance, which, however, cannot be treated as a dichotomy. Nonetheless, the TPL-TRL matrix offers a helpful steer towards focusing tech advancement and innovation at low TRL, remaining as open as possible to 'fundamental changes'. In a low maturity and rapidly evolving industry, this is particularly relevant, as Mocean can attest to.[13]

However, challenges remain even when implementing performance ahead of readiness trajectories. In particular, the estimation of TPL at low TRL, due to "uncertainties in the foresight of the mature system characteristics and limitations of the simulation and modelling capabilities." (Weber, 2012). In other words, experience, empirical evidence, and expert (ideally objective) judgement and/or assumptions are needed in order to estimate TPLs at an early development stage. Of these three, empirical evidence directly relates to physical model testing, which again speaks to this thesis' scope. In (Weber, Costello and Ringwood, 2013), reduced scale model testing is mentioned as an activity occurring to inform TPL at TRL3, to assess hydrodynamic power absorption, survival behaviour, and fatigue and load cases. However, several additional points can be made about its relevance in this context and in relation to some of the embedded assumptions:

- **Assumption #1: A major factor determining the increase in funding required across the *x-axis* in Figure 12 is the scaling up of the technology.**

[13] Dr Chris Retzler at the Ocean Energy Europe 2020 panel discussion: "At the moment, people building WECs tend to freeze designs very early. And in their rush to get steel in the water, tend to fix particular technologies at early stage - prematurely, we believe - therefore our approach has been to do a lot of numerical modelling and remain open to the different evolving technologies (e.g. for PTO) that do exist [or are being developed] and make sure we can accommodate these". This was also echoed by Matt Folley at the 2020 MORE-COER Wave Energy Workshop held in Turin (Italy), on 29th April 2022.

  - Thus, reducing the size of full-scale machines, and maximising the use of reduced scale physical models that are typically used early on, can reduce required funding during the technology development pathway. The latter suggests that small-scale physical modelling can play an important role in enabling this early-stage TPL boosting. This is revisited in Chapter 5.
- **Assumption #2: Performance can be significantly advanced at low TRL and should take into account a broad range of factors (e.g. through a metric like TPL).**
  - In other words, being able to measure as many performance factors possible, including with physical models (that are particularly used early on). Linked to the above is the possibility of widening the pool of variables from which performance[14] can be assessed. Thus, if enough sub-systems or performance characteristics can be incorporated in early physical models, this may help to capture more of TPL, and guide its amelioration early on.
- **Assumption #3: In order to facilitate changes / innovations that can result in early TPL advancement, it is preferable to keep WEC system design open at early stages.**
  - Thus, if physical models can be made cheaper and more rapid to build and test (e.g. through modularity), this can also help to keep options open in terms of evolving subsystems that enable fundamental TPL-improving changes; thereby aiding in raising TPL elements early on. See Appendix C.

In light of these points, a new proposition can be made in applying *the performance before readiness* paradigm to physical modelling:

> Not only is it important to iterate designs at lower TRL - where physical model scales are typically smaller, and where learning can be obtained at cheaper cost, time, and risk - but also to include as many of the

[14] See next section for what is meant by 'performance'.

‘performance’ elements as possible in the early-stage model(s) used, consistent with the way in which performance is defined, and with as low uncertainty as possible.

It is noted that a 2021 paper by Kerr et al. essentially mirrors the *performance before readiness* proposition from an overall industry funding perspective. Its analysis highlights that if policies focus on supporting step-change innovation first (akin to step-changes in TPL), then the incremental cost-cutting investments needed to reach hypothetical cumulative device deployment targets dramatically decrease, based on reaching competitive levels of cost of energy (CoE) (Kerr, Noble and Hodges, 2021). Once again, this points towards the need for step-change innovation early on in the development path. However, as is often the case, the analysis in Kerr et al. does not include the possibility of deployment supporting radical step-change innovation in the various considered scenarios. Here deployment is associated with gradual cost-cutting via slow learning, as opposed to sparking step-change innovation.

A further important point is made about the need for policy to support a portfolio of devices to enable cost of energy (CoE) step-change reduction. "Due to significant variation of resource in different sites, wave energy may not converge on one successful device concept. Developing and implementing a novel subsystem for a leading device will reduce the Levelised Cost of Energy (LCOE)[15] of that device. However, it may not reduce the LCOE of the whole sector" (Kerr, Noble and Hodges, 2021). This ties into expanding markets and applications discussed in Section 2.3, and an often more nuanced definition of performance based on different applications and stakeholder requirements (see Section 2.2).

Here it is worth noting that while policy makers have an important role to play in determining CoE outcomes, developers also have agency. Indeed, just as "these step-change cost reductions can be facilitated through policy that supports the development of radical innovations" (Kerr, Noble and Hodges, 2021), so too can

[15] Levelised cost of energy is prevalent across the energy sector and is typically defined as the cost per unit of energy generated over the whole lifetime of the energy producing asset.

they be facilitated through developers adopting design steps/processes that enable streamlined learning as early in the development timeline as possible. This can occur, for example, via small-scale representative tests.

The questions of how ‘performance’ is conceived or defined, how to measure it effectively based on developer objectives, and how to practically integrate such measurements within the technology development process naturally follow. These questions are picked up again over the course of the chapter. More broadly, this thesis provides an opportunity to apply the performance before readiness paradigm in a real developer context, and to observe whether, and how, it ‘holds up’ in practice.

The above reveals how a TPL-TRL matrix framework is relevant and helpful, but more guidance is required to render it practically implementable by developers. In particular, the less uniform the wave energy industry becomes (see Section 2.3) – reducing likelihood of overall sector convergence – the more nuanced these ‘goals’ are likely to become. In other words, the relative importance of performance or readiness will become less obvious. Both of these points are picked up by DNV, a global classification body for the maritime industry, even when considering TRL alone.

DNV firstly notes TRL-related difficulties in accelerating adoption of novel technologies, “due to vague and ambiguous definition of the TRL levels” (DNV GL, 2018). It further notes that “TRL definitions should be clarified […] by defining case-specific acceptance criteria and limits for attainment of targeted TRLs […] TRL attainment should be formulated as an adequate set of acceptance criteria and limits […] reviewed and accepted by all stakeholders prior to commencement of qualification activities”. This can be done via the defining of milestones, which then depend, for example, on whether the technology is regarded as ‘enhancing’ or ‘enabling’. Nevertheless, what is considered ‘adequate’ for the technology to be deemed to have achieved a particular TRL and thus to proceed to the next stage of technology qualification depends on the stakeholders – and is therefore partly subjective and partly application case-by-case specific. Finally, (DNV GL, 2018) states that the “attainment of TRL levels considers what has been accomplished in the past

more than future obstacles and efforts" – i.e. it is more useful in assessing how far one has come, rather than in objectively guiding future development.

In closing this section, it is hoped to have shown that TRL and TPL are helpful indicators of the boundaries within which a developer operates. Both are more helpful in comparing a WEC to its previous iterations, than to other, different, WECs. Finally, being quantitative and to an extent subjective, neither can be directly incorporated in an optimisation process, serving more as 'guide posts' and indicators of a technology status, than targets or metrics that can be explicitly aimed or optimised for. As such, the way a developer navigates through TPL and TRL remains a largely open question.

2.1.2 Measuring performance

In a 2019 paper, Weber et al. (Weber *et al.*, 2019) stated that "investment in both the determination of assessment criteria and their application has not been adequate, given their crucial importance in guiding technology development process to success in the most effective way." A scarcity of convergence on optimal performance metrics, as well as clear links of these to the design process, is particularly noteworthy (Caio, Davey and McNatt, 2019).

This is no small challenge. The way in which WEC performance is measured depends on a myriad of factors, among which:

- the definition of 'performance' itself – e.g. technical (how much energy), economic (how expensive), commercial (how attractive to stakeholders), and any combination of these;
- the data available to assess performance metrics – e.g. numerical/experimental models, their accuracy, refinement and associated levels of confidence;
- the development stage of the technology – e.g. how defined are the subsystems and their interfaces (i.e. TRL);
- the target market – e.g. grid-connected or off-grid, dictating WEC requirements based on end-user requirements;
- the developer's objectives and how performance is used – e.g. internally as part of an optimisation routine, for stage-gated assessment, or for external reporting;

- other stakeholder objectives – e.g. are investors more interested in cost or energy yield, reliability, minimum available power, etc. (Babarit *et al.*, 2017);
- the relative priority of performance aspects – e.g. survival and reliability are in a sense binary and thus arguably more important key performance indicators (KPIs) than LCOE or efficiency, particularly in a *developing* industry (Salter, 2005; Sheng, 2019; Villate *et al.*, 2020);

This is well demonstrated by the numerous (twenty-three) TPL categories identified in (Weber *et al.*, 2019), each consisting in a series of questions that lead to particular choices in terms of assessment criteria, tools, and methods employed. The study is comprehensive in terms of the questions it poses, but does not offer a means of prioritising or narrowing down the actual choice. Interestingly, (Trueworthy *et al.*, 2021) apply the methodology to a series of 'emerging' markets, including some extended questions in order to fit the stakeholders and energy end-use. Such an effort is crucial in order to motivate choice of assessment criteria, methods, and metrics utilised.

A major trade-off in the choice of metrics is fundamentally one of breadth versus accuracy (i.e. close to true value), particularly early on. TPL is a good example of this, where numerous factors spanning technicality and economics are included at the expense of being able to accurately quantify all of the required input parameters. On the other hand, more focused quantitative metrics tend to be easier to incorporate into iterative design processes that rely on numerical/quantitative assessment for optimisation (see Chapter 4). Whether the latter lead to satisfactory or better outcomes is an open question, which will be returned to in the discussion (Chapter 9). In practice, whatever path is followed, it is important to remember that metrics need to be used as part of a wider assessment and evaluation process leading to decision-making, as emphatically outlined in (Muller, 2018). One should not fall into the trap of considering quantitative metrics as being more objective, since there is an often subjective choice in what is going to be measured in the first place. In addition, one should resist the assumption that "what can't be measured does not exist", while ensuring that what *can* be measured at each stage *is*. In this sense, the earlier

this is done, and the more these quantities of interest can be validated experimentally, the better.

A comprehensive review and discussion of WEC metrics can be found in (Judge *et al.*, 2021) and (Hodges *et al.*, 2021). The remainder of this section focuses on metrics that can be feasibly used in early stages of development (refer to Figure 10 and Figure 11), where physical model testing can contribute to building empirical evidence, hopefully rapidly and economically, as advocated by Weber (Weber, 2012).

2.1.3 Linking metrics and performance

Based on the assumption that early, rapid, accurate, learning is essential to an effective technology development trajectory, two points are further explored here:

- What performance metrics can be used early on, such that they can be validated with empirically derived data available at that point in time?
- Are they suitable for integration within a streamlined design optimisation?

The latter point links to the choice of metrics in relation to how they are used – i.e. what process they inform. A distinction is made between *assessment* and *optimisation*. Optimisation is conceived as an ongoing process of improvement of the technology often boosted by iterative numerical models that quantify performance in order to drive *development*. Assessment, on the other hand, is considered as a global (to the extent possible) evaluation of a technology that considers a holistic techno-economic-commercial performance in as much depth as feasible at that point in time. This might be done more occasionally such as during critical design reviews. It uses metrics that look ahead at *deployment* potential. The former has a stronger onus on accuracy, the latter on breadth. To the best of the author's knowledge, there is a lack of literature on the relationship between metrics and performance, and assessment versus optimisation.

Returning to physical model testing, data collected during such campaigns should be able to talk to the chosen metrics, enabling (especially, but not exclusively) developers to optimise performance and track its progress. In a testing campaign, Quantities of Interest (QOIs) – that relate to metrics – are identified and measured; these are discussed in Chapter 3. The topic of metrics

applied to Mocean's optimisation routine and development process will be touched on again in Chapter 5. A final note is taken from (Vanegas-Cantarero *et al.*, 2022):

> "*Comprehensive* and *transparent* assessments are required that reflect the *complexity* and *multi-dimensionality* of the transition to low-carbon energy systems"

The above is interpreted as a reminder to return to all energy trilemma elements (see Figure 20) and beyond – not just the cost.

2.2 Early-stage metrics

The fundamental question in the context of early development stage metrics may be worded as: what is *fit-for-purpose* from a developer perspective? This relates both to the nature of the metrics used, and their integration within a multi-step and iterative development process (see Appendix C, Figure 183).

From a developer's perspective, it is worth considering how metrics might practically fit into the WEC design and optimisation process. At low TRL, cost estimates are difficult to make. Thus at early-stages, the most relevant metrics appear to be those that (small-scale) physical modelling can directly feed into. Nevertheless, they may be 'enriched' with additional aspects that - if not directly, at least indirectly - represent some other performance and cost elements. As found in (Nielsen, 2003) and (Babarit *et al.*, 2012), cost proxies such as structural mass, PTO force, volume, and surface area have been proposed. "The crudest measure of cost is volume - this sets the basic size of the structural elements and has a direct influence on the average and maximum forces that the system is likely to see" (Yemm *et al.*, 2012). (Babarit *et al.*, 2012) numerical benchmarking study considers (techno-economic) performance metrics (AEP, AEP/mass,) of 8 different WEC types across 5 different deployment locations via the author's own numerically developed models for each concept. More recently, (Jin, Zheng and Greaves, 2022) has expanded this database to 161 WEC cases, with practical CWRs values "achieved from field, laboratory, and numerical tests". However, the latter are not normalised by deployment location.

These feed into proxy techno-economic metrics such as *AEP/mass*, *AEP/rms PTO force*, *AEP/wetted surface area*, etc. (Judge *et al.*, 2021) points out that these fail to represent market size or grid compliance characteristics; while indeed limiting, these aspects may not be showstoppers depending on the metrics' use.

In theory, such techno-economic proxies can all be derived from appropriate experimental tank tests. Another potential proxy for cost (in the form of reliability or survivability) could be measures of operational or extreme climate structural loads, which again could be directly measured in tank tests via load or pressure sensors. Examples of this extend beyond academia into industry (Cruz Atcheson and ARUP, 2016).

Generally, PTO parameters and structural loads are harder to measure as a model gets smaller due to the need to include additional, often relatively bulky and/or heavy, sensors in the model without affecting its dynamic and kinematic responses. However, it is worth trying to incorporate these if possible, taking care to evaluate any adverse effects on data quality and uncertainties. The metrics implemented by Mocean in its optimisation process are returned to in Chapters 4, 5, and 9. Hereafter, a brief overview of metrics used or advocated at early stages of technology development is given from literature.

2.2.1 Nature of metrics

(Caio, Davey and McNatt, 2019) reviewed what performance metrics have been published by funding bodies, industry standards and research collaboration initiatives as of mid-2019. The review is not exhaustive but paints an accurate overall picture. It offers initial insights in terms of meaningful metrics for developer implementation, and metrics alignment between developers and funding bodies/organisations. (Caio, Davey and McNatt, 2019) first introduced and defined the *wave energy paradox*, as the negative reinforcement loop that exists in the wave energy industry and that has ultimately hindered industry-wide learning (see Chapter 5).

Organisation	Document	Scope	Suggested performance metric(s)	Reference
EMEC	Assessment of performance of wave energy conversion systems	Aimed primarily at post-prototype machines	- Capture length	(Pitt, 2009)
IEC	TS 114-62600-103:2018 Marine Energy – Wave, tidal and other water current converters	Guidelines for the early stage development of WECs	TRLs mentioned as stage gate definitions up to TRL6. Power performance to be measured by: - (TRL1-3) RAO from regular waves - (TRL4) Experimental power matrix produced to estimate AEP - (TRL5-6) Actual power matrix using scaled power capture and conversion	(IEC, 2018)
IEA-OES	Annex II – Recommended practices for testing and evaluation of ocean energy systems	Guidelines for testing, preliminary cost assessment and presentation of results	- AEP/Volume - AEP/Structural mass - Average capture width ratio	(Nielsen, 2003)
UK Department of Trade and Industry (DTI)	Preliminary wave energy device performance protocol	Focuses on supply of electricity to the network via single grid supply-point	None specific to hydrodynamic or techno-economic performance	(Smith and Taylor, 2007)
EquiMar	D5.3 – Protocols and guidance for device specification and quantification of performance	Performance metrics for device arrays in particular	- Capacity factor - Conversion efficiency - Capture width	(EquiMar, 2009)
Ocean Energy Forum	Strategic Roadmap	Establishes priority areas for technological progress with an associated implementation plan	None specific to performance. TRLs mentioned as part of stage-gated approach.	(Ocean Energy Forum, 2016)
ETIP Ocean	D2.1 – An integrated framework for ocean energy sector challenges	Highlights the challenges viewed as most critical to overcome in the pursuit of sector commercialisation	None specific to performance. Calls for “defining and enforcing standards for stage gate progression through scale testing”	(ETIP Ocean, 2016)

DTOceanPlus	D2.2 Functional requirements and metrics of second generation design tools	Introduces a suite of design tools to assist users in achieving optimsal design solutions based on information available at a particular stage of development	- AEP – as the output of 'system performance and energy yield' tools - LCOE – as one of the outputs of 'system lifetime costs' tools (used as inputs for stage gate and structure innovation tools)	(DTOceanPlus, 2018)

Table 2 – Summary of published performance metrics, as found in mid-2019 (Caio, Davey and McNatt, 2019).

From Table 2, and as mentioned above, many of these (particularly more historic) metrics are hydrodynamic in nature. Some, like capacity factor (CF), are more appropriate to wind and tidal energy[16].

Capture width (CW) and its non-dimensional equivalent - Capture Width Ratio (CWR) – are almost ubiquitously utilised to determine the power performance of a WEC from a hydrodynamic perspective (Jin, Zheng and Greaves, 2022). CW is defined as the ratio of power captured per energy flux (power in the wave per unit metre crest, and has units of length), while CWR is CW divided by the characteristic width of the device, which is usually taken to be the front width of the WEC orthogonal to the wave propagation direction. Under the assumption of linear waves, CW and CWR theoretical maxima have been established for different WEC typologies, including in (Budar and Falnes, 1975). CWR includes elements of power capture / device dimension, and is thus somewhat analogous to AEP/mass or AEP/volume metrics, with the advantage of non-dimensionality.

Techno-economic metrics that feature above are either proxies (e.g. *AEP/Structural mass*) or LCOE, which arguably is also a proxy depending on what stage of development it is estimated. A note on LCOE is due at this point.

[16] Capacity factor (CF) is defined as the achieved annual energy production (AEP), divided by the theoretically available energy throughout the year at a given site (hours per year multiplied by device nominal power rating). However, the nominal power rating is not universally defined, particularly in the case of WECs, which do not have a single clearly specified operating point (contrary to e.g. wind turbines). WEC nominal rating is typically assigned as the max operational power of the generators in the system, but does not give any information regarding the consistency of energy capture during the year, or the mean power captured. At Mocean, it is typical to run analyses to calculate continuously available power (CAP) as well as AEP. Specification of CF is avoided due to its somewhat arbitrary and site-dependent nature.

2.2.1.1 The LCOE trap

LCOE is arguably the most widely used metric in both academic and industry literature. This is partly because it enables a cost of energy comparison with other forms of energy (including non-renewable ones), which has been a long-term focal point for the wave energy industry in order to prove its competitiveness[17]. LCOE figures are therefore often quoted in the attempt to either demonstrate compliance, or lack thereof, towards a target cost of energy. This has associated potential pitfalls, since the result is highly sensitive to several assumptions that often lack clarity (Muller, 2018; Judge *et al.*, 2021). For instance, "it is important to note that the most common metric, currency/MWh, is site-specific and should be qualified as such" (Trueworthy and Dupont, 2020). This highlights the need for transparent and openly stated assumptions in its use.

LCOE's long-established and widely adopted use makes it a convenient comparative indicator, though some have pointed to its questionable accuracy for device optimisation in absolute terms and poor utility as an early-stage performance indicator (de Andres *et al.*, 2016) (Judge *et al.*, 2021). Since LCOE requires inputs covering the entirety of project costs, several assumptions are needed for its calculation especially at early stages when significant cost uncertainties exist (Caio, Davey and McNatt, 2019). For example, reliability and operations and maintenance (O&M) strategies are key determinants for cost of energy (Pascal *et al.*, 2018) that are difficult to estimate with confidence prior to at-sea testing. The contribution of OPEX, for example, was around 30% of overall lifetime costs as per the state of the industry deployment in 2015 (IEA-OES, 2015). Some authors have pointed out that LCOE has limited validity as an overall indicator of commercial attractiveness (de Andres *et al.*, 2017), particularly for a low maturity industry. However, "despite researchers' claims that LCOE is not the best metric for WEC performance, it is clear that designers do not see a viable alternative" (Trueworthy and Dupont, 2020). An underlying issue is that "the high costs inherent to current wave energy technologies derive

[17] This onus is growingly shifting towards the value of complementarity as part of a balanced overall energy mix.

from a *relative* perspective" (Daniel Clemente et al., 2021) (author's addition of italics), because wave energy technology is compared to more mature technologies via LCOE. One could say, therefore, that this is a problem of perspective in terms of the applications foreseen for WECs (Rodrigues *et al.*, 2020). Perhaps, given the more recent onus on the value of a diverse WEC portfolio (Kerr, Noble and Hodges, 2021) and complementarity of supply as part of a more balanced grid system (Pennock *et al.*, 2022) (see also the research project EVOLVE[18]), 'diversity' and 'complementarity' metrics may be usefully introduced as part of a technology's 'value'.

In its 2022 paper, (Vanegas-Cantarero *et al.*, 2022) demonstrate the slowly growing movement towards inclusion of environment and socio-economics alongside techno-economic considerations in evaluating the 'worthiness' or value of a particular technology. The use of techno-economic performance criteria alone often penalises emerging technologies. On the contrary, a multi-criteria approach provides a more holistic evaluation of merit. The author also points to the potential use of multi-criteria analyses for metrics assessment, which could well be combined with TPL related analyses and different stakeholder factor weightings such as in (Trueworthy and Dupont, 2020).

The above does not rule out useful scenarios for LCOE, such as in sensitivity analyses where learning is available even if inputs are not fully determined. See, for example, those undertaken in (Teillant *et al.*, 2012) for operational simulations, and (Henry *et al.*, 2021) for deployment location and lifetime costs. Highly capable tools such as WaveVenture software[19] have been developed to this end, recognising the significance of being guided by techno-economics and not just techno-capabilities. Both WES and the US Department of Energy (DoE) have used techno-economic metrics as part of competitive scoring processes of multiple devices – i.e. benchmarking. WES, for example, uses LCOE as part of its first stage-gated assessment at TRL 3 and for admission to the stream itself at TRL1. A recognition is required, however, of LCOE's suitability in assessing a

[18] EVOLVE project: https://evolveenergy.eu/

[19] http://www.wave-venture.com/software

project as opposed to a *technology*. LCOE is of limited use as a metric to improve a particular technology.

Recognising LCOE's shortcomings, the US DoE developed its own ACE (Average climate capture width to the Characteristic capital Expenditure), MMC (Manufactured Material Cost) and HPQ (Hydrodynamic Performance Qualifier) metrics for its Wave Energy Prize competition. ACE is applicable to low-TRL concepts and expressed in units of m/$ (Driscoll *et al.*, 2018). It represents the ratio of Average Climate Capture Width / Characteristic Capital Expenditure. In other words, the "equivalent wave crest width for which the WEC can absorb all incoming energy", per million dollars spent on the load bearing structure (Judge *et al.*, 2021).

- Its calculation relies on a parameter – Representative Structural Thickness (RST) – that is the mass/surface area * material density (US Department of Energy, 2016).
- The MMC parameter aims to include all the major material cost centres (e.g. PTO and moorings, not just prime mover)
- ACE is akin to *AEP/structural mass*, but includes material cost effects - e.g. in results shown in (Dallman *et al.*, 2018)
- (Dallman *et al.*, 2018) recommend that ACE be modified to include other cost proxies such as operational, installation, array costs. This can be done to an extent via the additional HPQ factors.

HPQ was also used in the Wave Energy Prize competition to complement the ACE metric, as well as including more factors that ultimately impact LCOE (Driscoll *et al.*, 2018), such as capital expenditure, operational expenditure and grid integration proxies (Dallman *et al.*, 2018), see Table 3. Crucially, most of the ACE correcting factors in HPQ are directly derived from "measurements and event counts made during basin testing" (Judge *et al.*, 2021). This is highly attractive in terms of their applicability to both numerical and experimental models. The list of 'performance impact factors' is as follows:

Impact factor	Performance characteristic accounted for	Associated measurement	Capex (C) / Opex (O) / Grid (G) proxy
I_mf	Mooring load intensity	Statistical peak mooring force	O
I_wc	Station keeping ability	Statistical peak of mooring watch circle	O
I_ap-p2a	Variability of absorbed power	Ratio of statistical peak-to-average absorbed power	G
I_es	Frequency and severity of end-stop impacts	Number of end-stop impact events	O
I_rs	Absorbed power in realistic seas	%	C
I_ac	Adaptive control effort	(observation)	O

Table 3 – Performance impact factors, adapted from (Judge *et al.*, 2021).

Table 3 shows interesting elements that could perhaps be integrated within design optimisation, and that could be derived from physical model testing. Further details as to how these were analogously adopted and incorporated by Mocean is discussed in following chapters (4, 5, 9). More details on the calculation of performance impact factors and ACE can be found in (Driscoll *et al.*, 2018). In a sense, a version of ACE is used by Mocean in its fitness function for optimisation (see Chapter 4).

Further potential weighting factors may be extracted from max-to-mean ratios. Recommended max-to-mean power ratios for different device types can be found in (Pecher and Kofoed, 2017). Here, the authors point to the undesirability of large fluctuations in absorbed power, which “increase the need for oversizing mechanical and electrical equipment and are one of the main barriers to achieve a reliable and cost-efficient technology”.

WEC type	Max-to-mean ratio
Single wave-activated body with one-way PTO	15-30
Single wave-activated body with two-way PTO	10-12
PWC with two-way PTO	10-15
10 side-by-side located wave-activated bodies (in the wave direction) with two-way PTO	3-7

Table 4 - Indication of the max-to-mean ratio on the absorbed power by a WEC with different configurations (Pecher and Kofoed, 2017).

Returning to TPL, this tries to account for “technical performance, life cycle costs, environmental and social impacts, safety aspects, and risks of a technology” (Mendoza *et al.*, 2021). The fact that such a large number of papers exist discussing its application suggests that its application may not be straightforward. While being a robust framework to set development trajectory, it is tricky to measure, hence why it is referred to here as an *indicator* instead. (Bull *et al.*, 2015) contains some guidance on TPL scoring, while a more recent publication contains individual TPL assessment questions is (Bull *et al.*, 2017). In the most recent TPL focused paper (Mendoza *et al.*, 2021), the authors list target use cases. Notably, among these geometry optimisation or iterative optimisation are not included. Rather, the end use for developers is to “find fatal flaws early […] and identify areas for improvement that will yield the highest return for investment”. The online tool to assist TPL scoring contains 88 questions that are both quantitative and qualitative. These also require modification depending on the end-use or target market of the energy. Participation from multiple stakeholders is also necessary to assess TPL, with assessors having to reach consensus when scoring the WEC in (Mendoza *et al.*, 2021). In short, it is very comprehensive, and thus requires many inputs and a significant time investment to assess it properly. On the plus side, it gives a holistic view, is flexible, encourages stakeholder engagement, but not easily implementable to guide optimisation from a developer point of view. More akin to a big design review – so useful in that sense. Indeed, “though TPL could become a comprehensive metric of performance, it cannot be used for device design optimization, while other metrics can” (Trueworthy and Dupont, 2020).

Emerging from this section is the recognition that objective performance assessment at early stages is needed (Weber and Laird, 2015), but optimal metrics or method is not yet clear.

2.2.4 Metrics integration within the design process

Mocean relies on a combination of numerical optimisation and physical validation to advance WEC design. To varying extents and levels of complexity, this is common across WEC developers. Optimisation needs to be supported by associated real world evidence.

The previous section has suggested that LCOE's use is more suited to scoring WECs against one another (benchmarking) - provided the assumptions are equivalent and transparent - than for iterating and optimising a particular design. In 2008, Salter argued the following (Salter, 2008):

> *"The traditional, and sound, engineering approach for many projects has been to measure or calculate all the loads on a structure before finishing the design and then to make a series of design modifications in the light of cost calculation before arriving at the final optimised result. But politicians and investors want to know the bottom line before making any initial investment and are in a position to enforce their wishes for continuous assessment and early figures for the cost of electricity. This is very much like people wanting to know the winning horse before placing a bet."*

The above can be interpreted as an argument against the use of LCOE, but, perhaps more importantly, as a statement in favour of involving investors in the design loop, and making that iterative process more apparent, transparent, and recognised. Interestingly, it is the more recent sources in Table 2 - (IEC and DTOceanPlus, 2018) - that tie metrics to the particular design development phase – this underlines the key of scoring for *development* as opposed to for *deployment*.

Since 2019, a number of new frameworks has been proposed – e.g. (Roberts *et al.*, 2021). This provides a scenario-based tool for techno-economic assessment "at the earliest stages of design" to score systems based on performance and costs, and is conceived to talk to both investors and developers. It stems from the Scenario Creation tool produced as part of the European Commission's Horizon 2020 funded DTOceanPlus project[20]. The tool allows users to benchmark their WEC concept against theoretical maximum performance, and is most likely to be used for very early conceptualisation stages ("identifying new avenues of innovation") and sensitivity analyses. It is also flexible, since users can augment the tool with proprietary information about the maximum performance of their own type of device. However, it is currently restricted to the comparative analysis of rigid single-body WEC comparisons with their theoretical

[20] https://www.dtoceanplus.eu/Publications/Dissemination-material/DTOceanPlus-Fact-Sheet

maximum performance (including LCOE) or state-of-the-art. The information contained in the tool does not allow 'evolution' comparisons of e.g. a two-body hinged raft WEC[21]. Thus the tool can help to explore the design space (valuable for performance ahead of readiness), but has limited value for 'optimisation', in that it would be difficult to integrate and streamline into a numerical optimisation routine.

A review of structured innovation tools for wave energy can be found in (Ruiz-Minguela, Nava and Hodges, 2020) and (Roberts *et al.*, 2021). Structured innovation is also discussed in (Weber and Laird, 2015) and in the WaveSPARC project (Costello *et al.*, 2019), which employs the TRIZ[22] technique, linked to a systems engineering approach used in the early design of WECs. This has also been fed into the DTOceanPlus collaboration (Tunga *et al.*, 2021). It also adds considerations on transparency being important for stakeholder confidence, and for wave energy developers to be able to know where they are in relation to one another in a realistic fashion. "We should all use common transparent costing methods, […] based on material weight and safe working stresses." (Salter, 2008).

When considering the integration of metrics in the design process and the comparison of performance between devices, (Aderinto and Li, 2019) offers some useful insights. It compares the efficiency and power performance of different WEC types based on 'characteristic length' as a common metric to score relative hydrodynamic efficiency. Interestingly, the authors point out that it is "difficult to quantify the progress of the advancement of wave energy-harvesting techniques". Three key challenges are identified: scaling issues (see Chapter 3, Section 3.5) and reliable inclusion of various system efficiencies – both of which hinder even individual WEC performance tracking – and the inherent site-dependency of performance assessment. In comparing different

[21] Communication exchange with lead author Anna Garcia-Teruel (21-01-2022), reported with permission.

[22] TRIZ is a particular structured innovation methodology, where 'structured innovation' involves applying ideation techniques in a structured and repeatable manner to creatively solve a given problem (Oxford Creativty, no date).

WECs, it is often simply assumed that each is operating at optimum conditions, particularly if site-specific performance in not known, which may in fact not be the case.

WES used ‘stage gate metrics’ to competitively assess the various WEC technologies involved in its PCP streams (Wave Energy Scotland, no date). These included AEP, CAPEX, OPEX, and LCOE, where AEP was often characterised for an EMEC wave climate, the deployment location mandated in the PCP program itself.

At international level, a metrics framework begins to appear in the IEA-OES Annual Report of 2017 (The Executive Committee of Ocean Energy Systems, 2017), where “Task 12 - Stage Gate Metrics International Framework for Ocean Energy” is set out. This work has continued through the following years and culminated in 2021 via a published framework (Hodges *et al.*, 2021). This represents a long-awaited consensus on actual metrics to be used in each of nine evaluation areas (see Chapter 9), though thresholds have not yet been identified (see also Chapter 3, Section 3.2). The methods to measure these metrics include (with IEA Stages in square brackets, refer to Figure 10):

- Tank testing of reduced scale models [up to Stage 2]
- Laboratory testing of key subsystems [Stages 2-4]
- Open water testing of relevant scale prototypes (including full-scale) [Stages 3-5]

Finally, it is noted that the IEA-OES 2017 Annual Report mentions as part of Task 12: “a final definition of success and metrics thresholds will, to some extent, be specific to a technology area and perhaps the type of market targeted” (The Executive Committee of Ocean Energy Systems, 2017). This is more than likely, as will expanded on in the following section.

2.3 Markets for wave energy applications

The essential distinction to draw out here is between grid-connected and non-grid-connected (i.e. off-grid) WEC applications. The associated target market affects both the design pathway and the technology assessment process. For example, there may be notable differences in size of WEC, cost thresholds,

length and number of deployments, end-use power demand and type, as well as the role of the public and other stakeholders (Trueworthy *et al.*, 2021). This, in turn, affects cost-performance metrics, prototype testing processes, optimisation objectives, among others.

Differing WEC requirements, design parameters, and performance priorities have an effect on metrics and a cascading effect on development aspects such as physical modelling. The link between metrics and physical modelling in the case of an off-grid WEC is revisited in greater depth in Chapter 5. However, everything starts from system requirements, whose early definition is crucial, as reported by (Ruiz-Minguela, Nava and Blanco, 2022). The report is based on a survey, where respondents highlighted that economic and political factors are dominant drivers for utility-scale WECs, while social drivers play greater role in remote community applications.

2.3.1 Emerging markets

Emerging markets are typically associated with applications within the "Blue Economy"[23] - see (Office of Energy Efficiency and Renewable Energy (EERE), 2019). An initial description and contextual introduction is given in Chapter 1 (see Section 1.2), given Mocean's near-term shift from a grid to off-grid focus. The implications of this shift are discussed in Chapter 5.

In essence, emerging market WECs ("EM-WECs" in (Trueworthy *et al.*, 2021), "off-grid WECs" elsewhere in this thesis) require a more carefully targeted development pathway because many aspects of the design and assessment depend on the specific WEC end-use, which in turn affects requirements and the type and priorities of the involved stakeholders. Some requirements/capabilities are common and have similar priority levels for both grid and off-grid – e.g. reliability and survivability (Sheng, 2019; Trueworthy *et al.*, 2021). The European Technology Integrated Platform for Ocean Energy (ETIP Ocean, 2016) points

[23] The Blue Economy refers to the sustainable growth of existing ocean uses alongside the emergence of novel economically beneficial ones (Office of Energy Efficiency and Renewable Energy (EERE), 2019). There are a wide range of both established and emerging sectors within it that ocean energy can support, such as: ocean observation, isolated communities, disaster recovery and resiliency, desalination, seawater mining, marine algae, marine aquaculture, underwater vehicle charging (IEA-OES, 2020).

out how these ought to be key performance indicators (KPIs) over and above LCOE, because they are essentially 'binary' in their nature. A WEC can either survive in the most extreme predicted waves or not. If it does not, it has no potential to generate any useful energy, and all other performance aspects fade into relative irrelevance. Salter, too, alludes to this (Salter, 2005):

> *"We must initially design devices which will survive and be reliable but eventually we will have to make them economical. Their initial productivity does not have to be maximised but it must be what was predicted by their designers"*

The above is critical, since it links to the ability of design and development tools (such as physical model testing) to rapidly and efficiently lead to better performing devices. Other requirements and capabilities require tuning or adapting – or are simply not relevant in the case of emerging markets – and can be revealed through the comprehensive TPL assessment lens. Examples are drawn directly from (Trueworthy *et al.*, 2021), which discusses this within a TPL framework using a technique called Quality Function Deployment[24]. The paper's focus is on the "changes that could be made to the current TPL assessment within the high-level capabilities, individual questions, and the information requested in order to perform the assessment." (Trueworthy *et al.*, 2021). As a result, some of the 'high-level capabilities' (cost of energy ('sub-capabilities' of performance and availability), grid integration, global deployability) are affected. Some 'capability' categories are transferable and some irrelevant. The clearest illustration is *grid integration* becoming *use integration*. Additional examples are given in the following paragraphs.

The requirement of *cost of energy* becomes *cost of concept* since there are cost factors to be accounted for distinct from the cost of energy. For example, "for an EM-WEC sold as a contained product, or through some other marketing structure […] the TPL assessment would need to reflect the cost at which one might sell or lease a device". Again, "for a smaller EM-WEC, the cost of a device might be used as a constraint rather than an objective". One needs to consider

[24] A "stakeholder-focused product definition process meant to help designers understand and organise a design problem". (Trueworthy *et al.*, 2021)

"how and how often a device is required to perform", such as the duty cycles of the loads to which the device is connected to and attempting to feed.

Further, *benefit to society* and *permitting and certification* capabilities need changing due to the different role of the public, who are no longer simply the energy off-takers plugging into the electrical grid, but direct or indirect beneficiaries of the activities enabled by wave energy off-grid. The above affects the sub-capabilities of *job creation*, *energy debt*, and *environmental impact*. *Job creation* measured in FTE/gigawatt may be transferable to FTE/project since deployments could be shorter. A greater distinction between local and non- job creation is required, since a device may be manufactured away from its deployment location.

Environmental impacts of the WEC may be minimal but those of the overall project may be high (e.g. if powering O&G platforms). However, if the project would go ahead regardless of the energy supply type, one could argue for an overall beneficial WEC impact. Finally, *energy debt*, i.e. the time to pay back the energy used to produce, operate, deploy, and decommission a device. This loses relevance if the WEC is enabling an activity that would not otherwise be able to happen.

A separate comparison between requirements for grid and off-grid can be extracted from (Babarit *et al.*, 2017), which identifies stakeholder requirements for grid-connected WECs. Requirements 1 (have as low CAPEX as possible), 3 (be reliable for grid operations) and 7 (be deployable globally) can be relaxed for Powering the Blue Economy (PBE) applications. One of the main challenges to moving to emerging markets is the difficulty of benchmarking devices against alternatives – we can no longer use a ubiquitous indicator like LCOE that is used for grid-connected devices across multiple sectors. In addition, not as much wave sector data available; thus, a developer is more reliant on market research and end-user engagement.

The first paper that explicitly discusses PBE, to the best of the author's knowledge, is (Mendoza *et al.*, 2021). Other papers have discussed the prospects, opportunities, and challenges in targeting 'alternative' markets.

Firstly, (Dalton and Ó Gallachóir, 2010) highlight the importance of building the industry based on innovation and deployment but with a bottom-up and stepped approach. PBE applications offer such an opportunity. The authors draw inspiration from the successful approach employed by Denmark in the wind sector. "Danish researchers took a bottom-up strategy of wind turbine development - a slow, crafts-oriented, step-by-step process including incremental learning through practical experience" […] "The strategy seemed superior to the top-down approach of science-oriented German and American researchers and manufacturers, who aimed at massive, centralized, quick and ambitious full-scale development" (Dalton and Ó Gallachóir, 2010). In addition, they highlight that the Danish Government's efforts to stimulate wind turbine manufacturing were prolonged. They began in the 1970s, and were based on high energy taxes and the ensuing oil crisis of the 1980s, which combined to raise domestic energy prices. Interestingly, the UK's wave energy development program began in the 1970s (Salter, 1974).

Commercial development pathways suggested in the literature vary. (Blažauskas, Pašilis and Knolis, 2015) specifically focus on developing small-scale WEC sub-systems (such as a linear generator) for wave energy converters in areas of low wave resource like the Baltic Sea, for applications such as navigation assistance and pier illumination. (Sandberg *et al.*, 2016) assess the viability of small-scale WECs in luxury resorts and small utilities. They identify the main barrier to be insufficient economies of scale to aid lowering of costs due to a relatively restricted number of devices, and other critical factors to include local infrastructure and supply chains. Nonetheless, technical and commercial viability is not ruled out.

The potential for small- to mid-size WEC applications in the provision of power to small islands and remote communities also appears in literature. For example, (Keiner *et al.*, 2022) assess the potential grid cost of energy for powering the Maldives islands with 100% offshore renewable technology including floating solar PV, wave, and wind. Costs of energy between EUR 120-132/MWh are predicted by 2030, potentially decreasing to EUR 78-93/MWh by 2050. The authors also conclude that wave energy will play an important role in the 'de-fossilisation' of small island states with limited land area.

(Clemente, Rosa-Santos and Taveira-Pinto, 2021) explore potential synergies and applications for wave energy, pointing to the opportunities of co-location or hybridisation of wave energy with other technologies, in order to drive down cost and raise commercial attractiveness. The authors highlight that it is "important to find **new perspectives** that **facilitate the development process** and **improve the chances of a successful deployment** and operation"[25]. This is precisely the approach sought and outlined in Chapter 5.

The authors in (Clemente, Rosa-Santos and Taveira-Pinto, 2021)c considers the following potential applications:

- Hybridisation and co-location with alternative sources of energy
- Autonomous vehicles
- Shipping and seaports
- Marine resources, ocean exploration and data services
- Coastal defence, surveillance and monitoring
- Water desalination
- Aquaculture
- Oil & Gas

Several papers exist supporting each of these. For example, (Green *et al.*, 2019) discusses opportunities for expanded ocean observation networks via marine renewable energy integration. For O&G, enabling ocean observation activities during decommissioning could be significant given the hundreds of platforms just in the North Sea that are reaching end of life (Jones *et al.*, 2019). In terms of alternative sources of energy, the Finnish wave energy company AW-Energy recently entered the green hydrogen market (Garanovic, 2021b).

2.3.2 Physical modelling implications

The shift from grid-scale to emerging or ‘alternative’ markets is also not straightforward from a technical perspective. Aside from understanding the implications on end-uses, stakeholder impacts and product requirements discussed above, technical barriers also exist.

[25] Bolding of text is the author’s addition.

The amount of power required from a WEC is often lower within an emerging market (Trueworthy *et al.*, 2021), affecting both the size of the full-scale WEC (some relevant consideration here (Pascal *et al.*, 2018)) and the choice of deployment location – and thus the desired wave resource topology. When considering the development process, such as reduced scale testing, a fundamental difference arises due to hydrodynamics of wave-body interactions not scaling linearly with the size of the body (i.e. the WEC). This needs to be carefully managed.

Alongside hydrodynamic impacts, physical modelling closely ties to overall development costs. In fact, while “the capital cost for a WEC farm is estimated in the millions of dollars per MW installed capacity” (Astariz and Iglesias, 2015), a smaller off-grid WEC is likely to have lower capital costs, which puts greater demands on developers to economise and accelerate the development process, since it’s a greater proportion of the overall cots. The standard, grid-scale approach to modelling, as pointed out in (Trueworthy *et al.*, 2021), is one of: computational simulation early on, followed by a multi-step physical modelling pathway with increasing scale. This is far from ideal in an emerging market context. For instance, it is relatively long and expensive, since the costs of physical models and test process scale with size of model and tank facilities. “For smaller size devices, developers can spend more time on physical models and prototypes” (Trueworthy *et al.*, 2021), implying desirability of these if the processes are cheap enough. Linked to this is the opportunity to “create a full-scale prototype earlier and so reduce uncertainty in both physical and numerical models” (Trueworthy *et al.*, 2021).

An important recommendation found in (Trueworthy *et al.*, 2021) is to support this using “an information deficit-driven approach to risk reduction through physical modelling”. Accordingly, tests can be established in order to gather the most information with the least uncertainty at the lowest cost. This can either take the form of early full-scale prototyping, or rapid turnaround at smaller scale. Ideally, it would be even better served by a sufficiently representative (i.e. with

most major sub-systems accurately incorporated) *all-in-one*[26] type physical model at reduced scale to streamline development, provided that uncertainty levels associated are deemed acceptable. Uncertainty with regards to physical modelling is covered in Chapter 3.

A final concept, which has not been encountered in the literature thus far, is the idea of 'integrated physical testing'. The avoidance of grid connection means that the 'fed' systems, which may be ocean sensors or AUV docks, could also be embodied at reduced scale and combined with a reduced scale WEC for a combined system demonstration. It is unclear how much scope exists in practice for a streamlined physical modelling approach at reduced scale, for an all-in-one type physical model, or for an 'integrated testing' campaign. These themes will be returned to at the end of this thesis.

Concluding remarks

This chapter hopes to have shown the lack of clear pathways to WEC development that currently exist. This translates into an open and ambiguously defined process of advancing both performance and readiness of a technology. The shift from grid to off-grid markets brings about both challenges and opportunities. From a developer's point of view, all these considerations need to relate to metrics that reflect value and enable optimisation and assessment. The gaps, challenges and opportunities highlighted lead to a strategic framework definition (the Wave Energy Paradox) for the development of the Blue Star WEC, and a choice of metrics for optimisation and validation. Both can be found in Chapter 5. What follows first, though, is a review of physical modelling (Chapter 3).

[26] i.e. a physical model that is able to fulfil multiple testing purposes, such as the gathering of validation, performance, and survival data (see further in Section 3.1).

Chapter 3. Physical Model Testing

This chapter explores the role of physical model testing, challenges and opportunities in its use with a focus on: small scale, PTO inclusion, and accounting for uncertainties. It also covers relevant testing and development standards. Considerations are limited to physical model testing with reduced scale 'models', as opposed to full-scale 'prototypes'. The theoretical underpinnings of physical model testing, such as Froude scaling and linear wave theory, are covered in Chapter 4. Chapter 3 aims to cover three broad themes within physical model testing: what data is typically gathered (for what purpose), in what way the data gathering process occurs, and what the quality of such data is.

An initial brainstorming exercise aimed at extracting key themes relating to physical modelling – in terms of opportunities and challenges of moving to smaller scales – is included Appendix C.

Figure 14 - A scaled model of Blue X at FloWave facility.

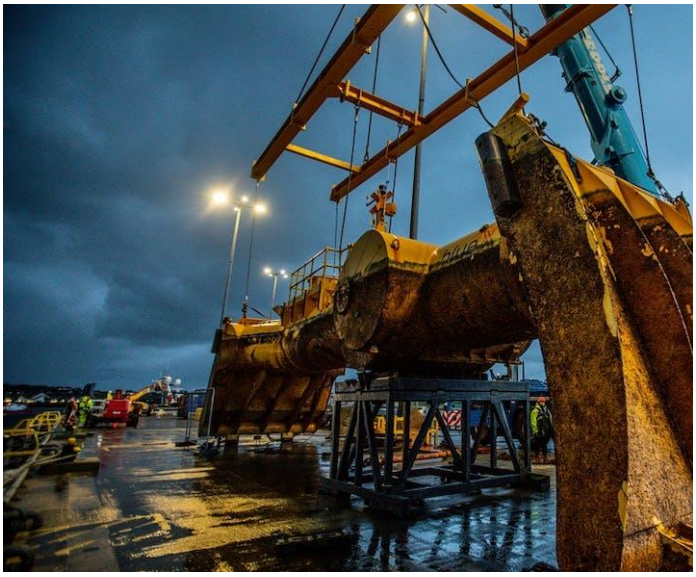

Figure 15 – Full-scale Blue X wave energy converter being lifted at Hatston Pier in Orkney (Scotland).

3.1 Role and purpose

The physical modelling and experimental testing (henceforth, just "physical model testing" or PMT) of a WEC is an essential link in wave energy

development, and viewed as a well-established practice. Even a miniature reproduction of a physical system can help to understand complex fluid behaviour (Hughes, 1993). It also allows developers to test their systems in a controlled and repeatable environment. The downside is the potential introduction of unwanted scaling effects and the need to balance often conflicting requirements ("PMT trilemma" – see final section). Developers "need to scale the dominant physical process(es) and compensate or reduce the errors in others" (Noble *et al.*, 2021). Traditionally, the approach has been to simplify environmental conditions as much as possible in order to obtain an initial understanding of the overall device behaviour and performance. In progressing through the development stages, more 'realism' and accuracy are added in the tests. The question of when to move from one development stage to the next largely remains an open one (Noble *et al.*, 2018, 2021) – as discussed in Chapter 2 – and is often device/developer specific, since the diversity of WECs means universal thresholds are not easily come by (Hodges *et al.*, 2021). The correlation between increasing TRL (development stage) and model scale is also not necessarily applicable universally.

One perspective is that numerical modelling overheads – in terms of computing power, coding time, and debugging time – ought to be weighed against physical modelling overheads in designing, building, and testing an experimental model. Nowadays, the latter typically outweighs the former, but it has not always been so – and smaller scale PMT could push the scale further towards a renewed middle ground. In a paper titled "Research requirements for 4th generation wave energy devices" published in 2003, S. Salter outlines some key advantages of testing physical models in wave tanks at small scale, among which: increased safety and ease of handling devices, the reduced cost of these devices, and the opportunity for effective learning (Salter, 2003). Here Salter additionally points out that: "Mistakes made at small scale in private do not damage the credibility of the entire technology. Indeed they can be very informative". On the contrary, testing of full-scale devices can be so expensive that "iterative problem-solving is ruled out" (Salter, 2003). As such, testing at small scale can mitigate some of the advantages accrued by numerical modelling over time due to developing computing technologies and tools.

The primary goal of physical model testing is to facilitate learning. We may classify the drivers of learning facilitation at reduced scale physical model testing PMT as falling within four categories: *cost*, *safety*, *practicality*, *insights*.

From the point of view of insights, the purpose of physical modelling spans (from (Hughes, 1993)):

- Validating numerical model predictions and tuning analytical parameters (*validation* model)
- Modelling complex behaviour (e.g. nonlinearities) without the simplifying assumptions embedded in analytical or mathematical representations (*design* model)
- Exploring specific response details that are not yet understood or theoretically modelled (*process* model)
- From a funder perspective, one might suggest that there is also an important visual (*demonstration* model) element, although full-scale is undoubtedly more compelling in its visual and confidence impact. Visual observation is also insightful for developers when attempting to decipher some of the underlying nonlinearities in behaviour via live or video footage of the model in water.

"The tank is the only place where data can be collected in a controlled environment, in the presence of a free surface" (DeBord Jr *et al.*, 2003). Considering validation in particular, the ability to validate a particular numerical model depends on the type of model and the quality and of tank measurements made. Sometimes a numerical model cannot be validated because of a lack of measurements or because key physical processes cannot be included numerically but turn out to be significant in tested conditions. In such cases, validation serves to identify the shortcomings of a numerical model and can suggest paths for future improvements.

Before continuing, the practice of PMT is framed historically, to provide a brief retrospective roadmap to the current state of play. This is relevant in terms of the availability of analytic tools (hardware and software), but also in terms of the spirit and mentality with which wave energy development has been approached.

3.1.2 Historical pathway

Wave energy development has been characterised by a series of start-stops. The first known wave energy patent was filed on July 12, 1799 by Pierre-Simon Girard (Girard, 1799), it was an early version heaving float, not too dissimilar modern day versions; it involved a lever arm actuating a pump. According to other sources, there had been more than 340 files related to wave energy filed in Britain alone by 1981, though most were not 'practicable' (Ross, 1981). Others claim that more than 1000 patents had been registered by 1980 (McCormick, 1981).

Yoshio Masuda, a former Japanese naval commander, was one of the pioneers of modern wave energy technology, whose studies originate from the 1940s (OES, 2008). He utilised the principle of the oscillating water column (OWC), where enclosed air pressure drives a turbine under the action of rising and falling water levels, to power navigational buoys. These were commercialised since 1965 (Masuda, 1971), but remained limited in terms of their size and applications.

The oil shortages following the Arab-Israeli war in the 50s and 60s, and the associated energy crises, were one of the sparks that raised interest in large-scale wave energy production (Ross, 1981). In particular, it encouraged the UK government to invest in a major wave energy R&D programme in 1975, following a proposal to the UK Science Research Council by Stephen Salter and others in 1974 (Salter, 1974). The Norwegian government soon followed suit. In the UK, Salter's proposal kicked off the structured empirical research efforts that led to the design of the "Edinburgh Duck" concept, using just a workshop and a borrowed narrow tank. The successive step-wise learning and innovations can be found in (Salter, 2008, 2016). Observational insights collected during this period were instrumental in making a considerable leap from a fundamental understanding point of view. Several landmark studies followed, such as (Salter, 1974; Budar and Falnes, 1975).

In 1981, D. Ross wrote, "we could be on the verge of a new industrial revolution in which we shall be able to obtain all the energy we need from the ceaseless motion of the waves" (Ross, 1981). However, UK funding ground to a halt in

1982 (OES, 2008), and “the [UK] government closed the wave-energy project” in favour of the nuclear industry; a political decision, according to (*Stephen Salter: pioneer of wave power*, 2007). It was also partly motivated by a drop in the oil price by the mid-80s. However, although UK wave activity stopped, it continued in Norway. In 1985, two full-sized shoreline prototypes were deployed near Bergen, rated at 350 kW and 500 kW (OES, 2008).

Momentum picked up again in the mid-90s due to growing climate change awareness (Day *et al.*, 2015). In 1991, the European Commission included wave energy in its R&D programme on renewable energies (OES, 2008); this can be considered the genesis of wider development and involvement at European political level. Ultimately, though, wave energy lost the race with nuclear, which received far more attention between the late 1980s and the late 1990s. A later resurgence at the onset of the millennium, with flagship companies like Pelamis Wave Power and Aquamarine Ltd developing large full-scale WECs, ended when both companies entered administration by the mid-2010s. At this stage, onshore renewables first, and offshore wind second, pushed wave power to the fringes once again. It is still unclear whether the ongoing gas crisis following Russia’s invasion of Ukraine will encourage or accelerate state support once more (February 2022). Towards the end of summer 2022, gas fired power stations were reported to produce electricity at £446/MWh in the UK, according to The Carbon Brief (Spencer, 2022) – in light of this number, wave energy support would not seem misplaced even if assessed purely on cost.

Returning to wave energy development itself, the shift towards numerical modelling was motivated - among other things - by developments in computing power and capabilities. A digital computer employed in linear Duck analysis work was reported in 1987 (Skyner, 1987). In addition, flexibility (one can vary more variables and more easily undertake sensitivity studies), and cost reduction (facilities and physical model costs) form other attractive elements. Two of these benefits can be potentially reproduced experimentally by fast-turnaround small-scale PMT. For example, it is not uncommon for facility costs to take up to half or more of overall experimental project costs, with the other being model build. A pragmatic balancing of budgets with expectations of type of data and quality of results is often required.

The level of emphasis placed on physical modelling depends much on the answer to the question, “can the investigated phenomena be captured numerically?” This is not always straightforward to answer, and, ultimately, experimental testing is a necessary tool for this purpose – not least because numerical models are typically limited in their ability to account for hydrodynamic losses due to viscous fluid effects, or to accurately model large amplitude water oscillations (Falcao, 2009). Empirically correcting for these effects is important, as it has been in other fields such as naval engineering and offshore structures.

3.2 Standards & Guidance

This section highlights the sources of standards and best practice guidelines available to wave energy experimentalists, but does not explore all of these standards in detail. Instead, the aspects most relevant to scaling, PTO/subsystem inclusion, uncertainty, and quantities of interest (related to metrics) are picked out. Aspects directly relating to tank operation and best practice are discussed in Part II (Chapters 6-8).

The fundamental premise is that marine renewable energy is still an ‘emerging’ technology, of which wave arguably the most nascent. As such, it has been difficult for wave energy to find an industry standard to “rally around” (Falcão, 2010). A totally converged set of standards does not currently exist (Noble *et al.*, 2021), though efforts led by the IEA-OES are building towards greater convergence (Hodges and Colby, 2022).

Standards are set by international standards bodies, intergovernmental organisations, as well as European, national and regional projects. The main sources of interest are outlined below.

The International Energy Agency (IEA) is an intergovernmental organisation, which includes Ocean Energy Systems (OES) as one of its Technology Collaboration Programmes. OES was founded in 2001, involves 25 countries, and can be considered to represent the overarching consensus in the sector. An IEA-OES guidance protocol on establishing common industry practices was published as far back as 2003 (Nielsen, 2003). OES focuses on 15 tasks, which drive its activities. Task 12, titled “Stage Gate Metrics International Framework

for Ocean Energy", is the most relevant here. The IEA-OES report from 2021 finds a "wide range of evaluation criteria …[but] does not set thresholds to indicate success at each stage – noting that these are specific to technologies, projects, markets, and investors" – hence 'standard' values cannot be specified (Noble *et al.*, 2021).

The same report finds that more detail is needed on *what* to test at each stage of development and *how* to determine whether to move to the next stage or not. For example, the lack of thresholds used to inform progression from small to larger scale tank testing – in the specific case, "what value of a particular metric is good enough and are we sufficiently confident in its obtained value?" Nevertheless, the IEA-OES framework for Ocean Energy Technology (Hodges *et al.*, 2021) is considered to represent industry consensus on performance metrics and ocean energy technology evaluation methodology. It is not a technical standard, but rather defines development stage activities and associated evaluation criteria. It was conceived to be complementary to the International Electrotechnical Commission (IEC) standards; IEA-OES essentially illustrate the "what", while the IEC the "how" (Hodges and Colby, 2022). For example, the IEA-OES document states that mean time between failures (MTBF) should be considered as part of Stage 3 (TRL 5-6) activities and evaluation, while the IEC illustrates how this quantity can be measured and/or calculated in more detail.

The IEA-OES framework is helpful in terms of its unification and clarification of evaluation criteria, but has some shortcomings, particularly in terms of:

- Not including social cost of energy as part of the evaluation areas
- Largely missing environmental considerations – 'disposability' is illustrated as one of the 'Process Efficiency' inputs (Hodges *et al.*, 2021), though 'recyclability' or 'sustainability' would likely better represent this element. Either way, these are outside of its scope[27].

[27] One of the IEA-OES framework lead authors stated in 2022 that both social and environmental cost of energy have been set as top priorities for future expansion of the framework, which includes Wave Energy Scotland (WES) as part of its stakeholders and document drafting personnel.

- Missing a clearly identified Technology Qualification step

The already mentioned IEC – an international standards-setting body – has a technical Committee (TC114) dedicated to Marine Energy, which produced what is arguably the most comprehensive experimental testing implementation protocol to date (IEC TS 62600-103, 2018). It recommends always using the largest possible physical model scale, and states in relation to hydrodynamic scaling:

> *"A model cannot meet both Froude [Fr] and Reynolds [Re] scaling criteria simultaneously. The Re number for a Fr-scaled model is smaller by a factor of $s^{1.5}$ [where 's' is the scaling coefficient]. Hence, while the prototype flow regime may be turbulent, the model may be laminar. The drag coefficients in laminar flow are normally higher than those found in turbulent flow. Hence the scale-up is generally expected to underestimate the true performance of the WEC. The level of underestimation is directly related to the dominance of viscous losses in the design.* ***Currently there is no guidance on the relation between underestimation, the WEC scale, and the WEC design elements.*** *The larger the scale of the WEC device, the less dominant the scaling mismatch will become." [bold is author's addition]*

However, accounting for uncertainty is largely not covered. On the other hand, the International Towing Tank Conference (ITTC) has a specialist committee on hydrodynamic modelling of marine renewable energy devices, including recommended practices for uncertainty analysis of WECs (ITTC, 2017). However, these are challenging and time intensive to apply in practice, and, consequently, rarely are.

IEC technical specifications have been widely adopted. An example being Deliverable D5.3 of the Horizon 2020 OPERA project, which applies these to open-sea data collection (Berque *et al.*, 2019). It identifies that more guidance is required for users working uncertainty evalutation, and that "more data is needed to provide reliable recommendations on yield prediction for scaled prototypes" (Berque *et al.*, 2019). The aim of the OPERA[28] project is to: collect, analyse, and share open-sea operating data and experience, taking a WEC from

[28] http://opera-h2020.eu/

TRL 3 to TRL 5. It also aims to make open-sea data publically available for wave energy research and development (R&D) and to reduce commercial costs of wave energy. Such a remit is invaluable for the industry.

The UK Department of Trade and Industry (DTI) published a preliminary wave energy device performance protocol in March 2017 (Smith and Taylor, 2007), in some ways a precursor to the IEA-OES framework, though only at UK level. It was published after £42m had been put aside for the Wave and Tidal-stream Energy Demonstration Scheme as part of DTI's Marine Renewables Deployment Fund. The funds aimed to support demonstrations of large-scale deployments, including WEC arrays that would supply energy to the grid network. The objective was to provide a protocol such that the supported technologies could be "assessed in a consistent manner", and which would ensure "the capture of data that will allow the varying power generated by WECs to be considered in the context of corresponding sea conditions" (Smith and Taylor, 2007). This effort is still ongoing and spearheaded by IEA-OES (as mentioned previously). The DTI protocol also refers to the European Marine Energy Centre (EMEC)'s 2004 guidance, which focuses on wave resource as much as full-sale device responses. It indicates the following mandatory device-record parameters at half-hourly intervals during at-sea trials:

- Mean, min and max power generated
- Power variability – i.e. standard deviation about average
- Device status – i.e. device available and operational, or offline for maintenance or other purposes
- System identifiers – i.e. records of events that may affect the performance data, such as sensors or associated software
- Device compass heading

The European Marine Energy Centre (EMEC), an open sea test centre for marine renewables, publishes guidelines based on experience. Its original publication came in 2004. In its latest version (Pitt, 2009), it gives guidance on performance assessment in open sea. It is similar to the DTI Protocol, but also includes a section on performance indicator sensitivities to factors such as wave height (specifically, H_s) and period (specifically, T_e). For example, it recommends

power matrix cells to be 0.5m wide for H_s and 1.0s wide for T_e. It points out the importance of specifying uncertainty in power output at each cell, because of the size of the cells and the variability of the waves in a set period of time that are statistically represented by each cell. In other words, "the power samples included in each cell are not identically distributed" (Pitt, 2009), as they vary with H_s^2 and T_e. Capture length (i.e. the ratio of electrical power output to the power in the sea state) is highlighted as the "advocated" measure of performance.

EquiMar, an EU-funded research project, having 9 deliverable areas, including one titled "Assessment of current practice for tank testing of small marine energy devices" (McCombes *et al.*, 2010). In 2011, it published its protocols for the equitable testing and evaluation of marine energy extraction devices, in terms of performance, cost and environmental impact (Ingram *et al.*, 2011). Those on tank testing include quality and accuracy of results, scale recommendations, and qualities of prototype models including PTO.

- Quality and accuracy: split between pre-test and post-test, and refers to ITTC recommendations.
- Scaling: "in performing tests of extreme conditions […] unlikely that the same facility will be able to produce the large waves required to test the prototype" at the same scale as tested for power performance. The recommendation is to move from Stage 1 to Stage 2 of testing, moving from a facility that can produce 1:50 testing conditions to one that can facilitate 1:10 testing, [such] that the small-scale prototype be reused in the large-scale facility"[29] (Ingram *et al.*, 2011).
- Qualities of model – geometric tolerances given in ITTC Procedures 7.5-01-01-01 and 7.5-01-02-02, and also PTO inclusion (see later section).

The Marine Renewables Infrastructure Network (MaRINET) – funded by the European Horizon 2020 program – provides practical guidance on testing and assessing wave energy converters, including model construction methods (Deliverable 2.28). Under 'scale selection', it highlights that "it is clear that the

[29] Underlined text is the author's addition.

larger the scale, the more accurate the results can be but also the higher the costs" (Thiébaut, Sutton and Johnstone, 2015). Scale is selected based on development stage, test objectives, and test location. Suggested scales for different objectives are revisited in Section 3.5.

MaRINET has been followed by MaRINET2. (Trueworthy and Dupont, 2020) discuss MaRINET2 best practices and appraise them in light of overall WEC design process, highlighting their aim in facilitating access to testing facilities and in standardising the testing process itself. On the latter, the so-called 'Round robin test program' (Davey *et al.*, 2021) is significant and worth mentioning, having the aim of providing "understanding on the causes of variation between facilities in order to develop a standardised approach to offshore renewable laboratory testing" (Thiébaut, Sutton and Johnstone, 2015). Another relevant piece of the MaRINET2 program has been a gap analysis and test recommendations report, D2.1 (Noble *et al.*, 2018). This helpfully contains a section summarising applicable general, technical standards and other guidance documentation.

For completion, Supergen Marine, a UK-funded research project, published in 2008 a guidance document for the experimental tank testing of WECs (Payne, 2008), which offers sound practical advice on aspects such as repeat time for each run and the inclusion of PTOs. This acted as a precursor to some of the aforementioned MaRINET deliverables.

Outside Europe, the US Department of Energy (DoE) ran a competition called Wave Energy Prize (Driscoll *et al.*, 2018) in 2014, involving 92 teams. It was run in 3 phases and developed not only assessment metrics (covered in Chapter 2) but also a specific testing methodology. In the final phase of assessment, all entry models were at 1:20 scale and included a model PTO. The evaluators included new power assessment metrics such as ACE and ACCW (see Chapter 2), as well as hydrodynamic performance qualifiers (HPQs) that are described in Chapter 2. The models were tested in 10 irregular sea states representative of 7 offshore locations in the US.

Also in the US, the National Renewable Energy Laboratory (NREL) – a national laboratory of the US DoE – ran a Marine Hydrokinetic Instrumentation Workshop

in 2017 (Driscoll, Mauer and Rieks, 2018), where it identified four themes relating to measurement methodology gaps, two of which are particularly relevant to this thesis:

- **High cost of measurement** that leads to undesirable trade-offs between quantity and quality of data captured – e.g. often sacrificing on the number of tests and quality of measurements (e.g. repeats) in order to be able to run longer or broader tests in terms of different parameters explored[30].
- **Better measurement capabilities at low TRLs** to facilitate reduced scale testing at or below 1:10 scale. The smaller the scale, the more difficult it can be to find capable and cheap enough sensors. The need for these sensors to be light can either drive up costs or drive down measurement capability, but is often crucial in order to avoid affecting the measurements themselves via altered model mass distribution properties or hydrodynamic characteristics and behaviour.

The other two themes consisted in limited knowledge transfer and a lack of open-source tools for unified data processing and analysis, both of which are significant, and the latter is picked up in Chapter 9.

Det Norske Veritas (DNV) also produces and publishes industry standards, mostly adapted from the O&G sector and broadly applicable across the offshore sector, including wave. Relevant documents include: DNV-OSS-312 on Certification of Tidal and Wave Energy Converters, DNV-RP-C205 on Environmental Conditions and Environmental Loads, and DNVGL-SE-0160 on Technology qualification management and verification, among others.

When thinking about future updates and changes to standards and guidelines, it is useful to note how frequently they are updated. For example, the IEC revision interval varies from several years to decades (Noble *et al.*, 2021). The next one in the 62600 series should be between 2021-24. With regards to the ITTC,

[30] This is partly why uncertainty analysis is not commonly performed in WEC physical tests.

Special Technical Committees meet 4 times between the triennial conferences where the Executive Committee can approve changes that are proposed.

3.2.1 Limitations

(Day *et al.*, 2015) maintain that, “much of the guidance is rather general and does not address the specific nature of many critical challenges of tank testing marine renewable energy devices”. This is echoed in (Rodríguez, Rosa-Santos and Taveira-Pinto, 2018), where the authors suggest that “guidance is still too general and does not address the more practical issues”. For example, as of 2015, ITTC material was more tailored to providing guidance on specific issues related to the execution of the actual tests. Some of their procedures can be adapted to uncertainty analysis for WECs (see Section 3.6).

Standards do exist, as has been shown, but "in many cases are not focussed on hydrodynamics aspects involving physical testing or numerical modelling of devices" (Day *et al.*, 2015). Programs like MaRINET have gone a significant way in addressing these gaps from a very practical perspective. An interesting paper on standardising marine renewable energy testing is (Noble *et al.*, 2021). This gives a comprehensive tabulated summary of topics covered by published marine renewable energy testing guidance documents in its Appendix. It identifies gaps and follows these up with stakeholder surveys to make recommendations. The gaps most relevant to the present work are:

- “Effective scaling and simulation of PTO at model scale, along with method for performance assessment” (Noble *et al.*, 2021), particularly at early development stages
- A “need for uncertainty analysis to become part of a standardised testing process” (Noble *et al.*, 2021)

Two additional secondary limitations are identified:

- Accounting for biofouling
- Accounting for combined wave and current conditions, particularly for floating devices

The authors note that: “existing IEC standards for performance assessment list the uncertainty items to include in studies, but limited guidance is given

regarding how these should be processed and presented" (Noble *et al.*, 2021). In addition, the potential to introduce bias in results and their uncertainty levels are also affected by the fact that different facilities use different procedures – several factors including tank capabilities and equipment available, as well as personal experience. This links to the round-robin testing programme of MaRINET2 specifically designed to "identify effects individual laboratory facilities have on performance results" (Noble *et al.*, 2021).

Specific aspects are highlighted in detail in the relevant sections that follow. Standards and guidance will be returned to when outlining methodology in Chapters 6 and 8. "Despite the acknowledged gaps in the standards, one benefit to O[ffshore]R[enewable]E[nergy] being a relatively young and evolving sector is that industry practice and academic research are closely aligned, unlike more established industries" (Noble *et al.*, 2021).

Fundamentally, no guidance exists for identifying the minimum acceptable scale to perform physical model testing, such that appropriate data is obtained at an appropriate degree of confidence/uncertainty. This remains in the hands of the developer. The main guidance is in terms of scale with increasing TRL, but it remains unclear when to move up, especially given growingly diverse target markets that, in turn, mean diversifying sizes of full-scale WEC and therefore of relative scales.

3.3 Quantities of Interest

One of the first steps in a testing campaign – particularly for validation – is to define the Quantities of Interest (QOIs): the measurements that are used to define the success of the campaign. Metrics are not the same as QOIs, they are rather *representations* of QOIs (Robertson, 2017). For example, the free surface elevation at a particular point in a wave tank can be a QOI, typically measured with a wave gauge. The associated metric could be the reflection coefficient of the tank for a given specified sea, or the response amplitude operator based on another QOI – e.g. the heave of the deployed model. Thus, the metric represents the physical behaviour – via QOI measurements – that enables the process of validation. The specification of metrics (see Chapter 2) can guide the choice of QOIs, and vice versa.

A non-exhaustive mapping of wave energy physical testing studies having either validation or performance goals is offered in Appendix C, to illustrate the range of model sizes, scales, PTOs utilised, and seas run. This summary shows that the majority of physical testing campaigns do include PTO representations, often do not include short-crested seas or uncertainty analyses, and involve large test basins with scaled models often weighing in the 100s of kilograms, and measuring greater than 1m in characteristic dimensions. In contrast, as will be seen in Chapter 6 and 8, the 1:20 scale physical models tested in this research weight a few kilograms and can be easily and safely handled manually.

Besides the above, it is worth picking out a paper by (O'Boyle *et al.*, 2015). A rare study that compares full-scale QOIs retrospectively with 'equivalent' (i.e. as-installed) experimental 1:40 scale and numerical (spectral domain and time domain) models. It is based on at-sea testing of a full-scale Aquamarine Oyster 800 flap-type WEC, where the test programme is specifically intended to maximise quality and learning – denoted as Performance Improvement Programme (PIP), even at the expense of maximising power generation.

The paper correlates prototype-model behaviour in terms of hydrodynamic power capture and flap dynamics. It reports that during actively damped operation of the full-scale machine, "friction in the entire [PTO] subsystem can typically be of the order to 10% of the total resistive torque applied to the flap" of the Oyster 800 WEC (O'Boyle *et al.*, 2015). No direct measurement of friction in the full-scale prototype means that this must be inferred from back calculations, and introduces uncertainty in power capture estimates. In the scaled physical model, a disc-brake damping mechanism is used, which "broadly represents the characteristics of the PTO", although "the transient subtleties of the [full-scale prototype] hydraulic system are not well represented" (O'Boyle *et al.*, 2015).

Although good agreement is demonstrated between as-installed experimental and numerical models in terms of prototype dynamics and torque curves, the nature of the experimental PTO means that the numerical model better matches prototype data as it includes parameters that describe the actual hydraulic system more closely, unlike the 40th scale representation.

EquiMar protocols highlight that PTO inclusion is important even at the first stage of development (proof of concept) but the power conversion chain does not need to be complete. The PTO may just be mechanically simulated. Since the relationship between any conversion stage input and the output is likely to be non-linear, it is desirable to directly measure performance at each conversion interface. The challenge is to arrive at “the best compromise between a meaningful and sensible power indicator, intrusion into the operation of the device, and the requirements of fabricating and instrumentation of the test prototype” (Ingram *et al.*, 2011). Some PTO inclusion studies and considerations are made in the following subsection.

3.3.1 Inclusion of power-take-off

If the power capture elements of a WEC are to be assessed, a physical representation of the PTO and associated measurable QOIs need to be included in the model. Device performance depends on the PTO behaviour, because this affects the motions and thus the hydrodynamic response of the prime mover, including the loads. "Hence appropriate simulation of the power take-off is essential during small-scale model tests to determine the performance of the system” (Day *et al.*, 2015).

For example, for heaving point absorbers, it has been shown that under uncontrolled conditions, viscous drag forces are negligible and the device behaves linearly as a wave follower. But under control conditions, viscous forces become fundamental (Giorgi and Ringwood, 2017) – thus the importance of including a physical PTO if possible. Generally speaking, the inclusion of PTO and control may expand the envelope of relative displacements and relative velocities between fluid and WEC, which has effects on flow regimes and thus nonlinearities encountered (Day *et al.*, 2015).

However, a key challenge is that “accurately simulating a PTO and quantifying the power production is difficult, particularly at small scale” (Noble *et al.*, 2018). This is primarily because power scales as length^3.5 according to Froude laws. Thus, a 100kW device at 1:20 scale would require measurements in the order of a few watts and thus measurements in the milli-watts range. In light of this fact, Salter argues that attempting to make a model scale PTO anything like a

"microscopic version" of the full-scale one would be a mistake. A radically different system is likely to be better suited to such small wattage (Salter, 2016).

Seven methods for representing and instrumenting the PTO are discussed in a MaRINET Report of Instrumentation Best Practice (Tetu *et al.*, 2013). These consist in: "friction based, weight lifting by rotating axle, eddy current brakes, pressure difference, overtopping flow, passive linear actuators, and advanced PTO systems" (Noble *et al.*, 2018).

A different type of model PTO used in (Rodrigues *et al.*, 2020) consists in triboelectric nanogenerators (TENGs). "A TENG is basically composed by two triboelectric materials with different polarity, an air gap between them and two metal electrodes. When two triboelectric surfaces with opposite triboelectric charges are contacted and separated, a potential difference is created, driving electrons to flow between two connected metal electrodes" (Clemente *et al.*, 2021). The maximum power generator by the TENG at 1:20 model scale was 1.50mV, corresponding to a maximum power density of 1.5W/m2 (model scale). These can be 3D stacked in order to increase available damping. However, the authors point out that the "Froude similarity criterion may not be the most suitable approach to upscale these outputs to prototype equivalent, given the predominance of electrostatic, triboelectrics and material-contact phenomena" (Rodrigues *et al.*, 2020).

Mechanical motion rectifiers (MMR) are used in (Li *et al.*, 2017; Liang, Ai and Zuo, 2017; Martin *et al.*, 2020). An MMR 'rectifies' (i.e. converts) bi-directional linear motion into unidirectional rotational motion. This is often needed in the context of point absorber WECs that are excited in, say, heave, but rely on rotational PTOs for mechanical-to-electrical energy conversion. The model used in (Martin *et al.*, 2020) has a gearbox, two one-way clutches, and a coupling – a relatively complex drivetrain. However, friction effects and other potential losses and uncertainties are not captured in the paper. The authors find that the optimal (target) PTO damping is unachievable at model scale due to PTO limitations. The maximum experimental linear damping (2.5 kN/m) cannot reach the 13-14 kN/m predicted by numerical models. It should be noted that the numerical

models can still be (at least partly) validated by lowering the damping values to compare like-for-like behaviour.

(Li *et al.*, 2017) study the dry-testing of an engagement/disengagement mechanism for an MMR, which results in a PTO efficiency of up to 80% at model scale. A more detailed analyses can be found in (Liang, Ai and Zuo, 2017).

In (Shahroozi, Göteman and Engström, 2021), a PTO model is incorporated at 30^{th} scale, based on contact friction between a Teflon block that is sprung against a rectangular Aluminium rod. However, the ball bearings of the linear guide as well as pulleys used in the PTO representation have non-zero friction, which limit the lower bound damping value that can be applied. The pulley friction value is estimated based on an operator moving the PTO translator at approximately constant speed, which is found to be 7N average based on half-stroke displacement. This is likely to vary with translation speed and rope tension, so is prone to error.

In (Cameron McNatt and Retzler, 2019), a 1:20 model of a 100kW rated hinged raft WEC is tested including a controllable motor used as PTO. In the irregular waves tested, agreement between powers measured and those predicted in the time-domain is within 10% for all seas and PTO damping values utilised. The study shows that in this case power absorption can be “reasonably captured using only a nonlinear viscous Morison model and a nonlinear torque limit”. In this set of tests, non-zero friction in the hinge, primarily due to the presence of a lip seal at the motor’s shaft exit, is not measured directly, exposing the results to some uncertainty. The motor is instead pre-calibrated in the dry to account for friction effects. Among others, the paper highlights the risk of power over-prediction at higher wave heights if nonlinear forces are not accounted for.

(Shahroozi *et al.*, 2020) suggest a rotary PTO system based on eddy current damping that increases with the applied current, is independent of mass, and is non-contact. The PTO consists in an Aluminium disc rotating between two sets of coils that provide magnetic braking. The induced magnetic current that is braking the disc increases with the disc’s speed of rotation. Damping can then be varied by hanging different masses from the rotary disc at a constant radial distance from the axis of rotation.

Other recommendations can be found with regards to the PTO inclusion. For example, (IEC TS 62600-103, 2018) states that in Stage 1 and 2 (corresponding to smaller scale tests):

> *"representational PTOs that capture dynamic-kinematic (force-velocity, torque-angular velocity, pressure-flow, etc.) characteristics are often used. However, these representational PTOs can introduce frictional effects, like stiction, or non-physical hysteretic effects. Further, these representational PTOs may not be able to imitate limitations that will exist in the prototype, such as max forces or slew rates*[31] *from the generator."*

The standard also recommends to:

> *"Consider the power conversion chain (PCC) carefully. A major issue is the inability to truly scale bearing surfaces such that frictional losses are also scaled. Thus, to improve power performance prediction, a friction analysis can be completed to determine the difference in performance that is being lost to the inability to scale frictional losses."*

Typically, the amplitude of motion in the device correlates to the amount of energy being converted, and this in turn typically correlates with the level of damping from the PTO. "Thus the simulation of the device requires that the model-scale PTO behaves in a manner which correctly represents the behaviour of the full-scale system over the range of oscillation amplitude and frequency. In addition it is important that the model-scale PTO allows the damping to be repeatably varied in order to allow systematic investigation of the power extraction" (IEC TS 62600-103, 2018).

It is acknowledged in various standards that at TRL1-3[32], the full-scale PTO detailed design is unlikely to be complete, but the ability to set a damping value and repeatability are often minimum requirements. In their state of the art review of marine renewable energy device hydrodynamic modelling, (Day *et al.*, 2015) offer some helpful guidelines on the inclusion of model PTOs in reduced scale WEC physical models. A preference is expressed for active (i.e. controllable) model PTOs, and to avoid friction-based systems where possible, since these

[31] Slew rate refers to the change in voltage or current per unit of time.

[32] i.e. research stages up to and including proof of concept.

are particularly sensitive to environmental factors such as temperature and moisture, which lowers repeatability (as well as friction not Froude scaling well in the first place).

For tests at TRL>3[33], active dampers with closed-loop control are preferred. One can still use relatively simple linear or quadratic damping strategies (to represent idealised PTOs).

Aside from parasitic friction loads, key limitations in implementing PTOs at small model scale include spatial constraints and mass limitations. In (Berriel *et al.*, 2021), the authors select a Froude scale of 1:5 based on the available off-the-shelf induction machine and its working range. This is an example of how PTO availability and characteristics can end up driving the overall scale of the physical model and the scope of associated test programs. If in loco measurements of load variables (e.g. torque or force) cannot be made, bench testing the PTO ahead of wet tests is possible but usually not recommended, since it is difficult to replicate inputs representative of wave excitations, as found in e.g. (Rodríguez, Rosa-Santos and Taveira-Pinto, 2018).

To overcome some of these limitations, so called ‘hybrid’ testing – involving a combination of physical experimentation and numerical behaviour emulation – is a growingly applied tool in the sector.

3.3.2 Hybrid testing

Temporarily stepping into the floating offshore wind domain, no ‘silver bullet’ approach exists for physical modelling of floating offshore wind turbines (FOWTs); the approach is either to do full physical tests or hybrid tests, where waves are physically generated but the aerodynamic loads are applied with a numerical substructure (Otter *et al.*, 2021). The hybrid testing approach is generally cheaper and more versatile than a ‘fully physical’ approach.

However, fully physical – especially with ‘performance scaled rotors’ that reduce scaling regime mismatch – can model all aspects and phenomena of the FOWT,

[33] i.e. component, sub-system, and system validation in laboratories and/or simulated operational environment,

including potential unexpected aerodynamic behaviour which influences overall dynamics and which is not captured numerically. Indeed, although a fully physical approach is expensive and requires a dedicated model for each design iteration, the authors in (Otter *et al.*, 2021) caution against doing away with physical testing stages in the bid to cost-cutting even if high-fidelity numerical models are available.

The above scenario from offshore wind is somewhat analogous to the hardware-in-the-loop (HiL) idea for wave energy. HiL couples parts of a real system with simulated parts of the same overall system, and is geared to facilitating development, including by reducing expense (Bacic, Neild and Gawthrop, 2009). It is widespread in automotive and aerospace applications (Bracco *et al.*, 2015) and became growingly used in wave energy from around the 2000s. The fundamental motivation for using HiL is to enable the inclusion of aspects of the WEC that are difficult to model (which might be implemented physically), and aspects that are expensive or difficult to manufacture (which might be simulated numerically).

HiL is predominantly used for ‘dry’ testing of PTO and control systems, most often to test large scale physical PTOs relatively late in the development process when the PTO systems are fairly well defined (Signorelli, Villegas and Ringwood, 2011; Bracco *et al.*, 2015; Berriel *et al.*, 2021). (Yemm *et al.*, 2012) mention the use of HiL to test real electronics hardware and firmware of the Pelamis WEC, with a virtual hydraulic PTO and hydrodynamic part of the system in order to investigate partial electronic system failures. HiL has also been used to emulate behaviour that is more representative of a full scale PTO in a physical model tank tested at reduced model scale (Giorgi *et al.*, 2018). (De Falcão *et al.*, 2010) adopt a ‘mid-way’ approach, where no tank is used but the use of a pressurised U-tube enables the physical representation of inertia and hydrostatic restoring forces in a laboratory setup. Even then, the flow properties in the U-tube rig are very different to those that would be encountered with a floating WEC model in a wave tank.

HiL data is validated with fully numerical (Signorelli, Villegas and Ringwood, 2011), or fully physical models (Bracco *et al.*, 2015; Berriel *et al.*, 2021). Bracco

et al. use HiL to test a 1:8 scale PTO physical model of the ISWEC[34] (including a physical gyroscope and flywheel), while Berriel et al. do so with a 1:5 scale PTO of a heave point absorber WEC. In Signorelli et al. the physical scale is unspecified, though the PTO is large and chosen for its simplicity, to be representative of the idealised numerical model with which the HiL system is compared. Other examples include (De Falcão *et al.*, 2010), where hydrodynamic behaviour can be simulated by means of a U-tube in a laboratory environment. PTO forces are applied to one side of the tube and controlled air pressure at the other tube end emulates wave excitation and radiation damping behaviour of the WEC. This is used to test a PTO and its control system at 1:5-1:4 model scales.

In most wave energy HiL testing, the hydrodynamic wave-body interaction is the simulated component. The motivation is to avoid more expensive, complete, large-scale WEC models having to be built, as well as the cost of accessing larger facilities for the tank tests. Other potential benefits include greater flexibility in terms of cycling through different 'virtual' WEC hull geometries or physical parameters such as inertia (De Falcão *et al.*, 2010; Berriel *et al.*, 2021).

Nevertheless, HiL can only be complementary to physical model testing. Hydrodynamic data inputs for HiL emulation typically come from wave tank tests. In addition, there are development costs associated with the design, build, and operation of the HiL test-rig itself, and likely limitations in its ability to emulate hydrodynamic behaviour and interactions. These can introduce additional uncertainties (Signorelli, Villegas and Ringwood, 2011; Berriel *et al.*, 2021) and may limit the platform to being used within a particular sea state operational envelope and limited DoFs, as is the case for (Bracco *et al.*, 2015).

Signorelli et al. use HiL to compare a 'dry' test bench setup that includes a real PTO and its control subsystem, with numerically obtained results for a heaving WEC (Signorelli, Villegas and Ringwood, 2011). They find close correlation between predicted and measured WEC body displacement signals. However,

[34] Inertial Sea Wave Energy Converter, developed by Turin Polytechnic and MORELab.

errors arise due to: (a) the physical properties of the actual emulator test-rig feeding back into the simulation, causing asymmetric vertical loading that would not occur at sea due to the presence of buoyancy forces; (b) the physical PTO exhibits non-linear behaviour due to friction and valve non-linearity, which is more representative of the real life scenario but is not fully captured in the numerical model. The latter makes this test more suited to performance evaluation than validation. In (De Falcão *et al.*, 2010), the former is avoided by including hydrostatic restoring forces in the setup. In Berriel et al. the friction force due to the roller wheels at the interface between the heaving buoy body and support rails is neglected (Berriel *et al.*, 2021).

Interestingly, Bracco et al. highlight the two different 'modes' that pitching motion can be applied to the physical PTO via their dedicated test-rig. 'Feed-through' means that the applied pitching motion is directly based on a historical pitch angle time-series. On the other hand, 'HiL simulation' mode fully models the ISWEC-wave interaction numerically, so pitch angle is determined real-time. 'Feed-through' is thus used to validate the ability of the test-rig to reproduce a given time history, while 'HiL simulation mode' is used to validate the hydrodynamic model.

Assessment of HiL performance is done via numerical or physical validation, comparing time-domain kinematic signals such as displacement or velocity. These are typically based on regular wave inputs.

(Bracco *et al.*, 2015) and (Berriel *et al.*, 2021) carry out the validation based on physical model data with regular waves, while (Giorgi *et al.*, 2018) and (Signorelli, Villegas and Ringwood, 2011) use pan-chromatic seas for numerical validation. None of the aforementioned studies focus on uncertainty analysis. (Bracco *et al.*, 2015) mentions 10x repeat tests for each sea to reduce random errors. It also assesses the error with respect to fully physical tests at the same scale as the PTO. The Feed-through mode has errors <5% in all measured quantities (average power, RMS pitch angle, RMS PTO torque, RMS angle of precession). These rise to up to 10% for HiL simulation mode. (Signorelli, Villegas and Ringwood, 2011) validate based on WEC body displacement and find a close correlation between numerical and HiL signals, better at high

velocities and worse at lower velocities. Berriel et al. satisfactorily validate based on mechanical speed, while Falcao measures pressures and displacement, finding that the U-tube rig “provides a reasonably realistic way of testing the PTO system” (De Falcão *et al.*, 2010).

Contrary to the previously cited studies, Giorgi et al. (2018) implement a hydraulic PTO emulator with a controlled actuator motor to be used for tank tests in combination with a real 1:16 scale WEC hull. They elect to have a “programmable” PTO based on the controller block of the system, as opposed to “programmable” waves or WEC physical properties. This is motivated by a desire to reduce PTO design effort and because real hydraulic hardware at the reduced scale required would not give performance representative of full scale PTO. Since the emulated PTO is modelled at full-scale, physical quantities need to be scaled up from 1:16 to 1:1 to link WEC prime mover model and the PTO model. The WEC hydrodynamic behaviour is assumed to be linear but potential scaling related errors are not discussed. Only the simulated performance of the HiL system is presented by comparing optimal to delivered PTO force signals. Of the papers discussed in this section, this is the only approach that can be applied to early-stage physical model testing.

In summary, HiL can help to mitigate reliance on expensive tank testing facilities or PTOs that are difficult to model at small scale. It can help to optimise control strategies with a more representative large scale PTO relatively late in the development process when the various WEC subsystems are more clearly defined, and when hydrodynamic interactions are already relatively well understood. The latter is particularly relevant since experimental inputs are not only needed to validate HiL platforms, but also to provide accurate emulation of WEC body-wave interactions that should include complex hydrodynamic behaviour such as nonlinear flow effects that occur in reality. This underlines the complementarity of physical testing to providing good quality emulator inputs, and highlights the benefits of carrying out small-scale physical tests at early stages that include as much of the overall system behaviour as possible (ideally including PTO). If, on the other hand, numerical models are used for validation of HiL, these in turn need to have been validated with reasonably accurate physical test data. In addition, depending on the extent of the foundational

experimental work, HiL results can be exposed to scaling errors even when the real part of the system is at large or even full-scale.

Finally, a currently active industrial project focused on HiL is IMPACT[35], where a 250kW rated dual HiL testing platform is being developed with the explicit aim of accelerating wave energy development, “reducing test duration by 50% with respect to a typical endurance test” (VGA *et al.*, 2021). This expands current HiL capabilities by combining a test rig for the entire drivetrain, and another for the moorings and structural elements.

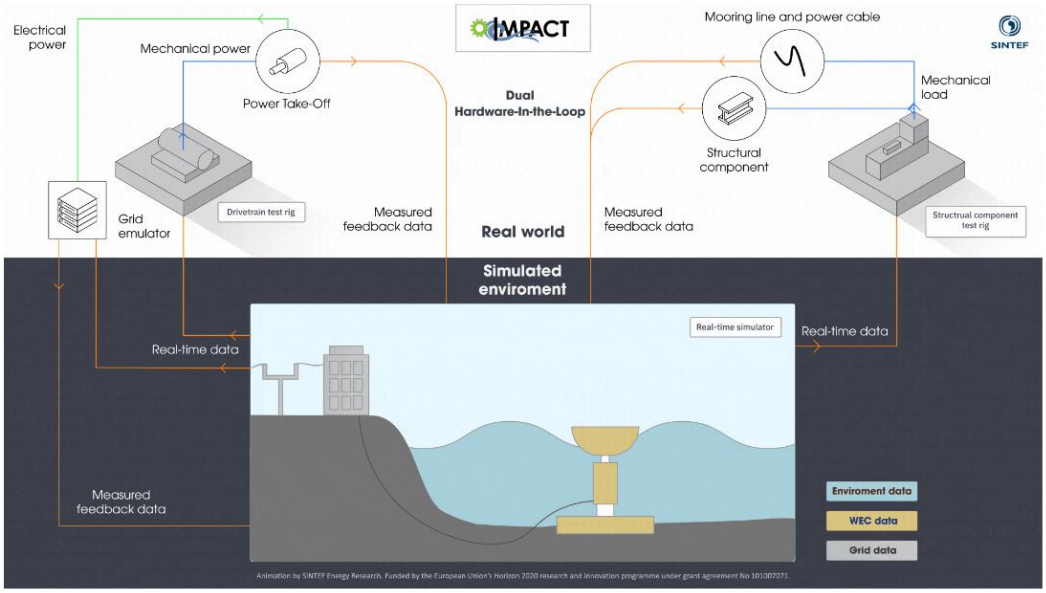

Figure 16 - IMPACT dual hardware-in-the-loop test rig diagram (VGA *et al.*, 2021).

3.4 Tank testing

In tank testing, the choice or availability of a particular wave tank informs the choice of scale – and vice versa. Often it is the former that dominates a developer decision, due to the greater expenses involved and the increased reliance on external staff. Borrowing from (DeBord Jr *et al.*, 2003), key factors for

[35] https://www.impact-h2020.eu/

the planning and execution of tank testing in the context of the America's Cup[36] include:

- Facility and scale selection
- Quality and history of test equipment
- Model construction
- Test procedures
- Data analysis techniques

These elements apply to wave energy tank testing as well. Some of the factors involved in the choice of wave tank are: depth, operational envelope, wavemaker control, staff, wave reflections, ability to produce currents as well as waves, ability to produce spread seas and associated angles, sea types, width, length, auxiliary (e.g. trimming basin), instrumentation, and costs. An example from (Martin *et al.*, 2020): "a 1:30 scale was selected to accommodate the wave tank capabilities", a very common reason for the choice.

Tanks have the unique advantage of allowing data to be collected in a controlled environment in the presence of a free surface. One "can command a calm to recover your model or zero a force sensor and then, a minute later, generate exact repeats of the wildest event of the wildest storm in a thousand years" (Salter, 2005). More modern facilities such as FloWave at the University of Edinburgh, also allow combined current and wave experimentation, as researched and characterised by (Noble, 2017), which offers dedicated recommendations for developers. This is particularly important to recreate specific loading scenarios relevant to slack moored devices, where most of the slack may be taken up by the current drift, and thus result in significant snatch loads that may not otherwise be reproduced and measured.

Since wave tanks are 3D basins with hard boundaries determined by walls, artificial beaches, or wave maker paddles, wave reflections occur and can be significant. Skyner (Skyner, 1987) points out that beaches have nonlinear absorption characteristics and that "reflection ratios are normally in the range 2%

[36] The oldest sailing competition in the world involving cutting-edge technology development. It is picked out here because, analogously to Formula1 car racing, rule changes introduced over time can restrict the use of physical modelling in the development of particular systems. This highlights its significance as a development tool.

to 20% with the lowest values available at higher frequencies and larger amplitudes." In addition, as per the "a good wave absorber is a good emitter" paradigm (Yemm *et al.*, 2012; Alves, 2016), wavemaker absorption improves when these are also generating waves: reflection ratios of 10% to 20% are typical (Skyner, 1987). However, smaller waves such as those generated by the physical model as it moves, tend to be less well absorbed, partly due to stiction in the wavemaker motors. These waves tend to be at high frequency but the tank's wavemakers are effective absorber where they are effective emitters, which is around a central region – around 1 Hz for the Curved Tank.

The evolution of wave tanks at the University of Edinburgh – a narrow flume tank, a wide tank, a quarter-circle Curved Tank, and a fully circular combined wave-current facility at Flowave – are fairly representative of the global picture. A crucial and recurring question is how to make best use of tank time, and this largely depends on the testing goals being pursued. In the case of comparing different configurations of a device, a streamlining test method is outlined in Section 3.4.2.

It is rare for a developer to have access to their own tank. If there is confidence that sufficiently accurate insights can be obtained at smaller scales, this can open up further possibilities in terms of the type of tests that can be performed for a given tank capability (i.e. operational envelope). The following section summarises available literature on the UoE Curved Tank, which was utilised in this EngD research.

3.4.1 The Curved Tank

The University of Edinburgh Curved Tank is given particular focus as it is the wave tank utilised in this EngD research - an example of working backwards based on available facilities. The Curved Tank was not heavily utilised and easy to operate. In fact, it risked being shut down during the course of the present research. A letter of support written to put forward a positive case for the tank is appended in Appendix A.

The pre-cursor to UoE's Curved Tank was the so called Wide Tank, built in 1977 (Taylor, Rea and Rogers, 2003) and later demolished in 2001. The Curved Tank that replaced it has been utilised in several studies and campaigns. It has a

curved section of 48 force-controlled wave makers, a glass side-wall, and an artificial beach composed of wedge-shaped steel mesh cages. The beach is built such that the front section has an impedance that matches higher and shorter waves to reduce reflections. The density of the mesh increases as you move back and down, which helps to reduce reflections of less steep waves. These are encouraged to bounce back between adjacent wedges (Taylor, Rea and Rogers, 2003). The glass wall is useful in allowing the operator to observe underwater behaviour, but introduces “long period transverse standing waves between the window and any other reflecting walls of the tank”, which are known as ‘seiche’ waves (Taylor, Rea and Rogers, 2003).

(Cruz, Pascal and Taylor, 2006) characterised the wave profile of the tank in 2006, pointing out that 14% of its perimeter is reflective. They used two sets of wave gauge arrays composed of 7 wave gauges made of two stainless steel rods with relative conductivity inversely proportional to the immersed depth. Their findings suggest that wave gauge calibration in the tank should be undertaken daily, since the wave gauge gain varied by 2.4% over the week of experiments. The study also identified the top left corner of the mapped area shown in Figure 17 as optimal, based on root-mean-square (RMS) and standard deviation (std) values of wave height.

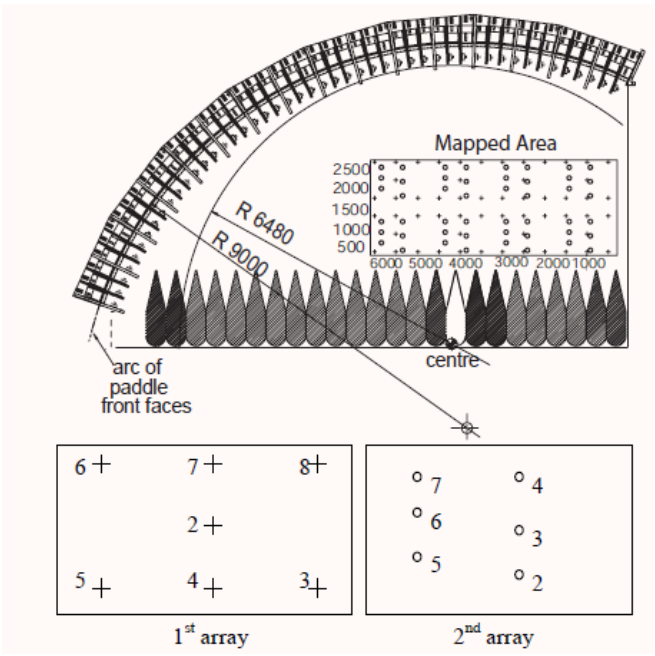

Figure 17 - Scheme of the curved wave tank and position of the gauges during measurements (Cruz, Pascal and Taylor, 2006).

(Lucas *et al.*, 2008) used the Curved Tank to test a 1:33 scale model of the Edinburgh Duck WEC. They carried out a reflection analysis using the (Mansard and Funke, 1980) method with three wave gauges, using wave amplitudes between 5mm and 10mm. Their findings were than incident wave amplitudes varied strongly with frequency, and more so at lower frequencies.

Finally, (Pascal *et al.*, 2009) built on previously discussed studies to investigate reflection coefficients in irregular waves and multi directional seas. Their results suggest that for irregular (i.e. polychromatic) waves, amplitude does not affect reflection coefficient, while for regular waves the coefficient decreases as steepness (and thus amplitude, given 1Hz fixed frequency) increases. A nominal +/-1% reflection coefficient error due to probe positioning is accounted for in all the presented results. These include a reflection coefficient less than 7.5% at amplitudes >20mm and steepness 0.02. The reflection coefficient doubles to 15% at a steepness of 0.005.

In addition, polychromatic waves (with components in range 0.7 to 1.4Hz) have reflection coefficients below 10%, which is deemed satisfactory, and "compares favourably with previous studies". In general, concordance is found between mono and polychromatic reflection coefficients, and low spatial variability in the tank.

In terms of multi directional seas, the tank is found to achieve a sub degree level of precision in the +/-20deg demand range.

The main recommendations offered by the authors are (Pascal *et al.*, 2009):

- Use of a minimum amplitude of 7mm for 1Hz waves in regular tests (below this the reflection coefficient is above 8%)
- Multi directional seas should be carried out in the +/-20deg range; above this dispersion and reflection do affect the waves, degrading tank performance

3.4.2 Reducing tank time

When testing physical models, there is a clear necessity to limit material expenditure, but perhaps even more so, to limit the time needed for testing. Since tank time is expensive, test plans tend to be very time constrained,

running limited numbers of sea states, as shown in Appendix C. Recently, Pascal et al. (Pascal *et al.*, 2021) have proposed a method, referred to as *Ir0*, whereby different configurations of a device can be explored more efficiently compared to traditional methods.

A device is typically characterised with regular waves, and then a few configurations are selected for irregular wave tests. However, behaviour under regular and irregular conditions might differ, and the resolution of irregular wave runs may not be sufficient to capture sufficient detail in the device's response characteristics or the optimal configuration. The authors therefore propose to characterise a device by obtaining the RAOs from irregular waves directly. In short, the method proposes to obtain a finer resolution in terms of wave period without increasing testing time.

In the paper, an early concept of the 'Seaturns' WEC is tested at 1:30 Froude scale. The numerous configurations arise from altering PTO damping, mooring, geometry, trim, water volume, and others; 52 configurations in total. The device is moored with a semi-taut system and has a PTO represented by an orifice that can be manually adjusted and is driven by a pressure differential.

The Ir0 method is as follows. A polychromatic sea composed of 25 components of a specific frequency and amplitude is assembled. The repeat period[37] is 256s. Each component has an integer number of repeats and a random phase. The selection of amplitudes is ad hoc, and depends on the overall spectral characteristics that are being represented. For example, an H_s-T_e combination more or less at the centre of the modelled site scatter diagram can be selected. The amplitudes are then selected as either 5mm or 7.5mm (tank scale) such that the sum of relevant spectral moments is as close to the H_s = 2.1m and T_e = 10.0s (full scale), i.e. the central point of the wave occurrence diagram. Higher amplitudes – resulting in better signal-to-noise ratios - are assigned to components around the middle of the frequency bandwidth, as these are deemed more important for the overall device performance.

[37] Repeat period is defined as the length of the time series command given to the wave tank, which typically contains a discrete number of wave cycles for the chosen wave frequencies.

The time for each Ir0 run comprising 25 frequency components is 11 minutes, including a repeat. This in comparison to 1 hour for 16 regular wave components without repeats.

There are further advantages to this approach over other test methods.

- Typical irregular wave tests might not provide enough energy over the full range of desired periods, and improving the spectral resolution means that longer runs are needed (i.e. increasing repeat period to reduce the delta frequency (df) interval)
- White / pink noise tests require additional tests compared to a typical test plan (i.e. they cannot replace irregular wave tests), and the energy in each frequency component needs to be kept low in order for the overall Hs to remain reasonable.

The method yields a satisfactory match of regular and Ir0 obtained RAOs of surge, pitch, normalised pressure, and normalised CWR, even in the presence of the nonlinear PTO. For mooring load RAOs, again the overall match between regular waves and Ir0 is satisfactory and closer for horizontal than vertical mooring lines. Compared to a relatively energetic irregular wave sea, where the effect of non-linearities should be relatively significant, Ir0 plots have a better match compared to regular RAOs, as well as giving broader frequency coverage. The results suggest that Ir0 sea captures the underlying nonlinearities of the system more than a regular wave characterisation. The Ir0 responses are between high-energy irregular and low-energy irregular obtained responses.

This method would not be suitable if the objective was to identify the best PTO control setting for each period. On the other hand, if, like in the case of Mocean's WEC, the control strategy is based on a single linear PTO damping setting across operational sea states, this method can be used to the developer's advantage. In terms of deriving a power matrix, if the assumption is one of pure linearity (mooring, hydrodynamics, PTO) and a constant PTO damping across all seas, then an estimate of the power matrix can be derived from the CWR curve, by multiplying the CWR value and associated spectrum in each occurrence matrix cell. However, it is likely that discrepancies would arise for sea states with a period and energy content away from the utilised Ir0 seas.

The Ir0 method is implemented and extended in Chapter 8. Another approach to reduce tank time is to pursue hybrid testing, as outlined in Section 3.3.2.

As seen in (DeBord Jr *et al.*, 2003), tank testing typically consumes a significant portion of the overall project resources. However, “effort expended on tank testing can be minimised if it is properly integrated into the overall design program”. One such way is to carefully consider scales used, as explored in the next section.

3.5 Scaling

The theory behind scaling – and in particular Froude similarity – is outlined in Chapter 4. A clear theoretical summary can be found in (Sheng, Alcorn and Lewis, 2014) and further in (Sheng, 2019). This section focuses on scaling implications found in relevant industry guidance and standards, and other academic studies. In particular, literature is reviewed with respect to the prospect of identifying appropriate scales, and quantifying scaling errors.

Choosing an appropriate model scale is not straightforward. As part of MaRINET2, different scales for different testing purposes are recommended. For power capture evaluation, a minimum scale 1:10-1:20 is recommended, for operating conditions tests, 1:30. For survival testing, the larger the scale the better “because extreme waves cause significant viscous forces which are greater at smaller scale” (Thiébaut, Sutton and Johnstone, 2015). For PTO testing, scales of 1:4.5 to 1:10 are recommended.

The latest IEC protocols indicate the following with respect to scaling (IEC TS 62600-103, 2018): “Stage 2: validate technical conclusions drawn from previous test programme (assumed to be at smaller scale) and identify potential scaling issues between the two stages”. However, no guidance is offered on how to identify (or quantify) such scaling issues. In fact, the standard recommends using the largest feasible scale for the available facilities to reduce the influence of potential scaling effects.

The 2021 issued IEA-OES Framework provides a helpful summary of scaling considerations, shown in Figure 18.

In the US DoE Wave Energy Prize, all models tested in the final assessment phase were at 1:20 scale during the final testing and evaluation stage of the competition (Driscoll *et al.*, 2018). These models were used for comparative purposes but also for absolute assessment, since the aim of the competition was to double the performance of WECs compared to current state of the art.

- **Maximising**
  - Learning
  - Risk reduction
  - Confidence building
  - Experience generation
  - Where appropriate, revenue generation
- **While minimising**
  - Safety risk
  - Cost
  - Technical risk

The scale or size must be appropriate to the parameters and characteristics being investigated and measured, but first, the importance of scale vs. size must be clearly defined:

- Scale – ratio of the model size to commercial-scale size
- Size – the physical dimensions of the device

Scale considerations:

- "What constitutes commercial-scale?" - a technology development trajectory could reasonably target numerous product sizes to address different markets
- The ability to scale the impact of natural parameters such as water density
- The impact of functional parameters that scale differently to the main functional charateristics of a device e.g. air pressure and material properties

Size considerations:

- The ability to integrate or otherwise represent a functional subsystem in a particular scale or size of device e.g. the size of a PTO and the size or force-generation capability of a model or actuator used to mimic such a PTO
- The ability to demonstrate an operation or process in a manner representative of commercial-scale e.g. installation or maintenance actions
- The ability of the particular technology to be built or function at smaller size
- The accuracy of extrapolating test results from a small scale to commercial scale
- The availability of appropriate sensing methods and instrumentation equipment to measure the parameter of interest with required accuracy

Considerations affecting both scale and size:

- For tank testing:
  - the water depth of the facility
  - the wave and current generation capability
- In the case of open-water deployment,
  - the ability to find a site with water depth and wave conditions which are comparable, at scale, to the selected commercial-scale including the expectation for extreme waves at the site during deployment

Figure 18 - Size and scaling guidelines from 2021 IEA-OES Framework (Hodges *et al.*, 2021).

Few experimental studies exist estimating effects of scaling between geometrically identical physical models in equivalent sea states. This is often incidental rather than part of a study, which makes cross-comparisons difficult or impossible as the WEC design and/or test conditions have typically evolved. Nevertheless, some studies do shed some light on this, usually supporting the feasibility of scaling down.

The “Edinburgh Duck” development work carried out at the University of Edinburgh is likely one of the most relevant to estimating hydrodynamic scaling effects with the same model at different scales. From (Salter, 2016):

> *"There were always anxieties about whether results from small models at around 1:100 scale could apply to full scale but the leading experts assured us that we just clear of the scale where surface tension becomes a significant restoring force and insects can walk on water. We did hire a 1:10 scale tank for a week. The results were within 2% of our narrow tank ones but while you could lift a 1:100 scale model with one hand and make it in a day, dropping a 1:10 scale model could easily kill somebody. The 1:10 scale tank took twenty minutes instead of forty seconds to settle. Everything was far slower and more expensive but, for shapes like those of most wave devices, no more accurate."*

In a previous publication, Salter (Salter, 2005) states that "Froude scaling rules work very well for wave effects on things with the shapes of typical wave devices even for things as nonlinear as breakwaters" (Pearson *et al.*, 2002). Another reassuring observation comes from one of the – arguably – most successful WEC devices in terms of size and commercialisation promise, Pelamis. Physical modelling was carried during the development process with models ranging from 1:80 to 1:7 scale in five different tank test basins (Yemm *et al.*, 2012) – no significant scaling issues are reported.

It is also important to note – as will be revisited in Chapter 4 – that some parameters do not Froude scale, e.g. friction and viscous damping, and thus may be overestimated for smaller models (Noble *et al.*, 2018). The relationship of scale to drag requires careful attention. Viscous effects can be separated in scale dependent and independent components (Palm *et al.*, 2018):

- **Scale dependent** - Viscous drag, dominated by Reynolds (Re) number, which does not scale according to Froude laws. There are typically included in parameterised form (e.g. Morison equation) and require calibration of drag coefficients.
- **Scale independent** - Other drag types such as form drag (e.g. around bilge keel of ships) and induced drag from geometrically induced vortices, e.g. around sharp corners.

Few detailed experimental scaling comparison found by author in literature search. However, some numerically based studies exist, often based on computational fluid dynamics (CFD). Such studies try to assess hydrodynamic scaling; a few focus on OWC type WECs and include (Dai *et al.*, 2019) and (Palm *et al.*, 2018). The latter numerically analyses nonlinear forces on a point

absorber WEC in resonance at 1:1 and 1:16 scale, by running three different CFD models that differently account for drag effects. It quantifies the Re dominated effects of viscosity, and finds that drag damping is responsible for a severe reduction in RAO at resonance when the wave steepness increases. It recommends to separate total drag into scale-independent and viscous (scale-dependent) terms, as well as accompanying experimental tests with RANS[38] simulations to quantify scale-dependent nonlinear effects (Palm *et al.*, 2018).

The study finds that a doubling of wave steepness causes an overall reduction in device response, of which:

- 3% drop is due to nonlinear mooring response and Froude-Krylov force (see Appendix D)
- 1-4% is due to viscous forces
- 18-19% is due to induced drag and nonlinear added mass and radiation forces, which “differ significantly depending on geometry, mooring design, and PTO complexity”.

As a result, it recommends carrying out Euler[39] and RANS based CFD to accompany experimental model tests, in order to separate viscous drag influence from induced drag. This is because Euler simulations are shown to be scale independent, so can be used to quantify uncertainties due to viscosity and scale. The difference between Euler and RANS results provides an upper bound on scale dependent effects at the particular tested scale; a smaller scale will have a greater upper bound.

(Stansby, Carpiteno Moreno and Stallard, 2015) perform an experimental investigation with a 1:8 and 1:40 Froude scale model of flat-bottomed floats. Although they use two different tanks, the RANS based CFD shows “small nut noticeable” difference in numerically obtained drag coefficients. Coefficients slightly decrease as physical size increases, and increase as amplitude of decay

[38] Reynolds-Averaged Navier Stokes; a numerical method that models turbulent flow with viscosity taken into account.

[39] Based on inviscid flow assumption.

motion increases - i.e. drag coefficients increase as the ratio of model size to motion amplitude decreases (i.e. as small motion linearity assumption breaks down). In (Schmitt and Elsäßer, 2017), CFD computations are validated with experimental tests with and without a mesh fixed to the wave facing side of the WEC flap to force turbulent flow transitions. Experiments in monochromatic waves “showed no measurable difference for test runs with and without the attached mesh”, though the limited flow around the flap sides limits confidence in this conclusion.

Another relevant study is (Giorgi and Ringwood, 2017), which gives recommendations based on studying a floating heaving point absorber. It points out the inconsistencies in Morison drag coefficient values for WECs found in literature, and the lack of consensus on which estimation technique may be best. If uncertain, the recommendation is to use a larger rather than smaller drag coefficient value, due to a lesser impact on errors. "The ideal drag identification test would be able to replicate the full complexity of the flow around the device, and concurrently isolate viscous forces." However, defining a single representative and comprehensive drag coefficient is very difficult; there is large variability of results due to the wide range of relative velocities for a surface piercing WEC excited by waves.

Aside from drag complications, the downscaling of PTOs is particularly challenging, as explored in Section 3.3.1. (Liu *et al.*, 2019) find that "the model size of the impulse turbine could not be reduced to match the optimal damping ratio obtained from the previous studies” due to manufacturing complexities, which then limited the comparison of the results with previous studies. Such practical limitations are not uncommon and typically ‘force’ developers towards larger scale models.

Finally, structural design is possibly the most difficult aspect to scale. It requires a detail of scaling above and beyond what is traditionally included via Froude, where the geometry is made to match, mass properties can be made to match full-scale as closely as possible (and are usually matched relatively closely), but structural properties are difficult to replicate exactly (e.g. stiffness, strength, other material properties). This is typically not a significant issue, because for

validation purposes the numerical model can be ‘retrofitted’ with ‘as-tested’ physical model properties, and structural loading is typically excluded from the validation and performance variables. Eventually, structural loads will be required to estimate fatigue life and different load limit states, when a shift to an ‘as-built’ prototype will be required to estimate full-scale machine structural responses.

It is worth remembering that, ultimately, the validation and performance that really matters is that at full-scale. Thus, any scaling errors should be ideally related to a full-scale data set; the extrapolation from, say, 1:10 to 1:20 does not necessarily represent that from 1:10 to 1:1. What augments this issue is that, much like the offshore wind sector, wave energy too suffers from few publicly available full scale data sets being available (Otter *et al.*, 2021). One such full-scale experimental data set (O’Boyle *et al.*, 2015) is touched upon in the next section.

3.6 Uncertainties

As well as specifying QOIs and metrics, the assessment (ideally via quantitative measurement) of experimental uncertainty should be undertaken. This is an important complementary step to appraise reduced scale testing methodologies (as well as numerical models) and to move forward with confidence in the development process.

Uncertainty bounds can be determined because the metrics of interest will themselves fall within a range, due to inevitable systematic and bias errors. In order to assign uncertainty to a response metric, the combination of random and systematic uncertainties should be known (Robertson *et al.*, 2018). Indeed, the success of a validation campaign depends on experimental metrics matching numerical metrics with sufficiently small uncertainty – though it is also possible that a bad physical model would be very closely matched by a bad numerical model. In general, the smaller the QOI in terms of the measured quantities, the greater the need to assess uncertainty because errors may prevent conclusions from being made (Lamont-Kane, Folley and Whittaker, 2013).

“Due to the mathematical assumptions and simplifications applied during numerical model development, uncertainty will exist in predictions made” (Lamont-Kane, Folley and Whittaker, 2013). Physical models typically provide a benchmark for validation, but there may be errors in the PMT itself, where measured values may not be the true values of QOI. One should ideally benchmark physical models against themselves, for example by testing more than one scale in the same testing campaign. However, little guidance for this exists in standards.

Uncertainties can be categorised in three types:

- Model – uncertainty in the way the model behaves
- Instrumentation – uncertainty in the measurements themselves
- Tank – uncertainty in tank performance and whether the demanded seas match those generated by the tank

Errors are inherent characteristics of experimental systems, and their sources are typically considered as:

- Random – typically accounted for statistically (e.g. mean and std)
- Systematic – typically accounted for by calibration

Measurement errors can also be amplified, as found in (Shahroozi, Göteman and Engström, 2021). Here friction computation requires a two-time derivation of displacement to calculate acceleration. “Therefore, the noise level and accuracy of the position sensor together with the low-pass filter applied on the data introduce some uncertainty […] the precise quantification of this uncertainty is rather difficult as it depends on both filter characteristics and measurement errors”.

(Wilkinson *et al.*, 2017) do carry out a partial uncertainty analysis and discussion of main systematic and random errors in PMT of a modular flap type WEC model:

- Torque sensor calibration slopes [systematic]
- Rotation sensor calibration accuracy (largest) [systematic]
- Model orientation [systematic]
- Variation of wave conditions and model behaviour [random]

The dominant source was identified as the second due to the way the various flap modules of the WEC model were calibrated. This affects mean absolute angular velocities by +8% to -7%, which are then used to evaluate power absorption. Other sources are mentioned as having magnitudes below 1%.

There are relatively few examples of “thorough uncertainty analyses of hydrodynamic tests and/or extrapolation to full-scale” (Day *et al.*, 2015). This is likely, at least in part, because few WECs have reached full-scale testing stages, and developers are often not inclined to share their data. It is also a huge task for relatively small developers to undertake given the vast amounts of data collected from even a few days in open sea.

A notable exception is (O’Boyle *et al.*, 2015), based on the Aquamarine Oyster WEC. In the study, the authors correlate prototype-model in terms of hydrodynamic power capture and flap dynamics, though it is unclear what subset of prototype, numerical, or experimental data is being compared, simply stating that “the numerical and experimental simulations that have achieved an RMS damping torque most similar to that estimated from the prototype are selected for comparison”. The authors also undertake an uncertainty analysis, where different parameter contributions are examined in isolation via sensitivity studies to assess the impact on hydrodynamic power. As in (Wilkinson *et al.*, 2017), calibration uncertainty has a significant contribution, as does the surface elevation measurement (see Figure 19).

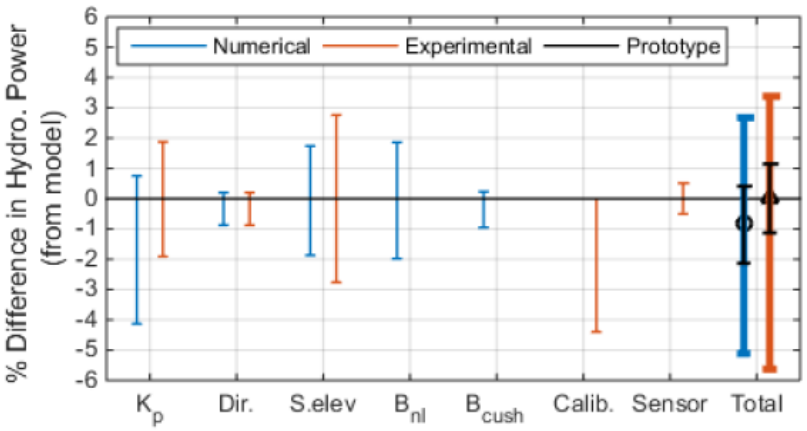

Figure 19 - Contributions of individual sources of uncertainty in numerical (blue) and experimental (orange) models relative to the model predication of hydrodynamic power for the case study sea state. The black data points indicate the difference in the prototype hydrodynamic power from the numerical and experimental predictions with associated uncertainties (O’Boyle *et al.*, 2015).

In Figure 19, K_p denotes pitch stiffness, *Dir.* is the incident wave direction, *S.elev* is the measured water surface elevation, B_{nl} is the nonlinear damping coefficient (numerical only), B_{cush} is the damping coefficient (numerical only), *Calib.* is the uncertainty from the calibration (experiment only), *Sensor* is the uncertainty of the sensors used (experimental only). However, it is important to recall that uncertainty is not invariant, but is both environmental conditions (e.g. sea state) dependent and device state dependent. This is one of the motivations for which uncertainty analysis is omitted from many tank testing campaigns, and also why Figure 19 only paints a partial picture.

No major innovations or updates have arisen since 2015, to the best knowledge of the authors, and uncertainty analysis of WECs remains relatively nebulous. The 28th ITTC Specialist Committee met in 2017 and produced updated guidelines for a WEC uncertainty analysis process (ITTC, 2017). However, little evidence exists of its uptake thus far.

The IEC adopted a more pragmatic approach to uncertainty quantification. It offers reference figures about what is an ‘acceptable level’ of uncertainty at each development stage. It provides aims but no steer to quantifying it in practice. A pragmatic 1-2-5-10% thresholds approach is offered.

Another effort that does not ‘compete’ with the ITTC has been via the MaRINET2 program. This also points to the significant of hydrodynamic and scaling errors in determining overall test campaigns uncertainty and thus validation outcomes. In a ‘round-robin’ test programme using the exact same physical model in different facilities, considering sources of variance from experimental setup, instrumentation, and post processing methodology. It found that model repeatability is good and most of the uncertainty is from tank calibration (and thus wave repeatability) differences across facilities (Davey *et al.*, 2021). Indeed, “differences in the wave conditions generated at different facilities can have a profound impact on the results” (Noble *et al.*, 2021).

Measurement uncertainty is low and the model seems to respond in the same way, such that if the waves have good repeatability, then overall response repeatability will also be satisfactory. Thus, assuming waves are calibrated, and measurement equipment is appropriately selected, this work points to the need

to focus on more fundamental hydrodynamic uncertainties to do with the model itself and its scaling, which is not covered in the MaRINET2 work.

The other notable inconsistencies arise from different post-processing practices at different facilities. For example, the choice of analysis intervals, which is determined by the different length of tests and the different reflection characteristics of each tank basin, can vary. “Existing guidance does not provide clarity on how the analysis interval should be selected” or “how waves should be calibrated so that target wave heights are achieved during the selected interval” (Noble *et al.*, 2021). Analysis methodology is also affected by different length of intervals, as may not be able to do fast Fourier Transform (FFT) analysis if the sampling interval is too short.

A recent OES benchmarking study refers to papers (Wendt *et al.*, 2019) and (Kramer *et al.*, 2021) in assessing scaling uncertainties. The objective is to examine different numerical models and compare them to highly rigorous experimental tests involving the free decay responses of a sphere dropped in still water from different heights. It points to a requirement for careful uncertainty analysis yielding 90% confidence intervals when validating.

An older IEA-OES work (Nielsen, 2003) recommends that accuracy of test conditions should exceed 5% for both H_s and T_z / T_p, while the uncertainty in spreading parameter (s) should be greater than 10% within the interval for wave periods from $0.5T_p$ to $1.25T_p$.

(Day *et al.*, 2015) discusses some of the specific challenges in the analysis of uncertainty of output power for marine renewable energy (MRE) devices, and their relevance when extrapolating to full-scale behaviour. "Whilst standard procedures specifically addressing MRE devices have not yet been developed, some aspects of uncertainty analysis for hydrodynamic tests of MRE devices may be inferred from existing ITTC procedures":

- Motions of floating WECs can be assessed by adapting approach found in ITTC Recommended Procedure *7.5-02-07-02.1 Seakeeping Experiments;*
- Measurements of flow around devices can be assessed *7.5-01-03-03 Uncertainty Analysis: Particle Imaging Velocimetry (PIV).*

(Lamont-Kane, Folley and Whittaker, 2013) defines ‘sufficient quality’ as the QOI changes compared to some baseline being greater order of magnitude compared to the uncertainty effects on that baseline. However, this is not discussed in standards. Results in (Lamont-Kane, Folley and Whittaker, 2013) point out that a 8-10% uncertainty in power capture estimation can drop to 2-3% if multiple tests are performed.

The paper considers and assesses five sources of experimental uncertainty:

- spatial variation within the wave basin
- temporal variation of wave-field between repeats
- repeatability of model response(s) with single WEC
- reproducibility of model response(s) with nominally identical WECs
- variation in time-series of an incident irregular wave train

It is challenging to obtain a homogeneous wave field in a closed basin due to reflections, spreading, and imperfect wave generation – this is more of an issue for array testing compared to testing at a single point. A set of draft protocols is presented for small-scale PMT, among which (Lamont-Kane, Folley and Whittaker, 2013):

- Use numerical model to estimate QOI sensitivity to relevant parameter uncertainties/variability;
- Consider most appropriate quantities for data presentation and numerical model validation;
- Complete uncertainty analysis for model and tank, including: wave-field spatial variability, wave-field temporal variability, model repeatability, model reproducibility, wave component phase relationship on model response;
- Design model, instrumentation and data acquisition (DAQ) so that uncertainties from model repeatability and reproducibility are acceptable;
- Employ repeat testing especially around resonance, and in very small and very large sea states.

Wave blockage effects can also be sources of error, though blockage is more relevant with larger models in narrower tanks. Its impact when testing arrays can

be accounted for by numerically simulating a row of mirror WECs to the side of the model WEC, where the tank walls effectively act as mirror planes, as found in (Ersdal and Moe, 2013). Finally, (Robertson *et al.*, 2018) emphasise the importance of the process of understanding where “design tool capabilities break down”. Before quantifying uncertainties, it recommends assessing this from the planning stages, pointing to commonly occurring uncertainties of both test and modelling types.

To conclude, uncertainty quantification is a challenging area in wave energy. Uncertainties are categorised as pertaining to the model, instrumentation, and the tank testing facility. Of these, tank errors are typically the largest source of precision uncertainty (i.e. repeatability), highlighting the need for careful calibration of seas in advance of model testing, as shown by the round-robin MaRINET 2 program. On the other hand, model uncertainty is a significant contributor to accuracy unknowns (i.e. how close to the true value), and is often the most challenging source to quantify and isolate. In the case of physical model testing, the ‘true value’ is that of the full-scale device in the real sea.

Uncertainty analysis is challenging to apply and rarely found in literature studies, not least because tank time is so precious and finite, so that this is not prioritised in typical test campaigns. A particular challenge is the dependency of uncertainty on the variation with environmental conditions. Another is the dependency on the scale of the physical model – i.e. scaling errors arising from the use of relatively small-sized physical WEC representations. Standards and targets outline uncertainty thresholds and targets but little practical advice on assessing these. Thus, it is key for developers to consider major uncertainty sources in advance, follow what guidance exists (e.g. repeat testing, particularly around resonance, as well as small and large seas; and tank pre-calibration), and consider using more than one physical model at different scales to help disinterring scaling related errors.

3.7 Another ‘trilemma’

Just as the classic – and now somewhat out-dated – energy trilemma, where a balance between affordability, security, and sustainability of energy needs to be found; for physical model, the tension is brought about by the competing

elements of cost, representation, and accuracy. The optical illusion of the Penrose Triangle – an impossible triangular object – is used to illustrate these.

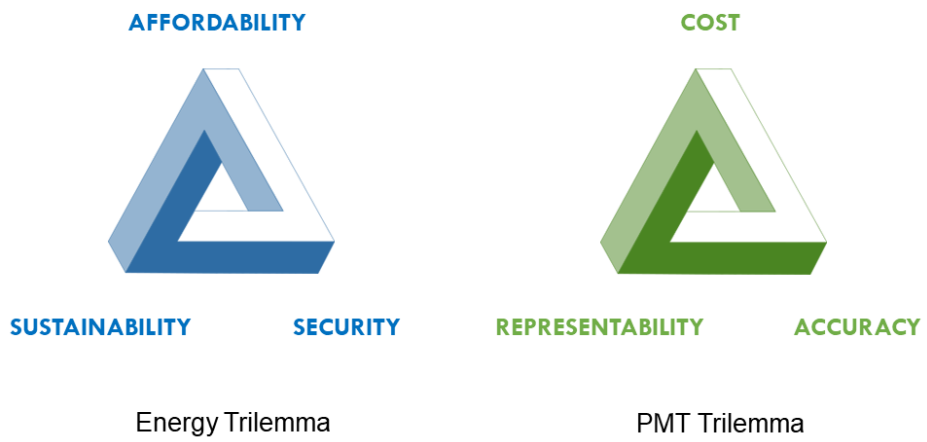

Figure 20 - The Energy Trilemma (left) and the analogous 'Physical Model Testing (PMT) Trilemma' (right).

The fundamental challenge lies in simultaneously addressing simplicity (reduce costs and maximise ease of manufacture, assembly, handling and testing), representability (including the most important aspects of the problem – i.e. the manifestation of insights), and accuracy (in order to minimise or at least measure uncertainty).

Drawing directly from (DeBord Jr *et al.*, 2003):

> *"When selecting a scale ratio, the specific objectives of the test program must be considered along with the increased viscous effects and the requirements for better absolute precision as model size decreased […] These factors should be weighed against the increase cost and time required for larger models."*

Traditionally, the complexity (and scale) of a physical model increases as the various subsystems forming the overall device crystallise – i.e. as TRL increases (see Section 3.2). This is accompanied by increasing predictive accuracy of – and confidence in – the obtained results. However, in practice, the evolution process is not linear; a development pathway is not a one-way street. Iteration and feedback are key because numerical models, physical models, product specifications, user-needs, and available subsystems technology (e.g. PTO), among other factors, are not static. On the contrary, they too typically evolve and

consolidate over time. The practicalities of what can be built evolve (e.g. the type of generator and associated max torque thresholds per PTO size), and thus the 'ideal machine' evolves accordingly, depending on manufacturing capability and technology innovation of a particular subsystem.

For Mocean, the above is especially true due to the following:

- Target markets are new and not yet well explored – requirements crystallise as commercial relationships are formed and develop. Many design inputs (e.g. minimum continuous power requirements, autonomous underwater vehicle (AUV) interfacing) will be more *ad hoc* compared to a grid connected WEC. [See Chapter 2, Section 2.3]
- Avoidance of premature freezing of the WEC design. This enables accommodation of different subsystems as their relevant technology develops (e.g. novel moorings (EMEC, 2020) and novel PTO (University of Edinburgh, 2018)), effectively embracing a *performance ahead of readiness* approach. [See Chapter 2, Section 2.1.1]
- Mocean's in-house optimisation routine rapidly generates new prime mover geometries based on input requirements and constraints (Cameron McNatt and Retzler, 2019). The underlying model is linear, so nonlinearities must be captured via physical testing. [See Chapters 4-5]
- Proximity to tank testing facilities – relatively available and economic in the case of Edinburgh University's Curved Tank (CT) (see Section 3.4.1) – makes physical model testing a more readily deployable design tool. [See Section 3.4, and Chapters 6, 8]

Hence, fast-turnaround and small-scale are attractive characteristics for Mocean's physical modelling strategy. Overall turnaround can be accelerated by including more subsystems at earlier development stages. At the same time, shrinking the physical models in scale allows cost reduction and maximisation of available testing facilities. In a sense, this mirrors the *Wave Energy Paradox* transformation, where the levers of markets and of scale are used to unlock more learning, more quickly (see Chapter 5). However, associated risks such as exposure to undesired scaling effects and similitude inconsistencies should be considered (Section 3.5).

Part II:
Frameworks & Approach

This part provides the necessary theoretical and practical approaches, applied to Mocean Energy's development context, to precede the physical model testing campaigns carried out in Part III. Chapter 4 lays out the fundamental features and theory underpinning Mocean's numerical model, focusing in particular on the numerical optimisation routine that leads to specific WEC geometries and performance predictions. The scaling theory utilised to move between laboratory to at-sea deployment, as well as different laboratory scales, is also outlined. Lessons learned from previous testing campaigns run by Mocean are extracted. Chapter 5, on the other hand, links commercial to experimental aspects of WEC development. It does so by proposing and formalising a new framework, which also identifies useful levers for supporting deployment and commercialisation pathways of WECs. Its implications in terms of physical model testing are then implemented in Part III.

"Every fresh idea for a way of doing this [WEC development] presents its own daunting new list of design variables. Somehow or other these have to be brought to some sort of collective optimisation before considering the risks of going to full-scale prototype." (Taylor, Rea and Rogers, 2003)

- J. R. M. Taylor, M. Rea, D. J. Rogers, 2003

"Levelised cost of energy needs to reduce but it will not happen without deployment"

- Kate Johannesen, 2019

Chapter 4. Underpinnings of WEC development

This chapter outlines the fundamental features and theory behind Mocean's numerical model and unique optimisation routine – i.e. linear wave theory. It also describes the fundamental theory behind reduced scale physical testing – in this case, Froude scaling. These are relevant since the numerical model leads to specific WEC geometries, with associated behaviour and performance characteristics that – to greater or lesser extents – require physical validation. Following the theoretical underpinnings, notable geometry evolutions are presented. Finally, physical modelling campaigns carried out by Mocean that preceded the present work are reviewed in terms of outputs and lessons learned. The idea is to provide a guide for the physical modelling activities that are core to the present thesis.

4.1 Theoretical underpinnings

"Optimisation requires a choice or combination of modelling techniques – analytic, numerical, physical" (Taylor, Rea and Rogers, 2003). This section provides a top-level summary of linear wave theory and of scaling regimes, focusing on Froude scaling. It primarily aims to draw out fundamental theories, assumptions and constraints that apply to Mocean's numerical model and the physical modelling undertaken in this research project.

4.1.1 Hydrodynamics of ocean waves

While often considered wildly novel and pioneering, the hydrodynamic theory underlying WEC development partly builds on previous studies on ship dynamics – e.g. (Newman, 1979) – that occurred prior to the onset of dedicated wave energy studies. Floating WECs, however, differ from ships in that, while their structure must station-keep[40] (i.e. remain more or less stationary if

[40] No autonomously wandering, un-moored, WEC has been developed at the time of writing. However, wave-powered drones exist (such as the WaveGlider) that convert wave motion into energy for their own propulsion. Clues pointing to unmoored WEC attempts are beginning to emerge.

anchored to the seabed), their hydrodynamic sensitivity to waves is encouraged to promote power-converting motions. The theory is further complicated by the influences of PTOs (Falcao, 2009).

In order to model a body's *response* to waves, one must understand and somehow represent the nature of waves themselves, to which the body is exposed. A brief outline of some fundamental wave features and characterising parameters follows in the next section. A comprehensive source for the theoretical hydrodynamics of wave energy is (Falnes, 2002). More recent reference texts include (Cruz, 2008), (Matt Folley, 2016), and (Pecher and Kofoed, 2017). Most theory illustrated in the next section will be based on particular chapters from (Matt Folley, 2016).

4.1.2 Linear wave theory

Though linear wave theory is extensively used in the sector, the real sea is actually not linear. However, linear theory helps to get an initial indication of device hydrodynamics with significantly reduced complexity, which in many cases is 'good enough' – at least as an initial starting point or approximation. As stated in one of the key references for modelling WECs, "The hydrodynamic interaction between wave energy converters (WECs) and ocean waves is a complex high-order nonlinear process that, under particular conditions, can be simplified" (Alves, 2016).

When assuming linearity (subject to assumptions discussed later), "all the physical quantities vary sinusoidally in time with the same frequency of the incident wave" (Alves, 2016). Reactive loads from moorings and the PTO are also assumed to follow simplified linear relationships. It is important to note that linearity assumptions apply to both hydrodynamics *and* responses; i.e. both to the waves and to the way the 'captor' behaves in response to them.

The most common framework used to apply linear wave theory is the frequency domain (FD). Other domains such as spectral and time domains are briefly discussed in Appendix D. The advantages of FD models include (Alves, 2016):

- Relatively fast calculation of response(s) and power capture;
- Easy inclusion of multiple degrees of freedom (DoFs)

- Relatively easy to production of hydrodynamic coefficients via boundary element methods (BEM), such as WAMIT (see more in section 4.2).

Among the many relationships that emerge from the linear theory framework, of particular note is the fundamental revelation from the Kramers-Kronig – there is "a relationship between the body's ability to radiate waves and the frequency dependence of the inertia increase due to the water displaced by the body motion" (Alves, 2016). This essentially means that a WEC's ability to absorb waves is inherently correlated to its ability to radiate waves – i.e. *a perfect absorber is a perfect emitter*. This can be counter-intuitive but a crucial consideration for maximising power capture. A detailed mindmap showing the relationships, assumptions, and derivations of fundamental FD model elements, including the Kramers-Kronig relation, is shown in Appendix D. Another fundamental principle is that "under the linearity assumption it is possible to describe the resultant wave field around a WEC or any other floating body as a superposition of an incident, a diffracted and a radiated wave field." (Alves, 2016). These wave field elements are also disinterred in Appendix D.

A few final notes are offered here. Firstly, waves transmit energy via the orbital motion of water particles, which are assumed to remain local relative to the travelling wave. However, water particles are also subject to drift, which is not typically captured in numerical models. In addition, wave pressure decays with increasing depth, such that the wave's presence is less 'felt' the further away from the free surface (illustrated in Figure 21).

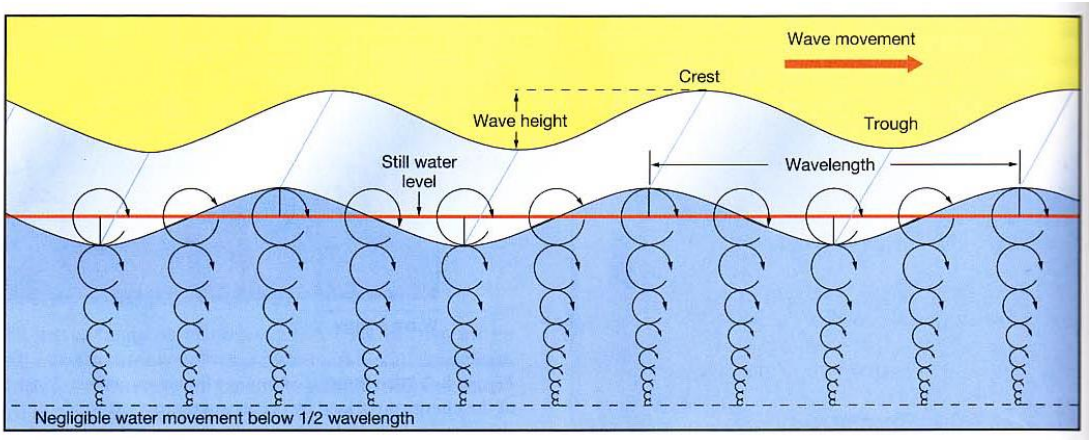

Figure 21 - Showing orbital motion of particles in water waves and basic definitions. Source: (Thurman, 1993).

4.1.2.1 Potential flow theory

Potential flow theory deserves a mention, being a foundational theory to FD modelling and beyond.

It is based on three assumptions:

- Inviscid (i.e. frictionless) flow
    - Viscous forces are the only forces that can dissipate energy in the fluid. For example, waves can be radiated away but the energy still exists within them.
    - Only normal stresses are experienced.
    - If the Reynolds number is high enough, viscous forces are relatively insignificant (Alves, 2016), so the assumption of inviscid flow is valid.
- Irrotational flow
    - Fluid elements or particles do not rotate relative to their own centre of gravity, albeit they have orbital motion trajectories
    - If a flow starts as irrotational, and is inviscid, it remains irrotational.
- Small amplitude waves and body motions – infinitesimal waves and responses (idealised system)
    - This goes with the inviscid flow assumption because under the influence of large or extreme waves, viscous effects increase and body motions are likely to become more nonlinear, potentially invalidating potential flow theory (Alves, 2016).

Under the above three conditions, the Laplace equation can be obtained:

$$\nabla^2 \varphi = 0$$

where φ is the velocity potential.

The additional boundary condition of limited water depth the leads to the dispersion relation:

$$\frac{\omega^2}{g} = k\ tanh(kh)$$

The above equations are cardinal pillars of potential flow theory applied to wave energy, and are shown in the mind-map in Appendix D.

4.1.2.2. Reality checks

Several aspects can be pointed out regarding how waves in practice differ from their idealised descriptions. It should be underlined that real world waves are non-deterministic in nature, and as such require statistical representation. This is typically approximated via different types or shapes of spectra, as will be visited later in the chapter.

In addition, there is nonlinearity to contend with. In practice, nonlinearity arises due to the relative displacement and the relative velocity between the WEC and the water (Giorgi and Ringwood, 2017), particularly when large motions occur. Nonlinearity fundamentally refers to effects that are not representable by the superposition of sinusoids, which prevents the decomposition of complex solutions into simpler linearly superimposed components (as per Appendix D).

This aspect is typically that which most affects predictions from FD models (such as WAMIT) mismatching with observed behaviour. For example, the non-perfectly sinusoidal shape as waves get steeper, and the shape of the water surface as it interacts with the device (particularly at the wave channel or around sharp corners or relatively narrow slits where jets and losses can form more easily when water moves through them – see Figure 22). Surface elevation effects such as breaking are another example of a nonlinear phenomenon, and water level heights predicted by WAMIT are sometimes not physically obtainable. This effect can be seen by observing the shape of the water surface elevation as it interacts with the model, including at the wave channel. Nevertheless, WAMIT is generally considered as giving satisfactory accuracy with relatively low computational effort (Alves, 2016), and is revisited in Section 4.2.

Figure 22 – Wave breaking at the forward wave channel for Blue X WEC at Scapa Flow (© Colin Keldie).

In short, "linear formulations in both the time domain and frequency domain allow much more rapid computation than nonlinear models; this is very useful for design scoping studies, but with loss of detail and accuracy in large waves." (Yemm *et al.*, 2012)

4.1.2.3 Wave definitions

For the purposes of this thesis, three wave definitions are outlined: regular, irregular long-crested, and irregular short-crested. These are increasingly complex and representative of wave conditions encountered at sea. All have an important role in modelling wave conditions in a lab environment.

Regular waves are the simplest waves to specify, having a constant period and height. Irregular waves are more complex, though still idealised as they are based on approximated or assumed spectral distributions compared to real sea conditions. A spectral distribution is shown in left side of Figure 23, while a series of regular waves superimposing together to form an irregular wave are shown on the right of the same figure. Note that once an irregular profile is obtained, this can be extended in the third dimension to obtain a long-crested irregular – i.e. one that does not vary along the wave crests (akin to the right hand side of Figure 24).

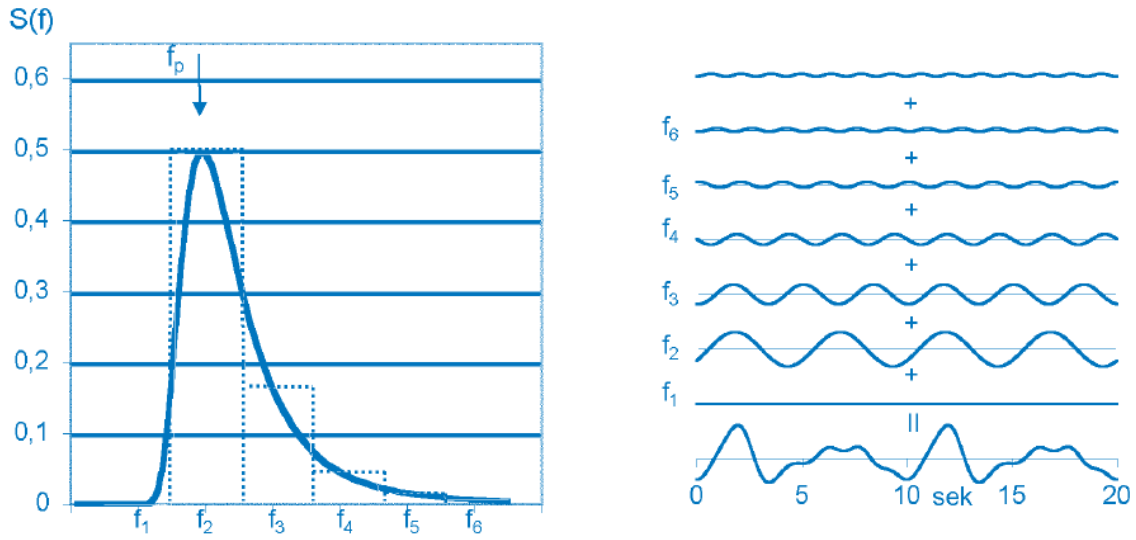

Figure 23 - Irregular wave spectrum and composition (Nielsen, 2003).

On the other hand, Figure 24 (left) shows a short-crested sea, one that is subject to directional spreading, and where the wave crests are scattered. A parameter (s), known as spreading factor, typically describes the extent of spreading. As well as directional spreading, waves can have varying dominant direction of propagation at a given location, where their direction is not singular but may vary between particular +/- angle ranges. In this case, the wave 'fronts' or 'crests' shown as straight vertical lines in Figure 24 (right) would actually be inclined at +/- angle relative to the horizontal direction of travel. Other 'types' of waves exist, such as focused waves, but are beyond the scope of this thesis.

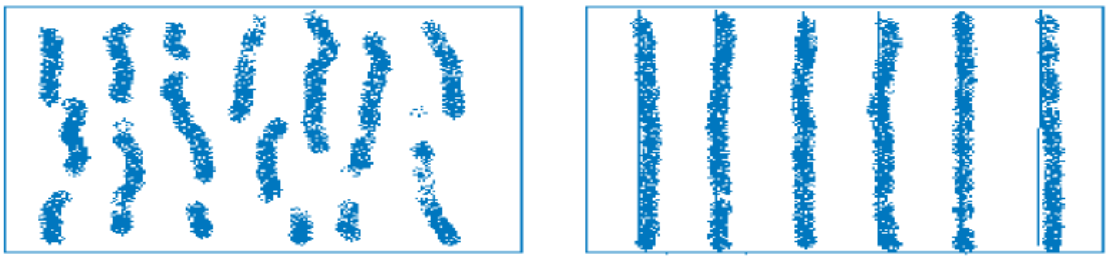

Figure 24 - Directional spreading (Nielsen, 2003).

In addition, it is common for seas to be multi-modal – i.e. composed of both shorter crested waves (from local winds) and longer crested waves (from longer fetch swells). However, when modelled, seas are typically represented by single types of spectra that cannot capture the full extent and complexity of multi-modal sea states. This too introduces uncertainty in WEC evaluation (see Section 3.6).

4.1.3 Links to Mocean's numerical model

As will be visited in Section 4.2, Mocean's optimisation was initially based on FD fully linear models and then on spectral-domain (SD) quasi-nonlinear models going into this thesis's scope of work. More recently, a time-domain (TD) multi-objective optimisation has been set up, but is not discussed here as outside the scope of the present work. Before describing the main features of the optimisation, a few more theoretical aspects should be mentioned.

There are three fundamental force components: hydrodynamic excitation force, hydrodynamic radiation force, viscous damping force. There are also three damping contributions: radiation damping, PTO damping, and viscous damping. The optimal PTO damping coefficient can be found as that which maximises the average power absorbed. The typical way of including viscous drag effects in WEC mathematical models is via a Morison-like term based on the Morison equation (Morison, Johnson and Schaaf, 1950). Additional notes on drag modelling, associated coefficients, and relevance to physical testing is given in Appendix D.

4.1.3.1 Power absorption

Wave energy conversion involves a chain of conversion processes. The first is the interaction between a WEC's hydrodynamically 'active' structure (i.e. the 'prime mover' or 'captor') with the incident waves, whereby the structure 'absorbs' some of the incident wave energy, and passes it on to the next conversion stage(s). Each conversion stage has its own associated efficiency.

- Hydrodynamic to mechanical
    - As well as the prime mover, this also involves the moorings and the PTO, since these affect prime mover motion
- Mechanical to electrical
    - Via PTO damping
- Electrical AC to electrical DC
    - Via power modulation

Going back to the idea of a perfect absorber being a perfect emitter, as stated in (Yemm *et al.*, 2012),"wave energy absorbers can be thought of as wave-makers, with their motion-radiations waves". The paper also illustrates how a WEC can absorb more energy than is contained within its frontal width, because it actually

interacts with the entire 3D wave field around it, not just with the wave crest and orbitals travelling directly in-line with the WEC. Two important definitions are given:

- *Capture width* is used to denote the width of oncoming wave that contains the same power as that absorbed by the WEC
- *Capture width ratio* (non-dimensional) is the capture width normalised by the WEC's characteristic dimension (typically the length of the dimension that faces oncoming waves)

In the mechanical-to-electrical conversion, "the amount of absorbed wave energy can be significantly increased by adequately controlling the PTO in order to achieve near-resonance" (Falcao, 2009). There are wide ranging methods to achieve optimal control. In broad terms, strategies can be resistive, where the PTO strategically breaks or resists the mechanical motion, or reactive, where some power is strategically injected back into the system to stimulate further motion in order to obtain overall greater power out. This is not discussed further, except to say that Mocean's control strategy up to and including the present work has been a linear resistive strategy, using a constant PTO damping coefficient across seas. Aside from the attraction of its simplicity, this is enabled by the already excellent tuning provided by the optimised geometry that gives broad bandwidth and high conversion efficiency. The mean power absorbed by the WEC is essentially the mean power consumed by the mechanical damper as part of the PTO. Over a wave period, the average contribution to absorbed power from the mechanical spring component is null.

The concept of *added mass* is an important part of Mocean's WEC performance, primarily caused by the wave channels. Since added mass is frequency dependent, this means one can have more natural frequencies than the DoFs, with the potential to expand and increase the response bandwidth. Added mass "accounts for the fact that when accelerating a water particle from rest, the surrounding fluid is also accelerated, and so it corresponds to an additional inertial effect due to the water displaced in the body vicinity when the body moves" (Alves, 2016). It is made up by a frequency-depended component and

an infinite component (as frequency tends to infinity, i.e. when no waves are radiated by the captor).

Mocean's WEC has 6 DoFs for the connected hulls, with an additional DoF for relative pitch (i.e. flex). Flex is the constrained motion of the two hull bodies at the hinge. Considering less than these can be justified if motions in the ignored modes do not (significantly) influence the captor's power capture response.

4.1.4 Scaling

It is worth recollecting that the governing equations used to study the interaction of waves and WEC that describe the flow field are:

- The continuity equation for conservation of mass
- The Navier-Stokes (N-S) equations for conservation of momentum

Ideally, a reduced scale model would be tested in a lab environment, maintaining geometric, kinematic, and dynamic similarities with the full-scale prototype. However, geometric similarity (i.e. proportionality of dimensions) alone is not sufficient to guarantee kinematic (proportionality of motions, i.e. velocity vectors) and dynamic similarities (i.e. proportionality of force[41] and moment vectors at corresponding locations) as well (Sheng, 2019). To satisfy the latter two, certain conditions must be met. These are embodied in two dimensionless numbers, Froude and Reynolds, defined as follows:

- Froude number: $Fr = {U}/{\sqrt{gL}}$
- Reynolds number: $Re = {\rho L U}/{\mu}$

where U is the characteristic velocity, L is the characteristic length, ρ is the fluid density, g is the gravitational constant, and μ is the fluid dynamic viscosity.

Fr can be regarded as describing the ratio of hydrodynamic to gravitational (or inertial) forces, while Re the ratio of hydrodynamic to drag forces. "Identical dynamic equations for the two geometrically similar systems can only be attainable if their Froude and Reynolds numbers are the same" (Sheng, 2019).

[41] Fluid flow pressure and the PTO are typically the major sources of force in the context of WECs.

However, there are conflicting requirements on L and U parameters. To keep Fr constant, U needs to decrease as L decreases; to keep Re constant, U needs to increase U as L decreases. Thus, either the viscosity of the fluid or the gravitational constant would have to change in order for both Froude and Reynolds similarity to be achieved at model scale, meaning that these conditions are fundamentally incompatible.

Therefore, in practice, larger models tend to be used to ensure a large enough Re number, such that the viscous force in the N-S equations, which is proportional to 1/Re, can be neglected. If this is the case, kinematic and dynamic similarities can be guaranteed by Froude similarity alone. A smaller model (lower L and thus lower Re number) is more likely to see a flow regime that is more laminar and less turbulent, which affects the proportionality of inertial to viscous forces in favour of viscous. The key is for Re to be above the critical threshold for laminar flow, and this is largely dependent on the problem of interest. For example, Fitzgerald and Bergdahl (Fitzgerald and Bergdahl, 2009) assume 10^5 as the threshold for Re. This is also model and application specific because, as pointed out in (Sheng, 2019), a WEC does not have a ‘prescribed travelling velocity’ (unless perhaps one is conducting a towing test), so it is difficult to define a U value to represent overall responses.

Viscous effects are smaller, outright, at smaller scales, but are much larger proportionally to the inertial forces, hence a low Re but a higher 1/Re (laminar) contribution in the N-S equations. On the other hand, at larger scales, inertial effects dominate, which are the cause of turbulence and vortex shedding. (Palm *et al.*, 2018) contains a helpful breakdown and description of different drag forces and their sensitivity to scale. For WECs, identification of drag is challenging because of: device dimensions, characteristic flow regimes, large motions, and presence of free surface (two fluid phases – water and air – and a non-constant wetted surface, radiation and diffraction forces) - see (Giorgi and Ringwood, 2017). The resulting flow regime is more complex than that described by Re alone.

4.1.4.1 Froude similarity

Physical modelling using Froude scaling has been widely accepted, as a "relatively large Re number in the scale model can be easily achieved in most cases" (Sheng, 2019). As further stated by Salter: "when a very small scale model is used, the worries may be those coming from the interaction of the cables and some other issues, such as instrumentations, balance of the model, etc., rather than the selection of the relevant similarity laws" (Salter, 2003).

A Froude scaling coefficient, *s*, can be defined as the ratio of prototype to model dimensions. For example, if the physical model is ten times smaller than the full-scale prototype, *s* would take a value of 10. Table 5 provides useful references for Froude scaling of different quantities in terms of *s*.

Quantity	**Scaling**
Wave height and length	s
Wave period	$s^{0.5}$
Wave frequency	$s^{-0.5}$
Power density	$s^{2.5}$
Linear displacement	s
Angular displacement	1
Linear velocity	$s^{0.5}$
Angular velocity	$s^{-0.5}$
Linear acceleration	1
Angular acceleration	s^{-1}
Mass	s^{3}
Force	s^{3}
Torque	s^{4}
Power	$s^{3.5}$
Linear stiffness	s^{2}
Angular stiffness	s^{4}
Linear damping	$s^{2.5}$
Angular damping	$s^{4.5}$

Table 5 - Froude scaling factors summary table, adapted from (McMaster, 2014).

It should be noted that Annual Energy Production (AEP) scales as power, even though it has units of energy, because it is the average power generated by a device multiplied by the number of hours in a year.

Froude number is proportional to U/L. According to Froude scaling, a WEC gets larger proportionately to volume, but also gets exposed to longer faster moving waves, and vice versa; this relationship favours laboratory test conditions.

One can also be reassured by relevant reflections found in (Salter, 2003):

> *"Froude scaling rules for force, velocity, acceleration and power work very well down to the point where surface tension takes over from gravity as the restoring force allowing insects to walk on the water surface. Gravity and surface tension become equal at a wave length of 17mm, four orders of magnitude down on a full scale ocean […] At scales down to 150, the only worries are the cross forces on cables, the steady drag forces from currents and the relatively higher viscous forces which will reduce measured efficiency by a few percent […] Scaling rules for forces work well over this range even for objects as non-linear as breakwaters in shallow water* (Pearson *et al.*, 2002; Salter, 2003)*."*

Finally, it is noted that as far as the FD numerical model is concerned, so long as the WEC and the wave conditions are scaled consistently, its linear underpinnings mean that the same hydrodynamic results will be produced. One reason for complementing the optimisation loop with PMT is that, theoretically, the Morison drag coefficient (viscous drag) should be tuned for each geometry revision. The same Morison coefficient as per previous Mocean testing campaigns is being assumed going into the present thesis.

4.2 Geometry optimisation

Mocean has developed an in-house numerical tool known as *Blue Insight* to aid the simulation, optimisation, and design of WECs. It comprises four elements, each based on a particular software package:

1. Geometry creation – via *Rhinoceros*
2. Hydrodynamics - *WAMIT*
3. Non-linear forces – *Simulink & Matlab*
4. Post-processing - *Matlab*

The output metric from the post-processing element is used to assess performance and has varied over time. Whatever metric or series of metrics are selected, they are then assembled as part of a fitness function or fitness score, which represents the ‘desirability’ or ‘attractiveness’ of that particular geometry (see Figure 25). The fitness function is optimised via an algorithm. This can have a single objective or multiple objectives. Two different metaheuristic[42] techniques - genetic algorithms and particle swarm algorithms - have been used in this step. A particle swarm type algorithm is shown in the lower box of Figure 25.

Mocean’s numerical routine uses object-oriented programming, which is suited to complex and actively updated programmes. As well as creating geometries, it can evaluate both wave and PTO forces, and it can calculate power capture. Both of these are coupled to the optimisation routine.

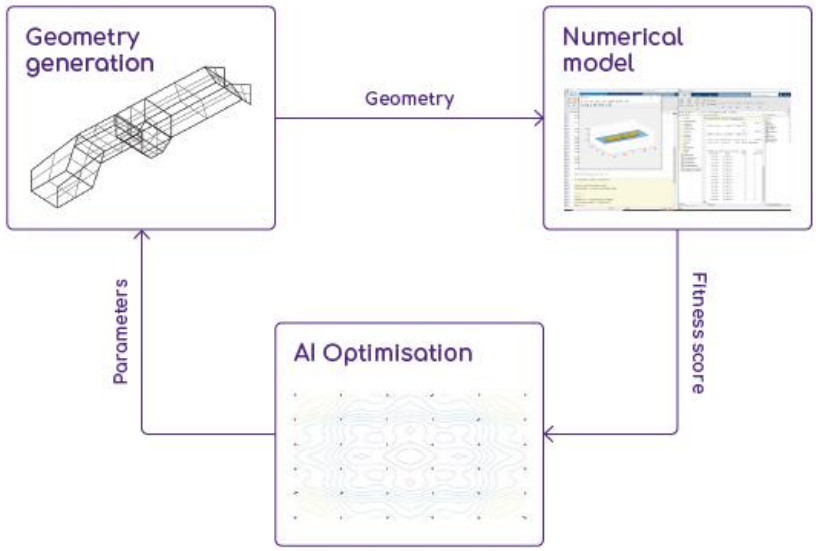

Figure 25 - A flow diagram representation of Blue Insight blocks.

[42] Metaheuristic refers to mathematical optimisation strategies that are used to explore a design space in order to find near-optimal solutions. No guarantee is given on a globally optimal solution being found, but these are suitable approaches to optimisation problems faced with incomplete information and/or limited computation capacities.

Initially, a rough programmatical realisation was constructed, which then evolved over time. Blue Insight code is more or less constantly evolving to improve its efficiency and expand its capabilities.

Once a geometry is determined, further refinements are manually implemented using CAD software. Engineering considerations are also made once an optimised geometry is yielded. These may go back as optimisation constraints (to the 'parameters') applied to the routine itself as part of an iterating process. For example, steel plate panel thickness of the hulls or wave channels may be altered, or perhaps PTO torque limits, or overall dimensional envelopes. New parameters may be introduced, or previously varied parameters may become fixed due to learning accumulation – e.g. manufacturing considerations.

4.2.1 Guiding the optimisation

Key features and constraints of the WEC can be specified at the optimisation's onset. Aside from geometrical constraints tied to coding capabilities in reproducing particular WEC prime mover shapes, these features might be engineering and/or O&M informed. Up to 30 parameters are used to define a geometry, typically – but not exclusively – assigned as a min-max range (see Appendix D). For example, an overall dimensional constraint such that the WEC fits into a standard shipping container; or a set panel thickness to withstand typical hull loads; or a minimum nacelle diameter needed to house a particular size of PTO generator based on best known velocity-torque profiles. Or again, one may want to set an overall draft limit to satisfy minimum depth requirements in the harbours where the machine may be wet commissioned or towed to/from; or a forward hull length limit to limit excessive wave channel loading or higher torques. At least some of these parameters remain fluid throughout a given development project, while others crystallise on their way to becoming 'frozen', such as by the end of a Front-End-Engineering-Design (FEED) phase.

With each variable continually distributed in a constrained range, there is a potentially infinite number of combinations. Even 20 variables that can each move 10 ways result in an impressive 200,000 combinations. For such an optimization problem, metaheuristic techniques, such as the particle swarm and genetic algorithm, are used. *These methods are derivative free so require no*

prior knowledge of the mathematical structure of a function. This is important since Mocean's in-house numerical model comprises several layers.

Sensitivity studies can be carried out but require progressively more time as the number of parameters increases and as the code becomes of higher fidelity and more complex, particularly once the optimisation moves into the time-domain, as has been more recently implemented – though outside of this particular research effort. The wave resource occurrence matrix is a major input driving the optimisation.

4.2.1.1 Fitness function

At the time of this research and associated testing, 'performance' was optimised via a fitness function defined as AEP/cost, where cost was represented by a combination of mass and torque (see more details in Appendix D). The original assumption with Blue Star was that we could just optimise for AEP without having to consider power delivered and battery size. Continuous available power (CAP) was not taken into account in the optimisation, but computed post optimisation. Among other reasons, this is because performance is optimised based on 24 synthetic wave climates to speed up the computation; this would not yield accurate CAP which required TD computation.

A few more optimisation considerations are outlined here. In selecting appropriate candidates, each hull is individually trimmed first – if that fails, then it is trimmed together so that one hull may support the other in mass and/or buoyancy. Independent trimming is desirable such that no moments are applied at the hinge when the WEC is at equilibrium. Other aspects are analysed post optimisation, such as roll stability and other engineering/structural/reliability considerations, and power production at different locations to that optimised for (the WEC is optimised based on a single location, i.e. occurrence matrix).

For the Blue Star geometry revisions presented in later chapters, 17 parameters (open variables) were used as inputs, though up to 30 can be used to describe the WEC if the variables currently held constant are included. The torque limit, for example, is set as a fixed threshold. More recently, the optimisation was switched to multi-objective, yielding what is known as a 'Pareto front' of possible solutions (as shown in Figure 26). In this manner, one can pick the optimal

solution/geometry based on post-processed characteristics that are not driving the optimisation itself, but that determine whether one geometry is more attractive than the other – e.g. roll responses.

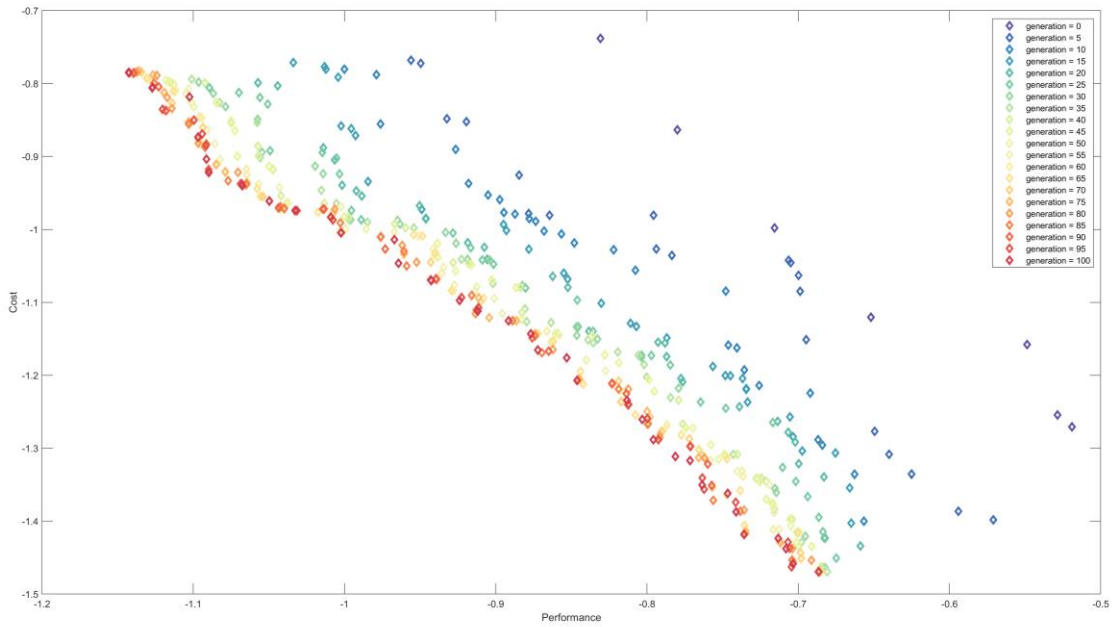

Figure 26 - Pareto front showing optimal solutions for different geometry generations distributed across cost (vertical) and performance (horizontal) axes.

4.2.1.2 Numerical representation of PTO

There are two PTO parameters in the numerical model used for optimisation: torque limit and PTO damping. This means that the PTO is relatively easily 'representable' physically, even with just a motor acting as a break. One should be able to adjust current limit for torque limit, and gain for damping value. In this sense, the numerical and physical models would be 'equivalent' and the physical model is not a radical simplification of the numerical model. It should therefore lend itself to validation purposes.

The optimisation yields a discrete power matrix for the resulting geometry, which combined with the input occurrence matrix, produces an energy matrix whose elements sum to AEP.

4.3 Progress to date

In the spirit of learning, the following questions are addressed in this section. What can be learnt from previous physical model testing campaigns?

Additionally, what can be deduced from particular geometry versions that have fed into, or arisen out of, these campaigns? This is the scope of the present section, to be used as a launching pad to inform and support the physical modelling pursued in the Part III.

4.3.1 Geometry evolution

Figure 27 shows the development of Blue X (M100P) through each geometry evolution corresponding to a particular stage of the NWEC programme run by WES. A distinction between geometry revisions and evolutions is found in Chapter 9.

Name	Approx. Size	Description	Image
NWEC Application	500 kW 1,900 te 95 m LOA	Version submitted with our NWEC1 application.	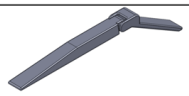
NWEC1	200 kW 720 te 80 m LOA	Version developed by the end of the NWEC1 project.	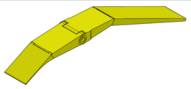
M100A	100 kW 220 te 37 m LOA	Version developed by NWEC2 M05.	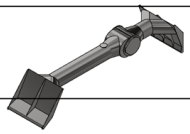
M100B	100 kW 270 te 36 m LOA	Further refinement of M100A. Full-scale version of the M100P.	
M100P **(the Prototype)**	10 kW 34 te 19 m LOA	M100 that is designed and built in the NWEC3 project. It is a half-scale version of the M100B. However, the M100B is actually based on scaling up the M100P.	

Figure 27 - Evolutions of the WEC developed via the NWEC programme.

The overall design process is iterative. It is important to note that numerical modelling of each geometry occurs sequentially, but physical testing activities can occur in parallel to it.

Numerically, each revision is generated over a period of time as a result of design insights, engineering considerations, and the set-up of the numerical code itself. The code is regularly refined, expanded, or updated. In essence, the numerical optimisation never stops – as the model is almost continuously refined and updated to include the latest learning, in order to extract as much value as possible heading towards the next project or development phase. Thus, in order to carry out testing of physical models to complement numerical results, one cannot always wait until the geometry has been ‘frozen’ at the end of the project. Theoretically, the numerical model can be made infinitely complex; there are

always numerical improvements that can be implemented. On the other hand, the physical modelling itself requires time and effectively represents a WEC 'frozen' in time, during which the numerical model can 'run on' and be further progressed. This can lead to a sense that the physical models are always lagging behind and 'chasing' the latest numerical simulations. Streamlining physical modelling would thus be beneficial.

4.3.2 Review of prior physical testing campaigns

Broadly speaking, the adopted process of physical testing can be summarised as follows:

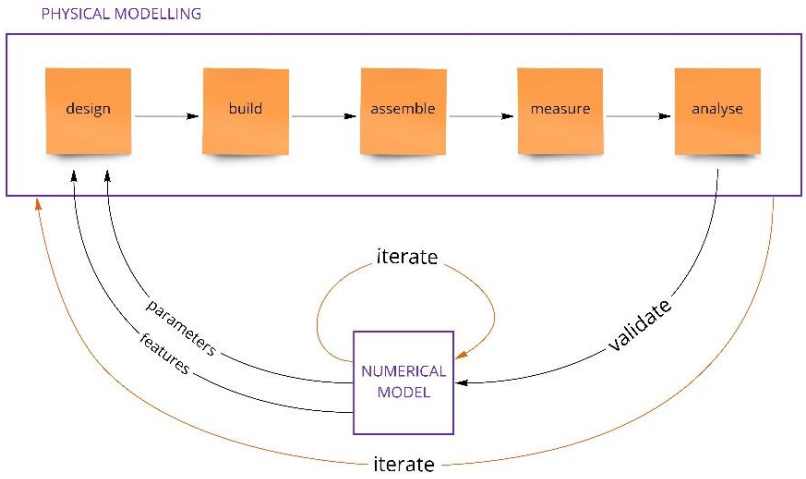

Figure 28 - Elements of physical model testing and their numerical modelling interfaces.

A physical model is designed on the basis of a numerically optimised geometry. It is then built, assembled, and deployed in a wave tank for testing. Measurements of its behaviour under controlled conditions are obtained, analysed, and subsequently used to check – and ideally to validate – the numerical simulations by results comparison of appropriate results data. Physical testing plays a particularly important role in capturing nonlinear (hydrodynamic and other) effects, as well as boosting confidence in the iterative development process. It can also be helpful to use physical models to advance a developer's understanding of aspects related to operations and handling of the WEC – e.g. towing behaviour and towing speed limits – that are typically trickier to model numerically.

Typically, Mocean has tended to use two numerical model set-ups for each test campaign. An as-designed model, and an updated as-built physical model to enable like-for-like validation and comparison.

Table 6 summarises the most practical aspects of the build of each model.

Campaign	Dimensions	Mass (kg)	Froude scale	Hinge	Gearbox	Cables	Tank
NWEC1	Length: 1.85-1.90m* Width: 0.30mm Draft: various*	28.1-36.9*	1:50	Active	Yes	Yes - 3	Curved Tank
“	Length: 3.86m Width: 50mm Draft: 0.9m (WC)	85.9 (dry) 121.9 (wet)	1:20	Active	Yes	Yes - 2	FloWave
NWEC2	Length: 0.95-1.23m Width: 0.189m (hinge and channels) Draft: 58mm (hull)	7.3	1:53***	Active	Yes	Yes - 3	Curved Tank
“	Length: 0.93m Width: 100mm (hinge); 225mm (WCs) Draft: 50mm (hull)**	3.7	1:40	Passive	No	No	FloWave
“	Length: 1.85m Width: 450mm (WCs); 200mm (hinge); Draft: 106mm (hull)**	32.6	1:20	Active	No	Yes - 3	FloWave

Table 6 - Summary of physical models tested ahead of 2019.

NOTES:

- *multiple models were tested with slight dimensional variations
- ** all hull draft values are ‘as-tested’ values, measured from the mean water line as opposed to the hinge axis
- *** does not match other NWEC2 scales as the underlying design geometry changed since the start of this development phase

Table 6 shows that model geometries and masses change, and dimensions don't quite add up (other than in the 1/20 and 1/40 NWEC2 models). This goes back to the fact that the background numerical model was evolving throughout the period of these tests.

The rest of this section is arranged according to previous programme development phases. These include stages 1-2 of the WES Novel WEC (NWEC) programme. Later phases include one funded by a Scottish-Enterprise (SE) SMART grant, and another by MaRINET2 run by the COAST Lab at Plymouth University focusing on mooring behaviour in survival seas. NWEC3 and Blue Star's Front End Engineering Design (FEED) funded by InnovateUK projects are also not covered here as these occurred during the course of the thesis, not before – info was therefore not available at the time of devising thesis work and methodology. Some of the associated results are relevant though and will be touched on in Chapter 9. The rest are presented chronologically in Appendix D. Only the main or major points from NWEC1 and NWEC2 are presented, so these sections should not be treated as exhaustive of all activities performed or learnings achieved. The reason why these Blue X learnings apply to Blue Star is two-fold: (a) the underlying technology and principles of hydrodynamic performance is the same despite more detailed geometry changes; (b) the underlying numerical model is also common, albeit constantly evolving.

Lessons broadly fall into four model-related categories:

1. *build* (relating to physical model design and operation);
2. *validation* (relating physical to numerical model predictions and tuning);
3. *performance* (characteristics of WEC behaviour);
4. *uncertainty* (confidence in measured WC behaviour).

4.3.3 Gaps and pointers

Major takeaways in each learning category are presented here. These read like a series of instructions or recommendations, with supporting bullet points. Additional supporting material for each can be found in Appendix D.

4.3.3.1 Build

Aim to avoid the use of a gearbox, which has introduced high levels of measurement uncertainty and hindered validation.

- It is preferable to sacrifice the (nominal)[43] achievement of the exact torque limit and PTO damping required, particularly if the primary aim is validation as opposed to performance.

Minimise the number of separate components in the powertrain, not dissimilarly to full-scale testing considerations to maximise reliability.

- Tends to reduce windup, compliance, and friction
- Best to have an encoder included in the motor, ideally incorporated in the controller set up also (all in one), or to use a Qualisys optical system instead of a separate encoder.
    - If so, beware of Qualisys effects on inertia and dynamics, particularly for relatively small models.
- In NWEC1 20th scale tests, although the motor and gearbox were selected on the basis of having sufficient nominal torque and damping available, the reflected motor inertia coupled with the shaft compliance affected the frequency response measured, ultimately causing less bandwidth, less gain, and less damping.

The use of a torque sensor is recommended but not essential.

- A trade-off exists between minimising powertrain components and the ability to measure the torque applied by the overall hinge, as opposed to just the motor itself, thus isolating the frictional component.

Wherever possible, the model ought to be sized based on active hinge spatial and torque constraints.

- E.g. NWEC1: without the constraint of having fixed the scale at 1:20, it would have been preferable to make a physical model of the PTO, check

[43] Have observed from certain campaigns that issues with backlash, powertrain windup, and/or shaft compliance mean that nominal values may not be achieved anyway.

what control performance could be achieved, and then use this information to select an appropriate scale.

- A Mocean report states: “The scale would have likely been smaller, reducing time and cost of the build and allowing higher PTO damping (relative to full-scale).”

Bear in mind the need to reduce time and expenditure, which can limit test scope and data quality.

- NWEC1 20th scale: needed more time to investigate effects of non-linearities and mitigation of energy losses (e.g. repeat runs with sidewalls added at slopes such as for smaller scale tests), but cost of FloWave was a major constraint.
- Avoid relying on 3D printed models with less than full density. These are prone to delamination, and eventually absorb water.

Design modular hinges for different scales compatible with a variety of different hull geometries.

- Producing exact values of predicted torque and PTO damping is not strictly necessary – particularly for validation models. The quality of the collected data is what is paramount.

4.3.3.2 Validation

There is room for improvement in terms of the numerical model validation.

The wave amplitude inside the wave channel is much higher than that of the ambient wave passing by on the outside.

- The 1/53 scale model shows that amplitude is limited by steepness wave breaking, a fluid jet formation, and overtopping as the wave reaches the top of the wave channel.
- Suggests that wave channel geometry causes a fluid resonance in the wave channel, which increases excitation forces.
- Linear models predict unphysical wave elevations because they do not inherently have constraints on wave elevation.

Within time and cost limitations, run planned seas in empty basin ahead of model deployment.

- Do not assume pre-calibration of tank is sufficient – accounting for reflections leads to more rigorous RAOs based on higher quality incident wave data.

A rigorous like-for-like physical model comparison at two different scales is missing (despite 20th and 40th NWEC2 models being geometrically equivalent). As of July 2020, validation has thus far been primarily based on visual comparison of RAOs, and comparison of average power values achieved in particular sea states.

4.3.3.1 Performance

Further exploration of the power/cost trade-offs based on a particular torque limit range and PTO damping range would be beneficial. For example, in the NWEC 20th scale model, a cost/benefit investigation was carried out in the 0.5-1.0MNm region. It was found that lowering the torque limit to 0.5MNm caused a 15% drop in power capture; increasing it to 1.5MNm caused no change (in given 6.6s T_e, 1.5m H_s sea). The predicted required torque limit was 1MNm, i.e. the design torque capability of the full-scale WEC (20th scale large model in NWEC2).

The use of sidewalls to limit lateral flow across sloped sections (i.e. wave-channels) boosts performance. However, the impact of different sidewall depth is not known. The NWEC2 validation concept exhibits deep side walls that extend above the mean water line. On the other hand, the NWEC2 performance concept has sloped plates but relatively narrow sidewalls.

A low freeboard and the presence of sloped sections enables diving and load shedding in steeper waves. The sensitivity of performance to wave channel slope angle and freeboard is largely unknown.

Finally, control strategies more complex than linear damping have not been explored or implemented thus far.

4.3.3.4 Uncertainty

Gearbox backlash compromised the power measurements, particularly for small motions, while friction introduced a degree of uncertainty in assigning an appropriate damping value to the numerical model.

In 1/53 Phase1a tests, uncertainty exists in whether it was hydrodynamic or hinge related nonlinearities that were being captured via the adjustment of the validation parameters. It is likely that the Cd value is not representing pure viscous drag but additional nonlinearities and is thus acting as an *equivalent* drag/damping coefficient[44], as outlined in (Giorgi and Ringwood, 2017).

It can therefore be beneficial in design tests (as in Phase1b) to reduce effects of hinge uncertainty, for example via:

- Single body runs (i.e. model with locked hinge);
- Force tests (locked hinge attached to load cell attached to fixed support overhead holding it fixed with respect to incoming waves);
- Free body tests (hinge free but PTO off).

These led to use of a complex damping-plate impedance. Results with the complex impedance were generally very good for all tests considered. However, particular values of damping plate coefficients are not yet fully understood or analytically formulated. Broadly speaking, there is higher confidence in the numerical model that now includes a partial theory on the hydrodynamic behaviour of the nose and tail of WEC based on ‘trapped’ modes (Ursell, 1951).

The effect of cables on measurements has not been investigated – the NWEC2 20th scale model has three cables while the 40th scale model has none. The effect is likely to differ depending on their arrangement – e.g. Figure 29 shows cables below the water line, and Figure 30 shows them draped above the model via a gantry. The NWEC2 20th scale model had three relatively large and heavy cables. The two nacelle cables weigh 0.2kg/m and there is a 2m drape of cable

[44] As flow becomes more complex, different sources of nonlinearities will combine -> leading to 'apparent' changes in the drag coefficient, in turn leading to an *equivalent* drag coefficient being estimated, incorporating viscous drag but not exclusively. As such the drag coefficient risks becoming a descriptor of all unmodelled effects/nonlinearities, as well as modelling errors and inaccuracies, making it less applicable to other experiments.

to the tank floor; total of ~0.4kg of mass. Cable diameters are 7mm and 9mm; the volume is 0.1L/m so the buoyancy of 2m drape is 200g; this gives net mass as opposed to buoyancy. The load cell cable was sheathed in watertight tubing that floated. To keep it from interfering with the model motion, it was ballasted with a weight that sat on the tank floor, but still allowed 0.5m of free movement to the model.

Scaling effects have not been explicitly investigated nor fully accounted thus far. For example, the pull-release test obtained natural period for the 40th scale model was 10.26s, but 6.19s for the 20th scale model. This was attributed to the presence of Qualisys markers having a greater relative impact to the response with a smaller model. On the other hand, flex natural frequencies (full-scale) were 8.85s and 8.87s

A final point of note is the effect of yaw angle of the model when exposed to waves and its effects on flex RAO measured. For the NWEC2 40th scale model, the mean yaw angles at each wave period during the sample time used to calculate flex RAOs vary between +15 to -30deg – this is considerable. It is preferable to limit this with a slack yaw alignment line that extends from the rear wave channel to the side of tank, also to limit yawing during the rest period between wave runs.

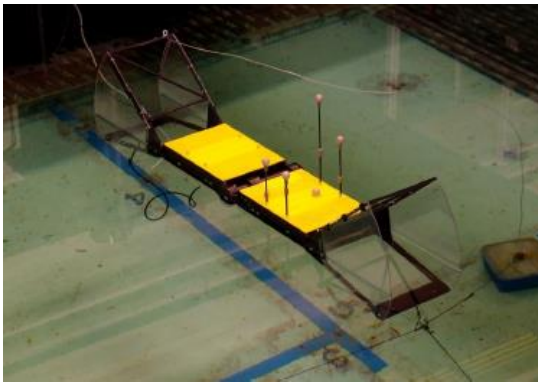

Figure 29 - 1/53 NWEC2 scale model in the Curved Tank (Courtesy of Mocean Energy).

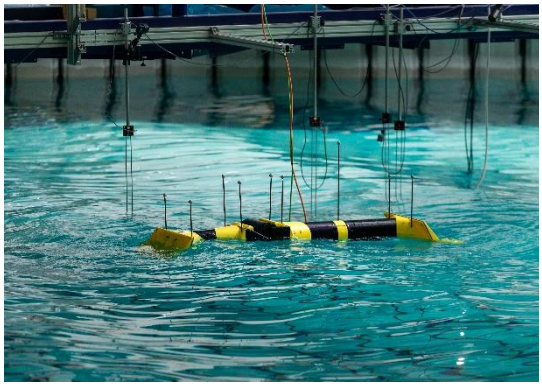

Figure 30 - 1/20 NWEC2 model in FloWave (Courtesy of Mocean Energy).

Chapter 5. The Wave Energy Paradox

This chapter first presents a framework – denoted *wave energy paradox* – formulated by the author on the basis of the examined literature and commercial context. This new framework informs both the choice of WEC to be developed (size and target market), and the approach to the particular activities that support this development within the boundaries of the present project (detailed in PART III). The approach is one of small-scale and fast-turnaround physical modelling in order to both maximise and accelerate learning as part of an enabling iterative development roadmap.

5.1 Definition of the wave energy paradox

Chapter 2 reviewed different aspects of the wave energy commercialisation challenge, including developer approaches to technology development, conceiving and measuring performance, and the choice of markets for energy end-use. The commercialisation discussion is rich and includes multiple angles, with numerous factors being highlighted in striving for commercial success. To an extent, this 'scatter' is the natural consequence of a challenging technology application within a novel industry and a perennially shifting commercial, policy, and public landscape. Nevertheless, a holistic/integrated synthesis is desirable to join up these factors and guide WEC development. Ideally, this is needed both at a 'higher' conceptual level and at a 'lower' practical level, applicable commercially but also technically, since all of these perspectives interlink and ultimately need to be present to maximise success of the industry and of individual developers within it. In the author's opinion, the fundamental requirement that ties all of these perspectives together is *learning*[45]. Learning, therefore, ought to be the underlying and continuous feature throughout development, particularly in a not yet established industry such as wave energy.

So, what has been – and currently still is – limiting learning?

[45] Different learning types are presented in (Kerr, Noble and Hodges, 2021), among which: learning by searching, doing, using, interacting.

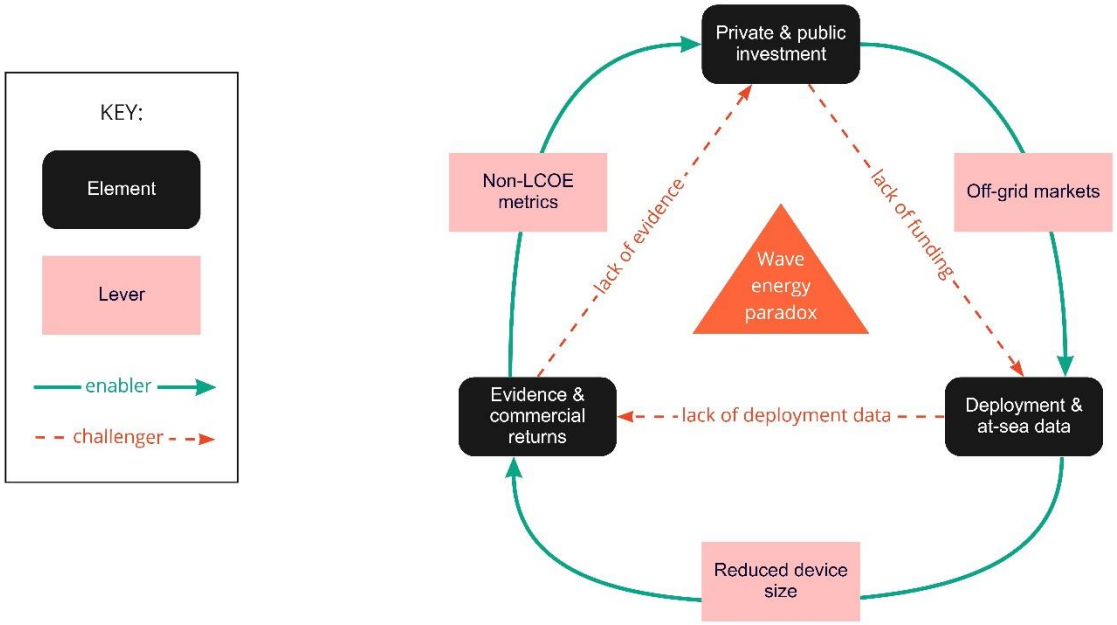

Figure 31 – Diagrammatic definition of the Wave Energy Paradox framework.

Key elements of the technology commercialisation roadmap are represented as the black boxes of Figure 31, which shows how the challenge is not singular, but rather a negative reinforcement mechanism. Initially following the red (dashed) arrows, it can be seen that:

- A lack of available capital and policy support hinders the ability of developers to deploy WECs at sea, from which performance and reliability data can be collected.
- This, in turn, does not allow the often-cited learning-by-doing process to occur, in order to build a performance evidence case and accumulate experience to cut costs, nor commercial returns since the device is not sufficiently developed to output monetary value.
- As a result, private investment is not forthcoming due to the high uncertainty and perceived risk, while policy tends to favour different renewable technologies that can already compete at utility-scale with more conventional forms of energy, such as offshore wind or solar.

The point at which one enters the loop is largely inconsequential; each element negatively feeds the others. The cycle repeats, but needs not remain a negative

one. Reversing the cycle is crucial to ultimate wave energy success, by enabling – and ideally accelerating – learning. How best to do so?

Following the green (block) arrows, the potential impact of specific levers in positively transforming the paradox is proposed. These levers are key areas of possible intervention that can 'bridge' across the (black-boxed) elements.

- **Markets** – off-grid markets that are outside utility, grid-connected, electricity generation offer several advantages, particularly in the shorter term. Developers can exploit the ever-increasing drive for 'greening' and the growing Blue Economy movement with its range of offshore power requirements. In so doing, they can access greater investment, reduce reliance on government support and opaque/evolving policy landscapes. They can focus on delivering a more self-contained technology solution, dodging grid compliance requirements and associated risks and costs. This can ultimately lead to faster deployment at full-scale, and influences both WEC size and metrics.
- **Size** – off-grid markets typically demand less power compared to utility applications. This means power requirements can be met with a smaller full-scale device, which implies a reduction in both CAPEX and OPEX. Not only is less material needed to build the WEC, but the requirements for handling the device and operating it (e.g. vessel size for towing and installation) also become more favourable. From a physical modelling perspective, this also means that for a given reduced scale, physical models are hydrodynamically more representative of the full-scale – as well as cheaper. This element links most directly to the activities undertaken in the present thesis.
- **Metrics** – necessary both in terms of optimisation and measuring 'attractiveness' of technology. By veering away from government reliance and the grid system 'rulebook', LCOE significance is reduced, and different values (not necessarily centred on techno-economic

performance)[46] begin to emerge. For example, carbon emission avoidance, supporting sustainability, 'greening', direct fossil fuel displacement, as well as social factors[47] that become more dominant (e.g. environmental protection, local job creation, not spoiling tourism with highly visible devices or occupying vast land area, energy security of remote island communities, etc.). Summarised in one concept, one could put it as: "different stakeholders; different needs; different values attached to wave energy".

Each of these levers facilitates movement along the fundamental development elements in Figure 31. It is suggested that the quicker one can move around the elements along the green arrows, the quicker one can learn. During the time of this project, the *wave energy paradox* framework has been adopted by Mocean to guide internal strategy, as well as to communicate with funders and investors.

5.1.1 Real life examples

As a practical illustration, the wave energy paradox has featured in several successful public funding applications by Mocean, among which Scottish Enterprise (SE), InnovateUK, Wave Energy Scotland's NWEC programme, EuropeWave, and more. The suggested progression is evidenced by the parallel – yet staggered – device development shown in Figure 32, with Blue X (10 kW), Blue Star (20 kW) and Blue Horizon (250 kW) WECs being shown left-to-right in order of descending TRL and corresponding descending device size and power rating. This timeline can be compared with Figure 33, which shows the development of the Orbital Marine Power (formerly Scotrenewables) O2 floating tidal energy platform (European Commission Joint Research Centre, 2019).

A few comments can be made when making the comparison, with some accompanying caveats. O2 is a 2MW rated tidal energy converter; Blue X is a

[46] Should underline that many prospective investors' initial question is: what TRL stage are you at? (again, out and out performance not necessarily the priority)

[47] In a recent report on "external forces influencing wave energy development", (Ruiz-Minguela, Nava and Blanco, 2022) conclude that different power markets considerably affect ranking of external forces. Also point well made by (Trueworthy *et al.*, 2021).

10kW rated WEC. As such, this is by no means a like-for-like comparison in terms of the finished product. It is also acknowledged that Scotrenewables was founded in 2002, while Mocean in 2015. The associated policy landscapes and available funding streams will have been different. Furthermore, this is a single case study involving one tidal developer and one wave energy developer. Nevertheless, the comparison reveals interesting features of the development pathways of two (more or less established) ocean energy developers. One (Orbital) has pursued a single large-scale utility device from the onset. The other (Mocean) has opted for a stepped approach via off-grid markets and smaller full-scale devices. Figure 32 and Figure 33 show that:

- O2 has taken 16 years to move from TRL 1-8, with TRL 8 signifying a single commercially ready device. Blue X is expected to reach TRL 8 in 2023, 8 years since its conception (TRL 1).
- O2 has taken 11 years from TRL 1-7 compared to Blue X's 7 years.
- Orbital Marine's first at-sea deployment was a 250kW scaled version of O2 in 2011, 8 years since beginning the overall development. This is a closer timeframe to Blue X, whose first-of-a-kind prototype was deployed at full-scale less than 6 years following its initial conception.
- Mocean's (grid-connected) Blue Horizon WEC may well be deployed in a similar overall timeframe if considering company-founding dates (2015 versus 2002). However, the key difference is that Mocean will have had a chance to accrue returns on investment via its off-grid devices in the meantime, used to support ongoing R&D activities including for its utility-scale WEC.

Thus, the comparison suggests that parallel development fundamentally unlocks shorter-term intermediate commercial returns and potentially accelerates ultimate utility-scale deployment.

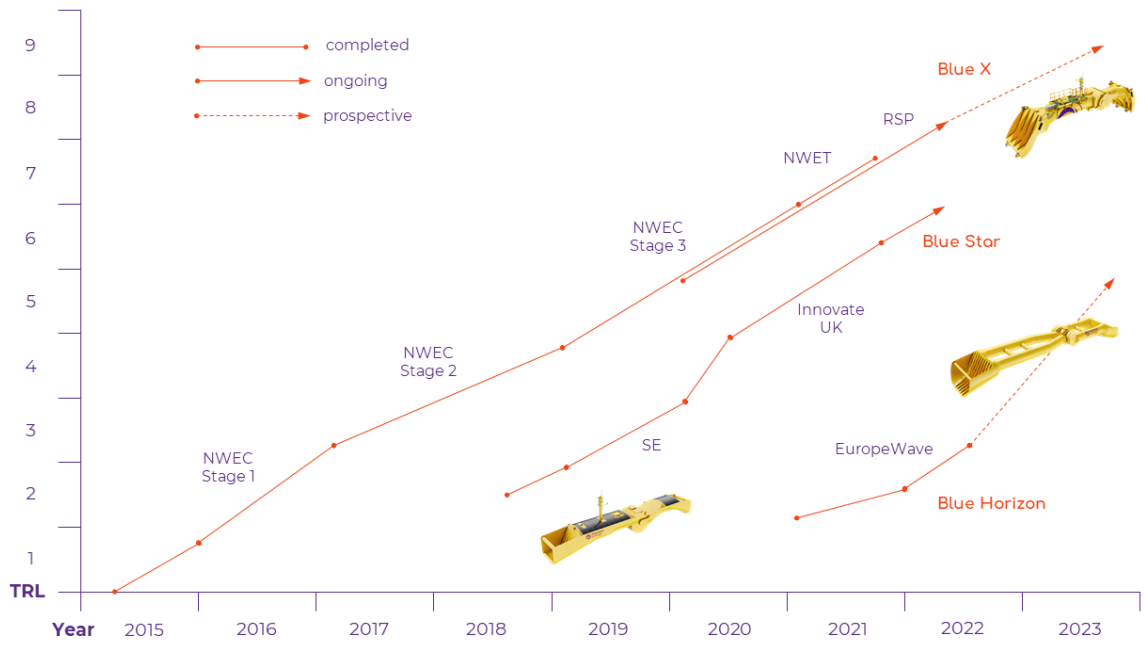

Figure 32 - Mocean WEC development across WEC device streams.

From Figure 32, note that (a) Blue Star and Blue Horizon do not start at TRL 1 due to commonalities in fundamental technology; (b) steeper TRL rise for Blue Star and prospected for Blue Horizon due to learning from Blue X and Blue Star developments. Technology scalability undoubtedly represents a major advantage in pursuing a stepped development approach.

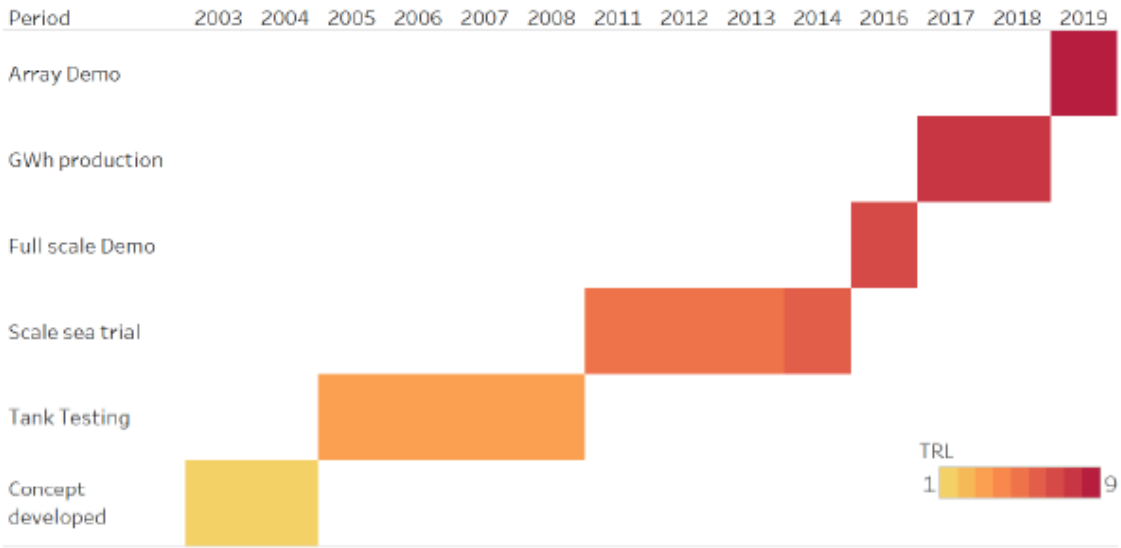

Figure 33 - Timeline of Scotrenewables / Orbital Marine development (European Commission Joint Research Centre, 2019).

Returning to the underlying framework, a particular benefit of the *wave energy paradox* representation is that it shows the iterative nature of WEC (and indeed most technology/product) development. One of the shortcomings of the TPL-TRL matrix (see Chapter 2) is that it portrays performance and readiness as linear and somewhat dichotomous, suggesting that a developer can – and indeed should – choose to pursue development (TPL) or deployment (TRL) in turn, while in practice each reinforces and is dependent on the other.

Finally, the *wave energy paradox* visually points to the importance of deployment in order to support TPL advance, not just TRL, as is often assumed. In the words of Kate Johannesen from the consultancy Black & Veatch: "LCOE needs to reduce but it won't happen without deployment"[48]. The value of deployment itself – in other words, the gaining of at-sea full-scale device experience[49] – is often missing from commonly used quantitative metrics. LCOE emphasis means that deployment is predominantly valued as an end-goal, as opposed to as part of a process that facilitates learning. Much of the focus in published reports has been on highlighting industry needs and priority areas for development in order to achieve accelerated deployment: learning by doing, cutting cost through design convergence, greater data sharing, supply chain development, etc. Yet none of these can occur without initial deployment of devices at sea.

The *wave energy paradox* was first introduced in (Caio, Davey and McNatt, 2019). It was then referred to by (Trueworthy and Dupont, 2020) and (Clemente *et al.*, 2020), and re-utilised by Caio et al. in the context of small-scale physical modelling (Caio, Davey and McNatt, 2021), and by (Trueworthy *et al.*, 2021) in the context of WECs transitioning to new markets. The most recent academic citation can be found in (Choupin, Henriksen and Tomlinson, 2022).

In the industrial domain, the framework aligns well with the historical narrative of the wave energy industry falling short of expectations. It provides a helpful

[48] Johannesen, K (2019). "Bridge markets for marine energy: gaining experience in non-utility markets," Black&Veatch Report. Glasgow: AllEnergy Conference.

[49] Can be equivalently understood as reducing uncertainty.

backward-looking perspective to consider notable, extremely large-scale, WECs that ultimately failed to reach commercial success (e.g. Pelamis and Aquamarine). Its relevance can also be gauged from regular ocean energy reports that OES has produced annually since 2002. The 2021 features “ORE and Offshore Aquaculture” as part of its achievements heading, while previous editions had far greater focus on including transmission and distribution network information. Up to the 2015 edition, a dedicated section outlined “electrical utilities involved in research & development and demonstration”. This is no longer a focus point in the reports.

The *wave energy paradox* therefore also provides a useful forward-looking vision of ‘slowly but surely’ growing industry prospects.

The following section gives more details on each lever’s potential impact, and relates these to Mocean’s development approach and the project’s methodology.

5.2 Tackling the wave energy paradox

In practice, the *wave energy paradox* informs and formalises Mocean’s choice of WEC concept – i.e. the decision to develop a 10s of kW rated WEC for off-grid applications, called *Blue Star*, as a stepping-stone to future larger power devices. Secondly, it informs the approach to physical modelling adopted in this project, aimed at maximising and accelerating learning, particularly at early stages.

In this section, further qualification of each lever is provided in turn, with explicit links to Mocean’s development approach, to underline each lever’s influence on the project methodology that follows in Part III.

5.2.1 Markets

(Caio, Davey and McNatt, 2019) first formulated the idea of exploiting different markets to overcome the *wave energy paradox*. This was followed by papers such as (Trueworthy *et al.*, 2021) that differentiate WEC requirements according to end-use in more detail, and (Jin and Greaves, 2021) that provided a more UK-centred overview of the industry’s trends. As found in the latter, “[the wave energy] market seems to be converging in two directions”: utility-scale, and sub-

utility scale off-grid (Jin and Greaves, 2021). The OES 2022-2026 Strategic Plan released in December 2021 provides evidence of broader uptake of this concept. Though pointing to grid-connected electricity as wave energy's main objective, it clearly recognises that offshore industries such as aquaculture, desalination and oceanographic research "offer a growing potential of direct use", and proposes that "islands and remote locations are the first opportunity around the world" due to their heavy reliance on costly fossil fuels (IEA-OES, 2021).

The idea of using WECs to provide off-grid power in remote offshore locations theoretically offers several benefits from a commercialisation perspective. In 2018, when Mocean's business plan already included the idea of off-grid WECs, this strategy was not so pervasive. However, a growing movement now views wave energy as a 'decarboniser' of offshore activities and an enabler of Blue Economy applications, both of which are gaining traction. These markets are typically referred to as 'alternative', 'beachhead', 'intermediate', 'emerging', 'niche', or 'off-grid', which is the term adopted henceforth as it groups all of the above and is the most objective. We use this term even when discussing grid-connected deployments in small island communities as the grids here are either not yet developed or typically very small.

A comprehensive discussion of how high capital costs can be offset to enable WEC development via off-grid markets can be found in (Foteinis and Tsoutsos, 2017). (MacGillivray *et al.*, 2014) also touch on this, highlighting how developers in the past have been tempted to fast-forward development from a single kW scale prototype to MW scale demonstration devices operating in highly energetic climates, "possibly omitting important intermediate development steps", and thus falling foul of survivability complications, a lack of experience, and the significant capital impact of iterative designs at large scale.

The possibility of avoiding grid-connection and compliance as a specific requirement also has notable advantages. (Magagna and Uihlein, 2015) mention grid integration as a particular issue: "one of the rising concerns for the ocean energy sector is the availability of grid in the proximity of proposed ocean energy projects". In 2015, a Cost of Energy report by OES pointed to grid integration

accounting for 6-8% of the LCOE for wave energy, and about 10% of overall CAPEX (IEA-OES, 2015). Similarly, OCEANERA-NET advises that grid connection for an ocean energy farm can reach up to 40% of total project costs (OCEANERA-NET, 2017), though of course this depends on multiple factors, among which site location and conditions. (Clemente, Rosa-Santos and Taveira-Pinto, 2021) points out that supplying a utility grid introduces "difficult regularization of the electricity output to meet the electricity demand variability", while also forcing a “direct competition with more robust and mature energy sources".

Pursuing off-grid applications overcomes ‘the chicken and egg scenario’ of what part of the system ought to be ready first: the grid or the WEC technology? This has undoubtedly contributed to some stasis. Finally, when considering external factors most impacting commercial success, moving away from utility-scale development shifts the focus from government and policy drivers to societal drivers (Ruiz-Minguela, Nava and Blanco, 2022). This typically grants a developer more agency in determining a successful outcome.

5.2.1.1 Chosen market(s)?

Mocean has adopted the “small-mid-grid” mantra. It initially explored the ocean observation market by engaging with the National Oceanography Centre (NOC) in Southampton, UK. At the time, in 2018, the WEC was envisaged as a floating communications platform that collected ocean data, for example used to service the decommissioning of a growing number of O&G platform reaching end of life in the North Sea (Jones *et al.*, 2019), potentially connected to an AUV dock. However, requirements from ocean observation market included a low power requirement <1kW and the ability to manually handle and deploy the WEC. AUV docks were also not yet ready for integration and to enable subsea docking at the time. As a result, Mocean veered towards O&G applications, in particular substituting umbilical cables that provide electricity to offshore fields to power electrically actuated systems. These cables can be very long and typically bring electricity from shore at great cost and environmental impact. The context of ageing offshore O&G platforms provides a big opportunity (Clemente, Rosa-Santos and Taveira-Pinto, 2021). The alternative is to meet power demands by burning fossil fuels. Offshore off-grid equipment provides an attractive

opportunity to provide that power (and communications) with more sustainable means like wave energy, even as production hopefully tapers down.

Two additional factors are noteworthy. The first relates to Mocean's business model, which involves licensing WECs to customers in order to service particular locations. Multiple applications in multiple sites represents a major opportunity, but also a challenge. It means that prospective customers typically require specific site assessments, whose available wave resource is best exploited by a specifically optimised WEC geometry in order to deliver optimal power. Power estimates and device behaviour requires validation and high-fidelity performance prediction. Hence, fast-turnaround is required to produce an optimised geometry and to validate its performance (including via physical models). A Basis of Design (BoD) for Blue Star is provided in the next section.

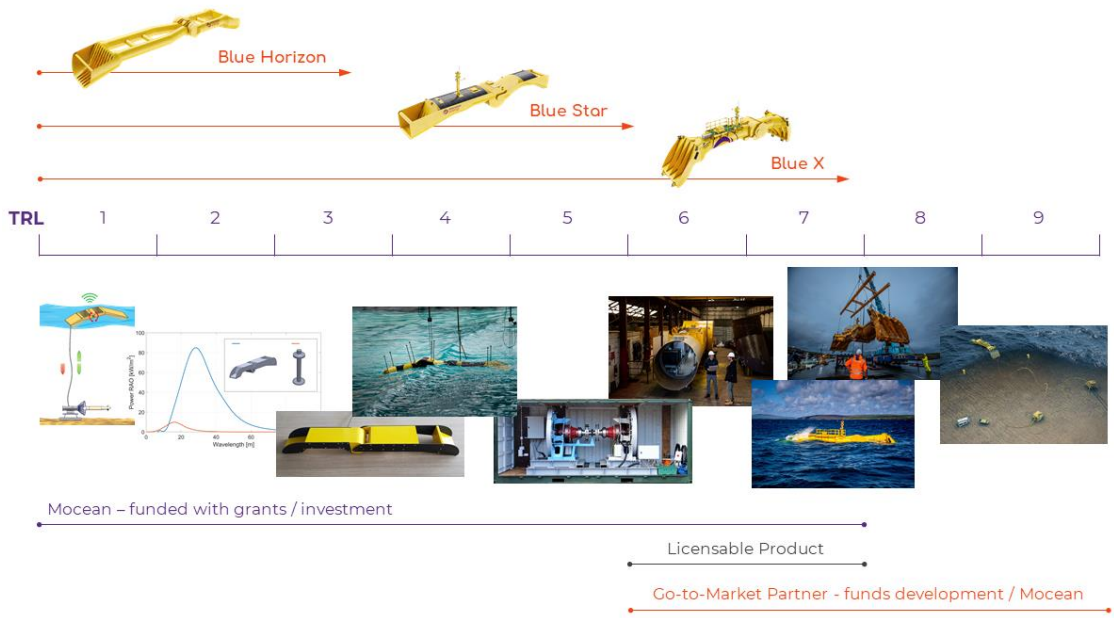

Figure 34 - Mocean's parallel development programmes - different sized WECs for different markets.

Figure 34 shows projects driving technology development through TRL stages up to a licensable product at TRL 5-7. Product development is maintained at different stages to ensure a pipeline. Combined with Figure 32, it goes some way to showing how the *wave energy paradox* is becoming a positive loop, with traction from each increasing device size positively influencing the development

of the next size up. What is not clearly shown on the diagram is that these parallel projects have inevitably fertilised one another.

5.2.2 Size & scale

The lever of ‘size’ (and equivalently physical model scale) is the most obvious in terms of reducing costs and risk for developers, as well as the most direct link between commercial and technical domains.

Commercially, the “start small, go big” philosophy/approach – involving the use of non-utility markets (see Section 4.2.1) as stepping blocks – is becoming central among wave energy developers, many of which are developing a range of WECs at different sizes to satisfy different applications – e.g. Columbia Power Technologies (C-Power)[50], and Ocean Power Technologies (OPT)[51]. Whether the technology learning involved is relevant for larger scales remains – to some extent – an open question, which will be returned to in the thesis discussion.

A parallel concept applies to the *technical* domain, particularly when considering physical models. Typically, the complexity and scale of the model increase as TRL increases. However, in practice this is not a linear process, and requires iteration. Thus, the more one can advance the performance of the model earlier on, the more economic and time costs one can ultimately save as a developer moving through the various development stages. In addition, the more sophisticated one’s reduced scale model, the more once can learn about the WEC’s overall performance. It follows that a physical testing process based on the principles of fast-turnaround and minimum viable scale can be highly enabling and very valuable.

There is an additional practical element when considering TRLs of key sub-systems such as the PTO. It is extremely challenging to scale novel generators such as C-GEN, the Vernier Hybrid Machine (VHM), or other non-contact direct-drive alternatives in one leap, from a relatively low TRL to their use in a very large utility-scale machine size. While the prime mover can be scaled relatively

[50] https://cpower.co/

[51] https://oceanpowertechnologies.com/

easily, this is not the case for other subsystems. Thus, a benefit of gradual scaling via intermediate markets is that one can not only learn at-sea with lower risk, but also incorporate the most promising ‘available at the time’ technology solutions for PTO, mooring connections, etc. as these also develop in maturity. Taking the PTO as an example, this is especially important because it is a fundamentally enabling subsystem in achieving the required performance/cost level.

5.2.2.1 Chosen size and scale?

Mocean’s embodiment of this approach is an off-grid WEC called Blue Star that targets 10 kW average power in the central North Sea climate, with applications including subsea O&G well component actuation, powering residential ROVs/AUVs, ocean sensing and monitoring, and powering CCS tiebacks. The chosen scale of physical model is outlined in Chapter 6. A 1:20 scale is chosen, in continuity with Mocean’s previous work and opportunities opened by Curved Tank availability and economising operation.

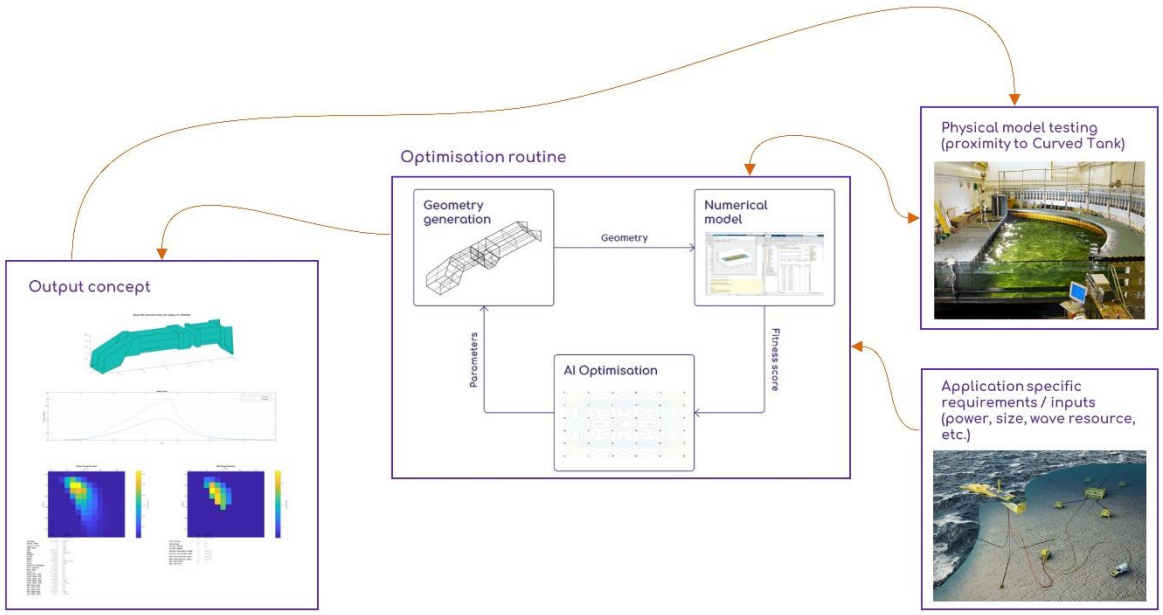

Figure 35. Showing integration of physical modelling within Mocean's development context.

5.2.3 Metrics

The dependency of metrics on a WEC’s end-use/application, and their limitation as objective indicators of comprehensive techno-economic performance –

particularly at early development stages – have been outlined in Chapter 2. This subsection complements these themes, guided by practical industrial context, to indicate how metrics are taken into account by Mocean's development strategy and the physical modelling that will follow. Three aspects that feed into metrics choice and methodology are considered: dimensionality; integration; alignment. It is noted that different metrics are likely be required to cover these three aspects, but this may well be a 'feature' as opposed to a 'bug'.

5.2.3.1 Dimensionality

Figure 36 has been constructed based on a hypothetical series of WECs of characteristic length 1, 2, 4, 8, 16 units. Device 'size' is associated to its characteristic length. A Froude scaling factor denoted as *s* is defined according to the ratio of characteristic lengths of hypothetical devices. When Froude-scaled, the corresponding scaling factor for a particular metric is proportional to a particular power of *s*. For example, mass scales as s^3. Chapter 4 provides a more detailed overview of Froude scaling theory and application. Here it can be seen (Figure 36) that:

- Length (or size) is taken as the baseline for the device comparison.
- Then the relative value of metrics in mass (or volume) (B), power[52] (C), and torque (D) categories is wildly different to length. This is also true for plot F, which is warped compared to plot A.
- A performance/cost metric such as AEP/mass (plot E) is less prone to scale warping. This is also the case for plot H and plot G, although for the latter plot the relative order of magnitude of its cells is inverted.
- Plot F is analogous to plot E (AEP/mass) though the relative cell size is inverted.

The issue of dimensionality becomes significant when comparing different device types, and even more so when comparing differently sized or rated devices. While it may be satisfactory to use dimensional metrics for a consistent

[52] According to Froude scaling, the scaling factor for power is the same as for AEP. This is because AEP is constructed as a summation of the powers achieved for each cell in the occurrence table of a given location.

WEC being internally iterated as part of an optimisation process, it is desirable to use a non-dimensional benchmark to compare a given WEC to others with which, for example, a developer is competing. If devices are optimised or designed for operation in different wave climates or locations, this adds another level of precision complexity.

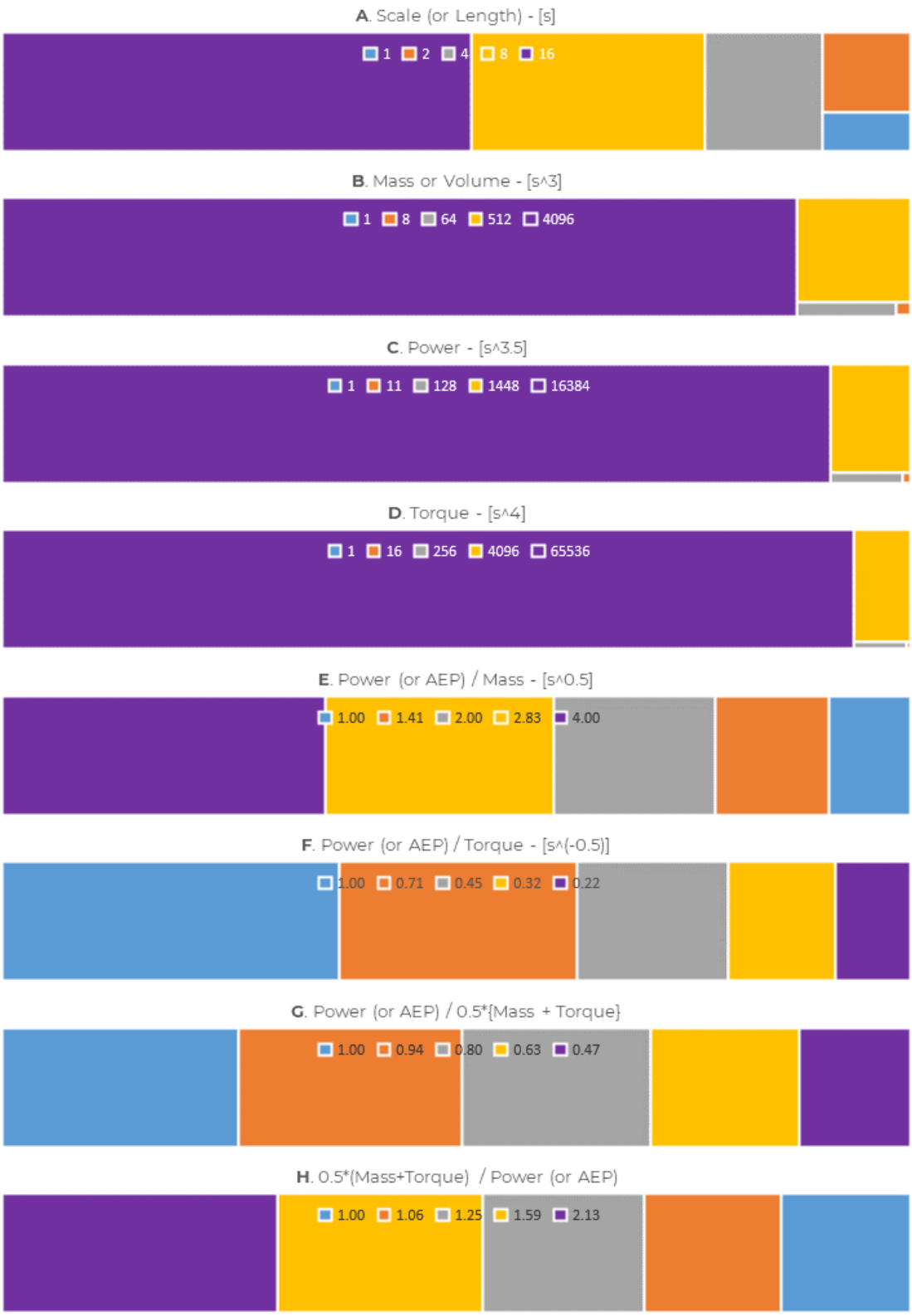

Figure 36 - Showing areas proportional to the Froude scaling factor associated with different metrics.

NB: Froude scaling is just an approximation; it is not at all the case that the power rating or torque limit (or max PTO force/torque or characteristic PTO force/torque or AEP will be actually proportional to s^3. This is an approximation. Only at the end of a development path involving different sizes of full-scale Mocean devices, with a backward looking perspective, will the degree of accuracy of this approximation be known. This is the only way to obtain an assured answer to the question.

It should also be noted that a larger WEC does not necessarily capture more power, or indeed, if it does, its CWR may actually drop after a certain threshold of scale. (Jin, Zheng and Greaves, 2022) find that the 'scalability'[53] of a WEC depends more on its orientation and size rather than its operating principle or typology, and is more complex than for mature wind turbine design. For an attenuator, such as the Mocean WEC, "the rate of increase in the maximum power extracted reduces with increasing length, because the theoretical CW does not increase linearly with device length" (Jin, Zheng and Greaves, 2022). The design length of an attenuator should consider the trade-off between increasing power and construction cost, which will not rise in direct proportion. Though largely outside of the thesis research scope, this links to the consideration of optimal WEC scale for arrays, where, depending on the CWR characteristics, it may be more beneficial to deploy a larger number of smaller WECs than fewer larger ones (de Andres *et al.*, 2016; Pascal *et al.*, 2018).

Of course, other considerations such as operations and maintenance will affect such choices. Practical – as opposed to theoretical – scalability is also affected by motion constraints, mooring effects, PTO, additional conversion efficiencies, control implementation, etc.

5.2.3.2 Integration

From a developer's point of view, a major challenge rests on the integration of comprehensive techno-economic metrics into the design process (including fitness score), as part of a trackable and optimisable strategic trajectory towards

[53] *Scalability* here is defined as power performance increasing with increasing device characteristic length.

commercial deployment. For example, these may be incorporated as fitness functions used to guide numerical optimisations, as is the case for Mocean. Mocean's choice and use of fitness functions is given in Chapter 4.

Chapter 2 outlined how the choice of appropriate metric(s) is important to set suitable goals and design trajectories. (Weber, 2012) states that, "depending on the fundamental definition of the objectives, development trajectories can diverge considerably subject to prioritisation of tech development". Chapter 2 also pointed to the difficulty and lack of consensus around which metrics to use. (Caio, Davey and McNatt, 2019) examined which metrics, among those published in design standards and guidelines at the time, could be used by developers to practically guide and optimise the design process. It pointed out that no clear choice emerges from current standards and guidelines.

Figure 37 shows different metric scores for floating WEC concepts featured in (Babarit *et al.*, 2012). Similarly to the analysis by (de Andres, et al., 2016), it can be seen that relative merit varies significantly depending on the chosen metric: there is no clear overall winner amongst the simulated device concepts, which are inspired by real WECs being developed at the time. In Figure 37, the deployment location of reference is an EMEC site. CWR represents capture width ratio, a measure of conversion efficiency. Different levels of uncertainty are associated with *Annual mean absorbed power*, which vary between -25% to +40%. The category *AEP/ rms PTO force* is missing two bars due to this metric not being always applicable. Thus, this too shows that attractiveness of a WEC concept depends on what metrics lens it is viewed through.

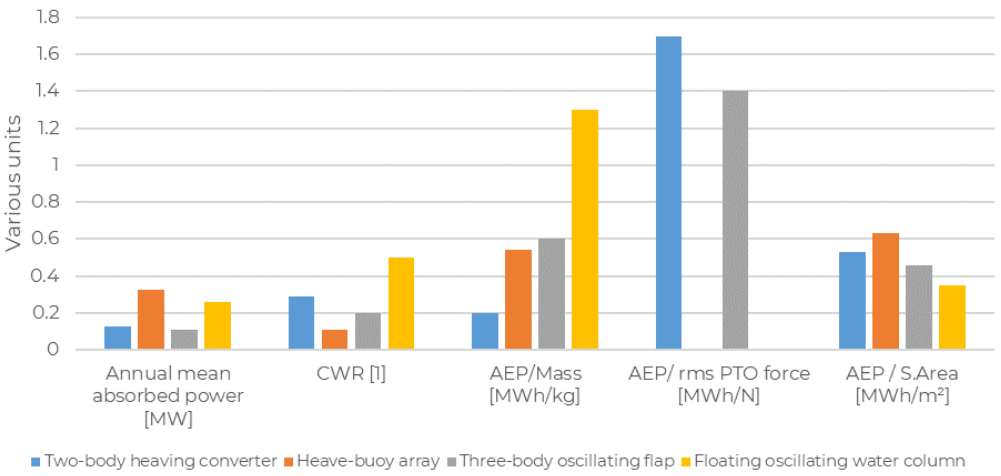

Figure 37 - Comparison of floating WEC concepts via numerically obtained metrics [adapted from (Babarit *et al.*, 2012)*].*

Mocean have primarily – though not exclusively – relied on some weighted combination of *AEP/Mass* and *AEP/PTO torque*$_{max}$ metrics to guide the design process. This is because they can be incorporated in device design with relative ease. For example, a key activity for Mocean during the second stage of the NWEC development program was the geometric optimisation of the WEC. Forming part of the fundamental design choices, this was run based on a genetic algorithm implemented in MATLAB, which aimed to minimise the following fitness function (discussed in Chapter 4):

$$F = C/P$$

where *C* is CAPEX of the prime mover structure and the power take off (PTO), and *P* represents *AEP* (based on a representative wave climate as input). Thus, the fitness function *F* essentially combines *AEP/Mass* and *AEP/PTO torque* metrics. Structural mass and PTO torque are selected as these typically make up for around 60-70% of CAPEX (The Carbon Trust, 2011). For the Mocean WEC, this percentage is 83% for the first-of-a-kind full-scale prototype. Although this function does not exhaustively cover techno-economic elements, it represented the most efficient way of including power per cost offering at an early stage of design, when large uncertainties remained in terms of reliability, lifetime, O&M, supply chain, etc.

5.2.3.3 Alignment

A clear disparity exists between external (i.e. set by external stakeholders such as investors and standards bodies) and internal (i.e. set by developers) performance metrics. This is significant when considering the *wave energy paradox*, since part of its resolution relies on a coherent set of metrics that can speak to developers, funding bodies and investors alike. Aligning internal and external performance goals would allow a greater understanding and appreciation of development progress.

Apart from the TRL indicator, shown in Figure 32 and Figure 34, it would be desirable to find metrics that could speak to both internal and external stakeholders regarding the ‘merit’ of a given device. One way to improve

alignment between stakeholders would be to involve more potential customers as project partners during the WEC development process, for example during WES and EuropeWave style programmes. The 2018 OES Annual Report contains two notable comments regarding the importance of internal (developer) and external (investor) metrics having a degree of alignment (The Executive Committee of Ocean Energy Systems, 2018):

> *"Performance metrics and technology evaluation process not only contributes to decisions made using DOE funding, but also attempts to* ***align [marine renewable energy] MRE performance metrics and evaluation criteria with private investor interests and concerns*** *as well." – L. Moraski, Technology Manager at the Water Power Technologies Office of the US Department of Energy (DoE) [bold text is the author's addition]*

> *"Importantly, both the development process and the stamps of approval have more effect on investor confidence if everyone agrees with the metrics for success."* [54] *– J. Hodges, Senior Innovation Engineer at WES*

In order for metrics to be effective during the development process, they ought to be integrated (common and feasibly obtained with appropriate confidence level) across development processes (including numerical and physical modelling). In order to act as appropriate 'stamps of approval/quality', they also ought to be as objective as possible. As explored in Chapter 2, this is not straightforward.

5.2.3.4 Chosen metrics?

(Weber *et al.*, 2019) identified 23 categories of metrics to guide WEC development, each consisting in a series of questions that lead to particular choices in terms of assessment criteria, tools, and methods employed. This particular study is comprehensive in terms of the questions it poses, but does not offer a means of prioritising or narrowing down the actual choice. (Trueworthy *et al.*, 2021) subsequently built on it by expanding such categories and questions to include emerging markets and applied them for desalination,

[54] Discussing the stage-gated process and how these stage gates connect to the integration of suitable metrics throughout the development process, as indicated by the *wave energy paradox*.

AUV charging, and ocean observation and navigation. Addressing these 23 categories is outside the bounds of this thesis, not least since significant commercial and stakeholder engagement would be required. Here, we instead focus on the following aspects as they most directly relate to physical modelling:

- CWR
- RAOs (especially flex, the power converting DoF)
- AEP
- Proxy indicators of reliability and survivability (e.g. mean-to-max power, mean-to-max mooring loads, Fwd hull stability, Flex / m wave height, etc.)
- Metrics related to uncertainty

Metrics such as AEP/mass and AEP/PTO torque will be informed by empirically estimated AEP but will require complementary numerical analysis. Of primary concern here is that these metrics can be validated during envisaged small-scale physical testing. A distinction is recalled between those metrics needed to talk back to the current optimisation (which therefore do not need loads such as mooring or structural prime mover loads; a PTO is sufficient), and those ideally required for an “all-in-one” model, which would require the latter load metrics also for completion.

For completeness, a Blue Star WEC block diagram is included in Appendix E.

Part III:
Methods & Results

This part outlines the design, build, and testing of two successive Blue Star WEC geometries: *Blue Star-baseline* and *Blue Star-folding*. These were optimised based on evolving numerical input criteria. The first round of tests is carried out using a passive model without power-take-off to provide a set of baseline results and to provide confidence that appropriate data can be collected in the chosen tank at the chosen scale, primarily for validation purposes (Chapter 6). Several model upgrades are then implemented, including a dedicated reduced scale powered hinge nacelle (power-take-off). This is designed, built, and dry characterised for calibration purposes (Chapter 7), and then incorporated in a new overall physical model with an expanded testing scope (Chapter 8). This part also summarises activities carried out to re-activate and somewhat re-characterise the Curved Tank test basin at the University of Edinburgh – given its recent period of inactivity – where the tank testing was carried out.

"It has been a long-term dream to design and test wave power devices in a computer with seamless links between the original drawing and the final results and with new ideas tried as quickly as [one] could change models in a narrow tank. It is a still a dream, but we may be getting closer." (Salter, 2016)

- Stephen Salter, 2016

Chapter 6. Blue Star – baseline

This chapter outlines the first round of physical model testing undertaken with an early model of the Blue Star concept, referred to as Blue Star *baseline* or *BST-baseline* for short. This model was utilised to set an initial reference for future testing rounds. As well as the physical model itself, useful activities included a partial characterisation of the University of Edinburgh's Curved Tank basin, which was used to conduct these tests. Although literature exists relating to the Curved Tank's performance – e.g. (Taylor, Rea and Rogers, 2003; Cruz, Pascal and Taylor, 2006; Lucas *et al.*, 2008; Gyongy *et al.*, 2014) – it is relatively out-dated, since the tank has been largely unutilised in the years leading up to the present work.

6.1 Background

Before doing so, the following aims are outlined:

1. To build modelling confidence, primarily by analysing the match between numerical and experimental data RAO curves – at this scale, with this tank (i.e. the Curved Tank).
2. To validate the effect of additional fins within the WEC wave channels.[55]
3. To begin examining how different factors affect the quality of experimental results:
    a. Whether a rotary sensor is sufficient to evaluate flex RAO behaviour, or whether Qualisys data is necessary (for a small model, Qualisys targets have a relatively large effect the model's mass properties; Qualisys system availability varies).
    b. The effect of wave reflections in the test basin.
    c. The effect of trimming errors.

[55] The original numerical model predicted a significant effect. It was later discovered that this was likely due to a modelling error, but experimental validation was deemed desirable.

6.1.1 Commercial context

The initial concept for BST-baseline was a WEC known as *Seabase*, ideated as a remote communications platform targeting the ocean observation market, including powering and data exchanging with autonomous underwater vehicles (AUVs) via dedicated AUV docks. Engagement was sought with the National Oceanographic Centre (NOC) in Southampton, UK, in order to begin gathering stakeholder feedback and end-user requirements. In fact, this physical model was used as a hands-on demo at the first NOC workshop run by Mocean on March 25, 2019.

The oceanography – or ocean observation – sector represented a promising existing market, not least due to its relative openness to innovation. The need for AUVs is both well-established and growing, with AUVs expanding in numbers and capabilities. Several references point to a likely increase in AUV use for O&M activities within oil and gas, aquacultures, and offshore wind markets (Addison, 2018; Hodson, 2018). However, the advantage of targeting ocean observation lies in its existing and – though still evolving – AUV activity. Secondly, the current early R&D development phase of BST-baseline magnified the importance of seeking industry inputs to define appropriate end-user requirements. This is further emphasised by ORE Catapult in its 2019 report on Robotics and Autonomous Systems in O&M (Fong, 2019). The combination of relevant expertise, openness in providing design guidance, and reduced emphasis of commercial sensitivity pointed to the NOC as an ideal partner compared to potential O&G and offshore wind players, both of which are also adopting AUV use. The above factors are needed to overcome key barriers to development, and additionally provide the opportunity of forming future partnerships with other industry players within NOC's Marine Autonomous and Robotic Systems (MARS) group. The remainder of this section briefly touches on the fundamental background of ocean observation, before detailing how BST-baseline intends to address major needs in the sector.

Ocean observation involves the monitoring – via in situ data collection – of the oceans. This forms an integral part of the 'Blue Economy': the sustainable growth of existing ocean uses alongside the emergence of novel economically beneficial ones. The fundamental role played by the oceans in sustaining life on

earth, as well as the global economy, means that the value of ocean data is growingly recognised worldwide. At the highest level, the significance of ocean observation is enshrined in the United Nations Development Programme (UNDP) sustainable development goals (SDGs), in particular SDG14: Life Below Water, which includes the increase of scientific knowledge, the development of research capacity and the transfer of marine technology among its targets (UNDP, no date). It also advocates for improving access to ocean science, an important social element picked up by UNESCO in its Global Ocean Science Report of 2017, which highlights that ocean science is expensive and only industrialised countries tend to afford it (Intergovernmental Oceanographic Commission, 2017). There is therefore an expanding need for integrated ocean data and information; exemplified, for example, by the recent set up of the Atlantic International Research (AIR) Centre, a network of international cooperation that aims to integrate space, atmosphere, climate, energy and data science[56].

At a more detailed level, much of this ocean science data is collected by unmanned or autonomous systems, among which AUVs are a growingly valuable asset. AUVs typically follow pre-programmed paths collecting data to depths of 6,000m, usually without involving any real-time operator control. Primary applications include long-term monitoring of: marine effects of climate change such as changes in ocean currents and ocean acidification, flora and fauna, and seismic activity. Apart from increased autonomy, AUVs offer additional benefits relative to other unmanned platforms. They can cover greater areas and travel faster than remotely operated vehicles (ROV), can move sensors closer to targets compared to unmanned surface vehicles (USVs), and provide better positioning and stability compared to towed bodies. Therefore, they ultimately produce better quality data at a higher resolution.

BST-baseline aims to address a fundamental constraint for AUVs: limited energy capacity. In general, the higher the capacity, the heavier, bulkier and more

[56] https://www.aircentre.org/about-us/

expensive an AUV will be to build and operate. Thus, energy tends to be capped, with detrimental effects on:

- **Range** – missions become limited in geographical distance and time duration
- **Communication** – intermittency to save power, efficiency losses due to the need to surface to communicate with operators
- **Payload** – use of less sensors that use less power, together with low duty cycles
- **Mission flexibility** – pre-programmed length and duration of missions, with no or limited reactive decision making
- **Control** – real-time operator control is energy intensive and requires more effective communications
- **O&M** – costlier and more frequent deployment and retrieval, often requiring dedicated vessels and cranes for larger AUVs.

BST-baseline is envisaged as a WEC that locally stores captured wave energy in a battery bank in order to provide in situ power for AUVs via a docking station. As well as power provision, it is hoped that it can overcome some of the aforementioned communication challenges by being surface located, thus providing a stable communications relay point for data exchange between AUV fleets and remote operators and data end-users. The potential valuation of the underwater recharge market is not well defined, however, in a 2017 report the U.S. Department of Energy (DOE) noted that a "best guess places the current market at tens of millions of dollars", potentially rising to hundreds of millions by 2030 (McShane, 2017). In particular, the drive is for longer-term power needs for applications such as monitoring: marine effects of climate change, ocean acidification, marine flora and fauna, and seismic activity (Joslin *et al.*, 2019). Other applications such as environmental monitoring during decommissioning of O&G platforms are also increasing, given the ever larger number of platforms that are approaching or reaching end of life (Jones *et al.*, 2019).

The fundamental triad for such applications is one of power, cost, and mobility. Thus, oceanography technology trends provide key opportunities for BST-baseline, providing power in situ at remote ocean locations via AUV docks,

reducing cost of missions by removing the need for manned vessels for retrieval, battery swapping, and data upload/download. A compact WEC can also enable mobility via mission flexibility. Overall, key opportunities relate to improved mission duration and flexibility, and improved communications and data exchange strategies. Other WEC developers, such as OPT and Fred Olsen, were also targeting such applications at the time.

In order to make the WEC more easily transportable (and thus more 'mobile'), a significant initial driver was the requirement to fit inside a standard shipping container, and to be handled by standard quayside equipment. This would facilitate both transportation and deployment. It was seen as a 'portable' WEC that could be deployed together with docks to provide an offshore network for AUVs to operate within, with more autonomy, flexibility, and mission duration.

Despite the potential benefits, after extended engagement with the NOC, this ocean science application was parked in favour of providing local power to subsea oil & gas equipment. This was primarily because BST-baseline was deemed to provide an excess of power for ocean researchers, who ideally required a smaller manually deployable WEC. In addition, AUV docking technology was not yet sufficiently developed and seen as a barrier, the market too small, and the opportunity too distant in terms of commercial outcomes.

Figure 38 - Concept of BST-baseline WEC inside standard shipping container envelope.

6.1.2 Numerical inputs and constraints

Based on the commercial context above, a numerical optimisation was run by Mocean (refer to Figure 25 in Chapter 4) with the following notable inputs:

- The fitness function simply relied on maximising AEP
- Bretschneider spectra to represent Central North Sea wave climate

- An overall size constraint to allow the WEC to fit into standard 40ft shipping container
- Box sections for the hulls

The shape generated via the genetic algorithm and its corresponding CAD realisation are shown in Figure 39 and Figure 40:

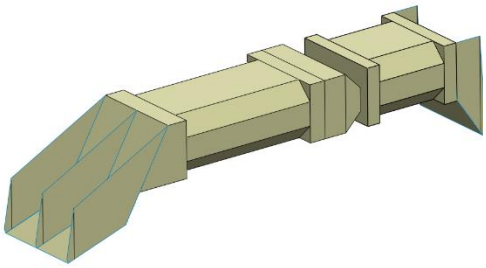

Figure 39 - Geometry generated using numerical model's genetic algorithm optimisation.

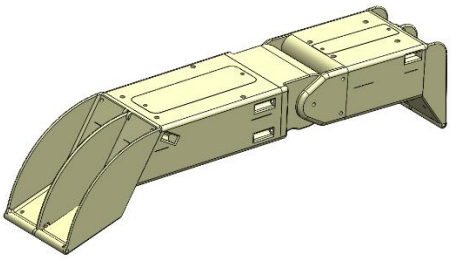

Figure 40 - CAD realisation of the non-instrumented geometry

The following section described the model build.

6.2 Model design and build

For this physical model, material selection was conducted based on previous learnings outlined in Chapter 4.

6.2.1 Choice of scale

The accommodation of the wavemaker generation envelope (of the Curved Tank) to the wave climate of the target site for the WEC dictates the (maximum) model scale. One could go smaller, though standards such as (IEC TS 62600-103, 2018) recommend using the largest feasible scale for the available facilities in order to reduce scaling errors (see Chapter 9 for energy matrix and facilities envelope comparison). A scale of 1:20 was therefore selected, also informed by this being a scale that Mocean have used in the past. In addition, it is relatively commonly occurring in published literature (as shown in Appendix C) and thus conducive for potential comparative assessments with other WECs. Notably, 1:20 was also the scale utilised in the Wave Energy Prize comparative WEC scoring (Dallman *et al.*, 2018).

In this case, the tank is a major driver for cost and ease of access, so it is preferable to let this guide scale as opposed to a particular model size driving facility selection. Note that, although the scale is the same as some previous models tested by Mocean, the latter were models representing larger machines and thus of larger size compared to the models tested during this research.

6.2.2 Build methodology and materials

The model was built for simplicity, cost minimisation, and fast turnaround. From Figure 41, yellow components are stereolithography (SLA) 3d-printed ABS material components, purple are anodised Aluminium alloy components. 'Lids' in each hull and nacelle are visible in Figure 43, covering a void that allows trim correction via appropriate placement of ballast. Ballast – in the form of dense Lead sheets or light closed-cell polystyrene cut-outs – can additionally be applied to the underside of each wave channel via bolts. Qualisys® motion tracking targets are included above each hull, and a 360° inductive non-contact rotary position sensor is placed within the nacelle. The latter was included for two reasons. It served as a complementary pitch rotation reading in case of Qualisys drop-outs, and would allow primary DoF measurement should the presence of Qualisys targets be deemed overly influential on model responses.

As a rule of thumb, the design included a mass allowance for ballast of at least 10% of the total scaled target mass, and to account for some uncertainty in the non-solid 3D printed parts density achieved in practice. Particular hydrodynamic amendments were also made compared to the numerically obtained geometry, such as: rounded edges all over with fillets, including the hull cross section; the addition of cylindrical bosses at front and rear edges of wave channels to smooth flow and mitigate vortex shedding. Personal communication[57] with Prof Stephen Salter confirmed the benefit of such an approach.

[57] Personal communication, date 2021-05-18: "David Evans told me that you start losing energy form vortex shedding when the wave amplitude is the same or bigger than the local radius of curvature. You might be able to see shedding by adding tufts of wool. There was a great improvement when we had soft corners to narrow tank ducks but we never had time for the wide tank ones."

The physical model was conceptualised to be as similar as possible in geometry to that generated by the genetic algorithm optimisation, shown in Figure 39. By observing Figure 39, it is likely that the forward (FWD) wave channel plays a more significant role in boosting power capture, and the rear (AFT) wave channel was somewhat 'sacrificed' by the optimisation as a result, due to overall length limit set. However, there are differences between it and its physical realisation, notably:

- Infinitely thin wave channel walls and central fin for hydrodynamic purposes (the numerical model then assigns these a thickness of 8mm to calculate mass characteristics);
- A gap between the nacelle and AFT hull.

Other differences between the two arise partly as a result of having to create a structurally sound model at a relatively small scale, partly due to considerations in the manufacturing, hydrodynamic drag and ballasting of the model, the inclusion of fixings, and other small changes in the evolution of the concept engineering. Note that the physical model is designed with removable fins at the FWD and AFT wave channels, in order to validate different configurations – e.g. Figure 39 shows no fin in the AFT wave channel while Figure 40 includes it. Figure 41 and Figure 42 show the instrumented model version, with a new nacelle and side flanges compared to Figure 43 (further details in Chapter 7).

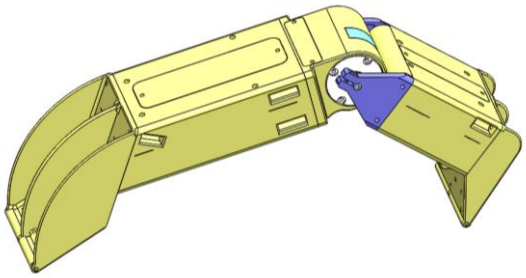

Figure 41 - Showing the FWD and AFT sections of BST-baseline during hinge flexing.

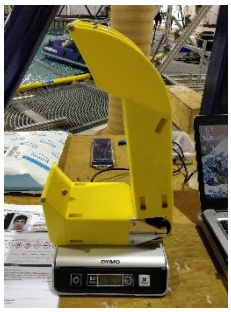

Figure 42 - Preliminary weighing of assembled model – full flex.

6.2.2.1 Model dimensions

The full-scale model is designed to fit in a 40ft open-top container, with approximate dimensional limits of: 11.5m length, 2.3m width, 2.3m height.

The theoretical total length of the 20th scale model is thus 577.85mm, and its actual CAD measured length is 576.54mm, with a beam of 115.00mm and overall height 126.81mm. The latter slightly exceeds full-scale height limits since the numerical model constraint was not strict enough in the overall height parameter. However, this is not critical as we are primarily concerned with comparing numerical and experimental results, so consistency between numerical and experimental models is the critical factor.

Space envelope parameters between numerical and physical models at different scales are compared here:

Property	**CAD 20th**	**CAD full scale**	**Numerical**	**Target (40ft container)**
Length [m]	0.57654	11.53	11.47	11.6
Height [m]	0.12681	2.53	2.56	2.3
Beam [m]	0.11500	2.30	2.28	2.3

Table 7 - Comparison of overall space envelope.

The various components of the model are shown in Figure 43 below, in exploded view. Materials are colour coded as follows:

Yellow – ABS (3D printed); Blue – Ballast (predominantly low density polystyrene blue); Purple – Anodised Al; Grey – stainless steel; White – Delrin plastic; Orange – Acetal copolymer

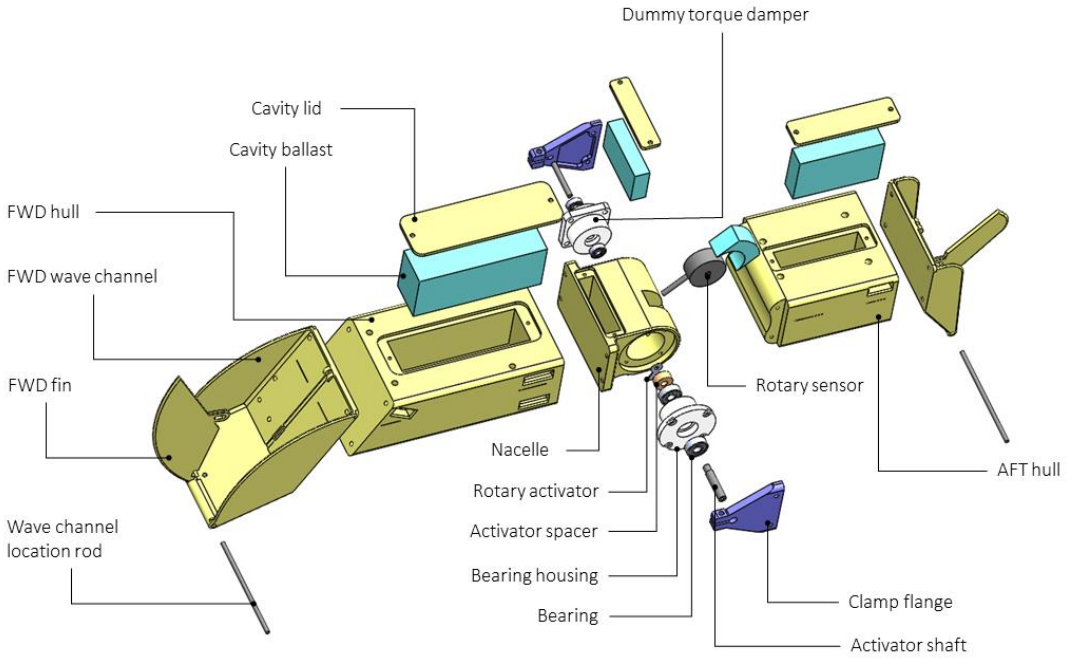

Figure 43 - Showing annotated exploded assembly view.

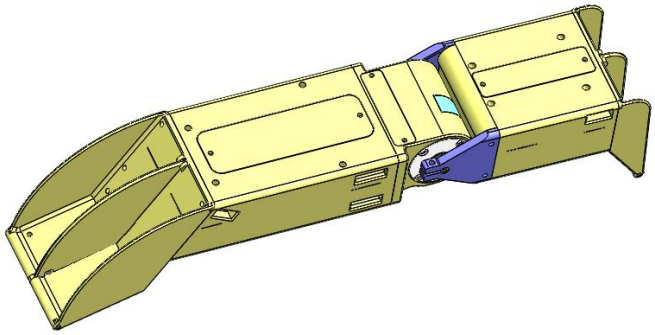

Figure 44 - Showing collapsed view of assembly, as built.

Wave channel fins and permitted angular flex range are outlined in Appendix F.

6.3 Detailed design

This section discusses additional design aspects of the model, including: detailed dimensional requirements, calculations used to estimate clamping forces between flanges and nacelle shafts, material density estimations; accounting for trimming requirements.

6.3.1 Dimensional reference table

A reference table between full-scale and model-scale parameters s provided:

Parameter	**Full-scale (numerical)**	**Model-scale**	**Unit**
Scale	1	20	-
Length	11.5	0.575	m
Width	2.3	0.115	m
Height	2.3	0.115*	m
Mass	14619	1.827	kg
Draft	1.99	0.995	m
Trim line (w.r.t hinge)	118	5.9	mm
Nacelle diameter	1.37	68.5	m
Max torque	50,000	0.3125	Nm
PTO damping	224,950	0.3144	Nms/rad

Table 8 - Reference values calculated from full-scale optimisation outputs.

The use of bearings at the hinge is particularly significant due to the model being Froude scaled w.r.t. the full-size WEC. Froude scaling implies that power scales

with the power of 3.5. Thus, a full-scale PTO rating of 10kW, would result in a scaled rated power of 10,000/(20^3.5) = 0.3W. The power dissipated due to friction should be kept orders of magnitude below this value, so minimising friction via the use of bearings becomes paramount.

Flange clamping forces, concept sketches, and a tolerance analysis for the rotary sensor interface are outlined in Appendix F.

6.3.2 Trimming and buoyancy

Undoubtedly, ballasting adjustments will be necessary in order to satisfy the target trim line. To this end, topside cavities are included in the FWD hull, Nacelle, and AFT hull. These can be easily accessed while the model is placed in a trimming tank, thus facilitating the process. The baseline scenario is for the cavities to be filled with low-density polystyrene blue foam, but lead cut-offs can also be added as necessary. In addition, lead sheets can be screwed to the underside of each wave channel to balance out the heavier hinge area. Being thin sheets, they should have minimal effects on model hydrodynamics.

6.3.2.1 Trimming calculations

Split line recesses are added on all sides of the model to provide a visual trim line reference in correspondence with the Mean Water Level (MWL), just above the hinge axis. Four such recesses on one side of the model are shown in Figure 45, in line with the target trim plane.

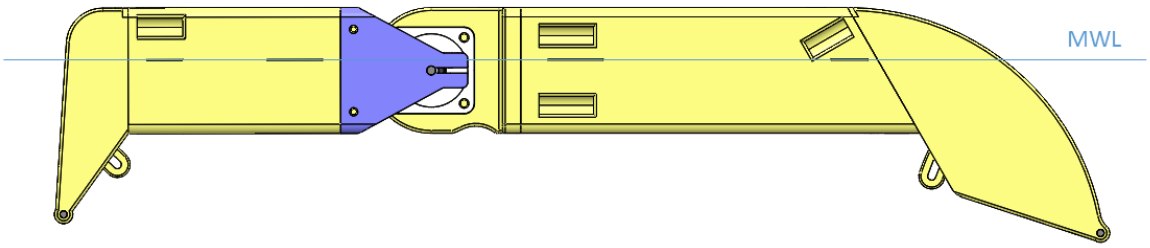

Figure 45 - Side view showing MWL recesses on each hull.

Each section (FWD and AFT) is to be trimmed independently. A ballast mass around 10% of the pre-ballasted mass is allowed for in the design. Ballast cavities are shown in Figure 43, while images of the trimming process are provided in Appendix F.

The following relationship is considered for trim line calculations:

$$V_{below} \times \rho_w = M_{below}$$

Where V_{below} is the volume of the model below the MWL (see Figure 47), ρ_w is the density of water. To achieve the desired trim, M_{below} should be equal to the total mass of the model, M_T.

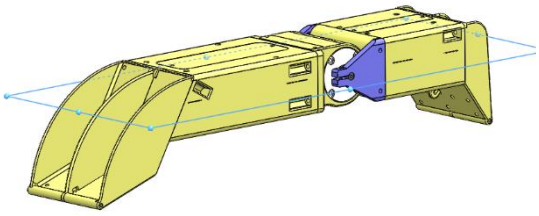

Figure 46 - Showing MWL plane.

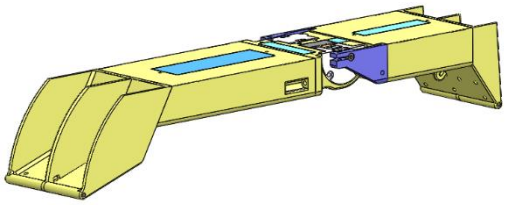

Figure 47 - Showing theoretical sub-surface volume.

The scaled target mass, M_{target}, is 1827g, as per Table 8. The non-ballasted mass without fixings or Qualisys targets (according to CAD model) is 1623g.

V_{below} = 2043217.6mm³, thus M_{below} = 2043.2g. This value is greater than 1623g so the trim line will be higher, as desired, since ballasting will be added to balance the model.

We note that this value is greater than M_{target} by around 216g. The differences between numerical and physical model can be accounted for by considering the main geometrical differences between the models and respective volumetric contributions:

- Octagonal hulls in numerical model
  - ΔFWD hull = 67600mm³; ΔFWD hull = 35200mm³
- "Infinitesimally" thin channel fins
  - ΔFWD hull = 59000mm³; ΔFWD hull = 2000mm³

A total volume difference of 181800mm³ multiplied by the approximate density of SLA material (1000kg/m³) results in a mass difference of 181.8g, close to the predicted value of 216g.

6.3.2.2 Trimming analysis in CAD

Achieving the correct trim of the model in practice is important, just as it is important to be able to predict where additional buoyancy or ballast may be

required, in order to adjust the main components of the model to permit its fixing/inclusion. This might be additional cavities in 3D-printed parts where lower density material needs to be placed, or appropriate fixing points to secure high density lead sheets for additional mass.

A methodology was developed in the SolidWorks CAD package, whereby the same assembly can be toggled between ‘Default’ (Figure 46) and ‘Buoyancy’ configurations (Figure 47). The assembly configuration is linked to individual part configurations. Individual part configurations are linked to a specific material property, which is whatever material in Default and ‘Water’ material in Buoyancy configuration.

In addition, the MWL is plan that is associated with an extruded cut operation in the ‘Buoyancy’ configuration, such that only the assembly sections below the MWL remain. Supressing and unsuppressing, mates, and material properties of components can be assigned to the assembly configuration. This methodology still involves some trial and error, but was found to be highly successful and accurate for both BST-baseline, giving confidence as an effective methodology for future physical model iterations. The implemented trimming procedure is discussed in Appendix N for the next geometry iteration, where the same process was followed for the present physical model.

6.3.3 Waterproofing

The use of 3D-printed parts was considered to improver logistical ease. Larger volume parts were printed in a non-solid build to limit their mass. This exposed them to additional water absorption in cases where cracks might form. The 3D-printed parts were thereby coated with a single layer of XTC-3D formulated epoxy resin (trade name: Smooth-On EpoxAxast/coat). This was found to be thin and easily applicable, and considered effective in rendering them watertight, in order to avoid the need for epoxy resin that had been utilised with some difficulty to waterproof the NWEC2 1:20 scale model (see also Section 6.3.3). Post curing time, the parts were fully submerged in a trimming tank for a period in the order of a few minutes in order to check for visible bubble formation and corresponding cracks or defects. None were identified, and although the immersion time was short, no mass difference was measured pre and post wetting. In hindsight, it

would have been beneficial to leave these parts submerged for 24 hours in order to fully flood them and reduce errors later on. This was done in the following model build (Chapter 8).

Assuming a maximum total fixings mass of around 100g, the total model mass should equate to approximately 1723g, compared to M_{below} = 2043g. The difference, corresponding to 18% of the model mass, allows for a 10% ballast mass 'headroom', and an additional extra 8% for potential water uptake. Finally, the Aluminium alloy flanges were black anodised, in order to protect them from adverse wetting effects, particularly in light of multiple contact points with stainless steel components such as rods and screws.

6.4 Instrumentation

A rotary sensor to measure hinge flex parameters, a torque damper to simulate PTO damping, and a Qualisys[58] optical motion tracking system are discussed in this section.

6.4.1 Rotary sensor

An induction (non-contact), submersible, rotary sensor (Product 1498 – Gill Sensors & Controls)[59] is included to provide in situ measurements of relative position, velocity and acceleration of the two hulls about the hinge. The recommended mounting arrangement is shown in Appendix F. The activator is secured onto the end a stainless steel shaft, with a plastic ABS spacer to provide a larger contact face and potential gluing surface in addition to the contact force provided by the end-screw (not shown in Figure 48). The sensor itself is inserted into the nacelle at a 51° angle from vertical, and includes a cable that is threaded through to the bottom surface of the nacelle via a dedicated cable slot. The sensor location within the nacelle is chosen based on a requirement for the cable to protrude in line with the model's long-axis. The sensor is mounted in a

[58] www.qualisys.com

[59] https://www.gillsc.com/products/position-sensors/1498-rotary-position-sensor/

rotated position to avoid clashing between the cable and the AFT hull at maximum flex.

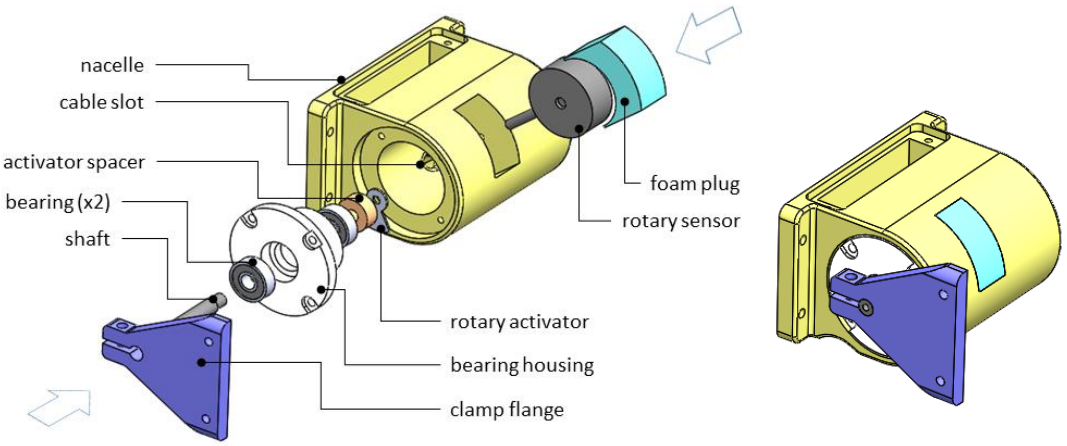

Figure 48 - Exploded (left) and collapsed (right) views of rotary sensor-activator layout.

The sensor is secured to the nacelle via 3x M3 screws, parallel to the hinge axis, inserted from the far side of the nacelle. A wire-cut foam block is used to cover the nacelle slot, provide buoyancy, and smooth the flow of water around the nacelle. Before the foam block is inserted, a hand-held 1mm thick spacer will be used to locate the activator w.r.t. the sensor's front surface.

The opposite side of the nacelle can accommodate a torque damper (see Appendix F), or a dummy torque damper with a bearing pair to simulate a free-hinge, as shown in Figure 49.

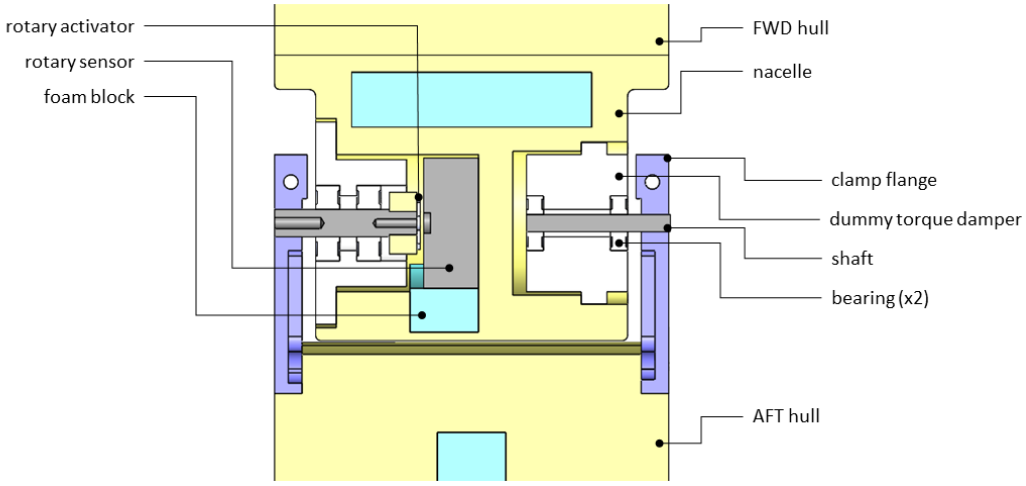

Figure 49 - Section view of hinge.

The potential of including a PTO damper was explored and later abandoned due to the unsuitability of available off-the-shelf dampers; relevant considerations are given in Appendix F.

6.4.2 Qualisys targets

6mmm diameter bores are included in the top of the hulls to accommodate carbon rods to which Qualisys reflective targets are mounted. The eight bores can be seen in Figure 43. The Qualisys system includes 4x cameras that optically track the targets as the WEC moves in the tank. Figure 50 below illustrates the Qualisys target layout.

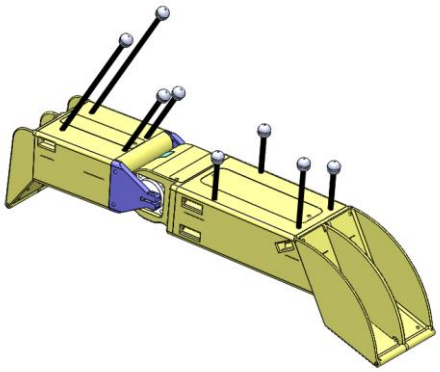

Figure 50 - Envisaged layout of 4 Qualisys targets per hull.

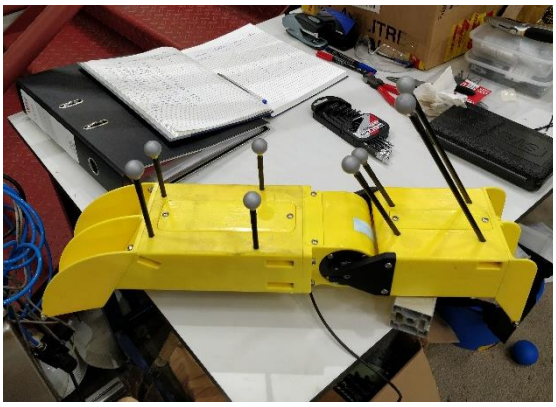

Figure 51 - As-built model showing 8 Qualisys targets.

6.5 Tank characterisation

The Curved Tank facility at the University of Edinburgh was used for this test campaign. It has a nominal water depth of 1.2m, and paddle depth of 0.7m. There are 48 wavemaker paddles across a 9m arc capable of generating uni- and multi-directional (+/- 30°) sea states. The tank manual quotes three nominal operating points (wave height, *H* / wave period, *T*): 0.220m / 1.0s; 0.075m / 2.0s; 0.060m / 0.5s; with an operating peak period around 1s.

Figure 52 relates to the Curved Wave Tank used throughout the tests. It shows the empirically derived operating envelope for regular waves. ‘CT specified’ points relate to nominal tank values, while ‘Interp’ is an interpolation curve of measured amplitude points along the stroke limit (with reflection effects

accounted for), and a steepness limited portion at frequencies greater than 1Hz. For further derivation details refer to Appendix F.

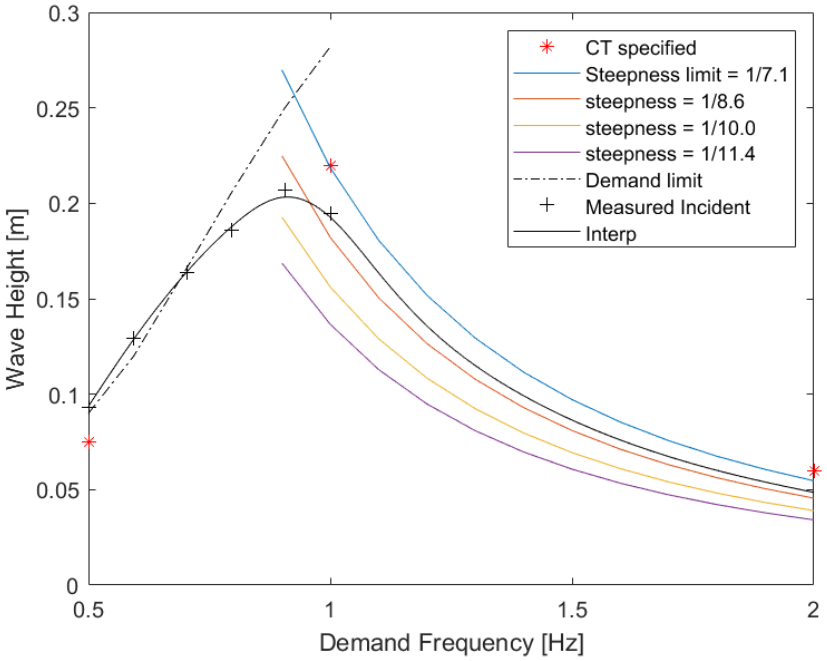

Figure 52 - Empirically derive Curved Tank operating envelope for regular wave generation.

As the wave field in the tank is not uniform, the wave profile is calibrated for an area of interest in the tank where the model is going to be located. Refer to Appendix J for sea calibrations.

6.6 Test plan

6.6.1 Tank set-up

Three wave gauges (WGs) were utilised for the BST-baseline tests in the CT. The wave gauges are made from two stainless steel rods, whose relative conductivity is inversely proportional to the immersed depth. These were found to offer satisfactory reflection analysis, with reflection coefficients greater than 0.1 detected primarily in very small amplitude waves.

Previous Mocean experience indicates that 3 WGs are sufficient, since a greater number does not appear to offer greater resolution. The main issue is the 3D nature of the tank. The Suryanto reflection analysis method (Suryanto, 2006) used assumes waves travel in two directions only (+*x* and –*x*), when in fact they

travel in all directions in the CT basin. Thus, if the WGs are in line with each other (along x direction), errors will likely remain even if 4 or 5 gauges are employed. An ideal scenario would involve deploying WGs on both sides of the model to enable a 3D reflection analysis – however, this is deemed out of scope. Other papers that discuss the use of the CT have used 3 WGs only without experiencing significant issues, e.g. (Lucas *et al.*, 2008).

The model will be placed in the tank with its rest (equilibrium) position approximating that shown in Figure 53. The WEC is shown as two orange rectangles, facing towards the curved paddle boundary.

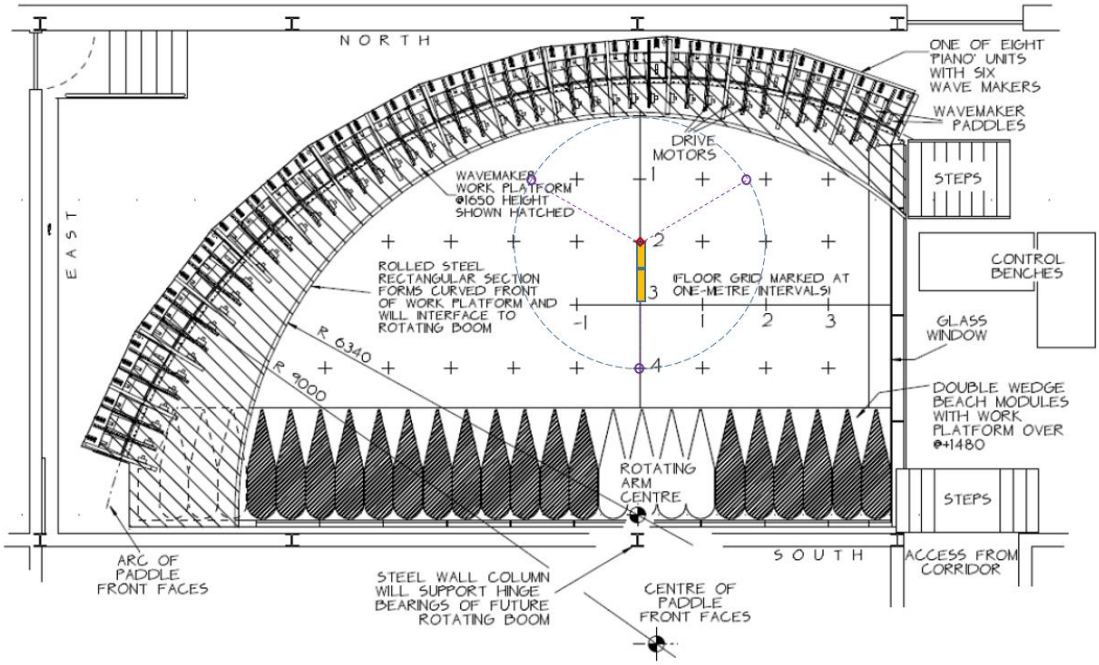

Figure 53 - Location of deployed model in Curved Tank. Red rhombus indicates mooring point. Purple circles indicate anchor locations. Blue circle corresponds to mooring circle with diameter 4m. (Waves travel north to south).

6.6.2 Sea states

Given limited available tank time, tests were conducted at transects though the frequency-amplitude space. In other words, the approach was that of sweeping across frequencies at a chosen amplitude, then sweeping in amplitude at a chosen frequency.

Regular wave sweeps were carried out at three constant steepness (height, H / wavelength, λ) values: 1/60, 1/180, 1/120. Running sweeps at constant steepness removes linearity changes by keeping the wave geometry constant.

Three values were chosen to give an indication of nonlinear wave effects and a trend to be captured. The values were selected based on previous wave channel tests (to enable direct comparisons) and on the wave climate steepness mode (1/53 for the North Sea location of interest). 1/60 steepness is estimated to be within the tank's capability range, but higher steepness values are not tested to avoid potential wave breaking and splashing effects.

Each sweep contained 20 sea states at frequencies between 0.53Hz and 2.00Hz. The peak response frequency at model scale was predicted to occur around 0.94Hz. The amplitude sweep was therefore carried out at this frequency, with a maximum demand amplitude of 36mm (non depth-corrected). The overall maximum depth corrected demand amplitude in the 1/60 sweep was 41.8mm at model scale (1.67m full scale wave height). Amplitude depth correction was applied, albeit minor.

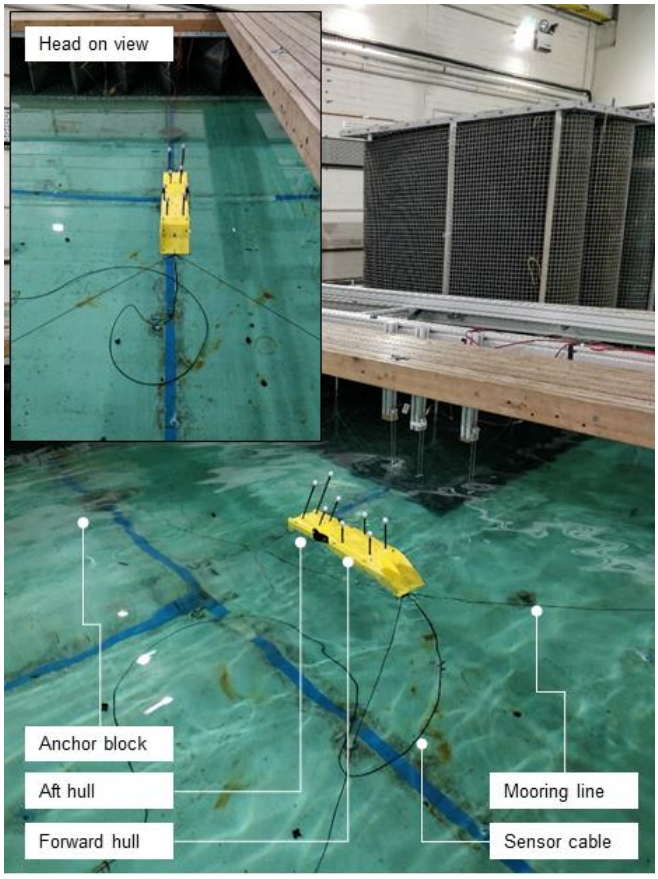

Figure 54 - Showing moored model deployed in the Curved Tank. Qualisys motion tracking targets are visible above each hull. Waves travel from the bottom right, and from the bottom in the inset image.

6.6.3 Mooring system

A generic station keeping system was used, since mooring behaviour is not an integral part of the device's hydrodynamic motion and energy conversion scheme (Cameron McNatt and Retzler, 2019). It consisted of three 2.1m length lines, equi-spaced at 120° around a mooring circle of 4m diameter.

Two lines extended in front of the model, each at 60° to the incident wave direction, and one line extended behind the model in line with incident waves (see Figure 53). Each line was anchored via simple gravity bases (concrete block with steel rings). The lines attach to the model via independent karabiners, which clip to a stainless steel ring at the lower lip of the forward wave channel. The lines were highly compliant and some pretension was applied in order to shift the operating point towards the linear section of their characteristically S-shaped load-response curve. The calculated resonant period of the mooring system was 12.9s.

6.6.4 Measurement set-up

Measured variables (and associated sensors) included: incident waves (via 3 wave gauges); 6 DoF model motion (via 4 Qualisys motion capture cameras); relative pitch angle between the hulls, referred to as 'flex' (via rotary sensor).

The first wave gauge was approximately coincident with the model mooring points, and the other two spanned the space occupied by the model in the tank. Wave gauge calibration errors throughout testing were around 1.0% and never exceeded 2.0%. Though approximately neutrally buoyant, the sensor cable had non-zero rigidity and torsional stiffness which affected the static yaw of the model. However, the model realigned with oncoming waves once they started travelling towards it.

The data acquisition sampling frequency was 128Hz, and a trigger signal was set up in order to synchronise wave gauges and model motion data capture.

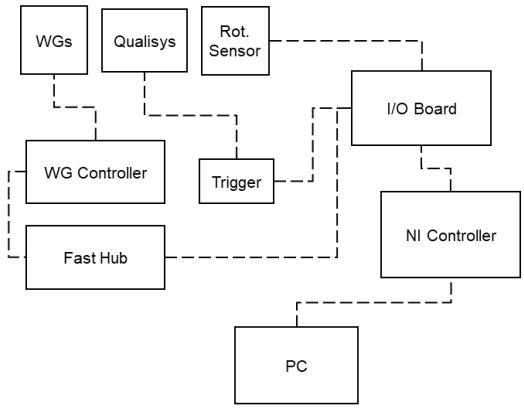

Figure 55 - Data measurement set-up.

- Electrical power supplies/sources not shown
- 2 channels for rotary sensor analogue
- I/O line to fast hub and Qualisys is the trigger line
- The data acquisition system (DAQ) is the combination of the I/O Board and the NI Controller
- Power supply is grounded
- NI Controller is grounded
- Sensor is grounded
- Controllers have plugs to mains

6.7 Experimental results

Regular wave sweeps allowed verification of response amplitude operators (RAOs) and a preliminary estimation of drag and nonlinear losses. A small number of long-crested irregular waves was also run to qualitatively observe the WEC's behaviour in more realistic seas – these are not discussed further.

Figure 56 shows the coordinate definition of the model; the power producing degree of freedom (DoF) being the relative pitch between forward and aft hulls. The overall mass of the model was 2,029g (including ballast and ~5% additional mass from water uptake during testing). It was 578mm long, 115mm wide, with maximum draft of 578mm below the mean water line (MWL). The hinge axis was nominally 5.9mm below the MWL (and increased to 7.5mm following trimming and minor water uptake).

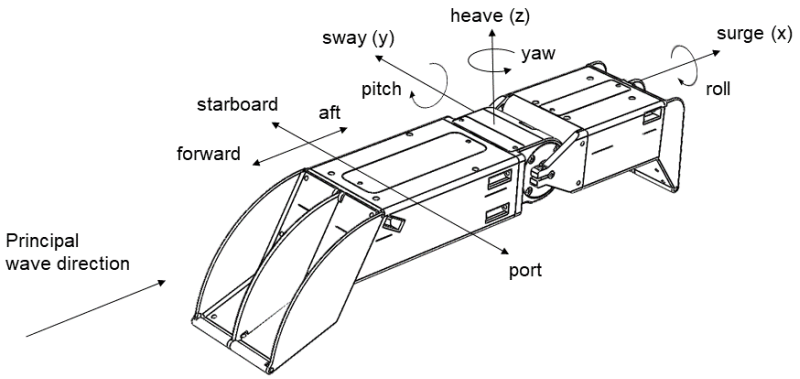

Figure 56 - Coordinate definition of Blue Star model; origin located at hinge (pitch) axis midpoint.

6.7.1 Reflection analysis

Being a finite body of water, the Curved Tank is subject to wave reflection effects. These were quantified ahead of model tests in order to estimate their effect on obtained RAOs, using the Suryanto method (Suryanto, 2006) and the (Mansard and Funke, 1980) embedded in WaveLab© software. Three in-line wave gauges were used, meaning that 3D effects were not captured. A reflection coefficient, *R*, is defined as the ratio of reflected wave amplitude over the incident wave amplitude. These 'open-tank' (i.e. model not present) incident wave amplitudes are then used to calculate RAOs, since the model's presence in the tank affects wave gauge signals during model response runs.

Reflection analysis yielded average values of *R* around 0.09, 0.10, and 0.13 for 1/60, 1/80, and 1/120 steepness sweeps. *R* values around 10% are deemed tolerable from a validation point of view. As expected, *R* values tended to increase at lower steepnesses given the lower amplitudes and thus greater noise sensitivity. Robust agreement was observed between the two analysis methods, and no significant difference was observed when comparing associated RAO plots.

Detailed reflection analysis is given in Appendix J.

6.7.2 Power producing degree of freedom response

The model's hydrodynamic response is characterised via RAO plots, where for a given DoF, the RAO represents the associated amplitude response, divided by the incident wave amplitude. The power producing DoF is flex (i.e. relative pitch

angle) and has units of degrees per meter (deg/m), though other RAOs are useful from a validation standpoint. Figure 57 shows that:

- Two peaks are detected. The first, larger peak around 3.5s full-scale period; the second, smaller peak around 5.5s.
- The peaks are higher at lower wave steepness, i.e. for waves that are more linear.
- There is a shift of the large shorter wavelength peak to wavelengths shorter still as the wave amplitude increases (i.e. as the steepness increases). This effect was also observed in testing carried out at École Centrale de Nantes (France) with a 1:10 scale *Blue Star* model.

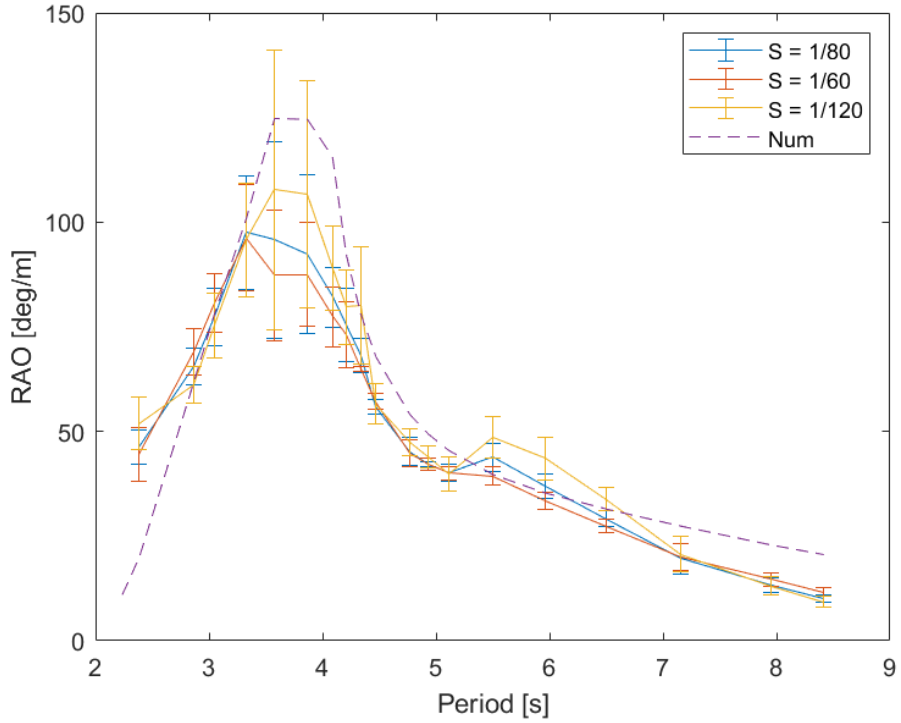

Figure 57 - Comparison between Flex RAOs obtained from rotary sensor readings at each steepness sweep, and numerical model predictions. Full-scale values shown.

Figure 57 also includes the numerically computed RAO. For a like-for-like comparison, the numerical model is updated with mass matrix values extracted from the CAD representation of the model as-built, including ballasting. A good fit can be observed between curves and the main tuning peak occurring just below 4s. Note also that excellent agreement was observed between Qualisys and rotary sensor flex measurements.

The numerical RAO includes approximated linear damping associated with the wave channels and viscous losses (Morrison's, i.e. fluid drag). It does not include PTO damping as the hinge is free during the experimental runs. There is no PTO with its nonlinear torque limit in this model, so the observed nonlinearity with wave amplitude is a consequence of the wave-body interaction alone.

The small peak at the longer wavelengths is very distinct in the tests but not in the numerical curve. Numerical results with no damping show this peak strongly so presumably this has implications for the assumed Morrison's damping coefficient, which is set to an initial value of 1.

Figure 57 shows error bars corresponding to the average *R* value for each sea state. There are significant, particularly in the case of 1/120 steepness where the error bar is approximately +/- 30% corresponding to +/- 34deg/m, around 3.58s full-scale period.

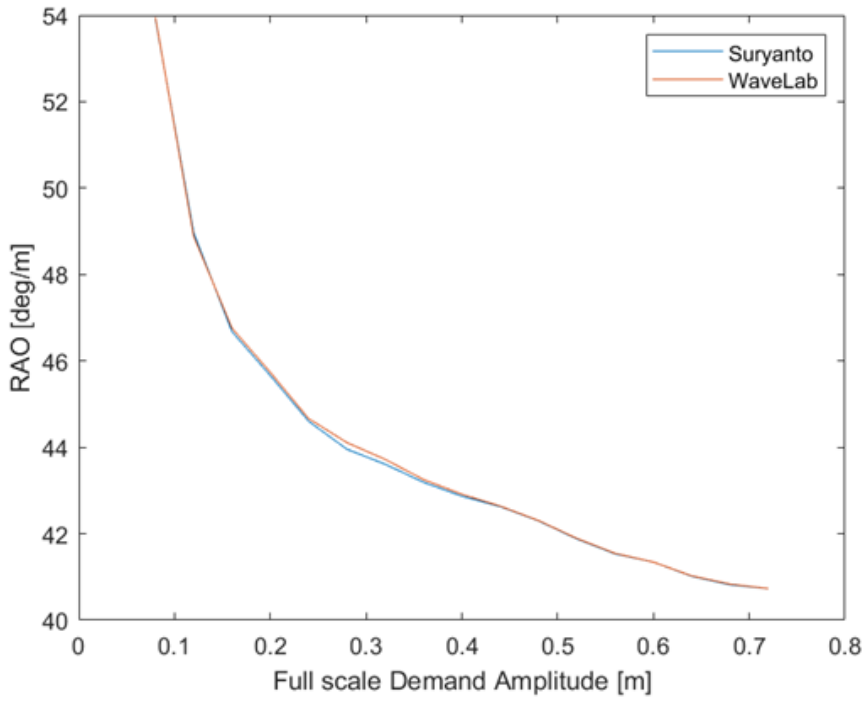

Figure 58 - Change in calculated Flex RAO at peak period over a range of demand amplitudes (based on R values from Suryanto and WaveLab methods).

Figure 58 shows RAO values dropping off as the demand amplitude (and the wave steepness) increase, for a set frequency of 0.94Hz at model scale, i.e. 4.77s period full-scale. This is due to waves becoming less linear as amplitude

increases, since the steepness is also increasing. For reference, full-scale demand amplitudes ran in the regular wave frequency sweeps were 0.30m, 0.44m, and 0.59m; pertaining to the flatter part of the curve in Figure 58.

6.7.3 All degree of freedom responses

The model responses in surge, sway, heave, roll, and yaw are compared, as well as pitch. Note that the pitch plot contains separate FWD and AFT hull responses. In all other cases, the response of the two hulls is identical since they are effectively behave as a single body.

Observed out of plane motions arise due to the centre of mass of FWD and AFT hulls not being aligned with the long axis of the model (see Figure 59). The inertia matrix exhibits cross terms, leading to non-zero values of yaw, roll and sway RAOs. In the case of yaw and sway, the experimental results are greater as the model is not perfectly aligned with incoming waves, as is instead the case in numerical simulations. Yaw (and to a lesser extend, roll) variation are affected by the electrical cable run-off path from model to tank floor. The cable moves most in the lowest frequency waves, and in the irregular wave sweeps. In these conditions, it very slightly rises off the tank floor (near the point where the cable initially meets the floor) as waves travel past the mooring attachment point and the forward hull pitches. Figure 60 again shows strong agreement between experimental and numerical hydrodynamic responses, based on the lowest steepness sea states.

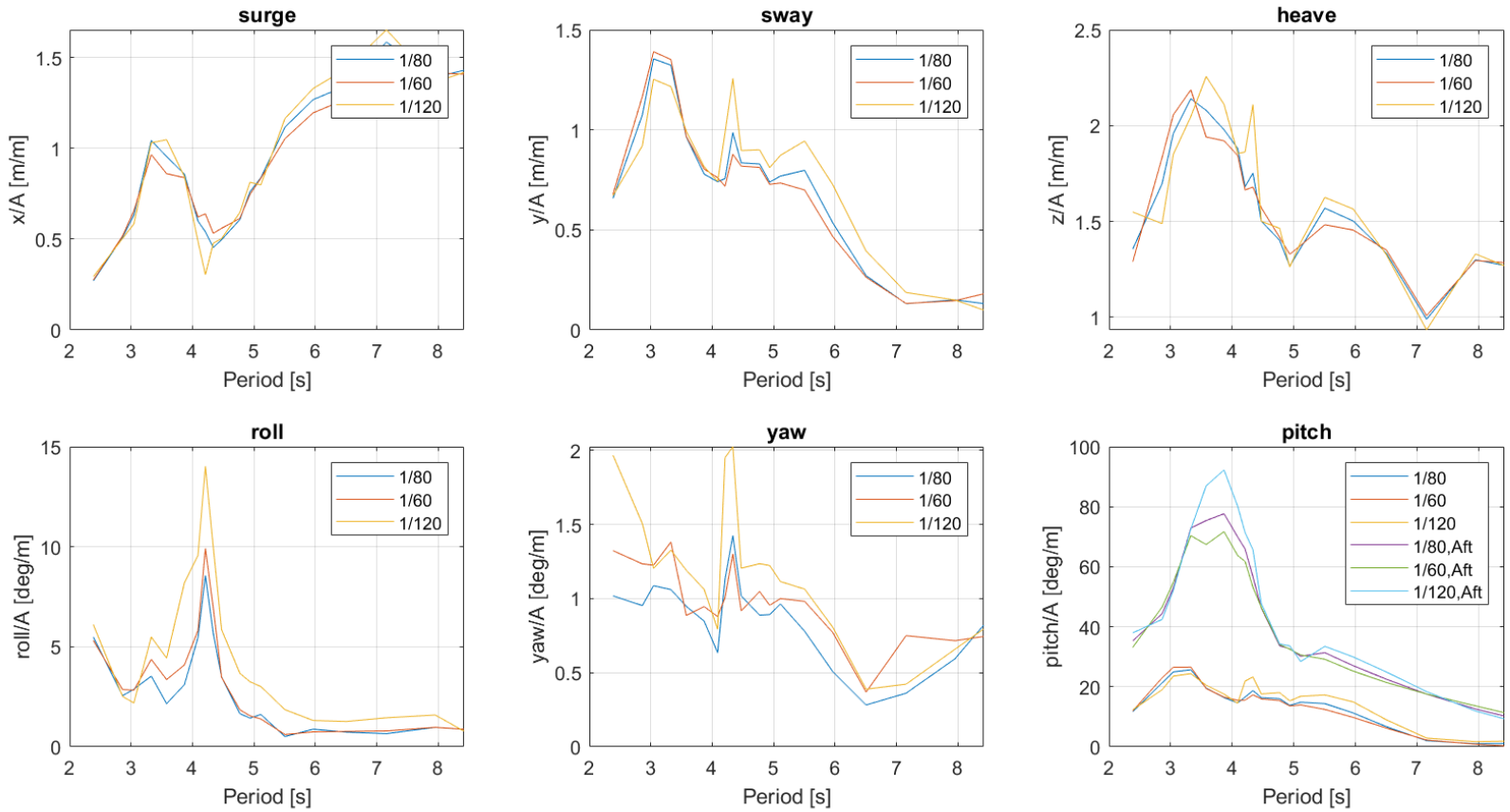

Figure 59 - Full-scale RAOs for all DoF's at each steepness, obtained from Qualisys data. 'A' refers to the wave incident amplitude.

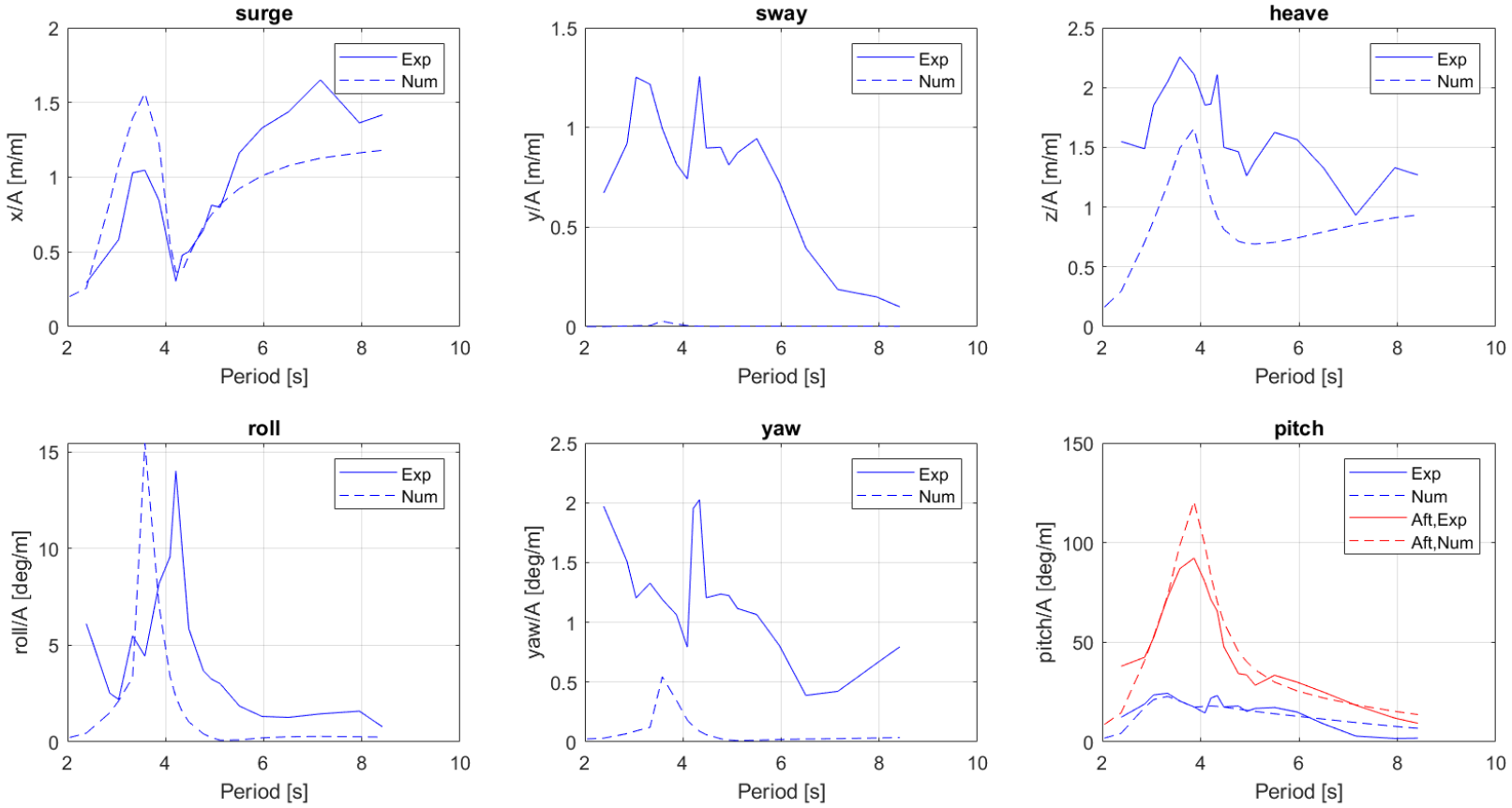

Figure 60 - Comparison of full-scale numerical and experimental RAOs for all DoFs at 1/120 steepness, obtained from QUalisys data. 'A' refers to the wave incident amplitude.

The flex RAO, as well as other DoF's allowed validation of the numerical model. Overall, there is good agreement between experimental and predicted RAOs, with lower steepness runs matching numerical results more closely, as expected from a wave linearity perspective. Particularly good matching is observed for the QOI of greatest relevance which is pitch, but also for surge, heave and roll. Sway and yaw match less closely, though experimental responses are minimal, and the close to zero nature of the numerical responses is due to the perfectly head-on wave assumption of the numerical model.

Robust agreement between rotary sensor and Qualisys data provides flexibility for future test set-ups. The two systems impact model mass and inertial properties differently. Qualisys targets raise the model's centre of mass (CoM), which increases the likelihood of roll instability that depends on the centre of buoyancy (CoB) being located vertically below the CoM. On the other hand, the sensor cable can affect roll and yaw even if neutrally buoyant, though these effects were found to be negligible in this particular set of tests. If testing in irregular waves, particularly spread seas, Qualisys inclusion is worthwhile in order to capture motion responses beyond flex. Additional DoF's can offer insights on survivability (e.g. dynamic instabilities) and overall hydrodynamic efficiency. The presence of the additional cable may also become more relevant for such tests with more dynamic responses. Static trimming errors can occur with a smaller model that offers less surface are and locations for trim adjustment via ballasting or model design. In this campaign, a static roll trimming error of ~1.5° – observable by eye – had a ~1% effect on the peak pitch RAO value, and was thus negligible.

In the case of Mocean's *Blue Star*, the round of testing presented in this chapter has provided a valuable baseline on which to build model complexity, by providing confidence that robust data can be collected at 20th scale, with an easily accessible wave tank. By conversion stages (i.e. hydrodynamic-to-mechanical, and the damping of relative pitch via a model PTO) in future tests, the idea is to shortcut towards assessing overall model performance via a *design* model that does not necessarily require larger scale or larger tanks; or at least delaying this need until performance predictions are deemed sufficiently high, and readiness becomes the driver for further testing.

Chapter 7. Model PTO

This chapter describes an advancement in physical model capability via model PTO design, build, and characterisation. The model PTO is to be included in the next iteration of the Blue Star WEC (see Chapter 8), and – ideally – designed as part of a modular nacelle that can be used with future geometry iterations. Starting from performance requirements, a suitable motor is selected to act as a PTO damper. The surrounding nacelle structure is designed, built, and the new motorised hinge is dry-tested to characterise damping and torque performance. It is then integrated with the rest of the physical model ahead of subsequent wet tests. More broadly, this effort represents the first step towards an "all-in-one" 20th scale model, having more of the WEC's major sub-systems represented and usable for validation, performance, and survivability testing in reasonably small wave tanks. Key elements such as friction behaviour and space constraints are addressed.

Chapter contributions

The following are acknowledged for their valued inputs to the work presented in this chapter: Chris Retzler of Mocean Energy for advice in set-up of the motor calibration and dry testing; Angus Spray and Iain Gold at the University of Edinburgh electrical workshop for their assistance in wiring the PTO motor within the nacelle; Charlie Westerling of Sequentec for setting up the motor controller; Martyn Lennon of FloWave for machining several physical model parts.

7.1 Performance requirements

The first element to consider is the desired torque-velocity relationship. Considering the comparison of experimental and numerical results for validation purposes, a linear relationship is appropriate being the one that the frequency-domain (FD) numerical model can correctly represent – e.g. as found in (Ersdal and Moe, 2013). A simple, linear relationship therefore suits the goal of implementing physical testing as part of a fast-turnaround validation. In addition, Mocean WECs display inherently broad bandwidths due to their geometries, even with simple linear control strategies. At this particular point in time, more advanced control strategies had not been thoroughly assessed. A later reinforcement learning study suggested that,

although scope for improvement exists, geometry itself goes a long way towards enabling optimum performance across a broad wave frequency range. Thus, the ideal regime for these tests is a linear damping strategy with a constant damping coefficient (i.e. a constant gradient in the plot of applied torque vs velocity). Nonetheless, it would be ideal to include a model PTO that has the potential to embody more advanced non-linear control strategies should these become more attractive in the future. For example, reinforcement learning strategies that rely on reactive control would require a model PTO that can supply power (or torque) to the prime mover of the WEC as well as damping it. It would also make the model PTO more representative of a real PTO system.

The target values for torque limit and PTO damping are obtained from the spectral-domain (SD) geometry optimisation output. Model-scale equivalents are shown in Table 9.

	Froude scales as s^ X	Full-scale	Model-scale (20^{th})
Torque limit (Tlim)	X = 4	65 kNm	0.406 Nm
PTO damping (Dpto)	X = 4.5	0.221 MNms/rad	0.309 Nms/rad

Table 9 - Target model PTO parameters for 20th scale model.

Additional key considerations include:

- Size constraints for the inclusion of a torque sensor and for the choice of motor/actuator
- Minimising friction
- Avoiding gearbox and backlash (as per Chapter 4 lessons learned)
- Minimising cost

The first two points above are explored in the following section.

7.2 Design

7.2.1 Choice of PTO damper

Referring back to Chapter 4 Section 4.3.3, which reviewed key take-aways from previous Mocean physical testing campaigns, the following guidelines are noted:

- Use of a gearbox should be avoided due to high levels of uncertainty introduced – this should be prioritised ahead of achieving the exact torque limit requirements;
- It is desirable to include an encoder in the motor and incorporate this in the controller set-up;
- Ideally, include a torque sensor in the nacelle subassembly to measure applied torque directly, though weigh this against a higher number of powertrain components (see following point);
- Minimising the number of powertrain components is desirable – to reduce wind-up, compliance, and cumulative friction;
- Size the model based on the hinge spatial and torque constraints (not possible in this case – geometry already existed).

Initially, a magnetic particle brake (MPB) was considered for the damping. An MPB is a non-contact brake where torque resistance is provided by supplying a current to energise magnetic particles[60]. This was encountered while reviewing Wilkinson's work on the Aquamarine Oyster concept and associated physical testing (Wilkinson *et al.*, 2015, 2017). Although Wilkinson aimed to apply a constant 'Coulomb' damping, the MPB displayed attractive cost and torque capabilities for a given size. However, controllability is relatively easy for constant damping regimes but becomes trickier for a linear regime, due to hysteresis and other factors. Though theoretically feasible, this presented an unknown. A detailed damper review can be found in (Wilkinson *et al.*, 2015) and is re-proposed here with an additional 'servomotor' line added based on the Kollmorgen AKM servomotor range[61]:

Damper type	Torque range (Nm)	Ease of control	Relative size	Relative cost
Braking clutch	Unknown - 1.3	Low	Low	Low
Disc brakes	0 - ∞	Medium	Medium	Low
Hydraulic (water)	Unknown	Low	Medium	Medium

[60] See associated papers for more detailed MPB working principles.

[61] https://www.kollmorgen.com/en-us/products/catalogs/kollmorgen-akm-servomotor-selection-guide/

Hydraulic (oil)	1.7 - 10.4	High	Medium	High
Linear motor	0.7 - 5.2	Medium	Medium	High
Magnetic particle brake	0.07 - 3.95	High	Medium	Medium
Electrical hysteresis brake	0.01 - 2.3	High	Medium/High	Medium/High
Servomotor	0.18 – 2.88[62]	High	Medium/High	High

Table 10 - Damper selection, adapted from (Wilkinson *et al.*, 2015).

Rotationality is a key requirement as well, which essentially rules out the top five options. MPBs and EHBs are more compact than the servomotor and also have lower unit cost. However, they both suffer from more significant hysteresis effects that complicate control, and are both heavier. Backlash may be another notable issue. The torque-current curves of candidate MPB (Placid Industries B6) and EHB (Magnetic Technologies Ltd EB-50M-2DS) options are shown below.

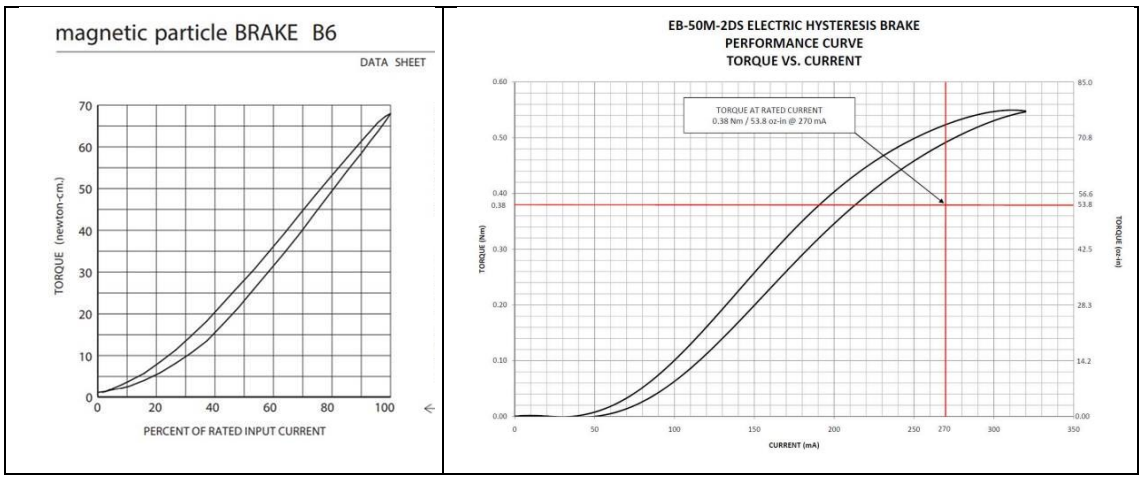

Table 11 - Torque-current plots for MPB (left) and EHB (right) damper options.

Through personal communication[63] with L. Wilkinson, it was disinterred that the MPB had not been trialled with a linear control strategy. To get around the hysteresis issue, Wilkinson implemented a control strategy in LabView that checked whether the voltage was being increased or decreased relative to the last

[62] NB: values of torque range are dependent on model and size of each damper, but here serve the purpose of enabling a comparison to be made across damper types for a given size. Servomotor data is added by comparing similar diameter Placid Industries MPBs and Kollmorgen AKM servomotors. MPB model B35 (85mm D), and servomotor model AKM33 (70 by 70mm). https://placidindustries.com/products/brakes/magnetic-particle-brakes/

[63] Personal communications in spring-summer 2020.

applied voltage, in order to decide what torque constant to apply (i.e. higher curve if voltage increasing, lower curve if decreasing). He also found the MPB to be quite fast to respond to changes in voltage, so would not exclude its suitability to a linear control strategy implementation. However, the degree of unknown, the potential controllability complications, and the size and backlash issues due to the need for a coupling meant that, ultimately, a servomotor was selected as model PTO.

Model PTO	Servomotor	MPB	EHB
Manufacturer	Kollmorgen	Placid Industries	Magnetic Technologies[64]
Model	AKM 11B	B6	EB-50M-2DS
Mass (g)	350	700	760
Cont. Torque (Nm)	0.19	n/a	0.38
Max stall Torque (Nm)	0.62	0.68	0.54
Diameter (mm)	46 (equivalent)	62.74	60
Length (mm) –excl. shaft	79	34.8	42.8
Rotor inertia (kg cm2)	0.017	0.026	0.167
Friction (Nm)	0.0011	None	n/a
Controllability	High	Medium	Medium
Encoder included?	Yes	No	No
Cost	£306 + £585 +£178*	£257 + shipping	£366

Table 12 - Summarising key characteristics of considered model PTOs.

*£585 for servo-drive controller, £178 for cables.

Once converged to using a servo-controlled motor as a brake, the candidates in Table 12 were identified and evaluated. An additional comparison table for different kinds of available motors is presented in Appendix G. Ultimately, the Kollmorgen AKM11 motor is chosen for the following reasons when compared to the other motor candidates:

[64] https://www.magnetictech.com/current-controlled-electric-hysteresis-brakes-with-double-ended-shafts/

- Positive experience in using AKM motors during previous Mocean test campaigns, albeit with larger models;
- Aerotech motor has a housing that is excessively long;
- Aeroflex Labs motor has the lowest stall torque, as well as a limit of +/- 25deg rotation (50deg overall), which makes it unsuitable given expected hinge rotations;
- AKM weighs only 350g making it the most lightweight – important for model trimming.

7.2.2 Minimising friction

To recap, the aim is to implement a model PTO in a 20th scale model that allows the user to apply "arbitrarily defined forces between the wave-driven and the reactive body-elements of the WEC" (Payne, 2008). In our specific case, there are wave-driven forces that cause the two WEC hulls to pitch relative to one another. The resistive body-elements of the WEC consist in the electromechanical generator, which damps this flex motion at the hinge.

In addition, the aim is to apply a damping force that “can be varied in function of an applied current or voltage that can be adjusted by the user” (Payne, 2008). Two factors complicate this objective: friction and the lack of a torque sensor in the nacelle, due to insufficient space being present in order to accommodate it. As a result, one has to infer torque from motor current, meaning that the current vs torque relationship needs to be predictable and reliable. The more friction is present, the less likely that this will be the case.

If there is no friction, the motor is only reacting against the rotating motion of the shaft induced by the waves (i.e. the relative pitch – flex – of the two hulls). If additional friction is present, there will already be a source of resistance to the flex motion. Thus, the same current setting on the motor will be producing a greater amount of overall damping than desired. Thus, in turn, adjusting the current (i.e. gain) of the motor will not guarantee that the torque ‘seen’ by the shaft will be the desired value.

The motor and its various connections need to be protected from water, and are thus housed within a nacelle with wet-proof cable glands allowing motor cables to

pass through, and a lip seal ensuring no water ingress at the motor shaft. The lip seal is predicted to contribute the most friction in the set-up. An alternative, as used by Wilkinson, is to avoid the use of a lip seal and utilise magnetic couplings instead. These can transmit torque across a gap but suffer from backlash in the region of a few degrees, and thus typically require over-specification of the coupling to minimise it, adding expense, volume, and mass.

To some extent, the above effect can be accounted for by pre-calibrating the motor and shaft seal arrangement, but this is not straightforward because:

- Friction is non-linear and uncontrolled
- Friction cannot be considered a pure damping term in the equation of motion (hinge torque) – it typically has a spring term as well
- Friction does not scale well – it depends on a range of factors, including: surface finish; fluid film thickness; fluid cleanliness; shaft run out; housing to seal co-axiality; vibration; shaft loading and unloading; changes in pressure; changes in speed; changes in temperature; wear; changes in shaft direction etc.
- Friction will alter the dynamics of the model when it is in the water – the torque from the wave excitation will need to overcome the friction at the hinge. For example, there will always be a glitch around zero velocity as the machine tries to move.

Although it cannot be fully mitigated, being able to measure friction *in situ* allows accurate torque measurements to be made during tests. Unfortunately, the model is relatively narrow at only 120mm width, meaning insufficient space exists for an off-the-shelf torque sensor to be included in the power train. Thus, a different methodology is sought in order to account for friction, as described in Section 7.3 and 7.4.

7.2.3 Inclusion in existing physical model and modularity

The idea is to swap out the old passive nacelle, composed primarily of a large 3D printed part, and housing and angular sensor, which a more complex active nacelle. The latter is made from a combination of anodised aluminium parts

(purple), 3D-printed components (yellow), and some polystyrene blue blocks (blue) for additional buoyancy.

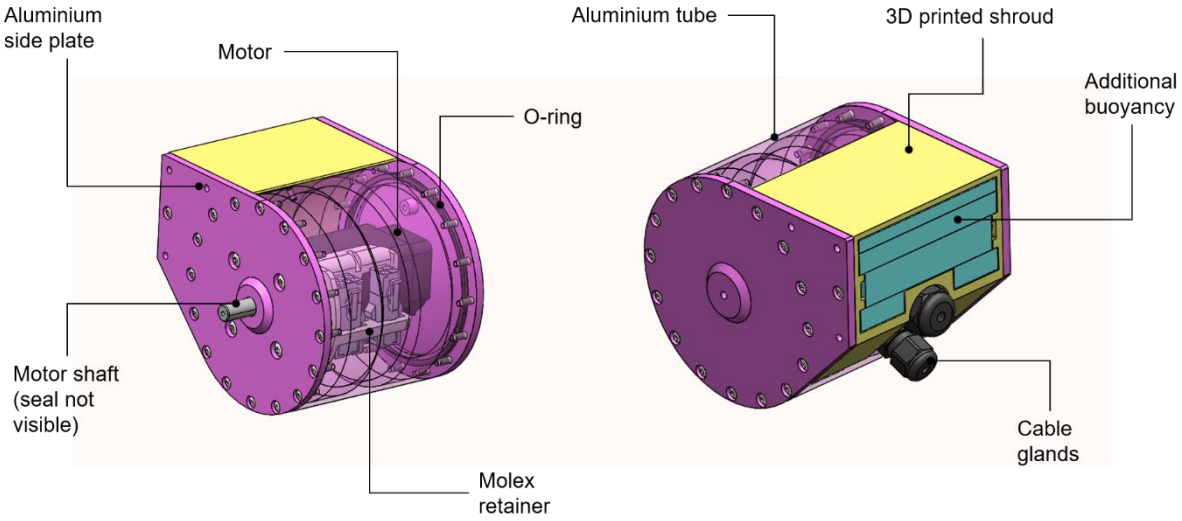

Figure 61 - CAD diagrams of nacelle subassembly (cables not shown).

7.3 Build

The overall hinge build presented several challenges from a spatial constraint point of view within the nacelle. It was assembled with assistance from Iain Gold and Angus Spray from the Edinburgh University School of Engineering's Electrical Workshop. Build images are available in Appendix G.

7.3.1 Nacelle

Available space within the nacelle was extremely limited. The need to safely and reliably connect the motor leads to the main cables needed a controlled connection. This was achieved via two pairs of Molex connectors. The only available reference surface to hold these in position was the motor body, so a custom Molex retainer was designed in CAD and 3D printed in PET-G material. Once the interface was checked and deemed satisfactory, it was held in position via small cable ties. A potential issue was the heating up of the motor body, with the risk of causing damage to the connectors and the Molex retainer. As such, the retainer was submerged in 100°C boiling water to check whether any damage or warping occurred. None did, and the design was found to work well.

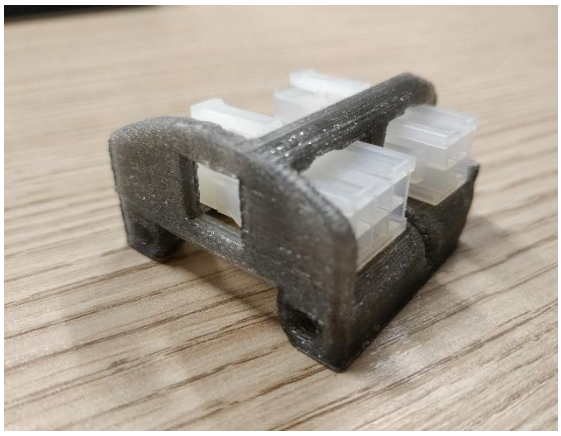

Figure 62 - Showing custom printed part (dark grey) and Molex connectors (light grey).

Figure 63 - A dedicated cable tie groove is visible between the Molex connectors.

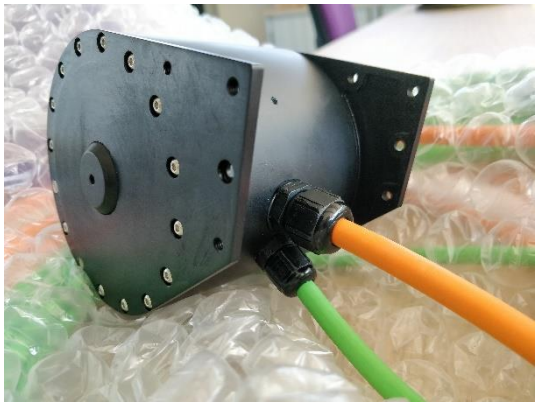

Figure 64 - Assembled nacelle, showing power (orange) and feedback (green) cable.

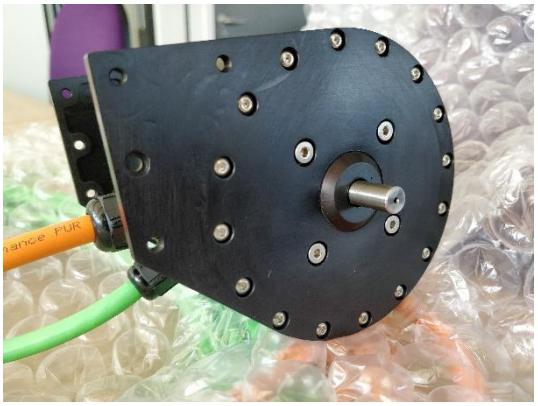

Figure 65 - Showing the shaft end of the nacelle, with the motor shaft protruding through a lip seal.

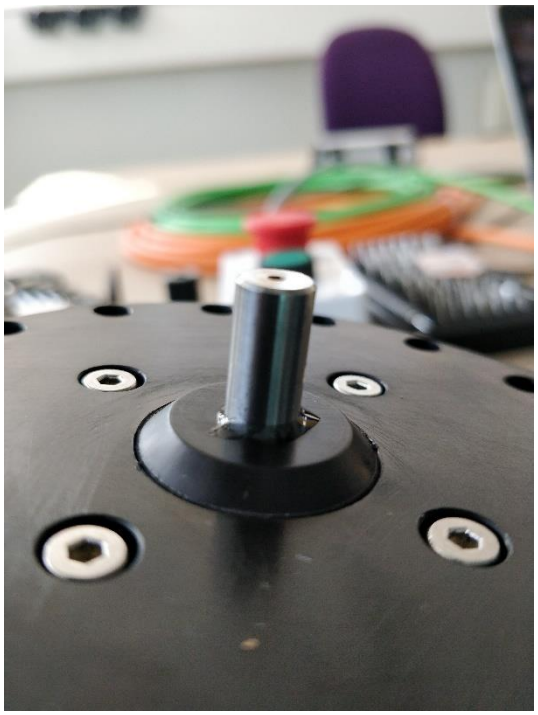

Figure 66 -Showing a meniscus of water around the motor shaft. Water is dropped around the seal, and the shaft rotated to check for water ingress. (lip seal not visible).

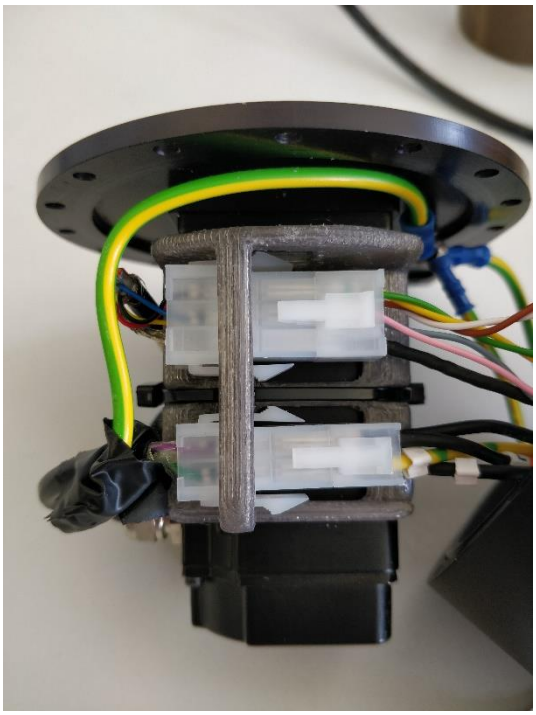

Figure 67 - Showing the Molex retainer part mounted to the motor body, which is in turn bolted to a mounting plate (top).

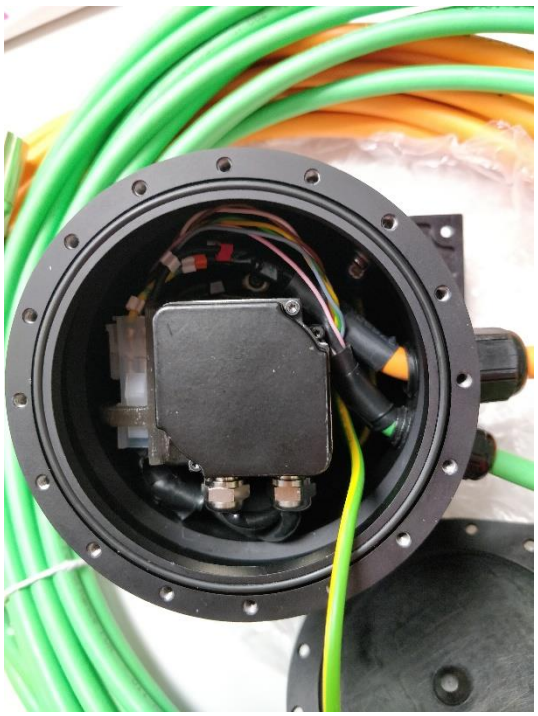

Figure 68 - Showing the back end of the motor and cable routing within the nacelle tube. O-ring also visible around the outside.

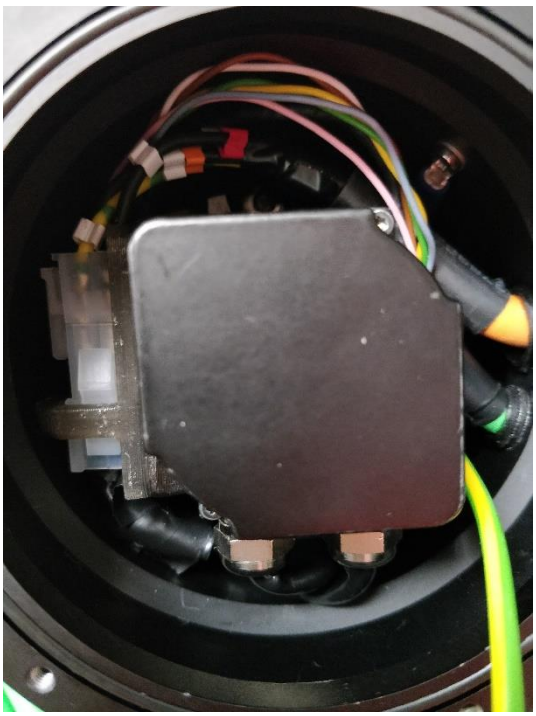

Figure 69 - A zoomed in view, showing the many cables and tight routing between motor and nacelle tube.

For earthing purposes, three tapped holes were made in the nacelle tube and each of the two end plates, with a screw into each, each screw retaining a solder tag. One tag (on motor plate) was chosen as the star earthing point, with all tags and motor earth wire connected to this star tag. By fully earthing the case, earthing regulatory requirements are satisfied in case of a live wire contacting the case (i.e. metal nacelle body).

The motor can be allowed to go to 100°C, but there is a danger that the 3D printed Molex mounting that is in contact with the motor body degrades at such high temperature. Thus, the PET-G part and cable tie are tested by immersion in boiling water, which is then allowed to cool. They were found to retain their shape and structural strength. The rotary (lip) seal utilised between motor shaft and mounting plate is Model 8X14X4_SC_VI from Simplybearings Ltd. More specifically, it is a 8x14x4mm SC/R21 Single Lip Viton Rubber metric rotary shaft oil seal. A temperature gauge was considered for inclusion in the nacelle, but abandoned due to both time and spatial constraints. This would sense energy dissipated as heat and provide indication of the temperature of the motor being close to or exceeding the maximum threshold set by the manufacturer. This would be a helpful input to the operator in order to allow the motor to cool off between longer wave runs featuring relatively high torques, and to gauge how much the default thermal safety settings can be manually overridden to reach desired torque during a set sea duration.

7.4 Proposed approach

Note that a similar motorised nacelle was previously characterised by Mocean in a model of roughly double the size of the present 20th scale embodiment. The past model is therefore termed “10th scale model”. For the 10th scale model, friction was of the order of 1% of typical torques. For this new 20th model, it will very likely be more, so following a similar procedure to characterise it will certainly be worthwhile.

The same material (Viton) and geometric arrangement of shaft seal is proposed for the 20th scale model. Assuming similar relationships between nominal and measured frictional values, the friction that the new model will experience can be

forecast to an extent. From Table 13, this is estimated as roughly 5% of the continuous motor torque capability.

Scale / Kollmorgen motor model	10th scale / AKM 43E	20th scale / AKM 11B
Nominal static friction [Nm]	0.109 (=0.038+0.071)	0.0221 (=0.0021+0.021)
Nominal dynamic friction [Nm/k_rpm]	0.017	0.0005
Measured static friction [Nm]	0.0419	0.00849*
Measured dynamic friction [Nm/k_rpm]	0.0041	0.00012*
Measured/nominal static ratio	38.4%	38.4%*
Measured/nominal dynamic ratio	24.1%	24.1%*
Continuous motor torque @100°C [Nm]	4.7	0.183
Static friction as % of cont. torque	0.9%	4.6%*

Table 13 - Parameter comparison at different testing scales.
*NB: ** indicates estimated value

From an observation of Table 13, friction is certainly not ideal in relative magnitude, but also should not be a fundamental barrier to the 20th scale model's utility. Ideally, the aim is to have complete control of the damping torque. The more linear the damping coefficient is with respect to rotational speed, the less concern associated with measuring the torque in situ (i.e. it is safe to assume that for a given velocity, there is a given damping coefficient and therefore torque).

Recall that when calculating power, one is multiplying how much the model actually moves with the current that is measured (torque proxy). This is then corrected by adding friction contributions that sum up to an estimation of the torque actually experienced by the model ($T_{effective}$). This will yield approximately the correct power, but it will not give the "correct" dynamics – i.e. it will yield the dynamics (v, in the equation below) including friction. In a full-scale device there will also be some friction, but typically with a lower contribution to overall torque.

$$P_{effective} = T_{effective} * v$$

When calculating power, one can no longer write a frequency-domain equation of motion, because this would be dependent on a linear solution, whereas there are nonlinear relationships at work. Instead, a time-domain equation of motion is required with a step function for the static friction.

When doing the power calculation: a time-domain equation of motion is written with all the contributing forces in order to get an effective torque, which is then multiplied by the measured velocity. The effective power removed from the waves is approximately the power absorbed by the model PTO and the power lost to friction. This applies to the torques as well, such that:

$$T_{effective} = T_{motor} + T_{friction}$$

Thus, we can also write:

$$P_{effective} = \left(T_{motor} + T_{friction}\right) * v$$

The motor torque can be calculated as the motor damping coefficient multiplied by the angular velocity, or the measured current (I) from the motor times the torque constant (T_{const}):

$$T_{motor} = (D_{pto} * v) + (k_{pto} * \theta) = I * T_{const}$$

Where the PTO damping coefficient is a function of the user-adjusted gain, G (i.e. the motor current value) and the normalised damping coefficient (D_{norm}):

$$D_{pto} = G * D_{norm}$$

and similarly the PTO spring coefficient is also a function of the user-adjusted gain:

$$k_{pto} = G * k_{norm}$$

The friction torque is the combination of static and dynamic friction:

$$T_{friction} = (sign(v) * C_{friction}) + (D_{friction} * v)$$

To calculate the torque experienced at the hinge of the physical model ($T_{effective}$), the applied motor torque is corrected with a torque signal equal to the sign of the velocity times the static friction ($C_{friction}$) contribution + the value of the velocity (v) times the dynamic (i.e. viscous) friction ($D_{friction}$).

Since the dynamic friction is deemed negligible, we are ultimately left with:

$$T_{effective} = (G * (D_{norm} * v + k_{norm} * \theta) + (sig(v) * C_{friction})$$

Appendix G provides a more detailed derivation of the equations utilised.

7.4.1 Calibration aim

The objective is to pre-calibrate the motor in dry conditions, in order to ensure that torque values can be reliably inferred from current readings during wet tests. Ideally, a torque sensor would be included within the nacelle itself, but there is insufficient space to accommodate it. We therefore use a torque sensor mounted outside the nacelle to characterise its performance ahead of wet tests. It is particularly important to do this to quantify and account for friction behaviour within the hinge. Ultimately, we would like to derive a value of PTO damping per unit gain (i.e D_{norm}), and a torque constant (T_{const}). The former has units of Nms/rad and the latter of Nm/A. We would also like to derive the spring constant (k_{pto}; units Nm/rad) and compare it with the hydrodynamic spring of the model (set-up outlined in Appendix G).

The available torque sensor is a 2Nm rated Interface Force Measurements Ltd. contactless torque transducer, model T8-2Nm, Serial No. 132662, Output +/-5V. Nominally, it has a +/-0.05% non-repeatability error and a +/-0.25% combined error, as specified on its datasheet. A 0.25% error translates to a 0.005Nm error, i.e. 1.3% of the peak demand torque of 0.375Nm.

7.4.1.1 Static calibration

It is very difficult to calibrate a contactless sensor. We can, however, conduct some ‘sanity checks’. We can first check its reading at torques lower than the static friction threshold of the combined motor and lip seal, when the shafts will remain static. When the torque sensor axis is in the horizontal plane (Figure 70), and only the lever arm is bolted to the torque sensor shaft, the theoretical torque reading (Tx) should just equal the mass of the lever arm multiplied by the distance of its CoG from the sensor shaft axis. The various steps followed for the static calibration are outlined in Appendix G.

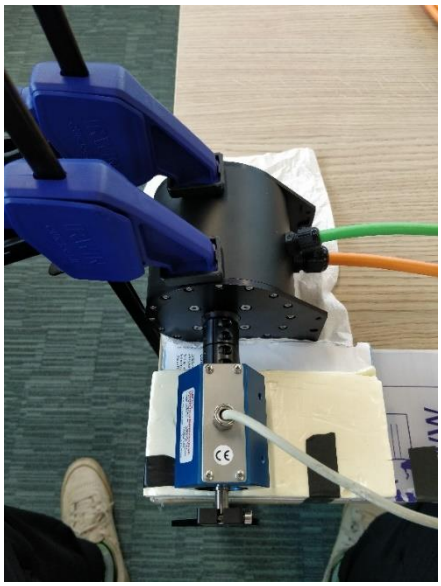

Figure 70 - Showing horizontal PTO 'train' set-up.

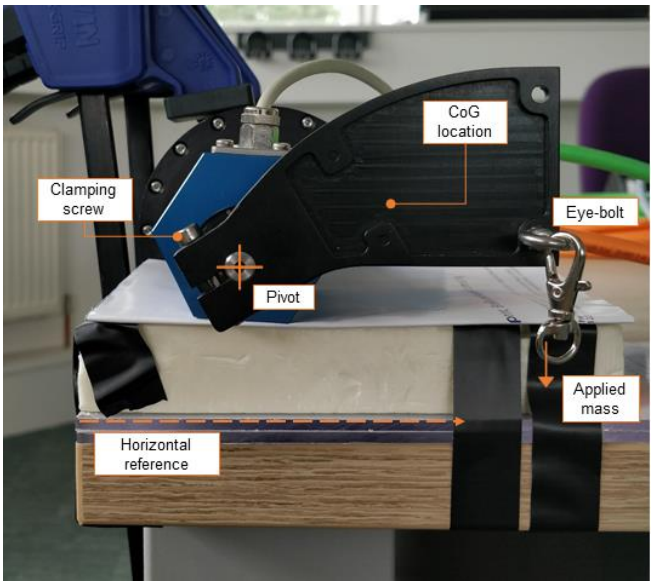

Figure 71 - Showing horizontal lever arm, clamping screw, eye-bolt, and key clip to apply known mass.

Two static friction threshold values are identified at the moment the shaft begins to move with different masses attached to it (as shown in Figure 71): 0.027919 Nm and 0.025663 Nm. The overall applied torque is 21.71g at 75mm plus the moment of the combined lever and screw: 0.015976+0.009766 = 0.025742 Nm, which is very close to the measured value. This value of static friction is also very close to the 0.0276 Nm measured in during the dynamic calibration in Section 7.4.3.1.

The static calibration is not perfect, but is the best that can be achieved with a contactless ‘floating’ sensor. However, as a further confidence check one can compare the values seen with the motor friction and check if they are consistent enough with the motor’s data sheet. We can also refer to the calibration values from the MSc thesis by Passas (Passas, 2016), where the author used this same torque sensor.

7.4.5 Controller

The controller, designed and built by Sequentec Ltd, also provides data readings from the Kollmorgen AKD drive for: motor shaft angular position, velocity, demand current, torque (derived from the current via nominal torque constant), timestamps, and a tank trigger.

One can set a maximum gain to set a maximum D_{pto} value, a max current to set a torque limit, alter PID control variables, and apply a low-pass frequency filter to the

demand output signal to the motor. This will introduce a spring coefficient in the damping, which should be constant with gain and thus not mechanical, arising from a time delay between the applied torque and velocity. Previously, Chris Retzler had applied a 50Hz low-pass filter in the demand output causing a delay of approximately 2 milliseconds. However, this spring component has little significance because power absorption depends on the damping – a spring can only store energy, not dissipate it. Furthermore, the applied spring effect is very small compared to the hydrostatic spring on the model.

The torque sensor, connected to the controller box, has an output that is filtered with a first order 50Hz low-pass filter. All the other inputs, including the torque feedback from the drive have a first order 500Hz low-pass filter applied. Therefore, the torque sensor and the velocity signals are filtered differently, which accounts for their phase difference observable via the plot below:

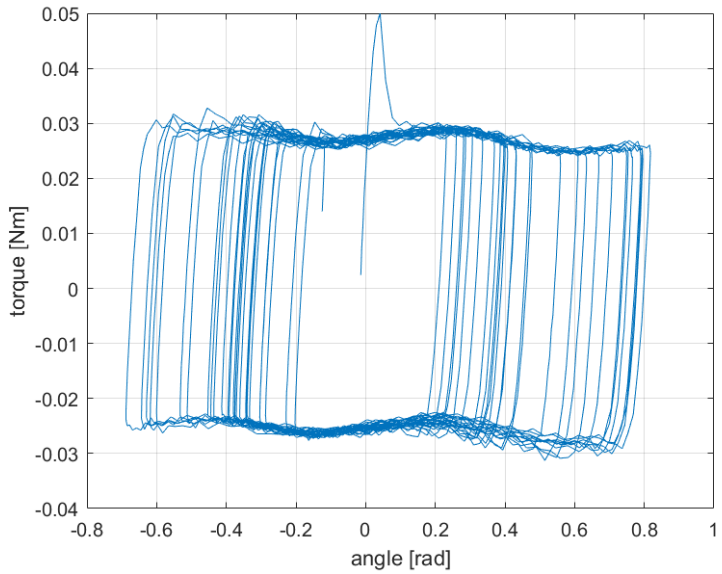

Figure 72 - Example of torque (from sensor) plotted over angle (from drive) for zero damping gain, showing phase difference.

The slight incline of each line in torque-angle plot (note that they are not vertical in Figure 72) implies either a real mechanical spring (unlikely) or a phase difference between the torque and angle channels because they are not filtered identically. The non-zero mechanical spring in the torque sensor observed when the sensor body is slightly displaced may contribute, but it probably has a minor effect.

The phase difference can also be observed when plotting torque (amplified by a factor of 10) and angle over time (see Figure below).

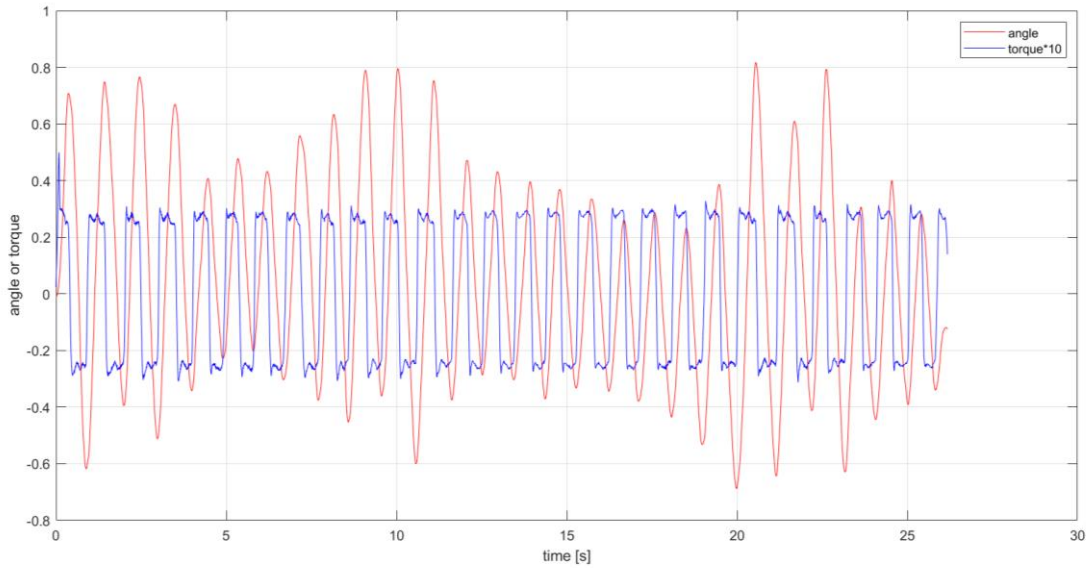

Figure 73 - Plot of angle and torque over time at zero damping gain, showing phase difference.

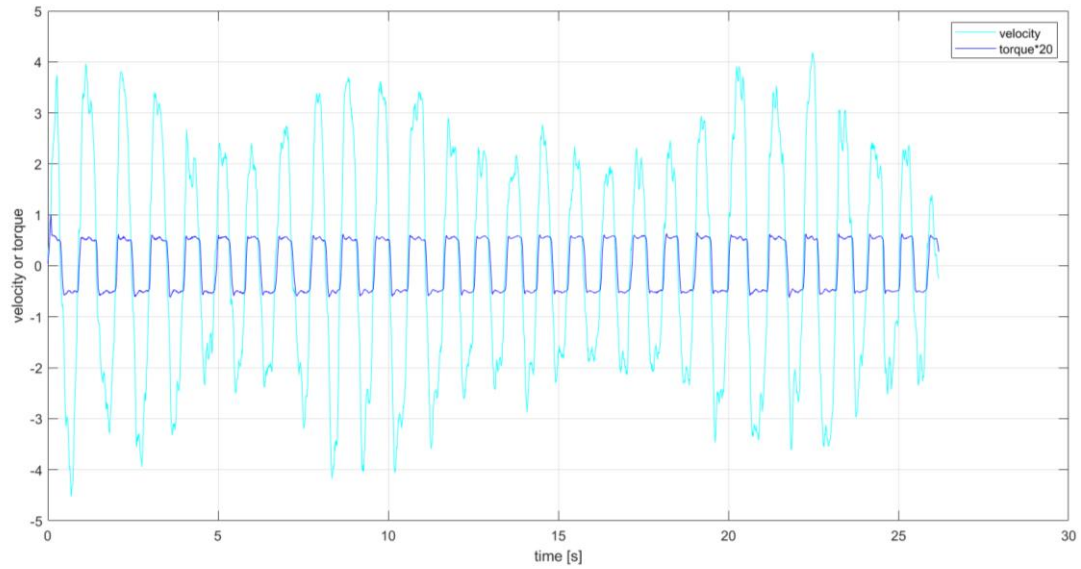

Figure 74 - Plot of velocity and torque over time at zero damping gain.

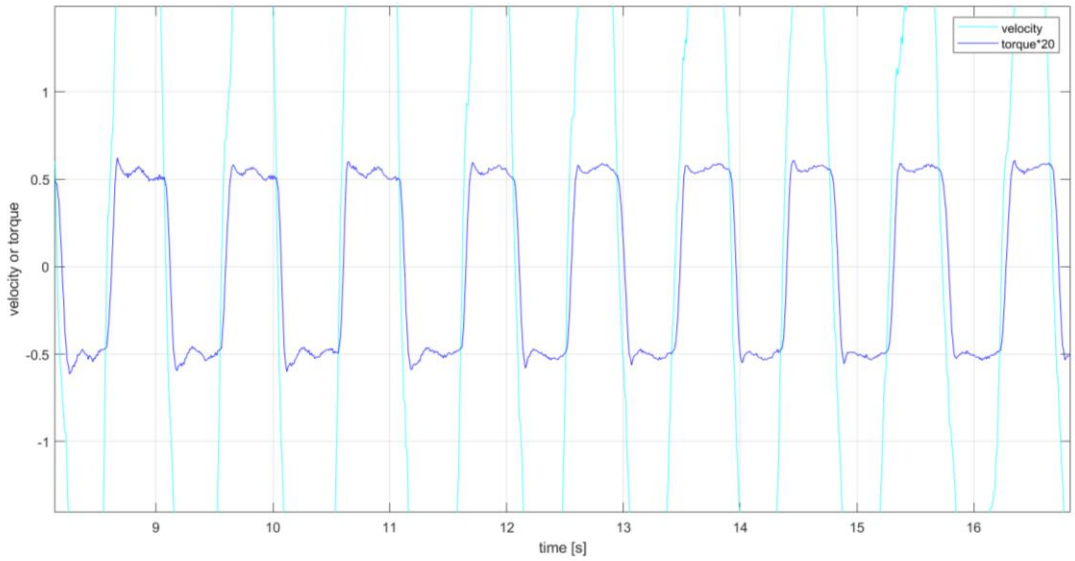

Figure 75 - Zoomed view of previous plot.

7.5 Dynamic calibration

7.5.1 Lever arm driving period

We should identify the average manual speed of excitation of the lever arm (also referred to as clamped arm) that corresponds to the desired peak period. The expected peak period is around 4s at full scale, i.e. 4/sqrt(20) = 0.9s at model scale; and the Curved Tank's central operating period is 1.0s.

A mean period of 1.00s +/-10% is chosen, attempting to keep this consistent across the range of gains that are identified as allowing the motor to function without introducing instability. The operating envelope of the Curved Tank is 0.5-2.0Hz (0.5-2.0s period), thus possible calibration values changes within this range can be checked. Note that this method more closely mimics regular as opposed to irregular seas in both manual exercising of the shaft and period over which this is done, which is approximately 20s, much less than an irregular wave run. We therefore cannot use this method to gauge what irregular wave conditions or length of tests may cause motor thermal limits to be reached in irregular seas. We could try to simulate such a sea manually, but it would be tricky to do, so we wait until the model is deployed in the tank and adjust our test plan to suit.

7.5.2 Identifying max gain

Without low-pass filtering, the maximum achievable gain, G, is around 7-8[65], at which point the output torque goes unstable, and vibrations are induced with a frequency around 50Hz. The instabilities reduce if the lever arm is driven more slowly, and depending on how tightly it is gripped. Tighter gripping when the lever arm is stationary or close to stationary can be detrimental as any involuntary rapid displacement (even if small – e.g. a slight tremble of the hand) can induce a significant reaction and then instability depending on the gain value. Thus, it is not so trivial to run the calibration manually as has been done in the procedure outlined here.

Note: initially this instability occurred at lower gains due to the lever arm not being clamped tightly enough over the sensor shaft, which caused it to slip slightly. The nacelle clamped horizontally was also not as stable as vertically, which likely did not help from a stability perspective.

By low-pass filtering at 20Hz, gains up to 52 can be reached. If the low-pass threshold is set to 10Hz, the max stable gain increases to 70 or so.

Following the dry calibration, the model will be placed in the tank. In this context, it is likely that stability will be achievable at higher gains, with an additional lower likelihood of reaching the thermal limit. The maximum achievable gain without the presence of waves was subsequently found to exceed 360. The model is closely observed in the tank to see whether the lever arm starts to vibrate in the water (check for ripples) as the gain is slowly increased. The presence of waves that excite the model will also improve stability at higher gains.

The difference between the dry and wet max gains is useful in informing future model builds. In future, one could also try to do the dry calibration with a disc/flywheel that has similar inertia properties as the model's hulls, and perhaps including water around the nacelle to aid heat dissipation.

---

[65] NB: the gain values quoted are actually (x1000) as displayed by the controller GUI, but will be consistently quoted in this thesis without the multiplying factor.

7.5.3 Zero gain

With the PTO ‘train’ mounted vertically, initial readings are taken by exercising the motor with a gain of zero (i.e. nominally free hinge), in order to quantify friction effects. The nominal static friction is 0.0221 Nm and the nominal dynamic friction (or viscous damping) is 0.005Nm/k_{rpm} = 0.0005236 Nms/rad.

An ‘offset’ reading is taken ahead of each run in order to account for the average offset value of Tx – i.e. a preliminary recording of the torque without the lever arm being touched.

NB: the torque acts in the opposite direction as the velocity, but is plotted as –Tx so that positive torque appears as positive velocity. Positive velocity is anticlockwise, as is position (angle).

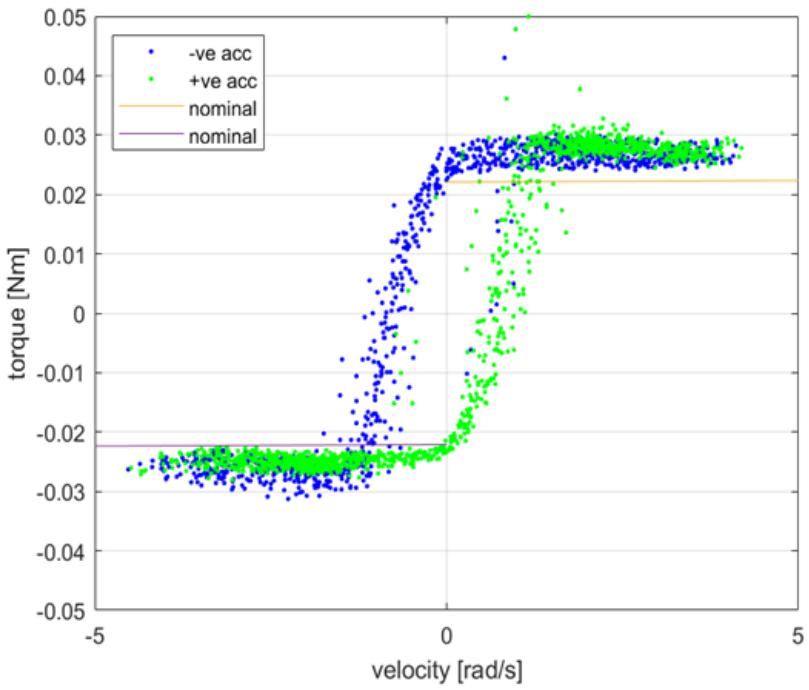

Figure 76 - Showing measured torque versus angular velocity, zero gain, mean period 0.96s.

The traces in Figure 76 are colour coded based on whether the lever arm is accelerating or decelerating. We plot the nominal friction lines based on a static friction y-axis intercept and a dynamic friction slope. Both nominal values appear close to the measured.

From inspection of one of the traces (say the blue points), we note that for negative velocities there appear to be both positive and negative torques, which is unphysical. It suggests a time delay on the torque, so that the torque reading lags the actual torque. This is likely a result of filtering, indeed the torque sensor output is filtered at 50Hz while velocity at 500Hz. Figure 72 confirms that this hysteresis is a phase effect due to filtering. Physical spring in the sensor could also give this effect, but is likely to be less significant.

7.5.3.1 Static friction

Since a clear y-intercept point from Figure 76 cannot be read, there are multiple ways in which it can be estimated. One is following the 'hysteretic' sections of the plot (Figure 77), and the other is interpolating the 'dynamic' sections at greater velocity magnitudes (Figure 78).

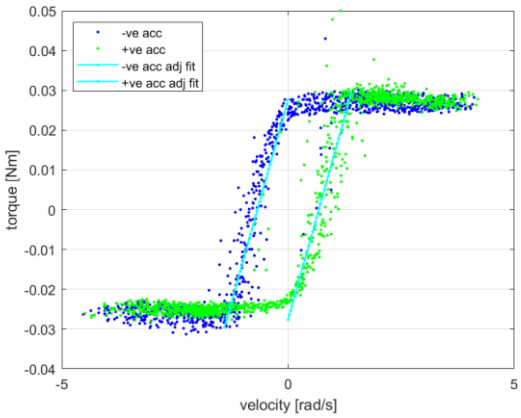

Figure 77 - 'Hysteretic' interpolation.

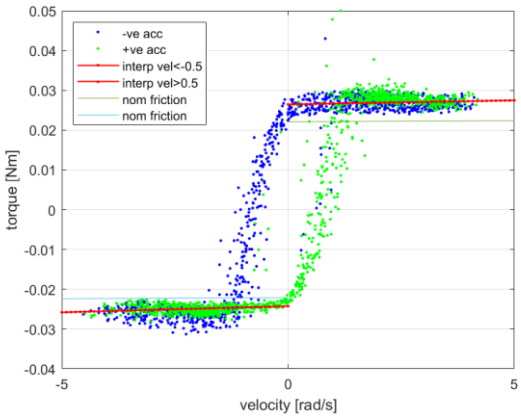

Figure 78 - 'Dynamic' interpolation.

Both methods are relatively arbitrary, in that their slopes and resulting y-axis intercept depend on the range of velocities used for the interpolations. The 'hysteretic' interpolation is carried out for velocities between 0 and |1.4| rad/s.

Interpolation fits:

- (-ve acc) Equation for Nms/rad @gain=0 is y = -0.042311*x + -0.03044
- (+ve acc) Equation for Nms/rad @gain=0 is y = -0.039206*x + 0.024815

Adjusted fits:

- (-ve acc) Equation for Nms/rad @gain=0 is y = -0.0408*x + -0.0276
- (+ve acc) Equation for Nms/rad @gain=0 is y = -0.0408*x + 0.0276

The obtained lines are then adjusted by averaging the respective *y=mx+c* terms *m* (-0.0408 Nms/rad) and *c* (|0.0276| Nm).

The 'dynamic' calibration is carried out for velocities lower than -0.5 and greater than 0.5 rad/s, by considering negative and positive acceleration points separately. It gives intercept values of 0.02647 and -0.02423, with an average of 0.02535 Nm. It is considered more arbitrary and thus a 0.0276 Nm is assumed for both positive and negative accelerations. The discrepancy between friction thresholds to clockwise motion and anti-clockwise motion is around 0.002 Nm. A **static friction of 0.0276 +/- 0.001 Nm** is finally assumed[66].

7.5.3.2 Dynamic friction

Interquartile ranges from Blue Star baseline experiments are initially checked, in order to gauge typical angular velocities of the hinge that might occur. The 95% quantile is considered in particular; there is less interest in the occasional sharp peaks as these ultimately have negligible effect on the power capture.

Tp [s]	Hs [mm]	Se	0.05, 5%ile [rad/s]	0.25 [rad/s]	0.5 [rad/s]	0.75 [rad/s]	0.95 [rad/s]	0.99 [rad/s]
0.75	18.20	0.0282	0.11	0.55	1.16	2.10	4.32	6.81
1.00	32.20	0.0282	0.14	0.64	1.38	2.44	4.54	6.67
1.25	50.50	0.0282	0.14	0.72	1.52	2.66	4.81	7.08
0.75	12.20	0.0189	0.08	0.47	1.05	1.91	3.96	6.25
1.00	21.70	0.0189	0.11	0.55	1.16	2.10	4.23	6.45
1.25	33.80	0.0189	0.11	0.58	1.27	2.24	4.32	6.61

Table 14 - Quantile thresholds of velocity from irregular seas run with BST-baseline 20th scale model.

By observing Figure 76, it is noted that the dynamic slope appears consistent with the nominal specified value of 0.0005236 Nms/rad. 95% of velocities are estimated to be lower than 5 rad/s (see Table 14). At 5 rad/s, dynamic friction adds 5*0.0005236 = 0.002618 Nm, which is 9.5% of the static value of 0.0276Nm. It is

[66] The gain=0 scatter plot is repeated on July 21st to check whether the static friction values have changed from seal wear or simply because it has been "broken in", by comparing them to values obtained on July 16th (plotted figures). These can be seen in Appendix C. The average appears to be approx. 0.002Nm lower than 0.0276, which could be the result of methodological errors, or a real decrease due to lip seal wearing in.

therefore decided to neglect the dynamic friction component. Indeed, dynamic friction is more significant during survival testing, where the PTO is switched off and the seas are most aggressive.

7.5.3.3 Variations with mean period

Zero gain runs are repeated around 0.5s and 2.0s mean period. The results are shown below.

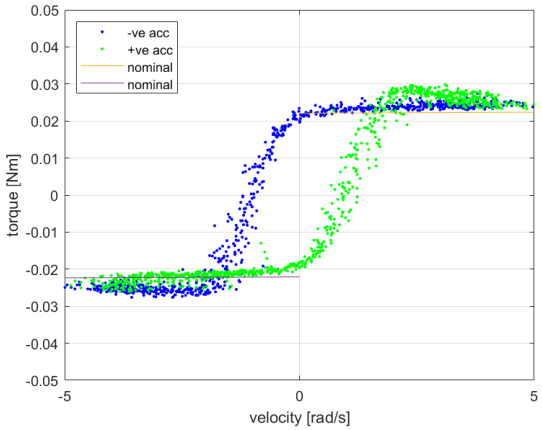

Figure 79 - Zero gain, mean T = 0.56s

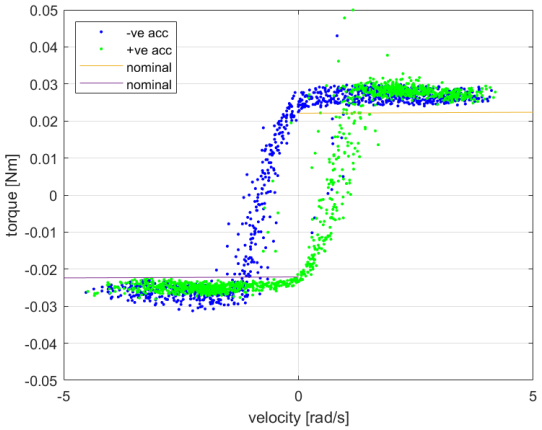

Figure 80 - Zero gain, mean T = 0.96s

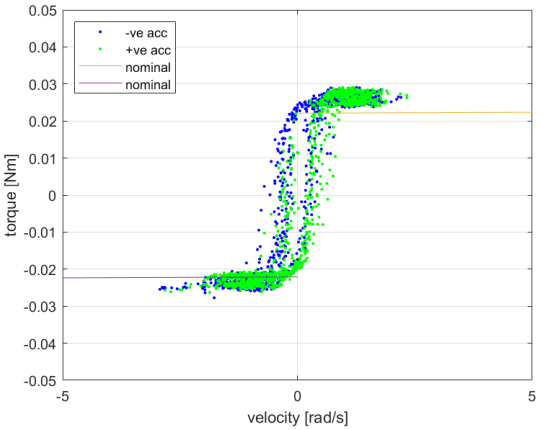

Figure 81 - Zero gain, mean T = 2.02s

The following observations are made:

- Relatively consistent y-axis intercepts
- Different amount of hysteresis opening up of the plot either side of velocity=0 region
- Friction not totally symmetric about x-axis; the torque that resists anti-clockwise motion appears slightly greater
- Slightly lower static friction value from the lower mean period. Note that plots for 0.56s and 2.02s were obtained one working day after 0.96s plot (this may explain slightly lower static friction due to longer exercising of arm and seal).

An example overall calibration dataset follows in Section 7.5.4.

7.5.4 Example calibration

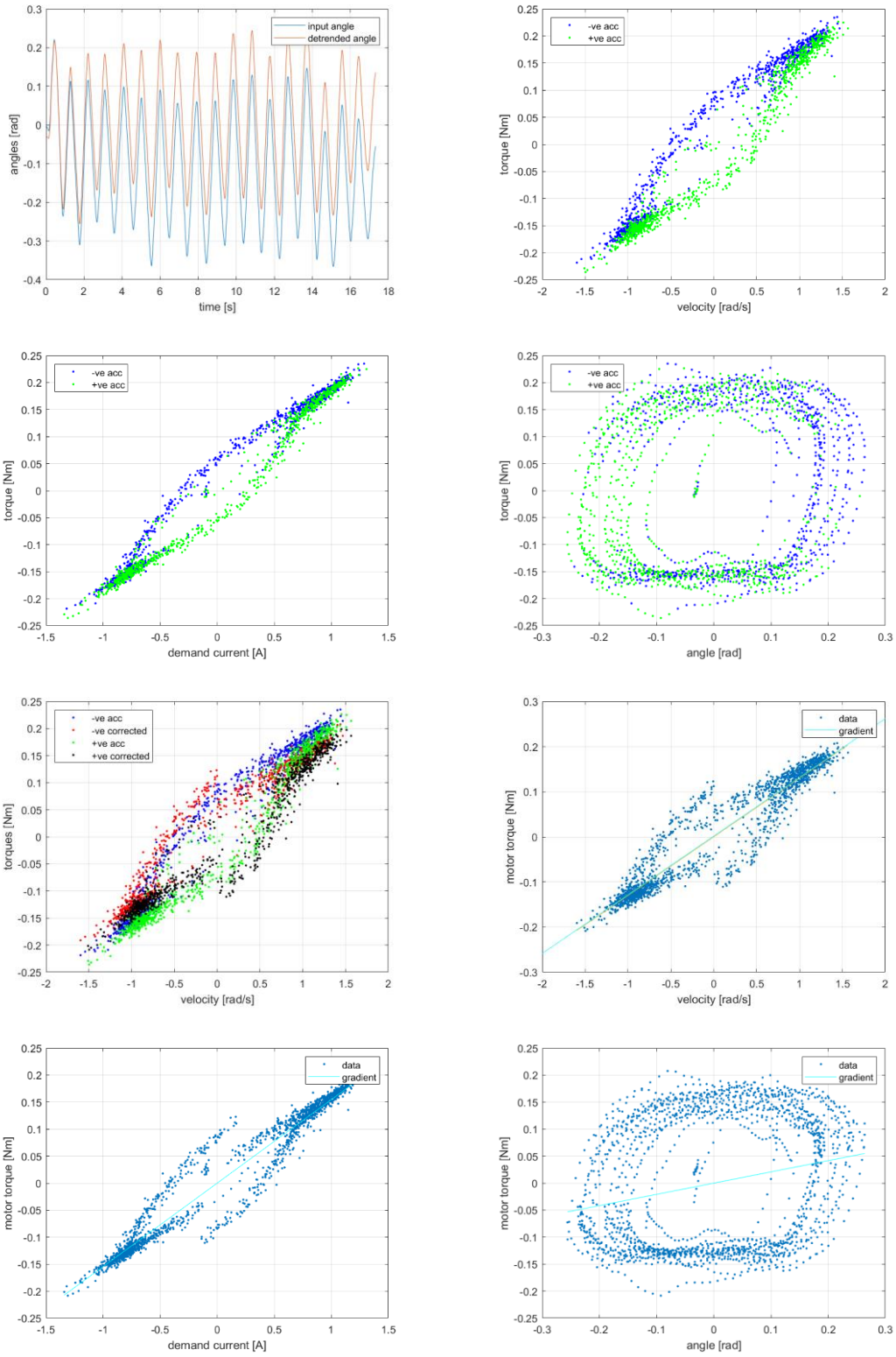

Table 15 - Example dataset obtained with gain 30, LP filter 20Hz, and mean period of 0.94s.

The data plotted in Table 15 corresponds to a dataset with gain set to 30, low-pass filter set to 20Hz, and a mean applied period of 0.94s.

The plots show the various steps involved in extracting the calibration variables from a given dataset. The D_{pto} value is obtained from the gradient of the motor torque-velocity plot, the T_{const} from the gradient of the motor torque-demand current plot, and the k_{pto} from the gradient of the motor torque-angle plot.

The above process for a gain of 30 is repeated for the gain range 2-52 at gain steps of 2, with a low-pass filer @ 20Hz between 2-42, and of 10Hz between 44-52. Associated plots are shown in Appendix G.

7.5.5 PTO damping per unit gain

A normalised damping value is obtained by dividing the D_{pto} by the associated gain. It still has units of Nms/rad. We note the more consistent normalised damping coefficient D_{norm} when friction is accounted for (Figure 83), the slight drop of D_{norm} at gains when LP=10Hz (gains of 44 and above, Figure 84), and the seeming lack of correlation with mean period (Figure 85).

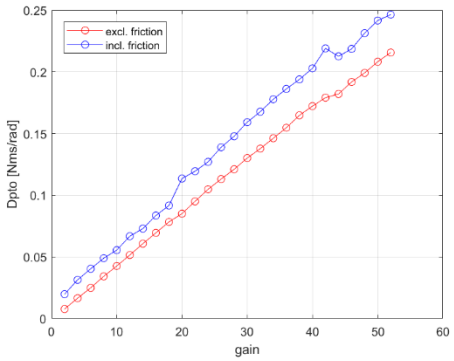

Figure 82 - Dpto terms obtained at each gain level.

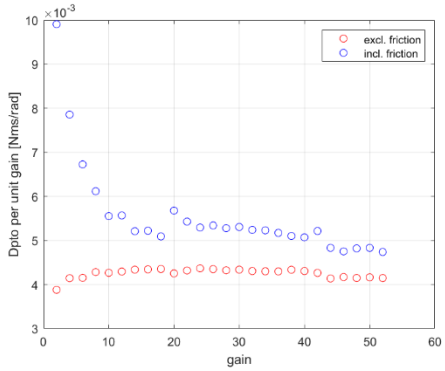

Figure 83 - Comparison of normalised Dpto including or excluding friction.

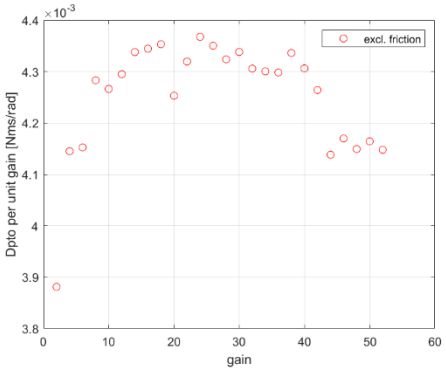

Figure 84 - Normalised Dpto when friction is accounted for.

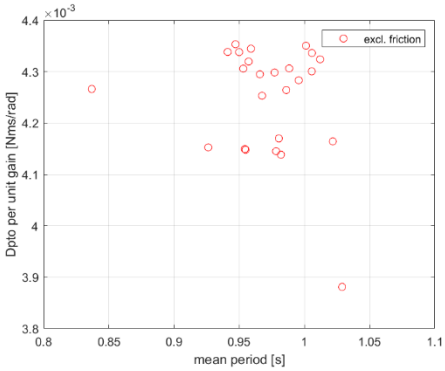

Figure 85 - Normalised Dpto versus mean period of excitation.

Observing Figure 85, and neglecting the point at gain=2, the scatter in D_{norm} is around +/-2% of the mean value of approx. 0.00425 Nms/rad per unit gain.

7.5.6 Torque constant

The torque constant specified on the motor data sheet is 0.158 Nm/A_{rms} +/-10%. This translates to bounds of 0.1422 and 0.1738 Nm/A_{rms}.

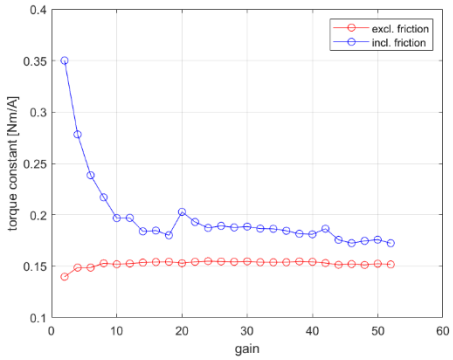

Figure 86 - Torque constant comparison including and excluding friction.

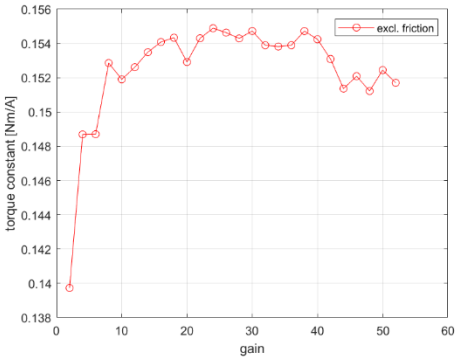

Figure 87 - Torque constant when friction is accounted for.

Observing Figure 87, and neglecting the point at gain=2, the scatter in T_{const} is around +/-2% of the mean value of approx. 0.152 Nm/A.

7.5.7 Spring coefficient per unit gain

The spring coefficient is not as crucial as the other two variables in terms of accurately measuring power capture in the wet tests. It is still worth deriving so that it can be compared with the hydrostatic spring coefficient of the physical model.

The plots show that k_{pto} values do not greatly vary when derived with the measured torque (including friction) or the motor torque (that is corrected for friction). They also show no particular correlation with gain or mean period.

Observing Figure 90, and neglecting the points at gain 2,4, the scatter in k_{norm} is around +/-20% of the mean value of approx. 0.0065 Nm/rad per unit gain.

This is the least consistent variable and perhaps most sensitive to methodological inconsistencies such as mean period and length of tests. One particularly relevant factor is the quality of the de-trended angular position and its mean being consistent about zero. This is difficult to produce manually, hence the need for de-trending to negate the drift in mean angle. The angles are de-trended using a power fit with power 3, but higher or lower powers could be used. The choice of power 3 is based on the sensitivity analysis presented in Table 16, and the choice of power that minimises standard deviation. The difference in standard deviation between powers of 3, 4 and 5 is deemed negligible and the lowest power among these is chosen.

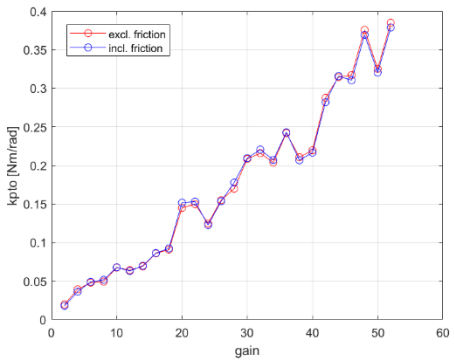

Figure 88 - Spring constant values including and excluding friction.

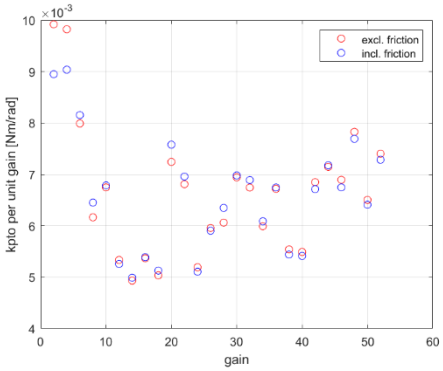

Figure 89 - Normalised spring constants including and excluding friction.

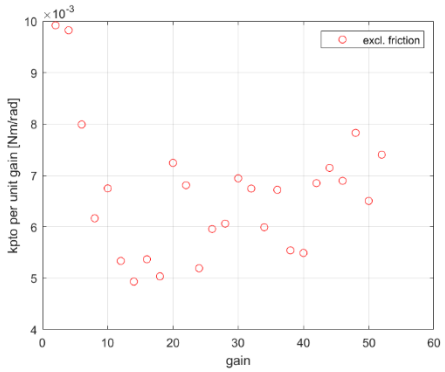

Figure 90 - Normalised spring constant variation with gain.

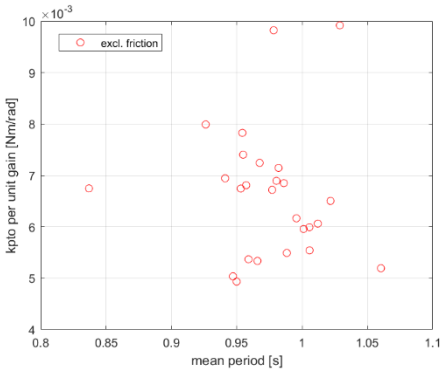

Figure 91 - Normalised spring constant variation with mean period.

Power	Mean (k_{norm}), Nm/rad	Std (k_{norm}), Nm/rad	Error (Std/Mean)
1	0.0065	0.0013	20.38
2	0.0065	0.0013	19.81
3	0.0066	0.0013	19.16
4	0.0067	0.0013	19.09
5	0.0067	0.0013	19.16

Table 16 - Sensitivity study around de-trending power.

Note – as would be the case in wet tests – that the angles reached at higher gains are smaller in order to maintain the required mean period of excitation.

7.5.8 Coarse calibration sweep with filtering

As well as the fine resolution calibrations shown in Appendix G for gain range 2-52 in steps of gain 2, additional measurements are taken at gains of 60 and 70, and

compared with the existing data spanning 10-50 in steps of 10. See Appendix G for a table with associated data entries. Note that the first 30 and the last 30 points are removed ahead of calibration calculation, as tighter holding of the lever arm at start and end of these tests at higher gain resulted in some instability. Only the plots for calibration variables are shown here for conciseness.

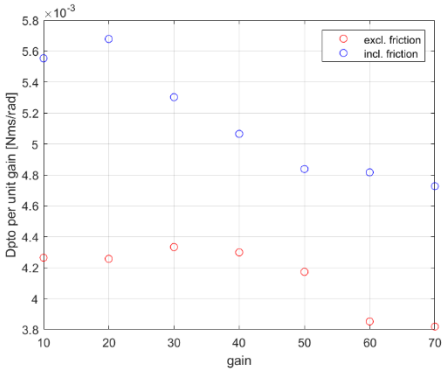

Figure 92 - Normalised damping coefficient including higher gains.

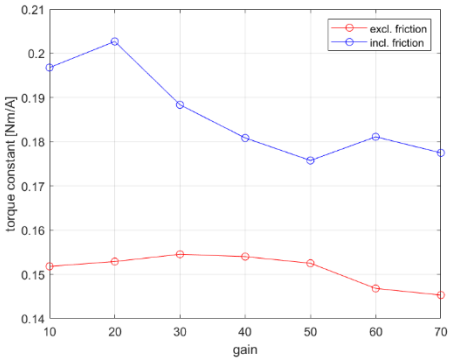

Figure 93 - Torque constant including higher gains.

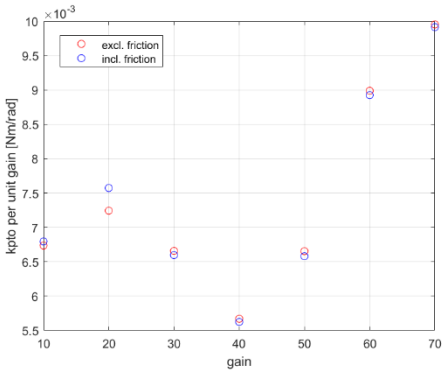

Figure 94 - Normalised spring coefficient including higher gains.

Of particular note is the lower value of D_{norm} and T_{const}, and the higher value of k_{norm}, at gains 60 and 70. Repeats in Appendix B suggest that while these may be real, their magnitude may be lower than captured in these plots, and that values of D_{norm} around 0.0040 and 0.0039 also occur at gains of 20.

7.5.10 Calibration variables summary

The following tables summarise calibration parameters in the range 2-52 and 10-70 using a static friction of 0.0276Nm, and range 2-52 using a static friction correction of 0.0223Nm.

Summary table for 'fine' calibration:

Calibration variable	Mean	Std	Error (Std/Mean)*100
D_{norm} [Nms/rad]	0.004254	0.0001085	2.55
T_{const} [Nm/A]	0.1525	0.003091	2.03
k_{norm} [Nm/rad]	0.006640	0.001272	19.16

Table 17 - Calibration variables from gains 2-52; static friction = 0.0276Nm.

Summary table for 'coarse' calibration:

Calibration variable	Mean	Std	Error (Std/Mean)*100
D_{norm} [Nms/rad]	0.004142	0.0002157	5.21
T_{const} [Nm/A]	0.1511	0.003608	2.39
k_{norm} [Nm/rad]	0.007415	0.001506	20.31

Table 18 - Calibration variables from gains 10-70; static friction = 0.0276Nm.

Using 0.0223 Nm as static friction correction instead of 0.0276Nm:

Calibration variable	Mean	Std	Error (Std/Mean)*100
D_{norm} [Nms/rad]	0.004501	0.0001085	3.71
T_{const} [Nm/A]	0.1611	0.003091	3.22
k_{norm} [Nm/rad]	0.006633	0.001272	18.69

Table 19 - Calibration variables from gains 2-52; static friction = 0.0223Nm.

7.6 Optimal Dpto value

The numerical optimisation (described in Chapter 4) uses both spectral domain (SD) and frequency domain (FD) models to derive an optimal geometry. A torque limit is applied in the SD model[67] by finding and applying a quasi-linear damping coefficient. The run that resulted in the built model version computed an optimal (quasi-linear) D_{pto} value of 0.221 MNms/rad. The linear D_{pto} value

[67] Applying a torque limit purely in the FD model is not possible as it is a square wave.

found by the optimiser is 0.254 MNms/rad. This is used as an initial value to find the quasi-linear coefficient needed to apply the torque limit, and is considered truer to the real value.

A time-domain (TD) model was also set up with this geometry (passive model version) to validate data acquired from Plymouth tests in 2020. It suggests an optimal D_{pto} value of 400 kNms/rad based on the July wave climate[68] and 410 kNms/rad with full wave climate. This is roughly double the optimiser prediction. The TD model also suggests that if this D_{pto} is halved, 96-97% of the performance is still obtained. If the full-scale value is divided by 4 (i.e. 0.100 MNms/rad), ~73% of the performance is retained. Historically, the July and full wave climate optimal D_{pto} values have been similar.

The Froude scaling factor for angular damping is s^4.5, where s is the scale (20). Thus, the target D_{pto} at model scale is 0.254*10^6/(20^.5) = **0.342 Nms/rad** (FD); 0.410*10^6/(20^4.5) = **0.573 Nms/rad** (TD). Assuming a D_{norm} value of 0.004254 Nms/rad per unit gain, the **target gains are 80 and 135**. Ideally, higher gains would be tested to ensure we have reached a peak along the power absorbed versus D_{pto} plot.

7.7 Additional considerations

7.7.1 Computational errors

The motor cuts out if it reaches its current limit. This occurs at non-zero velocity but the displayed torque value will be approximately 0 Nm when this occurs. Such points appear as anomalies in torque vs angular velocity plots, affecting the accuracy of associated Nms/rad gradients. Thus, care is taken to exclude such points from D_{pto} derivations. Torque constants are not affected since zero torque always equates to 0 current.

[68] The significance of July wave climates links to the requirement to provide continuous power for off-grid applications, which in the Northern Hemisphere is typically limited by the minimum wave conditions during the month of July.

7.7.2 Repeatability

Repeatability is explored by running repeats at the same nominal conditions, and also by comparing effects of different mean periods and different low-pass filtering frequencies (see Appendix G). Accordingly, the following observations can be made:

- No clear effect of low-pass filter frequency on any variable, though Figure 84 and Figure 87 suggest a slight drop;
- No clear effect of mean period on T_{const}, or D_{norm}; k_{norm} roughly doubles when mean period is halved to ~0.5s, and halves when mean period doubles to ~2.0s;
- No clear effect of gain on any of the calibration variables;
- Excluding k_{norm}, there is good consistency between calibrations with the same nominal inputs.

7.7.3 Water tightness

A check is undertaken to verify no water ingress inside the nacelle. The nacelle plates are removed to check the integrity of the O-rings, and to allow a silicone pellet dessicant bag to be placed within the nacelle tube, in order to check whether it would absorb any moisture during the submerged period. The O-rings maintained springiness as the plates were loosened, as desired. Cables, wires, and all other components around the motor looked intact. With the motor mounting plate detached, water was placed around the motor shaft and lip seal using a pipette and the shaft was rotated to check whether the seal worked. A meniscus of water formed around the shaft and none passed through the seal.

The O-rings were re-greased and the nacelle was re-assembled again. The cable glands were tightened, and silicone sealant was applied to the motor mounting plate counterbore holes, and to the tapped M3 hole in the nacelle tube. The sealant was applied at 8pm on July 21st, and left to dry overnight. A water tightness check was carried out on 22nd July 2021, the lever arm was re-attached and the nacelle was fully submerged in a large tray of non-saline water around 11:30am. No bubbles formed around the lip seal, even when the lever arm was exercised. No bubbles were visible around the metal casing either. A

few bubbles formed around the cable gland threads, which were checked later for slow leaks. None were identified.

The lever was exercised every half hour until 6pm, when the nacelle was removed from the water.

The external surfaces were dried, the nacelle was flipped with the shaft pointing downwards to see whether leaks occurred when the shaft was exercised – none were detected. The nacelle was left on paper towels on a desk and no further drainage was observed. Upon disassembly, all internal surfaces and components looked dry, including inside the cable glands, and the dessicant bag still weighed 2.11g. It was excluded upon re-assembly.

7.7.4 Controller

Some of the encountered issues are highlighted here, in particular the motor's response becoming unstable above a certain damping gain value when the lever arm is driven by hand during dry bench tests.

The controller applies an instantaneous torque. If there is any extremely high velocity fluctuation, the controller reacts with what it thinks is a suitable torque to resist it, which will push the response too far the other way, etc. One could tweak the PID loop to reduce the proportional term, which means the torque is applied over time rather than instantaneously. However, the problem is that the control loop would get fairly 'sloppy' and the user would feel 'sponginess' in the system while driving the lever arm.

In fact, once the hinge is in the water it should be far harder for the motor to do what it does when it is on the bench. There will be a moment applied from the rest of the model's hulls on the hinge, as well as damping from the water that mitigates the fast velocity fluctuations that cause the instability. In the tank, it is decided to gently wind up the gain when the model is at its resting state in the water, in order to identify the threshold of PTO damping gain at which it goes unstable. If necessary, this can be repeated while running some waves.

During dry testing, the low-pass filter function in the VNC (i.e. GUI) setup window is utilised. The frequency at which the lever arm begins to oscillate at during instability is identified, and a low-pass filter applied below this frequency. The

effects on device impedance are investigated in this chapter. Applying a 20Hz low-pass filter should be acceptable, as this is still much higher than the expected oscillations of the device (around 1Hz peak response) and of the tank, which can work up to a max frequency of 2Hz. It is noted that the low-pass filter is applied to the signal that goes out for the demand current.

7.8 Characterisation conclusion & next steps

A stable gain of 70 has been achieved during this calibration. The target gains are approximately 80 according to the FD model and 134 according to the TD model, though a gain of 67 should give 93% of the total absorbed power according to the latter. It is later found that a stable gain up to 360, and potentially higher, can be achieved in the tank.

Calibration parameters have been successfully obtained, with satisfactory levels of consistency.

- D_{norm} has a mean value of 0.004254 Nms/rad per unit gain
  - Ranges: [0.003881, 0.004368]; [0.004138, 0.004368] if gain=2 point is ignored.
- T_{const} has a mean value of 0.1525 Nm/A
  - Ranges: [0.1397, 0.1549]; [0.1487, 0.1549] if gain=2 point is ignored.
- k_{norm} has a mean value of 0.006640 Nm/rad per unit gain
  - Ranges: [0.009919, 0.004934]; [0.007991, 0.004934] if gain=2,4 are ignored.

7.9 Chapter conclusions

Ultimately, when the gain is set, the WEC does “see” the friction. At low gains in particular, the effective torque damping will be higher than the theoretical value from the calibration. However, by going through the steps above, we can more accurately ensure that the average damping coefficient assumed across the gain range is not skewed by the friction effects at low gains.

Furthermore, transitioning from a dry environment to a wet (tank) environment, it is assumed that friction in the dry is the same as in the wet. This is not exactly true. Although no water lubrication of the shaft seal should occur (since it supposed to keep water out of the nacelle), there may be more effective heat dissipation in water as opposed to in air; this may help to slightly reduce

frictional losses. Finally, it may be that the seal has not yet been ‘broken in’ during the dry characterisation tests, such that these represent an upper limit of the friction experienced at the hinge during testing. The lack of an in situ torque sensor ‘forces’ an assumption of consistent friction effects as measured in this chapter.

Chapter 8. Blue Star – folding

This chapter focuses on the second round of physical model testing undertaken at the Curved Tank basin (Edinburgh University) with a 20th scale model of an updated WEC geometry, referred to as Blue Star *folding* (henceforth just "BST-folding"). The model is an active – "powered" – version (i.e. having a motorised hinge) of the passive (i.e. free hinge) BST-folding 20th scale model previously tested at the Plymouth COAST Laboratory to investigate survival and associated mooring behaviour, as part of a dedicated external testing programme around moorings. A PTO representation is now included to enable the application of a linear torque resistance to hinge motions, in order to simulate power absorption by the WEC. This round of testing builds on the previous campaign with BST-baseline. Advances include model build, model capability, testing scope, and testing methodology. At the same time, sufficient consistency with baseline tests and previous Mocean campaigns (Chapter 4, Section 4.3.3) is sought, to enable appropriate comparisons and learning to be extracted and discussed more broadly.

Chapter contributions

Dr Gabriel Scarlett and Dr Alfred Cotten, both at Mocean Energy, are gratefully acknowledged for their valued inputs to the work presented in this chapter. They provided key numerical modelling contributions to this chapter, complementing the experimental data gathered and associated analysis. Their contribution included numerical optimisation of the geometry, frequency- and time-domain simulations, and numerical sensitivities carried out post physical model build.

8.1 Novel elements compared to baseline tests

From a model capability point of view, novel elements introduced in this testing round are:

- a new folding geometry including a gap in the aft hull;
- a motorised 20th scale modular hinge;
- the adaptation and application of an efficient testing methodology termed IR0, derived from (Pascal *et al.*, 2021);

- the inclusion of short-crested irregular seas (to cover more *performance* aspects, in addition to *validation*), which is not often found in literature where irregular sea testing tends to involve long-crested waves only;
- a direct comparison with a 40th scale geometrically equivalent model;
- a more thorough and comprehensive uncertainty analysis based on repeat runs and sensitivity to different configurations (including model geometry and test environment), which tries to identify and – where possible – quantify both systematic and random sources of error.

Detailed PTO characterisation work, involving dry bench tests, can be found in Chapter 7. This model and set of tests represent an attempt to move towards an 'all-in-one' 20th scale model concept, to be ideally utilised for validation, performance, and survival testing.

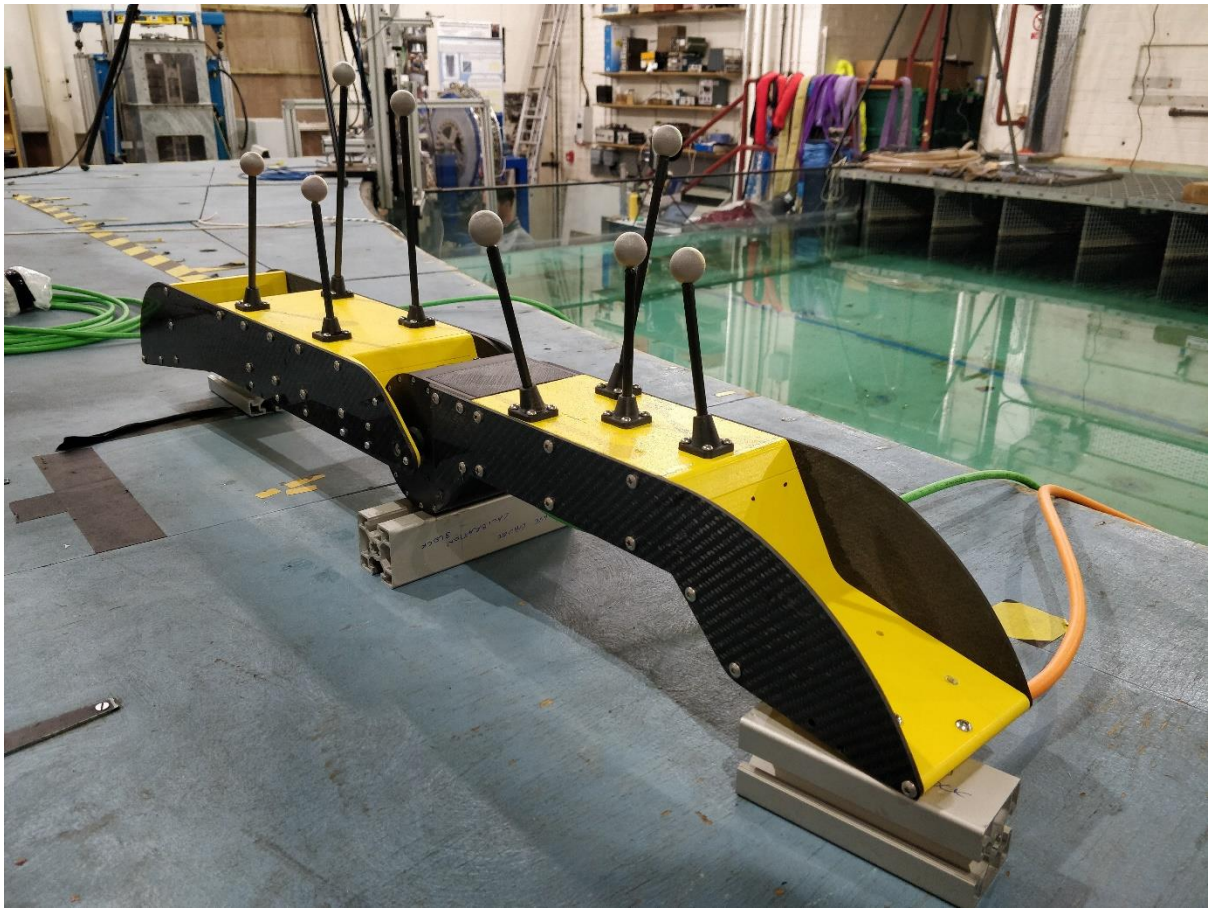

Figure 95 - BST-folding 20th scale motorised model at UoE's Curved Tank.

Figure 95 shows the active BST-folding 20th scale model at the side of the Curved Tank test basin, with orange and green cables (power and feedback).

Figure 96 and Figure 97 show different views of the passive version of this model (the nacelle is yellow and 3d-printed), illustrating it in its folded and unfolded configurations, as well as the smaller black cable from the rotary sensor. An additional figure can be found in the Appendix H.

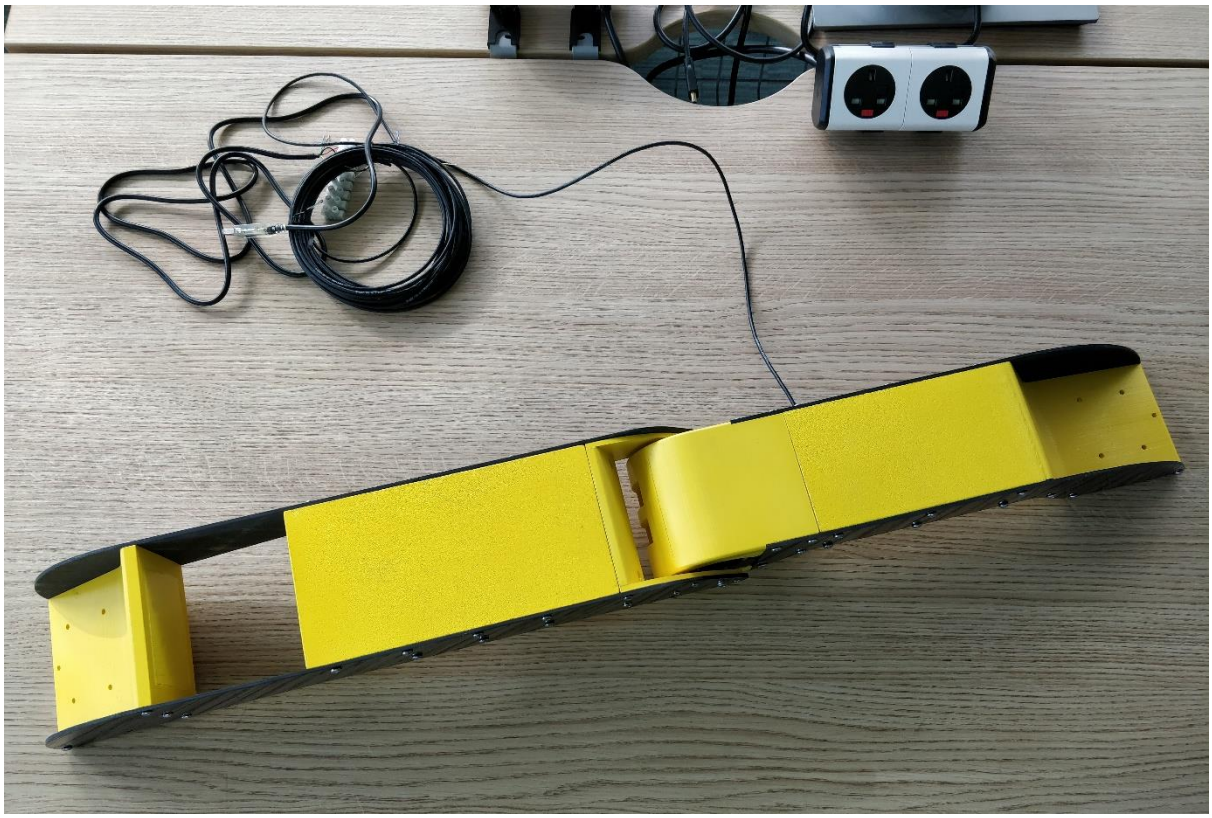

Figure 96 - Passive version of BST-folding 20th scale model.

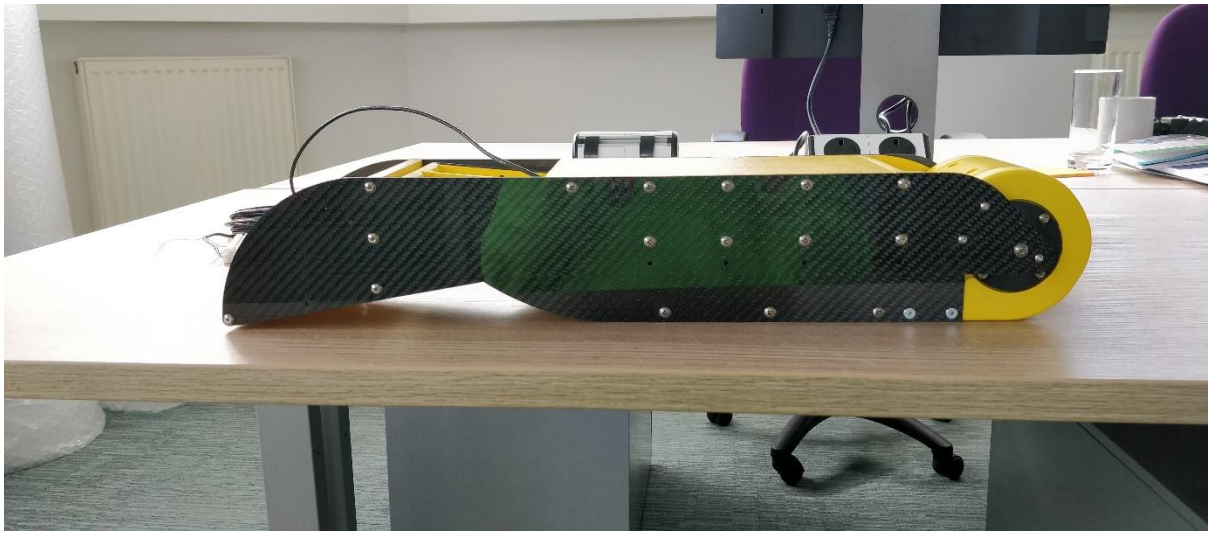

Figure 97 - Passive version of BST-folding 20th scale model - folded configuration.

8.2 Commercial model context

In accordance with Section 6.1, the overall dimensional envelope is maintained. However, the aim is to increase performance, of which device length is a major contributing factor. To facilitate transportation and general handling, the dimensions of BST are restricted to allow it to fit inside a standard-sized 40ft shipping container. However, the novel folding geometry enables a ~60% length increase (11.5m to 18.4m) when the WEC is unfolded, which, notably, results in a roughly doubled estimate of Annual Energy Production (AEP) according to the numerical optimisation – see Appendix H. It also increases survivability by accommodating the very large pitch angles that occur in extreme sea states. The WEC can now accommodate a range of flex angles from 105deg in sagging (aft hull pitches upwards relative to fwd hull) to 180deg in hogging (aft hull pitches downwards relative to fwd hull). The increased length of the machine also contributes to accommodating higher waves for a given hinge angle.

From a geometry perspective, aside from the wave channels, significant features include: a larger nacelle (now occupying the full cross-sectional area/draft allowed by the shipping container, and thus larger PTOs); and the large gap in the clevis (or aft) hull (Figure 98b), which accommodates the nacelle (or forward, “fwd”) wave channel when the device is in its ‘folded’ configuration (Figure 98a).

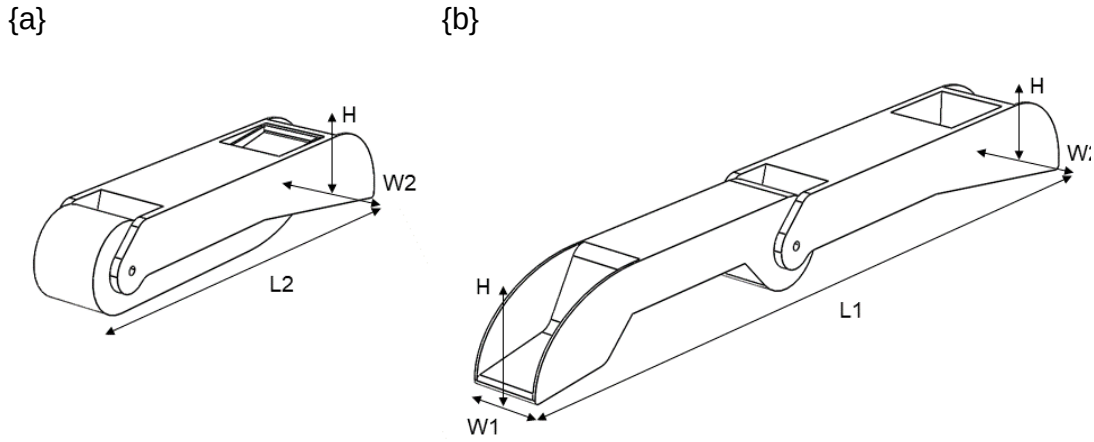

Figure 98 - Annotated views of Blue Star folded (a) and unfolded (b).

An overview of the specifications is provided in Table 20, where AEP and the average power values are quoted assuming a mechanical-to-electrical efficiency of 80%. This value is based on Mocean’s preliminary analysis of the PTO

system. A breakdown of the mass properties for each hull is provided in Table 21.

Property	Value
Material	Steel
Total mass	17,800 kg
Ballast mass	6,700 kg
Power take off	Generator with gear box
AEP	51 MWh
Average power	5.9 kW
Length, L1 (L2)	18.4 (11.5) m
Height, H	2.1 m
Width, W1 (W2)	1.6 (2.1) m
Draft	1.7 m

Table 20 - BST-folding spec table. Power is based on 80% mechanical-electrical efficiency.

Item	Mass
(FWD) Nacelle Hull	
Structure (steel)	4,538 kg
Hinge	500 kg
Clevis arms	500 kg
PTO	1,100 kg
Ballast (electrics)	1,500 kg
Ballast (concrete, etc.)	2,214 kg
Total	**10,352 kg**
(AFT) Clevis Hull	
Structure (steel)	4,404 kg
Ballast (concrete, etc.)	3,067 kg
Total	**7,471 kg**

Table 21 – Breakdown of mass properties.

Figure 99 – Views of the WEC folded inside a 40ft shipping container.

Figure 99 shows the folded WEC inside a 40ft shipping container. In this case, the forward hull is folded underneath the aft hull. The visible wave channel in the figure is at the aft section – in other words, the WEC is facing into the page. A use case for this version of BST can be found in Appendix B, where the WEC acts as a combined power and communication platform supporting subsea assets in cases of umbilical failures – one of the recurring issues faced by offshore platforms.

It is also noted that two patents were successfully filed by Mocean relating to this novel folding geometry.

8.3 Numerical inputs, constraints, and outputs

The power matrix and energy matrix evaluated by the SD numerical model are shown below in Figure 100, Froude scaled to 1:20. T02 is the zero up-crossing period derived from the input wave spectrum at the site of interest: Central North Sea. Full-scale equivalents are given in Appendix H.

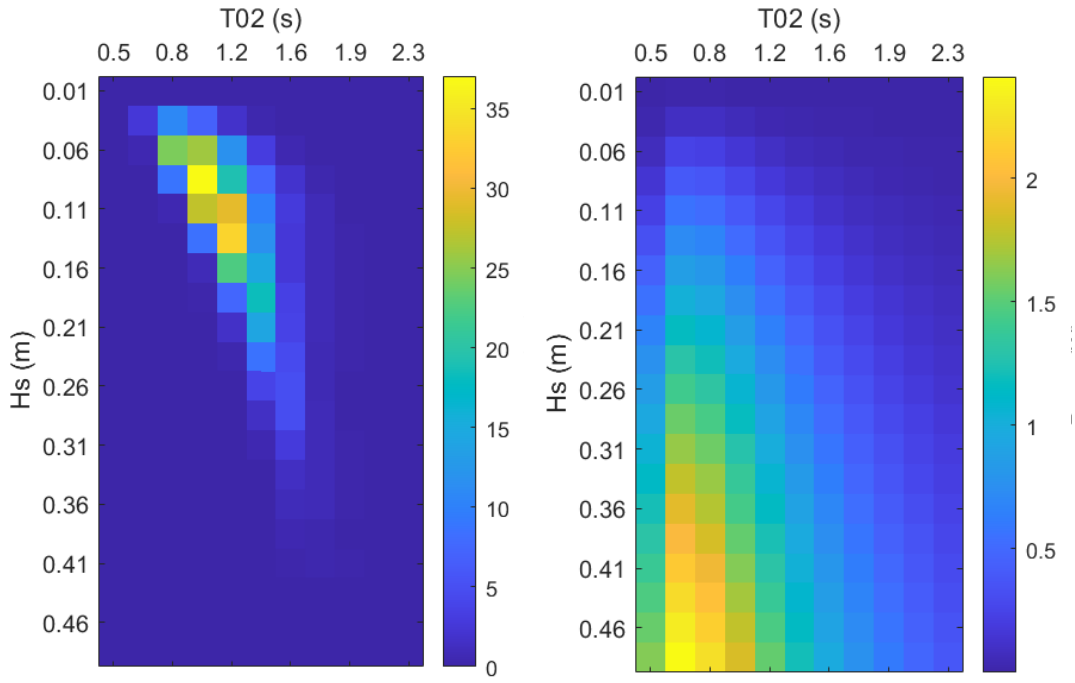

Figure 100 – Numerically predicted energy matrix (left) and power matrix (right) at 1:20 scale.

There are several points of interest going into the testing campaign, primarily relating to hydrodynamic scaling, and the effects of the gap in the aft hull (with potential associated 'moonpooling' effects).

8.3.1 Moonpooling effects

A 'moonpool' is typically an enclosed perimeter of water such as an opening in the hull of a marine vessel. It is often used as a miniature dock, to enable operations such as lowering equipment into the sea. The same term is used to refer to the opening or gap in the aft hull of the WEC.

Mocean's numerical model simulations in the frequency domain suggested that there was next to no difference in the hydrodynamics predicted by the numerical model when adding a patch to rigidly cover the gap in the aft hull, where some 'moonpooling' (i.e. sloshing) effects were observed during tests carried out at the

University of Plymouth COAST Lab. It is therefore of interest to run even just a few cases with the aft gap filled in, to check whether this concurs with WAMIT predictions.

Results from testing conducted at the Plymouth COAST Lab (with the passive model version) suggest a good match between numerical and experimental data without needing to consider the influence of the moonpool in a specific way; its geometrical presence seems to be sufficient to account for the model's hydrodynamics. Video footage should help to shed further light on associated effects (see salient behaviour section in Appendix H). Given the visible moonpooling behaviour indicated by the COAST Lab, it is decided to include a model version with the gap filled in to note any changes in behaviour.

8.3.2 Hydrodynamic scaling

A passive 40th scale model was also planned, in both gap and gapless configurations, to be compared with the 20th scale model with the hinge PTO switched off. In terms of the hydrodynamic scaling investigation, this could be a useful study because Mocean's numerical model assumes that drag coefficients do not change when scaling up, even though they may be very different in reality. As long as the geometries are sufficiently similar, mass properties can be accounted for in the numerical model. The expectation is to gain some insight into how well Froude scaling applies. This will also require a careful consideration of wave heights used – i.e. particular wave effects will only be visible, and will become more significant, when the waves are steep enough.

On the other hand, it can be argued that such scaling efforts may not yield sufficiently certain outcomes. This is because the impact of scaling is most relevant when extrapolating to a full-scale machine. Thus, if differences between 20th and 40th scales exist, it is not clear what this would imply about a 10th scale or even a full-scale machine. There will also likely be difficulties in assigning the measured differences to hydrodynamic scaling rather than other physical differences in the model – for example, hinge friction – or to the different wave quality at the two scales owing to, for example, differences in tank reflections.

Nevertheless, tank reflections will be measured in both cases, and other aspects of the tests will provide insight as to the effects of friction, e.g. by comparing the

20^{th} active model (with hinge switched off) to the passive model at the same scale. Another source of insight will be a comparison of gap and gapless responses at both 20^{th} and 40^{th} scales. An element to pay close attention to is the fact that the tank depth (i.e. absolute depth) remains constant, so wave numbers may not necessarily scale. One may have intermediate depth waves at 20^{th} scale that are effectively deep waves at 40^{th} scale. This has repercussions on the effective steepness and power associated with a given sea state (Noble *et al.*, 2017). An additional note on viscous loss effects from previous Mocean testing campaigns is provided in the Appendix D, confirming the proportionally greater influence of viscous losses at smaller scale.

8.4 Testing campaign aims

This test campaign encompasses the following test objectives (TOs):

1) Validate numerical model prediction of power absorption
    a) Power performance evaluated as per IEC Stage 1 (RAO from regular waves), Stage 2 (experimental power matrix produced to estimate AEP), and Stage 3 (actual power matrix using scaled power conversion chain) criteria.
    b) Verify whether the numerical model can predict physical behaviour accurately enough without an explicit wave channel hydrodynamic model
        i) Validation work carried out with Plymouth COAST Lab obtained data (and passive BST-folding model) suggest that damping plates were not necessary to calibrate the time-domain numerical model – is this still going to be the case here?
2) Evaluate possible errors introduced by non-zero friction in PTO (i.e. suitability of PTO physical model set-up)
    a) Quantify uncertainty introduced in power estimates given PTO dry characterisation (Chapter 7).
3) Provide mooring loads experienced by WEC under “operating” conditions (i.e. WEC actively extracting power from waves)
    a) Evaluate the effect of stiffer ‘taut’ mooring system on RAO response and power capture – in particular, whether the RAO peak is shifted to higher frequencies

   b) Evaluate effect of changing line angles in taut mooring system on WEC response and line loads
4) Provide comparison with Blue X 10th scale tests (to demonstrate design/performance progress)
   a) According to the following metrics:
      i) AEP; AEP/mass; AEP/max PTO force; CWR; max-to-mean power ratio; max angles; etc.
5) Provide comparison with BST-baseline 20th tests (to demonstrate design/performance progress)
   a) Metrics as above, though numerical results to be used for metrics that necessitate PTO presence
6) Provide comparison – and build on – Plymouth 20th tests with passive hinge (to check for consistency and repeatability)[69]
   a) Comparison of Plymouth RAOs with active model having PTO switched off
   b) Ideally compare natural response frequencies from pull-and-release decay tests
7) Provide comparison between physical model behaviour with and without hull gap (i.e. evaluate potential moonpool effects)[70]
   a) In particular, evaluate the degree of nonlinearity of the hull gap version. This assessment can also be observational (based on video footage in tank)
8) 40th scale passive test to provide hydrodynamic scaling comparison of:
   a) The variation in non-dimensional Morison damping coefficients at the two scales
   b) Whether their values are consistent with the two aft hull geometry variations (gap vs no gap)

[69] This depends on achievable waves in the CT and also on knowledge of waves ran in COAST Lab – unfortunately COAST Lab personnel was unable to confirm which irregular sea states were run, and no decay tests were performed.

[70] The latest Blue Star geometry from a Mocean FEED project is not dissimilar from the BST version being tested here, just without the hull gap. In addition, Mocean has not ruled out a folding WEC so this is also useful prospectively.

In general, the idea is to follow available/applicable standards while maintaining consistency with Mocean best practices and previous campaigns; wherever these clash is pointed out.

8.4.1 Design Statement

In accordance with IEC TS 62600-103 test standard guidance (IEC TS 62600-103, 2018), where words are underlined additionally by the thesis author,

> *"the basic rationale for the staged development process is to reduce the technical and financial risk of developing a wave energy device by investigating appropriate device parameters and the suitable geometric scale".*

This test programme aims to contribute to both investigations. Two questions immediately arise.

8.4.1.1 What are the appropriate device parameters?

This refers to what understanding is sought from these tests and about the device. The answer is those that enable power conversion measurement and those that help to validate the numerical model predictions - i.e. regular and irregular RAOs, power conversion vis-à-vis torque limit and PTO damping, mooring loads, etc. In addition, the presence of cables, friction and scaling effects (and nonlinearities, even more so due to hull gap); these are the parameters thought to be of interest and of relatively greatest impact.

8.4.1.2 What is the suitable geometric scale?

We hypothesise that 20th scale will be suitable in allowing the investigation of the above parameters with sufficient accuracy[71] (and - but not necessarily with - precision), in order to conduct smaller scale, faster-turnaround tests. We may find that the scale is too small (giving unacceptable levels of error), or not small enough (being unable to cover enough range of sea states with the Curved Tank, and would thus need a smaller PTO system that can be implemented). To address this question more satisfactorily, a 40th scale passive model is included

[71] Accuracy describes how close a measurement is to the 'true' value. This is differentiated from precision, which refers to how consistent or repeatable the measurement is. In other words, the former mostly relates to assessment, while the latter to optimisation.

in this testing campaign in the attempt to gauge scaling effects on measurement values and uncertainty. This question can only really be answered with test results in hand (see Chapter 9 and 10). A smaller scale is theoretically explored based on time, cost, and convenience.

Relevant guidance and applicability of IEC TS 62600-103 guidelines is given in Appendix H.

8.5 Physical model build

The figures that follow illustrate the overall physical 20th and 40th scale models as designed.

8.5.1 20th scale model

For reference, Figure 101 shows the direction of incoming waves with respect to the model and hinge axis, which is the axis of rotation between the two hulls. The moorings attach to a single point below the fwd wave channel. The overall model, including Qualisys targets and net mass of cables[72], weighs 3,109g. It has overall dimensions 'as designed' of 926.5mm length (unfolded), by 120mm width (of aft hull), by 100mm overall height (excluding Qualisys rods and targets). Appendix H contains the detailed mass and inertia properties as per the trimming analysis conducted in the trimming tank and via SolidWorks CAD (see Appendix N). Each hull can be independently trimmed, as is desirable. The same is true for the 40th model.

[72] The cables are not neutrally buoyant.

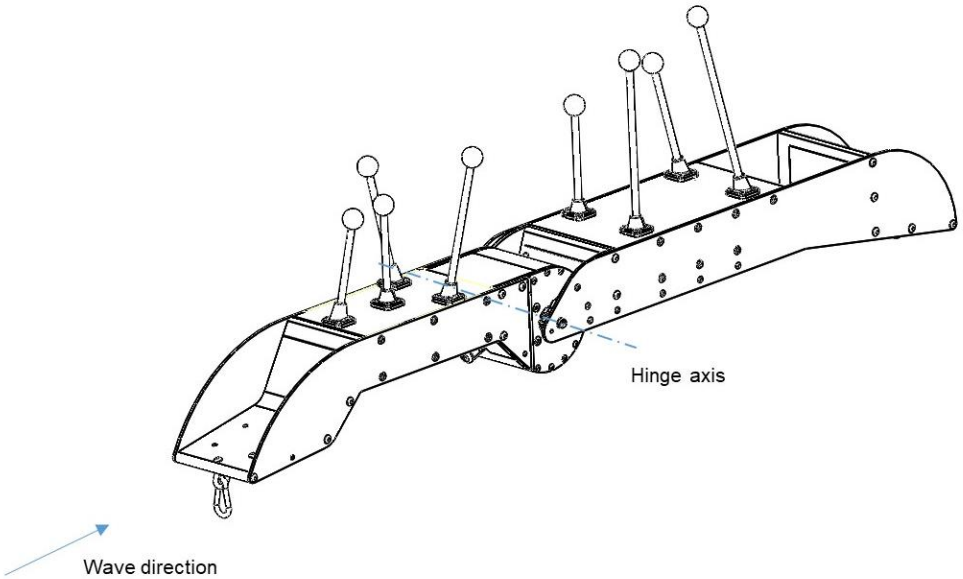

Figure 101 - Showing incident wave direction and location of hinge axis.

Figure 102 is an annotated diagram of the active 20th scale model, with materials shown in the key on the left-hand side. Additional material detail is given in the Appendix H. The model's PTO is housed within the nacelle. A gap in the aft hull is visible ahead of the aft WC, which enables the model to fully fold.

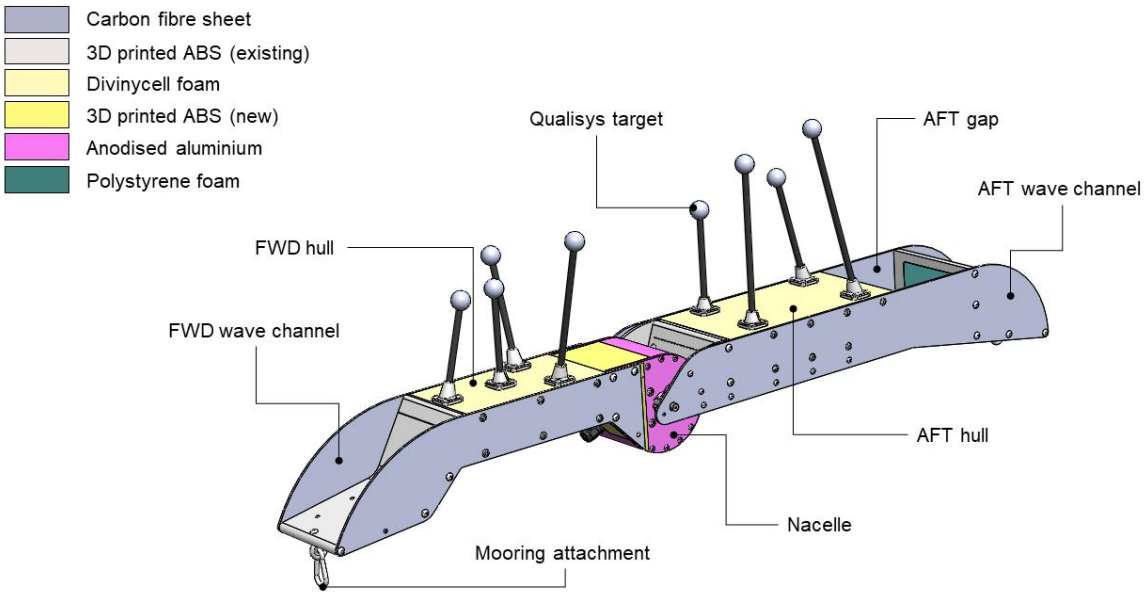

Figure 102 - Showing CAD representation of motorised model.

Appendix H contains a diagram showing more details regarding the mechanical arrangement around the nacelle, particularly in terms of the clamp arm.

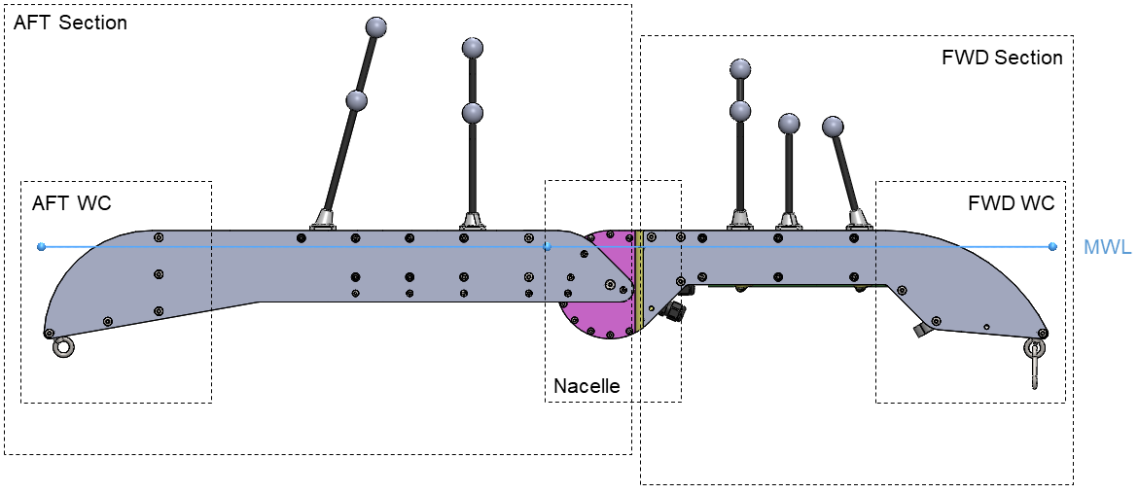

Figure 103 – Showing references to salient model areas (waves move right to left). The view is on the model's starboard side. The mean water line (MWL) plane is also shown, indicating the target trim above the hinge axis.

The target mean water line (MWL) is 35mm above the hinge axis, as shown in Figure 103. The estimated achieved trim was 36mm. The accompanying trimming analysis is outlined in Appendix N. As will be discussed further, the likely overall MWL variation during testing is approximately +/-2mm. However, an initial equilibrium point is calculated based on observation and CAD trimming analysis in order to obtain the MWL and associated wetted area required for numerical supporting analysis.

8.5.1.1 Power take off

Inclusion of a PTO relates particularly to *TOs 1-6* and *9*.

The PTO is located inside the nacelle, and modelled as a motor able to provide a braking torque that varies as a function of current input. Since no torque sensor can be included in the nacelle due to lack of sufficient space, the motor, its controller, and associated PTO parts (e.g. the rotary seal that prevents water ingress at the motor shaft perimeter) were characterised ahead of wet testing (see Chapter 7). Crucially, this enabled the measurement of friction behaviour, and assessment of whether this may affect the reliability of the braking torque being inferred from a current reading during wet tests, as opposed to direct measurement. Chapter 7 describes the motor characterisation in detail. Calibration parameters are reported in Table 22. Note that damping coefficient and spring coefficients are given per unit of PTO gain.

Calibration variable	**Mean**	**Std**	**Error (Std/Mean)*100**
D_{norm} [Nms/rad]	0.004254	0.0001085	2.55
T_{const} [Nm/A]	0.1525	0.003091	2.03
k_{norm} [Nm/rad]	0.006640	0.001272	19.16

Table 22 – Summary of motor calibration parameters.

The possibility of toggling power extraction on/off (by controlling whether the motor is engaged or disengaged) is relevant from a numerical modelling perspective, as well as experimental. An interesting aspect requiring further understanding is the impact of power extraction on the WAMIT results. In order to compute the second order hydrodynamic behaviour (e.g. mean drift forces), these are dependent on whether power extraction occurs, because they are also dependent on the WEC motions. Additionally, there is the direct effect of having power extraction active or not at the hinge, which determines the flexing behaviour of the WEC.

From a validation perspective, it is valuable to have a set of comparable tests with power extraction on and off. When power extraction is off, the model is effectively passive (albeit subject to some non-zero friction effects).

8.5.2 40th scale model

The 40th model as-built, including the AFT hull gap and Qualisys markers, is shown in Figure 104.

Figure 104 - The 40th scale model primarily build from black 3D-printed ABS material.

The green areas visible in Figure 104 are strips of thin tape whose upper horizontal edge is used to mark the target MWL. In the 20th model, MWL target markings are included as slight recesses in the 3D-printed components builds, which would not be visible here due to black ABS material. A trim analysis is provided in Appendix H, as well as more detail on its make-up and build. It has a 60mm wide aft hull, a 50mm diameter nacelle, and is approximately 463mm in length. The MWL is at 16.5mm above the hinge axis.

A summary of 20th and 40th model properties (with gap in aft hull versions) is given in Table 23 at equivalent full-scale values.

	1:20 model (eq. full scale values)			1:40 model (eq. full scale values)		
Dimensions [m]	Length	Width	Height	Length	Width	Height
Overall	18.53	2.4	2.0	18.53	2.4	2.0
Trim line [m above hinge axis]	0.72			0.66		
Mass [tonnes]						
Fwd section	13.83			13.11		
Aft section	11.04			10.52		
Overall	24.87*			23.63		
Centre of mass [m]	x	y	z	x	y	z
Fwd section	0.013	-1.234	2.280	0.002	-0.017	2.387
Aft section	-0.003	0.129	-4.764	0.004	0.224	-4.698
Overall	0.006	-0.629	-0.846	0.003	0.090	-0.766
Moments of inertia** [10^3 * kgm^2]						
Fwd section	x	y	z	x	y	z
x	452.820	0.177	-0.403	187.624	0.099	-0.006
y	0.177	185.408	-102.124	0.099	185.561	-10.342
z	-0.403	-102.124	277.899	0.071	-10.342	12.590
Aft section	x	y	z	x	y	z
X	365.343	0.311	0.436	327.808	0.069	-0.454
Y	0.331	370.842	-0.698	0.069	333.418	-9.992
z	0.436	-0.698	16.773	-0.454	-9.992	11.885
Overall	x	y	z	x	y	z
X	818.163	0.508	0.033	515.431	0.167	-0.382
y	0.508	556.250	-0.103	0.167	518.979	-20.334
z	0.033	-0.103	294.671	-0.382	-20.334	24.475

Table 23 - Summary of 20th and 40th model 'as-built' properties (full-scale equivalents, with gap).

NB: Table 23 values include ballast and buoyancy to achieve desired trim, as well as Qualisys kit and fasteners.

** Includes net mass of cables that hang to tank bottom (estimated as best as possible from trim analysis)*
*** taken from the model origin (centre of hinge axis) and aligned with the output coordinates (see Chapter6)*

8.6 Test set-up

8.6.1 Mooring system

The mooring system set-up choice is relevant for several aims of the test campaign, specifically: *TO3-6*. The choice and design of the mooring system are outlined in Appendix F. The slack mooring set up was the same as that used for BST-baseline (see Chapter 6). The taut mooring set up includes ad hoc fabricated poles that are mounted at the three desired locations in the tank, to maintain a 120deg spacing between them. Detailed annotated images are given in the Appendix. The model is placed in the tank with its rest (equilibrium) position as per BST-baseline (see Chapter 6). Ideally, the springs that link each line to the load cell would always remain above the water line, however, in some cases they penetrated the MWL. The mooring poles were built to enable line angles to be varied by making adjustments from the tank sides.

8.6.2 Equipment/sensors

The following sensors are utilised during this test campaign:

- Qualisys optical tracking system (4 cameras)
- 3x load cells to measure mooring loads
- AKM motor + drive (see Chapter 7)
- Controller to set required gain and other PTO parameters
- 3x wave gauges, as per BST-baseline tests

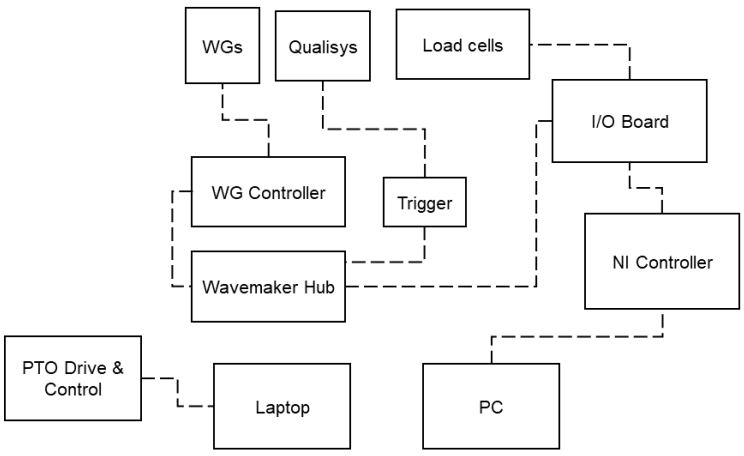

Figure 105 - Showing measurement set-up during active BST-folding tests.

8.6.3 Tank capabilities

A conservative Curved Tank operating envelope is investigated and reported in Chapter 6. Here the identified envelope is compared to the seas to be simulated in this testing round. IEC guidelines envisage wave measurements either while the model is in the tank or with an empty tank before the model is deployed.

In the former case:

- There is no need to carry out directional spreading waves in Stage 1
- For irregular long-crested waves in Stage 1: deploy at least 2 measurements during the tests, one in front and one flanking the device
- For irregular long-crested waves in Stage 2: deploy at least 4 measurements during tests: in front, behind, and flanking each side of the device.

In the latter case (characterisation with model absent):

- Special attention is to be paid to minimise reflections of scattered waves from the model.
- Approach is not recommended for testing when the model occupies a considerable part of the tank and therefore is more likely to contaminate incident waves via reflections
    - This is assumed not to be the case in this testing round (see Chapter 6 diagram) where model is shown approximately to scale).

An irregular wave envelope is derived from regular wave measurements collected in Chapter 6; supporting calculations for the envelope boundaries are provided in Appendix F. The envelope is shown later in this chapter in combination with occurrence and energy matrices. It is compared with FloWave tank boundary envelopes in Chapter 9.

8.7 Test plan

Table 24 summarises the series, runs, and sets. A *set* (e.g. IROa) contains a number of *runs* (i.e. IRO01 and IRO02), whose measured quantities are logged according to the *series* (i.e. names assigned to the measurements); in this case the 'R' series.

Series	Title	Runs	Experiment (or Set)	Cal run? [Y/N]	Series Duration	T. Mooring		C. Mooring		
						20th Gap	20th No Gap	20th Gap	40th Gap	40th No Gap
A01-16	Freq sweep, S50, Off	RR01-16	RRa	Y	58 mins	X	X (RR08 repeat)	X		
B01-16	Freq sweep, S100, Off	RR17-32	RRb	Y	58 mins	X	X	X	X	X
C01-16	Freq sweep, S50, d2	RR01-16	RRa		58 mins	X	X	X* (RR16 missing)		
D01-16	Freq sweep, S100, d1	RR01-16	RRb		58 mins	X		X		
E01-16	Freq sweep, S100, d3	RR01-16	RRb		58 mins	X		X		
F01-16	Freq sweep, S100, d2	RR17-32	RRb		58 mins	X	X	X		
G01-10	Amp sweep, peak f, Off	AR01-10	ARa	Y	36 mins	X	X	X	X	X
H01-10	Amp sweep, peak f, d2	AR01-10	ARa		36 mins	X*		X*		
G11-20	Amp sweep, second f, Off	AR10-20	ARb	Y	36 mins	X		X		
I01-05	Irreg sweep, long, S13, Off	IRL11-15	IRRa	Y	1 hr	X	X	X	X, with *IRRf.exp*	
J01-05	Irreg sweep, long, S13, d2	IRL11-15	IRLa		1 hr	X	X	X		
K01-04	Irreg sweep, long, S23, d2	IRL21-24	IRLb	Y	50 mins	X	X** (IRL23 only)	X		
L01-03	Irreg sweep, long, S33, d2	IRL31-33	IRLc	Y	35 mins	X	X*	X*		
M01-03 & 04-06	Irreg sweep, short6, S33, d2	IRS01-03 + IRS21-23	IRSa + IRSc	Y	1 hr	X		X		

N01-03	Irreg sweep, short10, S33, d2	IRS11-13	IRSb	Y	35 mins	X	X*	X		
O01-08	Irreg sweep, long, S13, d2, Ang2	IRL11-15	IRLa		1 hr	X				
P01-08	Irreg sweep, long, S13, d2, Ang3	IRL11-15	IRLa		1 hr	X** (01-04 error on STBD pole)				
Q01-05	Irreg sweep, long, S23, d2, seeds 1-5	IRL231-235	IRLd	Y	1 hr	X		X		
Q06-08, 09-10	Irreg sweep, long, S23, other d values	IRL23	IRLb		35 mins	X		X		
R01-02	Ir0, S sweep, Off, +repeat	IRO01-02	IROa	Y, 2x 3runs	32 mins	X	X	X		
S01-02	Ir0, S sweep, d2, +repeat	IRO01-02	IROa		32 mins	X	X	X		
T01-02	Ir0, envelope sweep, d2, +repeat	IRO11-12	IROb	Y, 2x 3runs	32 mins	X*	X*	X*		
U01-10; U11-13 (seeds)	Ir0 energy, d0-4 +repeats, d2 with seeds	IRO21-22; IRO211-213	IROc + d	Y, 2x 3runs, 1x 3runs	1.5 hr + 26mins	X* (no U05 or U10)	X (just d0-4 with IRO21)	X*		
V	Gain limit search	-	-		~ 30 mins	X		X		
Dsweep01-09	PTO damping scan, d1-11	RR20,RR25, RR30	Dsweep		30 mins	X	X*	X		
X01-08	T limit scan, d2, T1-4	IRX01, IRX02	IRLx	Y	1.8 hr	X		X		
Y01-12	Release tests, Off, d2, d3	-			~ 30 mins	X (no d3)	X	X	X	X
Z	{spare}					X				
Pcapture	Num model settings	IRX01 (and IRX03)	IRLx		~ 20 mins	X	X (no IRX03)	X		

Table 24 - Summary table for BST-folding test campaign.

KEY:

- d0-d4 = gains of 0, 20, 40, 60, 80
- Ang2-3 = mooring line vertical inclination is varied from the baseline to two additional angles.
- Yellow cells are incomplete runs, either due to:
    - *Means cut-outs occurred – thermally limited events; **Other errors

NB: IRX02 sea never reached torque limit, thus IRX03 was later introduced but not run in empty basin.

Tuning of the PTO-related parameters – PTO damping, torque limit, thermal limit – is also discussed in Appendix H. Power matrix coverage of the chosen sea states is outlined in Section 8.7.2. Prescribed and proposed seas are outlined in Appendix K (Irregular seas) and L (Ir0 seas). In short, the following seas were run:

Type of sea	**Repeat time [s]**	**Total run time [s]**	**Settling time [s]**	**Notes**
Regular	64	96	120	EIC minimum mandated number of waves, less than 50 run for lower frequencies; 3 wave amplitude sweeps in total as required
Irregular (long-crested)	512	544	240	EIC minimum mandated number of waves: 250 waves; Tp range 1.0-1.8s so can assume range of 1-(1/1.8) waves per second, as required.
Irregular (short-crested)	512	544	240	EIC minimum mandated number of waves: 1500; 512s repeat time equates to ~37mins full-scale, and 30s is typically considered to capture representative conditions for a given site data collection. Further info in Appendix.
Ir0	256	288	180	Not in IEC standards; further outlined in Section 8.7.1.

Table 25 - Summary of sea typology run duration parameters.

Note that this test plan was developed empirically, from a combination of tank limits, model PTO limits, and prior experience of testing Mocean physical models at similar scale(s).

8.7.1 Ir0 seas

The concept of ‘Ir0’ sea definition and implementation was introduced in (Pascal *et al.*, 2021). It was used to characterise the fundamental behaviour of multiple configurations of the same WEC concept in order to enable comparative assessments. It is adapted and adopted here as a promising avenue for streamlining future test campaigns. In the case of (Pascal *et al.*, 2021), it was used to select the best configuration among 51, over 2 weeks of tests (Refer to Chapter 3, Section 3.4.2).

For this research’s purposes, Ir0 would be a particularly useful method to quickly iterate between different PTO damping configurations more efficiently than by doing longer frequency and/or amplitude sweeps. It is also an opportunity to have greater measurement resolution at periods where the second undamped response peak occurs (around 5.3s Tz) and to extend the range of frequencies covered (i.e. more than the 16 frequencies for each regular wave sweep).

Ir0 seas are carried out with both compliant and taut mooring set-ups, to enable a comparison of load predictions obtained with different methodologies. The following principles are applied to the Ir0 methodology, building from those applied by the authors in (Pascal *et al.*, 2021):

- An amplitude spectrum is defined so as to be in the middle of the “scatter diagram” or occurrence table, and giving higher amplitude to more ‘important’ components – i.e. those with higher AEP contributions
    - Ir0 sea defined with 25 components and a 256s repeat period
    - Spectrum “shape” set up to have more energy in the middle period, but still enough range.
    - Target [Hs, Te] combination is [2.1m, 10.0s]
- Three calibration runs are performed in the absence of the model in the basin – all of these are run with the same random phases in each repeat run.
- Check whether the amplitude spectrum peaks are clear or whether too much spilling occurs.

- Repeat time of 256s + ramp up time of 60s for device to reach steady state. The latter can be ~30s in our case since the Curved Tank is shorter than the one used by the authors (Aalborg University test basin).
- Equivalent [Hs, Te] values of a particular sea are calculated from the discrete spectrum moments.

8.7.1.1 Proposed IR0 seas

All Ir0 seas are run three times in an empty basin first, to measure reflections and to check amplitudes of each fundamental frequency component that are achieved. It is also ensured that the [Hs, Te] combinations match some of the irregular seas in the long-crested sweeps to enable meaningful comparisons. For reference, in the case of the Central North Sea wave climate, the most commonly occurring sea in the occurrence matrix is [1.75m Hs, 6.5s Te], followed by [0.75m, 4.5s] and [2.25m, 7.5s].

Three sets of *Ir0* seas are hereby defined (all have a repeat time of 256s and a ramp up of 32s; thus 288s total run time):

1. 'Steepness' seas {IROa} – based on constant steepness frequency components (to isolate wave from WEC non-linearities)[73]; higher steepness corresponds to higher energy
2. 'Envelope' seas {IROb} – based on wave tank envelope limits, where the shape of the spectrum follows the shape of the tank envelope
3. 'Energy' seas {IROc} – based on a pre-defined target [Hs, Te] combination, based on the middle hot spot of the wave resource occurrence matrix or of the energy matrix of Blue Star-folding

Note that *Energy* seas are primarily informed by the WEC device characteristics, though some adjustment in period was required in order to respect tank envelope limits. The IROc is overlaid to the energy matrix of the device in Figure 106. In addition, 3 repeat seas of IR0c are defined but with different seed numbers in order to introduce different component phasing. IR0c has a seed

[73] For the waves, constant steepness maintains geometrical similarity and non-linearity content so it is a good metric to use. However, for the WEC non-linearity, it is the relative motion of the WEC to the water that is of more practical importance, and the load shedding, namely the relative reduction of power and thus stress to the WEC and PTO as wave size increases. For power, load shedding is probably more important at the WEC resonant period; for survival, it is the WEC response (and shedding) at the long high waves. Thus, choosing 3x Ir0 sets and running each over a range of steepness up to the maximum seems a valid and valuable approach.

number of 1, while the three seas in {IROd} experiment have seed numbers 4, 9 and 14. Some trial and error adjustment of the random phase for each Ir0 set was carried out in order to avoid power clipping from the tank generation software. As a result, IROa sets had a random seed number of 14, IRObof 7, and IROc (baseline) of 1.0. IROd series was then a copy of IROc but with altered seed numbers of 4, 9, and 14.

Refer to Appendix L for a methodology check of the seas used in (Pascal *et al.*, 2021), as well as the process carried out to identify suitable Ir0 seas that were compatible with Curved Tank generation capabilities. Demand and measured Ir0 conditions are also outlined in Appendix L. Equivalent demand Hs, Te combinations are summarised in Table 26, and shown in Figure 106 and Figure 107.

Ir0 sea type (& name)	**Gain**	**Equivalent Steepness**	**Hs [m]**	**Te [s]**
Steepness	0.50	1/17.2	2.18	6.13
Steepness	0.33	1/13.5	3.10	6.46
Envelope	0.05	1/12.7	2.19	5.27
Envelope	0.10	1/6.33	4.39	5.27
Energy	1.00	1/17.3	1.75	5.51
Energy	1.25	1/13.7	2.22	5.51

Table 26 - Summary of demand properties of Ir0 seas run. Hs and Te are given at full-scale.

It can be seen from the equivalent steepness values in Table 26 that the resultant Ir0 conditions are relatively high steepness seas. In the case of *Envelope* with 0.10 gain, they verge on the physically unfeasible boundary of ~1/7. Note that the seed sweep was run with an *Energy* sea having gain 1.0, thus [1.75m, 5.51s] equivalent conditions of Hs, Te.

8.7.2 Power matrix coverage

This section summarises the power matrix coverage of the seas run.

21 long-crested seas were run in total, including Ir0 runs, and excluding seed variation runs and repeats. A summary is provided in Table 27.

Type of sea	Wave run name	Hs (full-scale), [m]	Te (full-scale), [s]	Lim. Steepness
Bretschneider				
{IRLa}	IRL11	0.37	3.91	1/3
	IRL12	0.53	4.70	1/3
	IRL13	0.73	5.48	1/3
	IRL14	0.95	6.27	1/3
	IRL15	1.20	7.04	1/3
{IRLb}	IRL21	0.74	3.91	2/3
	IRL22	1.07	4.70	2/3
	IRL23	1.45	5.48	2/3
	IRL24	1.90	6.27	2/3
{IRLc}	IRL31	1.11	3.91	3/3
	IRL32	1.60	4.70	3/3
	IRL33	2.18	5.48	3/3
{IRLx}				
(highest occ. sea)	IRX01	1.25	6.50	1/2.6
(mode steepness)	IRX02	0.90	5.50	1/2.6
	IRX03	1.50	6.65	1/2.3
IR0				
(steepness), {IROa}	IRO01	2.18	6.13	1/1.24 = 0.81
	IRO02	3.10	6.46	1/0.98 = 1.02
(envelope), {IROb}	IRO11	2.19	5.27	1/0.92 = 1.09
	IRO12	4.39	5.27	1/0.46 = 2.17
(energy), {IROc}	IRO21	1.75	5.51	1/1.26 = 0.79
	IRO22	2.22	5.51	1/0.99 = 1.01

Table 27 - Irregular seas summary (long-crested).

Short-crested seas are also run at limiting steepness, with angle modifier *cos(2s)* where *s* is either 6 or 10. The phase seed is 1, the angle modifier seed is 3. In most cases, max and min angles are specified within -20deg to +20deg range as recommended by (Pascal *et al.*, 2009). The final two seas are specified to check the effect of greater angle variability (+/- 40deg) for the single components in the spectra.

Type of sea	γ	Wave run name	Hs (full-scale), [m]	Te (full-scale), [s]	s	Steepness limit[74]	Angle* [+/-deg]
Bretschneider	1.0	IRS01	1.11	3.91	6	Full (3/3)	20
Bretschneider	1.0	IRS02	1.60	4.70	6	Full	20
Bretschneider	1.0	IRS03	2.18	5.48	6	Full	20
Bretschneider	1.0	IRS11	1.11	3.91	10	Full	20
Bretschneider	1.0	IRS12	1.60	4.70	10	Full	20
Bretschneider	1.0	IRS13	2.18	5.48	10	Full	20
Jonswap	3.3	IRS21	1.75	5.86	6	0.70	20
Jonswap	1.0	IRS22	1.60	4.70	6	Full	40
Jonswap	3.3	IRS23	1.75	5.86	6	0.70	40

Table 28 - Irregular seas summary (short-crested).

** refers to the directional limits for single components in the spectra, not the mean directions of propagation.*

As well as the two Bretschneider short-crested sweeps, it is desirable to carry out a more 'realistic' short-crested run that can be compared with the others. To start with, a WES defined IR13 sea is chosen as that most likely to be achievable in the CT. This is a Jonswap sea with full-scale Te of 7.0s and 2.5m Hs, with a spreading factor of 6. However, when input to the CT, it yields 10.74% power clipping. Thus, the same steepness but of lower Hs is defined instead.

More specifically, the Tp of sea IRS21 is 6.69s, giving a steepness of Hs/Tp^2 = 1.75/(6.69^2) = 0.039. When normalised by the full limiting steepness (1/18), this gives 0.70, i.e. 70% of full limiting steepness. This yields 0.01% power clipping due to tank limits, which is minor and thus accepted.

[74] Note that North Atlantic steepness limit is used here (Hs = Te^2/13), as opposed to a literature informed steepness limit of S = 0.14 (for deep water waves, this is equivalent to Hs = Te^2/6.6, approximately double that observed in N Atlantic).

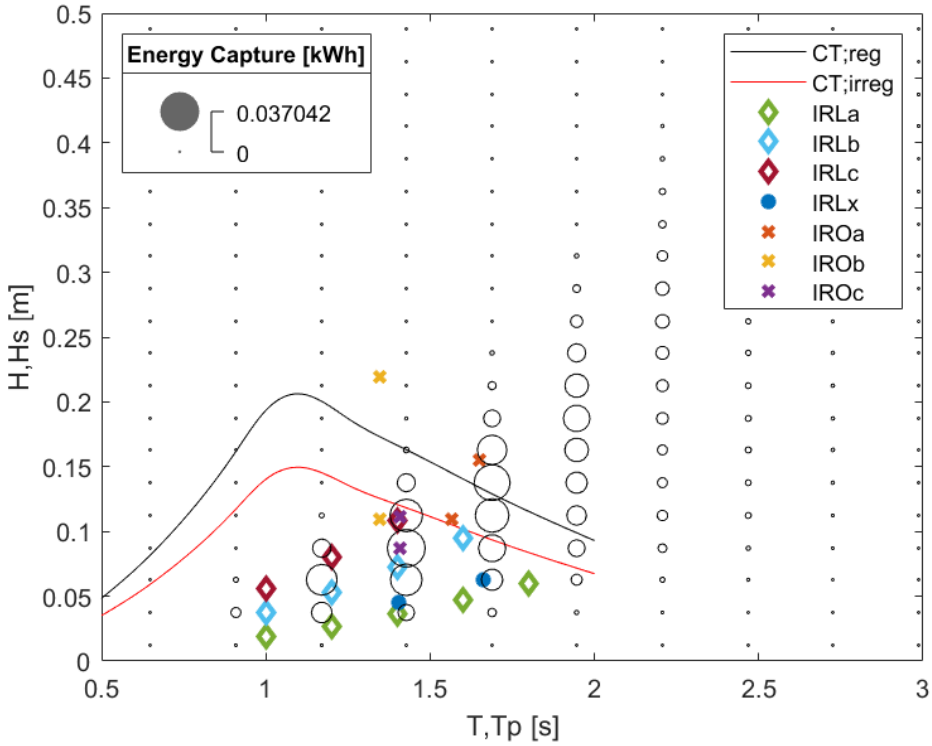

Figure 106 - Energy matrix coverage of long-crested and Ir0 seas, Central North Sea wave climate (1:20 scale). Energy scales as the size of the plotted bubbles.

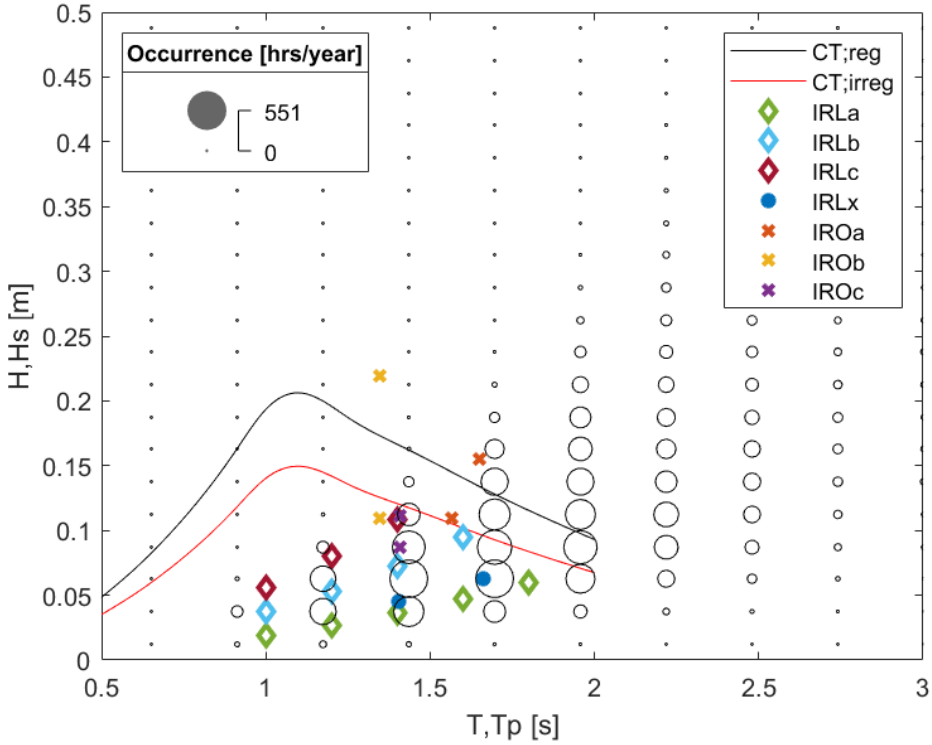

Figure 107 - Selected long-crested irregular and Ir0 seas are overlaid with the occurrence matrix of a Central North Sea wave climate (1:20 scale). Occurrence scales as the size of the plotted bubbles.

Note that IRX03 is missing from the above and below plots. However, observing Figure 107, the IRX03 sea (as defined in Table 26) almost exactly overlaps with the largest occurrence bubble (551 hours/year) around 1.7s, 0.075m. The rhombus shaped points, representing the long-crested sweeps at constant steepness, are also plotted {IRLa-IRLc}. IRO21 {IROc} and IRL23 {IRLb} seas are close and can be used to compare Ir0 results with long-crested approximately equivalents (see further in Chapter 9). Note that IRO02 and IRO12 seas lie outside the theoretical irregular capability envelope. They were still run although the tank flagged warning regarding power limits being reached.

8.8 Empty basin results

A thorough reflection analysis was conducted for regular and Ir0 polychromatic waves to ensure that reflection coefficients were within acceptable ranges for both monochromatic and polychromatic waves.

Sea	**Description**	**R_{coeff} range**	**R_{coeff} mean**
Regular, f sweep	S = 1/50	{2.9, 16.2}	11.1%
Regular, f sweep	S = 1/100	{2.3, 11.1}%	6.2%
Regular, A sweep	f = 0.9375Hz	{1.5, 10.3}%	2.8%
Regular, A sweep	f = 1.1560 Hz	{4.3, 7.0}%	5.5%
Ir0, steepness	Gain = 0.5	{2.4, 29.0}%	9.5%
Ir0, steepness	Gain = 0.33	{0.8, 19.4}%	7.1%
Ir0, envelope	Gain = 0.1	{1.5, 14.6}%	7.0%
Ir0, envelope	Gain = 0.05	{1.2, 20.6}%	8.2%
Ir0, energy	Gain = 1.25	{0.8, 15.3}%	6.9%
Ir0, energy	Gain = 1.0 (seed 1)	{1.3, 16.3}%	6.8%
Ir0, energy	Gain = 1.0, seed 4	{0.9, 14.0}%	5.9%
Ir0, energy	Gain = 1.0, seed 9	{0.8, 18.6}%	6.1%
Ir0, energy	Gain = 1.0, seed 14	{0.8, 18.6}%	6.1%

Table 29 - Summary of reflection coefficients.

NB: very large (>100%) reflection coefficients are yielded for f=2Hz Ir0 components in IROa (steepness) and IRObb (envelope) sweeps, and are therefore excluded from Table 29. IROc (energy) seas are more ‘robust’ due to the minimum amplitude component always being greater than 5mm demand.

Refer to Appendix L for more reflection analysis and calibration details, including demand and measured Ir0 seas.

8.9 Physical model results

An image of the active BST-folding model set up with the taut mooring arrangement is shown in Figure 108. Wavemaker paddles are shown in red along the curved boundary on the right hand side, while the artificial beach can be seen on the left as meshed metal sections jutting into the basin. The image is captured from the transparent flat glass edge of the tank.

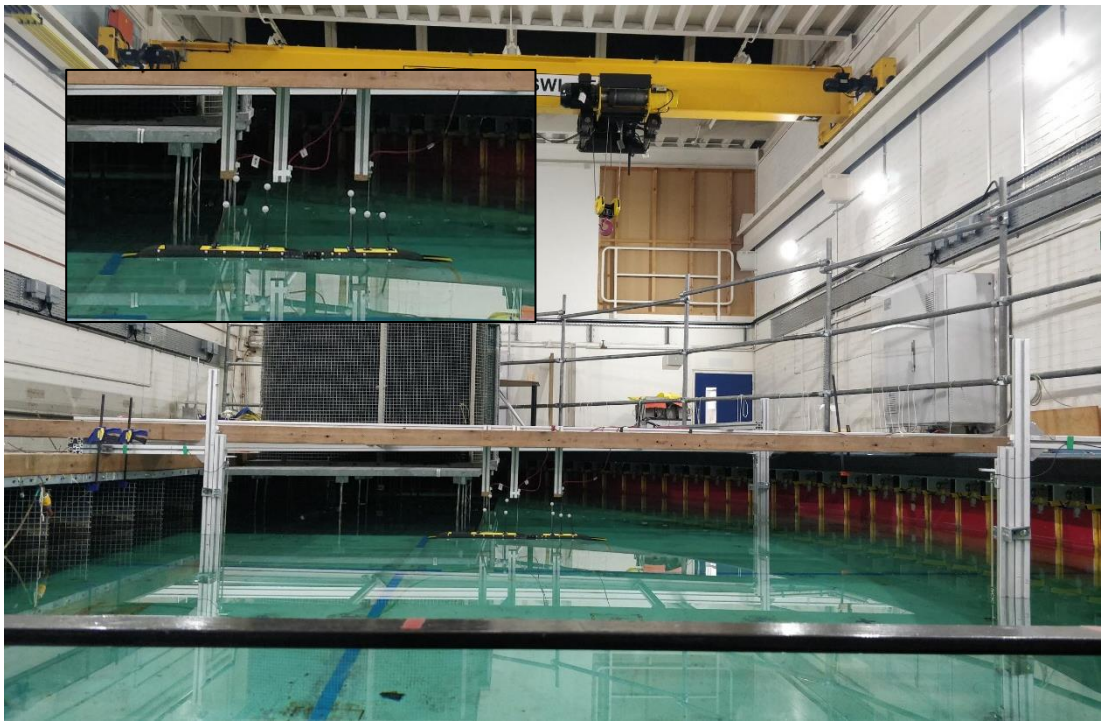

Figure 108 - The BST-folding model with taut mooring in the CT (zoomed section is shown top right with the three wave gauges behind the model).

Beyond validation and power performance, several additional aspects are explored in the test results:

- Effects of scale – by comparing with 40th scale RAOs
- Effects of cables – from decay tests and RAO comparison
- Effects of friction – by comparison with passive model
- Effects of hull gap – by RAO and power absorption comparison
- Effects of methodology (IR0) – by RAO comparison
- Effects of different moorings

8.9.1 Recap

The analysis begins with the default configuration: i.e. 20th scale, motorised, with the gap in the aft hull; and taut mooring. This is the case throughout, unless

explicitly stated otherwise. It is consistent with both Plymouth tests (apart from the passive hinge), and with the numerical validation run alongside.

Before unpacking the experimental data, the two most relevant plots from the SD numerical optimisation leading into this test campaign are presented again.

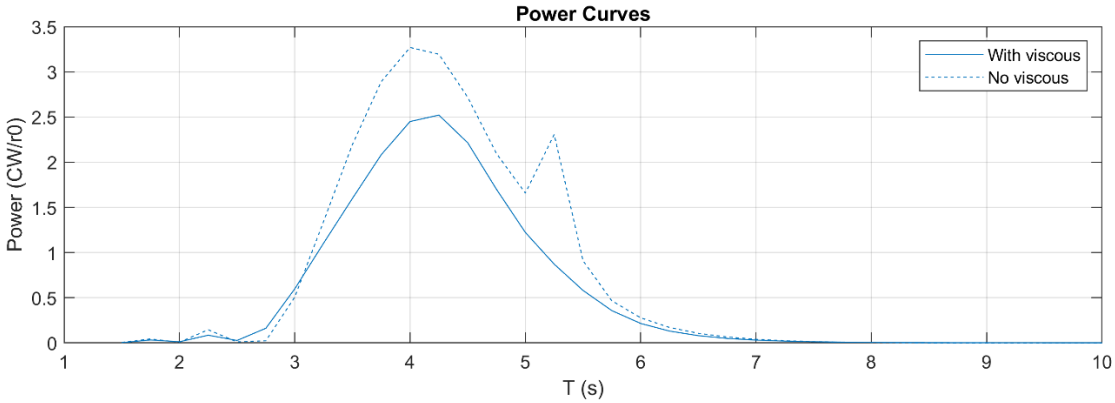

Figure 109 - Predicted capture width ratio (full scale) - with and without viscous damping.

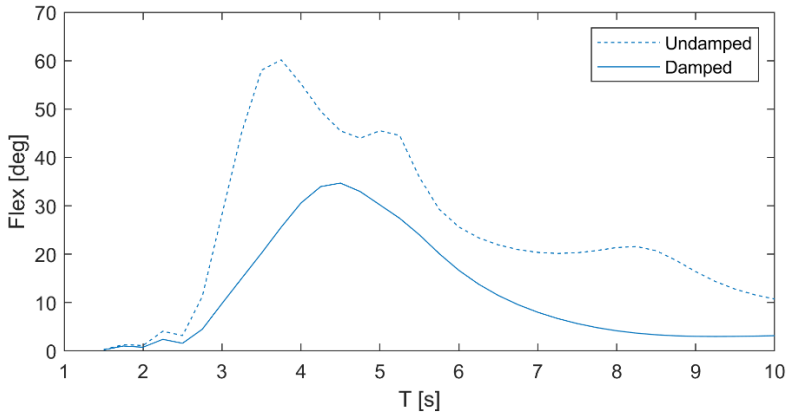

Figure 110 - Predicted flex RAO (full scale) - with and without viscous damping.

In both Figure 109 and Figure 110, the Morison's drag coefficient (Cd) is set to a constant value of 0.8, as calibrated via previous Mocean validation work.

8.9.2 Signal checks

Signal checks are initially carried out to verify the consistency between motor controller (AKM) and Qualisys (QTM) obtained measurements. These can be found in Appendix H. In short, a very close match between AKM controller angular position measurement and QTM Qualisys equivalent is measured, with typical differences being <0.1deg, including around the peak response frequency

of 1.09385Hz. Since the QTM signal (42Hz noise) is noisier than the AKM signal (50Hz noise), the position signal from QTM is low-pass (LP) filtered at 10Hz before differentiating, yielding a much closer match with the AKM velocity signal than its unfiltered counterpart. The effects are shown in Appendix H and in Figure 111. It should be noted that the velocity signals from the motor controller are LP filtered at 20Hz before being fed to the feedback loop in the controller that determines the application of the resisting motor torque.

As a final sanity check, the AKM position signal is differentiated to check that the resulting hinge velocity matches that computed by the AKM controller directly (raw). The raw velocity is also integrated to provide an angular position check. Both show excellent agreement - see Appendix H. Based on this preliminary analysis, it is decided to use AKM signals for hinge velocity related calculations, while it is deemed inconsequential to use QTM or AKM signals for position related calculations such as DoF RAOs.

RAOs are defined as the ratio of the magnitude of fundamental spectrum component for a given DoF response to the corresponding incident wave amplitude, net of reflections. All empirical data in this Chapter accounts for reflections via the Suryanto method (Suryanto, 2006); RAO values are computed based on incident amplitude spectra as opposed to overall amplitude spectra.

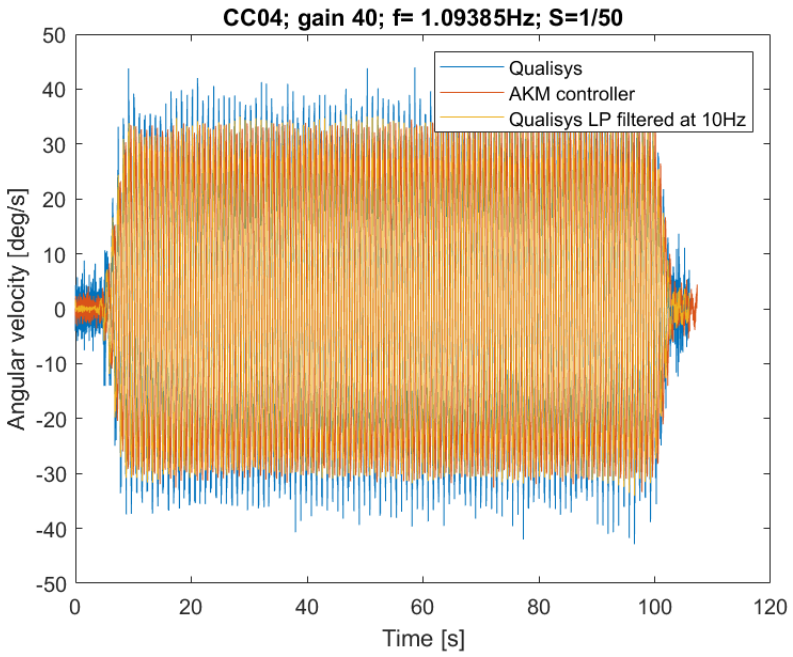

Figure 111 - AKM vs QTM velocity time series check; QTM is LP filtered at 10Hz.

8.9.3 Regular wave RAOs

Incident wave amplitudes and associated reflection coefficients are found in Appendix J. The following section presents flex degree of freedom RAOs.

8.9.3.1 Flex RAOs

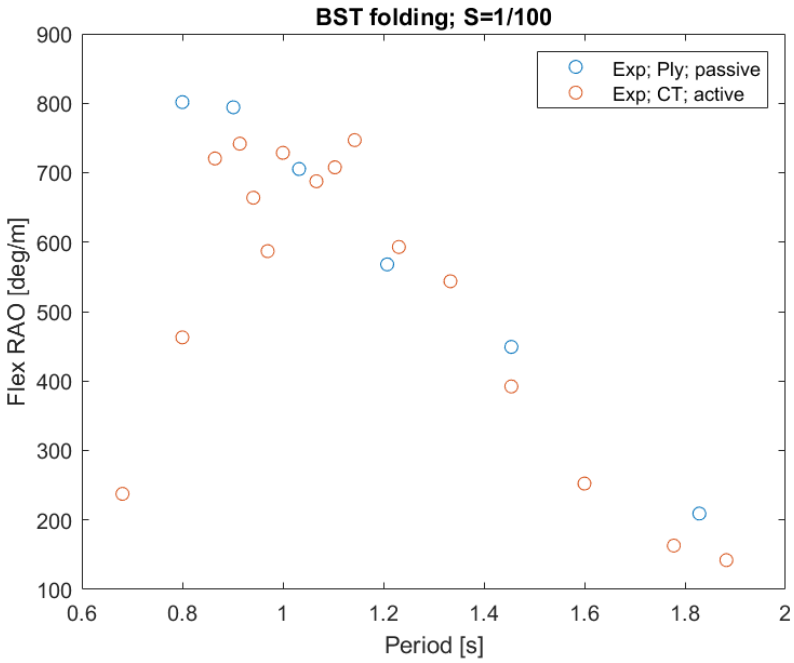

Figure 112 - Damping off comparison of active and passive BST-folding models.

Figure 112 shows a comparison between experimental data obtained via Qualisys, of the non-motorised (i.e. passive version) of the BST-folding model tested in the COAST Lab (in Plymouth, “Ply”) and the motorised model (i.e. active version) with PTO damping switched off, which was tested in the Curved Tank (“CT”). Both RAOs are obtained with regular waves of steepness 1/100, and the same depth-agnostic taut mooring set-up. We note that:

- The shape of the plots is broadly similar, with the ‘passive’ peak being slightly higher.
- There is a noticeable dip around 1s period in the ‘active’ version response; the ‘passive’ data is more sparse so it is unclear as to whether this is a model- or potentially tank-related effect.
- The ‘active’ response seems slightly narrower in bandwidth.

It may be concluded that some amount of friction in the hinge of the ‘active’ model version is limiting the flex RAO response, though this could also be the result of different mass matrices of the as-built models.

Therefore, both sets of experimental data are also compared with frequency-domain numerical predictions, as shown in Figure 113. This shows that the predicted response (which does not account for friction effects) has a narrower bandwidth, though slightly higher peak, compared to the ‘passive’ prediction. Thus, the narrower bandwidth is deemed to be an effect of the mass matrix as opposed to friction. The higher peak is visible in the ‘slack’ moored version of the ‘active’ model shown in Figure 113. Both sets of numerical predictions ‘Num’ are based on the taut mooring set-up and steepness 1/100 waves. There is greater discrepancy between the exp-num ‘active’ peaks, compared to the ‘passive’ counterparts.

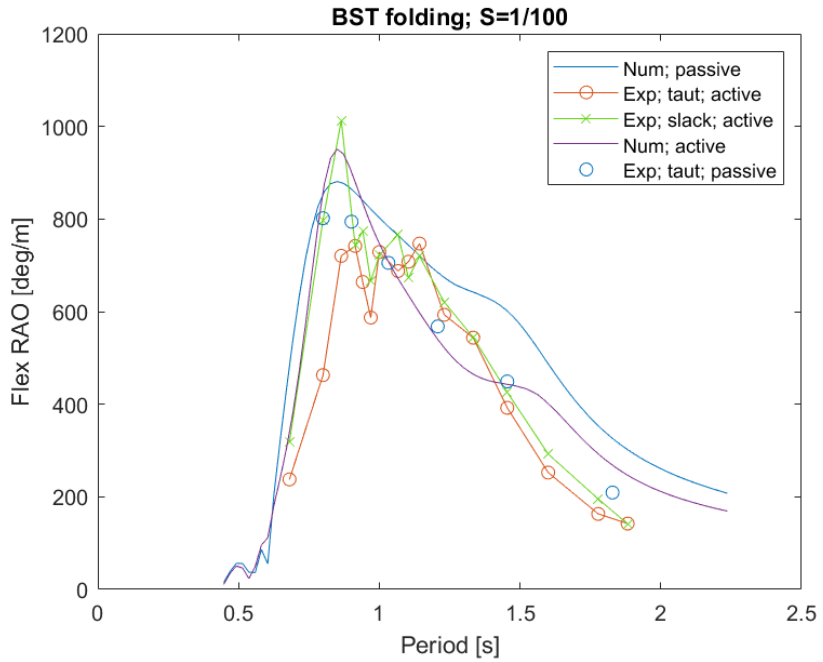

Figure 113 - Plot showing empirical flex RAOs from regular waves - passive and active model versions.

As previously mentioned, all empirical data in Figure 113 accounts for reflections; RAO values are computed based on incident amplitude spectra. The data is plotted at 20th scale. Comparing RAO flex values to Figure 110, we can divide the peak ‘Numerical’ RAO value of ~900 deg/m by 20 (the Froude scaling factor) to obtain a peak of roughly 45 deg/m, which lies between damped and

undamped curves of Figure 110. Cd, Morison's damping coefficient, is taken as 0.8 in above numerical curves. All numerical plots are calibrated for the as-built physical models.

Figure 113 suggests the following:

- Some - though limited - effect of friction and cables in the active model, observed via the greater discrepancy between the exp-num 'active' peaks, compared to the 'passive' counterparts. This, however, may also be partly due to some inaccuracy in the mass matrix of the active model, due to the effect of the cables, which is difficult to capture accurately.
- A generally good experimental response agreement with the numerically derived response, albeit with reduced bandwidth in both slack and taut cases.

Note that the active model data derived from a slack mooring set up does tend to give slightly greater responses compared to the taut mooring, as per the passive model. This, for example, is visible in the peak differences.

Figure 114 shows the first order RAO response in constant steepness sweeps at 1/50 and 1/100 steepness values, for the slack moored configuration. At lower steepness, the response is peakier and narrower; it also shows the second peak around 1.1-1.2s period. This is expected since this response will be less subject to nonlinear wave losses, and suggests some nonlinear effects occur from wave-body interactions, since the PTO is not actively engaged here. Figure 115 shows second order RAO responses, which are overall minimal, and only increase at longer periods where their value begins to approach that of the first order responses for the 1/50 steepness case. These are visible in asymmetric flex responses at longer periods (refer to Appendix H), but can be neglected in terms of their relative impact.

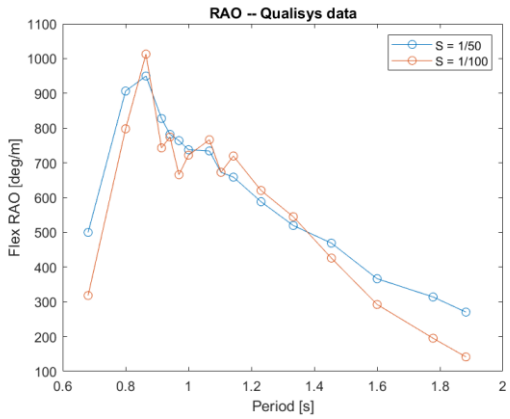

Figure 114 - First harmonic flex RAOs.

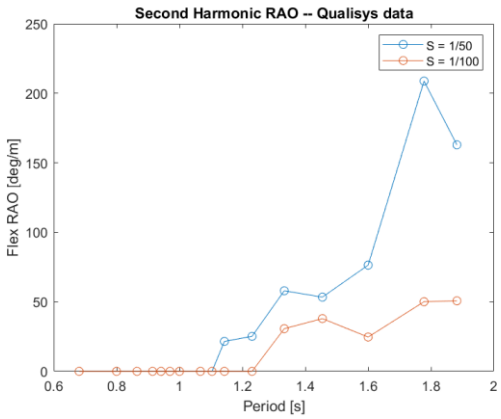

Figure 115 - Second harmonic flex RAOs.

Figure 116 shows the nonlinear nature of the WEC's response, which varies noticeably depending on the steepness of the incident waves used to produce it. Observing the points corresponding to 1.1563Hz frequency, there appears to be a maximum at a steepness value of 0.02. This may be artificial, but suggests that there may be a steepness "sweet spot", below which the motions of the WEC are limited by frictional losses (or other), and above which by load shedding via wave overtopping – as is indeed shown by other Mocean test campaigns.

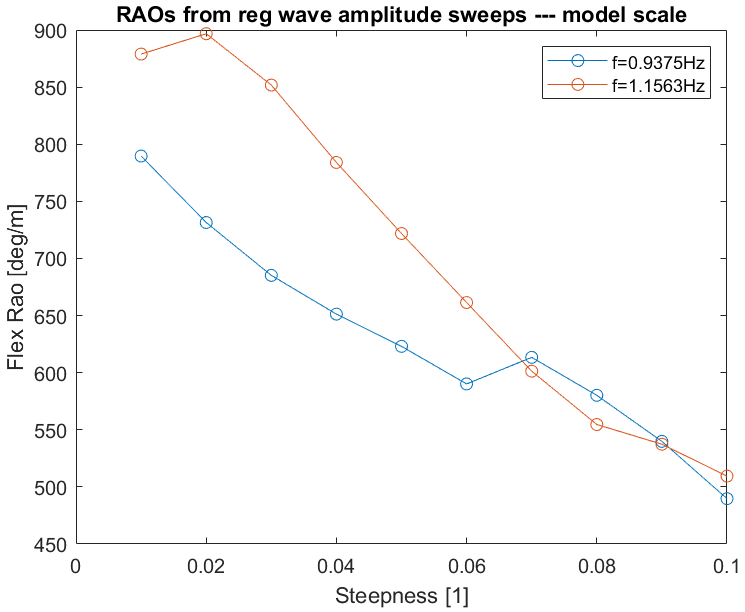

Figure 116 - Showing variation in RAO with demand amplitude wave steepness.

It is likely that at frequency of 0.9375Hz, the sweet spot is at a lower steepness, which is expected since the WEC is generally less sensitive to waves at this frequency. There appears to be a value of steepness at which load shedding is

such that the WEC's response becomes independent of frequency (around 0.07 or so). It can also serve to compare like-for-like points with RAOs above.

Run	Frequency	Steepness	Incident amplitude [mm]	RAO [deg/m]
RRa	0.9375Hz	0.02 (i.e. 1/50)	15.8	766.3
RRa	1.1563Hz	0.02	9.7	1012.7
RRb	0.9375Hz	0.01 (i.e. 1/100)	8.0	734.0
RRb	1.1563Hz	0.01	4.0	949.7
ARa	0.9375Hz	0.01	7.2	789.6
ARa	0.9375Hz	0.02	15.7	731.5
ARb	1.1563Hz	0.01	4.3	878.9
ARb	1.1563Hz	0.02	9.8	896.7

Table 30 - Summary table comparing equivalent seas run in frequency and amplitude sweeps.

8.9.3 Optimal PTO damping

Next, the optimal PTO damping value (D_{pto}) is explored. This is considered here as the PTO damping value that yields the highest power at frequencies around the peak response of the model. Recall that numerically, a constant damping coefficient value across occurrence matrix seas had been considered near optimal, or in any case "good enough". Thus, we explore the PTO damping space for a single damping value (or damping gain) to then utilise in irregular wave tests and power matrix validation.

In this chapter, the PTO damping coefficient is defined as: $D_{pto} = D_{norm} \times Gain$

D_{pto} values are varied by changing the PTO damping gain from a value of 20, in steps of 10 up to 80, and then in steps of 20 up to 160; thus 11 values in total. Such D_{pto} 'sweeps' were initially carried out at 1/50 steepness at five different frequencies, as shown in Figure 117. For each frequency, the tank is not stopped as the gains are stepped through. Instead, in order to carry out the process more efficiently, the PTO damping is turned on for a 10s duration, then off for a 5s duration, then on again at the next higher gain for 10s, then off again, etc. This 'cycling' of on and off damping can be seen in both Figure 117 and Figure 118, and allows the user to easily visualise the effect of different gain values. Instantaneous large spikes occur when the damping gain is switched on.

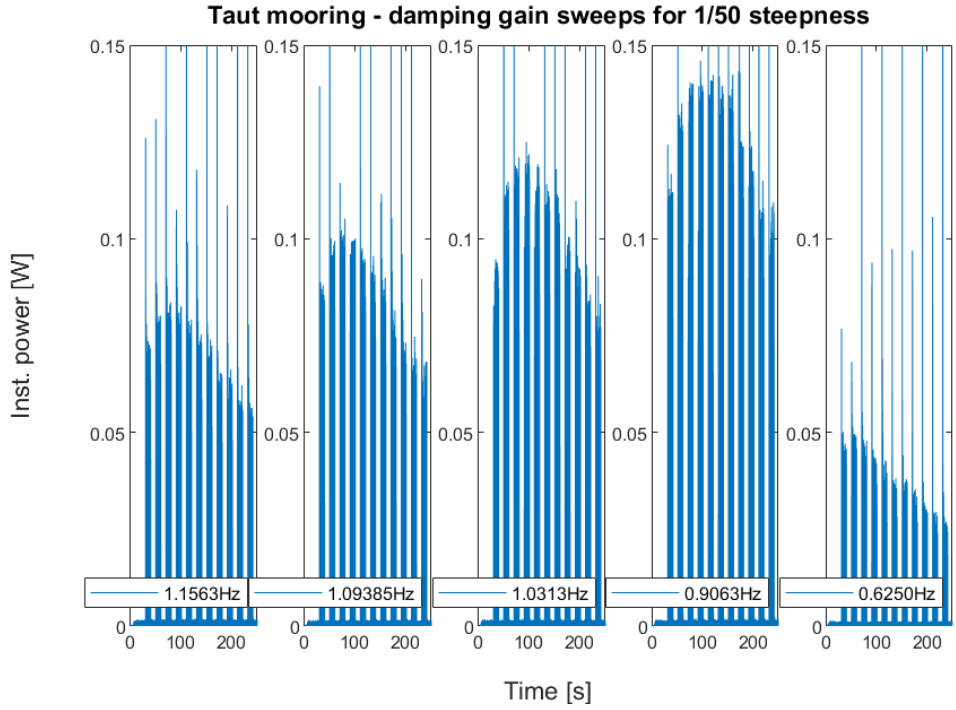

Figure 117 - PTO damping sweeps at 1/50 steepness; taut mooring.

The highest powers are measured at 0.9063Hz. Note that the actual power values here do not take frictional losses into account – they are instantaneous demand powers. This is acceptable for relative power comparison purposes. From Figure 117 (fourth plot from left) it is the 3rd to the 7th values of gain (i.e. gains of 30, 40, 50, 60, 70) that seem to yield the highest power values.

It is also necessary to explore power responses to different D_{pto} values for varying wave steepness and mooring set-up. Thus, D_{pto} sweeps at 1/50 and 1/100 steepness are carried out at – and either side of – the peak power frequency at model scale: 1.0938Hz, 0.9063Hz, 0.6250Hz (i.e. full-scale period of 4.09s, 4.93s, 7.42s). This was executed with both slack and taut moorings. The value of powers detected was lower for taut mooring, with the difference increasing at longer periods, as shown in Figure 119 (refer also to Appendix H). In addition, it is noted that the optimal D_{pto} value changes with wave period, as expected. From Figure 117, the optimal value (at which demand power is greatest), occurs at gain 30 for 1.1563Hz and 1.09385Hz, gain 40 for 1.0313Hz, a gain of 50 for 0.9063Hz, and gain 20 for 0.6250Hz. Ultimately, the optimal D_{pto} value is that which maximises overall energy yield, but all power matrix seas cannot be tested in the Curved Tank, and it would be uneconomical in terms of

time to cycle through D_{pto} values for all of these. Numerically, we know that a single D_{pto} value that maximises power capture at peak response is close enough to optimal for all power matrix seas.

Referring forward to Figure 124, which shows experimentally derived capture width ratio curves for damping gains of 20, 40 and 60, it can be seen that a higher gain of 60, compared to 40, does not appear to increase the response bandwidth, as may be expected. However, it may be that higher gains will and that the difference between these tested gains is not sufficient to show the effect.

Observing the 1/100 steepness plots in Figure 118, a gain of 40 seems optimal; while looking at the 1/50 steepness plots, a gain of 30 seems more optimal. A gain of 40 is provisionally chosen as the baseline of the optimal D_{pto}, since it is closer to the numerical model prediction, because it may broaden the response bandwidth to a minor extent, and because the model PTO should be able to safely handle it.

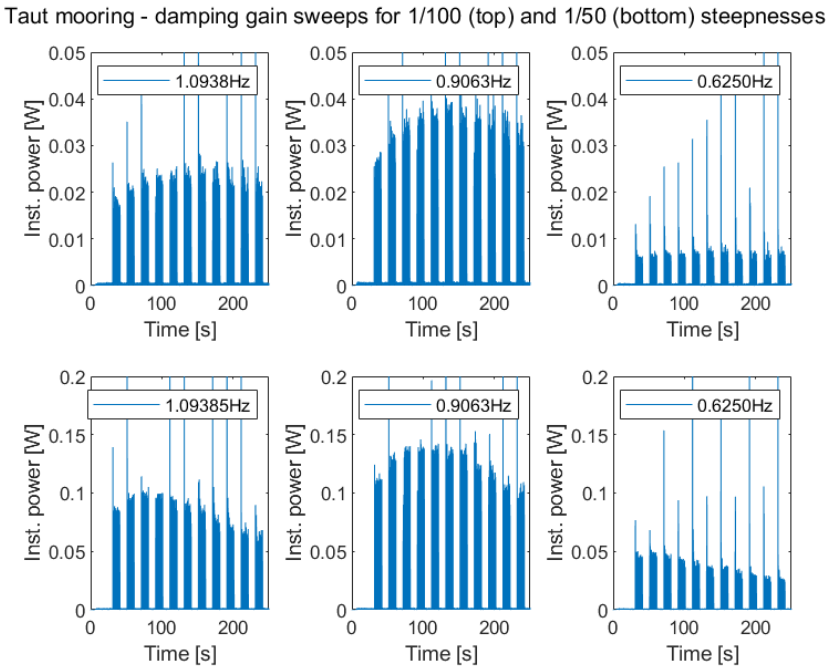

Figure 118 - Comparison of PTO damping gain sweeps at different wave steepness.

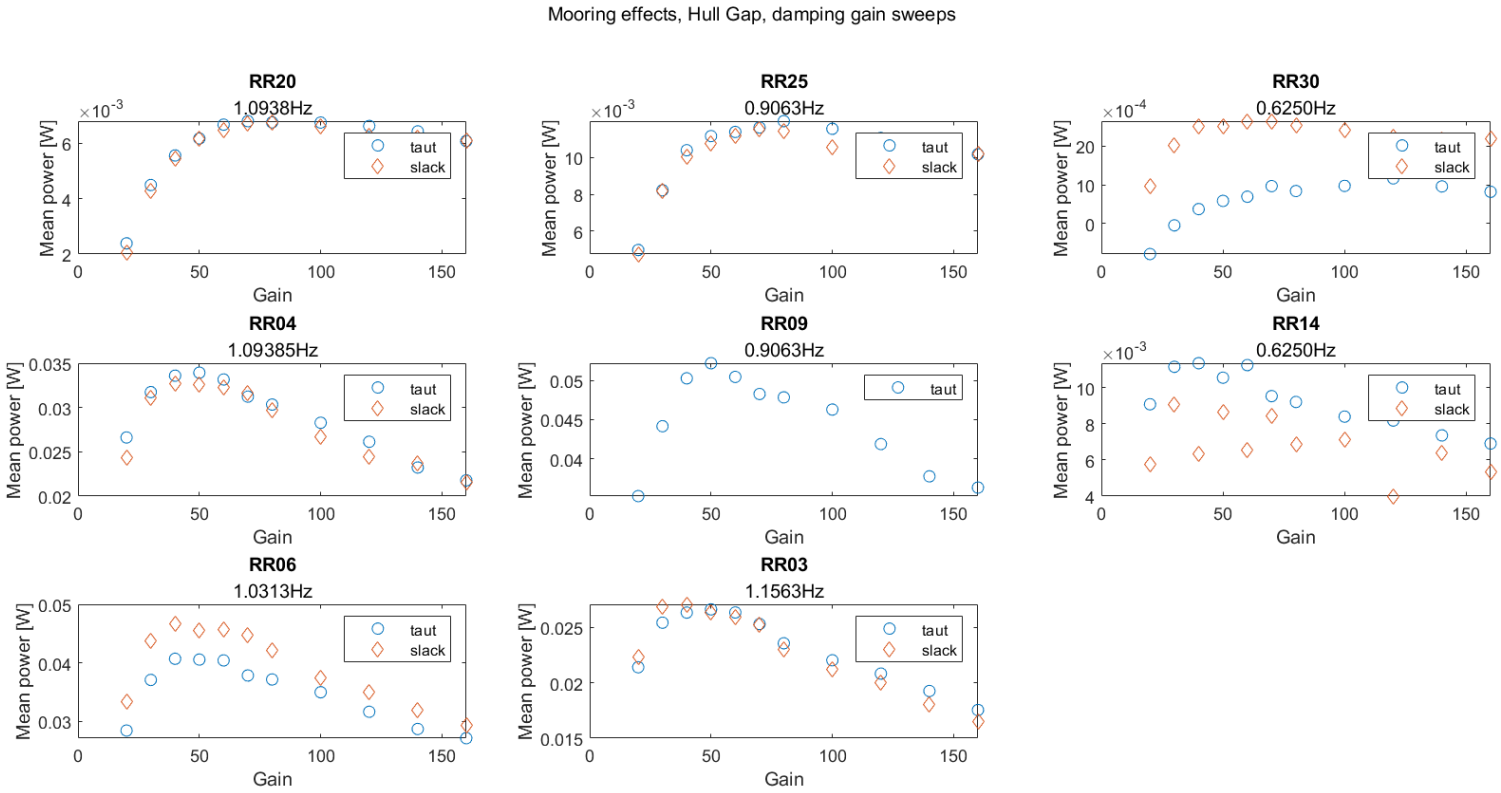

Figure 119 - Mooring effect on mean mechanical power.

The optimal D_{pto} value found experimentally is approximately half of the optimal value predicted by the SD numerical model (refer to Chapter 7). This is consistent with observations from the most recent Mocean testing campaign, with a model approximately double in size of a different geometry iteration (EuropeWave, 2022).

Whether slack or taut mooring setups are utilised to select the optimal gain value appears to be largely inconsequential, since the trends within each sweep are similar (Figure 119). It can be seen that for the 1/100 steepness sweeps, in which waves are more linear, the trends suggest an optimal gain higher than 40, and closer to 80. This is also visible in Figure 120, though with very minimal mean power gains. Again, since the disparity between mean power values between gains 40 and 80 seems minor, 40 is preferred as it would allow the model PTO (motor) to be active for longer wave runs with lower likelihood of thermal cut-outs.

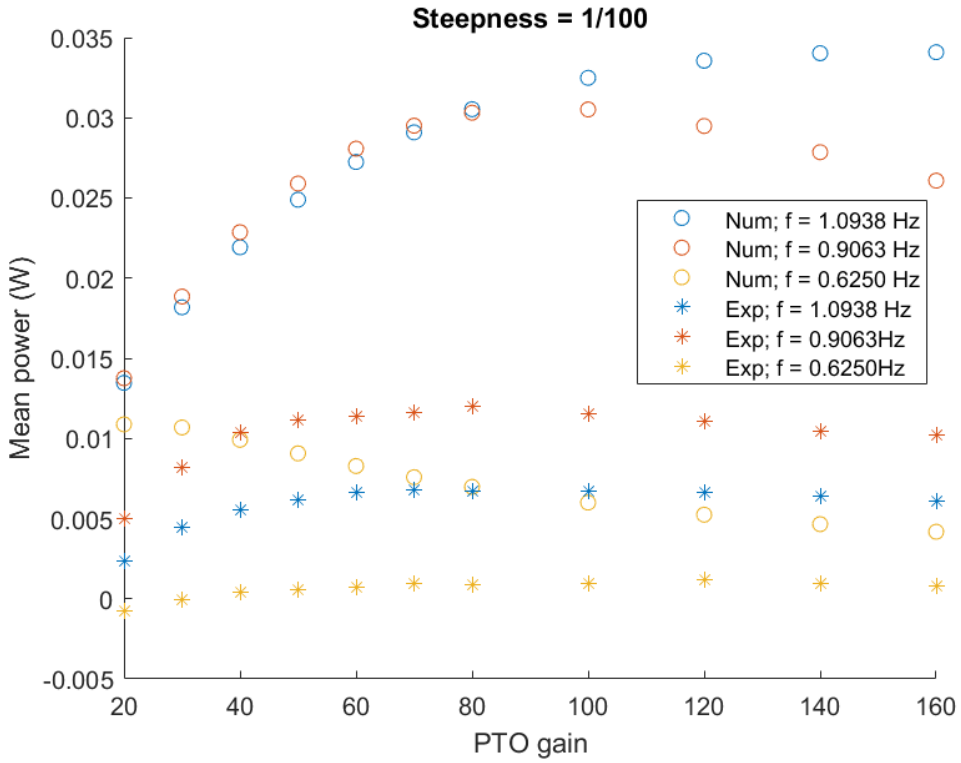

Figure 120 - TD model for mean power variations with PTO gain, shown for three frequencies at constant steepness (model scale).

Comparing Figure 118 and Figure 120, it can be seen that:

- Broadly, experimentally obtained values of mean power are significantly below those predicted
- For f = 0.9063Hz, the predicted peak mean power occurs at a gain between 80 and 90, while the experimental one shows similar mean

power for gains of 40 and 80, suggesting an optimal gain potentially around half the predicted value.

- For the highest frequency (1.09385Hz), the trend is totally different
- The trend for f=0.6250Hz is also different, though the experimental values are closer to the numerical ones compared to the other tested frequencies.

Experimental results suggest an optimal D_{pto} of 0.17 Nms/rad at model scale (0.004254 Nms/rad per unit gain * 40 gain), which is lower than the scaled down value yielded by the SD optimisation (0.225MNms/rad full scale, 0.31 Nms/rad at model scale). The TD predicted result is likely to be higher, probably twice or so the SD result. Experimental results also suggest a relatively low sensitivity of mean powers to the selected PTO damping value, which could explain some of the differences observed here. Once gain referring to Figure 124, it can be seen that CWR responses with gain 40 and 60 almost exactly overlap.

The TD model tends to select higher damping values when the torque limit is particularly constraining. For smaller waves, the torque limit is not reached, so perhaps the TD would predict lower values for smaller seas. The D_{pto} values obtained via TD optimisation look to optimise AEP over an entire wave climate; they could very well be a bit different if not considering the full range of sea states in finding the optima from tank tests. Indeed, the regular seas utilised in the tank tests are not representative of all potential seas encountered, nor of irregular sea behaviour. Analysis shows that the torque limit was never reached experimentally for the summarised D_{pto} sweeps (see Appendix H).

For the D_{pto} values to be comparable, one would ideally make sure the waves are high enough such that the torque limit is hit about as often as it would be in irregular waves. Thus, one reason why D_{pto} values are lower than TD simulated ones is the choice of seas in *Dsweep*. A more efficient and potentially more accurate way of obtaining D_{pto} values may be to do *Dsweep* experiments with IR0 seas, where seas are effectively irregular, wave heights are larger, torque limits more likely to be hit, and multiple frequency components are present at the same time.

8.9.4 Flex RAO comparisons

In this section, a few comparisons are drawn between flex RAOs obtained under different configurations and conditions, including wave steepness, PTO gain, and mooring arrangement.

8.9.4.1 PTO gain effect on RAOs

Firstly, Figure 121 shows RAO trends with different demand wave steepness and damping gain for the taut mooring set-up. For reference, in the legend 'S' refers to demand wave steepness, and 'dgain' to PTO damping gain. For 1/100 steepness, increasing PTO gain values result in diminished RAO values though with very consistent RAO shapes – as expected. A consistent dip just before 1s is also observed for these sweeps. At 1/50 steepness, the peak response is far higher at gain 0 while lower at gain 40. In both cases, the dip in RAO and the second peak observed for 1/100 steepness are less pronounced.

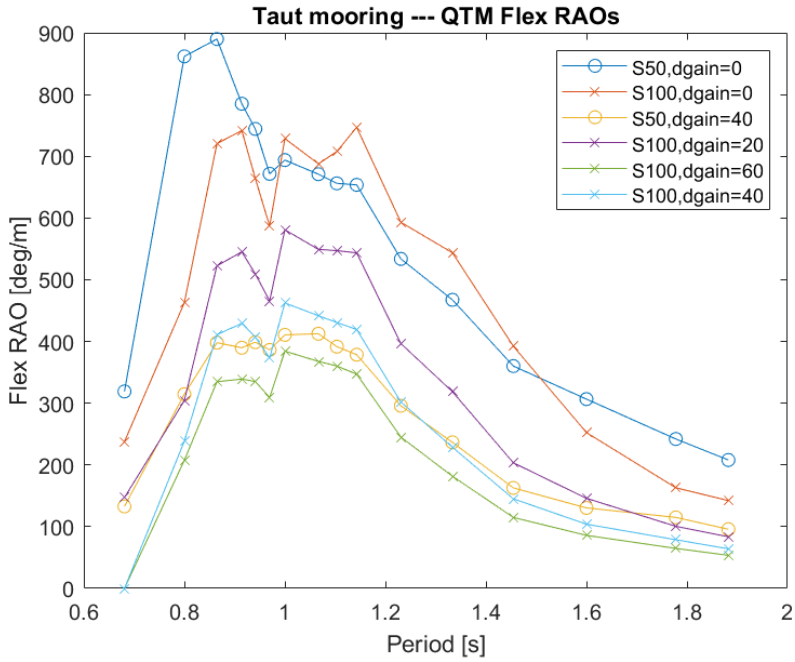

Figure 121 - Comparing Flex RAOs in regular waves under different generation conditions. [dgain = PTO damping gain; S50 = 1/50 steepness].

8.9.4.2 Mooring effects on RAOs

Effect of mooring on optimal Dpto identification was outlined previously. Here we briefly look at mooring configuration effect on the regular wave RAOs at wave steepness 1/100 and different PTO gains. Comparisons at gain 0 are shown in the section that compares Gap vs No Gap.

Once again, Figure 122 illustrates relationships that line up with expected trends:

- All slack RAOs exceed taut RAOs
- The discrepancies increase as gain decreases
- Taut response display less of a <1s peak and dip, compared to slack curves
- All flex responses reduce with higher PTO gains as expected

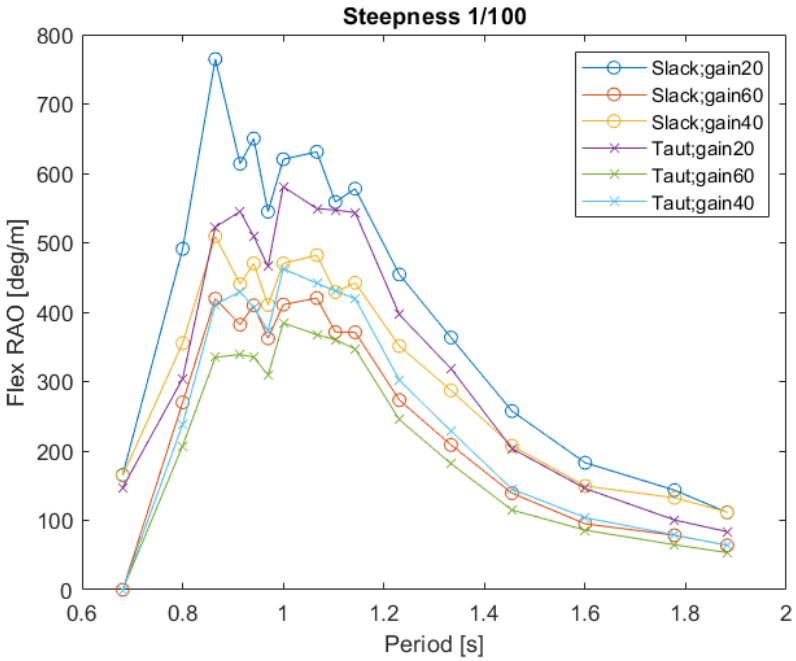

Figure 122 - Effect of mooring configuration on flex RAO at different PTO gains.

8.9.5 Power capture

The quantities of interest in terms of power capture are primarily the mean power values that enable power matrix element estimation and capture width, as well as its non-dimensional equivalent – i.e. capture width ratio. Mean powers are converted into equivalent CWR values for non-dimensionality purposes. The method is the same as that followed in (Ohana *et al.*, 2021) and is outlined in Appendix H. CW is the mean mechanical power absorbed by the WEC, divided by the power per unit crest of incident wave.

$$CW = \frac{P_{mean,absorbed}}{P_{wave}}$$

CW is converted to CWR by dividing by the following dimension: the equivalent radius of a submerged hemisphere of the same wetted volume (V_s) as the WEC, such that:

$$r_0 = \frac{3V_s}{2\pi}$$

$$CWR = CW/r_0$$

Mean powers in units of watts for regular frequency sweeps at 1/50 and 1/100 steepness are shown in Figure 123. As expected, the values obtained with 1/100 steepness waves are significantly lower than at 1/50 steepness. A peak value of 0.04W is recorded for 1/50 steepness, equivalent to ~ 1.4kW at full scale.

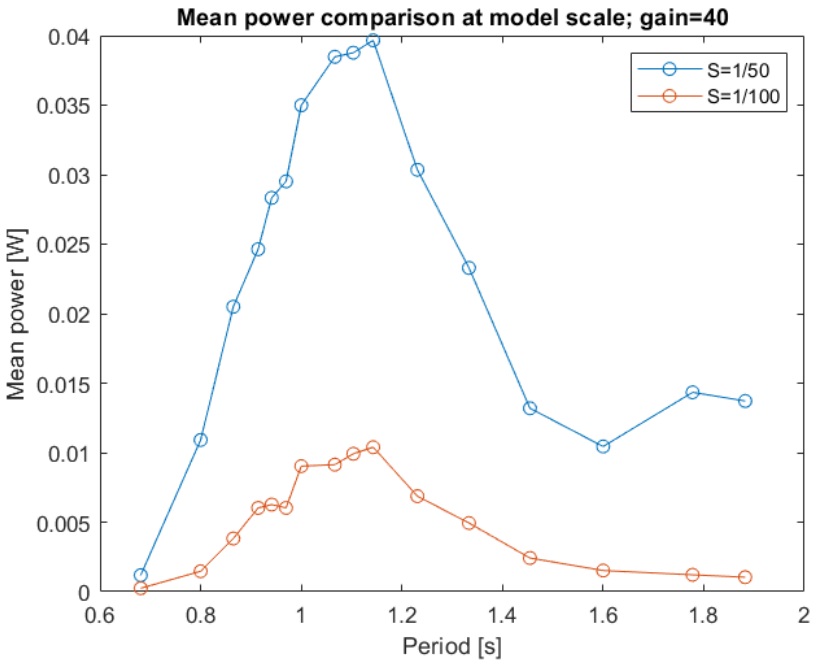

Figure 123 - Mean powers with taut mooring at different steepness regular waves.

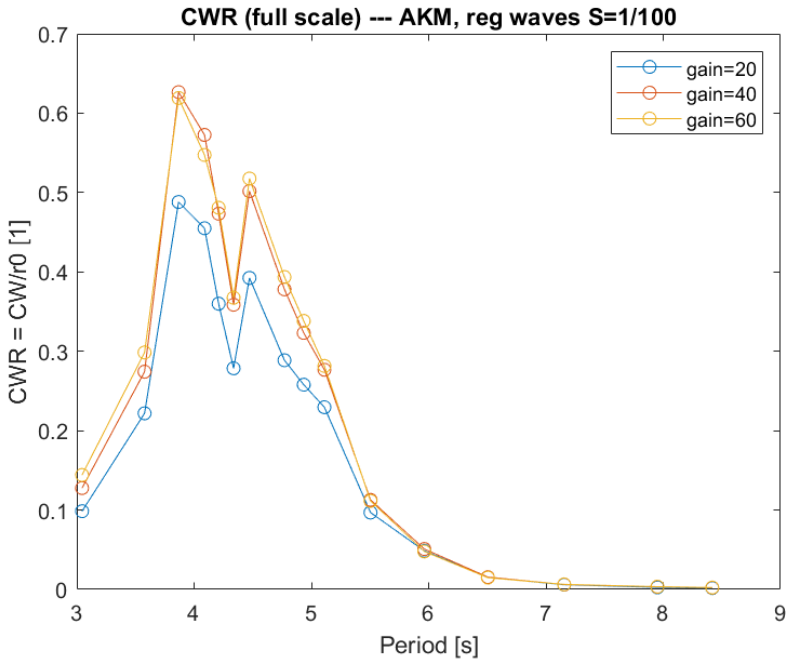

Figure 124 - Experimental CWR plotted at different PTO gains (AKM data).

Figure 124 confirms that a PTO damping gain around 40 to 60 is optimal for peak power capture. It also shows a CWR response with two peaks (more akin to the undamped numerical prediction – see Figure 109), but with CWR values approximately 5 times lower than those predicted, which displayed a peak at ~2.5 including viscous behaviour. This therefore suggests that the model is converting far less power than predicted at each period. The cause(s) for this discrepancy could be several:

- Torque losses greater than the static friction measured in Chapter 7
- Hinge velocity losses that are unaccounted for
- Numerical model over-predictions
- Measurement inaccuracies or analysis errors, including e.g.
    - Check QTM vs AKM data (AKM is filtered) – Appendix H
    - Check velocity match between numerical and experimental – Section 8.9.5.1
    - Check whether the central dip could be caused by tank behaviour (e.g. reflections) – Appendix H

The most likely cause is due to velocity losses.

8.9.5.1 Power checks

A check is performed on the QTM velocity and AKM velocity signals compared to the numerical prediction, for conditions: gain=40, taut mooring, S=1/100, f=0.9365Hz (model scale). This is shown in Appendix H, and confirms sensible phase relationships between hinge angles, hinge velocities, torques, and power. It also shows coherent values of power based on the measured velocity and torque. This largely rules our measurement inaccuracies as well as analysis errors.

Next, hinge velocity discrepancies are investigated, particularly with regards to potential friction effects and inconsistencies between numerical predictions and experimental measurements. Relevant experimental data obtained at f=0.9375Hz, S=1/100, and different gain values, is shown in Appendix H. The equivalent numerically obtained data from TD simulations, with and without friction effects included, is outlined in Appendix O. A summary of both experimental and numerical data is given below in Figure 126 (hinge flex velocity) and Figure 125 (hinge flex position). Numerical min and max exactly overlap both for ‘friction’ and ‘no friction’ simulations, and this is largely true of experimental data as well.

At gain 0, the numerically predicted peak angles are approximately 50% higher than those measured experimentally, dropping to 30% higher when friction is accounted for. As expected, the inclusion of friction affects numerical predictions uniformly across PTO gains. This inconsistency at gain 0 suggests that: (a) friction is having a significant effect; and (b) that friction is affecting responses more than the numerical model can predict, or that other non-friction effects are at work.

Inconsistency at gain 0 also suggests friction having a significant effect, even before PTO nonlinearities begin coming into effect at non-zero PTO gain values.

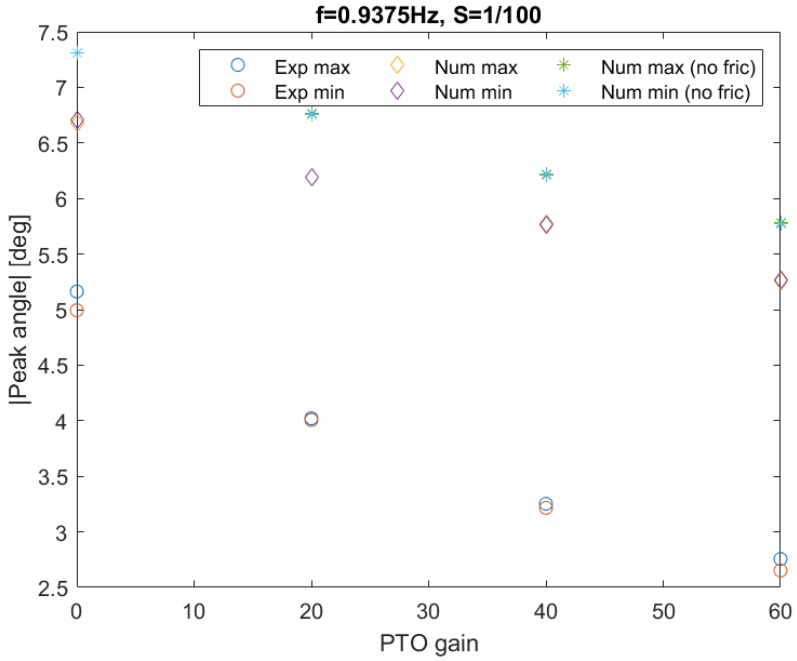

Figure 125 - Comparison of peak angles measured and predicted (with and without static friction).

Figure 125 shows that the mismatch between measured and predicted angles increases as PTO gain increases. This is also true for velocity values, as shown in Figure 126.

Figure 126 shows that the rate at which peak velocities drop with increasing PTO gain (experimentally and numerically) is linear. The gradient is slightly greater for the experimental data. However, it can also be seen that the difference between peak velocities obtained experimentally and numerically (accounting for static friction effects) are significantly different. There is a drop of about 9.5deg/s at gain 0, rising to 11.4deg/s at gain=60. This mismatch has a greater effect on power estimates, the higher the PTO gain is, since velocities are lower and therefore the ~constant offset has a greater relative impact.

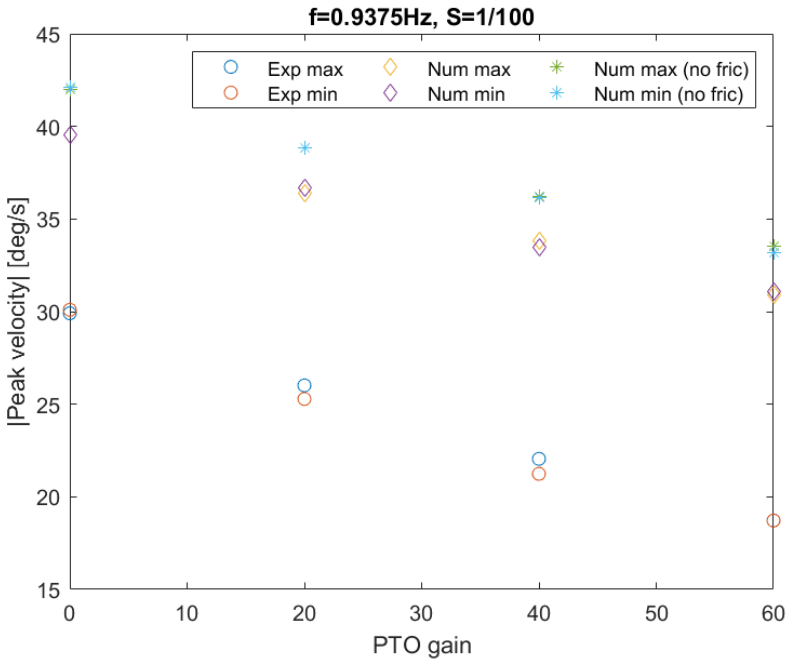

Figure 126 - Comparison of peak velocities measured and predicted (with and without static friction).

In the case of a 0.9375Hz wave with 1/100 steepness, gain 40:

- Peak hinge flex velocity, numerical (no friction) = 36.2 deg/s
- Peak hinge flex velocity, numerical (with friction) = 33.7 deg/s
- Peak hinge flex velocity, experimental (with friction) = 21.6 deg/s

Thus, the velocity measured is roughly 64% of that predicted numerically, taking friction into account, and 60% when not accounting for friction. The effect on power will be this disparity squared; i.e. 41% and 36%, since power is calculated as D_{pto} multiplied by the velocity squared.

The following plots attempt to verify whether this velocity disparity can account for some – or indeed most of – the power measurements disparities.

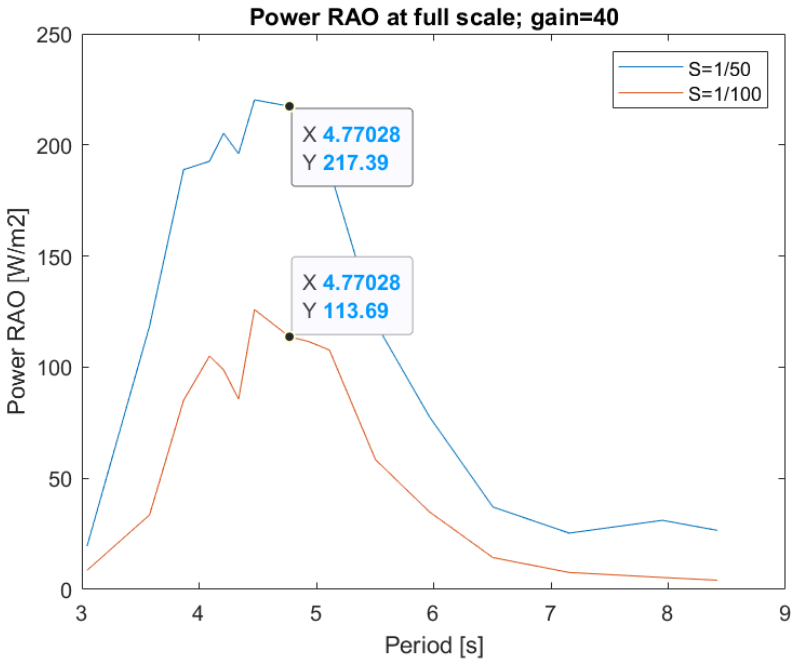

Figure 127 - Experimentally obtained Power RAOs at two wave steepness values (full-scale equivalent).

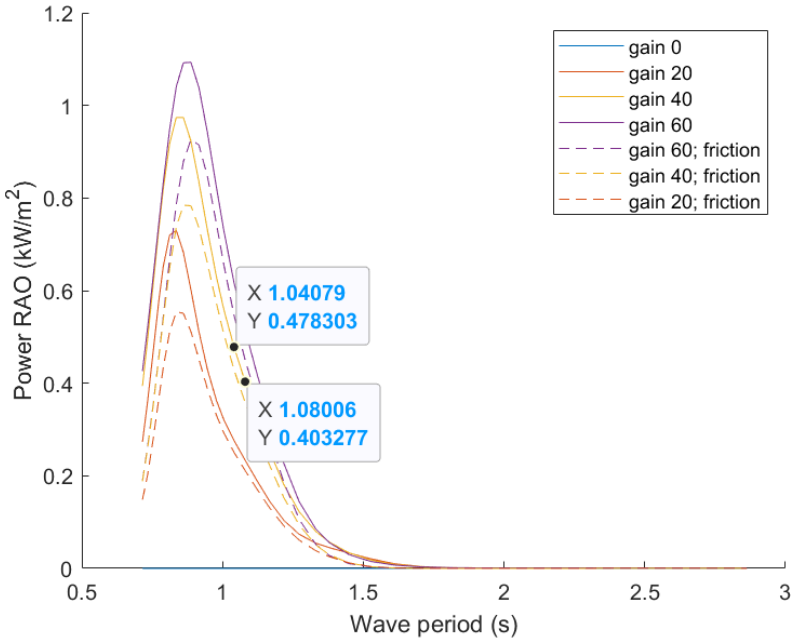

Figure 128 - Numerically obtained Power RAOs at S=1/100, with and without friction included.

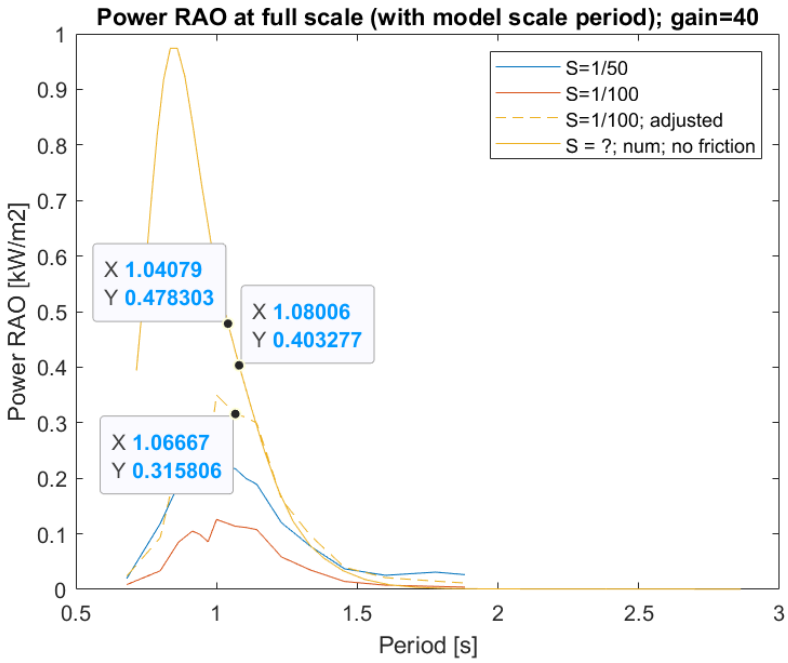

Figure 129 - Experimental power RAOs, including adjusted experimental data based on velocity disparity %, compared with numerical predictions.

In Figure 129, the adjusted experimental curve has been obtained by dividing the S/100 (red curve) by 0.36, which is the hinge velocity difference estimated at this period (see Figure 126). Of course, this 0.36 factor is only valid at the specific period 1.067s, and therefore this is the only point that can be reasonably compared. Indeed, the difference between the yellow curves is significant at periods below 1.067s.

Interpolating the power RAO values along the numerical curve to estimate a value at period ~1.067s, yields 0.403+ ((0.478-0.403)/(1.08-1.04) * 0.027) = 0.454. The difference is therefore 0.316/0.454 = 0.696 → 70% at a period of 1.067s. It is far greater at periods below this.

8.9.7 Hull Gap and No Gap

The figures shows ‘damping off’ responses at 1/50 steepness for Gap and NoGap configurations with different moorings. It shows that the flex RAO of NoGap-Taut is higher than Gap-Taut, across most periods, even more than Gap-slack. This is also largely true for S=1/100, as shown in Appendix H.

From Figure 131:

- NoGap configuration has a slightly higher response than Gap for both steepnesses – minimal effect; the gap versions have slightly wider tails at higher periods and narrower tail at low periods
- S=1/100 double peak and more pronounced dip like for Gap configuration

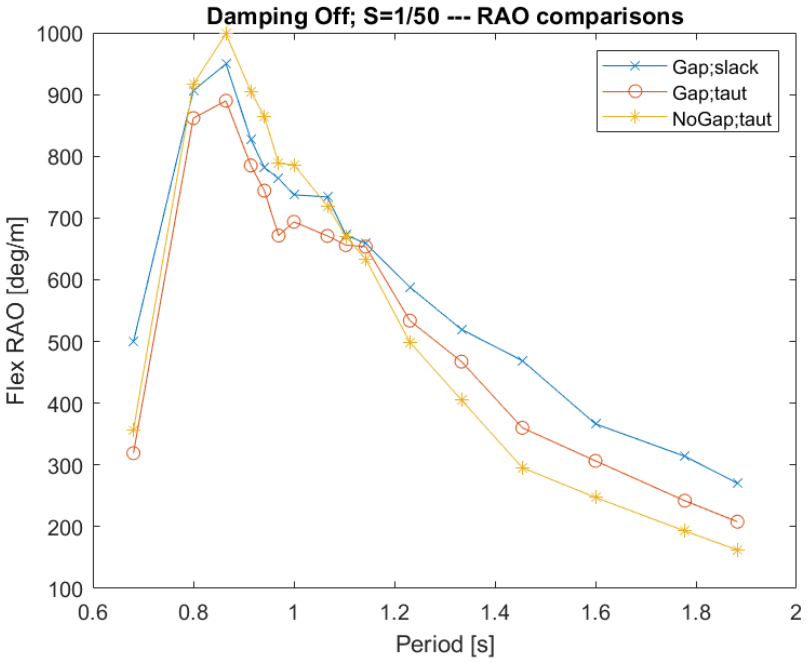

Figure 130 - Gap and NoGap flex RAOs for regular wave frequency sweep at 1/50 steepness.

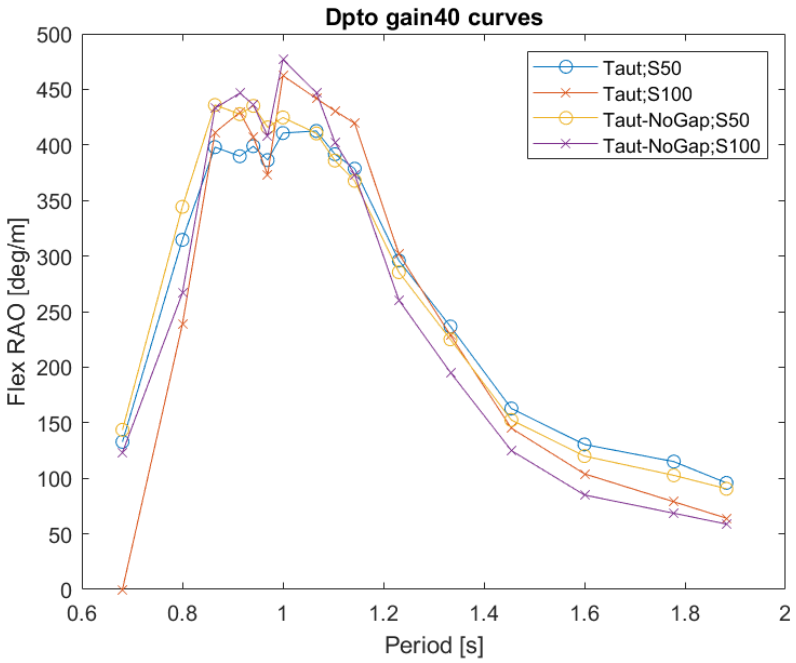

Figure 131 - Comparing Gap and NoGap flex RAOs for different steepness under power extraction (PTO gain 40).

8.9.8 Irregular waves

Guidelines and technical documents typically specify power matrix validation based on 15 standard sea states. Indeed, 15 sea states were run (IRLa,b,c,x), though the overall occurrence matrix coverage is not ideal. Power matrix validation is also hampered by the fact that recorded mean powers, analogously to those used to calculate CW plots and power RAO, are significantly lower than predicted ones, limiting results confidence.

As anticipated, the mean mechanical power at the hinge during irregular wave runs is compared to the relevant predicted power matrix entries. However, this is likely to be subject to greater uncertainty than power RAOs, for example, due to the limited time duration of each tested irregular sea. Before exploring power performance, irregular wave flex RAOs are considered. These are calculated as the amplitude ratio of fundamental frequency components, without taking reflections into account.

Figure 132 shows hinge flex RAO responses derived from long-crested irregular seas at 2/3 limiting steepness, with the PTO switched off. The data also has a 1Hz LP filter applied for smoothing purposes. Spurious RAO values below 5 rad/s can be observed for the Hs=0.74m equivalent full-scale sea. The key gives demand Hs values at full-scale, while flex RAOs and wave frequencies are at model scale. Data is plotted with rad/s units on the horizontal axis to facilitate comparison with Plymouth obtained data (passive model) – see Figure 133.

Figure 132 can be compared with Figure 133, which shows equivalent results for the passive BST-folding model tested at Plymouth's COAST lab. The comparison is limited, since Plymouth data is provided with unknown demand steepness values. This brings to light the importance of correct data management. Nevertheless, it can be seen that the shape and the peak of the responses align well, despite the Hs trend seems reversed. For the active model, increasing Hs gives slightly increasing flex RAO values, while the opposite is true for the Plymouth model. This may be a result of different wave steepness or of the mass property differences between the two models. It could also be a result of tank reflections, which are not taken into account in the active

model, and may or may not be taken account in the Plymouth passive model data provided.

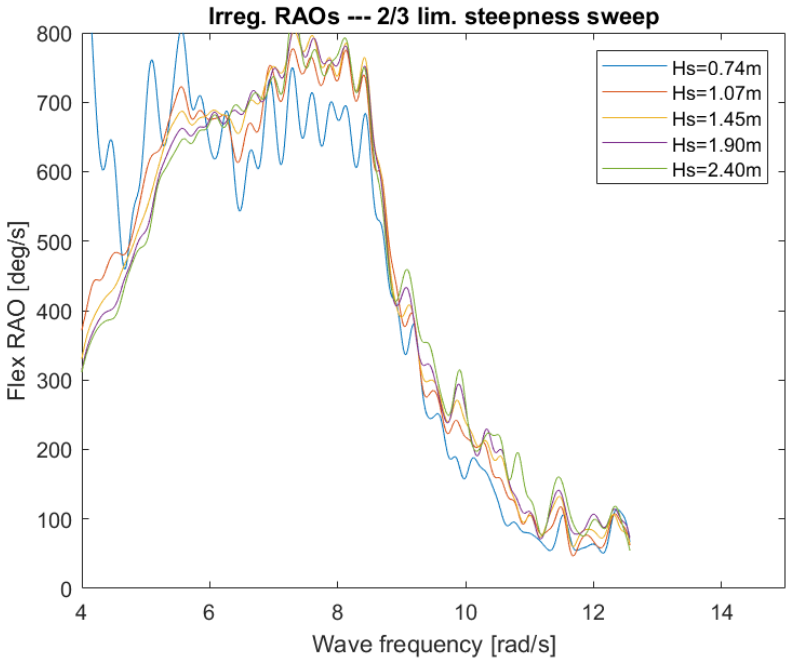

Figure 132 - Irregular wave RAO curves from CT - 2/3 limiting steepness (model scale).

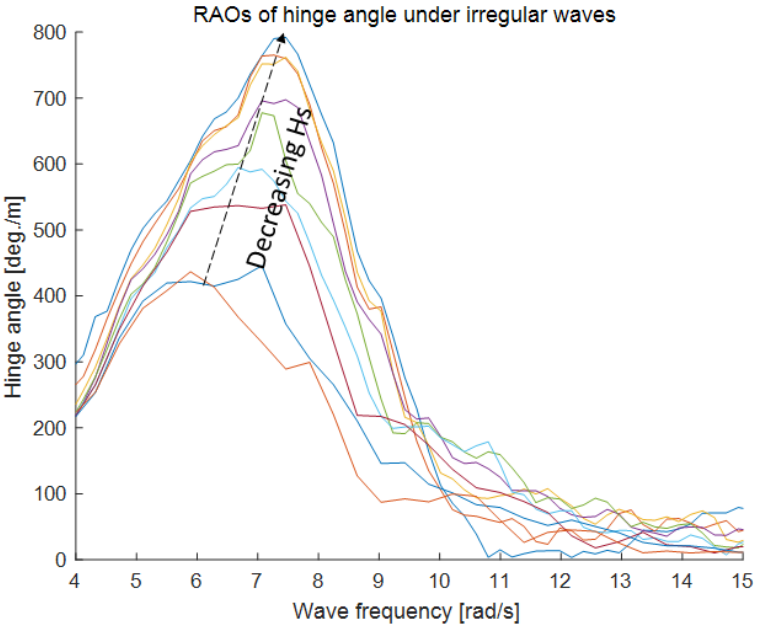

Figure 133 - Irregular wave RAO curves from Plymouth test campaign - unknown steepness. Note incorrect labelling of vertical axis.

Next, the variation of mean power with demand wave steepness and PTO damping gain is presented.

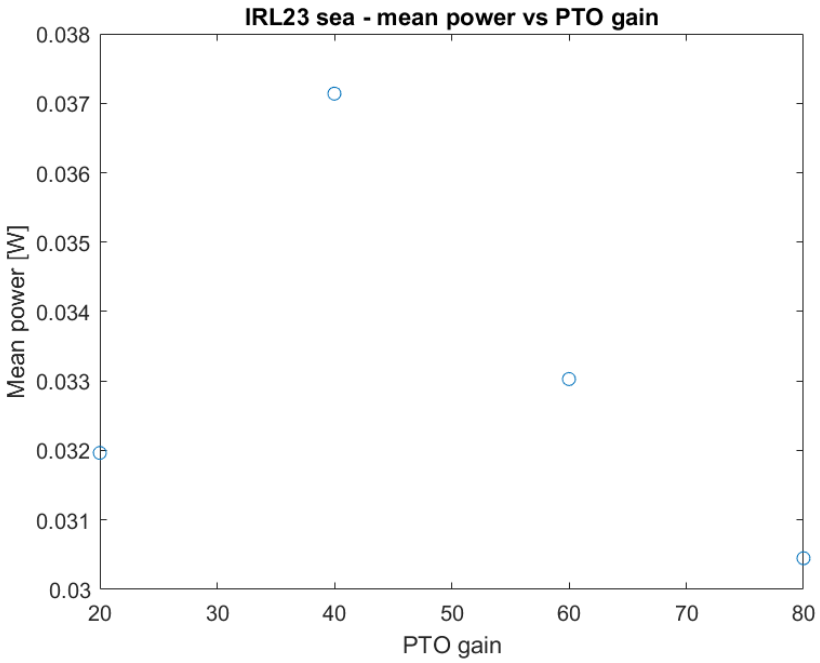

Figure 134 - Mean power variation with PTO gain; IRL23 sea.

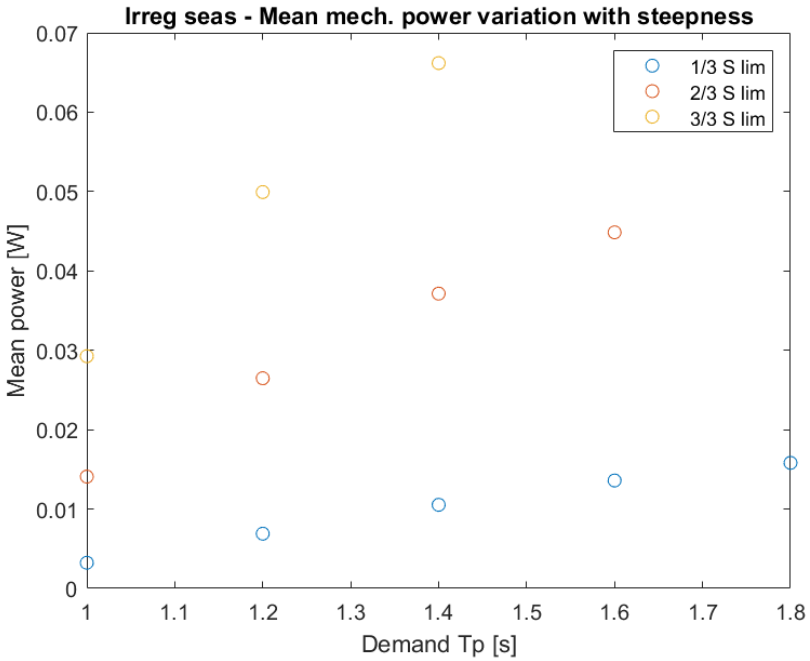

Figure 135 - Mean mechanical power for PTO gain=40; long-crested seas.

Recalling that 2/3 limiting steepness waves result in the highest energy contributing seas for BST-folding, Figure 134, obtained with such a sea, confirms the choice of PTO gain 40 to set optimal D_{pto} value as appropriate.

Using a PTO gain of 40, mean mechanical powers are obtained for each long-crested steepness sweep, as shown in Figure 135.

The effects of short-crested seas, of angular spreading, and directionality, are explored in Appendix O. The effects of applying a torque limit to mean power captures in long-crested irregular seas is explored in Appendix O. In short, results suggest that halving torque limit has a minor effect on mean power, which drops by approximately 10% as measured via IRX01 and IRX03 seas, respectively the most frequently occurring sea in the occurrence matrix, and the sea closest to the energy matrix 'hot spot'. This is, of course, only partially representative of the overall relationship between AEP and torque limit, since the higher end seas are not executable with the Curved Tank.

8.9.9 40th scale flex responses

A passive 40th scale model is tested, with the ability to add or remove the aft hull gap, just as for the larger 20th scale active model. The 40th model was tested in a slack mooring configuration only.

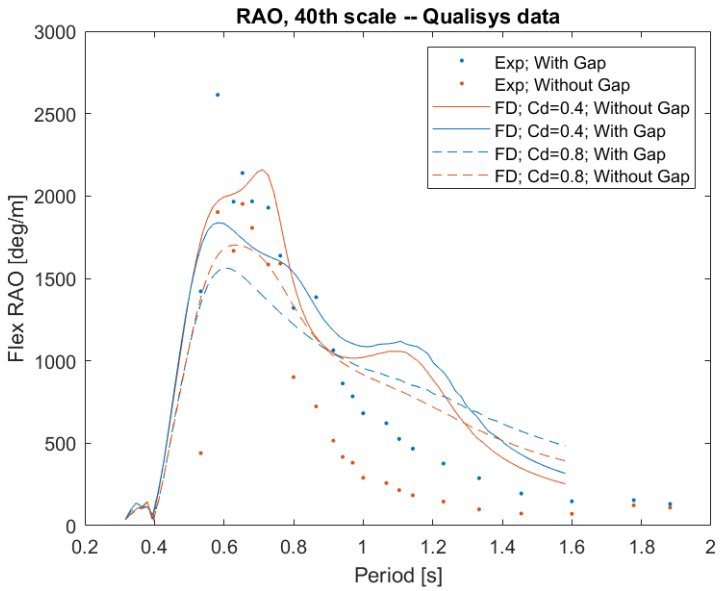

Figure 136 - Flex RAO at 1:40 model scale; experimental versus frequency-domain numerical comparison.

While Figure 136 shows FD obtained numerical predicted responses, Figure 137 does so within the TD. Note that experimental data is obtained with frequency sweeps at a constant steepness of 1/50 only, such that empty basin data from 1/100 steepness for the 20th model could be directly re-used, maximising tank

testing time. In the time-domain, the match is better with Cd=0.4; this is also the case for the FD data, especially at shorter periods. For longer waves, the match degrades in both domains. It may be that the second peak would be visible with 1/100 steepness experimental wave data, which is, however, unavailable.

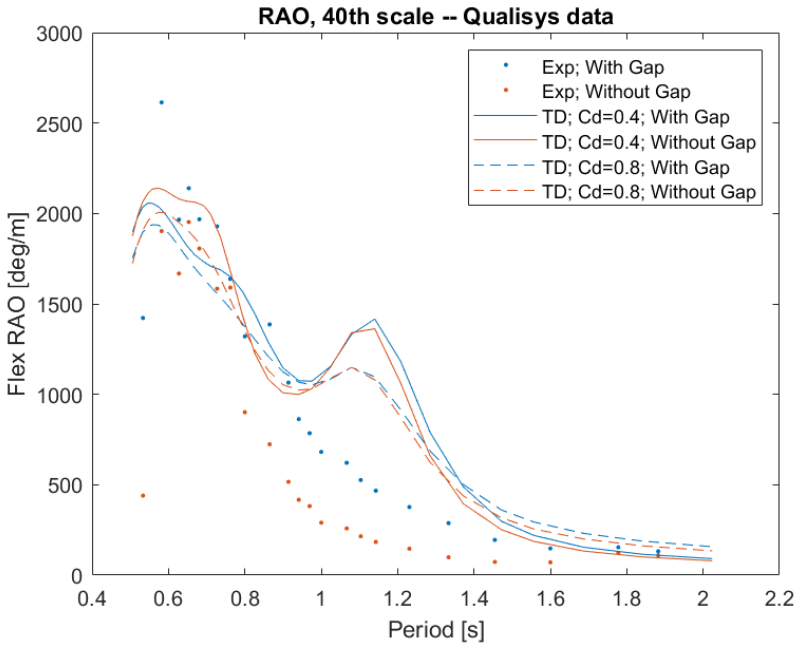

Figure 137 - Flex RAO at 1:40 model scale; experimental versus time-domain numerical comparison.

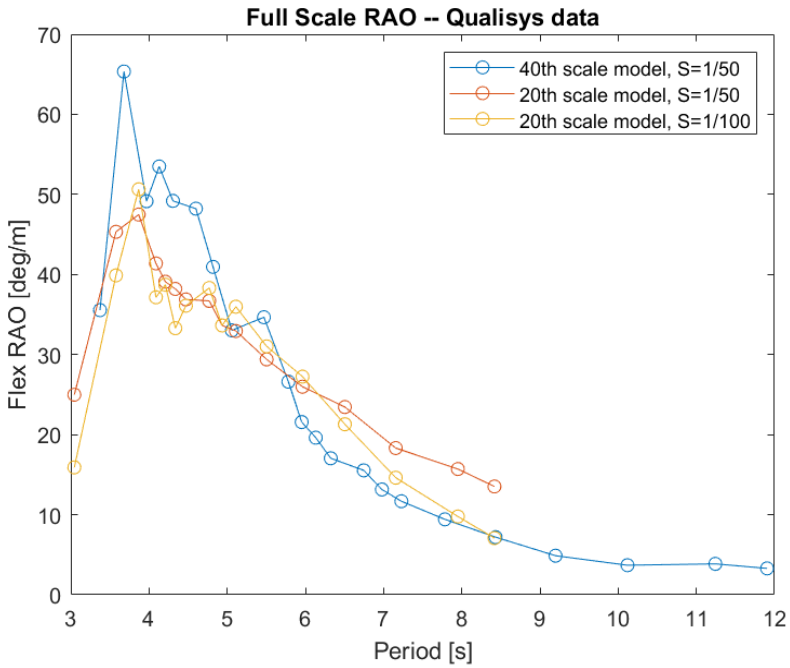

Figure 138 - Showing 1:40 scale and 1:20 scale RAOs plotted at full-scale for comparison.

It is also the case that a different Cd value would be required for different wave periods (and potentially wave heights), as highlighted by other data collected by Mocean outside of this research effort. Cd has been historically calibrated based on longer period, higher energy seas, while the seas ran in this test campaign are relatively short and of contained height, due to CT operational envelope limitations.

Figure 138 is derived for Hull Gap configurations of the two models. It shows that it would have been beneficial to carry out more short period runs instead of long period runs. It also shows that the 40th model gives considerably higher RAO values around the peak region. At least two peaks are visible, analogously to the 20th scale responses at 1/100 steepness, suggesting less Flex RAO at 40th model scale; experimental versus frequency-domain numerical comparison losses are occurring at this smaller scale. Finally, the 40th model has a comparatively reduced response at longer periods.

In terms of nonlinearity exposure, Figure 139 shows that the 40th model (particularly the Gap configuration) appears to have a shallower gradient compared to the 20th model data points, which seem to drop at a faster rate with increasing steepness. This somewhat agrees with the previous point regarding lower losses.

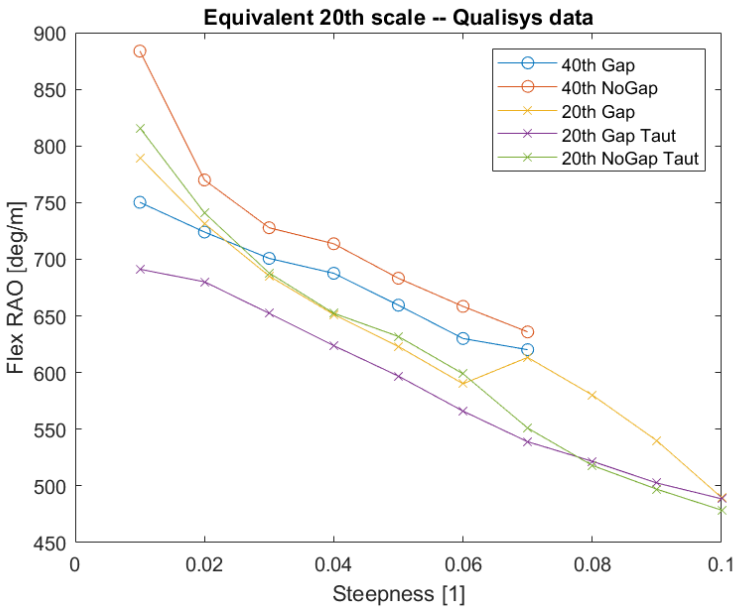

Figure 139 - Sensitivity of Flex RAO to wave steepness.

Increasing wave steepness causes greater viscous losses and also load shedding via nose diving, meaning the WEC does not follow surface elevation. Broadly speaking, Figure 139 suggests that the response of the WEC to differently linear waves is largely independent of scale, at least in the range of wave steepness values tested.

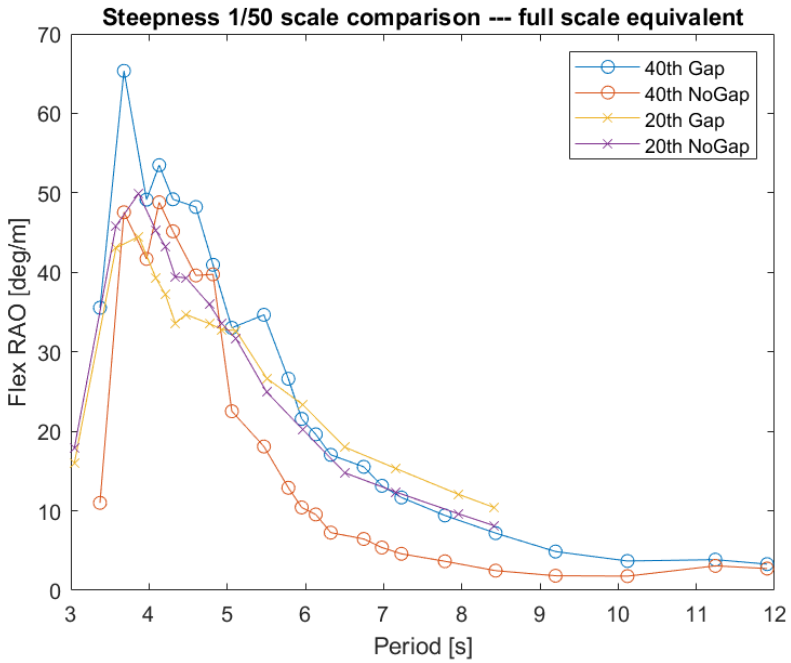

Figure 140 - Gap and NoGap response comparison at both model scales.

When observing Gap to NoGap data in Figure 140, the trends somewhat differ. Gap versions have consistently higher responses at the longer periods. For the 40th model, this remains true at all periods, while for the 20th model shorter period responses are greater without hull gap.

8.10 Uncertainty analysis

For a given RAO plot, x-axis and y-axis potential errors are considered in sequence. Errors in period can be ignored – these are negligible because of tight tank frequency control, and because frequencies are chosen for regular waves and for IRO components to give an integer number of waves during each wave run, resulting in no rounding being necessary in the periodic processing done by the tank. Thus, we can focus on y-axis error bars only. Y-axis (deg/m) errors occur due to wave height and pitching measurements, but are likely dominated by wave height.

Wave height is associated with wave gauge (WG) measurements, which can assumed to be +/-1mm as a worst case. WG calibration errors had means of 1.1 to 1.25%, with standard deviation ranges of +/- 0.6%. These values are calculated from collective calibrations carried out at the start of each test day, following a period of 5 minutes during which the tank water was mixed (by having active tank paddles near max wave length) in order to mitigate temperature gradient effects on WG sensitivity.

We can also assume that the motor drive is giving exact pitching measurements, which can be plotted against Qualisys measurements for a large regular sea. This error is identified as <0.1 degrees (see Section 8.9.2 and Appendix H) and thus considered negligible. Note that this is a set-up error, not an error arising from the system being measured (i.e. the model).

Repeatability of RAO plots is explored for a maximum motion scenario: a 1/50 wave steepness frequency sweep, with PTO damping off, slack mooring, for the 20th model. The results are shown in Figure 141. The difference at the peak is (949.7-879.5)/949.7 = 7.4%

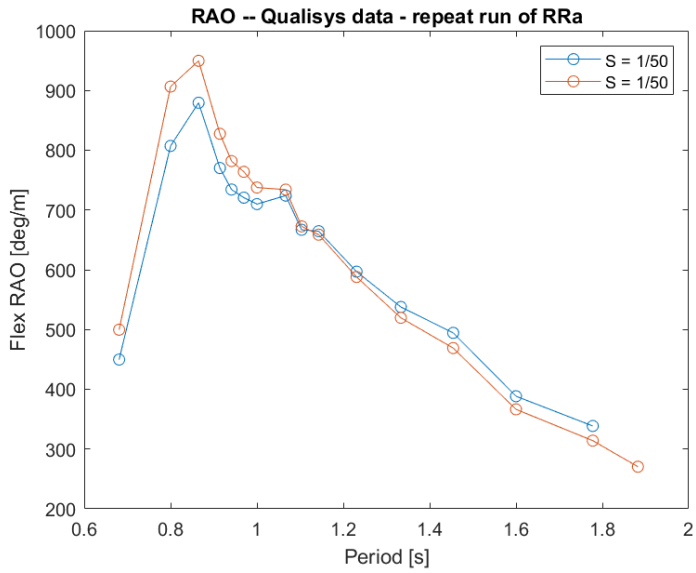

Figure 141 - Showing repeat RAO based on 1/50 wave steepness (20th scale model; PTO damping off).

Figure 142 is provided to compare starting positions in all the DoFs to check whether any patterns emerge relating to the repeat run (see Figure 141). The data shows the maximum drift during a 'ZeroRead' measurement ahead of run – i.e. a 10s measurement made in still water after the settling time between each run, which acts as a baseline for the 'equilibrium' conditions ahead of a particular run. Position 0 is the nominal position set at the start of each test day. The analysis relates to a slack mooring set-up so can be viewed as a worst-case.

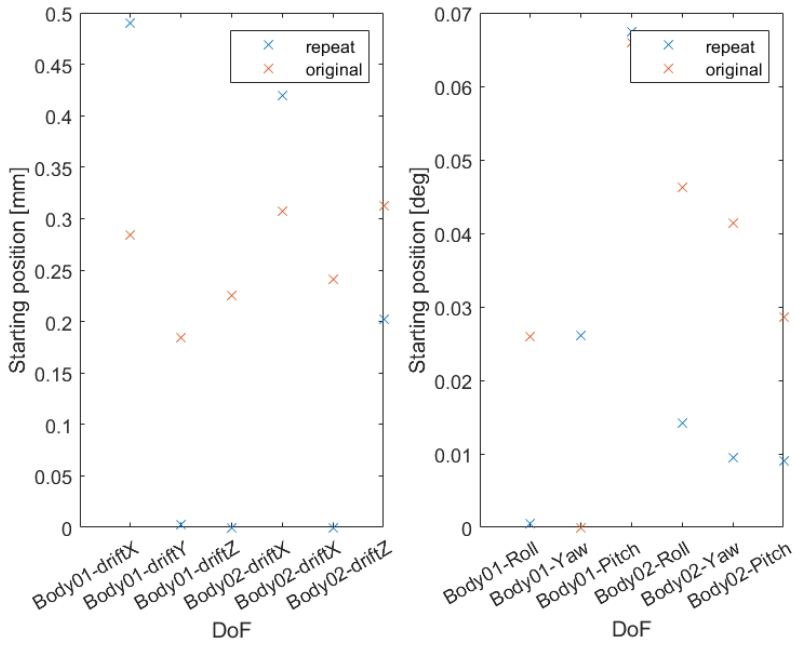

Figure 142 - Comparing model starting positions ahead of 1/50 steepness wave sweep.

8.10.1 Trimming error effects

Table 31 shows estimated effects of trimming line drift on submerged volume, V_s, and the characteristic dimension parameter, r0. V_s is an input to the WAMIT hydrodynamic simulation, while r_0 affects CWR calculations. r_0 is defined the radius of a hemisphere of equivalent volume as V_s (see Section 8.9.5), in accordance with Mocean best practices.

MWL (relative to target)	**20th model (Gap)**	
	V_s [mm^3]	Δr_0 [mm]
-15% (-5.4mm)	2786497 (-10.3%)	110.0 (-3.6%)
-10% (-3.6mm)	2894076 (-6.9%)	111.4 (-2.4%)
-5% (-1.8mm)	3001178 (-3.4%)	112.7 (-1.2%)
0% (i.e. 36.0mm above hinge axis)	3107725 (0%)	114.1 (0%)
+5% (+1.8mm)	3213853 (+3.4%)	115.3 (+1.1%)
+10% (+3.6mm)	3319403 (+6.8%)	116.6 (+2.2%)
+15% (+5.4mm)	3424706 (+10.2%)	117.8 (+3.2%)

Table 31 - Summary of MWL error on submerged volume and characteristic dimension.

Negative values indicate that the MWL is closer to hinge, positive indicates it is further away (i.e. the model is more submerged). Approximately +/-2mm variation of MWL was observed during the testing campaign, corresponding to V_s errors below 5% and r0 errors around 1.5%. For the repeatability comparison plot above, the drift in Z position (i.e. vertical) was within 0.25mm.

8.10.2 Adjusting Morison's damping

Currently, Mocean's numerical model approximates WEC responses by applying a single value of Morison coefficient, Cd (i.e. the non-linearity representation) to all seas. This is far from ideal, because the particular value of Cd used is tuned to larger waves and means numerical predictions are poorer in smaller waves. Cd should ideally change depending on the incident sea. Flex response sensitivity to Cd values in both FD and TD numerical domains is shown in Figure 143 with supporting figures in Appendix O.

Figure 143 shows that an FD based Cd change from 0.4 to 0.8 causes an approximately 14% reduction in peak flex RAOs, while TD-based Cd change from 0.8 to 1.2 results in approximately 2% reduction – in both cases, PTO gain does not seem to have significant effects on the delta. It makes sense for the TD model to be less sensitive to Cd variation as it is inherently taking more nonlinear behaviour into account, which are to an extent embedded in the Cd term as part of the FD model.

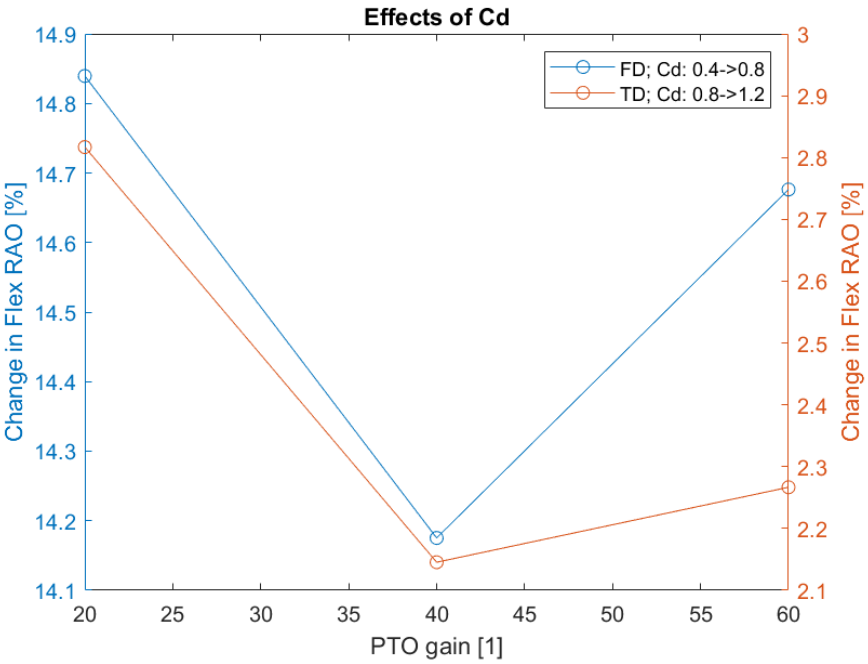

Figure 143 - Percentage differences in peak Flex RAO based on Cd variation.

8.10.3 Effects of friction

This section shows results from a numerical TD model, where the static friction value measured in Chapter 7 was included numerically. This is shown in Figure 144 and supported by plots in Appendix O. As previously, the numerical TD model was run by Alfred Cotton.

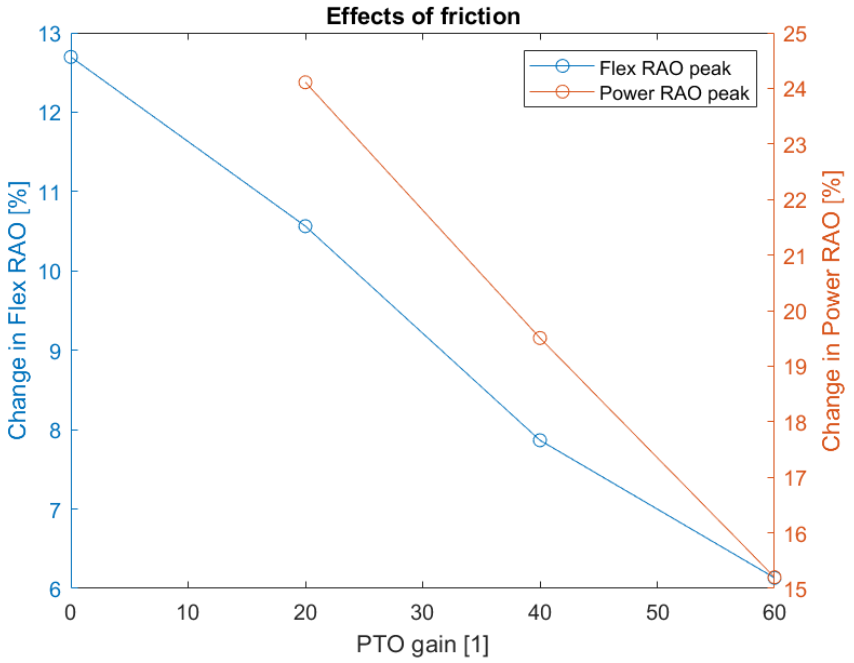

Figure 144 - Percentage differences in peak Flex RAO based on friction inclusion (TD numerical model).

Figure 144 shows that the power RAO peak value is more significantly affected by friction than flex RAO peak, as PTO gain increases from 20 to 60. At a gain of 40, it shows that an 8% decrease in flex RAO peak is equivalent to an almost 20% decrease in power RAO peak, which is significant.

8.10.4 Irregular waves

IEC guidelines recommend running irregular seas with series of 250 and 1500 waves minimum (long-crested and short-crested respectively), though this is likely to drop to 1000 waves for the latter in the upcoming revision of IEC technical specifications. For short-crested seas, the 1500 waves recommendation was not satisfied due to limited testing time available. A value closer to 500 waves was run, which still exceeds the half-hour interval often considered representative of spectrum at full-scale.

Long and short crested power comparisons can also be seen in Appendix O.

Repeatability is explored via IRL13 and IRL23 seas; with 3 repeats each. The resulting mean power data in watts was: [mean, +/-mean std], [0.0365 +/-0.000805], [0.0104 +/-0.0000156]. Seed effects to explore power sensitivity to wave component phasing are shown in Table 32.

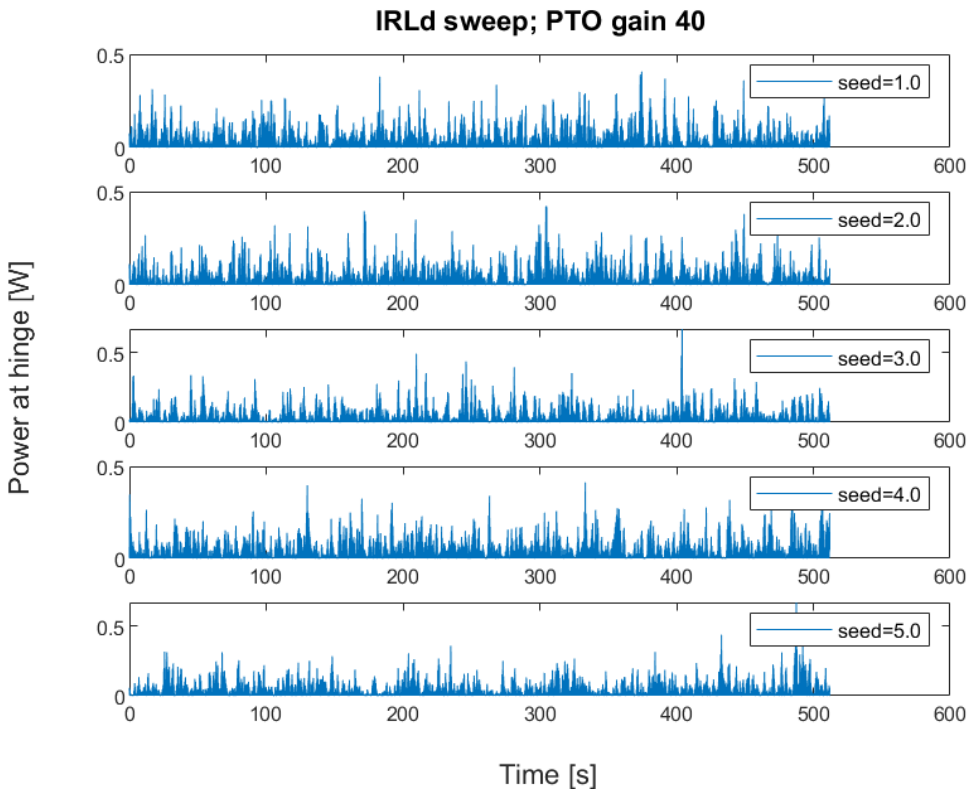

Figure 145 - Time series of IRL23 repeats with seed number variation (PTO gain 40).

Back up pots are shown in the relevant section of Appendix H. While seed effects on power time series are observable from Figure 366, the mean power figures closely match, with the largest difference being around 3.2% above the baseline value with a seed number of 1.

Seed	1	2	3	4	5
Mean power [W]	0.0355	0.0351	0.0344	0.0357	0.0348

Table 32 - Mean power measured with different seeded IRO23 runs.

When analysing the irregular waves to compare demand and measured parameter values, we only look at frequencies up to 2Hz, which is the tank's maximum. This technically implies that any higher order effects may occur at frequencies higher than 2 Hz (model scale) are ignored, though this is deemed acceptable.

8.10.5 Ir0 seas

Ir0 analysis is detailed in Section 8.12 and Appendix L. Here the repeatability of repeat segments within each IROa run is explored. The underlying intent is to verify whether repeat time can be further decreased when running such seas, while still ensuring sufficient precision. A 'segment' is a shorter repeat period (32s) within the nominally defined 256s repeat period for each run. Responses in both IROa seas more or less evens up from the fifth segment onwards, i.e. from 160s onwards, with an additional 32s of run up time.

In Figure 146, the asymmetry in flex response is visible from the fact that positive peaks (max_p) exceed negative flex minima (max_n). IRO02 has higher segment variability than IRO01, which is expected due to it being a larger sea with more reflections. Figure 147 shows broadly equivalent *intra* (segment) variation and *inter* (run) variation, suggesting that Ir0 runs can either be shortened, or repeatability analysis can be carried out within a 256s repeat time Ir0 run itself. Both bear relevance on streamlining the test method, which is picked up again in Chapter 9.

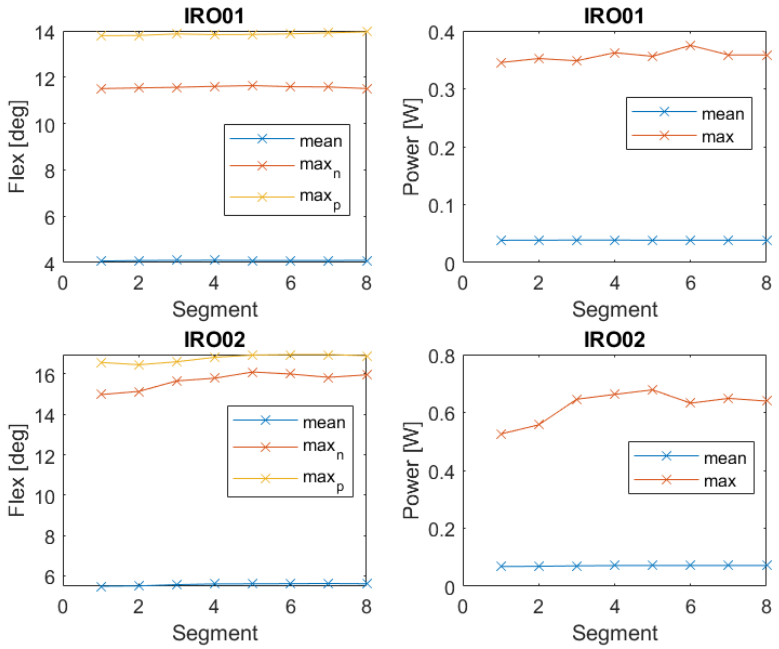

Figure 146 - Intra segment run repeatability for IROa series.

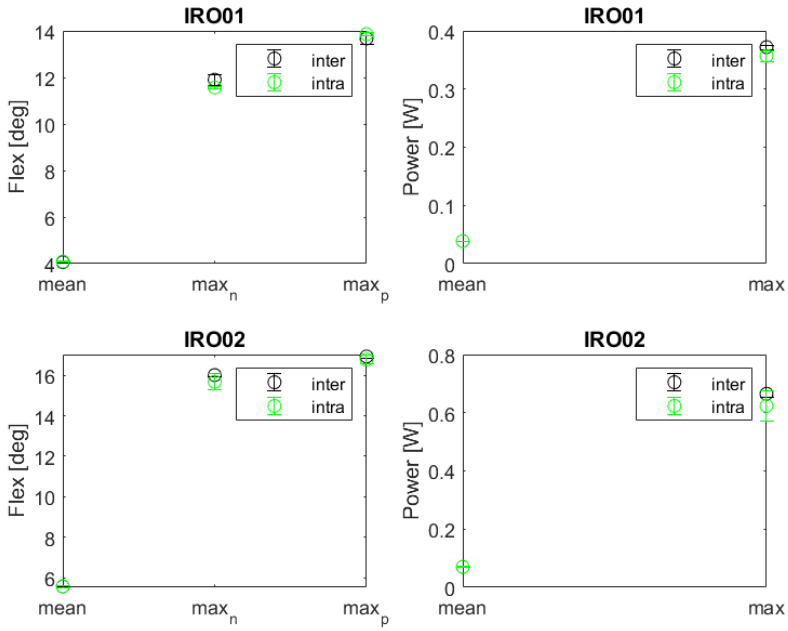

Figure 147 - Intra and inter repeatability of IROa series (flex and power).

8.11 Decay tests

Natural frequencies describe the response in the undamped system (i.e. just accounting for system inertia/mass and stiffness). Natural periods were experimentally obtained from decay (i.e. pull-and-release) tests in still water. The model is displaced from the equilibrium position in one DoF, and then released until it returns to equilibrium. This is done for surge, roll, flex, and yaw. For each DoF the initial displacement is applied sequentially in both directions. Periods reported in this section are in fact pseudo periods, approximately measured by measuring zero-crossing periods from the time traces (e.g. Figure 148) and averaging when more than one period can be measured for a given trace.

The figures below show results for 20th scale model in different configurations; more details are given in Appendix H. No PTO gain is applied in this case. Cases with PTO damping gain varied are given in the same Appendix. Natural periods are not dependent on PTO damping. However, adding damping can shift the frequency of the peak response such that the power RAO peak may occur at a slightly different period than the natural periods.

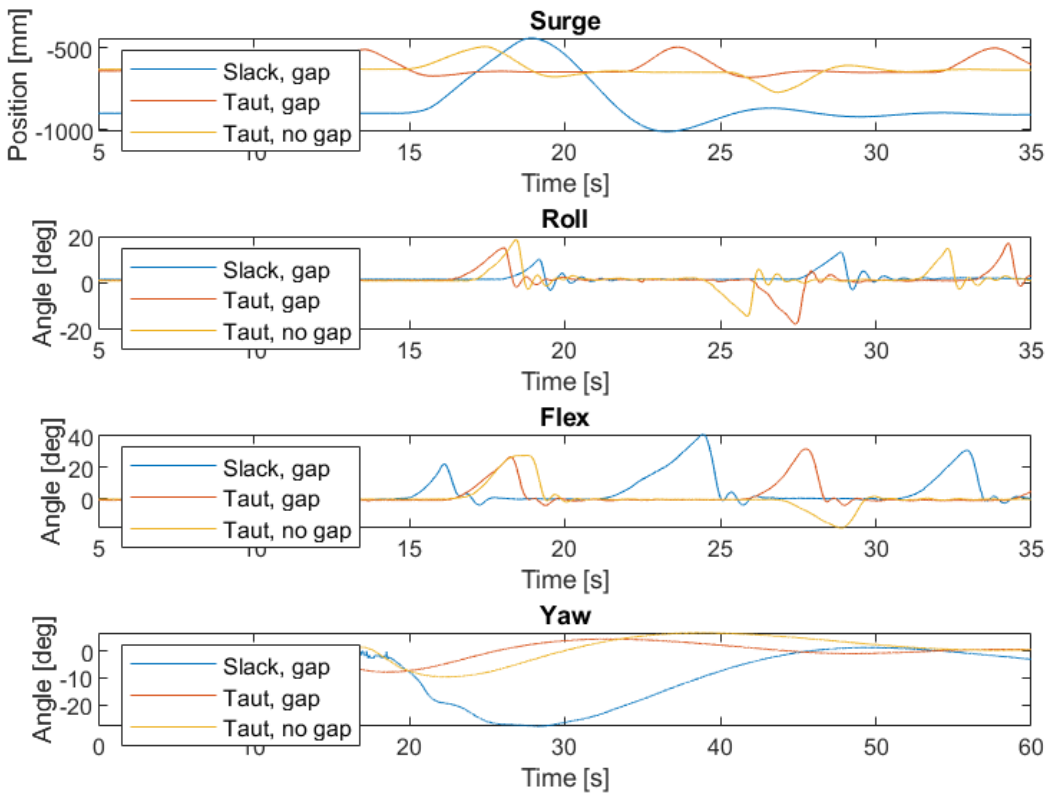

Figure 148 - Pull-and-release tests for 20th scale model - different configurations; no damping gain.

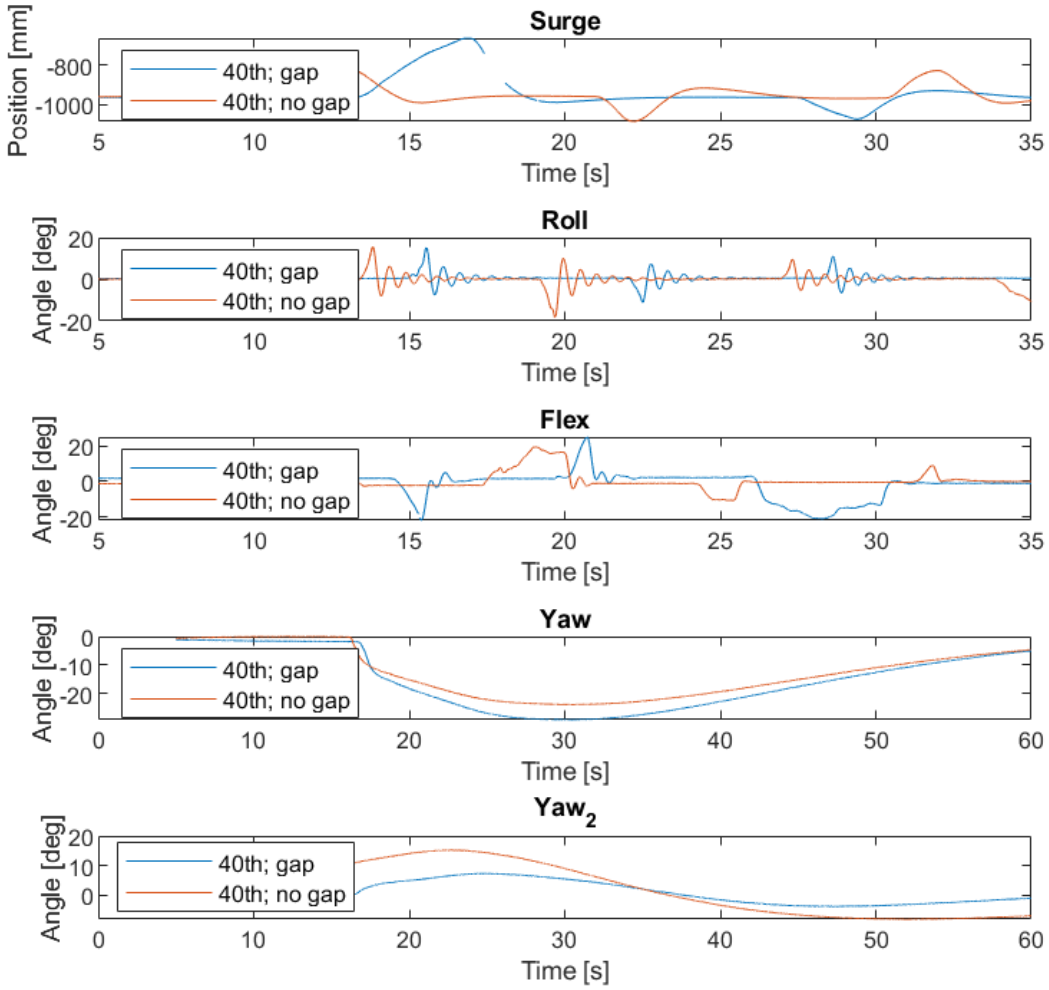

Figure 149 – Pull-and-release tests for 40th scale model - different configurations; no damping gain (slack mooring).

Note that Yaw_2 in Figure 149 is a repeat of Yaw but exciting the model with an opposing stimulus.

Model configuration	**Mooring**	**Natural period, full-scale equivalent [s]**			
		Surge	**Roll**	**Flex**	**Yaw**
20th, Gap	Slack	27.24	2.99	2.82	194.99
20th, Gap	Taut	14.53	2.82	2.50	141.59
20th, No Gap	Taut	17.44	2.59	2.68	147.04
40th, Gap	Slack	26.06	3.42	2.78	273.60*
40th, No Gap	Slack	28.08	3.48	2.85	336.97*

*Table 33 - Natural periods from pull-and-release tests at equivalent full-scale. NB: *indicates lower quality estimate.*

It is expected that the orange power and green feedback cables for the motor (Figure 150) will have an effect on the natural (i.e. undamped) period responses of the WEC. Similarly, the taut mooring with increased stiffness should also alter natural responses. The following observations can be made from Table 33:

- Natural periods for the 20th model under taut mooring are lower than under slack mooring in all DoFs, particularly surge and yaw, as expected.
- Surge natural periods for 20th and 40th models are very similar, despite the 40th model not having any cables – suggesting that cable influence is negligible in surge.
- Roll natural periods for 40th scale are higher than 20th, suggesting a higher hydrodynamic stiffness for the 20th model, as expected due to the influence of the cables.
- In yaw, the same as the above is true.
- All flex DoFs are remarkably similar – suggesting minimal effects of mooring, scale, or cables in this response.

As far as the last point, it is important to consider that scaling itself may be affecting responses, though this is unlikely since displacements and velocities in these decay tests are very low. It also assumes that the mass matrix elements are perfectly scaled between 20th and 40th models – i.e. that the ‘as-built’ model mass distributions are equivalent, which is not the case in practice.

When considering previous Blue X and different Blue Star geometry tests, the dominant flex responses involved significant aft section motion and a more static fwd section. If this is the case for BST-folding also, and given that the cables are attached to the fwd section, the cables may be having minimal impact on overall flex DoF responses. In surge and yaw, there is no hydrostatic restoring force, so one would expect any decay tests to be solely dependent on the mooring properties. However, if initial displacements are large in one of those directions, there is a possibility of accidentally introducing small amounts of other motions too.

It is posited that the effect of the cables would be strongest in roll. Having said this, out-of-plane modes of motion would have to be analysed to verify which mode corresponds to a response with significant roll motion.

8.11.1 Natural period as computed numerically

The following are computed based on hydrodynamic coefficients and as-built mass matrices for both 20th scale model with active hinge switched off, and passive 40th model (Table 34). This computation was run by Alfred Cotten to enable a numerical-experimental comparison.

Scale	Configuration	Mooring	Natural periods [s] – full scale equivalent
20th	Gap	Slack	1.44, 2.32, 2.60, 2.67, 5.18, 7.13, 7.62
			Roll only: 1.44, 1.44, 8.39 (other DoFs locked)
			Flex only: 2.38, 2.61, 5.25 (other DoFs locked)
20th	Gap	Taut	1.44, 2.32, 2.59 2.66, 5.08, 6.85, 7.08, 10.10, 13.35
20th	No Gap	Taut	2.58, 4.63, 6.95, 13.77
40th	Gap	Slack	1.44, 2.32, 2.59, 3.56, 4.06, 5.15, 7.49
			Roll only: 4.22 (other DoFs locked)

Table 34 - Numerically obtained natural periods.

(Key: blue – in-plane DoFs only; red – roll or flex DoFs only.)

NB: it is not possible to compute yaw period numerically because of the incredibly low frequencies needed.

Note that there are multiple natural periods, and these correspond to particular modes of motion of the device. Most modes involve coupling amongst multiple degrees of freedom, so it is not strictly possible to separate out a single NF for e.g. roll, or flex. In adding out-of-plane DoFs for the 20th Gap/taut configuration, notice that three new NFs appear; it is uncertain what sort of motions they correspond to.

However, surge and yaw are odd cases because there is no restoring force due to the WEC (only a bit due to the mooring system), so the NF at 13.35s when the mooring system is present in the model may correspond to the surge natural period. It is interesting that this is shorter than measured, implying a potential overestimation of the mooring stiffness in the numerical model.

When locking all DoFs apart from flex, there are natural periods at 2.38, 2.61 and 5.25s. Flex in the numerical model is basically defined as the pitch of the aft hull relative to the forward hull, so it is as if the fwd hull is fixed in place, and the aft hull then pitching on its own about that. It is difficult to know which numerical value corresponds to the experimental one because any flex motion in practice will be accompanied with surge and heave strongly coupled.

Perhaps there are also nonlinear effects at play here; the numerical model assumes small displacements.

Sometimes there are more NFs than degrees of freedom, and so it can be confusing to work out “what is what” when trying to compare to decay tests. Locking all DoFs apart from roll turns out to be wrong as it only allows for rolling about the centre of gravity – Mocean WECs probably end up rolling about the centre of flotation in practice, so sway and heave are also required in the numerical models to describe this sort of motion. Typically, this means one should end up with a natural period a bit lower, and so for the Blue Star case, this might explain some of the discrepancy observed.

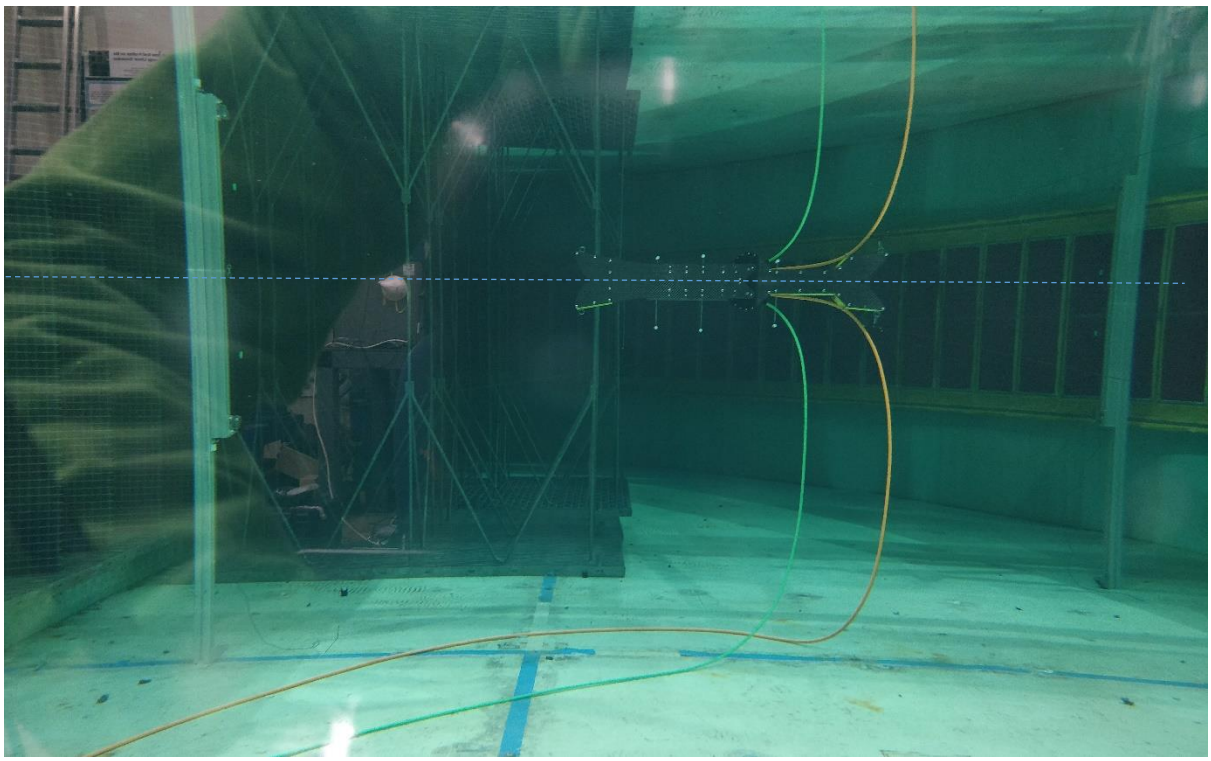

Figure 150 - Underwater view of BST-folding, showing cable pathway below model (MWL marked in dashed blue).

Figure 150 shows that the cables more or less lead out along the central axis of the model (along wave propagation direction) and have a natural backward ‘C’ shaped bend.

8.12 Ir0 sea responses

Incident Ir0 parameters (net of reflections) are analysed and outlined in a dedicated Appendix L. Here, their utility for RAO measurement, optimal PTO damping gain selection, and mean power estimation, is presented.

8.12.1 RAOs from Ir0 seas

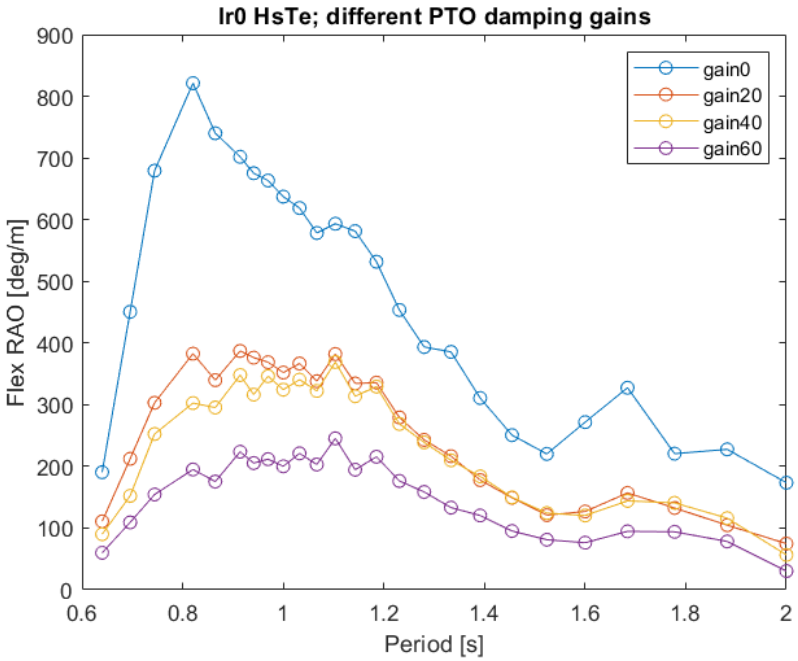

Figure 151 - Variation of flex RAO with different damping gains, under IRO21 sea.

Figure 151 shows that gain 20 and gain 40 give similar dynamics – this suggests that optimal damping is around those two values, as is the case for regular wave equivalent plots. Using IROc series, it can be seen that the PTO damping gain that yields maximum mean power is 40; this too is consistent with regular wave results with damping gain sweeps. The Ir0 result presented here gives greater confidence because the sea is more akin to real sea conditions, including different phasing of wave components.

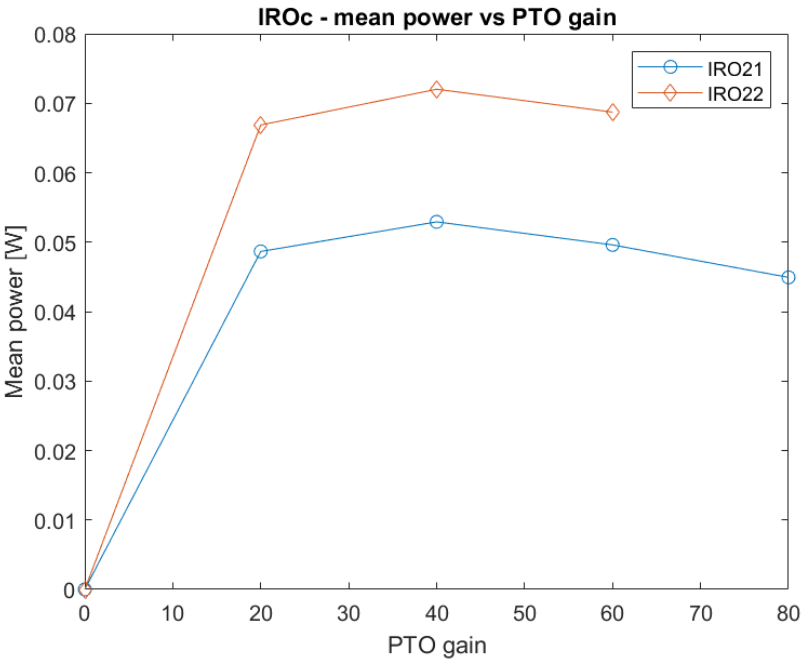

Figure 152 - Variation of mean power with PTO gain; IROc seas.

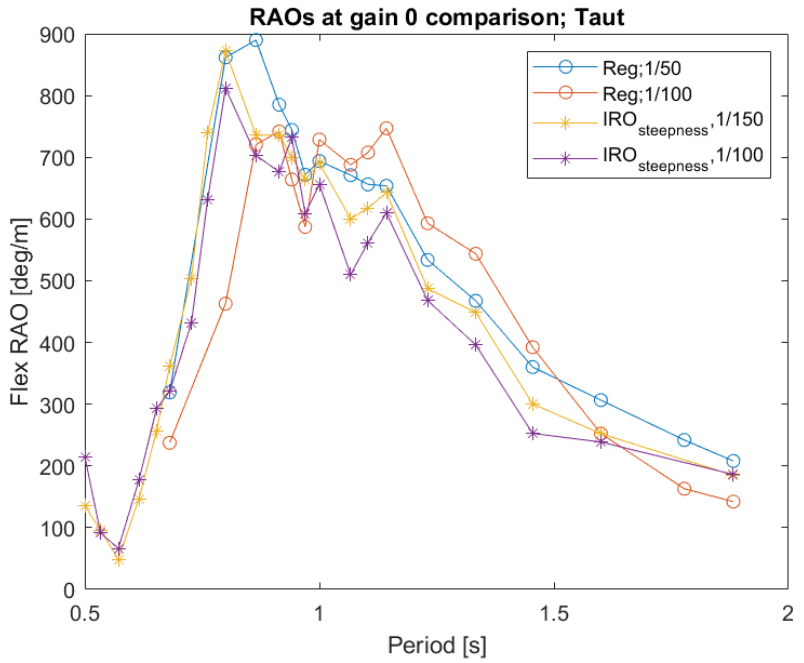

Figure 153 - Comparison of flex RAOs obtained from regular waves and 'steepness' type IRO seas; PTO off.

Figure 152 suggests an optimal PTO damping gain value of 40, the same as that deduced from regular wave PTO gain sweeps. Figure 153 compares regular wave obtained RAOs, with RAOs obtained with Ir0 seas having components at equivalent constant wave steepnesses. Interestingly, both Ir0 seas line up more

closely with the 1/50 steepness regular wave RAO and lie within its envelope. Unlike the regular wave plots, 1/150 steepness Ir0 data is consistently above 1/100 steepness Ir0 data.

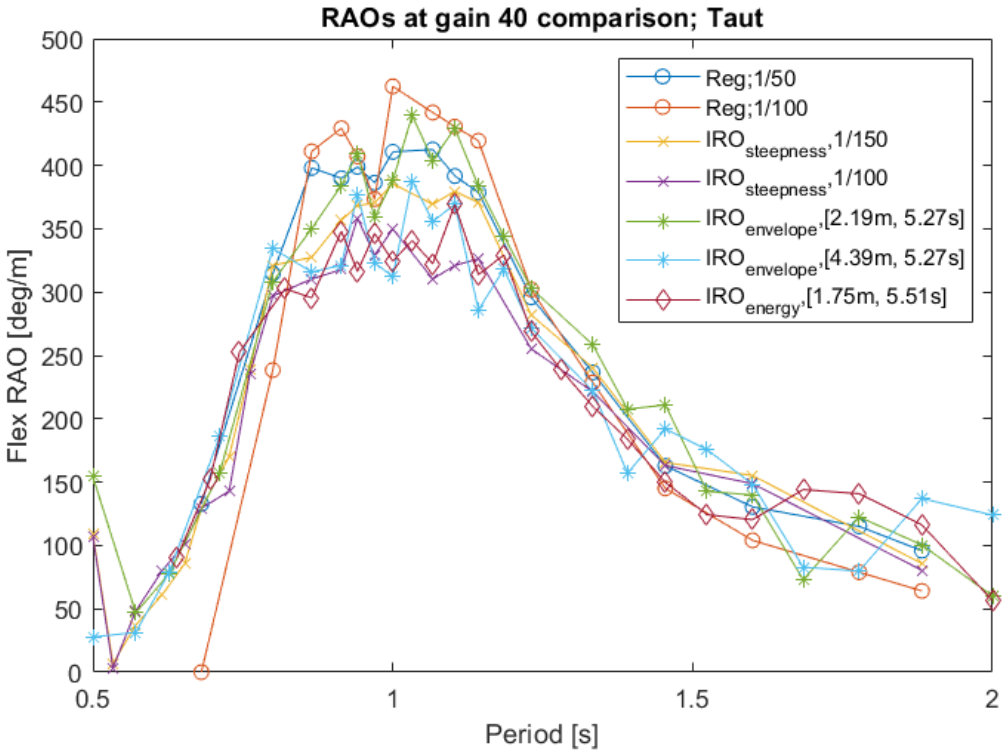

Figure 154 - Comparison of flex RAOs obtained from regular waves and IRO seas; PTO gain 40.

Figure 154 points to the following:

- IRO envelope [2.19mm, 5.27s] data matches regular wave data most closely, followed by the IRO steepness 1/150 sea.
- IRO steepness 1/100, IRO envelope [4.39, 5.27s] and IRO energy [1.75, 5.51s] are quite close to one another in terms of RAOs – no clear 'winner' exists among them.

Figure 155 shows the repeatability of different IRO seas at different PTO gains, with standard deviation error obtained from 3 repeat runs of each. Accordingly, the following points can be made:

- Higher PTO gain runs have better repeatability, as expected due to lower magnitude motions.

- Repeatability of gain 40 data appears better than the seed repeatability of IRL23 sea with PTO gain 40 (see Appendix O).

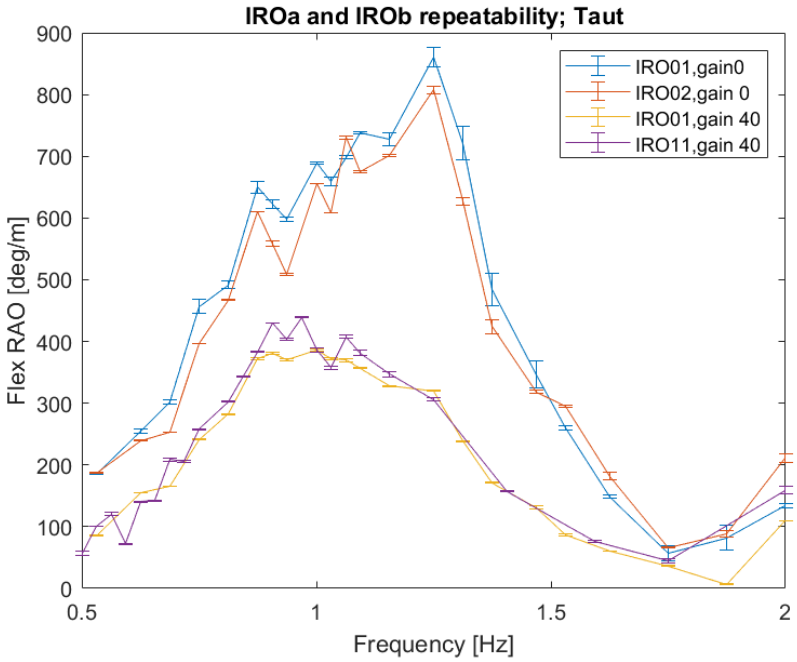

Figure 155 - RAO repeats with IROa and IRObb seas; PTO off.

Seed number sensitivity of both IRL and IR0 seas is explored in the following section and in Appendix L. Although irregular wave data is presented without taking reflections into account, the levels of repeatability are of the same magnitude, suggesting Ir0 is as reliable from a repeatability perspective.

8.12.2 Comparing moorings and gap effects via Ir0

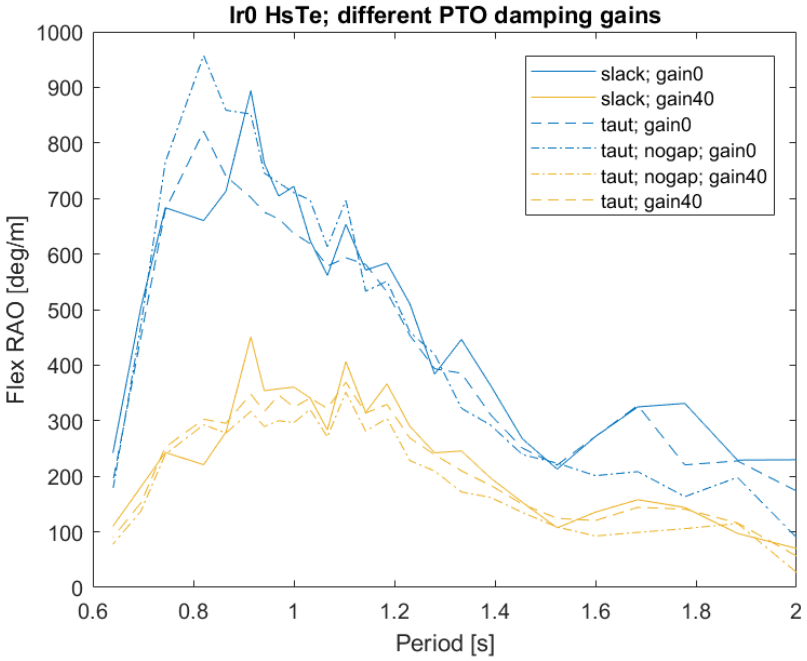

Figure 156 - Comparison of flex RAO responses for different geometry and mooring configurations.

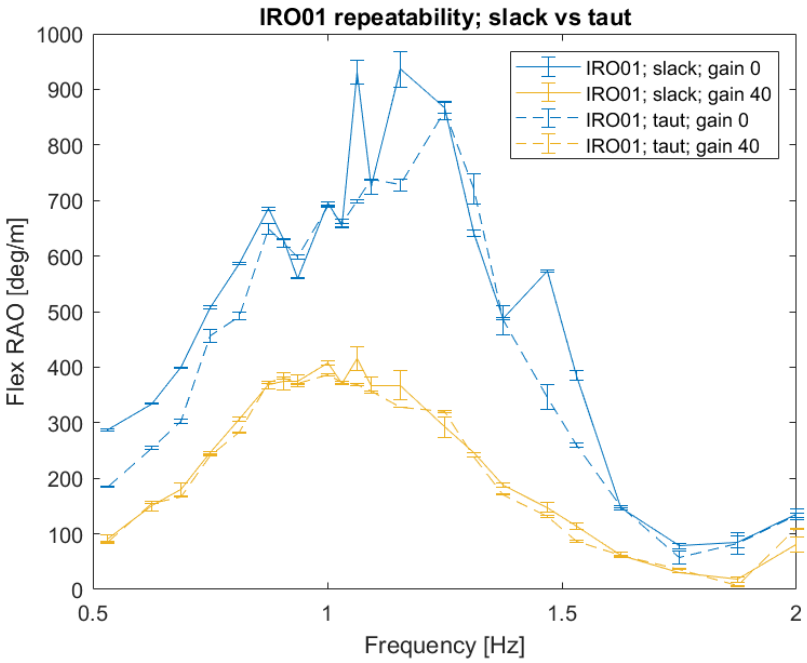

Figure 157 - Repeatability of IRO01 in slack and taut moored configurations.

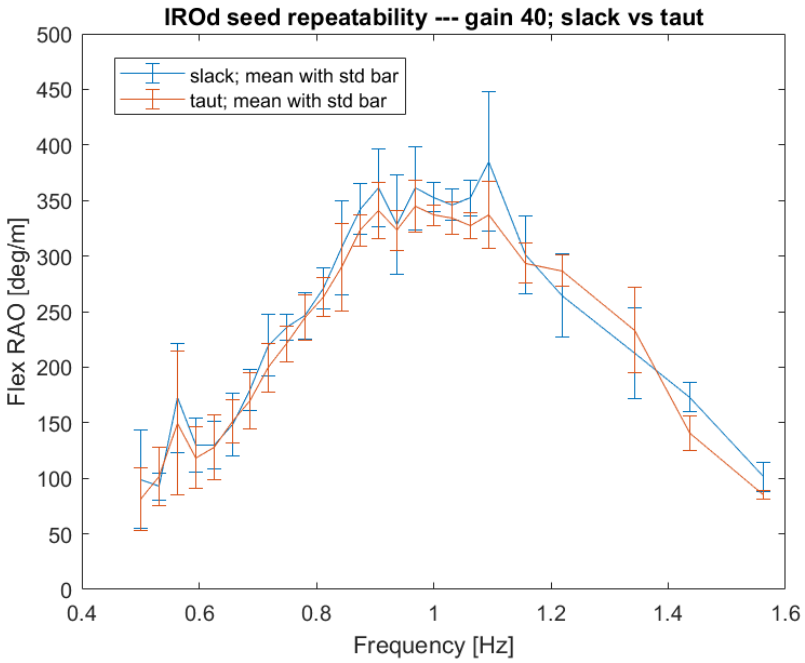

Figure 158 - Comparison of seed repeatability in slack and taut mooring configurations.

Implications of the Ir0 obtained results in this section are outlined and expanded upon in Chapter 9, particularly in terms of recommended testing methodologies for future physical testing campaigns.

Part IV:
Appraisal & Closing

This final part discusses results obtained via physical model testing in Part III and their link to metrics, particularly in terms of enabling performance evaluation, device evolution, and the integration of physical testing in the overall design and optimisation process (Chapter 9). In Chapter 10, findings relating to EngD goals are presented across metrics, method, and uncertainty areas. The impact of this research is then summarised and framed within Mocean Energy's as well as wider wave energy's context.

"[There is] no one technique, such as tank testing, or specific analysis tools that will insure success of a design optimization program" (DeBord Jr *et al.*, 2003)

- Frank DeBord Jr, John Reichel, Bruce Rosen, Claudio Fassardi, 2003

"Apparent simplicity will often turn out to be the extent to which the difficulties can be hidden" (Salter, 2005)

- Stephen Salter, 2005

Chapter 9. Discussion

This chapter discusses implications of the results obtained in the two physical model testing campaigns outlined in the previous Part III. Traditional and more novel metrics are applied to the two Blue Star WEC iterations for device comparison, and discussed in the context of off-grid markets. Integration of physical model testing in the design process is also discussed with respect to its merits, limitations, and ability to complement numerical methods. Also discussed is the ability of the followed framework and methodology in tracking progress and improving the Blue Star WEC as a product. Test methods are discussed in terms of accelerating testing and in quantifying scaling effects. Finally, areas of future work are offered, alongside recommendations to improve both WEC performance and development process.

9.1 Metrics application

Over the last five years or so, a growingly adopted industry standard for assessing WECs has finally emerged. A precursor of this was the stage-gated process pioneered by Wave Energy Scotland's PCP streams, then developed and published by IEA-OES (Hodges *et al.*, 2021). It has now been more fully implemented in the recent EuropeWave PCP program, which explicitly requires participating developers to use common evaluation areas (Figure 159) – e.g. reliability, controllability, and other parameter *-ities* – to establish ambitions and review development progress.

The fact that this is now common, established, and widely accepted, is positive news for the wave energy sector in terms of guiding inter and intra device comparisons. Aside from providing a useful framework to establish goals and review progress, the framework also defines sets of evaluation criteria for each area. However, many of these are qualitative indicators, as opposed to quantitative metrics, and difficult to evaluate at early development stages – a recurring problem.

Figure 159 - Evaluation areas included in the IEA-OES Evaluation and Guidance Framework. Source: (Hodges *et al.*, 2021).

Affordability (highlighted in red; Figure 159) – considered the paramount requirement and ultimately expressed via LCOE – is the combination of all other evaluation areas. From an early-stage development point of view, the set of practically measurable metrics overlap with quantities that can be obtained experimentally and at reduced scale – i.e. *power capture*. Thus, Figure 159 also provides a visual illustration of how much of 'performance' gets left out at early stages, at least from a quantitative perspective.

Other evaluation areas, such as reliability, availability, and survivability can be proxy measured, likely via device behaviours or characteristics highly specific to different WECs. For example, Mocean may measure and track self-referencing behaviour (affecting mooring loads), steep wave load shedding (affecting structural loads), roll stability (affecting seal wear), free hinge angles (affecting risk of hull-to-hull pitching impacts). These, too, are not easily encapsulated in a single industry-common metric.

While it is difficult to include more aspects (i.e. evaluation areas) of performance in the optimisation fitness function – it may possible to include some of these as part of the Pareto front evaluation criteria post optimisation. As a developer, just as we consider, "can the two hulls be independently trimmed?" (desirable from a

point of view of reducing static loading on the hinge), we can ask, “what is the roll response or max-to-mean angle ratio in a representative sea?” (via post-processing). Some of these aspects can be measured via physical tests; these are summarised for BST-folding in the following section, comparing configurations with and without aft hull gap.

9.1.1 Device comparison via metrics

The initial comparison is made between like-for-like models, i.e. BST-folding with and without aft hull gap. Initially, power elements are compared, relating these to the non-dimensional metric of CWR. Experimentally obtained CWRs with the optimal PTO damping gain of 40, smoothed with spline curves, are shown in Figure 160.

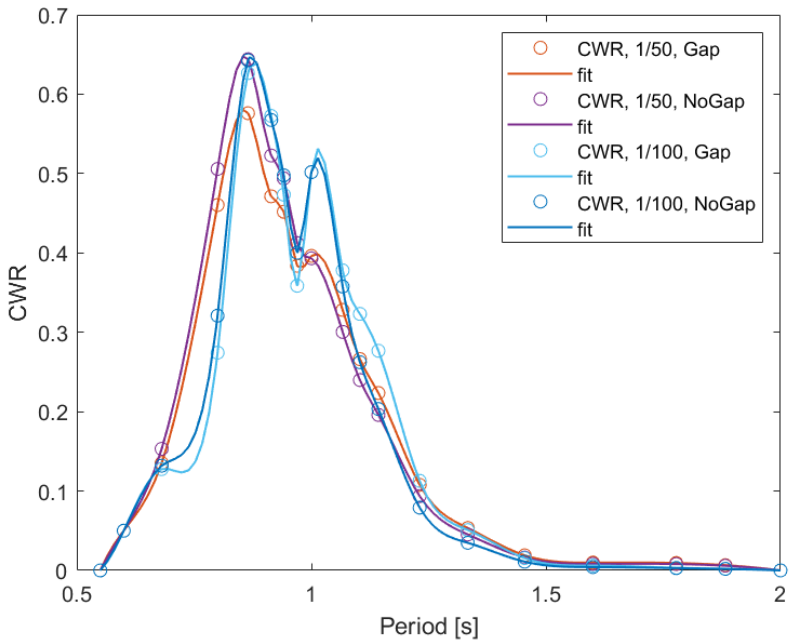

Figure 160 - CWR plots of different configurations and wave steepness.

From the above, quantities of interest can be extracted and plotted for comparative purposes. The following are specified:

- Peak CWR (Peak) – representative of the maximum power values that the subsystems will have to handle (related to transmission/modulation effort). It also relates to the max potential if applied to a particular sea.

- Area under CWR, normalised by appropriate value for visual representation ($Area_{norm}$) – representative of the overall energy the WEC can capture over the full range of seas (related to AEP).
- Bandwidth above a certain CWR threshold[75], normalised by tank bandwidth ($Bandwidth_{norm}$) – related to the versatility of the device to different climates (its power capture potential in different locations)
- Ratio of peak-to-width above a certain CWR threshold (PtW Ratio) – representative of the 'peakiness' of the CWR plot and thus of the consistency of the WEC in capturing power (related to CAP)[76].

In a continuously available power (CAP) driven scenario or application, one would ideally seek a 'square' shaped CWR, at the power value required by the asset or application where it is fed to. This allows for less reliance on battery storage capacity to compensate for variability of power generation, including due to seasonality. Additional power captured beyond that required simply 'stresses' the system and adds cost and capability to relevant equipment ratings without benefit to the customer. The above seems a reasonable approach, though requires further exploration to identify where the CWR threshold should lie, based on 'good enough' CAP performance.

[75] CWR threshold can be set in different ways, e.g. such that 95% of the area or bandwidth is covered. A nominal value of CWR>0.05 is chosen here.

[76] Better than CAP, as this would rely on a set battery capacity which can vary.

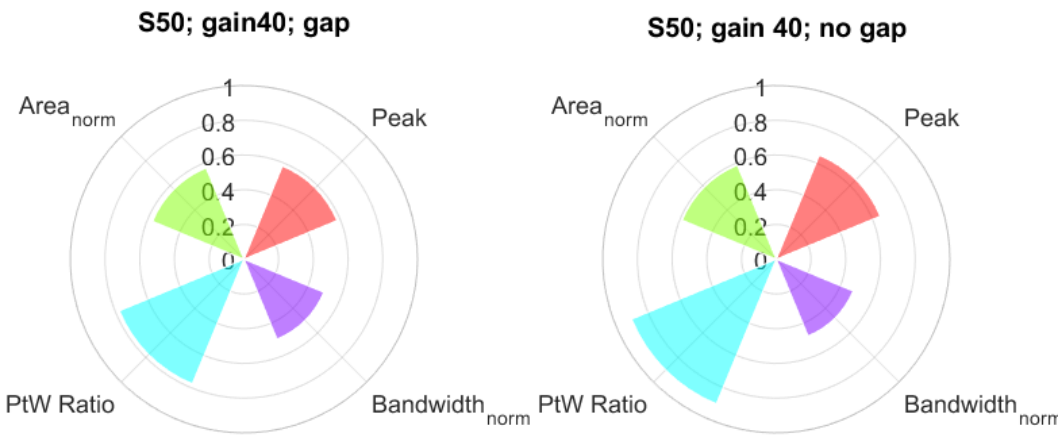

Figure 161 - Power capture elements; wave steepness 1/50.

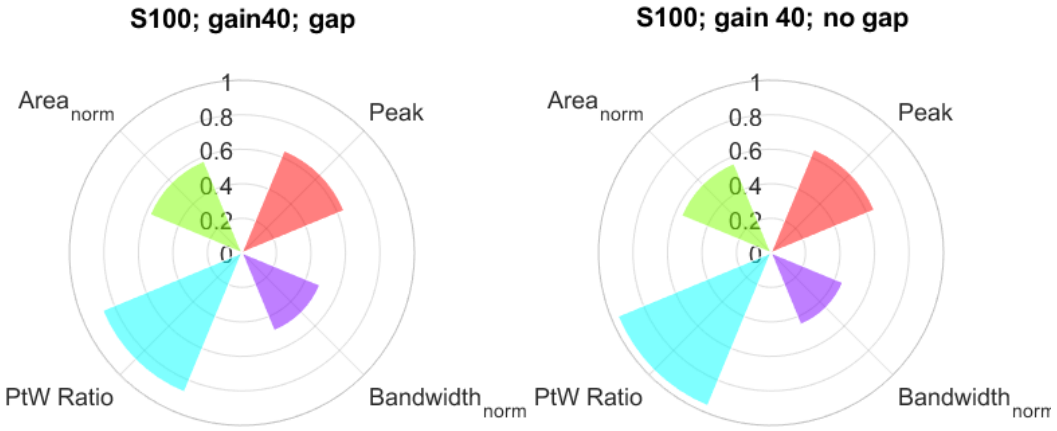

Figure 162 - Power capture elements; wave steepness 1/100.

The elements mapped in Figure 161 and Figure 162 all speak to the ‘power capture’ evaluation area of the IEA evaluation framework (see Figure 159). They are mapped here in order to compare the ‘gap’ and ‘no gap’ configurations. However, these elements could also be compared with numerical predictions to visually map the extent of validation. From Figure 161, it can be seen that ‘no gap’ configuration has a greater peak and area, but lower bandwidth, and a peakier overall response. Figure 162 agrees, except the area is now lower for the ‘no gap’ configuration. Since the areas are very similar and the bandwidth is greater for the ‘gap’ configuration, this may be chosen as the winner if consistency in power delivery is desirable, as it is for Blue Star. These

configurations are actually very similar, but it can be imagined how, in other scenarios, differences may be more significant.

In order to cover more of the IEA evaluation areas, additional proxies are extracted and compared. These are related to the 'I factors', or Hydrodynamic Performance Qualifiers (HPQs) utilised during the DoE Wave Energy Prize assessments, which are computed in a range of ten seas: 6 regulars, 2 large irregular storm seas, and 2 further multi-direction irregular seas (Driscoll *et al.*, 2018) – refer to Chapter 2 and Chapter 5.

Quantity/behavior of interest	Description & relevance	Related IEA Evaluation Area
Sensitivity of flex[77] angle to wave height and steepness	• WEC 'survival mode' involves the disengagement of the PTO, and free rotation of the hinge to avoid large loads through the powertrain • Large angles are expected as the WEC hulls contour the waves and are less constrained by applied damping	Survivability
Self-referencing behavior	• Historically, a longer forward hull and a shorter aft hull have enabled a stable forward hull and most rotation occurring at the aft hull (i.e. "self-referencing") • This alleviates mooring loads (including snatch loads) and enables use of more compliant mooring system	Reliability; Availability
Limited roll sensitivity	• Roll responses can be induced under wave excitation, potentially even with head-on waves. • Associated "snaking" behavior can limit towing speed and the lifetime of seals around the PTO shafts / power train	Reliability; Availability

Table 35: Additional proxy metrics for desirable WEC characteristics

A similar approach is pursued here, where the following HPQs are chosen:

- Mean-to-max (MtM) flex angle (relating to *survivability*)

[77] The relative pitch of the forward and aft hulls – i.e. the overall angular rotation at the hinge.

- Mean-to-max power (relating to *controllability*)
- Mean-to-max mooring loads (relating to *reliability*)

The seas chosen to compute these are IRL23 (long-crested, [Hs, Te] = [1.45m, 5.48s]), and IRO21 (Ir0 type, [Hs Te] = [1.75m, 5.51s]) – refer to Chapter 8. IRL23 is the sea closest to the 'hot spot' of the energy matrix, while IRO21 is the closest to IRL23 in terms of equivalent [Hs, Te] parameters.

The idea is that this provides a useful way of accounting for more 'performance' in a way that ties to both numerical and experimental data, as well as supporting particular WEC design and geometry decisions. Roll stability is not included here, but theoretically could be, and would provide another measure of reliability and/or survivability in relation to e.g. seal wear. This can take the form of mean-to-max indicators, and checking how far away the natural resonance frequency in roll is to pitching (the further away the better). Mooring load is taken as the vertically resultant tension from the three mooring lines.

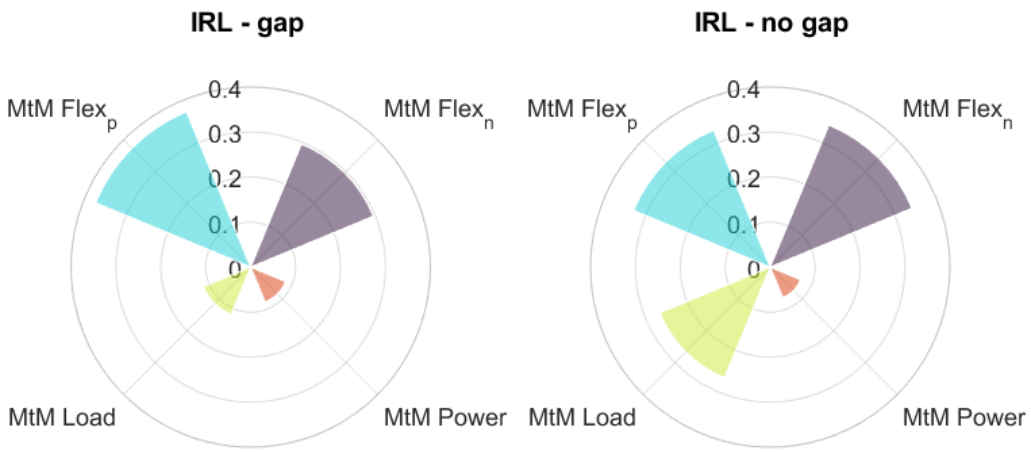

Figure 163 – Proxy performance indicators; based on long-crested sea.

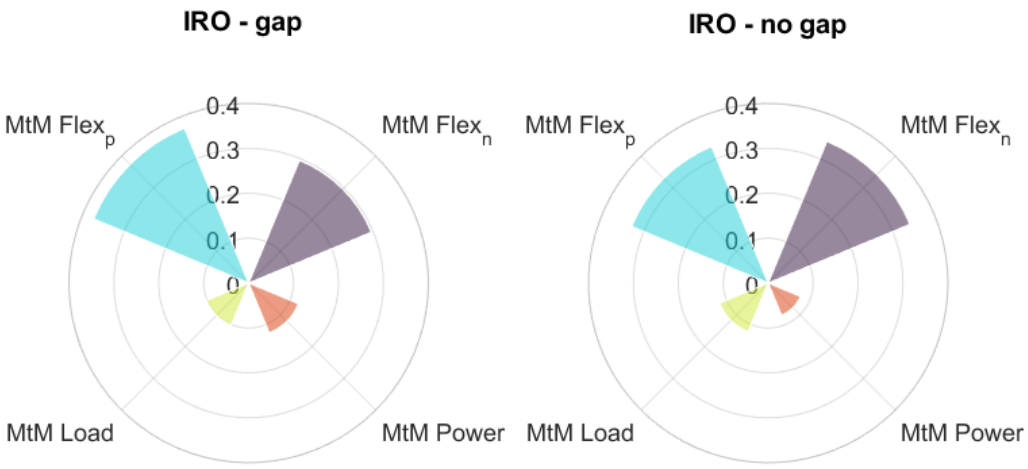

Figure 164 - Proxy performance indicators; based on Ir0 sea.

Both power capture elements and the additional proxies are plotted in polar chart format to facilitate visual comparisons but also to mirror the IEA evaluation area framework; this is the ultimate goal: to map the evaluation framework areas to a particular device. The framework proposed here is an attempt to do exactly that, in the context of Mocean WECs.

Similar trends are picked up from both IRL-based and IR0-based comparisons in Figure 163 and Figure 164. Values closer to 1 are preferable, as they indicate a lower degree of variability in the quantity of interest (e.g. flex, load, power). The figures suggest more balanced sag and hogging flex variability for the no gap configuration; and better loading variability. However, power variability is slightly better for the gap configuration. There is no clear winner. Some of the raw data plots from which metrics are extracted are given in Appendix I.

9.1.2 Device evolution

The previous evolution of Blue Star, i.e. *BST-baseline*, is compared with *BST-folding* in order to determine the impact of optimisation on WEC performance. This is done both numerically and experimentally, to the extent possible.

9.1.2.1 Impact via experimental data

The experimental comparison is limited by both sea states tested, and the fundamental build of the two models, which have different hinge properties, which effectively voids experimental comparisons (see Figure 165).

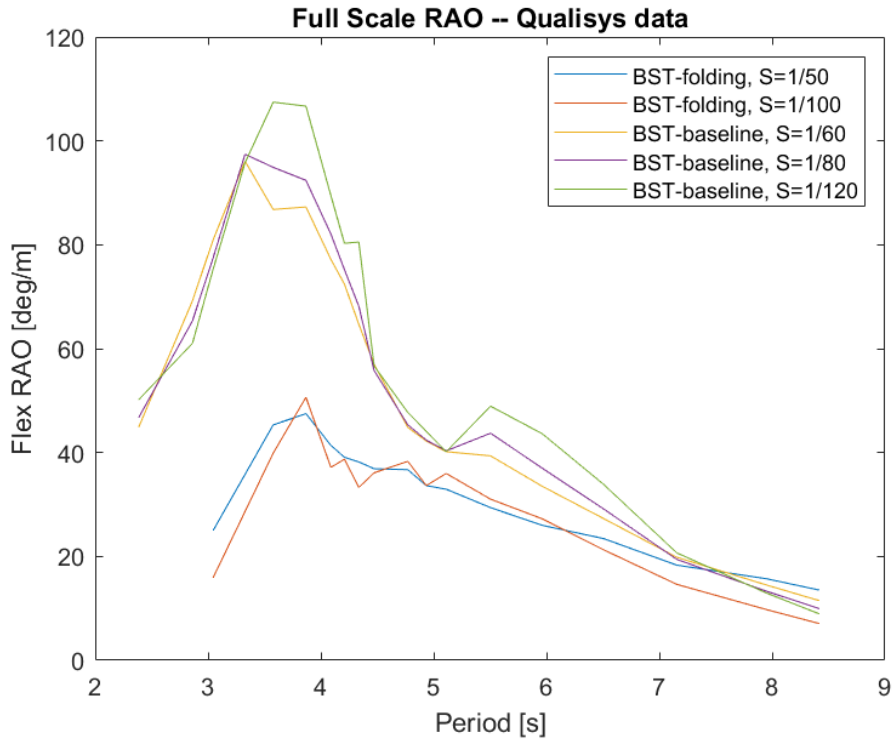

Figure 165 - Comparison of Flex RAOs (full-scale equivalent). S indicates wave steepness.

Figure 165 shows a greater flex response for BST-baseline compared to BST-folding, across all tested wave steepness values (S), despite numerically predicted capture widths for BST-folding exceeding those of BST-baseline. There are two potential explanations for this result:

- Since BST-baseline and BST-folding have different levels of hinge friction – due to the different hinge design and build – the comparison is not like-for-like. Friction is intrinsically different in the baseline and folding models, and likely to be much greater in the latter.
- However, results in Chapter 8 indicate that BST-folding with PTO damping switched off gave a similar flex response as BST-folding passive tested in Plymouth, thereby pointing to hinge friction (whose lip seal in the active BST-folding version is thought to be a major contributor) not being

the main source of flex RAO disparity. This may correspond to a different reason.

- Even if the friction and the hinge build were the same in both models, a higher RAO associated with a lower CW is possible because RAO behaviour obtained with damping off does not correspond to the realistic productive mode of the device. This is because the curves in Figure 165 are obtained without any PTO damping, only a small amount of parasitic friction associated with bearings and/or seals, which does not correspond to the realistic productive mode that is modelled numerically. This underscores the importance of including as many power conversion stages as possible in testing to capture their cross-influence. No damped RAO data is available from the baseline model, due to its lack of PTO.
- Incorrect reflection coefficients for baseline – though this is ruled out based on detailed Chapter 6 work.

Aside from the somewhat unsatisfactory experimental comparison, we can compare numerically derived performance elements, similarly to Figure 161 and Figure 162, given the same nominal scale of the physical models.

9.1.2.2 Impact via numerical optimisation data

In this case, BST-folding indicators are normalised by baseline values; same steepness; including viscous damping. The CWR threshold for Bandwidth and Ratio indicators is selected as 0.5 in this case. Figure 166 suggests an improvement across all indicators apart from Ratio, which suggests a peakier response for the folding evolution.

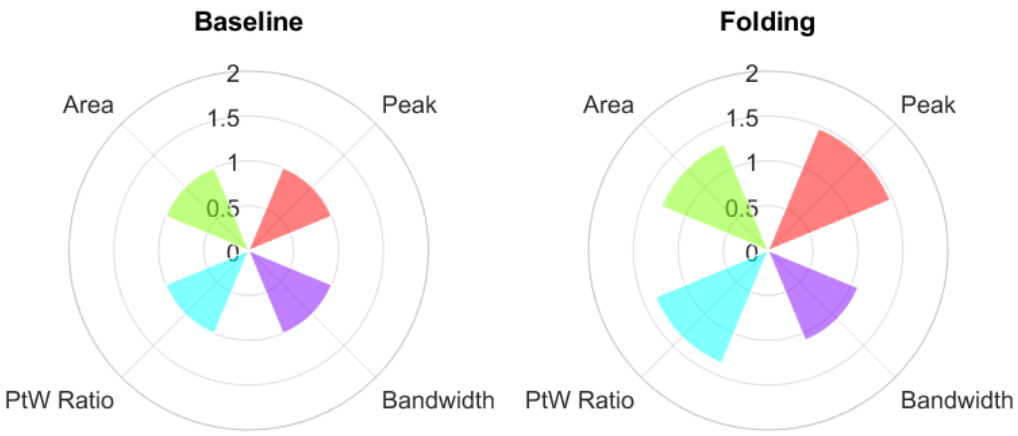

Figure 166 - Impact of numerical optimisation on power capture indicators.

9.1.3 Comparing different devices

Assuming that the underlying numerical models are accurate and representative – or at least accurate to the same extent – what do they tell us about performance comparison of these devices, and how these metrics vary if we had just Froude-scaled metrics down without optimising?[78]

A comparison of BST-folding with *M100* follows, a 100kW rated WEC that was initially conceived as the full-scale version of the Blue X prototype (rated at 10 kW) during the WES NWEC program. In Figure 167, metrics are normalised by *M100* values in order to preserve confidentiality of the absolute numbers. In comparing devices at different full scales, use of non-dimensional metrics is desirable, wherever possible (refer back to Chapter 5), where it is shown how dimensional metrics scale automatically as size/rating of device changes. Thus, Figure 168 attempts to account for scale differences, by scaling down *M100* metrics to Blue Star scale (according to nominal power rating):

[78] In other words, if instead of following a rigorous optimisation process, we had simply Froude scaled NWEC2/M100 WEC metrics to Blue Star power rating, what would have their values been? As such, is this a reasonable way of estimating them or is specific optimisation especially worth it (assuming that the performance criteria is the same)?

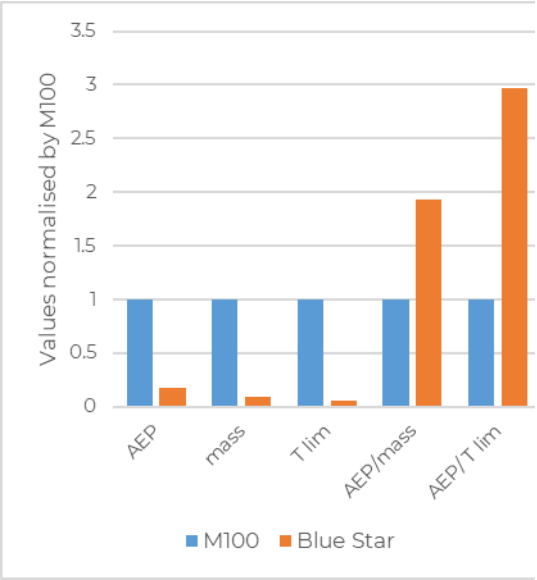

Figure 167 - Metrics comparison between M100 and Blue Star WECs, normalised by M100 parameters.

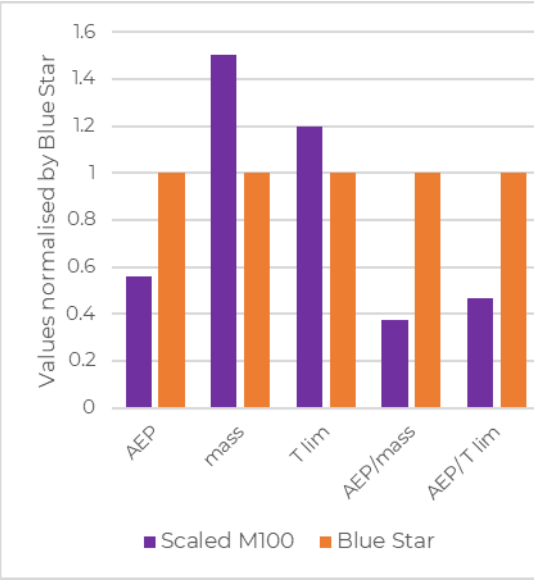

Figure 168 - Metrics comparison between M100 scaled to 10kW nominal power, and Blue Star (both normalised by Blue Star parameters).

In Figure 168, metrics values for *M100* at the end of NWEC Stage 2 (ahead of build and commissioning of Blue X ½ scale prototype of *M100*) are scaled down to a nominal 10kW rating, via Froude scaling. The scaling factor is therefore the ratio of nominal powers to the power of 1/3.5; i.e. (100/10)^(1/3.5) = 1.93. Note that 'T lim' stands for torque limit. Figure 168, which depicts more of a like-for-like comparison, shows that the Blue Star development route has led to an improvement of metrics across the board, compared to nominal values arising from a simple scaling exercise from *M100*. Mass and torque limit have decreased (reducing costs), while AEP has increased. Associated AEP/mass and AEP/torque have thereby also increased.

A number of caveats should be mentioned:

- *M100* was optimised for a more energetic wave climate (EMEC Billia Croo), while *Blue Star* has been optimised for a Central North Sea (CNS) climate.
- *M100* is at pre-FEED level (TRL4) of development while *Blue Star* is not (TRL2-3), thus masses may rise as engineering takes place for BST.
- AEP for both WECs may drop – potentially by different extents - when additional power conversion efficiencies are taken into account.

9.1.4 Effect of markets on metrics (and process)

From the point of view of power, off-grid applications for Blue Star require a minimum continuous amount of power to be available year round. In the Northern Hemisphere, this is limited by summer (in CNS July) wave climate, when wave resource is at its lowest – see Figure 169. This can be helped by the inclusion of a subsea battery, which can store energy during periods of high resource, and fill in gaps during periods of low capture. The greater the battery capacity, the greater the CAP – to a limit. A performance vs cost is at work too, of course. From a numerical optimisation point of view, there is a greater emphasis on CAP than AEP – though there is likely to be correlation, as indeed found by other work conducted by Mocean. Considering the optimisation fitness function, there is therefore not so much of an argument for including battery storage from a power point of view, but more so from a cost perspective.

However, the effect on experimental measured QOIs is minimal in practice, because both CAP and AEP rely on validation of power matrix cell values. CAP ideally requires a time-domain computation, while AEP can be calculated with sufficient fidelity in the frequency domain. A move to CAP would be feasibly validated with a smaller tank that can only reproduce the lower end of wave resource, which is likelier to occur in (Northern Hemisphere) summer as opposed to winter. However, a smaller tank would then rule out undertaking survivability testing with the same size/scale model.

Prospective customers tend to ask for TRL, (continuously) available power, and costs. From a customer confidence point of view, perhaps more seasonality investigations could be done to validate this aspect in particular. This is more about the test method than the metric that is being measured in and of itself. The number of power drop-outs in a given period would also be a useful factor to consider for validation.

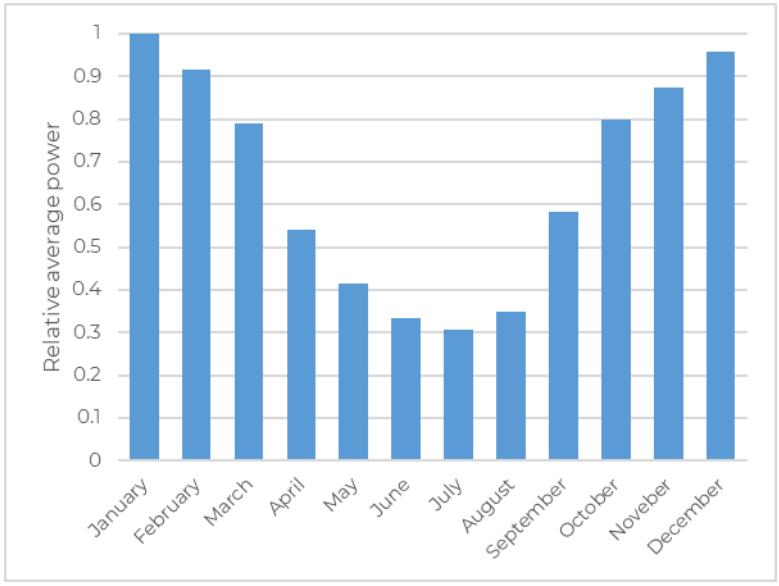

Figure 169 – Example average power seasonality of Blue Star WEC at a specific CNS location.

9.2 Integrating physical model testing

Integration of the physical model testing in the design process is key – specific aspects and reasons are given below.

A fundamental assumption is that once a numerical model is set up, it is easier (faster and cheaper) to verify the effect of design changes numerically rather than experimentally. The issue, however, is that numerical models are rarely 'complete' or static, and – at least in the case of Mocean's – are frequently being updated, revised, and expanded.

It is also not always the case that changes are more easily implemented in a numerical, rather than physical, model. For example, if concept changes are proposed that affect the WEC's characteristic shape (such as: tubular or rectangular section hulls, specific wave channel features, additional buoyancy modules to enable better trim, etc.), then the definition of new geometry components – or elemental shapes – can take considerable numerical effort to set up, verify, and debug. There are also numerical model capability limitations. For instance, curved surfaces are not currently implementable numerically – tubular hulls are approximated as an octagonal cross-section. Such shape numerical misrepresentations will not be without error, though this is not explicitly evaluated here.

Switching over to physical modelling, the most significant time expenditure occurs during the design, and even more so the manufacture/delivery time, of custom or longer lead time parts (such as the motor, drive, and cables) to arrive. Once these arrive, the build and testing process can happen relatively quickly. The whole testing program for BST-folding lasted around 20 days[79], while the design, procurement, manufacture, and assembly process occurred over a couple of months, and up to 6 additional months were spent on the design, assembly, and characterisation of the bespoke PTO model nacelle.

A significant number of tests can be carried out in a few weeks, which one would likely need for both numerical model geometry changes and test runs, at least in the time-domain. In order to reduce time further, it is essential to: (a) make the model as modular as possible; (b) ensure the underlying design includes a robust 'frame' to provide stiffness and load bearing capabilities. These can then enable an efficient use of 3D printed parts that can quickly add even complex geometry features but are not suited to withstanding significant loads. In the case of BST-folding, the nacelle is an example of a modular component, while carbon fibre side flanges provide strength and stiffness.

One can also pick up on a theme introduced in Chapter 3 (Section 3.1) around the scope of physical model testing (PMT) – physical testing's contribution of *insights* or, from a more practical perspective, 'surprises' arising from PMT. These point to the importance of tighter integration as part of the overall design process, avoiding exclusive or over-reliance on numerical models. Some such 'surprises' or insights are offered here (not necessarily from the specific BST-baseline and BST-folding campaigns):

- Comparison of average (measured versus predicted) power in unidirectional irregular waves, shows that under-predictions occur across the occurrence matrix – the most significant of which at low Hs and long Te combinations.

[79] It could be shortened further with a more optimal test methodology; the scope of this test programme involved identifying a better methodology as well as testing the model itself.

- The above is also visible via the CW plot. Depending on the steepness value, there is a mid-steepness at which the device seems to behave most linearly and the experimental and numerical curves align well. At steepness values below this, the CW drops off. At steepness values above this, it begins to shed loads via wave overtopping. This latter behaviour is intended but the former is not.
- The numerical model seems to suggest suboptimal PTO damping (D_{pto}); both when SD and TD based, with TD yielding even higher D_{pto} values. This is the case for BST-folding, and has been confirmed in other physical testing that Mocean undertook later in, at approximately double the Froude scale, using the same type of PTO, but where PTO seal friction was only about 2% of the specified torque limit. Thus, this effect seems to be unrelated to the relative effects of PTO friction.
- From numerical plots, there is initially a sharp rise in power with increasing D_{pto}, then from the optimal[80] value onwards the rise is of the order of 10% as D_{pto} goes up by an order of magnitude.
- Experimentally, D_{pto} optimal is chosen based on varying PTO gain across a finite selection of regular seas. However, ordinarily the D_{pto} is optimised for AEP, as opposed to power in a selection of regular seas.
- Besides friction in the physical model, it also does not seem to be the case that the TD model over-predicts D_{pto} because of the torque limit not being hit during physical tests (i.e. impact of torque limit increases optimal D_{pto} value predicted). In fact, the TD model over-predicts D_{pto} even when numerically simulating regular waves only. However, since the difference in power prediction is only ~10% (relatively small) for large increases in D_{pto}, it is possible that slight inaccuracies in the numerical model can cause the optimal D_{pto} value identified to be incorrect by 2 or 3 times quite easily.

[80] 'optimal' refers to best value for money – i.e. the point at which raising the torque limit gives diminishing returns in additional power for the additional required cost to implement such torque.

There is also an issue around Morison damping coefficient (Cd) – Cd is currently implemented as a constant, but should ideally vary across sea states. It is found from numerical simulations run by Mocean with a different model geometry that adjusting Cd does not significantly bridge the gap between predicted and measured average power discrepancies.

Another aspect is the fictitious damping plate method (refer to Chapter 4) – including this source of damping lowers the power in steeper, more energetic waves. It would likely yield better agreement at the higher end of Hs but that is where agreement is relatively good already, i.e. this would likely not improve the discrepancy at longer, lower waves.

From a cost perspective, too, numerical modelling does not always trump physical testing. For example, when analysing the budget for NWEC Stage 3 of the WES programme, physical modelling costs (which included use of a relatively expensive tank, FloWave) were about 60% of numerical modelling costs. This is of course also subject to the relative scope of each tool. Much more of the design space was explored numerically, with physical modelling serving predominantly for validation and for survival testing purposes. Further discussion of physical model cost variation with scale is given in Section 9.2.1.3.

Some key benefits of PMT integration have been highlighted, but these do not come without challenges in the integration effort. Above all, it is tough for physical modelling to keep up with numerical model optimisations, also due to ever increasing numerical model capabilities, as well as inputs and constraints. For instance, even with the TD optimisation, multiple optimisation runs can be performed in the same week, yielding different designs. This can be overcome with modularity and with quicker data post processing (see Section 9.5).

Generally, in advancing along the development phases, both the numerical and the physical model should get more complex and reach a greater degree of certainty/confidence. It is difficult to do this for one without the other. In addition, Mocean’s philosophy and design process is very much based on - and advocates – a highly integrated loop of numerical, physical, and engineering steps as part of WEC optimisation.

9.2.1 Relative merits of small-scale

When it comes to streamlining development, particularly the inclusion of physical model testing in the design iteration loop (as is the case for Mocean – see Chapter 5), moving to smaller scales of physical models can be a significant enabler. More specifically, one can ask: "what is useful to Mocean as outcomes of small-scale physical tests?"

Drawing from Chapters 6-8, several useful outcomes emerge:

- Relevant degree of freedom (DoF) RAOs predicted by the numerical model can be validated, and can be used to begin tuning an overall Morison damping coefficient.
- Inclusion of a model PTO can be used to obtain more realistic hydrodynamic responses based on a greater number of energy conversion chain elements, validate preliminary power capture estimations, and more so the optimal D_{pto} value.
    - We can be relatively confident in the empirically obtained optimal value, even though it appears approximately half that predicted by the FD model. Since the PTO behaviour in the numerical model is only characterised by a damping coefficient and a torque limit, the WEC 'prefers' a D_{pto} value towards the top of the range. However, in practice, lower PTO damping values are required due to the lower PTO efficiencies at lower hinge speeds. This means that predicted D_{pto} values do not Froude scale well, as also observed in previous and subsequent Mocean testing campaigns. In addition, findings from a recent testing campaign at larger scale once more yielded an empirical optimal D_{pto} about 4 times lower than the numerically predicted value.
- The running of wide irregular wave sweeps allows observation of dynamic behaviour that is useful in, for example, informing mooring fatigue loads.
- Comparisons of different device configurations that incorporate unique (likely nonlinear) geometry elements, such as the moon-pool for BST-folding, can be made efficiently.

    - BST-folding's moon-pool (gap) may introduce non-linearities and un-modelled hydrodynamic behaviour that are not apparent from the numerical model. The testing carried out enabled an efficient comparison to a configuration without hull gap.
    - These types of geometry re-configurations are common in early development stages, or in a development approach where a developer tries to freeze the geometry and various subsystems as late on as possible in order to exploit the best available technology that may be emerging (see Section 9.2.1.1).
- Extreme tests to further inform mooring and survival characteristics, as per the research undertaken in (Tosdevin *et al.*, 2021) with a passive version of BST-folding at the COAST Lab facility in Plymouth – see Appendix I for relevant figures. This is the traditional use of smaller scale models (i.e. to test extreme wave responses) but no a priori barrier exists to expanding their use more broadly.
- Costs can be significantly reduced (see Figure 172).

9.2.1.1 Reacting to available technology

From the point of view of the full-size WEC product, one benefit of scaling up gradually is that a developer can incorporate the most promising technology for, say, the PTO, as it also develops in maturity – especially if this is a fundamentally enabling aspect in terms of achieving the required performance/cost level (as is the case for the VHM[81] generator that Mocean is concurrently developing). Both VHM and C-GEN generators, the latter being already used in Blue X, cannot easily be scaled up to a utility-machine in one leap given their relatively low present TRL. It is therefore preferable to keep WEC design as open as possible until suitable enabling technology can be included. The prime mover structure can be scaled relatively easily, but this is not necessarily the case for other key subsystems.

[81] A hybrid of permanent magnet and variable reluctance machines, with unique benefits in converting reciprocating high-torque low-speed motion, and with inherent over-voltage protection and gearing.

From the point of view of a reduced scale model, a smaller, modular, yet still capable model, enables a developer to react to such design updates more efficiently and effectively. This is not least due to expanded sea state coverage from a given tank, as will be touched on in the following section.

9.2.1.2 Tank related aspects

Beyond the model related aspects, working at smaller scale also allows Mocean to exploit its proximity and access to the Curved Tank (CT) in several ways. Figure 170 shows that FloWave can comfortably cover all energy producing seas of interest – i.e. the larger bubbles in the plot corresponding to BST-folding energy matrix entries for a CNS location, Froude-scaled to 1:20. However, the CT is also able to cover a reasonable proportion of high energy yielding seas up to around 0.1m Hs and 1.5s Tp, equivalent to 2m Hs and 6.7s Tp full-scale. This is enough to enable validation of the device under relatively benign operating conditions that cover approximately 43%-54% of a typical year's occurrence[82]. However, some limits remain; for example, in irregular long- and short-crested seas the torque limit was hardly ever reached, so device behaviour around this could not be explored. The Ir0 method fictitiously reproduces more aggressive seas, partly circumventing this issue.

Note that the 'irreg' curves are obtained by multiplying regular wave height (H) by 0.725 to obtain Hs. This is the rule of thumb employed by FloWave staff based on accumulated experience running the tank, and was applied to the empirically obtained 'CT, reg' curve for comparative purposes. The energy capture bubbles represent energy matrix entries scaled to 20th Froude scale, and are based on the BST-folding power matrix combined with a Central North Sea (CNS) wave climate, for which the WEC was numerically optimised.

[82] Obtained from the occurrence matrix (Figure 171): 3796/8760 hours/year ratio (irreg); 4757/8760 hours/year ratio (reg).

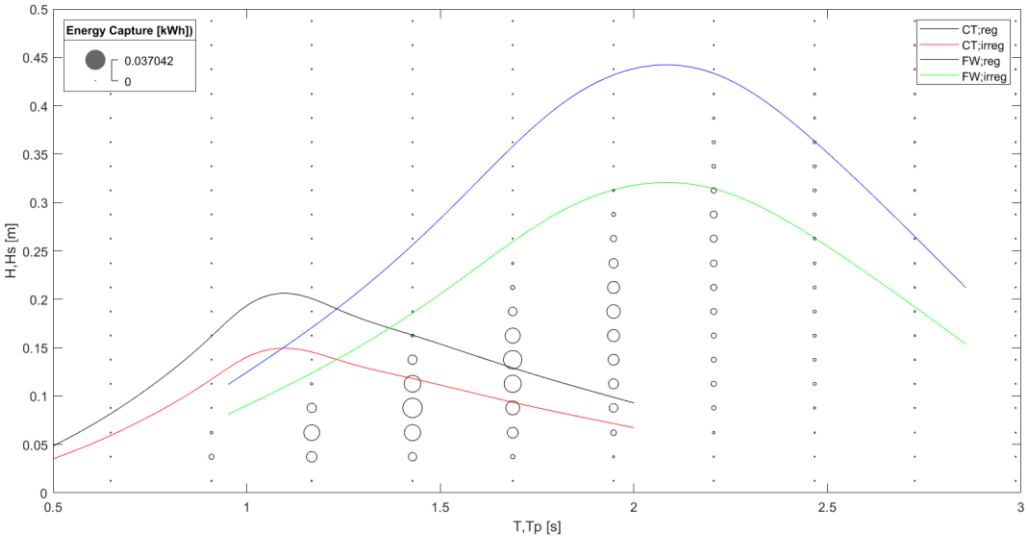

Figure 170 - Scaled energy matrix for BST-folding at CNS location, with Curved Tank (CT) and FloWave (FW) tank envelopes.

It should also be noted that the CT is 1.25m deep while FloWave is 2m deep; translating to 25m and 40m respectively at full scale. This means that in the CT some of the longer waves are verging on the threshold of intermediate depth waves, as opposed to deep water waves. This is not a significant issue, though it becomes more so when testing specific mooring designs optimised for deep water. In this case, a depth-agnostic mooring design was utilised to enable validation. Figure 171 shows that for a CNS climate, which is more benign than e.g. EMEC, the CT gives satisfactory levels of coverage, while FloWave comfortably covers all seas encountered.

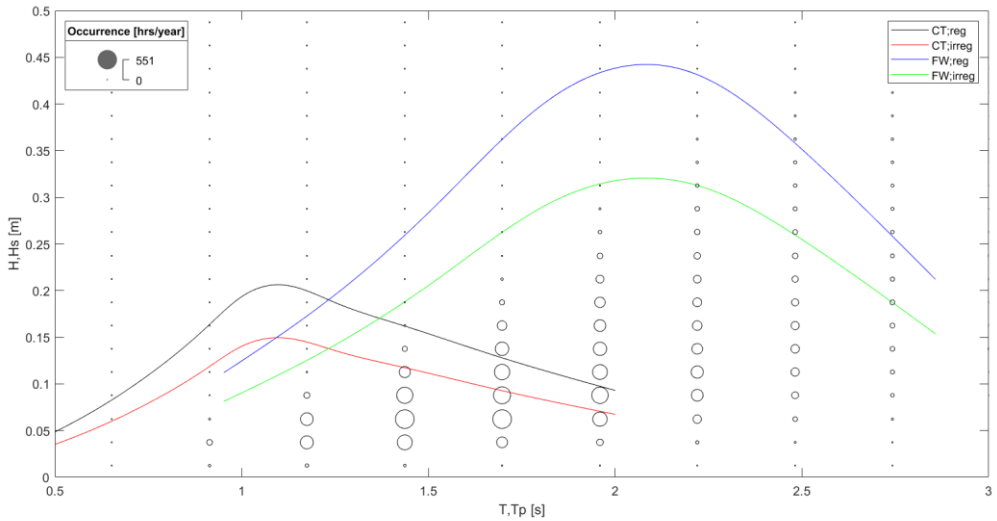

Figure 171 – Scaled occurrence matrix for CNS location, with Curved Tank (CT) and FloWave (FW) envelopes.

9.2.1.3 Model costs

Two observations arise from plotting the CAPEX of a 20th scale (Blue Star), a 10th scale (NWEC2), and a full-scale (Blue X) physical model/prototype:

1. Overall CAPEX rises approximately exponentially as scale increases;
2. The ratio of PTO to prime mover structure costs drops as scale increases.

The CAPEX rises by a factor of ~4 from 20th to 10th scale, and by a factor of ~40 from 10th scale to full scale.

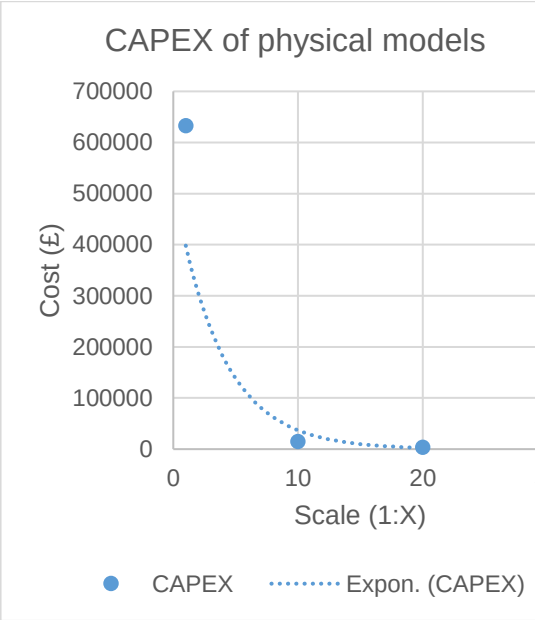

Figure 172 - CAPEX at different scales.

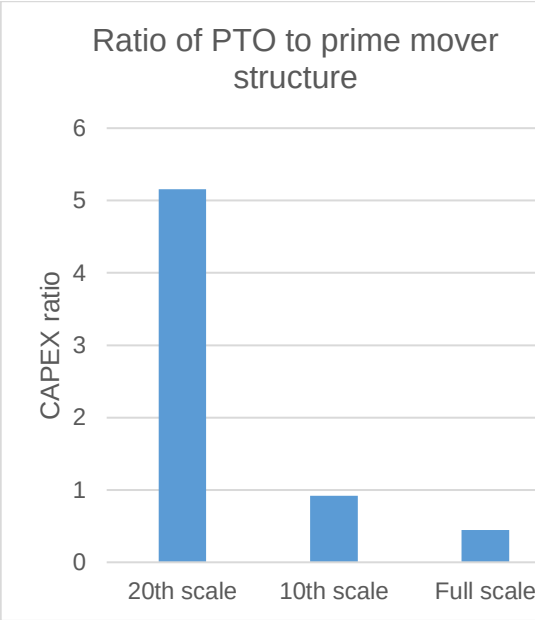

Figure 173 - CAPEX ratio at different scales

NB: the equation describing the curve in Figure 172 is *y=518465e^(-0.264x).*

Note that costs are just based on materials – fabrication – and on motor, with its drive and controller. The above cost data does not include mooring costs, development costs or operational costs. For a fairer comparison, certain costs for the 20th scale and 10th scale models have also been excluded, such as the cost of a large load cell used as part of one of the 10th scale model hulls, the costs of Qualisys (sensors and equipment), the cost of sensors other than the motor controller for the PTO. Most notably, this means that neither the costs of Qualisys (sensors and equipment), nor of a large load cell present as part of the 10th scale model have been included. VAT, on the other hand, is included in all costs. Figure 172 is somewhat in agreement with a piece of advice received

directly from S. Salter in 2020: “Model cost and time goes up by far more than the cube of scale. The only problem with sensible scales is getting the confidence of investors."[83]

In absolute terms, it is the tank running and operating costs that dominate overall physical modelling campaign expenditure. The CT is roughly an order of magnitude cheaper to run than FloWave, if the user is able to run the tank for themselves, which is a possibility. When comparing a like-for-like scenario, including support staff, the CT is still about four times cheaper than FloWave.

9.2.2 Addressing numerical modelling limitations

The most significant numerical limitation is unsatisfactory accounting of nonlinear effects. The WEC is much more nonlinear than even the nonlinear time-domain models show. For example, there is a strong ‘tail off’ in power capture in high waves, and there is also a threshold below which it is not very efficient in small waves.

An additional issue encountered with numerical modelling has been that, once the numerical code gets to a certain degree of complexity, it has at times proved difficult to be confident that no more ‘bugs’ exist within it. This can be illustrated via a few examples:

- Ahead of BST-baseline tests (as highlighted in Chapter 6), the numerical model displayed significant differences in energy capture performance for a version of the WEC with a central fin splitting each wave channel, and a version without fin. In this case, it was relatively straightforward to suspect a bug to be the cause, given the stark difference of >30% predicted AEP, but there may be more nebulous instances.
- Another specific numerical issue concerned the static stability of the WEC at low submergence values (i.e. device sitting ‘high’ in the water), which therefore constrained the limit of the hinge location vertically below the mean water line. In running the optimisation, the water line position had

[83] Based on personal correspondence – reproduced with permission from S. Salter.

to be restricted to no lower than 0.5m below the hinge to temporarily fix the issue. Checks were needed for static stability to ensure no coding errors or bugs were present. In such cases, it can be beneficial to be able to run some sensitivity studies with a physical model as well as – or instead of – exclusively relying on the numerical model.

Just as a physical model can be hampered by measuring inaccuracies and uncertainties, so can a numerical one. For the sake of increasing confidence, physical model validation is always recommended.

9.2.3 Mitigating physical modelling limitations

The main limitation encountered has been the model PTO and the presence of large stiff cables for powering and controlling the motor used as brake. It has not been possible to fully evaluate the impact of each of these, not least because their effects are very challenging to isolate.

Numerical inclusion of static friction in the time-domain model, as run by Alfred Cotten, using the empirically measured value of friction (see Chapter 7), revealed ~20% peak power capture impacts in terms of predicted power RAOs at the tested PTO damping value. It suggested friction as a non-dominant effect in explaining the significant discrepancies in measured power capture, even in smaller heights and longer periods.

Similar discrepancy trends, though of lesser overall impact, were found in a separate physical testing campaign run by Mocean. The above combine to suggest additional underlying causes for discrepancy that are likely linked to additional velocity related over-predictions. Inclusion of a torque sensor in the model would be highly beneficial, in confirming the effects of friction that were extrapolated from dry bench tests. In the present research with BST-folding, static friction was measured as ~10% of torque limit, so a numerical torque correction will account for more of the error, but is still unlikely to account for the total (large) power differences between measured and predicted observed in Chapter 8. Besides the loss in applied torque, the effects of friction on hinge angular velocity are particularly important to measure, since these have an effect on both power output, and are also used as inputs to generator (.g. VHM) design and development. Thus, hinge velocity validation is particularly key.

The issue of friction is not unique to Mocean. At the 2022 WES Annual Conference, a representative from the wave energy company AWS Energy pointed out that significant unknowns remained following the tank testing programmes and leading into at-sea prototype tests, as part of the final stage of NWEC. The major one being the rolling seal between the two heaving buoy halves. The question of its scaling was pointed out as particularly important in terms of friction and fatigue life.

In terms of mitigating the effect of power and feedback cables, it may be preferable to route these above the nacelle instead of below the waterline. Hog angles tends to be greater than sag angles, so impact on restricting max flex during survival testing is likely avoidable. However, it will still be challenging to avoid their inertial effect on model behaviour due to their mass and especially stiffness.

Another limitation in the recent past was the porosity and water uptake of 3D printed components. However, ABS material is now being fused as it is printed, which makes it is non-porous and almost completely avoids water ingress. If this was not the case, one would need to coat and/or seal all 3D printed parts, which adds mass, cost, and time to the overall process. A practical recommendation is to soak all 3D printed parts ahead of assembly, to reach water uptake saturation and limit mass (and thus trimming) variability during tank tests.

Finally, results have highlighted the high complexity of validation, which will require closer collaboration between physical and numerical efforts. Examples of avenues that may be further exploited include: decay tests to try to validate natural frequencies; and driving the hinge in still water while measuring generated waves in order to derive some viscous drag coefficients more accurately (see Section 9.5).

Having been fortunate enough to interact directly with Stephen Salter during this EngD and in the run-up to testing campaigns, an illuminating extract from a particular email exchange is reported here with his permission:

> *"I started wave energy work in almost complete ignorance but was fortunate enough to meet Michael Longuet-Higgins almost at once because his brother was in Artificial Intelligence as I was. He told me*

> *that our 100 mm diameter 300 mm wide models would be fine. Everything else he told me about waves was exactly correct. You just have to be careful about air compressibility for oscillating water columns. Making an accurate power conversion dynamometer with low friction is the key to success. Choose the scale which is convenient for that even if you have to use watch-maker skills and let this decision drive the other dimensions. Model cost and time goes up by far more than the cube of scale. The only problem with sensible scales is getting the confidence of investors."*

9.2.3.1 Uncertainty

An attempt has been made to identify major sources of uncertainty, as listed in Chapter 8. Some of these have been evaluated, while others are difficult to disinter. An idea of their relative significance can nonetheless be formed.

A likely major uncertainty would be due to discrepancies between incident and demanded seas due to tank reflections and wavemaker calibration. Calibration of regular seas and Ir0 seas, as advised by (Davey *et al.*, 2021), was undertaken. Reflection coefficients are summarised in Appendix J and L. However, there is also a potential discrepancy introduced by the presence of the model itself. In regular waves, amplitudes are calibrated when the tank is empty. The presence of the model appears to affect reflection coefficient (R_{coeff}) measured incident amplitude at peak response frequency of f=1.038Hz, by 0.1mm in both cases. The reflection coefficient change is +0.5% for RR04 and -2.0% for RR20. This suggests that the assumption of the model as ‘small’ in terms of its influence on wave conditions is indeed satisfactory.

The above percentage differences are slightly greater than the repeatability error found across empty basin repeats with RR04 and RR14 seas (3 repeats each). For RR04, R_{coeff} variation of -0.1% to +0.2%; for RR14, R_{coeff} variation of -0.0% to +0.1%. Not accounting for tank reflections would have caused the largest error in flex RAOs to be -11% for a 1/50 wave steepness sweep, and -17% for 1/100 steepness sweep. From a measurement error point of view, wave gauge percentage calibration errors had mean values of 1.1% to 1.25%, with standard deviation ranges of +/-0.6%. These can therefore also be considered negligible.

Potential uncertainties introduced by utilising a non-modelled slack mooring as a ‘quick and easy’ option versus a taut mooring with known spring stiffness, has also been evaluated. Negligible power difference at peak RAO response were

found (f=1.038Hz); but disparity increases as one moves to longer periods. For steepness 1/100, and PTO damping gain=40, at f=0.9063Hz disparity is 15% lower power with taut mooring, and at f=0.6250Hz, disparity is greater than 50%. Whether slack or taut mooring setups are utilised to select the optimal PTO damping gain value appears to be largely inconsequential, since the trends within each sweep are similar, suggesting an optimal gain of 40.

Trimming errors throughout the campaign were kept within a few millimetres of the target, and found to have minimal impact on power absorption estimated via numerical sensitivities. Discrepancies between the as-built mass and the target mass matrix can be taken into account numerically for validation, but not in terms of extrapolation to larger scale (especially full-scale) where equivalent mass matrix may differ considerably due to practical constraints. This can only be determined with full-scale data.

9.3 Impact of Wave Energy Paradox approach

In the Novel Wave Energy Converter (NWEC) pre-commercial procurement stream, Wave Energy Scotland (WES) has run what is widely recognised as a successful development programme, also evidenced by its replication at European level in the form of EuropeWave[84]. From a developer's commercial perspective, a crucial enabler is the significant financial support towards building a large-scale prototype and the inclusion of open water trials as part of the final funded phase. However, despite acknowledging LCOE scoring limitations, the WES methodology still includes LCOE as part of its stage-gated assessment in order to gauge commercial potential as part of the competitive funnelling process. The underlying assumption is that if LCOE drops enough (the current administrative strike price for Contracts for Difference (CfD)[85] allocation in the

[84] https://www.europewave.eu/

[85] Contracts for Difference (CfD): a support scheme to support low-carbon energy generation where the government guarantees a revenue for the developer, in the form of a flat payment of the different between a set strike price and the average price for electricity in the GB market. Administrative Strike Prices (ASPs) are the maximum strike price (£/MWh) for a project deploying a particular technology. CfD auctions are to be held annually as of 2023. The ASP of £258/MWh for wave energy projects is set assuming a delivery year of the project in 2025/26 and 2026/27; the ASP may drop after that on the assumption of cost reductions with increasing maturity.

UK is £258/MWh (BEIS, 2021)), then investors will gravitate towards such companies and the technologies will be taken up and deployed. In reality, considerable risk remains at the end of the programme in terms of achieving commercial status and gaining investor confidence. Relatively little deployment experience has been accumulated by the end of the programme (with what is in theory a half-scale prototype). In a sense, more time in the water is more of a confidence boost to investors than a lower *projected/estimated* LCOE.

Thus, a question that doesn't seem misplaced would be: is it more reasonable to try to lower LCOE by 10% with limited at-sea experience, or in accumulating a higher certainty of its value (even if it is actually 10% higher), but having an extra 6 months or 1 year of reliable deployment experience? The argument for the latter becomes stronger when considering that climate change demands rapid progress, as do investors. In particular, one of the first questions typically asked by investors is: what TRL is the technology at? Perhaps it is best to deploy sooner and iterate based on learning that has been accumulated. In discussing LCOE certainty and LCOE weight in decision-making, it would seem beneficial to calculate and report LCOE data as ranges with associated confidence intervals. This in order to: (i) more accurately represent the metric itself as an estimate that contains approximations and a degree of educated guess work; (ii) help decision-makers to appreciate the former, thereby introducing more nuance in the ranking or selection of the 'worthiest' technologies to support, whether with policy or investment.

Conversations with other investors have highlighted a desired emphasis for "more time in the water", again pointing to value of clocked days and months at-sea as opposed to additional performance gains (pointing to TRL ahead of TPL – see Chapter 2). This leads to practical observations that add to Weber's "performance ahead of readiness" approach. There will be a point in the development trajectory when further R&D efforts (e.g. optimisations) gives diminishing TPL returns, at which point a switch to TRL focus is recommended – i.e. the performance is good enough. If – and it is a significant 'if' – this point is recognised, deployment should be prioritised to continue to learn and attract investment, leaving finer refinement for latter stages or device embodiments. It leaves the central crux of the problem: how does one know when performance is

good enough? For off-grid markets, this can be disinterred by speaking with potential customers and by collecting application scenarios and running feasibility studies of power provision for them based on particular site locations, power demands and duty cycles. For grid-connected markets, once can consider utility electricity prices and e.g. CfD strike prices in the UK.

There is little doubt that WES has had a significant positive impact on Mocean's technology development as well as the development of wave energy more generally via its "technology push"-type programme. It is also noted, however, that Phases 3 of the various programme streams end at a pre-commercial IEA Stage 3 development (i.e. TRL 6). From then on, a developer is expected to be in the position to attract sufficient investment to progress through the following Stages 4 and 5: commercial-scale single device and array demonstration stages. The transitions from Stage 3 to 4 and from Stage 4 to 5 cannot be taken for granted, and both remain key areas of challenge and debate in the industry.

A rigorous stage-gated development programme includes the due diligence that WES has carried out, which can act as a 'stamp of approval' and inspire greater investor confidence. However, the activities and efforts required to move from a 'device' to a 'product' have fundamentally remained in the hands of developers, and form the key piece of the path towards commerciability (e.g. stakeholder engagement). Mocean has found its own market for commerciability purposes. Shortcutting this process with a smaller off-grid device like Blue Star has undoubtedly helped Mocean to approach commercial status.

In relation to metrics alignment and the *Wave Energy Paradox*:

- One way to improve alignment between stakeholders would be to involve more potential customers as project partners during the WEC development process, for example during WES and EuropeWave style program stages. For EuropeWave's second phase, Mocean has proposed the formation of an industrial advisory panel to advise and feed in to program from a potential customer and stakeholder point of view, to gather inputs to steer the program but also expose panel members to the technology development itself.

- Linking to Section 9.1, a crucial benefit of a *Wave Energy Paradox* approach that accelerates build and deployment, is that it can put the developer in the position to address and obtain data (if not numbers) to the other parameter *-ities* evaluation areas as soon as possible and at lower cost with a smaller machine. The learning can then be applied when scaling up, as is being found via Mocean's current Blue Horizon 250 WEC development (EuropeWave, no date).
- It follows that the TRL-TPL matrix introduced in Chapter 2 and applied in Chapter 5 can be used for individual WEC iterations but also, crucially, for a product range roadmap such as Mocean's that includes several different WECs (currently Blue Star 10, Blue Star 20, and Blue Horizon 250) – i.e. each later WEC builds on the learning from the previous, and intermediate returns are expected in each loop.

9.3.1 Streamlining design and tracking progress

The central thread to the proposed overcoming of the *Wave Energy Paradox* is the ability to accelerate learning. Undeniably, it is important to capture learning as much as it is to create new knowledge and understanding. This is key to avoid work repetition and to make sure insights are retained and applied as development progresses. However, the development process can be messy, and prone to ad-hoc shortcuts given time and budget limitations. A geometry tracking framework (Figure 174) has been proposed by the author during the course of this research, in order to assist Mocean with its learning capture. This is an attempt to close the loop on the *wave energy paradox* by helping to streamline learning by making it more structured and ideally more efficient, and has been taken up by the company.

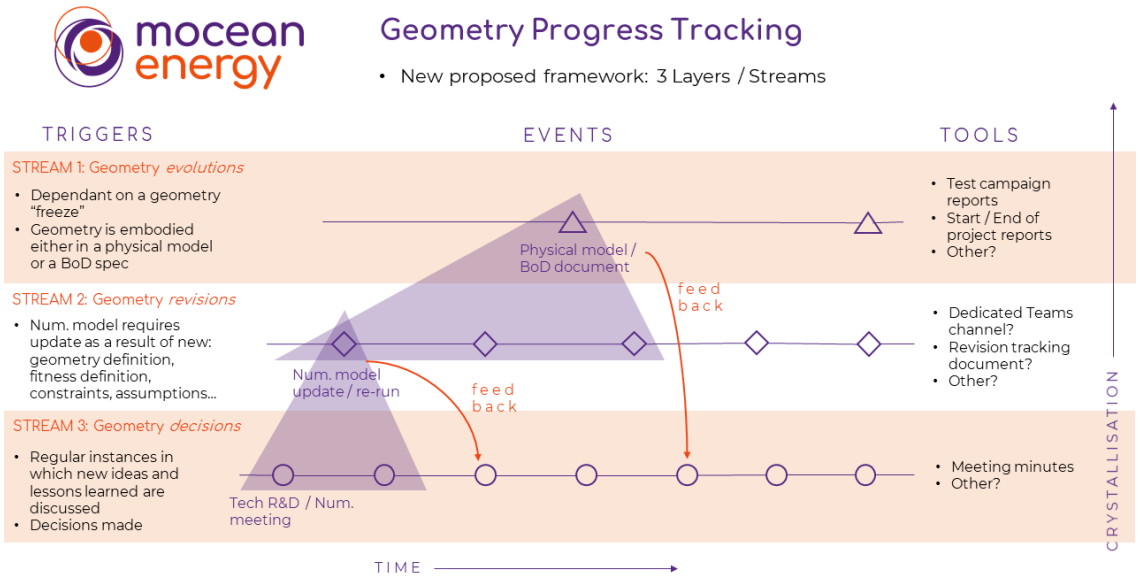

Figure 174 - Proposed geometry tracking framework – produced and presented to Mocean by author.

Observing Figure 174, *triggers* make *events* occur; *tools* capture the ***events'*** outputs. Information travels up and down but with varying frequency for each stream. This framework can be applied to any of the Mocean WECs, or indeed any other WECs being optimised.

Triggers include geometry *decisions*, *revisions* and *evolutions*:

- *Decisions* – instances when optimisation outputs are reviewed and decisions are made in terms of input parameter changes to be made informed by requirements and/or engineering considerations; these are more frequent than revisions and evolutions.
- *Revisions* – instances when geometry is updated as a result of an optimisation, see Figure 175; these are more frequent than evolutions.
- *Evolutions* – instances when a geometry is 'frozen', leading to a physical model being built or basis of design (BoD) being drawn up; these are less frequent than the above and may correspond to a stage-gate assessment in a structured development programme, such as during WES or EuropeWave PCPs.

Geometry evolutions from the WES NWEC programme were shown in Chapter 4. A subset of revisions for the Blue Star WEC is shown in Figure 175.

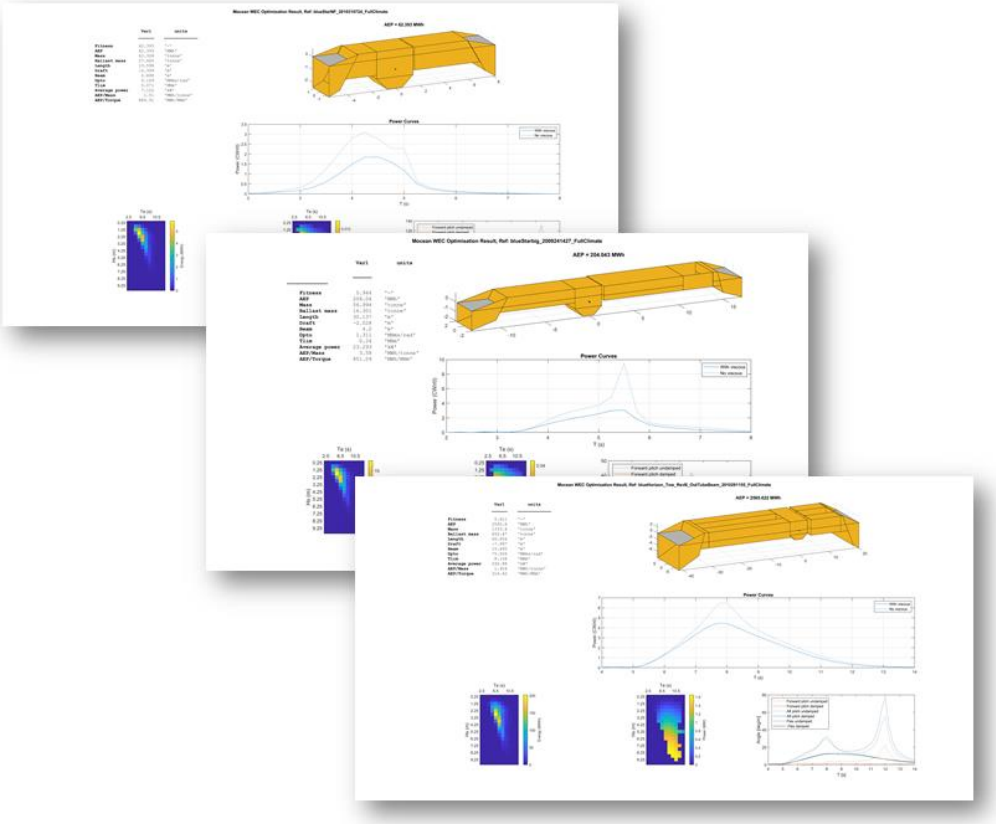

Figure 175 - A subset of the revisions of the Blue Star WEC.

Physical modelling needs to keep up with evolutions but ideally also with revisions. BST-baseline and BST-folding are examples of geometry revisions. Some of the numerical optimisation summary output for different revisions of BST-folding are shown in Figure 175 for illustrative purposes.

9.3.2 The Blue Star WEC

Currently, the Blue Star WEC is showing promise and gaining market traction. As stakeholder engagement progressed, a relaxation of mass and length requirements occurred, alongside an increase in power. This led to further revisions and a different geometry evolution that has now passed a FEED stage of development. This does not include an aft hull gap, but does include solar panels on the top hull surfaces, and a Vernier Hybrid Machine based PTO system different to Blue X's. These development steps, outside the scope of this thesis but building on development work that included the physical testing herein, have led to a machine that delivers roughly twice the power for the same size (20 kW rating) to Blue X. The Blue X prototype, meanwhile, has been

rebranded as *Blue Star 10*, successfully transitioning it to a product. The latter shows that the approach of scaling is valid and that, what was originally intended to be a half-scale version of the M100 WEC (100kW nominal rating) is showing promise as a 10 kW WEC product, and that no fundamental barriers exist to scaling the technology up or down and still having a commercially viable WEC.

The idea of a folding geometry for Blue Star has been developed during this thesis and has been shown to be viable – retaining self-referencing, nose diving, and broad bandwidth characteristics. It remains an option for extending the capture bandwidth without limiting transportability; it may well be utilized for future evolutions depending on market requirements. The ‘gap’ versus ‘no gap’ comparison has been particularly relevant, since more recent development work and stakeholder engagement is leading to the strict requirement on standard shipping container fit being abandoned or at least relaxed. This, in turn, relaxes the need for the gap and folding ability, although it could be useful in other transport and storage scenarios such as enabling the storage of redundant/spare WECs at nearest harbour, reducing quayside costs and facilitating handling.

Notably, as illustrated in Figure 166, the increase in length enables the capture of longer waves. As a rough rule of thumb, a standard raft with axisymmetric hulls and no wave channels has a peak power capture at wavelengths approximately equal to its total length. The overall aim is to widen the bandwidth, ensuring as much of the lower height, more frequently occurring waves can be captured (i.e. sensitive to short wavelengths) while being able to ‘hide’ from (or be insensitive to) extreme steep waves that give little energy contribution over the year (particularly in summer months) but introduce large loads. The ability to nose dive is a way to enable this load shedding.

The paradigm of “good enough” has been applied here via the verification of “enough power” being available, achieved from stakeholder inputs and feasibility studies for particular off-grid subsea infrastructure application scenarios. There is still some investigation to do in terms of other performance aspects, which will come about with further operational time at sea. The robust linking of HPQs to non-proxy reliability and survivability metrics remains to be undertaken once

sufficient full-scale data will be accrued. Power performance is also tied to subsea battery performance, which Mocean is not directly involved in and collaborates with an industry partner on, evidencing additional complexities.

It should be noted that other wave energy companies, most notably CorPower[86], have taken a different route to Mocean and aimed straight for utility scale WECs utilising a roadmap that relies on dedicated large scale accelerated dry testing facilities (e.g. to test for survival and reliability) instead of relying so much on operational time in the water. At this stage, it is difficult to say which approach will ultimately be more successful or whether indeed there is a single 'winner', though CorPower development seems to have yielded excellent techno-economic performance metrics, at least 'on paper'.

In Blue Star's wider development context, ongoing engagement with industry players (e.g. in the O&G industry) requiring power for off-grid applications has shown that the beachhead market/stepped roadmap message, of which Blue Star is the first nearer-term piece, is well received and a trajectory that makes immediate sense to them as stakeholders and potential customers (Garanovic, 2022). This reinforces how the "small-mid-grid" message should be one of providing solutions more broadly than just electrons. For example, addressing the challenges of decarbonisation, reducing vessel use and manned vessels in general, improving energy access, providing greater marine domain awareness, etc. as part of the value added as opposed to purely cost of energy. This approach is resonating with off-grid market stakeholders and an ever greater number of feasibility studies to assess power performance capabilities in different application scenarios is being submitted to Mocean. This has led – and will hopefully continue to lead – to FEED projects, investment, and joint demonstrator projects, as evidenced by the Renewables for Subsea Power (RSP) project (Garanovic, 2021a; Beckman, 2022; Offshore staff, 2022). RSP, carried out with several industry partners, will culminate in the at-sea demonstration of a fully integrated power and communications system that can provide continuous power and wireless communication links to operate subsea

[86] https://corpowerocean.com/

systems autonomously. The combined system includes: Blue Star 10 WEC; a subsea battery; an AUV with docking station; and an all-electric subsea XT (i.e. well head). The combined system is to be deployed in Orkney waters over winter/spring of 2022/23 for a period of up to 5 months, during which actuation, monitoring, and communications will be demonstrated using wave energy as the power source.

9.4 Test methods

Some overarching testing principles have been successfully followed in this work, such as maximising tank time by running repeats of wave runs at multiple gains, enabling interpolation of results. These have been used for both regular and Ir0 seas. However, one needs to be wary of effects that might invalidate interpolation. For example, below a certain wave steepness, RAO curves may show discrepancies due to higher relative effects of friction, while at the high steepness end the machine tends to dive through the waves and load shed, thus reducing RAO values due to wave overtopping. This suggests a potential ‘sweet spot’ in terms of matching numerical and experimental results, which has not been clearly identified yet. More specific aspects related to Ir0 and scaling are discussed below.

9.4.1 Application of the Ir0 method

As reviewed in Chapter 3 (Section 3.4.2), the motivation behind the Ir0 method is to more efficiently explore a design space via tank testing. More specifically, the method involves obtaining RAOs directly from a synthetically assembled polychromatic sea, of [Hs, Te] properties defined by the developer. For example, [Hs, Te] combinations that match high power potential or high occurrence seas for the location of interest. Ir0 seas should yield more realistic WEC behaviour than regular wave conditions, while also allowing greater resolution and greater energy spread across frequency components compared to typical spectrally defined irregular seas. One of the fundamental advantages should be to maximise frequency resolution while reducing overall testing time.

To assess the impact of Ir0 seas, general trends in comparing different device configurations based on regular wave or Ir0 sea data are discussed first. Relevant plots can be found in Chapter 8, Appendix L, and Appendix O.

To assess the taut versus slack moorings relationship, flex RAO is considered. Regular wave data shows taut response falls below slack; for Ir0, this is also the case.

To assess the ‘gap’ versus ‘no gap’ relationship, flex RAOs are again considered. Regular wave data shows that the ‘gap’ response is below ‘no gap’ around the peak period and then above it at longer periods. For Ir0, this is also the case when the PTO gain is off, while for a PTO gain of 40, ‘no gap’ is consistently below ‘gap’.

To assess the identification of the optimal PTO damping value, power RAOs are considered first. The same trend can be seen from Ir0 as regular waves for power RAOs, with curves for PTO gains 20 and 40 being relatively close. Then considering mean power, Ir0 seas suggest this is maximised by a PTO gain value of 40, as per data obtained from irregular wave sweeps.

Considering the effects of wavemaker gain (and thus wave steepness), flex RAOs at PTO gain 0 and 40 are considered. For regular waves, the 1/100 steepness curve is below the 1/50 around the peak period, but then rises above it at longer periods. On the other hand, Ir0 derived RAO with 1/100 steepness is consistently above the 1/150 steepness curve. For a PTO gain of 40, both regular and Ir0 derived trends are the same, with higher steepness waves causing consistently higher flex RAO responses.

Secondly, the impact of Ir0 tests on test time is discussed. Running a full 16 frequency component regular sea took 58 minutes, including 2 minutes of settling time between each run, and excluding repeats. On the other hand, each Ir0 run lasted approximately 5 minutes; thus, for 3 run repeats and a 4-minute settling time between each run totals 27 minutes. The additional resolution benefit is also notable, given that IROa seas were composed of 22 frequency components and IRObb and IROc of 25 components.

Compared to running irregular seas, the impact is less obvious because the mean power estimations from a long-crested irregular sea and an equivalent [Hs, Te] Ir0 sea are not necessarily comparable. However, it appears that Ir0 seas can usefully substitute regular and irregular seas in the determination of optimal D_{pto} values. They are preferable to regular seas since higher torques are achieved, giving greater confidence in the identified optimal gain. The optimal gain found is 40, as per regular sweeps and irregular sweeps.

Three different types of Ir0 seas were run, termed: *steepness*, *envelope*, and *energy* seas based on the different philosophy of their compositions. Overall, the recommended Ir0 type of sea is the *envelope* type (IROb) whose component amplitudes follow the tank envelope. This displayed less spilling than the *energy* type, with lower mean reflection coefficients compared to the *steepness* type.

The above elements confirm that Ir0 is highly attractive for comparison of different configurations, and is thus well suited to the idea of integrating physical modelling further into development process, particularly at early stages where multiple designs (e.g. geometries) may still be explored and the parameter space is generally broader. A trade-off exists between increasing the resolution and range of *Ir0* bins, with decreasing amplitude and longer test time. For the Curved Tank, 25 components appear to be the maximum.

An additional less expected potential benefit of Ir0 seas was also disinterred. Since each component in the Ir0 seas has an integer even number of waves in the repeat period, this can be exploited to further speed up tests by either: (a) reducing the time of each run to 32s, in order to still have integer number of runs for all frequency components; or (b), by keeping 256s repeat time and analyse this as one 32s run with 7 additional intra-run repeats (8 in total). Comparison with inter-run repeats shows comparable standard deviations of mean max flex angles measured, particularly at lower wavemaker gains.

In terms of reflections, maximum reflection coefficients across Ir0 sea components were generally higher than for regular waves, though mean values are actually very close. No notable reflection downside has emerged from Ir0 use. Repeatability of individual Ir0 seas is very high and satisfactory. Seed number variations were run to further extend the methodology proposed in

(Pascal *et al.*, 2021). Reflection coefficients were found to vary consistently across frequency components for each seed run. In terms of measured power with varying seeds, 4 different seed runs with an Ir0 sea (IRO21) yielded a mean power of 0.0532W and a standard deviation 0.0015W (2.8%), while 5 seed runs with an irregular long-crested (IRL23) sea yielded a mean power of 0.0351W and a standard deviation of 0.000529W (1.5%).

9.4.2 Experimental scaling investigation

This section re-proposes two Figures found in Chapter 8 to facilitate the discussion. This comparison is based on 20th and 40th scale model regular wave RAOs, amplitude sweeps, and natural frequency from decay tests.

Mocean's numerical model assumes that drag coefficients do not change with scale, though in practice the relative viscosity of water increases at smaller scales and is linked to viscous losses.

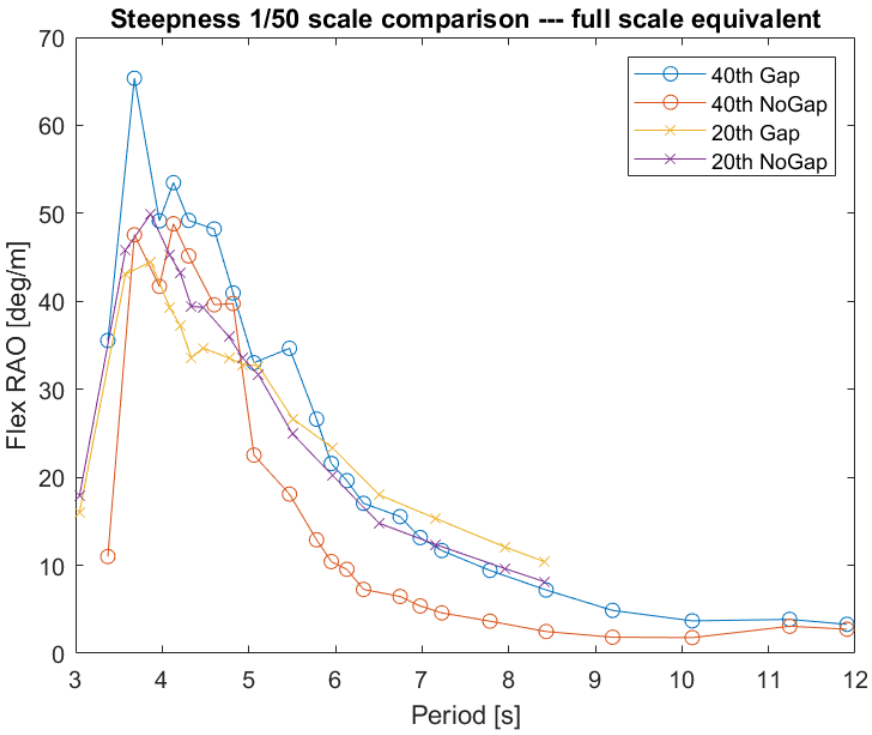

Figure 176 - Comparison of 40th scale and 20th scale Flex RAOs with different aft hull configurations.

In Figure 176, 40th scale results are obtained with a slack mooring, while 20th scale with a taut mooring. Nevertheless, the peak of the 20th scale RAO curve with the gap and slack mooring lies between the yellow and purple peaks shown

above, but with greater RAO values at periods above 5s. Results at both scales show that the presence of a gap raises the response at the longer periods and broadens the bandwidth.

If one considers the shift from ‘gap’ to ‘no gap’ to render the model behaviour more linear, one could infer that the effect of hydrodynamic scaling is not significant – though we bear in mind the mooring and hinge construction differences, including in the level of friction there.

Figure 177 shows RAO response variation depending on the steepness of incident waves. In other words, how does flex response vary as waves become less linear? The overall slopes are similar, showing broadly equivalent amounts of load shedding and other losses occurring.

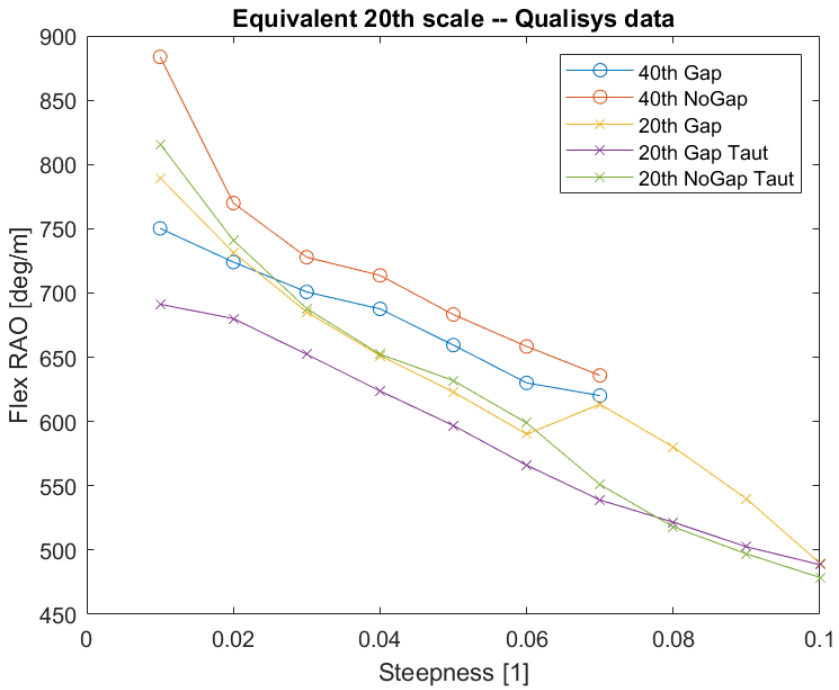

Figure 177 - Sensitivity of Flex RAO to wave steepness.

The above is by no means a guarantee – but an encouraging sign – that downscaling is reasonable in terms of capturing fundamental performance in ‘operational’ (relatively linear) waves. This may not be the case with steeper/extreme survival waves, though Figure 177 is promising in that sense also, at least in terms of hydrodynamic flex responses. In addition, natural periods in flex are almost identical at the two scales (refer to Chapter 8, Section

8.11.1), though differ a little more in surge, roll, and especially yaw. For slack moored configurations in flex, natural periods are 2.82s for 20th and 2.78s for 40th scale, both with the hull gap. Both show minor effects of gap being filled in, slightly increasing the natural response period in flex: 2.50 to 2.65s for 20th, 2.78 to 2.85s for 40th. This is positive news, though recall that DoFs cross-couple and there will be additional mixed DoF responses contributing to the overall response RAO.

Scaling effects on power and mooring loads may differ and have not been captured. As-built property differences and effects of cables will be affecting this data and are difficult to isolate and untangle from available data. Other scaling effects complicate the comparison, such as friction (which does not obey Froude scaling) and the waves. Care was taken to use relatively low steepness waves, to avoid nonlinearity effects and have higher quality waves too. Friction is fundamentally different in the models due to their different build and materials.

This initial scaling investigation attempt has shed light on the suggested approach within standards to pick the largest scale possible for physical testing, prompted by the fact that scaling effects are challenging to isolate and understand. Indeed, the exercise to try understand the best “value for money” scale of model is a highly complicated one, more so than initially anticipated by the author. However, it is also noted that for survival testing it is common practice to use a model half the scale of a performance model – the behaviour is likely to be even more nonlinear due to greater nonlinearity of the waves themselves. It seems sensible therefore that a scaling assessment should be included in the standards.

For an all-in-one model implementation, 20th scale is appropriate but would need to carry out such testing in a larger tank such as FloWave, not Curved Tank due to power matrix and extreme seas coverage, and limited depth – all of which limit performance and survival testing. Such a testing plan would only be possible in the CT if a 40th scale is used for power matrix coverage and even smaller for survival testing, though the focused wave CT envelope has not been explored.

Although well outside the scope of this testing campaign, it is also likely that what drives the structural loads at different scales is different. For a smaller device/model, loads are likely to be primarily driven by moorings and hinge forces. For a larger device, hydrodynamic pressure loads become more dominant in terms of affecting overall integrity of the structure. This ought to be considered if structural loading is included as part of the test program.

Finally, computational fluid dynamics (CFD) should be considered as a potential tool to evaluate scaling effects more accurately. As per (Palm *et al.*, 2018), Euler (scale independent) and RANS based CFD simulations can complement experimental scale tests in order to separate viscous drag influence from the induced drag.

9.5 Future work recommendations

This section spans recommendations arising from the present work to improve WEC performance, test methodology, and physical modelling integration.

Of primary interest is the link between metrics and physical testing, and the scope to expand measured performance criteria (Figure 159). As more full-scale data is accrued via Blue X deployments, one can try to link early-stage proxies to at-sea performance metrics. However, even without validated links between proxies and full-scale prototype absolute performance, identifying and agreeing on specific proxies for non power capture evaluation areas would be a significant step forwards. For example, a possible linear survivability metric could be the ‘Fwd hull stability’ as mentioned in Table 35; it has been observed from other tests that a trade-off exists between more stability and a higher AEP, requiring further exploration. There may be scope to include these in the numerical optimisation itself or post-process calculate them to screen geometries after optimising (some of these have been suggested in Section 9.1.1). It is likely that at early stages these would be hydrodynamically derived indicators, as these are the empirically measurable ones. Loading indicators would only be possible to integrate for the moorings via small load cells; it would be more difficult to measure loads on the small prime mover structure, also due to its lower likelihood of scaling appropriately (as discussed in Chapter 3).

9.5.1 Improving the physical modelling process

Improving the physical modelling process is primarily about making tests more representative, efficient and accurate.

Representability in this case concerns moorings and PTO. A PTO has been incorporated in the 20th scale model, though uncertainty is an open issue. For moorings, the difference in measured behaviour between slack and taut arrangements underlines its importance; not only in including a representative mooring system, but also one that can be reproduced numerically (cannot really do so with slack bungee lines). This ought to be included as early as possible in testing, given its impact on the overall conversion chain, but is an often overlooked part especially at earlier development stages. A 20th scale, a single-line-mooring was designed and built but the depth of the CT limited its application. Conversely, the poles-spring system proved very useful because it is depth agnostic and provides known stiffness properties suitable for validation. Besides the depth, and limited wave occurrence matrix coverage, no major barriers were identified in the use of a smaller facility like the Curved Tank for this scale of model. In assessing tank envelope, one should look at the energy matrix, as often the largest AEP contributions are not captured at the highest sea states. Reflections exist but can largely be accounted for. The other barrier was the tank not being well maintained, which slowed and complicated progress.

A more efficient test methodology would make further use of Ir0 seas. These can be used instead of regular waves to obtain RAOs, and also to sweep PTO damping gain values for identification of optimal damping coefficient. This would take longer than using a single regular wave, though technically this should be calculated for each combination of period and wave height present in the occurrence matrix. Ir0 seas would expose the model to more realistic seas including higher torques, which were missed during optimal PTO damping gain coefficient identification in the current testing campaign. Ir0 use as representative operational seas (as opposed to longer long- or short-crested irregular seas) to enable calculation of HPQs is promising, but requires further evidence accrual. Including decay tests in a given physical testing programme is also recommended given its value-for-time utility.

Setting up standard post-processing scripts would streamline the overall PMT process. This has been a major barrier to streamlining the whole process – doing it on the go would be incredibly valuable and enabling in terms of guiding the test programme. This is something standards could help with or focus on, for example. On the other hand, trimming via CAD method developed using two configurations (*Default* and *Buoyant*) of the same assembly in SolidWorks has proved highly effective and reproducible in practice.

Modularising as much of the model as possible would also aid iterative testing. Here the hinge with PTO has been modularised, being the longest lead-time item and the most expensive. Adding a temperature gauge within the nacelle itself would enable thermal monitoring and more confident thermal limit over-riding to temporarily achieve higher torque damping values with the same motor. Testing two different scale models at the same time, even passive versions, but with as similar hinge characteristics (i.e. build) as possible, is recommended to get an initial handle of scaling effects. These can be passive versions to isolate drag effects from PTO nonlinearity complications.

Improvements to accuracy and reducing uncertainty estimation is a significant effort, which has been partially explored in the present work. Friction has been assessed via dry testing pre-calibration of the active nacelle. Ideally, this should be re-measured at the end of the wet tests and ahead of future testing rounds in order to check for any variability. For example, in an active nacelle with similar construction but roughly twice the size of that used in the 20th model, static friction roughly four times after the nacelle had been unutilised for 2 years between one set of tests and another, though still remained about 4% of torque limit at full-scale. Seal friction may be reduced by utilising a flanged seal of PTFE material as opposed to a Viton lip seal[87]. Either way, torque should ideally be measured in situ, but lack of available space seriously constrained this. A relatively small, but costly (£659), custom thin-walled torque-gauge tube was used in (Wilkinson, 2018). This was included because the magnetic particle brake (used as model PTO of that particular testing campaign) response

[87] As advised by expert reviewers at Parker Plastics.

degrades over time and thus the torque response will vary for given current/voltage setting. Such a bespoke torque gauge ought to be investigated.

Model mass matrix properties (centre of gravity, centre of buoyancy, inertia moments, etc.) were extracted from CAD measurements – this is relatively common in literature, e.g. (Shahroozi, Göteman and Engström, 2021). To reduce associated uncertainties in practice one could use a bifilar pendulum method on each individual hull, or a quicker method utilising a dedicated vibrating platform as found in (Gabl *et al.*, 2021).

More generally, it is recommended to list all potential (at least major) sources of uncertainty and explicitly include targeted empirical sensitivities in the test programme to isolate and estimate their effects. Identifying consistent uncertainty metrics would enable Mocean to continue to accrue valuable data points to try to estimate where the optimal crossover lies between cost, uncertainty, and model scale.

9.5.2 Improving WEC performance

This can be summarised in three key areas[88] needed to design a novel WEC:

- Continue to understand the hydrodynamics of the device
    - Being aware of solutions that are contingent since based on limited modelling results – e.g. more detailed testing and understanding of wave channel behaviour, which can be relatively easily built and tested via 3D printing.
- Distinguish between *fundamental* and *practical* constraints, where fundamental constraints cannot be addressed and are inherent to the device, and practical constraints can be mitigated via design
    - Thus far, practical constraints such as risk of end-stop impacts and limited allowable flex angle have been overcome based on the new geometry.

[88] These were formulated by Dr. Matthew Folley in a presentation titled: *Challenges in the design of lift-based WECs*, during the 2022 joint MORELab-COER Wave Energy Workshop, held in Torino (Italy) on April 29th, 2022.

    - Continue to tackle the constraints that fall in the ‘practical’ category – e.g. width of wave channels is partly limited by the use of steel, which increases mass and risks increasing ballast requirements for trimming. This can set off a vicious cycle where moorings need to be made heavier to station-keep a heavier machine. Wave channel build from composite material should be explored for this purpose.
    - More sophisticated PTO control strategies could be explored, implementable with the currently available 20th scale motor and controller – thus far indication is that linear damping is optimal at shorter wave periods but can be improved for longer periods above 4s or so.
- Consider future technologies and try to remain open to them (as per generator technology discussed in Section 9.2.1.1)
    - Prospective inclusion of solar panels on the Blue Star WEC that leads to flatter top hull benefits, since more solar panels would be able to be fitted, yielding benefits to feeding hotel loads of the device but also aiding continuous available power performance by boosting power availability in lower wave resource periods (e.g. Norther hemisphere summers).
    - Battery technology will also be relevant in boosting efficiencies, reducing mass, and enabling greater continuous available power applications, but at a cost and not necessarily via sustainable materials – this is a quickly evolving space.

Finally, advancing performance is inherently linked to advancing learning. Thus, the question of how that learning is effectively and efficiently captured at each stage becomes very relevant. This can be implemented by implementing knowledge capture methodology suggested in Section 9.3.1.

Chapter 10. Conclusion

This chapter gives concluding remarks for the overall thesis, relating them back to the research questions outlined in Chapter 1. Findings are contextualised in relation to this EngD's goals – interlinked to Mocean Energy's objectives in terms of impact and implications – and extended to the wider wave energy sector wherever possible and relevant.

The present research has shown that there is indeed scope for accelerating testing and further optimising the physical modelling process. It has also supported Mocean's "small-mid-grid" approach internally - by linking metrics to physical modelling - and externally, by formalising messaging to investors and other stakeholders. The Blue Star WEC is on the cusp of commercialisation. Its prospective time at sea will enable further evidencing of the approach outlined in this work via the necessary and indispensable full-scale validation offshore.

10.1 Research recap

This research investigated the impact of small-scale, fast-turnaround, physical model testing in WEC technology development. In particular, the feasibility of accelerating and economising physical model testing in relation to Mocean's first off-grid WEC, *Blue Star*. The overarching goal is to maximise learning while minimising costs, time, and uncertainty. This process bears relevance to the metrics with which performance is defined, the ability to measure them experimentally, and the degree of confidence in their validation at reduced scale. Crucially, it also ties back to a developer's commercial roadmap that aims to unlock commercial returns and learning with smaller sized WECs before moving to larger grid-connected machines.

Examination of the reviewed literature provided little information regarding the identification of a minimum viable scale for physical model testing. In technical specifications and official guidelines, this is typically guided by TRL, but almost no guidance on scaling effects or uncertainty quantification is offered. In practice, this is important because working at smaller scale enables use of smaller tanks with significantly reduced costs. For example, use of the Curved Tank approximately halves costs of a testing campaign of equal duration

compared to the FloWave tank. It is also important because it allows more flexibility for developers in making design decisions that deviate more or less radically from previous device iterations, and that therefore are in greater need of validation to provide confidence that they perform as intended. The significant expense and time involved, as well as an inertial lean towards numerical models, can lead to a reluctance in conducting tests as often as would be desired during a development program.

In order to address this knowledge gap, two 1:20 Froude scale physical models of Mocean's off-grid WEC, *Blue Star*, have been designed, built, and tested as part of this research. This was done in the context of Mocean's wider design optimisation activities, embodying two successive geometry iterations of the WEC. Mocean uses an in-house code to programmatically generate geometries and simulate their hydrodynamic and power capture behaviour; this is wrapped inside an optimization routine to maximise particular metrics defined as a fitness function, typically AEP/cost, where cost is a combination of mass and torque. The process then relies on tank testing to validate the resulting geometry and PTO parameters, as carried out in this research. Novel test methods based on emerging literature were applied in order to accelerate the testing process.

10.2 Outcomes relating to the sector

In referring back to the research questions, and the impact of this research for the wider wave sector, the following findings are offered, broadly organised across: metrics (1), method (2), and uncertainty (3).

10.2.1 Metrics

a) No consensus exists on what techno-economic performance metrics should guide WEC design at early development stages. For Mocean, a blend of AEP/mass and AEP/torque is a reasonable means of capturing techno-economic performance. Emerging from this research is the need to ensure that chosen performance metrics can be validated experimentally, in order to boost internal and external stakeholder confidence and to enable continuous improvement of the WEC being

developed. Inclusion of a physical model PTO is key to enable a robust link between the numerical optimisation and experimental validation.

b) It has not been possible to validate AEP or the WEC's power matrix from measured mean power capture values here due to low precision and confidence (see later points in 10.2.2 and 10.2.3). However, additional power capture related metrics have been proposed, in the context of an off-grid WEC that relies on broad bandwidth in order to be deployable globally and capture enough energy during the lower resource months to satisfy continuously available power (CAP) driven requirements. These are based off CWR plots – widely adopted and non-dimensional – to infer other attractive power capture characteristics beyond AEP: e.g. bandwidth at a certain CWR threshold. This approach requires further exploration to identify what CWR threshold should be used; for example, by linking it to July month climate conditions, which represents the dominant underlying limit to CAP performance (at least in Northern Hemisphere and North Sea in particular).

c) Observing flex DoF RAOs is insufficient for enabling performance comparisons between device iterations, because of hinge property differences, but even more so because of incomplete power conversion stages being included. If flex RAOs are used for comparison, they should include PTO effects. Since the BST-baseline model does not include a PTO, comparison was made via numerically predicted CWR plots; BST-folding outperformed BST-baseline across these power indicators. An experimental comparison is possible between configurations of BST-folding with and without aft hull gaps. Results are very similar; the 'gap' version has broader bandwidth but slightly lower peak and overall area, and is thus likely preferable in a CAP driven scenario.

d) An attempt is made to propose metrics beyond just power capture, to address a greater number of the nine IEA evaluation areas that have been recently consolidated in the ocean energy sector. These are analogous to the Impact Factors or Hydrodynamic Performance Qualifiers (HPQs) utilised in US DoE Wave Energy Prize, providing mean-to-max indicators in seas of greatest interest; these act as proxies for e.g. reliability, controllability, and survivability. In comparing the 'gap'

vs ‘no gap’ configurations, BST-folding with the gap shows less favourable characteristics for power but better mooring load responses, and more even maximum angles between hog and flex. The comparison is presented in a polar char format, which visually mirrors the IEA evaluation framework.

e) Use of proxies, such as HPQs, is inevitable at early development stages, since no direct (validated) data exists yet to inform evaluation areas such as reliability, maintainability, survivability, etc., which ultimately contribute to LCOE (i.e. affordability). Such proxy indicators can vary depending on the type and application of a WEC. Identifying reasonable proxies is both important - to guide and track design progress - and necessary, since applications for funding programmes such as WES NWEC or EuropeWave require quantifiable ambitions and subsequent assessment to measure progress and impact within the IEA framework. Neither depends on model scale outright, save that model and method need to be capable of yielding relevant data.

f) Quantifiable parameters alone paint an incomplete picture. Other elements, arising from stakeholder engagement and requirements, are less measurable but just as important in determining the attractiveness of a WEC offering. It is important to follow a rigorous method to assess this and obtain relevant inputs – the TPL framework (e.g. as implemented by Trueworthy et al. 2021) can be a valuable as a guide to identify value and stakeholder priorities within a wider conception of performance (not just power and cost). This is still rarely found in literature. In off-grid markets, LCOE is usually not the best metric to steer development; CAP is more relevant. Optimisation work carried out by other Mocean team members suggests that AEP and CAP are highly correlated for the Mocean WEC, likely to its characteristically broad response bandwidth. Within a multi-objective optimisation that yields a Pareto front of solutions, there may be different requirements embodied in the fitness function and how an ‘optimal compromise WEC’ is selected.

10.2.2 Method

As well as reducing the CAPEX (and thus size / scale) of physical models, economising physical testing requires accelerating a given test programme and collecting data more efficiently to minimise operational (tank related) costs, while maximising the value of the data collected. The primary methodology findings are as follows:

a) A gap in standards and available testing guidance exists in terms of quantifying uncertainty, scaling effects (see 10.2.3), and identifying the smallest viable scale for a particular WEC. This leads to the current paradigm of using the largest tank that can be afforded, and the largest model scale that enables testing of scaled operational seas. A separate, smaller model is typically used to test survivability behaviour in larger seas. However, the fact that downscaling is not an absolute barrier is evidenced by the fact that models at smaller scales (half or lower common) than performance models are utilised for survival testing. Thus, here too guidance on evaluation of scaling effects would be highly relevant - even more so considering the generally greater nonlinearity involved due to typically larger induced model motions.
b) The recommendation found in the IEC specifications for testing a physical model at the largest possible scale seems to be justified from an accuracy and uncertainty limitation point of view but pushes developers towards use of larger tank facilities, which often limit testing scope. This guidance is not necessarily given because smaller scale models cannot viably enable the collection of required data, but because it is difficult to isolate various sources of associated error. Specifications are guided by the objective of reducing potential scaling errors, as opposed to understanding and quantifying them. However, it has been found that the use of a small tank facility is recommended particularly at early stages, even if it cannot cover the whole occurrence matrix at the location of interest, since it can more cheaply enable the exploration of inaccuracies from different parameter sensitivities. Developers approaching IEA-OES Stage 1 testing should consider both active and passive PTO model versions. The active version should be guided by the smallest viable

model PTO that can be included – ideally with a direct PTO load or torque sensor. Passive versions are recommended at the same scale as the active and also at a reduced scale, to enable some initial hydrodynamic scaling sensitivity.

c) Some errors arise due to measurement and practical limitations (e.g. lack of torque sensor), as opposed to fundamental scaling effects themselves. The method used here to characterise nacelle friction is only partially satisfactory in accounting for friction effects in operation. It can account for torque difference but not for hinge velocity effects, both of which feed the power calculation. This limitation is more significant the greater proportion of torque limit is made up by hinge friction (thus, more so with a smaller model). Characterisation should be repeated before and after each test campaign to quantify how friction changes; a larger nacelle with same type of motor and seal (though larger model) one year following initial characterisation revealed that the value of static friction had approximately doubled.

d) 1:20 Froude scale has been identified as appropriate for CT use. For Mocean, the lower limit is driven by inclusion of model PTO, while higher limits are driven by the tank's envelope. The shift to off-grid markets, where CAP is the main driver for performance requirements, means tank envelope upper bound is less limiting; of greater significance is the power produced in the lowest seasonal seas. Thus, the 'all-in-one' model hypothesis has not been fully dismissed – though different tanks would still be required, or a single larger tank. For example, at FloWave both survival and performance testing would have been feasible with the BST-folding 20th scale model.

e) The 20th model capabilities have been expanded, particularly via inclusion of a model PTO that allows +/-120deg relative hull pitch requirement. A new nacelle has been designed, bench-tested and characterised. Its modular design allows it to be re-used in future small-scale model revisions/evolutions – this is significant since the model PTO is by far the most expensive (five times more than the rest of the prime mover structure) component and time intensive to design, build, and characterise. Application of damping and torque limit were satisfactory; a

damping gain of up to ~4 times greater than the FD numerically predicted target was applied in the tank environment while maintaining response stability. Greater ‘overhead’ torque allowance would be desirable, to reduce the impact of thermally limited cut-outs encountered. Inclusion of a temperature gauge within the nacelle would give greater confidence when overriding the motor’s thermal limit set by the controller for short periods of time, and given that the motor can dissipate heat through the water via the nacelle. The use of an inertia disc or equivalent to drive the motor during characterisation would also be beneficial in order to mimic hydrodynamic damping encountered in tank, since in a dry environment the motor response became unstable around a gain of 80, which approximated the optimal damping value predicted by SD simulations.

f) The new nacelle enabled successful application of both linear damping and torque limit elements of PTO behaviour, the two key elements given Mocean’s relatively simple control strategy, since the device is already well-tuned via its geometry. Only two PTO parameters require validation: damping coefficient and torque limit, both of which are constant by design. An optimal PTO damping of 0.17 Nms/rad has been identified (equivalent to a PTO gain of 40), about half of that predicted numerically via SD (0.31 Nms/rad). One can be reasonably confident in this because Mocean test campaigns with larger models, where the relative influence of friction is lesser, similarly show a noticeably lower value of optimal damping found experimentally compared to numerical predictions. The torque limit in BST-folding tests was only partly validated, given that few seas were energetic enough to induce large enough torques.

g) Testing of two Blue Star geometries has revealed the importance of including PTO damping in the physically modelled power conversion stages. Observing power-producing DoF (flex) RAOs only may lead to incorrect conclusions regarding the power performance of a device iteration, particularly if the hinge characteristics are not comparable due to different builds. This is the case for BST-baseline and BST-folding; experimental and numerical flex RAOs are greater for BST-baseline, but numerical power RAO and CWR are greater for BST-folding.

h) An Ir0-based method was implemented and found to enable accelerated comparisons of different model configurations/iterations, including identification of an optimal PTO damping gain with higher torques being achieved. This method is based on artificially assembled polychromatic seas aiming to provide irregular sea 'realism' responses, with regular sea levels of 'control'. In line with its objectives, the Ir0 method was found to yield higher frequency resolution, to be more representative of real sea conditions (e.g. phasing influence), and require less run time compared to equivalent regular wave frequency sweeps (78mins versus 7.8mins), for a 22 frequency component RAO). Altering the gain of the overall Ir0 sea then also allows faster amplitude sweeps. Run (and settling) times of 94s (2mins), 288s (3mins), 288s (4mins) were used in the BST-folding campaign. Thus, the impact of Ir0 is one of acceleration and higher resolution, without sacrificing on precision (see 10.2.3). Given the even number of waves in each component specified in the overall 256s repeat period, 8x shorter repeat periods (32s) exist, giving scope to either: (i) reduce Ir0 run time further, say to 96s or 128s; or (ii) analyse each 32s repeat period segment as a 'run within a run', yielding additional repeatability data "for free". Initial analysis of *intra*- and *inter*-repeatability of IROa runs suggests that repeatability is very similar for the mean and max variable values measured.

i) Gain scaling of Ir0 seas once is encouraged as an easy way of gauging nonlinearity effects; two gains were used but using three is encouraged to obtain a more complete trend. Though power capabilities of the tank need to be taken into account (e.g. paddles cutting out near the limit of what the tank can produce), as well as potential amplitude components becoming too small and thus prone to error. It was found that 5mm was an acceptable threshold for the CT; below this amplitude there was more variability between demand and measured components. This is not too limiting as it can be quantified via reflection analysis, as long as spilling is limited. Demanded amplitudes were as low as 1.8mm, with in some cases similar R_{coeff} values as per >5mm amplitude components. More spilling occurs at overall higher demand gains, likely because tank capability limits are being approached. Large R_{coeff} values were found

near the top frequency (2Hz) limit of the tank, though the very small demand amplitudes likely contributed to this trend. More spilling was observed for *energy* (IROc) seas, compared to *steepness* and *envelope* seas. Thus, the recommendation is to set up Ir0 sea components to follow the tank envelope if possible; these are the most 'linear' seas with the least visually observed wave breaking and measured spilling.

j) Further acceleration would be enabled by additional guidance or 'off-the-shelf' data post processing material – enabling live processing of data to make better informed decisions "on the fly" during testing campaigns. Some of this has been set up during the course of this test campaign, as well as having access to an up-to-date CT envelope, which was not available before this research – both will aid future campaigns. The CT was re-characterised because of lack of recent use and maintenance, in particular because a few paddles (mostly around the far side of the tank and thus away from the zone of interest where the model was located) were not performing optimally due to belt wear, limited range, and lack of synchronisation.

10.2.3 Uncertainty

A trade-off is typically assumed between data quality and costs with model scale. As scale increases, so do the costs, while uncertainty drops. Identifying the crossover point, or the optimal trade-off between the two has been proven to be highly challenging. Not least because it would require rigorous identification and assessment of uncertainty indicators. An initial uncertainty analysis sheds light on where the trade-offs might be for Mocean's Blue Star WEC, and in understanding what constraints are fundamental and what are practical.

a) The contribution of various elements to the disparity between numerically predicted and experimentally measured mean power values was not conclusively ascertained. Hinge friction only partially explains the disparity in the case of BST-folding. Numerically accounting for friction suggests that its effects are unlikely to explain the full extent of power capture measured-predicted disparity. In particular, the disparity between measured and predicted hinge velocities suggests that other mechanisms

may be contributing, for example, the presence of relatively stiff and not neutrally buoyant cables for motor power and feedback affecting model dynamics. Accounting for hinge friction in the predicted max absolute hinge velocities during regular wave runs, suggests drops of 5-7% across PTO gain range (0-60), while in practice drops of 25-35% are measured (regular waves, peak response frequency). At PTO gain 40, the mean powers measured in 1/100 seas are between 10% to 43% of those predicted across a range of frequencies. Nevertheless, the shapes of CWR and Flex RAO plots align with expectations, as well as the trends with varying PTO gain; this gives sufficient confidence in terms of the underlying mechanisms. It is recommended to more actively include thorough isolation of uncertainties in the test programme - e.g. passive versus active model comparisons at the same scale in the same tank.

b) Some of the uncertainty rests with the numerical model, as this has not been fully calibrated and validated at the time of testing and writing. In the most recent physical testing with a 25th scale model of Mocean's Blue Horizon 250 WEC, discrepancies up to ~30% in mean power were found in some irregular sea states. Measured-predicted agreement improved as Hs increased and period decreased. Thus, the occurrence matrix area covered in BST-folding tests, in terms of lower Hs and longer period, would likely give the greatest inaccuracies with respect to numerical values, notwithstanding the influence of other errors. A notable limitation is the constant Morison's damping assumed, which should actually vary across different seas, and which is numerically tuned for larger waves.

c) The effect of friction and cables can be inferred - to an extent - by comparing the BST-folding model with its passive version tested at the Plymouth COAST Lab. Due to mass matrix differences in the as-built models, the numerically predicted curve for the active model has a narrower bandwidth and higher peak than the passive one. In both cases, the match between numerical and experimental data obtained with the PTO switched off is good, particularly in the case of slack moorings. Comparing the experimental data only, peak RAO does drop in the active case by roughly 10% relative to the passive case, though the passive data is more sparse. All curves are obtained with 1/100 steepness waves

and reflections accounted for. The comparison suggests that some effects are introduced by the active model nacelle, though these do not appear overly significant. In addition, the shape of active and passive irregular wave RAOs matches; further conclusions are not attainable since the actual Hs parameters from the data obtained in Plymouth are unknown. No decay tests were run at the COAST Lab, so no data for natural frequency response comparisons exists.

d) Natural frequency comparison is instead possible – yet more complex – by comparing 40th passive and 20th active (hinge switched off) decay tests. Considering slack moored active 20th and passive 40th models at full-scale, natural periods measured for the flex DoF were 2.82s and 2.78s respectively. In both cases, filling in the aft gap slightly raised the natural period. On the other hand, the roll period differed with 2.99s for the active 20th and 3.42s for the passive 40th (full-scale equivalents). This implied higher hydrodynamic stiffness for the 20th model could be due to cables adding stiffness. Unfortunately, we cannot disinter the effect due to the different as-built mass matrix itself. Comparison with numerical predictions is difficult, because the type of motion that each natural period corresponds to is not obvious due to multi-mode coupling. If some DoFs are locked to isolate e.g. roll, this should be set to occur about the centre of buoyancy as opposed to the centre of mass. Furthermore, the above is not necessarily representative of real motions in waves as it is based on small displacements. Nonetheless, inclusion of decay tests in all test campaigns is encouraged, despite these being found missing in standards and guidelines examined.

e) Seed sensitivity and the use of short-crested seas, as well as angular spreading, tend to be omitted at early stages of physical model testing. Thus, sensitivities for repeatability of each were run. In irregular seas of full limiting steepness and Tp=1.0-1.4s, gamma=1, introducing a +/-20deg spreading angle resulted in mean power dropping by 3.4-4.1%. Changes in spreading factor from s=6 to s=10 have negligible influence on mean power measured (full limiting steepness seas of gamma=1 and +/-20deg spreading angle). For gamma=1.0, increasing spreading angle from +/-20deg to +/-40deg, has negligible effect on mean power. For

gamma=3.3, increasing the spreading angle from +/-20deg to +/-40deg decreases mean power by ~14%.

f) The effect of different seeds on mean power and flex RAO responses in long-crested irregular and Ir0 seas was measured, choosing IRL23 and IRO21 being as close as possible seas in terms of equivalent Hs and Te parameters[89]. Relatively low Ir0 sensitivity to seed effects for flex RAO and mean power was found. IRL23 yielded values that ranged {-3.1 +0.6 %} about the mean of 0.0355 W. The 'energy' IRO21 sea yielded values in the range {-2.6 +3.8} % about the mean of 0.0532 W. *Energy* Ir0 seas were the least 'linear' among IRO types, so it is likely that *envelope* and *steepness* Ir0 seas would be less seed sensitive.

   For a PTO gain of 40, IRO21 seeds sweeps yield mean and std flex RAO of 287 +/-14 deg/m at peak frequency (f), and maximum variation at f=0.5625Hz which is 149 +/-64 deg/m. IRL23 repeats appear more consistent though here reflections are not taken into account.

   Ir0 seas tested have been found to be highly repeatable in terms of incident amplitudes of underlying frequency components, with comparable – and in some cases improved – levels of repeatability compared to regular RAOs. Flex RAO 7.4% peak variation from regular wave repeat run with 1/50 steepness and gain 0 (2 runs). IRO01 has flex RAO variation of 2.7% at peak, gain 0 (2 runs).

g) An initial identification of various uncertainty sources in terms of type and likely significance has been undertaken, though not all have been exhaustively quantified. The highest contributing sources of uncertainty relate to the model itself: the influence of hinge friction, the dynamic influence of the cables, vortex shedding at sharp corners, moonpooling at the aft hull gap. The BST-folding model had sharper corners than previously tested models, due to its carbon fibre sheet sandwich structure, where energy begins to be lost from vortex shedding when wave amplitude is the same or bigger than the local radius of curvature.

[89] IRL23 is [Hs=1.45m, Te=5.48s], IRO21 is [Hs=1.75, Te=5.51s].

h) Uncertainty sources of likely low significance include: trimming line errors, use of idealised compliant moorings, static friction estimation errors, dynamic friction contribution, Qualisys measurement, motor torque measurements, tank reflections (since quantified). Some difference is found between results achieved with slack versus taut mooring, but the shapes of responses and trends identified are the same, thus giving confidence for past obtained data with slack mooring only. A depth agnostic mooring set-up with known stiffness properties, such as that implemented via the sprung taut lines, is recommended for validation.

i) Two geometrically identical models of the folding geometry – in 'gap' and 'no gap' configurations – were tested at 20th and 40th scale in equivalent full-scale seas in order to estimate downscaling effects. Factors considered to evaluate scaling effects are: flex RAOs, sensitivity to wave amplitude variation, natural periods, value of Morison's damping that most closely matches experimental data.
    - Flex RAO responses show similar locations of the main response peak, though the 40th scale data shows a higher peak and narrower bandwidth. The peak obtained with 40th scale model is ~35% higher than equivalent 20th scale, and shows a clearer second peak around 5.5s period full-scale.
    - The rate of drop of Flex RAO with increasing wave steepness is similar for both 40th and 20th scale obtained data. However, while flex RAO values without hull gap are lower than with gap at 20th scale, the opposite is observed at 40th scale.
    - Natural frequency (NF) comparison of flex DoFs of slack moored models (20th active and 40th passive) suggest no significant scaling effects at work. Similar NF in flex, and drops for both when filling aft gap. However, how representative of more dynamic coupled behaviour is a decay test? Any flex motion in practice is likely to be accompanied with surge and heave strongly coupled. Displacements in decay tests are small so effects of scaling would be less pronounced anyway.

Significant downscaling is typically accepted for extreme survival sea tests, but less so for operational ones. In Mocean's case the survival

strategy entails disengaging the PTO and thus the hinge being passive, meaning that a lack of PTO in the smallest model does not affect its representability. However, associated hydrodynamic nonlinearities will remain and are worth trying to quantify.

j) Ultimately, validation, along with a more representative grasp of uncertainty, are achieved at large-scale subject to open water trials. Blue X trials offer a unique opportunity to do this. However, the upshot are the significant complexities related to accurate measurement and representation of waves at sea, away from the controlled lab environment (where complexities such as current drift, directionality, and wind effects are at play). A backward process should be attempted to shed light on whether scaling from 40^{th} to 20^{th}, or from 20^{th} to 10^{th}, is equivalent as 10^{th} to full scale. In reality, models at those scales should be built with equivalent scaled mass matrix as the full-scale. This is never the case in practice when working towards full-scale, and is a typically accepted error. It can be accounted in numerical to experimental step, as done in this research, but not in comparing like-for-like different scales of built physical models.

10.3 Outcomes relating to commercialisation pathway

The following outcomes relate to the commercial impact of the research and are grouped between the WEC product – Blue Star – and its associated development process.

10.3.1 The Blue Star WEC

The Blue Star WEC has been designed and developed. In particular, a new folding geometry was ideated and patented, geometrically optimised by the rest of the Mocean team, and physically tested via this research.

a) Numerically, significant improvement has been shown between BST-baseline and BST-folding evolutions. Experimentally, validation has been limited by some factors, which are difficult to disinter in terms of error

contributions. With regards to power capture, it is noteworthy that for off-grid applications, a broader bandwidth like Blue Star's is important. This can be tracked by continuous available power (CAP) numerically, which given its numerical correlation with AEP, can be validated in tank testing via power matrix cell contributions. However, an empirical QOI representing performance in the lowest resource wave climate could be valuable (e.g. July AEP in Northern Hemisphere locations).

b) Blue Star performs well against AEP/mass and AEP/torque limit metrics, achieving 2.3-2.7 times more than a purely scaled version of the original M100P WEC, of which Blue X was a half-scale prototype. Accounting for scaling effects on metrics, the optimised Blue Star folding evolution displays significant benefits over a scaled version of Blue X (more than double AEP/mass and AEP/Torque limit) though these metrics have not been exhaustively validated with experimental data. Ultimately, finding out if inaccuracies lie predominantly in the numerical model or the experimental testing needs full-scale data (e.g. from Blue X). This is caveated by the fact that accurate measurement and characterisation of at sea conditions is much more challenging that in the tank controlled environment; one of the biggest barriers from an open water point of view.

c) The folding geometry is an example of radical redesign that was initially considered, discarded, and could now be reintroduced. It evidences the need to be able to react to this quickly and at minimal cost, in order to avoid overly slowing down TRL. It is important to have an available tool that is highly responsive, adaptable, and with low - or at least known - uncertainty (to go hand in hand with fast turnaround optimisation capabilities) such as small-scale fast-turnaround physical model testing.

10.3.2 The development process

The process has enable significant learning to be captured.

a) The optimisation fitness function, or at least Pareto front assessment, should include more indicators of performance that is not power capture related – e.g. including roll stability, which has been identified as an important element to maximise for hinge seal lifetime and reliability.

Related to proxy metrics identified with consideration of what data can be obtained experimentally for their validation. For off-grid, different drivers commercially, though their effect on testing is not so significant: (CAP vs AEP), or focusing on AEP and associated power matrix validation for the lower seasonal climates – e.g. July in North Sea, but still want to validate as much as possible of it. Optimisations have not been optimised for CAP yet, though post processing suggest strong positive correlation between CAP and AEP, as found by other Mocean personnel.

b) The commercial impact of the Wave Energy Paradox framework has been ascertained during research period, particularly in providing traction and as a useful means of linking technical development to the “small-mid-grid” commercial roadmap. For a developer, it especially underscores the importance of learning, especially within a *maturing* sector such as wave energy. The positive impact of the “small-mid-grid” trajectory is partly evidenced by Letters of Intent (LoIs), a triparty Memorandum of Understanding (MoU), and a joint industry demonstrator project, Renewables for Subsea Power, RSP (Beckman, 2022; Thomas, 2022), for Mocean via its “small” scale WEC (BlueX and Blue Star). This has then fed forward to the Blue Horizon 250 positive funding and lessons learned implementation outcomes (i.e. the “mid” scale). It is highly likely that a successful campaign with Blue X played a part in progressing through to EuropeWave Phase 2, and hopefully onwards to Phase 3 in summer 2023 – showing cross-pollination and enabling scale up.

c) The research has underscored the importance of not only generating new knowledge, but retaining it through trackable decision-making and related outcomes and optimisation parameters. A framework/architecture has been suggested and implemented during this research, which includes geometry *iterations*, *revisions*, and *evolutions*. For example, this mitigates the risk of repeating design process steps via suitable recording of what performance changes a particular parameter change led to in the past.

d) Emerging strongly from this research is the need to address the question: what is “good enough”? The key to address is this are known targets, capturing wider value beyond cost of energy. These can only be obtained via stakeholder engagement, for which the TPL framework is useful.

These are crucial to guide design and can be applied in a systematic manner, though are not easily implemented in optimisation. The “good enough” question also directly relates to the *performance before readiness* paradigm. At what point of ‘performance’ does a developer switch to ‘readiness’ focus (and thus deployment) in order to build external confidence – i.e. where is the inflection point of the TPL-TRL matrix? Again, stakeholder engagement is essential in identifying this.

e) In considering the TPL-TRL matrix, TRL and costs are almost always the most sought after characteristics, at the forefront of questions from prospective customers and investors. The research somewhat challenges the *performance ahead of readiness* paradigm, suggesting that this is not necessarily the best route if learning is the paramount goal. One needs to build a full-scale device, and accumulate at sea ‘time on the clock’ to really understand and quantify OPEX and thus LCOE. A developer can do so more easily if development occurs at smaller scale (for models) and smaller size (for devices), providing a key lever for investor confidence and wider industry credibility and traction.

Borrowing from (DeBord Jr *et al.*, 2003), "success of the design optimization process will be highly dependent on how available resources (money, time and personnel) are allocated among the available techniques used to evaluate candidate designs."

This research has demonstrated the challenges in identifying the optimal trade-off between physical model scale, costs, and quality of results. Its applicability to different sizes of full-scale WECs bears relevance to wave energy’s evolving market, where numerous developers are shifting towards offering a range of WECs with different power capabilities for a range of applications. The present research suggests that this can be an effective approach, benefitting a developer like Mocean in a context where overall industry confidence from investors is still generally low. One could imagine that if the opposite were the case – i.e. confidence, recognised need, and risk exposure willingness were high – the intermediate development steps could theoretically be skipped and developers could go straight to a very large built machine. However, the needs for smaller scale power delivered by wave would continue to exist, and lessons

from the past suggest that a straight jump to utility-grid scale is a highly risky endeavour, particularly since the industry cannot afford another confidence knock-back.

Appendix A – Chapter 1

This Appendix is in support of Chapter 1.

A.1 Origin of ocean waves

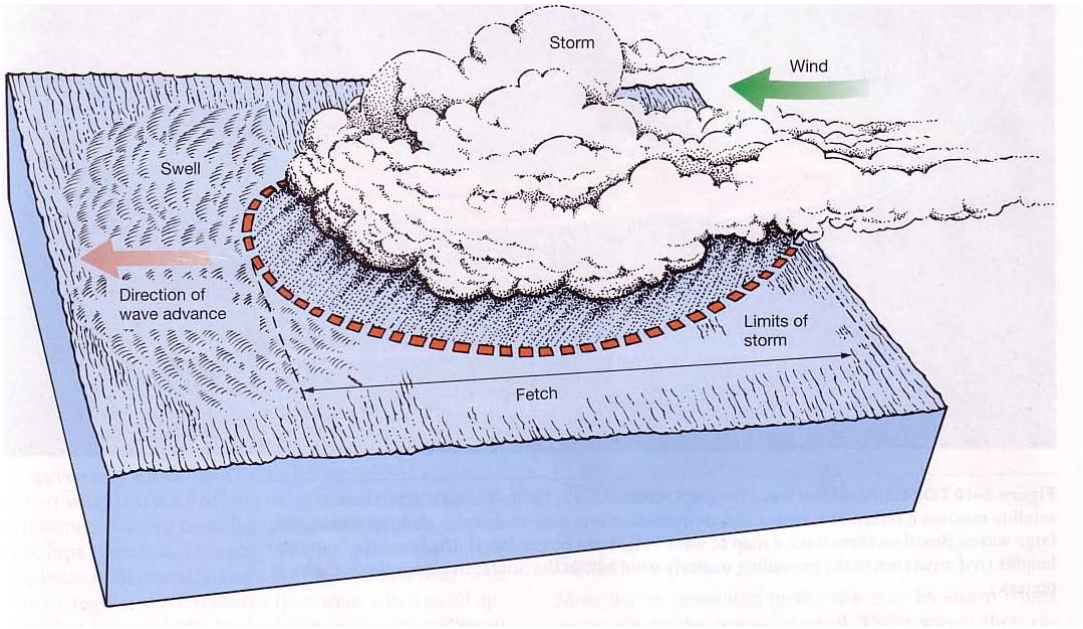

Figure 178 – Showing waves origin and long-distance propagation. Source: (Thurman, 1993)

A.2 Curved Tank Letter of Support

The following letter of support was submitted to the University of Edinburgh as part of the evidence gathering process to keep the Curved Tank operational.

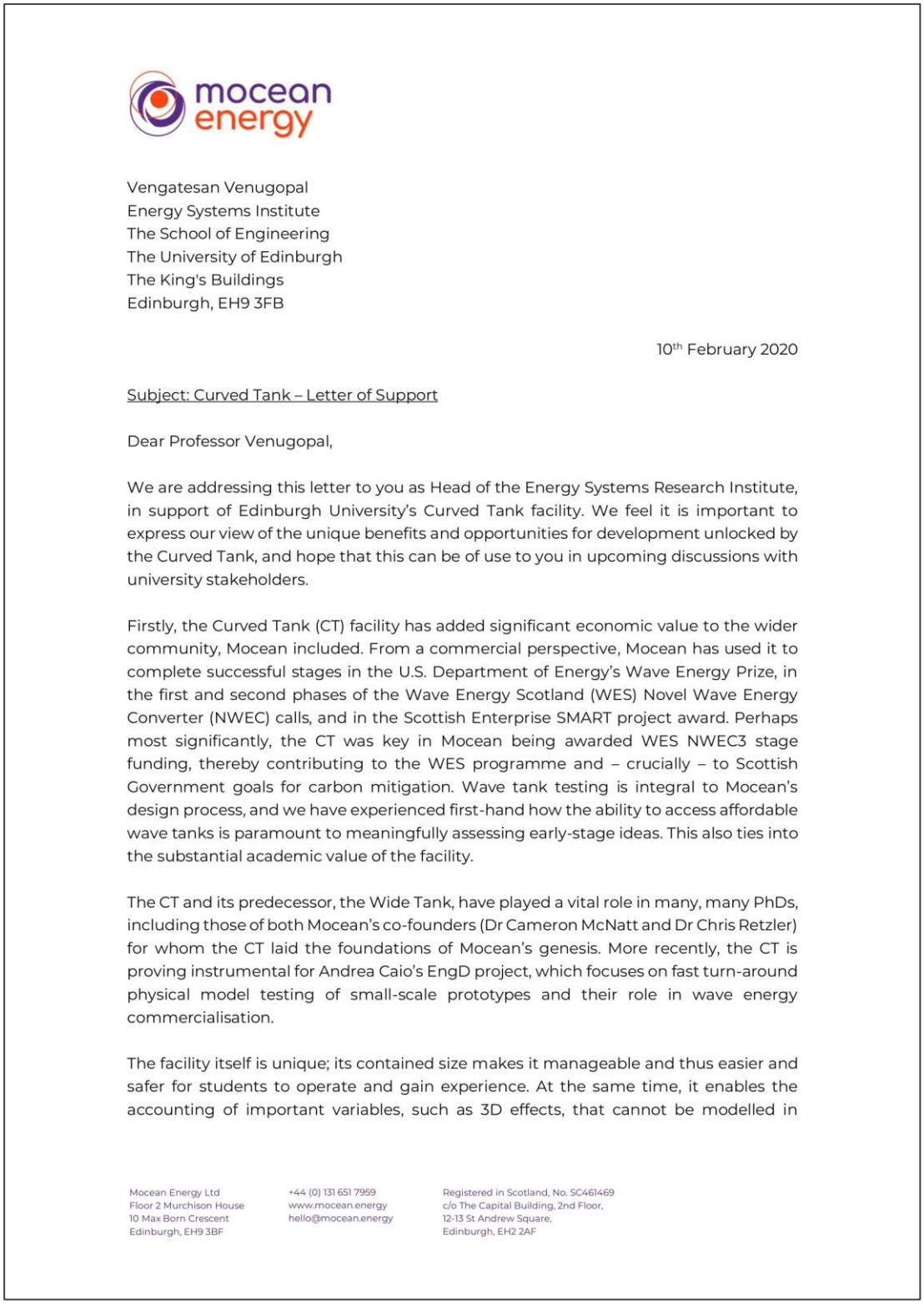

mocean energy

Vengatesan Venugopal
Energy Systems Institute
The School of Engineering
The University of Edinburgh
The King's Buildings
Edinburgh, EH9 3FB

10th February 2020

Subject: Curved Tank – Letter of Support

Dear Professor Venugopal,

We are addressing this letter to you as Head of the Energy Systems Research Institute, in support of Edinburgh University's Curved Tank facility. We feel it is important to express our view of the unique benefits and opportunities for development unlocked by the Curved Tank, and hope that this can be of use to you in upcoming discussions with university stakeholders.

Firstly, the Curved Tank (CT) facility has added significant economic value to the wider community, Mocean included. From a commercial perspective, Mocean has used it to complete successful stages in the U.S. Department of Energy's Wave Energy Prize, in the first and second phases of the Wave Energy Scotland (WES) Novel Wave Energy Converter (NWEC) calls, and in the Scottish Enterprise SMART project award. Perhaps most significantly, the CT was key in Mocean being awarded WES NWEC3 stage funding, thereby contributing to the WES programme and – crucially – to Scottish Government goals for carbon mitigation. Wave tank testing is integral to Mocean's design process, and we have experienced first-hand how the ability to access affordable wave tanks is paramount to meaningfully assessing early-stage ideas. This also ties into the substantial academic value of the facility.

The CT and its predecessor, the Wide Tank, have played a vital role in many, many PhDs, including those of both Mocean's co-founders (Dr Cameron McNatt and Dr Chris Retzler) for whom the CT laid the foundations of Mocean's genesis. More recently, the CT is proving instrumental for Andrea Caio's EngD project, which focuses on fast turn-around physical model testing of small-scale prototypes and their role in wave energy commercialisation.

The facility itself is unique; its contained size makes it manageable and thus easier and safer for students to operate and gain experience. At the same time, it enables the accounting of important variables, such as 3D effects, that cannot be modelled in

Mocean Energy Ltd
Floor 2 Murchison House
10 Max Born Crescent
Edinburgh, EH9 3BF

+44 (0) 131 651 7959
www.mocean.energy
hello@mocean.energy

Registered in Scotland, No. SC461469
c/o The Capital Building, 2nd Floor,
12-13 St Andrew Square,
Edinburgh, EH2 2AF

mocean energy

hydraulic flumes. Therefore, the CT represents an ideal stepping stone between flumes and larger, more complex, tanks like FloWave. The CT is also unique to Edinburgh University's spirit of innovation – it is not only part of its rich history but should also be part of its exciting future.

Finally, significant effort was devoted to re-activating the CT over the past year, working alongside Prof Tom Bruce, Dr Tom Davey, and with the help of many others who feel invested in the facility. Recent upgrades have increased the attractiveness of the tank as a working environment, and Mocean would be happy to support its continuing operation – e.g. by contracting for a minimum annual payment in return for an agreed number of testing weeks and a small storage/workshop area.

We trust that any upcoming decisions will carefully consider and take into account the aforementioned points, and very much hope that the CT will continue to enable key innovation in the wave energy industry and beyond.

Yours sincerely,

Andrea Caio
IDCORE Student

Cameron McNatt
Managing Director

Chris Retzler
Technical Director

Mocean Energy Ltd
Floor 2 Murchison House
10 Max Born Crescent
Edinburgh, EH9 3BF

+44 (0) 131 651 7959
www.mocean.energy
hello@mocean.energy

Registered in Scotland, No. SC461469
c/o The Capital Building, 2nd Floor,
12-13 St Andrew Square,
Edinburgh, EH2 2AF

Figure 179 - Copy of the letter of support for the Curved Tank basin.

A.3 Publications

The following publications are reproduced here back-to-back:

- ISOPE 2019
- EWTEC 2021
- POSTnote (2021)

Tackling the Wave Energy Paradox – Stepping towards Commercial Deployment

Andrea Caio[1], Thomas Davey[2], Cameron McNatt[3]
[1]School of Engineering, Industrial Doctorate Centre for Offshore Renewable Energy, The University of Edinburgh, Edinburgh, UK
[2]School of Engineering, Institute of Energy Systems, The University of Edinburgh, Edinburgh, UK
[3]Mocean Energy Ltd., Edinburgh, UK

ABSTRACT

For the wave energy industry, the leap from R&D to commercial deployment remains considerable and arises as part of the 'wave energy paradox', defined here as a negative reinforcement cycle involving a lack of investment, deployment, learning and returns. In this context, we review performance metrics set by funding bodies, industry standards and developers, examining how existing practices can result in sub-optimal design targets due to current specifications and misalignment of metrics between developers and external stakeholders. This paper offers initial insights – via a case study – to demonstrate how the integration of meaningful and aligned metrics throughout the design process represents a key lever in overcoming the paradox.

KEY WORDS: wave energy; commercial deployment; performance metrics; LCOE; design process; scale; markets.

INTRODUCTION

The vast potential of wave energy as a renewable source of power has been advocated for several decades (Isaacs & Seymour, 1973), (Cruz, 2008). Although nearshore wave energy potential has been estimated to be in the TW range, e.g. (Gunn & Stock-Williams, 2012), global deployed capacity as of 2017 was lagging at only 8MW (Ocean Energy Systems, 2017). Many observers argue that the shortfall is a result of the failure of wave energy converters (WECs) to converge to a single optimal design, though this can be viewed as both a cause and an effect (see following section). In 2016, O'Hagan et al. highlighted that "more than 50 types of WECs have been designed, but less than 20% have reached full-scale prototype stage" (O'Hagan, Huertas, O'Callaghan, & Greaves, 2016). Two notable (Edinburgh-based) projects that showed great promise, but ultimately failed to achieve commercialization, have been Pelamis and Aquamarine Power, which fell into administration in 2014 and 2015 respectively (The European Marine Energy Centre Ltd, 2015). Subsequently, Wave Energy Scotland (WES), a public funding body backed by the Scottish Government, purchased the know-how of these companies and set up a competitive procurement programme to streamline development of wave energy in several key technology areas. These events testify how, from a development perspective, "there is a clear need for research that outlines the pathway required to achieve LCOE[1] and deployment goals" (de Andres, MacGillivray, Roberts, Guanche, & Jeffrey, 2017).

The ultimate aim of the wave energy sector can be summarised as follows: to provide utility scale electricity at commercially competitive prices. Indeed, the majority of policy and industrial focus thus far has primarily centred on developing utility[2] scale WECs, with the benchmark cost of energy targets for offshore renewables largely set by the success of the offshore wind industry. (ETIP Ocean, 2016) defines a 'commercial' sector as one that "has the potential to be sustained solely on the basis of private investment by offering a sufficiently attractive investment opportunity". For wave energy, this proposition essentially reduces to minimising peak loads (i.e. costs) and maximising annual average loads (i.e. revenues).

However, major barriers to wave energy commercialisation exist, which have contributed to the sector failing to meet the anticipated progress. Challenges include: high capital costs (and thus investment); an often opaque policy landscape; complex spatial planning; consenting restrictions; grid availability; and harsh operating environments. Moreover, there may be additional factors related to the optimality of the design process and the way this links back to device performance measurement as well as the specific performance objectives that are chosen.

This paper focuses on these 'additional factors', examining the design process from the perspective of a WEC developer, i.e. Mocean Energy (MOE). The proposed analysis considers 'device-specific' elements that centre on *development* as opposed to broader 'industry-specific' elements associated with *deployment*. The scope is therefore limited to factors that have a directly quantifiable impact on techno-economic performance, without considering those outside of developer control –

[1] Levelised Cost Of Energy, i.e. the net present value of a unit of energy estimated over the lifetime of the energy generating asset.
[2] Utility scale implies grid connection and typical rated capacities in the MW range. In this paper, 'scale' is used to refer to the physical size or rated capacity of a WEC, as opposed to the scaling up from a single device to an array of devices.

such as political will, public support, consenting constraints, country resources and financial incentives – though they will too, of course, ultimately affect commercialisation outcomes.
The paper is structured as follows. The second section frames and formalises the negative feedback loop hindering commercialisation of wave energy technology. The third reviews existing design guidance in terms of WEC performance metrics, which is then analysed in the context of a specific WEC developer (fourth section). Concluding remarks, together with further research suggestions, are made in the final, fifth section.

THE WAVE ENERGY PARADOX

When considering the commercial challenges faced by the wave energy industry, we note that they are significantly interlinked. This has led to the definition of the *wave energy paradox* as a diagrammatical representation of the underlying negative reinforcement mechanisms at work (see Fig. 1). Not only is this representation useful to succinctly frame device-specific (and industry-specific) challenges, but it is also helpful in identifying key areas of possible intervention or 'bridges' required to transform this cycle into a positive one.

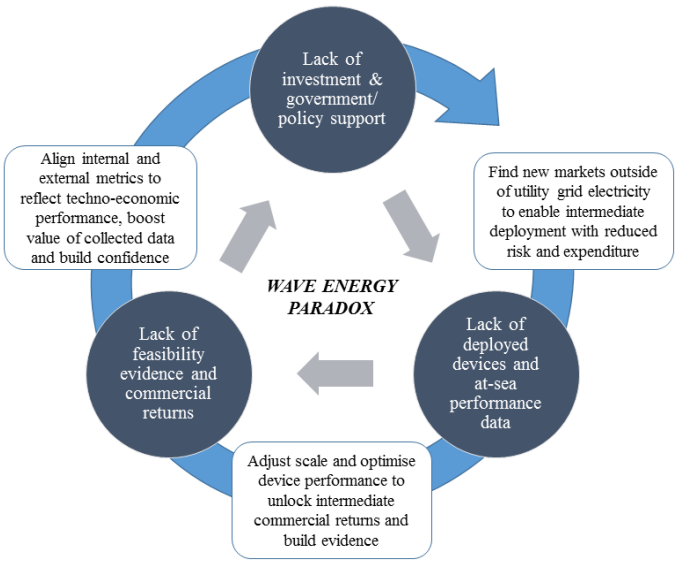

Figure 180. The wave energy paradox: negative loop elements (circles) and potential 'bridges' (rectangles).

Historically, high-perceived technology risk and high upfront capital expenditure (CAPEX) have contributed to a limited investor pool, particularly from the private sector. From a public perspective, this is reflected in the lack of ring-fenced funding for ocean energy in general from the UK Government, as demonstrated by its allocation of Contracts for Difference (CfDs) in 2017 (BEIS, 2017), favouring more established industries such as offshore wind instead.

This is a major cause behind the limited deployment of WECs, boosted by notable utility scale prototype failures, as previously mentioned. Similarly, Oceanera-NET report that "technical problems of some of the most promising devices have contributed to the loss of confidence of the investors and the current state is similar to the one in 2014" (Ocean Energy ERA-NET, 2017). Thus, as noted by (Magagna & Uihlein, 2015), there is evermore a "clear need for the sector to identify ways to facilitate technology development and deployment".

Unfortunately, the lack of deployed WECs also translates into a lack of returns for developers. This manifests in two ways: (i) a lack of monetary returns due to the inability of selling electricity; (ii) a lack of evidence accumulation in terms of at-sea performance. These both hinder the sector's ability to attract investment, and simultaneously create a heavy reliance on public funding. The latter in particular is held back by LCOE estimates that show the sector not being 'competitive' enough – in terms of cost of energy – with other renewable sources such as solar and wind. The cycle perpetuates and past evidence suggests that the R&D to utility scale commercial jump may be too ambitious.

Much of the focus in published reports has been on highlighting industry needs and priority areas for development in order to achieve accelerated development: learning by doing, cutting cost through design convergence, greater data sharing, supply chain development, etc. Yet none of these can occur without initial deployment of devices at sea. How to break the cycle? Several fundamental factors exist within wave energy paradox mechanisms that can act as positive 'bridges': metrics, markets, and scale.

The second and third are highly interdependent. Scale (i.e. the size or rated capacity of a device) has a significant impact on CAPEX and affects the target market for energy outputs. E.g. larger WECs would be required to power a national electricity grid (utility-scale) whereas smaller WECs would be suitable to more local, or off-grid, applications. Naturally, a smaller scale WEC would require lower CAPEX, while allowing quicker deployment and accelerated returns. Whether the technology learning involved is relevant for larger scales remains an open question.

The first bridge (metrics) – which this paper focuses on – relates in particular to *techno-economic* performance indicators. From a developer point of view, a major challenge rests on the integration of such techno-economic metrics into the design process, as part of a trackable and optimisable strategic trajectory towards commercial deployment. The next section examines which metrics, currently published in design standards and guidelines, can be used by developers to practically guide and optimise the design process. These are then related to a developer case study in the fourth section.

EXISTING DESIGN GUIDANCE

Existing WEC performance metrics are primarily outputs from a range of industry organisations, standards bodies and research collaboration initiatives. They are highlighted in Table 1. Here it can be seen that, wherever metrics are indicated, they mostly relate to device hydrodynamic performance, as is the case for: *Relative Amplitude Operator (RAO)*, *Annual Energy Production (AEP)*, *Capture Length*, *Capture Width Ratio (CWR)*, *Conversion Efficiency* and *Capacity Factor*. We preliminarily also note the lack of significant overlap and their dimensional dependence.

Accounting for Economic Performance

Though hydrodynamic metrics are of course highly relevant to inform device development, the authors note that most guidelines miss *economic* aspects of performance. As early as 2009, the EquiMar review report highlighted the lack of 'an accepted standard approach for calculating cost of electricity from large-scale marine energy projects' (EquiMar, 2009). This apparent void contrasts with much of the academic research published in the area, which typically advocates for the establishment and inclusion of techno-economic metrics as part of a more systematic performance measurement methodology (ETIP Ocean, 2017), (SET

Plan, 2018), (Ocean Energy Forum, 2016). There are some exceptions, such as the recent DTOceanPlus D2.2 Deliverable (DTOceanPlus, 2018) that refers to LCOE, and the older IEA-OES Annex II Report 2003 (OES, 2003), which points to *AEP/Mass* and *AEP/Volume* metrics, where energy capture is normalised by mass and volume acting as cost proxies (further discussed in the fourth section).

Metrics such as these are crucial to the development process both externally, as a more representative indicator of device potential for commercial stakeholders; and internally, by influencing a developer's ability to set appropriate design targets and measure performance progress. They therefore bear particular relevance in light of the previously defined wave energy paradox.

A study by (Weber, 2012) reinforces this idea by introducing the concept of Technology Performance Levels (TPLs) to complement TRLs, stressing that development trajectories should aim to rise up TPL prior to TRL, i.e. to achieve 'performance before readiness'. Simply put, using TRLs as design targets can lead to a technologically mature device that can, however, be commercially unattractive, since TRLs do not allow tracking of performance, and because meaningful cost reductions due to design changes become more expensive and technically challenging at higher TRLs.

Identifying Appropriate Techno-economic Metrics

Having established that techno-economic performance assessment is paramount at all stages of development, the challenge shifts to identifying the most suitable metrics. There is much debate in this regard. LCOE is the most widely used both in academic literature and industry reports.

Table 36. Summary of published performance metrics.

Organisation	Document	Scope	Suggested performance metric(s)	Reference
The European Marine Energy Centre (EMEC)	Assessment of Performance of Wave Energy Conversion Systems	• Aimed primarily at post-prototype machines.	• Capture length	(EMEC, 2009)
The International Electrotechnical Commission (IEC)	TS 114 – 62600-103:2018 Marine Energy – Wave, tidal and other water current converters	Part 103: Guidelines for the early stage development of wave energy converters – Best practices and recommended procedures for the testing of pre-prototype devices.	TRLs mentioned as stage gate definitions up to TRL 6. Power performance should be measured by: • (TRL1-3) RAO from regular waves • (TRL4) Experimental power matrix produced to estimate AEP • (TRL5-6) Actual power matrix using scaled Power Capture and Conversion •	(IEC, 2018)
International Energy Agency (IEA) - OES	Annex II – Recommended practices for testing and evaluation of ocean energy systems	• Guidelines for testing, preliminary cost assessment and presentation of results for ocean energy technologies.	• AEP/Volume • AEP/Structural mass • Average capture width ratio	(OES, 2003)
Department of Trade and Industry (DTI)	Wave energy device performance protocol	Focuses on supply of electricity to the network via single grid supply-point.	None specific to hydrodynamic or techno-economic performance.	(DTI, 2007)
EquiMar	D5.3 – **Protocols and guidance for device specification and quantification of performance**	• **Focuses on performance metrics for device arrays in particular.**	• Capacity factor • Conversion efficiency • Capture width	(EquiMar, 2009)
Ocean Energy Forum	Strategic Roadmap	Establishes priority areas for technological progress with an associated implementation plan.	None specific to performance. TRLs mentioned as part of a stage-gated approach.	(Ocean Energy Forum, 2016)
ETIP Ocean	Deliverable 2.1 – An Integrated framework for ocean energy sector challenges – Final report	Highlights the challenges viewed as most critical to overcome in the pursuit of sector commercialisation.	None specific to performance. Calls for 'defining and enforcing standards for stage gate progression through scale testing'	(ETIP Ocean, 2016)
DTOceanPlus	D2.2 Functional requirements and metrics of 2nd generation design	• Introduces a suite of design tools that aim to assist users in achieving optimal	• AEP - as the output of 'system performance and energy yield' tools • LCOE - as one of the outputs of 'system	(DTOceanPlus, 2018)

	tools	design solutions based on information available at a particular stage of development.	lifetime costs' tools (used as inputs for stage gate and structured innovation tools)	

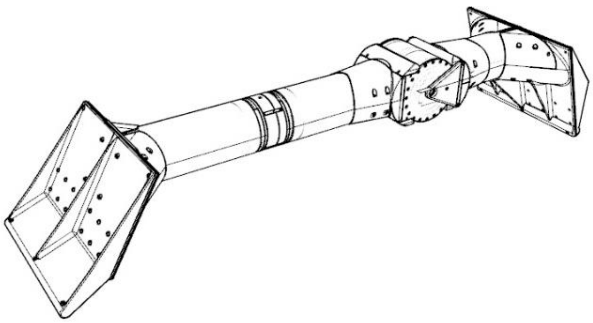

Figure 2. Rendered image of 20th-scale model of the MOE WEC used for tank testing during NWEC Stage 2.

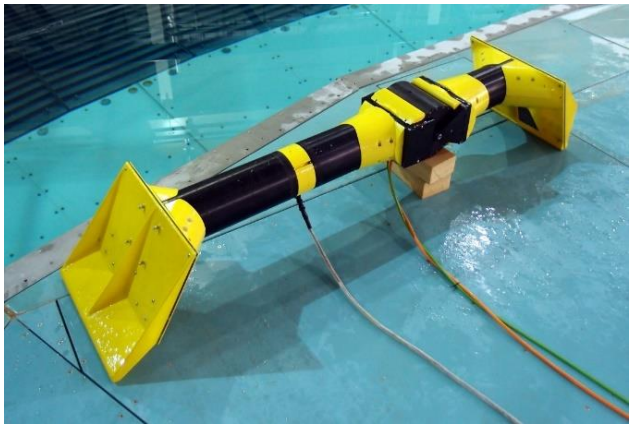

Figure 181. As-built 20th-scale model of the MOE WEC, ready for testing at FloWave research facility.

Its long-established use makes it a valuable comparative indicator, though it has questionable accuracy for device optimisation in absolute terms and poor utility as an early stage performance indicator (de Andres, et al., 2016). Since LCOE requires information on the entire project costs, several assumptions are needed at early stages of design when there are significant cost uncertainties. In particular, reliability and operations and maintenance (O&M) strategies are key determinants for cost of energy (Pascal, Payne, Gorintin, & Cliquet, 2018) that are extremely difficult to estimate with the necessary confidence prior to at-sea testing. Some authors have also pointed out the limited validity of LCOE as an overall indicator of commercial attractiveness (de Andres, MacGillivray, Roberts, Guanche, & Jeffrey, 2017).

As we have seen, just as it is crucial to estimate techno-economic performance at low TRLs to ensure an effective development trajectory, doing so accurately and effectively is a considerable challenge on which the sector hasn't yet reached consensus.

Interestingly, only two of the above sources focus on linking performance measurements to particular phases of the design process (IEC, DTOceanPlus) despite a key function of metrics being within the design process, as opposed to just for comparative assessments. The fact that they are the most recent sources (both published in 2018) suggests that the industry is increasingly confronting this requirement.

To this end, several stage-gated processes have been proposed, among which Wave Energy Scotland's Novel Wave Energy Converter (NWEC) programme[1], the U.S Department of Energy's Wave Energy Prize, and Europe's Strategic Energy Technology (SET) Plan. The latter aims for the prospective 'development of stage gate metrics (both technical standards and guidelines) for wave technology evaluation' by December 2019 (Action 1.6) (SET Plan, 2018), partly emulating the WES model.

All of these rely mainly on a TRL framework but still require "standardised and commonly understood performance indicators to allow monitoring and comparison of development between technologies" (ETIP Ocean, 2016). WES relies on LCOE from the very beginning of the programme when technologies are still at low TRLs, while the Wave Energy Prize uses ACE[2] as a techno-economic indicator, which relies on a parameter – Representative Structural Thickness (RST) – that lacks clarity and transparency (US Department of Energy, 2016). The IEC document in its current form does not specify design targets even though it mentions that these should be defined for each goal-oriented stage of development, and even though it is intended for a variety of stakeholders that includes private investors and funding councils. The most promising and comprehensive approach that looks to integrate metrics within the design process is DTOceanPlus, a tool that is however still in its infancy. For now, it acknowledges the need for a cost assessment at all project stages and that LCOE can only be used at higher readiness, mentioning that "for low TRL and or high-level device analysis, other economic metrics will be developed" (DTOceanPlus, 2018).

Having scanned the current metrics landscape, the following section discusses how a developer may practically navigate it and embed relevant metrics within their design process.

A DEVELOPER'S PERSPECTIVE

It is useful to examine how metrics feed into the design process through

[1] Among others, WES performance criteria is based on: reliability, capacity factor, availability, and LCOE from TRL1.

[2] Average Climate Capture Width / Characteristic Capital Expenditure, expressed in units of m/$.

the practical perspective of a developer. MOE's core technology is an asymmetric floating hinged-raft with wave channels at the forward and rear hulls (refer to Fig. 2 and Fig. 3). It captures energy via a single degree of motion; the induced rotation of the hulls at the hinge produces torque, which is converted to electricity via a magnetic contactless generator located within the nacelle.

Wave Energy Scotland (WES) Metrics

As previously mentioned, the WES NWEC programme relies on LCOE as an overall performance metric used for external assessment from the first stage-gate at TRL 3. However, LCOE is heavily dependent on: (i) capacity factor, which relies on the device rated power (there is no industry wide agreement on its definition); and (ii) availability, which in turn depends on reliability, operating costs (OPEX) and maintenance strategy, all of which can only be realistically assessed following sea trials with a larger scale model. These are typically measurable only at later TRLs 5-6 (IEC, 2018), see Fig. 4, and are not negligible elements of LCOE. The contribution of OPEX, for example, is typically around 30% as per the stage of industry deployment in 2015 (OES, 2015).

LCOE also relies on several parameters – discount rate, policy measures such as FITs, industry learning rates, bulk discount rates, device scaling – that are difficult to estimate and that lie outside of the developer's sphere of influence (de Andres, MacGillivray, Roberts,

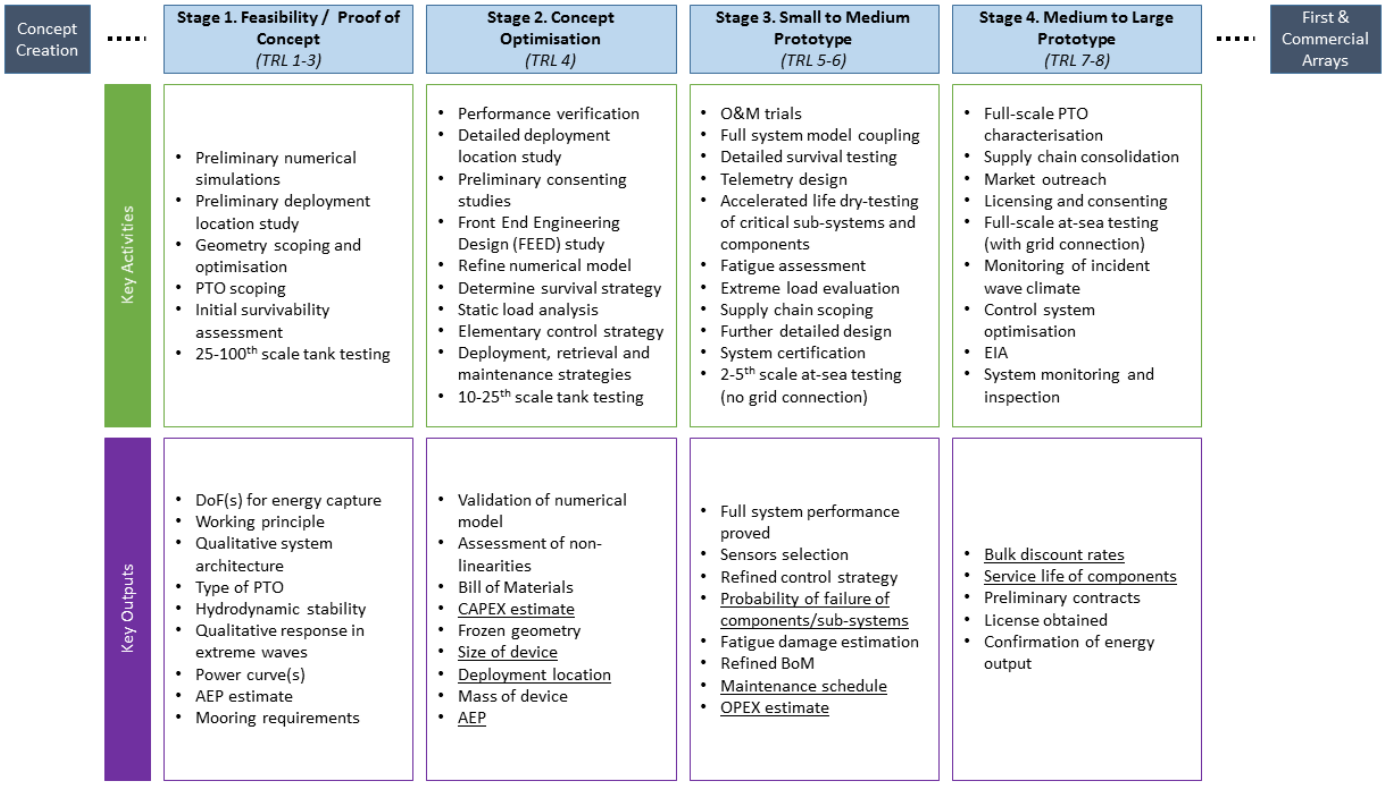

Figure 182. High-level breakdown of WEC development activities per TRL (Ruehl et al., 2012; HIE, 2015; IEC, 2018). NB: underlined outputs are required for LCOE calculation.

Guanche, & Jeffrey, 2017). Ultimately, LCOE is intended to measure the performance of a *commercially ready* device. Therefore, in practical terms, estimating the CAPEX of a full-scale commercial device from a low TRL is not straightforward, and can be a fairly malleable process due to ambiguous estimates. Can such a metric as LCOE really be relied on if it is to convince typically risk averse funders and investors? One might argue that funders and investors 'understand' LCOE because they have become familiar with it, and this in itself has some value. While this is a reasonable assumption, such stakeholders would also be interested in the degree of certainty of the metric. Persisting with its use would likely 'force' the funding model to remain: public body finance and grants up to TRL 6; private investment after TRL 6 once LCOE estimates can be made with sufficient confidence, thus limiting the ability of developers to deploy devices for sea testing without the support of public funds.

MOE's Approach

Contrarily to the above, MOE have primarily relied on *AEP/Mass* and *AEP/PTO torque* metrics to guide the design process. This is because they can be incorporated in device design with relative ease. For example, a key activity for MOE during the second stage of the NWEC development programme was the geometric optimisation of the WEC.

Forming part of the fundamental design choices, this was run based on a genetic algorithm implemented in MATLAB, which aimed to minimise the following fitness function:

$$F = C / P, \quad (1)$$

where C is CAPEX of the prime mover structure and the power take off (PTO), and P represents *AEP* (based on a representative wave climate as input). Thus, the fitness function F essentially combines *AEP/Mass* and *AEP/PTO torque* metrics. Structural mass and PTO torque are selected as these typically make up for around 60-70% of CAPEX (The Carbon

Trust, 2011). For the MOE WEC, this percentage is 83% for the first-of-a-kind full-scale prototype. Although this function does not exhaustively cover techno-economic elements, it represented the most efficient way of including power per cost offering at an early stage of design, when large uncertainties remained in terms of reliability, lifetime, O&M, supply chain, etc.

Thus, a clear disparity exists between external (i.e. set by external stakeholders such as investors and standards bodies) and internal (i.e. set by developers) performance metrics. This is significant when considering the wave energy paradox, since part of its resolution relies on a coherent set of metrics that can talk to developers, funding bodies and investors alike. Aligning internal and external performance goals would allow a greater understanding and appreciation of development progress.

Table 37. Metrics comparison for metrics of floating concepts operating at EMEC site reference climate (Babarit, et al., 2012).

Concept	Basis	CWR[a]	AEP/ Mass, kWh/ kg	AEP/ RMS PTO force[b], kWh/N	AEP/ Surface area, MWh/m²
Two-body heaving converter	Wavebob WEC	0.29	0.20	1.70	0.53
Heave-buoy array	Pontoon Power WEC	0.11	0.54	N/A	0.63
Three-body oscillating flap	Langlee WEC	0.20	0.60	1.40	0.46
Oscillating water column	OE Buoy	0.50	1.30	N/A	0.35
Single-hinge attenuator	MOE WEC	0.16	1.42	1.60	0.50

[a] Capture width ratio, a measure of WEC hydrodynamic efficiency.
[b] N/A indicates missing results.

MOE's decision to combine *AEP/Mass* and *AEP/PTO torque*, by translating mass and PTO torque into a cost, seems an appropriate starting point to include techno-economic elements.

$$C = Cost_Str + Cost_PTO \quad (2)$$
$$Cost_PTO = f(x) \quad (3)$$
$$Cost_Str = g(x) \quad (4)$$

In MOE's case, the control variable, represented by x, related to device geometry. However, this can be flexible depending on the optimisation required. This approach enabled MOE to improve *AEP/Mass* by 50% during Stage 1 and by a further 80% in Stage 2, while achieving a three-fold increase in *AEP/PTO torque*. These formed internal performance targets that primarily drove development and, ultimately, allowed MOE to progress to Stage 3 of the WES NWEC competitive funding award (WES, 2019). Equivalent metrics will also be used in future phases, refining their detail in accordance with the latest available data as development activities progress.

Choosing appropriate metric(s) is also important to set suitable goals and design trajectories. As Weber states, "depending on the fundamental definition of the objectives, development trajectories can diverge considerably subject to prioritisation of tech development" (Weber, 2012). Table 2 shows different metric scores for floating WEC concepts in (Babarit, et al., 2012) compared with the MOE WEC. Similarly to the analysis by (de Andres, et al., 2016), it can be seen that relative merit varies significantly depending on the chosen metric: each metric is maximised by a different device concept. Fig. 5 provides a visual representation of these variations.

CONCLUSIONS AND FURTHER RESEARCH

The study allows the following concluding remarks to be made:

- A review of the metrics landscape in current design guidance/standards has highlighted a lack of convergence in terms of which metrics should be used to assess WEC performance, while failure to account for economic performance aspects reduces the utility of such metrics for developers. This is augmented by the scarcity of clear links between techno-economic performance metrics and the design process, despite this being a crucial factor in overcoming the wave energy paradox and achieving commercial success.

- Though widely used, LCOE is likely a sub-optimal metric at early stages of design (below TRL 5-6) due to significant uncertainties in its input variables arising from insufficient available performance data. It therefore contributes to a misalignment between internal and external performance metrics, since developers are likely to avoid using it as an performance indicator throughout the design process. An over-reliance on LCOE may also lead to sub-optimal design trajectories and stop developers from ever reaching at-sea deployment, where key data is collected to collect performance evidence and inform device potential prospects; a key element within the wave energy paradox.

- It is not yet clear what alternative, early TRL proxies would be optimal, although a combination of *AEP/Mass* and *AEP/PTO torque or PTO force* appears to be an effective indicator, as it is relatively easy to include in the design loop and drives the design process more directly than LCOE. It may be that a *combination* of metrics, as opposed to a single indicator, is ultimately the best approach, so long as these can be integrated within the design process.

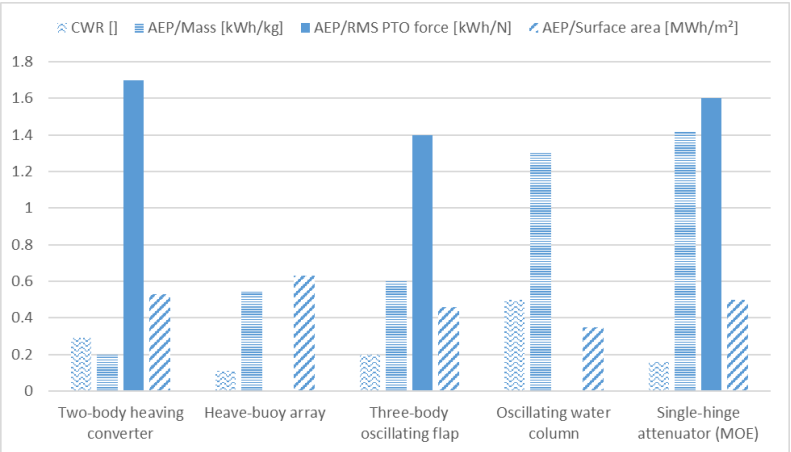

Figure 183. Metrics comparison for floating concepts at EMEC site (Babarit, et al., 2012).

Markets and scale are two other important 'bridges' that haven't been explored in this paper, yet worthy of further research focus in future. For example, off-grid applications can be a promising approach for developers that are hoping to relax the restrictions of LCOE requirements in cases where they are not directly competing with other renewable energy sources. In this regard, MOE are pursuing ocean observation market applications via a 10s-of-kW rated device, with the aim of providing a wave energy powered charging station for ocean-going drones. Such a beachhead market can be an effective intermediate development target, in order to: accelerate commercial returns, decrease reliance on heavy external investment, and allow quicker at-sea deployment to measure real sea performance and provide key reliability data for the ultimate LCOE offering.

If LCOE is to be used, a key requirement becomes component and sub-system accelerated life testing as early as possible in the design process, to alleviate LCOE assumptions that may reduce accuracy of the measure. Thus, metrics and standards would need to reflect such a requirement.

Lastly, the dimensional dependence of many of the discussed metrics bears significance, particularly when different markets and WEC scales are considered. Non-dimensional metrics would be better suited to cross-scale comparisons of performance.

ACKNOWLEDGEMENTS

This study was funded by the Engineering and Physical Sciences Research Council (EPSRC) IDCORE award EP/J5000847/1. The views in this paper are not necessarily those of EPSRC. The authors also gratefully acknowledge the support and data access granted by Mocean Energy Ltd.

REFERENCES

Babarit, A, Hals, J, Muliawan, MJ, Kurniawan, A, Moan, T, and Krokstad, J (2012). "Numerical benchmarking study of a selection of wave energy converters," *Renewable Energy*, 41: 44-63.

BEIS (2017). "Contracts for Difference (CFD) Second Allocation Round Results," Retrieved from Gov.uk: https://assets.publishing.service.gov.uk/government/uploads/system/uploads/attachment_data/file/643560/CFD_allocation_round_2_outcome_FINAL.pdf

Cruz, J (2008). *Ocean Wave Energy: Current Status and Future Perspectives.* Springer.

de Andres, A, MacGillivray, A, Roberts, O, Guanche, R, and Jeffrey, H (2017). "Beyond LCOE: A study of ocean energy technology development and deployment attractiveness," *Sustainable Energy Technologies and Assessments*, 19: 1-16.

de Andres, A, Maillet, J, Todalshaug, JH, Moller, P, Bould, D, and Jeffrey, H (2016). "Techno-Economic Related Metrics for a Wave Energy Converters Feasibility Assessment," *Sustainability*, (11)8.

DTI (2007). "Preliminary wave energy device performance protocol," Department of Trade and Industry.

DTOceanPlus (2018). Deliverable D2.2 - Advanced Design Tools for Ocean Energy Systems Innovation, Development and Deployment," Edinburgh: DTOcean.

EMEC (2009). "Assessment of Performance of Wave Energy Conversion Systems," London: British Standards Institute.EquiMar (2009). "Deliverable D1.1 - Global analysis of pre-normative research activities for marine energy," Commission of The European Communities.

ETIP Ocean (2016). "Deliverable 2.1: An integrated framework of ocean energy sector challenges," Brussels: European Commission.

ETIP Ocean (2017). "Metrics and stage-gate development programmes," European Technology and Innovation Platform for Ocean Energy.

Gunn, K, and Stock-Williams, C (2012). "Quantifying the global wave power resource," *Renewable Energy*, 44: 296-304.

HIE. (2015). "Wave Energy Scotland," Retrieved from Highlands and Islands Enterprise: http://www.hie.co.uk/common/handlers/download-document.ashx?id=078117ef-26d1-4144-aa34-88eaff0d0fec

IEC (2018). *TS 114 - 62600 - 103:2018: Guidelines for the early stage development of wave energy converters.* British Standards Institute.

Isaacs, JD, and Seymour, RJ (1973). "The ocean as a power resource," *International Journal of Environmental Studies, 4*(3), 201-205.

Magagna, D, and Uihlein, A (2015). "Ocean energy development in Europe: Current status and future perspectives," *International Journal of Marine Energy*, 11: 84-104.

Ocean Energy ERA-NET (2017). "WP2 - Deliverable 2.6: Annual study of EU-OE sector development and opportunities," OCEANERA-NET.

Ocean Energy Forum (2016). "Ocean Energy Strategic Roadmap 2016, building ocean energy for Europe."

Ocean Energy Systems (2017). "OES Annual Report."

OES (2003). "Annex II Report 2003," IEA, Ocean Energy Systems.

OES (2015). "International Levelised Cost of Energy for Ocean Energy Technologies," Ocean Energy Systems.

O'Hagan, AM, Huertas, C, O'Callaghan, J, and Greaves, D (2016). "Wave energy in Europe: Views on experiences and progress to date," *International Journal of Marine Energy*, 14: 180-197.

Pascal, RC, Payne, GS, Gorintin, F, and Cliquet, V (2018). "The right size for a WEC: a study on the consequences of the most basic design choice," *International Ocean Energy Conference.* Cherbourg: ResearchGate.

Ruehl, K, and Bull, D (2012) "Wave Energy Development Roadmap: Design to Commercialization," *Oceans '12 MTS/IEEE.* Hampton Roads, VA: USA.

SET Plan (2018). "Ocean Energy - Implementation Plan," Set Plan Temporary Working Group.

The Carbon Trust (2011). *Accelerating marine energy: The potential for cost reduction.* London: The Carbon Trsut.

The European Marine Energy Centre Ltd. (2015). "Pelamis wave power," Retrieved from EMEC: http://www.emec.org.uk/about-us/wave-clients/pelamis-wave-power/

US Department of Energy (2016). "How does the Wave Energy Prize calculate ACE?" Retrieved from Wave Energy Prize Blog: https://waveenergyprize.wordpress.com/2016/08/18/how-does-the-wave-energy-prize-calculate-ace/

Weber, J (2012). "WEC Technology Readiness and Performance Matrix - finding the best research technology development trajectory," *17th International Conference on Ocean Energy*. Dublin: ICOE.

WES (2019). "Two Scots Firms Secure £7.7m Funding," Retrieved from Wave Energy Scotland: https://www.waveenergyscotland.co.uk/news-events/two-scots-firms-secure-77m-funding/

Preliminary hydrodynamic assessment of Mocean Energy's *Blue Star* WEC via fast-turnaround physical model testing

Andrea Caio, Thomas Davey, and J. Cameron McNatt

Abstract—**Wave energy developers are increasingly moving towards beachhead markets that do not require megawatt-scale machines, as a strategy to overcome commercialisation barriers, by accelerating deployment, learning, and intermediate returns. Mocean Energy's embodiment of this approach is an off-grid 10kW rated wave energy converter (WEC), Blue Star. This paper focuses on the tank testing of a 1:20 scale physical model as part of Mocean's wider route-to-market strategy. Experimental results from an early geometry iteration are presented. Tests were carried out at the University of Edinburgh Curved Tank facility and centred on validating the WEC's predicted hydrodynamic response, involving regular waves of full-scale equivalent conditions up to 8.4s in period and 1.7m depth-corrected wave height. Results are compared to numerical predictions and linked back to Mocean's design targets, leading to a discussion on the role of small-scale physical model testing in accelerating WEC performance optimisation. Tentative technical solutions are proposed to improve the efficiency and effectiveness of such testing during future design iterations. The role of physical model testing in accelerating commercial deployment is also considered.**

Keywords—**Accelerated innovation, beachhead markets, commercial deployment, off-grid devices, physical model testing, wave energy.**

INTRODUCTION

ALTHOUGH wave energy research has primarily aimed to culminate in utility scale[95] devices capable of supplying TWh of electricity to national grids, no grid-connected wave energy converter (WEC) was operating at the time of writing, to the authors' best knowledge. A definition of 'commercial' is found in [1] specifying the "potential to be sustained solely on the basis of private investment by offering a sufficiently attractive investment opportunity".

Commercial success has been elusive for the wave energy sector. Numerous concepts and implementations have been attempted [2], but few without public financial support, and even fewer with sustained commercial returns. The UK flagship projects of Pelamis and Aquamarine Power fell into administration in 2014 and 2015 respectively [3]. The Pico WEC in Portugal, and Wello Oy's Penguin are examples of locally grid-connected demonstration projects, but neither is currently active [4], [5]. Many other, more or less advanced WEC prototypes are being developed around the world; the above is by no means an exhaustive list.

To help identify the challenge, the key elements of the commercialisation roadmap are represented in Fig. 1 (circles). The associated *wave energy paradox* illustrates how the challenge is not singular, but rather a circular negative reinforcement mechanism [6]. A lack of available capital and policy support hinders the ability of developers to deploy WECs at sea, from which performance and reliability data can be collected. This, in turn, hinders the often cited *learning-by-doing* process that allows performance evidence building, cost cutting, and commercial returns since the device is not sufficiently developed to output monetary value. As a result, private investment is not forthcoming due to high associated uncertainty and risk, while policy tends to favour different renewable technologies that can already compete at utility scale with more conventional forms of energy, such as

ID Number 1951, Track WDD. This work was supported by the Engineering and Physical Sciences Research Council (EPSRC) under grant EP/J5000847/1. The views in this paper are not necessarily those of EPSRC. The authors also gratefully acknowledge the support and data access granted by Mocean Energy Ltd.

A. Caio is an EngD candidate at the Industrial Doctorate Centre on Offshore Renewable Energy (IDCORE), researching in collaboration with Mocean Energy, and based at the School of Engineering, The University of Edinburgh, Sanderson Building, Robert Stevenson Road, Edinburgh, EH9 3FB, U.K. (e-mail: andrea.caio@ed.ac.uk).

T. Davey is Senior Experimental Officer at the FloWave Ocean Energy Research Facility, at The University of Edinburgh, Max Born Crescent, King's Buildings, Edinburgh, EH9 3BF, U.K. They are also a member of Edinburgh University's Institute for Energy Systems. (e-mail: tom.davey@flowave.ed.ac.uk).

J. C. McNatt is the Managing Director and co-founder of Mocean Energy Ltd., Murchison House, West Mains Road, Edinburgh, EH9 3LA, U.K. (e-mail: cameron.mcnatt@mocean.energy).

[95] Utility scale implies grid connection and typical rated capacities in the MW range. In this paper, 'scale' is used to refer to the physical size or rated capacity of a WEC, as opposed to the scaling up from a single device to an array or farm of devices.

offshore wind. The challenge is to transform this feedback cycle into a positive one.

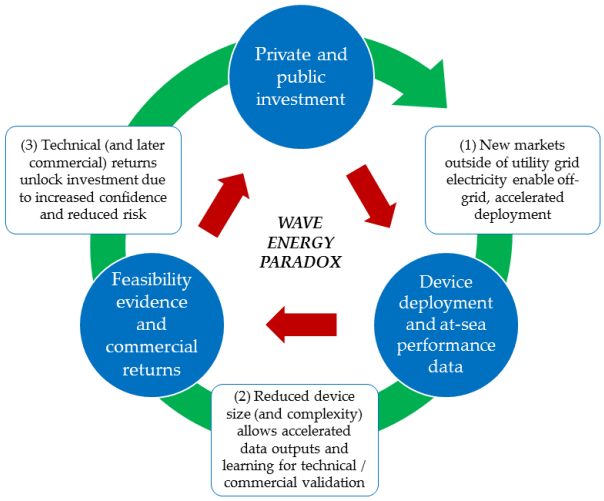

Fig. 1. The wave energy paradox: primary elements are circled; boxes represent potential enabling bridges that can arise from targeting 'beachhead markets'.

A fundamental way of tackling the paradox is via what are often termed 'alternative', 'intermediate', or 'beachhead' markets – i.e. the idea of using sub-utility-scale WECs for off-grid applications. This approach theoretically offers several benefits, illustrated in the boxes of Fig. 1: lower capital costs and risk due to reduced WEC size; accelerated learning via facilitated deployment; sooner revenue generation due to greater independence from public funding. A comprehensive discussion of how high capital costs can be offset to enable WEC development via alternative markets can be found in [7]. Reference [8] highlights how developers in the past have been tempted to fast-forward development from single kW-scale prototypes to MW-scale demonstration devices operating in highly energetic climates, "possibly omitting important intermediate development steps", and thus falling into the trap of survivability complications, a lack of at-sea experience, and the capital impact of iterative designs at large scale. Off-grid advantages such as avoiding grid integration cost can also be significant, as found in [9] and [10]. However, a key prerequisite to this approach is engaging appropriate and willing end-users that necessitate kilowatts of energy in offshore locations (see Section II).

Though still pre-commercial, Scotland-based Mocean Energy (henceforth just "Mocean") is making promising strides towards commercial deployment. The next section builds on this context by introducing Mocean's means of targeting beachhead markets, via a novel WEC called *Blue Star*. The paper then turns to a specific aspect of *Blue Star*'s development: early-stage physical model testing, with a focus on fast-turnaround (Section III). Section IV briefly describes the testing methodology and set-up for a hydrodynamic assessment of an early *Blue Star* iteration. Section V presents experimental results. Tentative conclusions that point to future focus areas are offered in the final section, where the role of small-scale physical testing in streamlining design process and performance optimisation is also considered.

Case Study – Blue Star

Mocean seeks to tackle the wave energy paradox by targeting the oil and gas (O&G) and ocean observation markets, effectively treating these as beachheads to exploit the enabling bridges enclosed in the boxes of Fig. 1. In this context, *Blue Star* would provide in-situ power to: (i) improve monitoring and communication strategies at sea (data gathering and exchange); (ii) charge autonomous underwater vehicles (AUVs); (iii) act as a source of primary of back-up power by replacing O&G 'tiebacks' (i.e. power cables that feed subsea wells).

Market details and *Blue Star*'s potential within them are not discussed here in-depth. However, the ability to provide uninterrupted in-situ subsea power in remote locations is a distinctive feature of wave energy that feeds into numerous sectors forming the much acclaimed and ever-expanding Blue Economy [96] [11]. Aquaculture, navigation, climate change forecasting, marine protected areas (MPAs), deep sea mining, offshore platform decommissioning; all these activities fundamentally rely on the availability of power and ocean data-gathering capabilities.

Blue Star builds on Mocean's original WEC concept – initially referred to as *M100* – currently in the third stage of the Wave Energy Scotland (WES) competitive procurement programme for Novel WECs (NWEC3). The WEC is a floating hinged raft, featuring asymmetric hulls with a submerged nose and tail ("wave channels") that project into the wave flow. When excited by waves, the induced relative motion of the hulls is converted into electrical power by an electro-magnetic generator located at the hinge, parallel to the wave crests, as seen in Fig. 2. The implemented geometric innovations have the combined effect of broadening the frequency response, as the WEC is sensitive to wavelengths that far exceed its total length. The geometric innovations and operating principles are described in greater detail by Mocean's co-founders in [12] together with an overview of numerical modelling, optimisation and past experimental validation.

[96] Defined as: "the sustainable use of ocean resources for economic growth, improved livelihoods and jobs, and ocean ecosystem health".

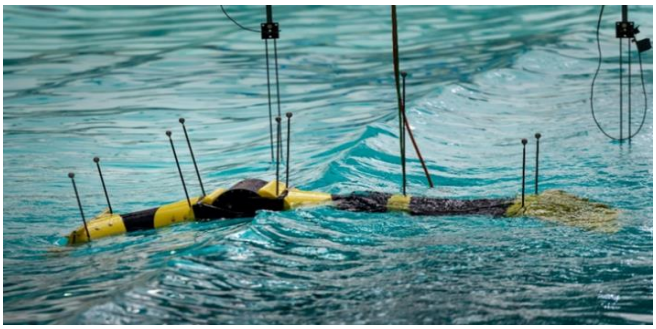

Fig. 2. Scaled model of the *M100*, tested at the FloWave facility in Edinburgh (waves travel right to left). [Courtesy of Mocean Energy]

Having been awarded over £3m by public body WES [13], Mocean is deploying a half-scale 10kW-rated prototype WEC – *Blue X* – for open water testing at EMEC during spring-summer 2021 [14]. Following NWEC3 testing completion, it will be used as part of a demonstrator project alongside companies Chrysaor, EC-OG, and Modus [15]. Mocean has also recently closed a £850k investment round [16]. *Blue Star* is effectively an evolved version of *Blue X*, also rated at 10kW.

Fig. 3. *Blue X* prototype during final assembly at Rosyth, Scotland (The front wave channel is visible on the quayside). [Courtesy of Mocean Energy]

Role of Physical Model Testing

The physical modelling and experimental testing of a WEC is an essential link in wave energy development. Even a miniature reproduction of a physical system can help to understand complex fluid behaviour. The purpose of physical modelling spans (from [17]):

- Validating numerical model predictions and tuning analytical parameters (*validation* model)
- Modelling complex behaviour (e.g. nonlinearities) without the simplifying assumptions embedded in analytical or mathematical representations (*design* model)
- Exploring specific response details that are not yet understood or theoretically modelled (*process* model)

The fundamental challenge lies in simultaneously addressing simplicity (reduce costs and maximise ease of manufacture, assembly, handling and testing) and representability (including the most important aspects of the problem). Traditionally, the complexity (and scale) of a physical model increases as the various subsystems forming the overall device crystallise – i.e. as Technology Readiness Level (TRL) increases. This is accompanied by increasing predictive accuracy of – and confidence in – the obtained results. However, in practice, this is not a linear evolution process. Iteration and feedback are key because numerical models, physical models, product specifications, user-needs, and available subsystems technology (e.g. PTO) typically also evolve and consolidate over time. For Mocean, this is especially true due to the following:

- Target markets are new and not well explored – requirements crystallise as commercial relationships are formed and develop. Many design inputs (e.g. minimum continuous power requirements, AUV interfacing) will be more ad hoc compared to a grid connected WEC.
- Avoidance of premature freezing of the WEC design. This enables accommodation of different subsystems as their relevant technology develops (e.g. novel moorings [18], and novel PTO [19]), effectively embracing a *performance* ahead of *readiness* approach [20].
- Mocean's in-house optimisation routine rapidly generates new prime mover geometries based on input requirements and constraints [12]. The underlying model is linear, so nonlinearities must be captured via physical testing.
- Proximity to tank testing facilities – relatively available and economic in the case of Edinburgh University's Curved Tank (CT) (see Section IV) – makes physical model testing a more readily deployable design tool.

Hence, fast turnaround and small scale are attractive characteristics for Mocean's physical modelling strategy. Overall turnaround can be accelerated by including more subsystems at earlier development stages. At the same time, shrinking the physical models in scale allows cost reduction and maximisation of available testing facilities. In a sense, this mirrors the wave energy paradox transformation, where the levers of markets and of scale are used to unlock more learning, more quickly. However, associated risks such as exposure to undesired scaling effects and similitude inconsistencies should be considered (Section VI).

Testing Methodology

A 1:20 Froude-scaled validation model was tested to verify the numerically predicted hydrodynamic response of *Blue Star*'s prime mover. Testing was carried out in accordance with IEC published guidelines for testing of pre-prototype devices [21], specifically Stage 1 ("Concept model"; TRL 1-3).

Regular wave sweeps allowed verification of response amplitude operators (RAOs) and a preliminary estimation of drag and nonlinear losses. A small number of long-crested irregular waves was also run to qualitatively observe the WEC's behaviour in more realistic seas – these are not discussed further. The model is passive; it has a freely rotating hinge with two roller bearings at port and starboard sides of the nacelle (see Fig. 4), and no PTO

damping. A paper discussing mooring behaviour in survival seas with a later geometry iteration of Blue Star is also being submitted based on tests carried out by the COAST Laboratory at Plymouth University [22].

Testing was carried out in late 2019. *Blue Star*'s geometry has since evolved, though this represented an important anchor point for physical assessment. Fig. 4. Shows the coordinate definition of the model; the power producing degree of freedom (DoF) being the relative pitch between forward and aft hulls. Fig. 5. Shows the model as built. The overall mass of the model was 2,029g (including ballast and ~5% additional mass from water uptake during testing). It was 578mm long, 115mm wide, with maximum draft of 578mm below the mean water line (MWL). The hinge axis was nominally 5.9mm below the MWL (and increased to 7.5mm following trimming and minor water uptake).

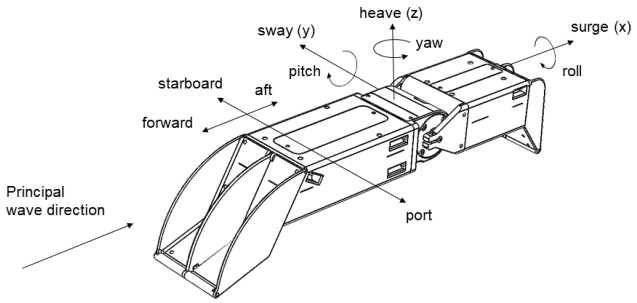

Fig. 4. Coordinate definition of Blue Star model; origin located at hinge (pitch) axis midpoint.

Model build

The model was built for simplicity, cost minimisation, and fast turnaround. From Fig. 5., yellow components are stereolithography (SLA) 3d-printed ABS material components, black are anodised Aluminium alloy components. 'Lids' in each hull and nacelle are visible in Fig. 4., covering a void that allows trim correction via appropriate placement of ballast. Ballast – in the form of dense Lead sheets or light closed-cell polystyrene cut outs – can additionally be applied to the underside of each wave channel via bolts. Qualisys® motion tracking targets are included above each hull, and a 360° inductive non-contact rotary position sensor [23] is placed within the nacelle. The latter was included for two reasons. It served as a complementary pitch rotation reading in case of Qualisys drop-outs, and would allow primary DoF measurement should the presence of Qualisys targets be deemed overly influential on model responses.

Wave tank

The Curved Tank facility at the University of Edinburgh was used for this test campaign. It has a nominal water depth of 1.2m, and paddle depth of 0.7m. There are 48 wavemaker paddles across a 9 metre arc capable of generating uni- and multi-directional (+/- 30°) sea states [24]. The tank manual quotes three nominal operating points (wave height, H / wave period, T): 0.220m / 1.0s; 0.075m / 2.0s; 0.060m / 0.5s; with an operating peak period around 1s. An empirically derived tank operating envelope for regular waves, with plotted stroke and steepness limited curves, is shown in the Appendix Fig. 10.

Sea states

Given limited available tank time, tests were conducted at transects though the frequency-amplitude space. In other words, the approach was that of sweeping across frequencies at a chosen amplitude, then sweeping in amplitude at a chosen frequency.

Regular wave sweeps were carried out at three constant steepness (height, H / wavelength, λ) values: 1/60, 1/180, 1/120. Running sweeps at constant steepness removed linearity changes by keeping the wave geometry constant. Three values were chosen to give an indication of nonlinear wave effects and a trend to be captured. The values were selected based on previous wave channel tests (to enable direct comparisons) and on the wave climate steepness mode (1/53 for the North Sea location of interest). 1/60 steepness is estimated to be within the tanks capability range, but higher steepness values are not tested to avoid potential wave breaking and splashing effects.

Each sweep contained 20 sea states at frequencies between 0.53Hz and 2.00Hz. The peak response frequency at model scale was predicted to occur around 0.94Hz. The amplitude sweep was therefore carried out at this frequency, with a maximum demand amplitude of 36mm (non depth-corrected). The overall maximum depth corrected demand amplitude in the 1.60 sweep was 41.8mm at model scale (1.67m full scale wave height). Amplitude depth correction was applied, albeit minor.

The sampling frequency was 128Hz, and a trigger signal was set up in order to synchronise wave gauges and model motion data capture.

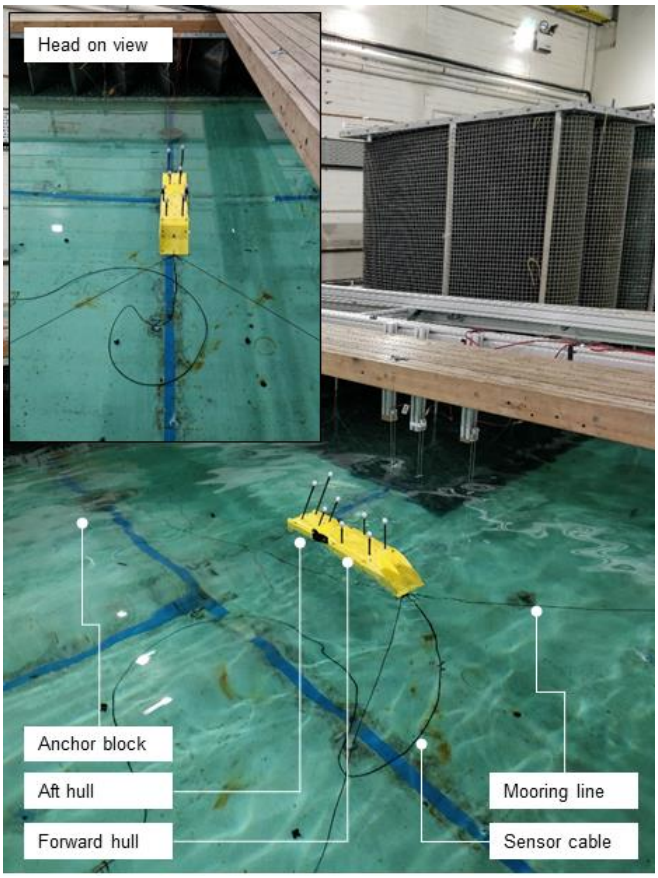

Fig. 5. Showing moored model deployed in the Edinburgh University Curved Wave Tank. Qualisys motion tracking targets are visible above each hull. Wave travel from the bottom right, and from the bottom in the inset image.

Mooring system

A generic station keeping system was used, since mooring behaviour is not an integral part of the device's hydrodynamic motion and energy conversion scheme [21]. It consisted of three 2.1m length lines, equi-spaced at 120° around a mooring circle of 4m diameter.

Two lines extended in front of the model, each at 60° to the incident wave direction, and one line extended behind the model in line with incident waves (see Fig. 11. Appendix). Each line was anchored via simple gravity bases (concrete block with steel rings). The lines attach to the model via independent karabiners, which clip to a stainless steel ring at the lower lip of the forward wave channel. The lines were highly compliant and some pretension was applied in order to shift the operating point towards the linear section of their characteristically S-shaped load-response curve. The calculated resonant period of the mooring system was 12.9s.

Measurement set-up

Measured variables (and associated sensors) included: incident waves (via 3 wave gauges); 6 DoF model motion (via 4 Qualisys motion capture cameras); relative pitch angle between the hulls, referred to as 'flex' (via rotary sensor).

The first wave gauge was approximately coincident with the model mooring points, and the other two spanned the space occupied by the model in the tank. Wave gauge calibration errors throughout testing were around 1.0% and never exceeded 2.0%. Though approximately neutrally buoyant, the sensor cable had non-zero rigidity and torsional stiffness which affected the static yaw of the model. However, the model realigned with oncoming waves once they started travelling towards it.

The data acquisition sampling frequency was 128Hz, and a trigger signal was set up in order to synchronise wave gauges and model motion data capture.

Experimental Results

Reflection analysis

Being a finite body of water, the Curved Tank is subject to wave reflection effects. These were quantified ahead of model tests in order to estimate their effect on obtained RAOs, using the Suryanto method [25] and the Lin and Huang method [26] embedded in WaveLab© software. 3 in-line wave gauges were used, meaning that 3D effects were not captured. A reflection coefficient, *R*, is defined as the ratio of reflected wave amplitude over the incident wave amplitude. These 'open-tank' (i.e. model not present) incident wave amplitudes are then used to calculate RAOs, since the model's presence in the tank affects wave gauge signals during model response runs.

Reflection analysis yielded average values of *R* around 0.09, 0.10, and 0.13 for 1/60, 1/80, and 1/120 steepness sweeps. *R* values around 10% are deemed tolerable from a validation point of view. As expected, *R* values tended to increase at lower steepnesses given the lower amplitudes and thus greater noise sensitivity. Robust agreement was observed between the two analysis methods, and no significant difference was observed when comparing associated RAO plots.

Power producing degree of freedom response

The model's hydrodynamic response is characterised via RAO plots, where for a given DoF, the RAO represents the associated amplitude response, divided by the incident wave amplitude. The power producing DoF is flex (i.e. relative pitch angle) and has units of degrees per meter (deg/m), though other RAOs are useful from a validation standpoint. Fig. 6. shows that:

- Two peaks are detected. The first, larger peak around 3.5s full-scale period; the second, smaller peak around 5.5s.
- The peaks are higher at lower wave steepness, i.e. for waves that are more linear.
- There is a shift of the large shorter wavelength peak to wavelengths shorter still as the wave amplitude increases (i.e. as the steepness increases). This effect was also observed in testing carried out at École Centrale de Nantes (France) with a 1:10 scale *Blue Star* model.

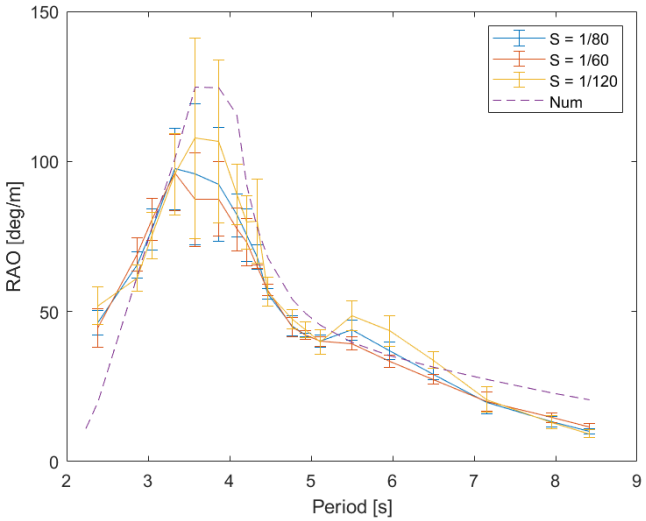

Fig. 6. Comparison between Flex RAOs obtained from rotary sensor readings at each steepness sweep, and numerical model predictions. Full-scale values shown.

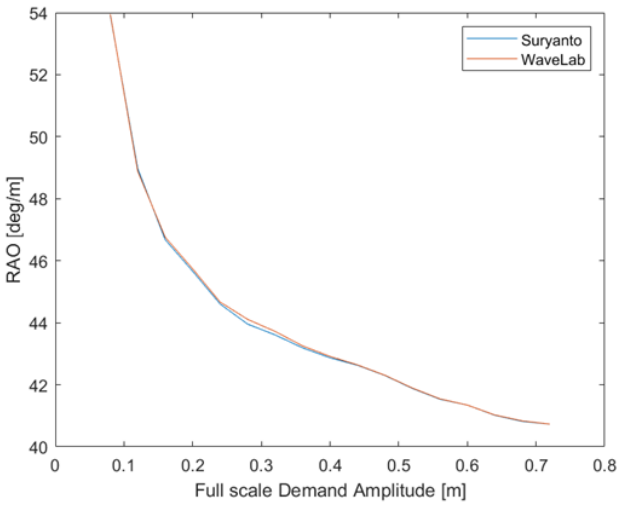

Fig. 7. Change in calculated Flex RAO at peak period over a range of demand amplitudes (based on *R* values from Suryanto and WaveLab methods).

Fig. 6. also includes the numerically computed RAO. For a like-for-like comparison, the numerical model is updated with mass matrix values extracted from the CAD representation of the model as-built, including ballasting. A good fit can be observed between curves and the main tuning peak occurring just below 4s. Note also that excellent agreement was observed between Qualisys and rotary sensor flex measurements.

The numerical RAO includes approximated linear damping associated with the wave channels and viscous losses (Morrison's, i.e. fluid drag). It does not include PTO damping as the hinge is free during the experimental runs. There is no PTO with its nonlinear torque limit in this model, so the observed nonlinearity with wave amplitude is a consequence of the wave-body interaction alone.

The small peak at the longer wavelengths is very distinct in the tests but not in the numerical curve. Numerical results with no damping show this peak strongly so presumably this has implications for the assumed Morrison's damping coefficient, which is set to an initial value of 1.

Fig. 6. shows error bars corresponding to the average *R* value for each sea state. There are significant, particularly in the case of 1/120 steepness where the error bar is approximately +/- 30% corresponding to +/- 34deg/m, around 3.58s full-scale period.

Fig. 7. shows RAO values dropping off as the demand amplitude (and the wave steepness) increase, for a set frequency of 0.94Hz at model scale, i.e. 4.77s period full-scale. This is due to waves becoming less linear as amplitude increases, since the steepness is also increasing. For reference, full-scale demand amplitudes ran in the regular wave frequency sweeps were 0.30m, 0.44m, and 0.59m; pertaining to the flatter part of the curve in Fig. 7.

All degree of freedom responses

The model response in surge, sway, heave, roll, and yaw are compared, as well as pitch. Note that the pitch plot contains separate forward and aft hull responses. In all other cases, the response of the two hulls is identical since they are effectively behave as a single body.

Observed out of plane motions arise due to the centre of mass of forward and aft hulls not being aligned with the long axis of the model (see Fig. 8.). The inertia matrix exhibits cross terms, leading to non-zero values of yaw, roll and sway RAOs. In the case of yaw and sway, the experimental results are greater as the model is not perfectly aligned with incoming waves, as is instead the case in numerical simulations. Yaw (and to a lesser extend, roll) variation are affected by the electrical cable run-off path from model to tank floor. The cable moves most in the lowest frequency waves, and in the irregular wave sweeps. In these conditions, it very slightly rises off the tank floor (near the point where the cable initially meets the floor) as waves travel past the mooring attachment point and the forward hull pitches. Fig. 9. again shows strong agreement between experimental and numerical hydrodynamic responses, based on the lowest steepness sea states.

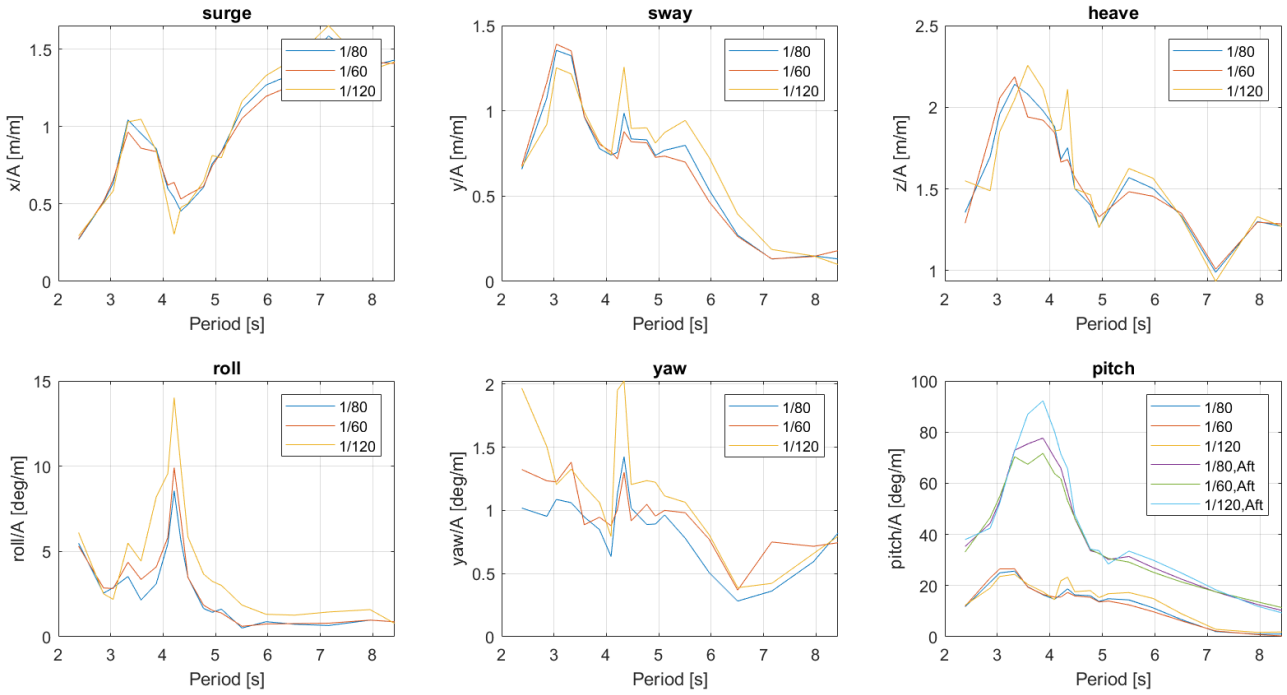

Fig. 8. Full-scale RAOs for all DoF's at each steepness; obtained from Qualisys data. 'A' refers to the wave incident amplitude.

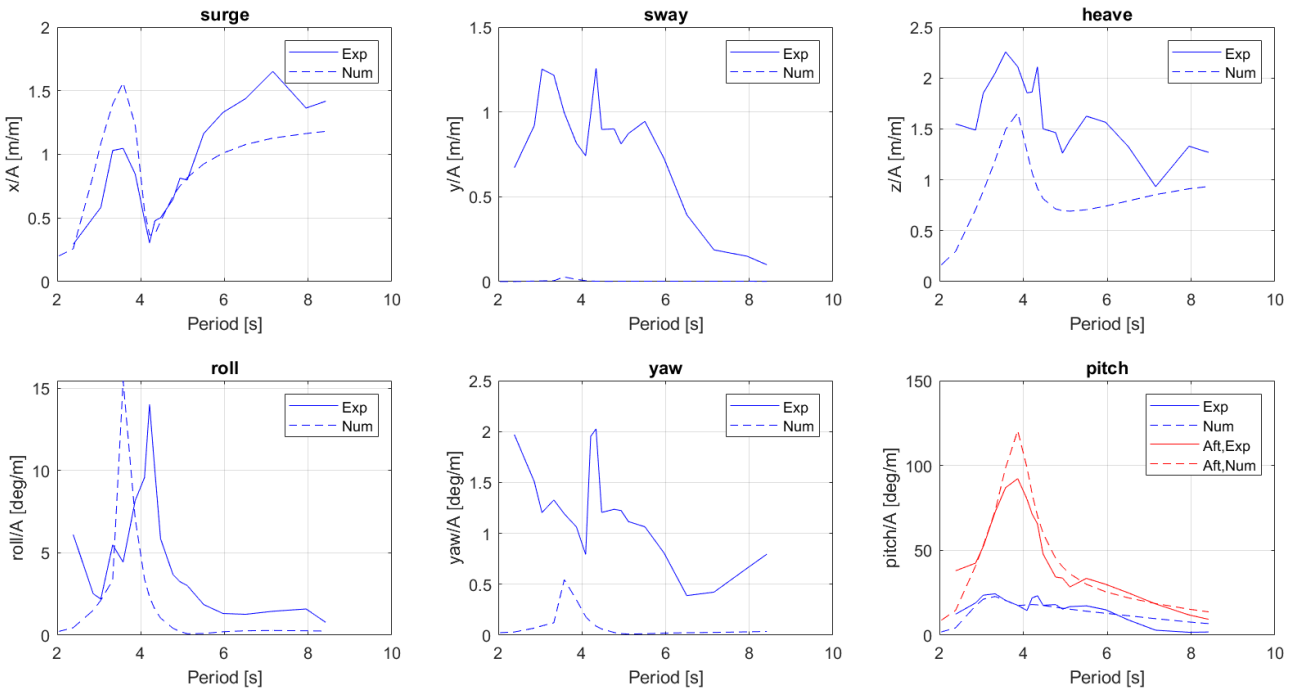

Fig. 9. Comparison of full-scale numerical and experimental RAOs for all DoF's at 1/120 steepness; obtained from Qualisys data. 'A' refers to the wave incident amplitude

Discussion and Further Study

The flex RAO, as well as other DoF's allowed validation of the numerical model. Overall, there is good agreement between experimental and predicted RAOs, with lower steepness runs matching numerical results more closely, as expected from a wave linearity perspective.

Robust agreement between rotary sensor and Qualisys data provides flexibility for future test set ups. The two systems impact model mass and inertial properties differently. Qualisys targets raise the model's centre of mass (CoM), which increases the likelihood of roll instability that depends on the centre of buoyancy (CoB) being located vertically below the CoM. On the other hand, the sensor cable can affect roll and yaw even if neutrally buoyant, though these effects were found to be negligible in this particular set of tests. If testing in irregular waves, particularly spread seas, Qualisys inclusion is worthwhile in order to capture motion responses beyond flex. Additional DoF's can offer insights on survivability (e.g. dynamic instabilities) and overall hydrodynamic efficiency. The presence of the additional cable may also become more relevant for such tests with more dynamic responses.

Static trimming errors can occur with a smaller model that offers less surface are and locations for trim adjustment via ballasting or model design. In this campaign, a static roll trimming error of ~1.5° - observable by eye – had a ~1% effect on the peak pitch RAO value, and was thus negligible.

The following next steps are considered:

- Performing a reflection analysis using 4 or 5 wave gauges, as well as deploying 3 wave gauges on the port or starboard side of the model along the incident wave direction, would allow a more accurate mapping of reflection coefficients, and to capture associated 3D effects. Though mostly approximating 0.1, reflection coefficients introduced relatively large error bars in the flex RAO.
- A set of tests in Edinburgh University's 2D Flume Tank to reduce reflection – particularly 3D – effects, allowing greater confidence in the obtained RAO curves and a more accurate tuning of the Morrison's damping coefficient used in the numerical model.
- More detailed evaluation of the impact of Qualisys targets on hydrodynamic responses. According to the model's CAD representation, Qualisys targets added 74.0g to the overall mass, and shifted the model's CoM by 1.12mm, -0.15mm, and 4.21mm along positive x, y, and z axes (refer to Fig. 4.). The latter is of particular significance.

In the case of Mocean's *Blue Star*, the round of testing presented in this paper has provided a valuable baseline on which to build model complexity, by providing confidence that robust data can be collected at 20th scale, with an easily accessible wave tank. By combining conversion stages in future tests, the idea is to shortcut towards assessing overall model performance via a *design* model that does not necessarily require larger scale or larger tanks; or at least delaying this need until performance predictions are deemed sufficiently high, and readiness becomes the driver for further testing.

APPENDIX

The following figures relate to the Curved Wave Tank used throughout the tests. Fig. 10. shows the empirically derived operating envelope for regular waves. 'CT specified' points relate to nominal tank values, while 'Interp' is an interpolation curve of measured amplitude points along the stroke limit (with reflection effects accounted for), and a steepness limited portion at frequencies greater than 1Hz. Fig. 11. shows a circular area overlaid in the tank's water basin. The centre of the circle indicates the model's static location, the perimeter and dotted lines show the mooring line orientation and mooring circle diameter.

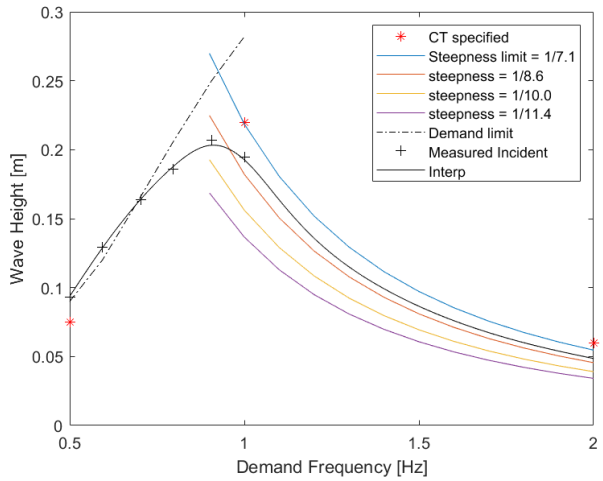

Fig. 10. Empirically derived Curved Tank operating envelope for regular wave generation.

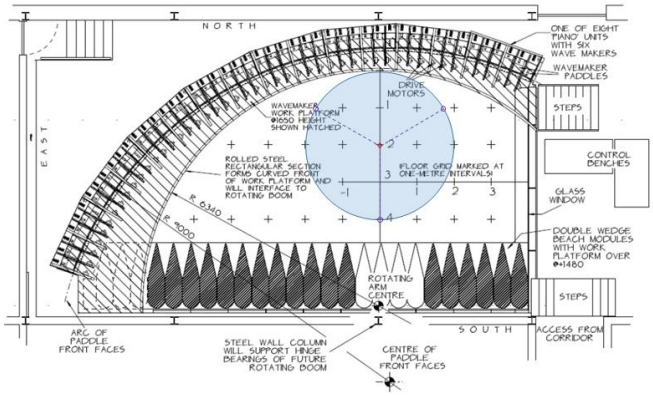

Fig. 11. Showing Curved Tank layout, with model position and mooring layout overlaid. [Adapted from: Curved Tank operating manual]

ACKNOWLEDGEMENT

This study was funded by the Engineering and Physical Sciences Research Council (EPSRC) IDCORE award EP/J5000847/1. The authors gratefully acknowledge the support and data access granted by Mocean Energy Ltd. Chris Retzler provided extensive inputs to the physical model design and planning stages. FloWave staff members also provided valuable assistance during the test setup process, particularly Roman Gabl with the Qualisys system. The physical model build was funded under a Scottish Enterprise SMART grant.

REFERENCES

ETIP Ocean, "Deliverable 2.1: An integrated framework of ocean energy sector challenges," European Commission, Brussels, 2016.

N. Blažauskas, A. Pašilis and A. Knolis, "Potential implementations for small scale energy converters," *Renewable and Sustainable Energy Reviews,* vol. 49, pp. 297-305, 2015.

The European Marine Energy Centre, "Pelamis wave power," 2015. [Online]. Available: http://www.emec.org.uk/about-us/wave-clients/pelamis-wave-power/. [Accessed 18 3 2021].

MarineEnergy.biz, "Pico wave power plant caves in," 23 4 2018. [Online]. Available: https://marineenergy.biz/2018/04/23/pico-wave-power-plant-caves-in/. [Accessed 18 3 2021].

Wello Oy, "Wello launch Penguin WEC2 for H2020 CEFOW array," 7 12 2018. [Online]. Available: https://wello.eu/2018/12/07/wello-launch-penguin-wec2-for-h2020-cefow-array/. [Accessed 18 3 2021].

A. Caio, T. Davey and J. C. McNatt, "Tackling the wave energy paradox: stepping towards commercial deployment," in *29th International Ocean and Polar Engineering Conference*, Honolulu, Hawaii, USA, 2019.

S. Foteinis and T. Tsoutsos, "Strategies to improve sustainability and offset the initial high capital expenditure of wave energy converters (WECs)," *Renewable and Sustainable Energy Reviews,* vol. 70, pp. 775-785, 2017.

A. MacGillivray, H. Jeffrey, M. Winskel and I. Bryden, "Innovation and cost reduction for marine renewable energy," *Technological Forecasting & Social Change,* vol. 87, pp. 108-124, 2014.

D. Magagna and A. Uihlein, "Ocean energy development in Europe: current status and future perspectives," *International Journal of Marine Energy,* vol. 11, pp. 84-104, 2015.

OCEANERA-NET, "Deliverable 2.6 – Annual study of EU-OE sector development and opportunities: Updated 2017," 2017

The World Bank, "What is the Blue Economy?" 6 6 2017. [Online]. Available: https://www.worldbank.org/en/news/infographic/2017/06/06/blue-economy. [Accessed 18 3 2021].

J. C. McNatt and C. H. Retzler, "The performance of the Mocean M100 wave energy converter described through numerical and physical modelling," in *European Wave and Tidal Energy Conference*, Naples, Italy, 2019.

Wave Energy Scotland, "Two Scots firms secure £7.7m funding," 8 1 2019. [Online]. Available: https://www.waveenergyscotland.co.uk/news-events/two-scots-firms-secure-77m-funding/. [Accessed 18 3 2021].

Offshore Engineer, "Mocean to test Blue X wave energy converter at EMEC," 29 01 2021. [Online]. Available: https://www.oedigital.com/news/484926-mocean-to-test-blue-x-wave-energy-converter-at-emec. [Accessed: 18 3 2021]

Offshore Energy, "Mocean's wave power for subsea tiebacks and AUVs," 10 02 2020. [Online]. Available: https://www.offshore-energy.biz/moceans-wave-power-for-subsea-tiebacks-and-auvs/. [Accessed 18 3 2021]

Energy Voice, "Scottish start-up Mocean Energy raises £850k to bring wave power to subsea oil and gas," 18 11 2020. [Online]. Available: https://www.energyvoice.com/renewables-energy-transition/279796/scottish-start-up-mocean-energy-raises-850k-to-bring-wave-power-to-subsea-oil-and-gas/. [Accessed 18 3 2021]

S. A. Hughes, "Physical models and laboratory techniques in coastal engineering," in *Advanced Series on Ocean Engineering – Volume 7*. World Scientific, 1993.

European Marine Energy Centre, "Press Release: WES awards £1.4 million for wave energy connection systems," 17 7 2020. [Online]. Available: www.emec.org.uk/press-release-wes-awards-for-wave-energy-connection-systems/. [Accessed: 18 3 2021]

Mocean Energy, "Mocean Energy selects C-GEN technology for wave power take-off," 20 08 2019. [Online]. Available: https://www.mocean.energy/mocean-energy-selcts-c-gen-technology-for-wave-power-take-off/. [Accessed: 18 3 2021]

J. Weber, "WEC Technology Readiness and Performance Matrix – finding the best research technology development trajectory," in *17th International Conference on Ocean Energy*. Dublin, Ireland, 2012.

IEC. Marine energy - Wave, tidal and other water current converters - Part 201: Tidal energy resource assessment and characterization, IEC TS 62600-201:2015.

T. Tosdevin, S. Jin, A. Caio, D. Simmonds, M. Hann, and D. Greaves, "Extreme responses of a raft type WEC," in *14th European Wave and Tidal Energy Conference*; under review, Plymouth, UK, 2021.

Gill Sensors & Controls, "1498 Rotary Position Sensor," [Online]. Available: https://www.gillsc.com/products/position-sensors/1498-rotary-position-sensor/. [Accessed: 18 3 2021]

The University of Edinburgh, "The Curved Wave Tank," [Online]. Available: https://www.eng.ed.ac.uk/research/facilities-and-resources/small-research-facilities/curved-wave-tank. [Accessed: 18 3 2021]

A. Suryanto, "Estimation of incident and reflected waves in irregular wave experiments," *Journal of Indonesian Mathematical Society*, vol. 12, pp. 141-152, 2006.

C-Y. Lin, C-J. Huang, "Decomposition of incident and reflected higher harmonic waves using four wave gauges"," *Coastal Engineering*, vol. 51, pp. 395-406 , 2004.

UK Parliament POST

POSTNOTE

Number 642 April 2021

Sustainable cooling

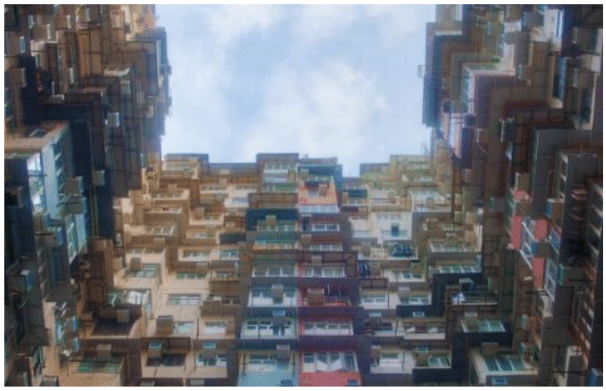

Cooling in buildings, industrial processes and supply chains accounts for 7% of global greenhouse gas emissions (GHGs) from the use of energy and refrigerants. Demand for cooling is forecast to rise further, presenting challenges for meeting climate change goals.

Overview

- Cooling is key to public health, food security and productivity. It provides thermal comfort in buildings, prevents overheating, avoids food waste, and keeps vaccines safe.
- Cold can be provided by avoiding heating (through buildings' design) or using technologies such as air conditioning. The latter result in greenhouse gas emissions from refrigerants and power generation.
- Cooling is key to sustainable development, but access to it is unequal. The UK funds sustainable cooling projects abroad.
- There is relatively little cooling-specific UK policy beyond overheating and device efficiency. Building and cold chain policy changes can improve UK cooling provision.

Background

Cooling is a process that addresses a range of society's needs.[1] It provides thermal comfort in buildings, preventing risks from overheating, and is required to keep food fresh and medical products safe. A lack of access to cooling is a barrier to development and cooling has a role in all UN Sustainable Development Goals (SDGs), though it does not feature explicitly in any of them.[2–4] Recently, potential disruptions to food and vaccine provision have also increased awareness of the value of cooling in the UK and developed nations with milder climates.[5]

Under existing international emission pledges, average global temperatures could reach 3°C above pre-industrial levels by the end of this century.[6] Around 1°C of global warming has already taken place, with increasing severity, duration and frequency of extreme events, such as heatwaves, leading to localised spikes in temperature.[7–9] As the climate warms, global demand for cooling, including in the UK, is forecast to rise.[10] In developing countries often located at warmer tropical latitudes, socio-economic trends such as population growth, urbanisation and rising prosperity are further driving demand for cooling.[3,11–13]

Conventional cooling contributes to climate change in two ways. First, it often requires electricity or diesel, with associated carbon dioxide (CO_2) emissions (a GHG). Estimates of global cooling-related CO_2 emissions tripled from 1990 to 2018 (to 1,130 million tonnes, equivalent to the CO_2 emissions of Japan).[14] Second, many cooling systems use fluorinated gases (F-gases), which can be potent GHGs when they leak.[15] Cooling accounts for over 7% of global GHG emissions, compared with around 2% from aviation.[16–18] Inefficient cooling devices (like air conditioners) are common, and it has been predicted that global energy demand for cooling may match that of heating by 2060.[11,19] There has been relatively little focus on the growing energy demand for cooling compared with that of heating.[2,14] Reducing F-gas use in line with international agreements could avoid 0.4°C of warming by 2100.[20] Increasing global access to cooling therefore challenges GHG emission reductions if policy does not incentivise the use of approaches that minimise energy demand and F-gas use.[21,22]

Sustainable cooling includes approaches that aid climate change mitigation and adaptation, are affordable and accessible, and support the SDGs.[2,23] The UK has significant cooling research and innovation expertise and is a major contributor to cooling programmes abroad.[24–26] This POSTnote examines UK and global demand for different forms of cooling, ways of meeting it, and technology and policy options to do so more sustainably.

Demand for cooling

Cooling is used for indoor space cooling and cold supply chains ('cold chains'). It is also used in industrial processes and power generation.[27] In 2018 the size of the global market for refrigeration and air conditioning exceeded that of solar panels.[3] Global electricity demand for space cooling alone is forecast to triple by 2050.[14] Residential cooling is currently the largest source of total global demand. However, cooling demand is expected to grow fastest within the industrial and

The Parliamentary Office of Science and Technology, Westminster, London SW1A 0AA
02072192840 **post@parliament.uk** **parliament.uk/post** **@POST_UK**

transport sectors before 2030, mainly due to expanding cold chains,[3] particularly in India and other developing economies.[28] Cold chains currently account for 2–4% of UK GHG emissions.[28] The use of data centres in the UK may grow by 70% before 2050 with an associated growth in cooling demand.[29]

Box 1: Overheating risks and impacts

Overheating is difficult to predict with accuracy due to demographic, behavioural and building type dependencies.[30] UK risks in dwellings and public buildings are currently not well quantified.[8] Thermal models can be used to assess the likelihood of overheating in new and existing buildings; direct measurement is often more accurate but also more complex and time consuming.[31,32] Warmer locations and dense urban areas are typically exposed to higher risk.[33]

Health risks from heat stress

Extended periods of temperature above 25°C are associated with increased mortality, heatstroke and hospitalisation.[34] Chronic illness, older age and certain disabilities can increase risk,[33,35] and infants and rough sleepers are also vulnerable.[36] The Climate Change Committee (CCC) estimates that 2,000 heat-related deaths occur in the UK annually and project that this could grow to 7,000 by the 2050s without intervention.[8] It also found that 20% of UK homes currently overheat, even in mild summers.[37]

Productivity risks from thermal discomfort

Thermal discomfort is determined by factors such as air temperature and humidity,[38] as well as a person's subjective tolerance to heat.[39] It can negatively impact workplace and learning productivity, and sleep.[37] The 2003 heatwave is estimated to have cost £400–500m in UK manufacturing output.[8] Heatwaves are expected to intensify in the future.[40]

Loss in efficiency and capacity of infrastructure

Some IT and energy infrastructure relies on cooling. Thermal power plants (gas and nuclear) need cooling to function efficiently and a warmer future climate would reduce plant efficiency.[41] Servers in data centres also rely on cooling.[42]

Space cooling

Space cooling involves reducing indoor temperatures in response to heating from sunlight or internal sources (such as occupants, lighting and machinery). High temperatures can lead to overheating risks for occupants and infrastructure (Box 1).[27] Some cooling measures can improve indoor air quality by reducing humidity, aiding ventilation, changing airflow patterns or purifying air inflows.[43] This can mitigate indoor spread of airborne pathogens.[44] Space cooling accounts for nearly 20% of global electricity demand in buildings.[14] A 2016 study estimated that 10% of total UK electricity demand is for air conditioning (AC) – mostly in non-domestic buildings such as offices – and AC use in the UK grew an estimated 2% per year between 2012 and 2019.[45–48] Data on cooling demand is not routinely collected and modelling is often used to estimate demand.[30,33,47]

Cold chains

A cold chain is a system of temperature-controlled logistics in the supply chain of perishable products, primarily food and pharmaceuticals. These are cooled to maintain quality and prolong shelf-life. Cold chains comprise food processing plants, refrigerated warehouses ('cold stores'), supermarket cabinets and domestic refrigerators, as well as temperature-controlled vehicles.[49] UK cold chains include around 700 large cold stores and 30,000 vehicles,[50] and support more than 100,000 direct jobs.[49] Cold chains use chilled, frozen, and cryogenic (-70°C and lower) temperature ranges. Most food is chilled, but demand for frozen food is growing.[49] Cryogenic stores are mostly used in the medical sector (e.g. for certain vaccines).[51]

Cold chains underpin population health and security.[1,52] 70% of food in the developed world relies on cold chains.[1] In 2018, UK food trade included £24.5bn imports and £5.9bn exports of temperature-controlled products.[53] Globally, 25% of liquid vaccines and 200m tonnes of food are lost annually due to limited cold storage and refrigerated transport.[54,55]

Cooling and sustainable development

Cooling is needed to achieve each of the SDGs.[2,4] Over 1 billion people lack access to cooling,[5] which disproportionately affects less affluent groups in the Global South.[3] Worldwide, 72m full-time jobs are predicted to be lost as a result of climate induced heat stress,[56] and 90% of medical facilities lack access to modern cold chain equipment.[57] Broken cold chains lead to food loss and, in turn, malnutrition, as well as income loss.[54] In developing contexts they can lead to a widening gender gap, as a large proportion of agricultural workers are women and cold storage reduces time burdens from food provision trips.[58,59]

Approaches to cooling provision

Spaces and products can be cooled either by avoiding heat gains (through passive strategies or changing behaviour), or by actively sourcing, storing and distributing cold thermal energy.

Passive cooling strategies

Space cooling can often be provided passively, without using mechanical systems that require energy inputs.[60]

Building design

The combination of heat exposure, internal heat sources, insulation and ventilation affects a building's cooling demand.[45] Most heat enters a space via glazed areas (windows) and poor ventilation reduces the capacity to dissipate it. Shading (from blinds or shutters), and to a lesser extent light-coloured external surfaces, can reduce heat gains.[61] Novel types of glazing can also be effective thermal barriers.[62] Dense building materials such as brick can reduce temperature fluctuations during short-term heatwaves. Orientation also affects heat gains due to varying sun exposure.[61] High-rise flats are less able to reject heat due to their lower ratio of external surfaces to floor area.[63] When these are situated in less affluent areas,[64] poorer residents are often exposed to overheating risks,[61,65] and have the least ability to install and run cooling measures.[66]

Passive strategies depend on the local climate and raw material availability.[67] In many warmer countries, traditional architecture developed over generations uses passive cooling strategies.[67,68] In the UK, multiple tools exist to help planners identify and mitigate overheating risks in early-stage building projects.[66,69]

Urban heat islands and green infrastructure

Globally, cities are on average 5–9°C warmer than rural areas, due to the urban heat island (UHI) effect.[70–72] Artificial surfaces, such as concrete and tarmac, store heat during daylight hours and slowly release it, raising night-time temperatures.[36] Increasing urban vegetation (re-greening) has been shown to lower air temperatures.[73–75] Parks, street trees, green walls and

roof gardens ('green infrastructure') can provide the co-benefits of improved air quality, biodiversity, and physical and mental health (PN 538).[20,76,77] Nearby bodies of water, such as rivers, can also contribute to cooling.[66] Access to green space in England is correlated with income and ethnicity.[78]

Occupant behaviour

Occupant interactions with buildings and equipment, which are influenced by social norms and personal preferences, can affect cooling demand.[2,79,80] Different cultural expectations, and uses of behavioural strategies such as looser clothing[81] and consumption of cold food and drink products, can reduce active cooling demand.[63,82,83] A key aspect is occupants' knowledge of how best to use passive tools such as opening windows and internal doors for cross-ventilation.[84] Night-time ventilation is most effective for cooling but security, air pollution, and noise can be barriers.[36,85] Proposed government guidelines ask developers to produce a Home User Guide on a dwelling's overheating, ventilation, and energy efficiency strategy.[86] The NHS and Public Health England provide heatwave advice.[36,87] Occupants typically adapt to wider temperature ranges in naturally ventilated buildings without AC.[88,89] Use of smarter control systems, such as thermostats with flexible thresholds, can be more effective while also lowering energy demand.[90–94]

Box 2: Refrigerants

Refrigerants are chemicals that can exist either as a gas or liquid at relatively low temperatures. They absorb heat when evaporating to a gas and release it when condensing to a liquid.[14] Many refrigerants are GHGs if released to the atmosphere. Global Warming Potential (GWP) typically describes the warming effect of the gas compared to the same mass of CO_2 (whose GWP is 1) over 100 years.[95,96]

Fluorinated gases (F-gases)

Most refrigerants are manufactured F-gases, with estimated GWP values ranging from less than 1 to 23,500.[97,98] 35% of global cooling-related GHG emissions come from F-gases.[99]

- **Hydrofluorocarbons (HFCs)** make up 95% of F-gas emissions.[100]
- **Hydrofluoroolefins (HFOs)** generally have lower GWPs than HFCs. Some concerns have been raised around marine ecosystem damage when HFOs degrade, but there is no evidence of environmental and health risks.[101–103]

Natural refrigerants (NFs)

NFs are increasingly used to avoid F-gases. Commercially available NFs include water, CO_2, air, ammonia and hydrocarbons (isobutane, propane). They have GWPs of between 0 and 3, are less energy intensive to produce than F-gases (including HFOs),[104] and can reduce indirect emissions. Some carry separate risks, for example hydrocarbons are flammable, ammonia is toxic and CO_2 needs higher operating pressures.[105]

Active cooling technologies

Active cooling uses an energy input such as electricity.[38] Most active devices work by circulating a refrigerant (Box 2) in a closed system.[14] Heat from the environment is absorbed at one location (where cooling is needed) and released at another.[14] The most commonly used active technologies include:

- **Air conditioners (ACs)**. Can be fixed electricity-powered units used to cool buildings,[45] or mobile fossil-fuel (e.g. diesel)-powered units in refrigerated transport vehicles.[104]
- **Chillers** are often thermally-driven units that deliver cooling via chilled water for larger buildings and industrial processes, often within a district network (PN 632).[14]
- **Refrigerators.** Including smaller electric domestic fridge-freezers and the centrally-cooled cabinets found in larger supermarkets and cold stores.[106]

Globally, 135 million AC units are sold each year and the International Energy Agency estimates that most of these have energy efficiencies less than half of the highest achievable.[11] Several lesser-used active cooling technologies can result in lower GHG emissions.

Heat pumps

Heat pumps (HPs) are primarily used as an energy-efficient way of providing heat to a building but many can also work like an AC unit to provide cooling ('reversible' types).[107] HPs are not widely used in the UK but their deployment is expected to rise significantly under low-carbon heat policy.[108,109] They use electricity and a refrigerant to extract heat from (or, when cooling, reject heat to) outdoor air or the ground.

Ground-source systems

The temperature tens of metres beneath the ground remains relatively constant throughout the year.[110] This can be exploited by circulating water through the ground to provide both heating (extracting heat from the ground into a building) and cooling (depositing heat from a building into the ground).[111] Ground-source systems use a standard water pump and, in most cases, an HP to boost heat transfer. High up-front costs make ground-source systems more suited to commercial or communal settings.[112–114] The Climate Change Committee's (CCC's) Sixth Carbon Budget advice suggested that ground-source HPs could account for 20% of HPs installed in the UK by 2050.[115]

Waste cold

Cold that is produced as a by-product of an industrial process or power production can be captured and used for cooling. The most common examples are chillers in 'combined cooling, heat and power plants', which recycle waste thermal energy to chill water used for AC or refrigeration.[116,117] A more recent prospect is to exploit liquefied natural gas (LNG),[118] which is stored at -162°C,[27] shipped by tanker and converted back into a gas at destination, releasing cold that is typically wasted.[10] Waste cold is a central part of the wider Cold Economy (Box 3).

Making cooling more sustainable

There is relatively little specific policy for sustainable cooling in the UK. Broad aims to mitigate risks from overheating are outlined in Defra's 2018 National Adaptation Programme (NAP) and, as of 2019, the National Planning Policy Framework.[119,120] More specific policy is focused on the energy efficiency of AC devices and reducing F-gas use. Academic researchers suggest that improving the sustainability of cooling requires measures beyond device efficiency and electricity use. They advocate a greater focus on passive and behavioural strategies, and a circular economy approach that considers the whole life cycle from designing to disposing of systems (PN 536).[2] Doing so could reduce the need for active cooling. Several data gaps exist, presenting barriers to understanding future demand and creating and implementing policy.[114]

Box 3: Cold energy storage and the Cold Economy
Academic and industry groups have developed the concept of a 'Cold Economy': an economy-wide system that uses waste and surplus cold as a way of storing and transporting energy for use in a range of applications other than cooling to reduce environmental impact.[4,118,121] Cold energy can be stored for long periods using 'phase-change materials' (PCMs) such as specialist gels. PCMs can accumulate cold during periods of low energy demand and release it at a different time or place as needed. This can help reduce electricity demand during hot peaks and improve energy system flexibility (PN 587).[55] PCMs can also be used in parts of cold chains, such as shipping containers, to reduce reliance on diesel or the power network.[118,122] Compared with electrical batteries, cold energy storage can be cheaper to run and longer-lasting, and relies less on rare or toxic materials, but its use to date has been limited. Cooling can further enable energy system flexibility:

- Using 'demand-side response', electricity system operators can pay large AC or refrigeration users (such as hotel chains or supermarkets) to briefly turn down their systems in periods of peak electricity demand without compromising food safety or thermal comfort.[123,124]
- 'Liquid air energy storage' uses electricity to cool air to cryogenic temperatures that can later be used to generate power.[125,126] The first commercial project is under construction near Manchester.[127]

Using more efficient cooling devices

Standards and labelling

Efficiency gains in AC units and other active devices can be made by raising minimum energy performance standards and incentivising high-efficiency equipment through voluntary measures.[11] Small cooling units sold in the EU must bear energy efficiency labels and comply with 'ecodesign' standards;[128,129] similar standards exist elsewhere.[130] Several UK industry and government guides for increasing efficiency also exist.[131,132]

Cooling as a service

More efficient systems often have higher up-front end-user costs. Reducing electricity consumption also relies on better operation and maintenance.[16,45] New business models such as 'cooling as a service' (CaaS) can address these, and promote innovation and circular economy practices. In CaaS, the end-user pays a specialist provider an ongoing fee to install, run, maintain and decommission its cooling system.[133,134]

Policy for combining heat and cooling

Combining heating and cooling systems (such as by using HPs) can increase technical and cost efficiency.[107,112] The 2020 Energy White Paper outlines a target to increase HP deployment from 30,000 to 600,000 per year by 2028.[108] System design and installation that accounts for reversible operation is key to delivering intended efficiency benefits,[107,135] but the UK skills base to do so is currently lacking.[136,137]

Reducing F-gas use

The UN Montreal Protocol and its Kigali Amendment (Box 4) aim to reduce global HFC use by 80-85% by 2047.[138] In the UK, the retained EU F-Gas Regulation requires a 79% reduction in HFC sales by 2030 relative to 2015,[100] which is more stringent than the Kigali target in the near-term. Defra is assessing how the Regulation's ambition could be increased.[139] Because fixed and mobile ACs have typical lifetimes of around 10 years that 'lock in' associated emissions,[140] as well as illegal HFC trading and historically low leakage and disposal compliance, a shift to natural refrigerants (NFs, Box 2) is advocated by environmental stakeholders.[95,105,141] In the UK, many cold stores and domestic and supermarket systems already use NFs,[105,106] while most AC devices and heat pumps still rely on F-gases.

Promoting passive cooling strategies

Building codes and wider planning laws are the main tool for improving building design and green infrastructure. The UK currently has no formal requirement to increase the use of passive cooling strategies,[83] and the CCC recommends new statutory requirements to reduce overheating in new-build homes.[37] Most existing UK buildings will need to be made more energy efficient to meet decarbonisation targets for heat, but an exclusive focus on retaining heat can lead to summer overheating if cooling is overlooked.[142–146] Embedding passive cooling in new dwellings has been proposed by the 2021 MHCLG Future Buildings Standard consultation,[147,148] but does not cover existing buildings.[37] The 2018 NAP encourages actions to deliver more, better quality, green infrastructure.[119]

Improving cold chains

In 2013 the UK Government renewed the voluntary Food Chain Climate Change Agreement, to incentivise the uptake of energy efficiency measures in the UK cold chain.[146] Its 2020 efficiency targets were surpassed and the scheme has been extended until 2025.[131,149] Few commercialised technologies exist for decarbonising refrigerated transport.[150,151] Aggregating food and medical cold chains via facilities and data sharing can increase resilience and efficiency but would require coordination and cost sharing across multiple actors.[28,152]

International cooling programmes

Globally, cooling programmes relate to both aid and climate finance efforts. The UK Government's ODA has provided around £26m for cooling-related projects since 2011,[153] which includes the BEIS-funded £15m Sustainable Cooling Innovation Fund.[154] Cooling is also part of the £1bn Ayrton Fund, which promotes clean energy technology innovation in developing countries.[155] In 2020/21, Defra co-funded the African Cooling Centre of Excellence (ACES).[156] The UK Government has a leading role in the Cool Coalition (Box 4),[117] and the "Affordable heating and cooling of buildings" challenge for Mission Innovation, a global public-private initiative.[157] Analysts suggest that development finance institutions such as the World Bank Group are key to delivering sustainable cooling projects internationally.[158,159]

Box 4: International efforts for sustainable cooling
Relevant international programmes or agreements include the 2015 Paris Agreement on climate change;[160] the 1987 Montreal Protocol and its 2016 Kigali Amendment, which aim to prevent ozone layer depletion and reduce HFCs (Box 2);[161] and the UN SDGs.[2] The Kigali Cooling Efficiency Programme (K-CEP) is a philanthropic programme that supports the aims of the Montreal Protocol. It helps nations develop National Cooling Plans (NCPs): roadmaps for reducing F-gas use, developing sustainable cooling, and linking these with wider energy, climate and development targets. A tool to identify cooling needs is being developed to support this.[162–164] In 2019, the UN Environment Programme created the Cool Coalition, a global network to promote sustainable cooling.

POST is an office of both Houses of Parliament, charged with providing independent and balanced analysis of policy issues that have a basis in science and technology. POST is grateful to Andrea Caio for researching this briefing, to EPSRC for funding his parliamentary fellowship, and to all contributors and reviewers. For further information on this subject, please contact the co-author, Jack Miller. Parliamentary Copyright 2021.

Endnotes

1. Peters, T. *et al.* (2018). *Clean Cooling Landscape Assessment*. Heriot Watt University; Birmingham University; K-CEP.
2. Khosla, R. *et al.* (2020). Cooling for sustainable development | Nature Sustainability. *Nature Sustainability*,
3. Economist Intelligence Unit (2019). The Cooling Imperative: Forecasting the size and source of future cooling demand.
4. Birmingham Energy Institute (2016). *Clean Cold and the Global Goals*. University of Birmingham.
5. Gross, L. (2020). Building back better: How climate-friendly cooling can support a clean, resilient Covid-19 recovery. E3G; Kigali Cooling Efficiency Program.
6. UNEP (2020). Emissions Gap Report 2020: Executive Summary. UN Environment Programme.
7. Masson-Delmotte, V. *et al.* (2018). Summary for Policymakers — Global Warming of 1.5 oC. IPCC.
8. Climate Change Committee (2017). UK Climate Change Risk Assessment 2017: Synthesis Report.
9. Lowe, J. A. *et al.* (2019). *UKCP18 Science Overview Report*. Met Office; DEFRA; BEIS; Environment Agency.
10. Carbon Trust (2015). The Emerging Cold Economy. Carbon Trust.
11. IEA (2018). The Future of Cooling: Opportunities for energy-efficient air conditioning. International Energy Agency.
12. Peters, T. (2018). A Cool World - Defining the Energy Conundrum of Cooling for All. Birmingham Energy Institute – University of Birmingham.
13. Davis, L. W. *et al.* (2015). Contribution of air conditioning adoption to future energy use under global warming. *PNAS*, Vol 112, 5962–5967. National Academy of Sciences.
14. IEA (2018). The Future of Cooling: Opportunities for energy-efficient air conditioning. International Energy Agency.
15. Greenhouse Gas Protocol (2016). Global Warming Potential Values.
16. Kigali Cooling Efficiency Program (2018). *Optimization, monitoring, and maintenance of cooling technology*. K-CEP.
17. Green Cooling Initiative (2018). Green Cooling Initiative (GCI II). Deutsche Gesellschaft für Internationale Zusammenarbeit (GIZ) GmbH.
18. Ritchie, H. (2020). Sector by sector: where do global greenhouse gas emissions come from? *Our World in Data*.
19. Isaac, M. *et al.* (2009). Modeling global residential sector energy demand for heating and air conditioning in the context of climate change. *Energy Policy*, Vol 37, 507–521.
20. Cool Coalition *et al.* (2021). Sustainable Cooling in Support of a Resilient and Climate-Proof Recovery. 28.
21. IEA *et al.* (2020). Cooling Emissions and Policy Synthesis Report: Benefits of cooling efficiency and the Kigali Amendment. Cool Coalition.
22. Economist Intelligence Unit (2020). The Power of Efficient Cooling. The Economist.
23. Costanza, R. *et al.* (1992). Natural Capital and Sustainable Development. *Conservation Biology*, Vol 6, 37–46.
24. University of Oxford [online] Future of Cooling Programme. Accessed 27/04/21
25. London South Bank University (2017). Centre for Air Conditioning and Refrigeration Research. London South Bank University.
26. University of Birmingham [online] The Cold Economy - Birmingham Energy Institute. Accessed 27/04/21
27. IIR (2019). *The Role of Refrigeration in the Global Economy*. International Institute of Refrigeration.
28. Ravishankar, M. *et al.* (2020). Net zero cold chains for food. Carbon Trust.
29. National Grid ESO (2020). Future Energy Scenarios. National Grid ESO.
30. Peacock, A. D. *et al.* (2010). Investigating the potential of overheating in UK dwellings as a consequence of extant climate change. *Energy Policy*, Vol 38, 3277–3288.
31. Roberts, B. M. *et al.* (2019). Predictions of summertime overheating: Comparison of dynamic thermal models and measurements in synthetically occupied test houses. *Building Serv. Eng. Res. Technol.*, Vol 40, 512–552.
32. CIBSE (2017). Using TM59 to assess overheating risk in homes. *CIBSE Journal*.
33. Crawley, J. *et al.* (2020). IVUGER Report: Domestic Air Conditioning in 2050. UKERC.
34. Building Research Establishment (2016). Guidance Document: Overheating in dwellings.
35. Health and Safety Executive [online] Heat stress - Temperature. Accessed 27/04/21
36. Public Health England (2015). Heatwave plan for England - making the case: the impact of heat on health now and in the future. Public Health England; NHS England; Local Government Association; Met Office.
37. CCC (2019). UK housing: Fit for the future? Committee on Climate Change.
38. ESMAP (2020). Primer for Space Cooling. Energy Sector Management Assistance Program.
39. Damiati, S. A. *et al.* (2016). Field study on adaptive thermal comfort in office buildings in Malaysia, Indonesia, Singapore, and Japan during hot and humid season. *Building and Environment*, Vol 109, 208–223.
40. Christidis, N. *et al.* (2015). Dramatically increasing chance of extremely hot summers since the 2003 European heatwave. *Nature Climate Change*, Vol 5, 46–50. Nature Publishing Group.
41. Coffel, E. D. *et al.* (2020). Thermal power generation is disadvantaged in a warming world. *Environ. Res. Lett.*, IOP Publishing.
42. Roach, J. (2020). Microsoft finds underwater datacenters are reliable, practical and use energy sustainably. *Microsoft - Innovation Stories*.
43. McKinsey (Advanced Industries Practice) (2020). Can HVAC guidance help prevent transmission of COVID-19?
44. Health and Safety Executive (2021). Ventilation and air conditioning during the coronavirus (COVID-19) pandemic. *HSE*.
45. Abela, A. *et al.* (2016). *Study on Energy Use by Air-Conditioning: Final Report*. 39. BRE on behalf of Department of Energy and Climate Change.
46. CIBSE (2016). A tenth of UK electricity used for air conditioning. *CIBSE Journal*.
47. McLachlan, C. *et al.* (2016). Air conditioning demand assessment. 46. Tyndall Centre for Climate Change Research, University of Manchester.
48. Maidment, G. *et al.* (2019). Reducing energy demand using cooling efficiently (REDUCE). in *The 25th IIR International Conference of Refrigeration*.
49. Cold Chain Federation (2020). The Cold Chain. CCF.
50. Savills (2020). *UK Cold Storage Sector*. 6. Cold Chain Federation.
51. UNEP (2020). COVID-19 vaccine could revolutionize cold storage around the world. *UN Environment*.
52. Bakalis, S. *et al.* (2020). Perspectives from CO+RE: How COVID-19 changed our food systems and food security paradigms. *Current Research in Food Science*, Vol 3, 166–172.
53. Defra [online] Food Statistics in your pocket: Food Chain. Accessed 27/04/21.
54. Miller, A. *et al.* (2020). Chilling Prospects: Providing Sustainable Cooling for All. SEforALL.
55. Peters, T. *et al.* (2016). The Cold Economy – Why? What? How? Birmingham Energy Institute – University of Birmingham.
56. ILO (2019). Working on a warmer planet: The impact of heat stress on labour productivity and decent work.

57. Gavi (2020). Cold Chain Equipment Optimisation Platform: Technology Guide.
58. UNIDO (2019). Gender Equality in the Sustainable Energy Transition - Guidance Note.
59. SEforALL (2021). Cooling for All and Gender - Towards Inclusive, Sustainable Cooling Solutions.
60. Bhamare, D. K. *et al.* (2019). Passive cooling techniques for building and their applicability in different climatic zones—The state of art. *Energy and Buildings*, Vol 198, 467–490.
61. PEEB (2020). Better design for cool buildings. Programme for Energy Efficiency in Buildings.
62. Aguilar-Santana, J. L. *et al.* (2020). Review on window-glazing technologies and future prospects. *International Journal of Low-Carbon Technologies*, 112–120.
63. Baborska-Narożny, M. *et al.* (2017). Overheating in retrofitted flats: occupant practices, learning and interventions. *Building Research & Information*, Vol 45, 40–59. Routledge.
64. MHCLG (2019). English Housing Survey - Households report 2017-18. Ministry of Housing, Communities & Local Government.
65. CABE (2010). Community green: using local spaces to tackle inequality and improve health.
66. Good Homes Alliance (2019). Overheating in New Homes: Tool and guidance for identifying and mitigating early stage overheating risks in new homes.
67. Mazzone, A. (2020). Thermal comfort and cooling strategies in the Brazilian Amazon. An assessment of the concept of fuel poverty in tropical climates. *Energy Policy*, Vol 139, 111256.
68. Kubota, T. *et al.* (2015). Application of Passive Cooling Techniques in Vernacular Houses to Modern Urban Houses: A Case Study of Malaysia. *Procedia - Social and Behavioral Sciences*, Vol 179, 29–39.
69. Cobb, R. (2018). Making energy calculations more accurate, using HQM – Home Quality Mark. *BRE Group*.
70. UNEP (2019). Cities can fight climate change and improve lives by finding new ways to be cool. *UNEP*.
71. Watkins, R. *et al.* (2002). The London Heat Island: results from summertime monitoring. *Building Services Engineering Research and Technology*, Vol 23, 97–106. SAGE Publications Ltd STM.
72. Cheung, H. K. W. (2011). An urban heat island study for building and urban design. University of Manchester.
73. Abohorlu Doğramacı, P. *et al.* (2019). Experimental study of the potential of eucalyptus fibres for evaporative cooling. *Renewable Energy*, Vol 131, 250–260.
74. Wang, X. *et al.* (2021). Tree species richness and diversity predicts the magnitude of urban heat island mitigation effects of greenspaces. *Science of The Total Environment*, Vol 770, 145211.
75. Dong, J. *et al.* (2020). Quantitative study on the cooling effect of green roofs in a high-density urban Area—A case study of Xiamen, China. *Journal of Cleaner Production*, Vol 255, 120152.
76. Public Health England (2020). Improving access to greenspace: A new review for 2020.
77. Ward Thompson, C. *et al.* (2016). Urban green spaces and health - A review of evidence. World Health Organization Regional Office for Europe.
78. Friends of the Earth (2020). England's green space gap - How to end green space deprivation in England.
79. Behavioural Insights Team (2011). *Behaviour Change and Energy Use.*
80. Policy Learning Platform on Low-carbon Economy (2018). Behaviour Change for Energy Efficiency. Interreg Europe, European Union.
81. Takagi, H. (2015). The Japanese Cool Biz Campaign: Increasing Comfort in the Workplace. *Environmental and Energy Study Institute*.
82. Mavrogianni, A. *et al.* (2014). The impact of occupancy patterns, occupant-controlled ventilation and shading on indoor overheating risk in domestic environments. *Building and Environment*, Vol 78, 183–198.
83. MHCLG (2019). Research into overheating in new homes - Phase 1 report. UK Government.
84. BRE (2016). Solutions to Overheating in Homes - Evidence Review. Zero Carbon Hub.
85. Roberts, B. M. (2020). Ventilation and shading to reduce overheating in UK homes: an evaluation using matched pair test houses with synthetic occupants. Loughborough University.
86. Ministry of Housing, Communities & Local Government (2021). Home User Guide Template: Building Regulations Part L, F, and Overheating - England.
87. NHS [online] Heatwave: how to cope in hot weather. Accessed 28/04/21
88. Zhu, Y. *et al.* (2016). Dynamic thermal environment and thermal comfort. *Indoor Air*, Vol 26, 125–137.
89. Ghiaus, C. (2003). Free-running building temperature and HVAC climatic suitability. *Energy and Buildings*, Vol 35, 405–411.
90. Khalid, W. *et al.* (2019). Investigation of comfort temperature and thermal adaptation for patients and visitors in Malaysian hospitals. *Energy & Buildings*, Vol 183, 484–499.
91. Sajjadian, S. M. *et al.* (2020). An Expandable, Contextualized and Data-Driven Indoor Thermal Comfort Model. *Energy and Built Environment*, Vol 1, 385–392.
92. Brusey, J. *et al.* (2018). Reinforcement learning-based thermal comfort control for vehicle cabins. *Mechatronics*, Vol 50, 413–421.
93. Aguilera, J. J. *et al.* (2019). Thermal adaptation in occupant-driven HVAC control. *Journal of Building Engineering*, Vol 25, 100846.
94. Dounis, A. I. *et al.* (2001). Design of a fuzzy system for living space thermal-comfort regulation. *Applied Energy*, Vol 69, 119–144.
95. Environmental Investigation Agency (2017). Chilling Facts VII: Are Europe's supermarket ready to quit HFCs?
96. GWP can be calculated either using the warming effect of the gas over a 100-year or 20-year timeframe (GWP100 or GWP20), which accounts for the rate at which the gas breaks down or escapes the atmosphere. Most F-gases have a 10-20 year lifetime and hence a higher GWP20.
97. Ozone Secretariat [online] Annex F: Controlled substances. Accessed 28/04/21
98. IPCC (2014). Fifth Assessment Report WGIII: Technical summary.
99. Zolcer Skacanová, K. *et al.* (2018). Technical report on energy efficiency in HFC-free supermarket refrigeration. Environmental Investigation Agency; shecco; K-CEP.
100. CCC (2020). The Sixth Carbon Budget: The UK's path to Net Zero.
101. EIA (2020). New family of synthetic refrigerant gases poses potential dangers to human health and the environment.
102. Fleet, D. *et al.* (2017). Study on environmental and health effects of HFO refrigerants. Norwegian Environment Agency.
103. UN Environment Programme Ozone Secretariat (2018). *Environmental Effects and Interactions of Stratospheric Ozone Depletion, UV Radiation, and Climate Change. 2018 Assessment Report.*
104. Blumberg, K. *et al.* (2019). Mobile air conditioning: The life-cycle costs and greenhouse-gas benefits of switching to alternative refrigerants and improving system efficiencies. The International Council on Clean Transportation.
105. Environmental Investigation Agency (2018). Summary: Technical Report on Energy Efficiency in HFC-free Supermarket Refrigeration.

106. Green Cooling Initiative [online]. Cooling subsectors. Accessed 27/04/21.
107. Carbon Trust (2020). Heat pump retrofit in London.
108. BEIS (2020). Energy White Paper: Powering our Net Zero Future.
109. BEIS (2016). Evidence Gathering - Low Carbon Heating Technologies. Domestic High Temperature, Hybrid and Gas Driven Heat Pumps: Summary Report.
110. Sanner, B. (2017). Ground Source Heat Pumps - history, development, current-status, and future prospects. in *12th IEA Heat Pump Conference*. IEA Energy Technology Network.
111. BGS Research [online]. Geothermal energy. Accessed 27/04/21.
112. GSHPA [online]. Ground Source Heat Pumps - Commercial. Accessed 27/04/21.
113. BEIS (2018). *Clean Growth - Transforming Heating: Overview of Current Evidence*.
114. DECC (2015). European Commission Heating & Cooling Strategy Consultation - DECC Commentary.
115. Element Energy Ltd (2020). Development of trajectories for residential heat decarbonisation to inform the Sixth Carbon Budget (Element Energy).
116. CIBSE [online]. Case Study London Olympic Park Energy Centre. Accessed 27/04/21
117. Carbon Trust (2017). UK Leadership on Sustainable Cooling: From Covid-19 to COP26.
118. IMechE (2014). A Tank of Cold: Cleantech Leapforg to a more Food Secure World.
119. Defra (2018). The National Adaptation Programme and the Third Strategy for Climate Adaptation Reporting: Making the country resilient to a changing climate.
120. MHCLG (2019). *National Planning Policy Framework*.
121. Birmingham Energy Institute (2014). Doing Cold Smarter.
122. Birmingham Energy Institute (2019). Passively cooled containers being delivered for integrated rail and road cold chain transportation following world's first commercial demonstration.
123. Ambrose, J. (2019). Cool running: supermarket fridges could help power UK. *The Guardian*.
124. Grundy, A. (2019). Tesco trials offering up fridges for frequency response. *Current News*.
125. Highview Power Storage (2017). Liquid Air Energy Storage.
126. CORDIS (2021). Pioneering CryoHub technology of cryogenic energy storage to harness renewables for carbon-neutral refrigeration and power supply. *CORDIS | European Commission*.
127. EEOnline (2020). Highview Power Breaks Ground on 250MWh CRYOBattery Long Duration Energy Storage Facility. *Electric Energy Online*.
128. European Commission [online]. Air conditioners and comfort fans. Accessed 27/04/21
129. European Commission [online]. Air conditioners. Accessed 27/04/21.
130. UN [online]. Top Runner Program. Accessed 27/04/21.
131. Cold Chain Federation (2020). *Energy Efficiency In Cold Stores: A Practical Guide*. 17. Cold Chain Federation.
132. BEIS (2020). HVAC: heating, ventilation and air conditioning equipment - A guide to energy efficient equipment listed on the Energy Technology List (ETL).
133. BASE (2020). Cooling as a Service Initiative.
134. EPEE [online]. Service-based business models for heating and cooling as a way to save energy and contribute to a circular economy. Accessed 27/04/21.
135. Guertler, P. (2020). Getting on track to net-zero - ten million heat pumps for homes by 2030. E3G.
136. Heat Pump Association (2020). Building the installer base for net zero heating.
137. HMG [online]. Green Jobs Taskforce. Accessed 27/04/21.
138. UN Environment Programme (2017). Frequently asked questions relating to the Kigali Amendment to the Montreal Protocol.
139. Lords Parliamentary Question UIN HL13854 (2021). Greenhouse Gas Emissions.
140. Gluckman, R. *et al.* (2019). *Assessment of the potential to reduce UK F-gas emissions beyond the ambition of the F-gas Regulation and Kigali Amendment*. Ricardo Energy & Environment.
141. EIA (2019). Doors wide open: Europe's flourishing illegal trade in hydrofluorocarbons (HFCs).
142. McLeod, R. S. *et al.* (2017). Chronic overheating in low carbon urban developments in a temperate climate. *Renewable and Sustainable Energy Reviews*, Vol 74, 201–220.
143. McGill, G. *et al.* (2017). Meta-analysis of indoor temperatures in new-build housing. *Building Research & Information*, Vol 45, 19–39. Routledge.
144. Foster, J. *et al.* (2016). Scottish Passive House: Insights into Environmental Conditions in Monitored Passive Houses. *Sustainability*, Vol 8, 412. Multidisciplinary Digital Publishing Institute.
145. Fletcher, M. J. *et al.* (2017). An empirical evaluation of temporal overheating in an assisted living Passivhaus dwelling in the UK. *Building and Environment*, Vol 121, 106–
146. Tink, V. *et al.* (2018). Measuring and mitigating overheating risk in solid wall dwellings retrofitted with internal wall insulation. *Building and Environment*, Vol 141, 247–261.
147. MHCLG (2021). The Future Buildings Standard: Consultation on changes to Part L (conservation of fuel and power) and Part F (ventilation) of the Building Regulations for non-domestic buildings and dwellings; and overheating in new residential buildings.
148. MHCLG (2021). Approved Document [X] - Overheating. Consultation version.
149. BEIS (2020). *Climate Change Agreements: Scheme Extension Statutory Guidance*. UK Government.
150. UK Government [online]. Budget 2020: Delivering on our promises to the British people. Accessed 27/04/21.
151. Cold Chain Federation [online]. Cold Chain Net Zero Project. Accessed 27/04/21.
152. Cold Chain Federation (2020). *Shaping the Cold Chain of the Future: The Road to Net Zero*.
153. SEforALL (2019). *Chilling Prospects: Tracking Sustainable Cooling for All*.
154. TechEmerge *et al.* [online]. Sustainable Cooling. Accessed 27/04/21.
155. Mission Innovation (2020). UK announces plan to double efforts in developing nations to boost clean energy innovation.
156. UNEP (2020). Centre of Excellence in Rwanda aims to support African farmers and rural communities.
157. Mission Innovation IC7: Affordable Heating and Cooling of Buildings.
158. Orozco, D. *et al.* (2020). *Cool Developmet Banks: Rising to the Challenge of Cooling a Warming World*. 25. E3G.
159. Warren, P. (2020). Blind spots in climate finance for innovation. *Advances in Climate Change Research*, Vol 11, 60–64.
160. UNFCC [online]. Paris Agreement - Status of Ratification. Accessed 27/04/21.
161. EIA (2016). Kigali Amendment to the Montreal Protocol.
162. K-CEP (2019). Principles for National Cooling Plans.
163. SEforALL *et al.* (2019). Cooling for All: Needs Assessment - Working Paper.

164. Cool Coalition (2019). UN Secretary General Summit: Government Action on Efficient, Climate-friendly Cooling.

Appendix B – Chapter 2

B.1 Use-case for oil & gas applications

The figure below shown Blue Star employed as a combined power and communications platform to support subsea architecture in cases of umbilical failure. The WEC uses its own, much shorter umbilical to transfer converted power. NB: EFL = electrical flow line; HFL = hydraulic flow line. The WEC is shown facing into the page.

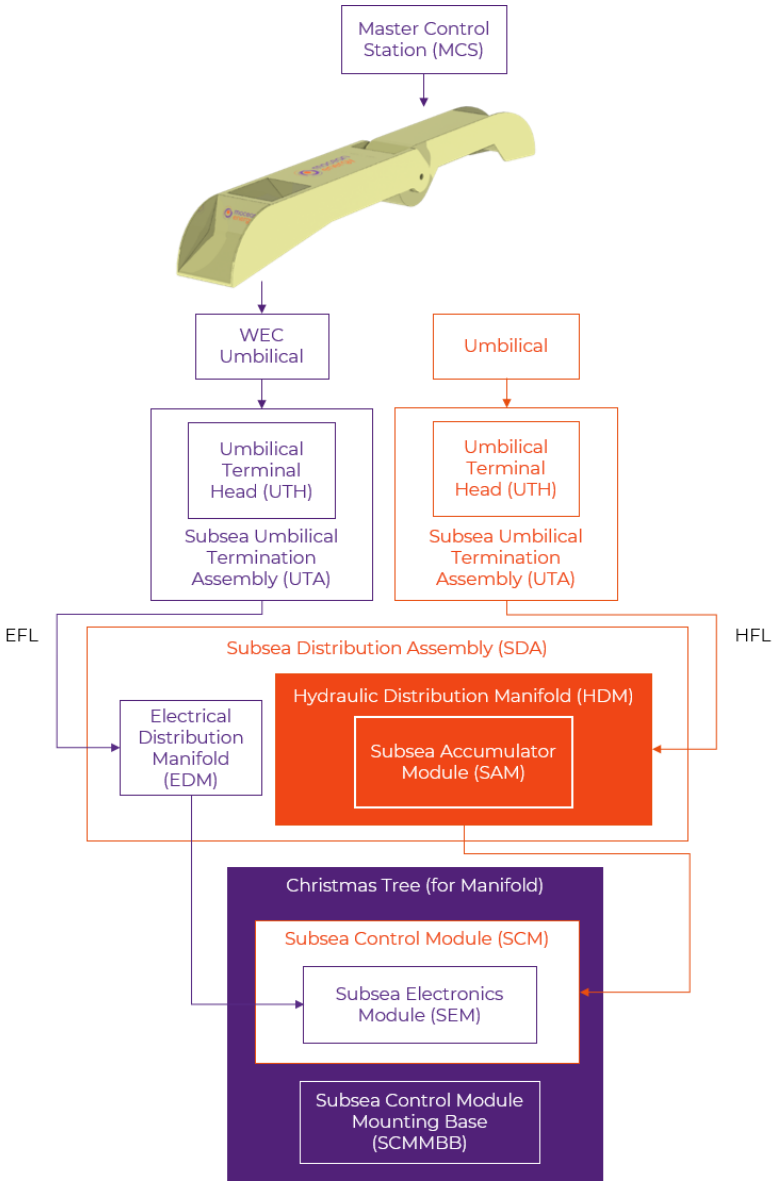

Figure 180 - Interfacing architecture for an existing subsea electrical system (umbilical failure event).

B.2 Mocean’s design process

The cyclical interplay between design requirements, numerical optimisation, physical testing and validation, and design review based on engineering considerations, is illustrated below.

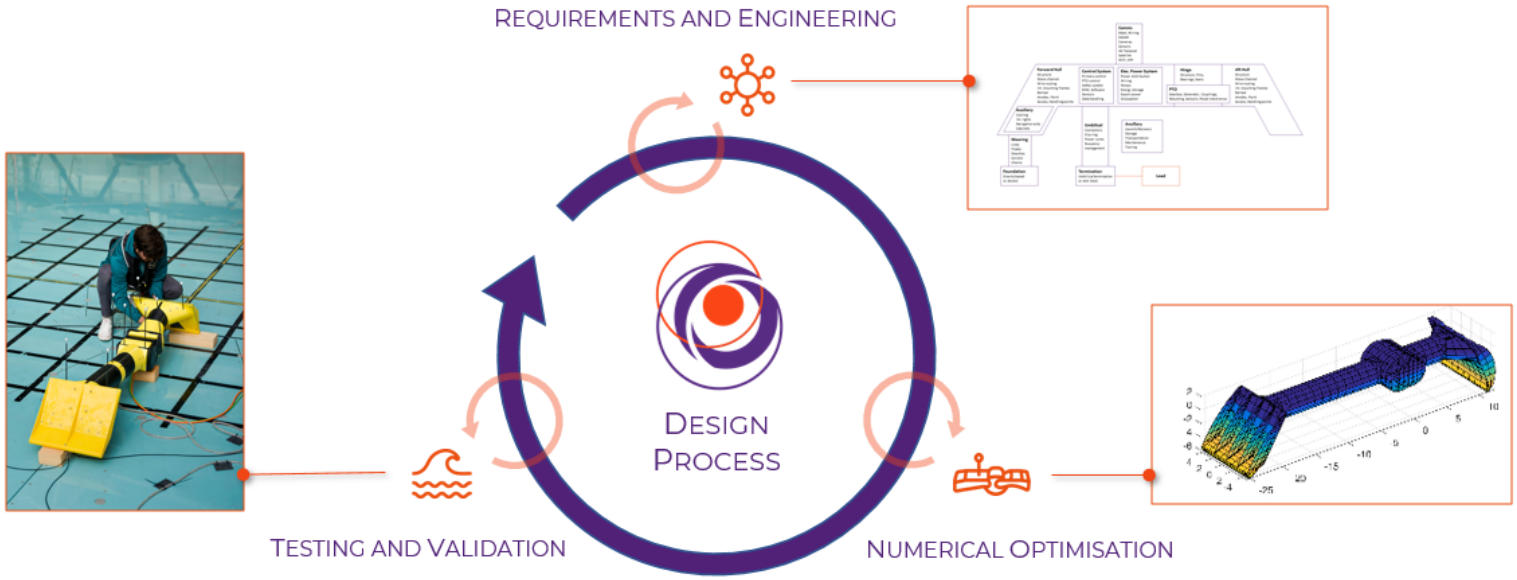

Figure 181 - Diagrammatic representation of Mocean Energy's design process.

Appendix C – Chapter 3

C.1 Initial mind-map

Prior to the literature review and to the testing campaign definition, the following mind-map was composed in order to draw out all potential elements related to small-scale physical model testing.

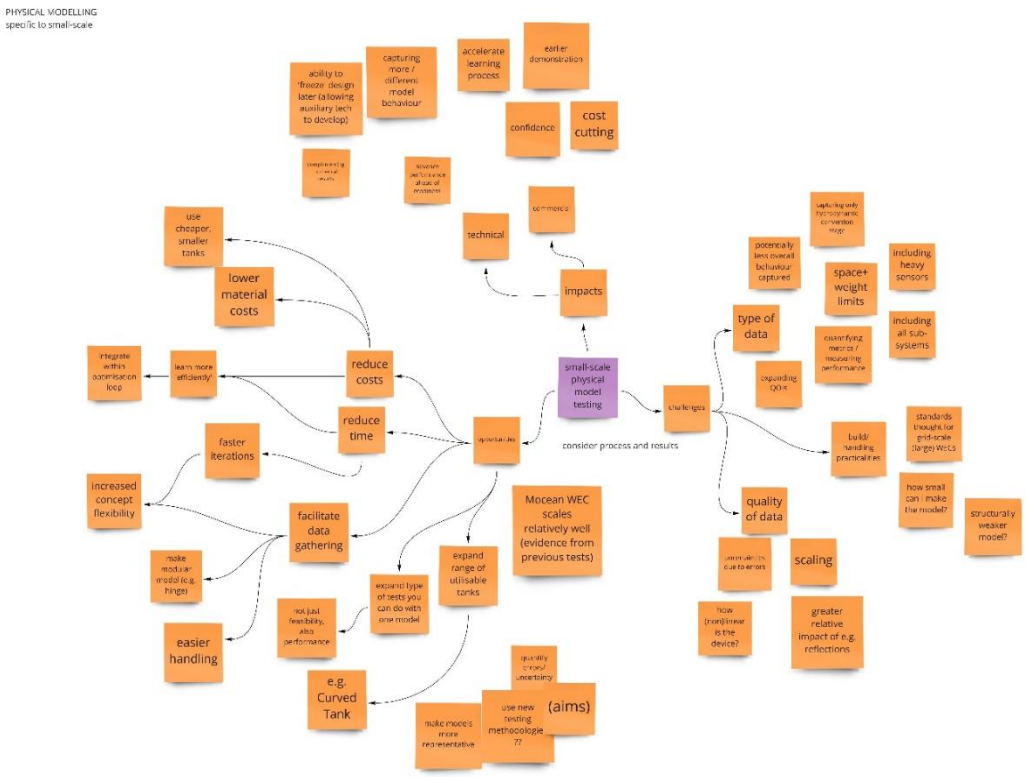

Figure 182 – Mind-map to capture initial physical modelling themes from brainstorming purposes.

C.2 Design process

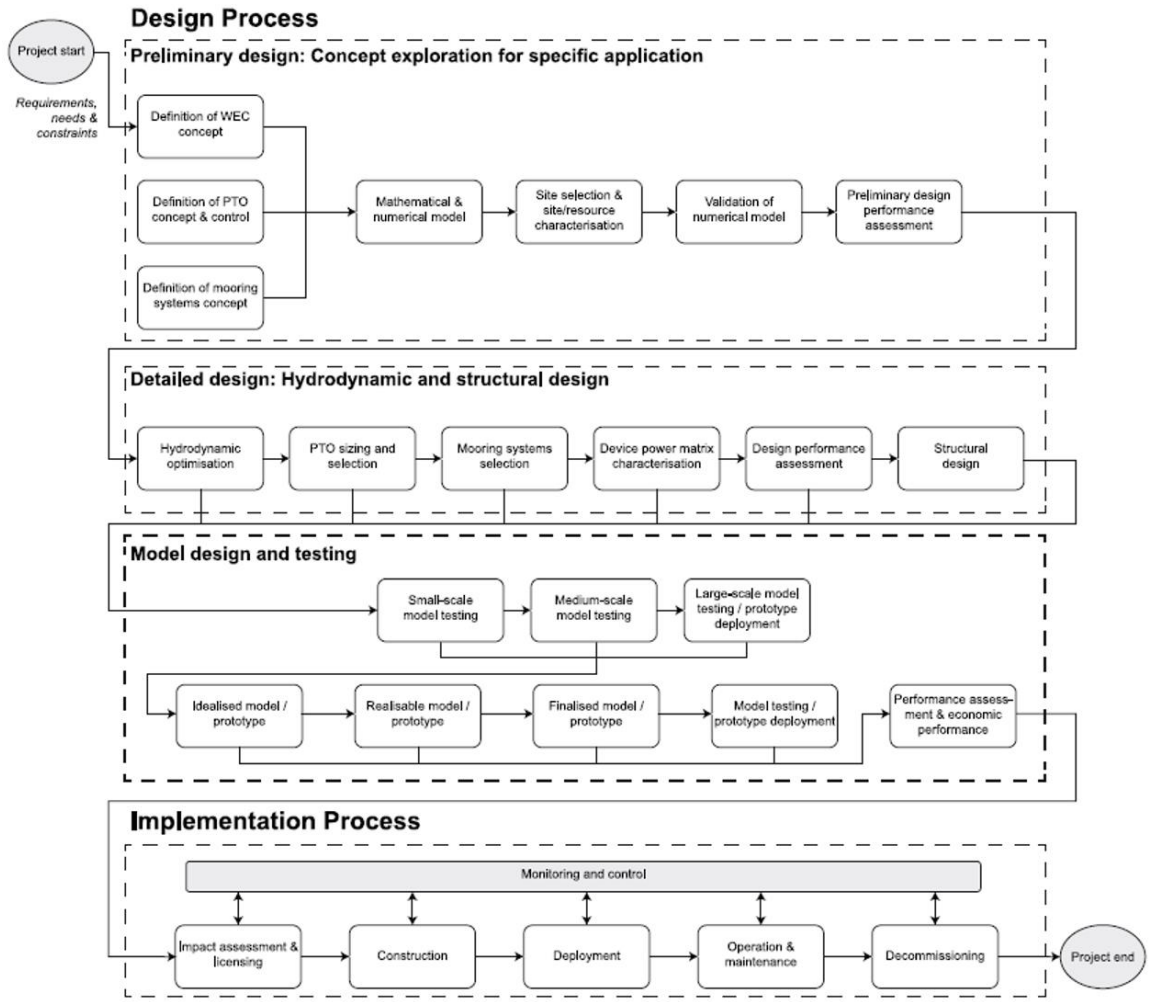

Figure 183 - Schematic representation of the life cycle of a wave energy project, as found in (Portillo *et al.*, 2020).

Figure 183 shows many of the steps required in a design process, which in practice are not static, but rather iterative. It is particularly odd that the *Model design and testing* block - including 'small-scale model testing' - occurs after *Detailed design* – not least given its fundamental relevance in 'Numerical model validation' in the first block. Such discrepancies in the conception of the design process are clearly pointed out in (Trueworthy and Dupont, 2020), which highlights that "the steps designers should take to make the next iteration better than the last once they have simulation results are missing from [the figure], as well as from the literature more generally".

C.3 Summary of QOIs and types of physical model testing

A non-exhaustive list of literature focused on physical model testing is offered, to paint a representative picture of the sizes, scales, objectives, PTO inclusions, and sea states utilised in typical reported testing campaigns.

Paper	WEC type	V / P	Scale	Mass (kg)	Dims (m)	PTO (Yes/No, type)	Other (waves, damping, sensors)
(Clemente *et al.*, 2021)	Roll-based floating single body	P	1:20	56.5	1m L 0.5m r 0.125m D	Y – triboelectric nanogenerators (TENGs)	7 irregular seas
(Martin *et al.*, 2020)	Two-body point absorber	V	1:30	60.1 (buoy) 334.2 (submerged body)	Overall: 3.23m L 0.60-0.75m d	Y – mechanical motion rectifier (MMR); gearbox; two one-way clutches, coupling.	7 regular, 1 irregular; 6 PTO damping values Quite complex model drivetrain; friction effects and uncertainties not captured.
(Zanuttigh, Angelelli and Kofoed, 2013)	Wave activated body (floating 2-hull attenuator)	P	1:30	33kg (of which 10kg PTO)	2.10m length; 0.81m width	Y – metal bar with slot, wheel with wound metal wire that is welded to the ends of the slot; bar connected to one hull and wheel to the other; electric motor provides varying resistance to wheel rotation – linear damping (PTO totally above water line)	10 reg to identify optimal PTO rigidity; then 10 Jonswap irreg Load sensor to measure forces via strain gauge; ultrasonic sensor for displacements and velocities. 17 different PTO ‘rigidities’ tested
(O’Boyle *et al.*, 2015)	Oyster 800 (bottom-fixed, flap-type)	V, P	1:40	n/a	n/a	Y – friction-based	Retrospectively compares full-scale data to scaled model built to as-installed full-scale properties.
(Shahroozi, Göteman and Engström, 2021)	Point absorber	V	1:30	15.73kg for the buoy only	380mm height; 330mm diameter	Y – friction-based, linear guide and damper based on Teflon-sprung block for contact friction; non-zero friction in ball bearings of linear guide	Regular, irregular, focused waves; 4 PTO damping levels explored 2 repetitions per sea state Issues highlighted: no measurement uncertainty in PTO friction is quantified; explores viscous drag

							coefficients in heave and surge via decay tests
Paper	**WEC type**	**V/P**	**Scale**	**Mass (kg)**	**Dims (m)**	**PTO (Yes/No, type)**	**Other (waves, damping, sensors)**
(Cameron McNatt and Retzler, 2019)	Mocean M100P hinged raft	V	1:20	32.68	1.84m length; 0.30m draft	Y – electromagnetic controllable motor brake; non-zero friction in lip seal of hinge nacelle assembly	3x Reg sweeps, 2x irreg seas Variation of PTO torque limits; free hinge & 2 PTO damping values; no torque sensor
(Rahmati and Aggidis, 2016)	Point absorber	V, P	1:100	140g (collector body)	0.15m height 0.26m width 0.10m length (collector body)	Y – two available brakes (Coulomb friction damping force and hung weights)	Irregular (Bretschneider)
(Wilkinson *et al.*, 2017)	Near-shore, rigid/modular, flap type WEC	P	1:30	n/a	0.21m height 11.1m width 0.13m length	Y – Coulomb damping via magnetic resonance break (MRB), with magnetic coupling.	8x regular; range of Dpto; Backlash; Torque measured in loco including friction effects via bespoke torque pin with strain gauges
(Rodríguez, Rosa-Santos and Taveira-Pinto, 2018)	Floating point absorber (surge and heave DoF)	P	1:20	n/a	0.20m radius 0.25m width (floating module)	Y – direct-drive PTO connected to external variable resistance for damping variation (rack + gear, DC generator)	9x regular; 9x irregular (JONSWAP); 6x damping levels; 52 wave conditions per damping level
(Lopes de Almeida, Mujtaba and Oliveira Fernandes, 2018)	REEFS WEC (multi-flap type)	P	1:66.67	n/a	0.132 length 0.15m height 0.30m width	Y - hydraulic	83x regular waves
(Liu *et al.*, 2019)	Oscillating Water Column (OWC)	V	n/a	n/a	(air chamber) 0.6m length; 0.8m width; 1.2m height	Y – air impulse turbine controlled by servomotor;	Regular waves only; based on 4 wave heights and 5 wave periods.
(Clemente *et al.*, 2020)	E-motions WEC concept (roll based)	V	1:40	14.8-19.7kg (ballast dependent)	15mm diameter half-tube; 0.2m draft, 0.76m width	Y – sliding PTO with springs on superstructure above float, relatively complex dynamics that influence WEC response	2 wave heights, then regular, irregular long-crested and irregular short-crested sea states (6 in total); 3x PTO damping values

Paper	WEC type	V/P	Scale	Mass (kg)	Dims (m)	PTO (Yes/No, type)	Other (waves, damping, sensors)
(Ersdal and Moe, 2013)	Aker WEC (articulated floating body)	V, P	1:30	106kg (barge) 8kg (absorber)	1.7m length 0.54m width 0.30m height (overall)	Y – direct drive servomotor (with drive for control)	28x irregular; Non-zero friction in motor; torque sensor at shaft
(Lamont-Kane, Folley and Whittaker, 2013)	Heaving buoy	P	n/a	n/a	0.25m D; 0.5m height	Y – electromagnetic clutch to restrict motion of tensioned cable that runs over pulley	21x regular; 8 irregular Single-axis load cell to measure instantaneous force; Standard deviation of applied damping force always within +/- 10% of target 0.4N
(Davey *et al.*, 2021)	Symmetric hinged-raft attenuator	V	1:25	200kg	1.44m length 0.87m width 0.31m height	Y – direct drive motor; real time controlled	12x irregular seas; Measurements of power output, hinge angles, mooring loads, 6 DoFs
(Pecher, Kofoed and Larsen, 2012)	WEPTOS WEC (A-shaped floating structure with attenuator flaps)	P	1:8.33	1150 kg for complete model	7.4m length (each leg of support frame); 0.2m D for each of the 40 rotors	Y – two electrical motors; constant a linear PTO damping applied; 1:3 gearbox used for each motor	12x irregular seas (JONSWAP); extreme wave states; peak enhancement factor and directional spreading effects explored for two wave states. Torque sensors mounted to each leg
(Pascal *et al.*, 2021)	Seaturns WEC (floating cylinder with pneumatic PTO)	V	1:30	n/a	0.31, 0.41, 0.51m lengths; diameter X	Y – adjustable orifice size (nonlinear damping)	Regular; irregular (JONSWAP), and 'Ir0' polychromatic

Table 37 - Summary of QOIs and types of reduced scale physical model tests found in literature (NB: the primary objective of the testing performed is denoted by: V = validation; P = performance). D = diameter; Dpto = PTO damping.

Appendix D – Chapter 4

This appendix provides additional context and details to support the theoretical underpinning highlighted in Chapter 4.

D.1 Key equations

The equations presented here are extracted from (Alves, 2016) and visually contextualised in a mind-map found below in this appendix. They are not exhaustive; we simply refer to those that are most fundamental and useful for the work presented and discussed in the rest of the thesis.

Equation of motion (given here in 1 DoF) from Newton's second law:

$$m\ddot{\varepsilon}(t) = F_{pe}(t) + F_{re}(t)$$

Where m is the total inertia of the captor, ε is the captor displacement (thus ε is the acceleration), F_{pe} are the external pressure forces (hydrodynamic/hydrostatic), and F_{re} are the reaction forces (PTO/mooring/end-stop).

A fundamental aspect of frequency-domain modelling is then that ε can be expressed as sinusoidal signals:

$$\varepsilon(t) = Re\{\hat{\varepsilon}(\omega)e^{i\omega t}\}$$

Where the $\hat{\varepsilon}$ is the complex amplitude of ε.

These can then be subsequently broken down as follows:

$$\hat{F}_{pe}(\omega) = \hat{F}_{hd}(\omega) + \hat{F}_{hs}(\omega)$$

$$\hat{F}_{re}(\omega) = \hat{F}_{pto}(\omega) + \hat{F}_{m}(\omega)$$

where $\hat{F}_{hd}$ is the hydrodynamic pressure force, $\hat{F}_{hs}$ is the hydrostatic pressure force, $\hat{F}_{pto}$ is the PTO reaction force, and $\hat{F}_{m}$ is the mooring reaction force. We omit the (ω) from here on.

The pressure forces can be further broken down as:

$$\hat{F}_{hd} = \hat{F}_{e} + \hat{F}_{r}$$

Composed of excitation and radiation components, where excitation can be further decomposed into incidence and scatter. The hydrostatic force can be expressed as a function of the hydrostatic coefficient, G, which acts as a spring stiffness term:

$$\hat{F}_{hs} = -G\hat{\varepsilon}$$

Radiation is related to the inherent impedance, Z, of the WEC, which can be expressed as:

$$Z = R + i\omega A$$

resulting in:

$$\hat{F}_r = -i\omega R\hat{\varepsilon} + \omega^2 A\hat{\varepsilon}$$

where R is the hydrodynamic damping coefficient, and A is known as the added mass.

$\hat{F}_{hd}$ and $\hat{F}_{hs}$ can then be broken down further – refer to mind-map.

Moving on to the reaction forces, in a linear form, the PTO force can be expressed as:

$$\hat{F}_{pto} = -i\omega B_{pto}\hat{\varepsilon} - K_{pto}\hat{\varepsilon}$$

and the mooring reaction force as:

$$\hat{F}_m = -K_m\hat{\varepsilon}$$

where B_{pto} is the PTO damping, K_{pto} is the PTO spring, and K_m is the mooring spring term.

Coming on to power absorption, the mean absorbed power over a wave period is expressed as:

$$P_a = \frac{1}{2}B_{pto}\omega^2|\hat{\varepsilon}|^2$$

[Mean incident power = power transported per unit of time and width of a wave]

$$J_w = \left(\frac{\rho g^2 D(kh)}{4\omega}\right)|A_w|^2$$

Where $D(kh)$ is the depth function (which defined the effect of sea bottom proximity to orbital motion of water particles), ρ is the density of water, g is the acceleration due to gravity, and A_w is the incident wave amplitude.

Capture width is then defined as the ratio of absorbed to incident power:

$$CW = \frac{P_a}{J_w} = \frac{2\omega^2 B_{pto}}{\rho g}\left|\frac{\hat{\varepsilon}}{A_w}\right|^2$$

Where the term $\left|\frac{\hat{\varepsilon}}{A_w}\right|$ is commonly referred to as the response amplitude operator (RAO), and is the ratio of the captor's response to the incident wave amplitude. To give an example, in heave DoF, if the RAO is equal to 1 at a particular frequency, it means the captor is moving exactly with the water surface.

Finally the absorption bandwidth:

$$\Delta\omega = \frac{B_{pto} + R}{M + A}$$

where M is the mass. In general, bandwidth tends to increase with size due to lower relative weight of the denominator ($M + A$) reactive term. The wider the bandwidth the lower the need for optimal control to maximise power capture away from the resonant frequency (Alves, 2016).

D.2 Theory mind-map

The following mind-map has been assembled by the author, with reference to (Alves, 2016) – ‘Frequency-domain Models’, Chapter 2 in Numerical Modelling of Wave Energy Converters. Edited by M. Folley. Elsevier Ltd.

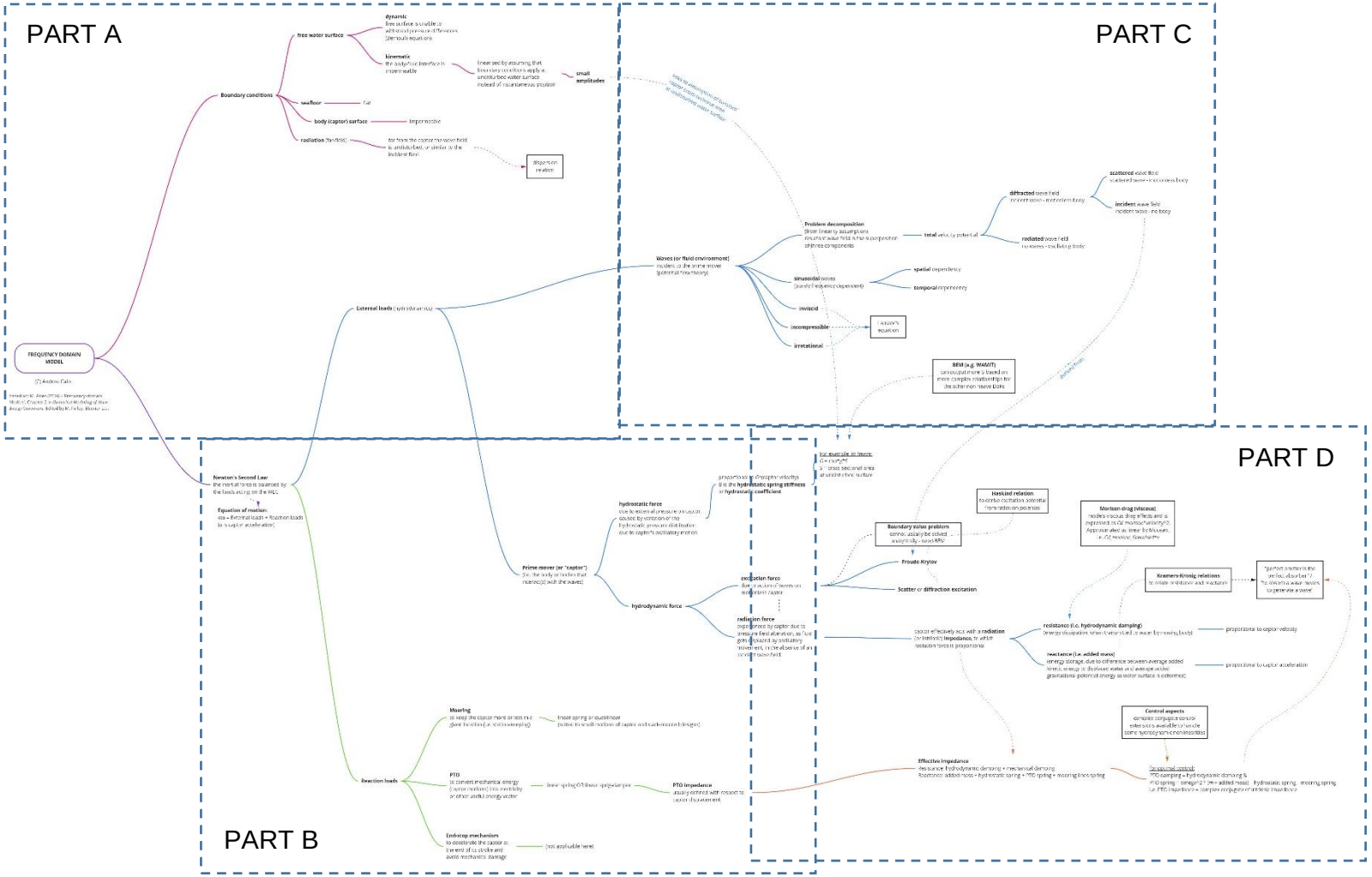

Figure 184 - Mind-map showing frequency-domain model elements, assumption, and key relationships.

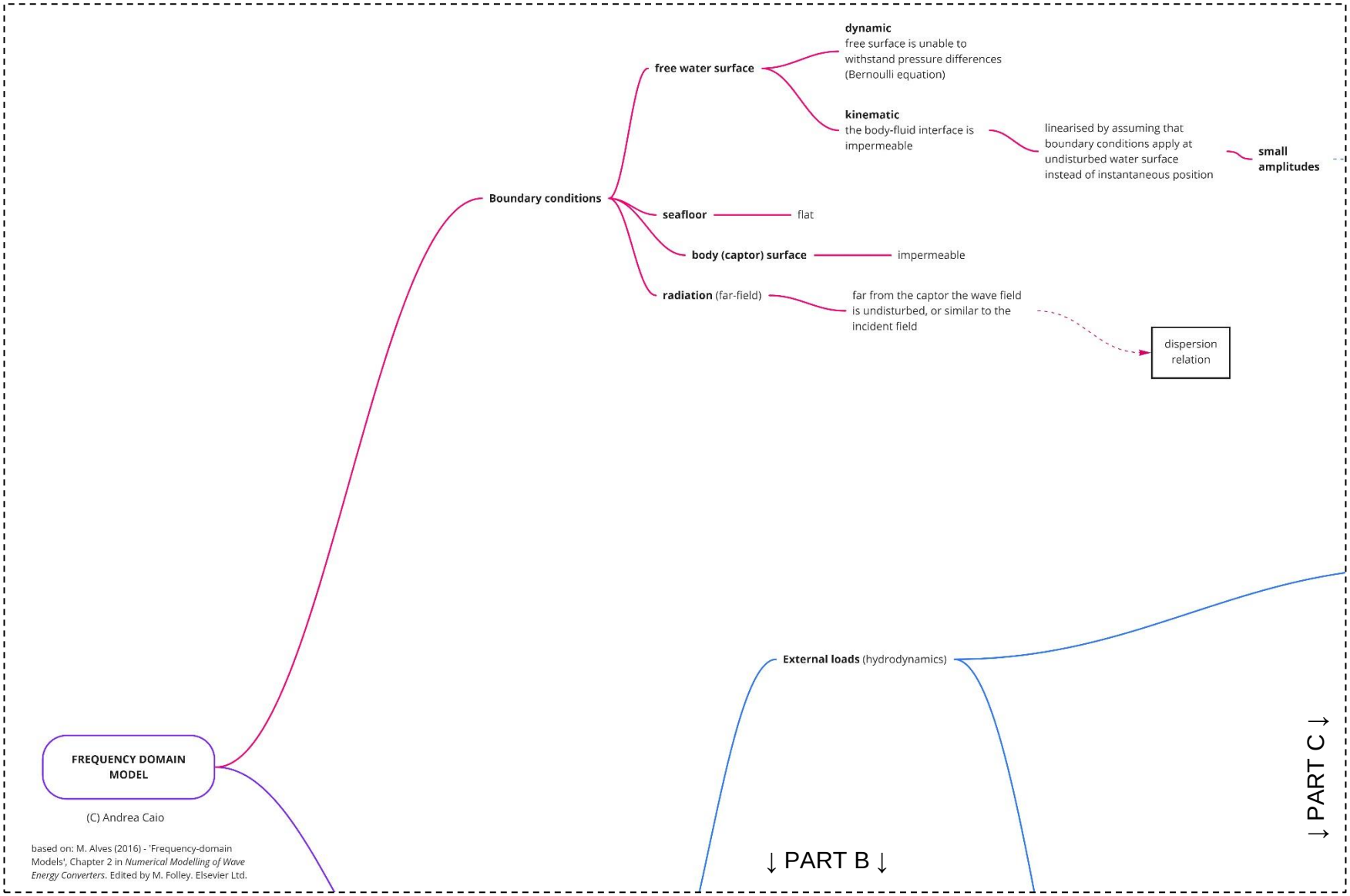

Figure 185 - Mind-map breakdown – PART A.

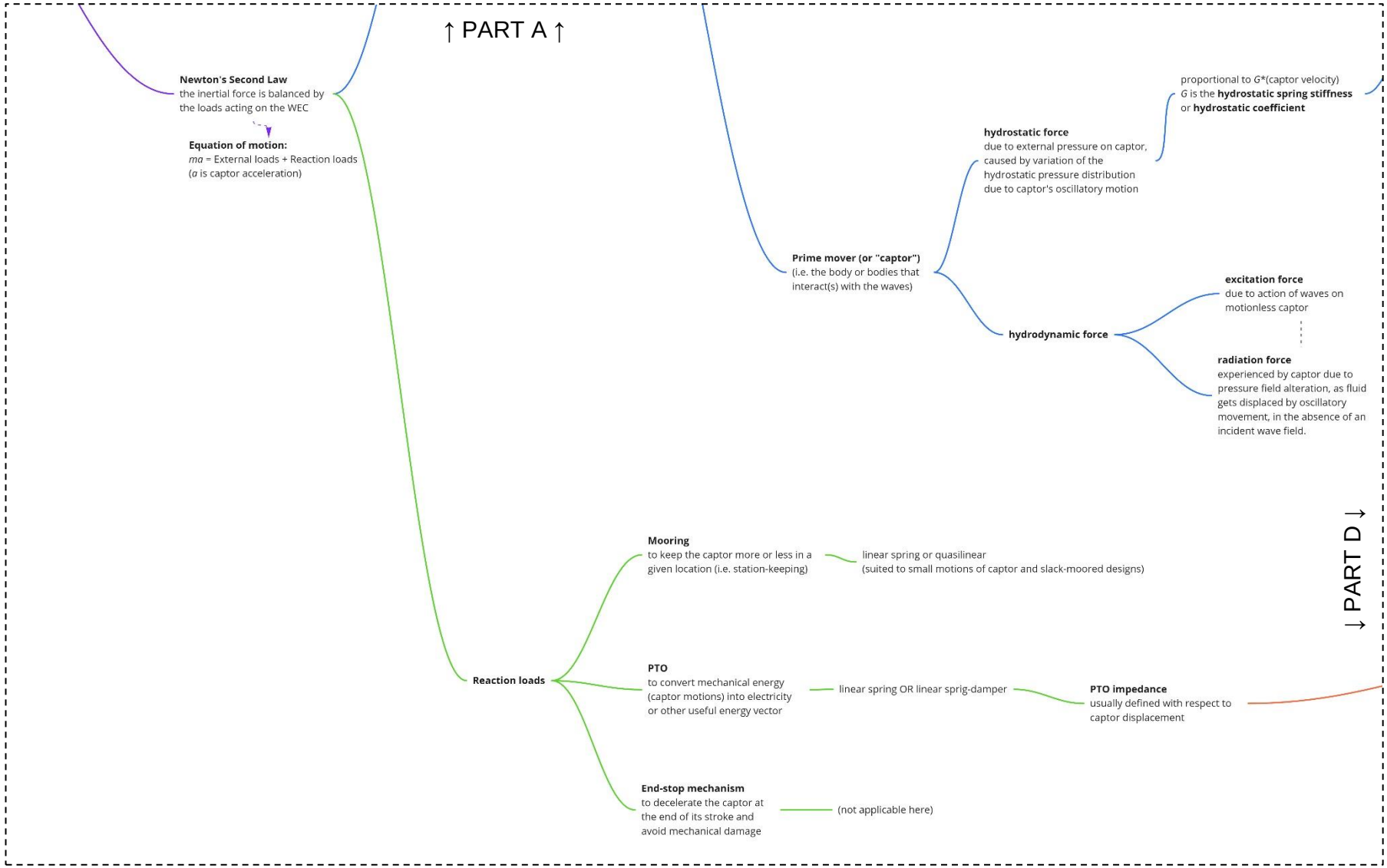

Figure 186 - Mind-map breakdown – PART B.

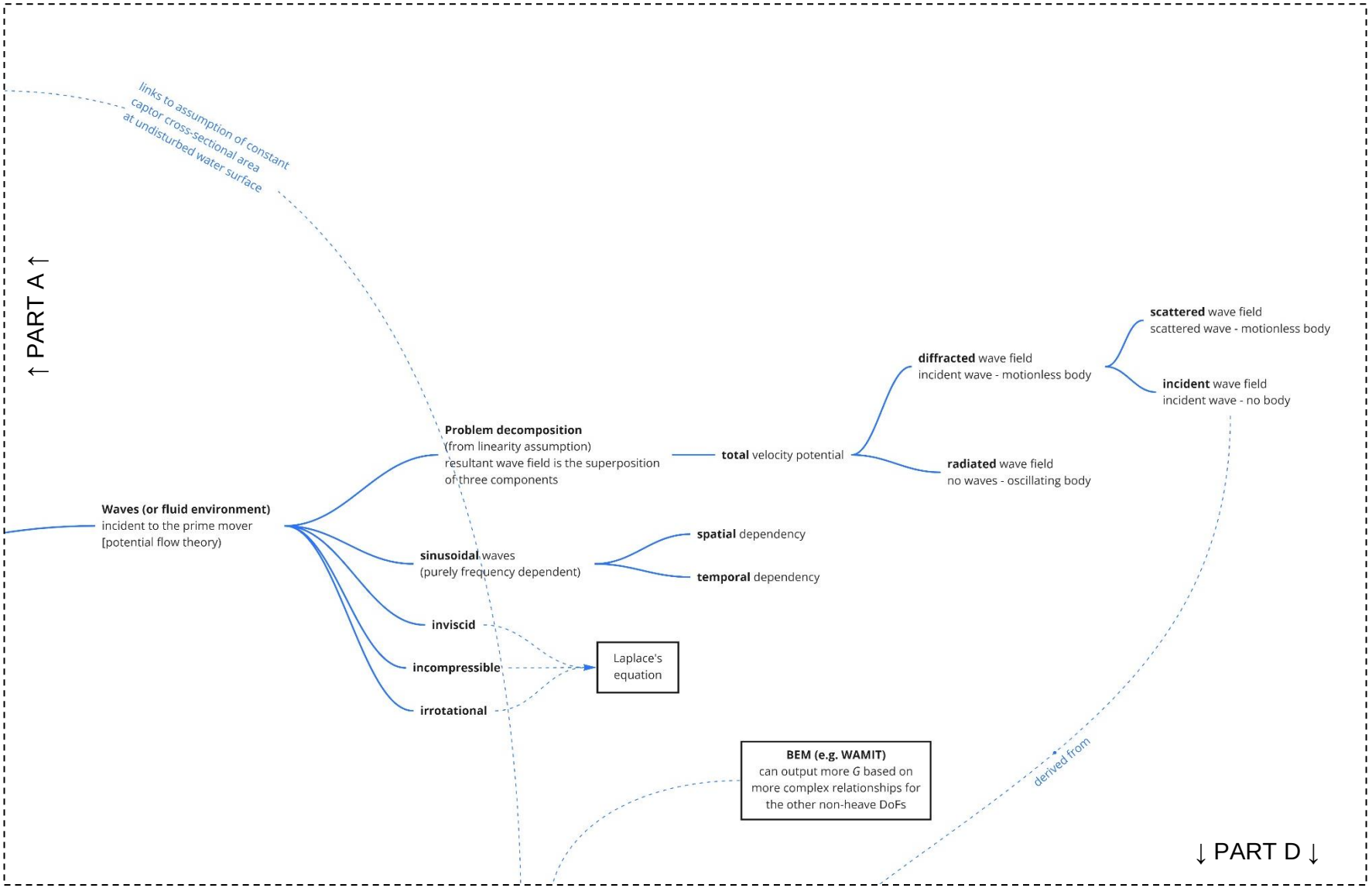

Figure 187 - Mind-map breakdown – PART C.

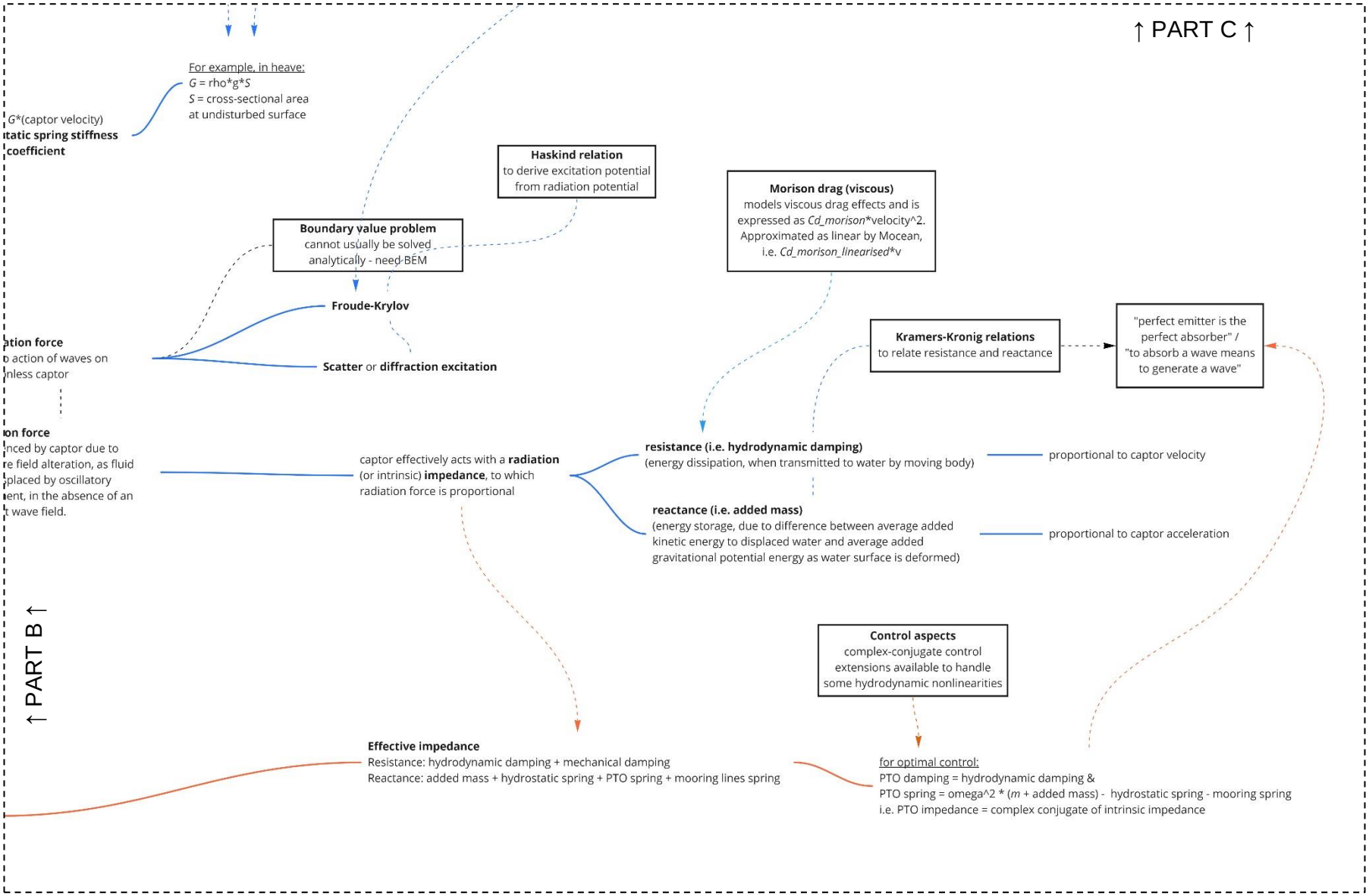

Figure 188 - Mind-map breakdown – PART D.

D.3 Wave characterisation

Some notes on different spectra & different domains are given below.

A general reference for different domain applications to numerical modelling is (Matt Folley, 2016). Frequency-domain (FD) is the most relevant to WAMIT (Alves, 2016). FD is usually always the first step in modelling WECs. The primary component of most frequency-domain models is the wave-body interaction (usually computed with WAMIT/NEMOH because of the lack of analytical solutions). WAMIT is an example of a Boundary Element Method (BEM) used “to estimate the hydrodynamic coefficients of added mass and damping, and the excitation force per unit wave amplitude” (Alves, 2016).

FD analysis is enabled by linearization of governing equations.

On the other hand, TD is necessary for inclusion of non-linearities. These arise from energy chain elements (PTO, power conversion, friction, moorings), more complex fluid interactions, and more complex control mechanisms. The other key differentiator is in the ability to model transient phenomena, which is not possible in FD (because assumes stationarity) (Ricci, 2016). The quadratic nonlinear viscous drag model is quite common amongst modelling WECs in the time domain. From (Ricci, 2016), the other main take-aways relating to TD models are:

- Fundamentally based on the Cummins equation (Cummins, 1962)
- TD models are more computationally demanding than FD models and “the uncertainty in expected power capture and WEC response decreases with the square root of the simulation duration” (Ricci, 2016)
- A higher risk of significant errors in predicted response due to model formulation errors.

SD is discussed more in relation to PTO modelling – it is more efficient for computing statistical parameters such as average power capture.

The fundamental difference from TD and FD is its use of a “probabilistic model of the system dynamics,” while both FD and TD are deterministic in solving the equation of motion. It is based on the assumption that the wave spectrum

chosen is a “reasonable statistical representation of the waves”. This statistically represents a large number of sinusoidal waves, with spectral energy density (in J/Hz) varying with both frequency and direction, though direction is often not considered – at least initially. Limited because: it excludes the phase relationship between the waves.

If it is assumed that this phase relationship is random, the waves can be modelled as a Gaussian process. Nonlinear forces are also therefore modelled as probabilistic processes, with often satisfactory results. For example, it is” the standard model used for large-scale modelling of wave propagation processes” (M Folley, 2016). (Folley and Whittaker, 2010) showed that statistical linearization of drag forces and large-angle rotations for a flap-type WEC closely aligned with TD model predictions.

In summary, from (M Folley, 2016):

- Just as the wave resource, the WEC responses are also probabilistic. For example, can use SD to compute an expected average power capture.
- Cannot be used for extreme responses modelling
- Linear potential flow solution is typically used to obtain hydrodynamic forces, and the SD solution is typically an iteration of an FD model, and especially suitable when large numbers of simulations are required (e.g. optimisation routine, and indeed this is what Mocean uses in its numerical code).
- Assumes nonlinear forces can be linearised and that the WEC response is usually Gaussian
- Can model quadratic damping and Coulomb friction nonlinear forces

Within a given sea state, the computation of hydrodynamic responses is linear. However, the theory used to create the power matrix for a given WEC iteration is quasi-nonlinear. In other words, coefficients related to the viscous damping and PTO damping are varied as a function of sea state. The determination of the coefficient variation is given by Folley’s spectral WEC theory (Folley and Whittaker, 2010).

- *"Spectral domain (SD) modelling is a means of including nonlinear forces in a fast FD-like computation. It is based on assumptions about the statistical independence of the wave components that make up a wave spectrum, and as such it is only appropriate to apply it to spectral seas (i.e. not regular waves)."*

Generally speaking, the SD model is a fast way of incorporating nonlinear forces into the numerical model, and is therefore applied within Mocean's optimisation effort. In particular, the SD model can evaluate statistical parameters (e.g. power) for spectral seas in a fast manner. Mocean verified case study SD results with an equivalent TD model. The agreement was very good, demonstrating the advantage of the SD model over FD in terms of accuracy, and over TD in terms of computational time. As such, the inclusion of nonlinear forces should significantly increase the accuracy of energy production estimates, while adding negligible computation time. The exact SD model theory is not discussed further. The following references are provided, on which the SD model is based upon: (Folley and Whittaker, 2010, 2013; Matt Folley, 2016).

AEP is calculated by a spectral computation, in which the viscous damping changes with each different sea state. This is not so for the frequency domain computation. The spectral domain computation is essentially interpolating the FD computation.

D.4 Limitations

This subsection is once again extracted from (Alves, 2016).

The limitation of FD modelling stem from the linearization assumptions, which restrict their use to linear problems. Accuracy around resonance is a key area of limitation, since this is where small amplitude assumptions are likeliest to be unsatisfied. Another aspect that FD modelling cannot account for is viscous effects, such as flow separation and vortex shedding due to the inviscid flow assumption.

Aside from nonlinearity of the captor's response, nonlinearity of the waves themselves is not accounted for either; this results from assuming that the

amplitude is small relative to the wavelength. It means that waves are assumed to be well below the steepness at which breaking occurs. The shape of the waves, assumed to be monochromatic and sinusoidal, is also a limitation in terms of accurately representing real waves. For example, these tend to be 'peakier' at the crests and shallower at troughs.

Finally, there are control-related limitations, since control strategies able to maximise power capture tend to be complex and nonlinear. The only real possibility with linear control strategies is applying constant PTO coefficients since no real-time information is available to implement anything more advanced. However, in Mocean's case and in terms of this thesis work, this is not as significant because simple "quasi-linear" control strategies are implemented both in the numerical optimisation routine and purely linear in the physical tests themselves.

D.5 Drag coefficients

Drag forces are typically included in parameterised form as in Morison equation, but require calibration of drag coefficients. A few notes on drag coefficients are given below:

- WAMIT is based on potential flow theory and thus cannot explicitly account for form drag, induced drag (vortex shedding) or viscous drag forces.
- In the time-domain (TD), the Morison forces are computed proportional to the square of the velocity, and are therefore nonlinear. In the frequency-domain (FD), a linear approximation is used by tuning a non-dimensional coefficient that is combined with water density and body surface areas to compute dimensional Morison coefficients.
- For Morison damping:

$$Fd = 0.5 * Cd * rho * A * v\text{^}2$$

  where Cd is the Morison coefficient and A is the submerged area
- In the numerical model, the only drag forces accounted for are perpendicular to the body surfaces, but the calibration process essentially groups all of the physically present drag forces into one coefficient.

- This coefficient has never been tuned in the FD. The non-dimensional coefficient is only tuned in the TD, and then transferred across as a linear ‘equivalent’ term to the FD.
- In the NWEC2 tests, the scope was trying to tune the Morison Cd value, the plate damping coefficients (phase and magnitude), and the number of Morison points used.
- However, in the latest BST-folding, according to TD validation work with Plymouth results, damping plate inclusion did not seem necessary, and has not been included in the BST-baseline or folding models.

Thinking about the specific geometry of BST-baseline and BST-folding, is there a penalty in terms of viscous losses in the numerical model if the model is boxy? No, a boxy cross-section means likelier flow separation which cannot be quantified using potential flow.

Viscous losses are modelled via wave channel ‘plate damping’ and Morison damping. The Morison damping coefficient Cd is chosen based on validation work in the tank. There are errors from A also, which is assumed to be a constant submerged area but in reality changes dynamically. In the FD, however, one is always working with mean values for a given wave frequency.

A key aspect of the validation from experimental models is choosing the correct Cd.

D.6 Numerical optimisation

D.6.1 Fitness function

The reference figures in the updated fitness function have usually represented targets.

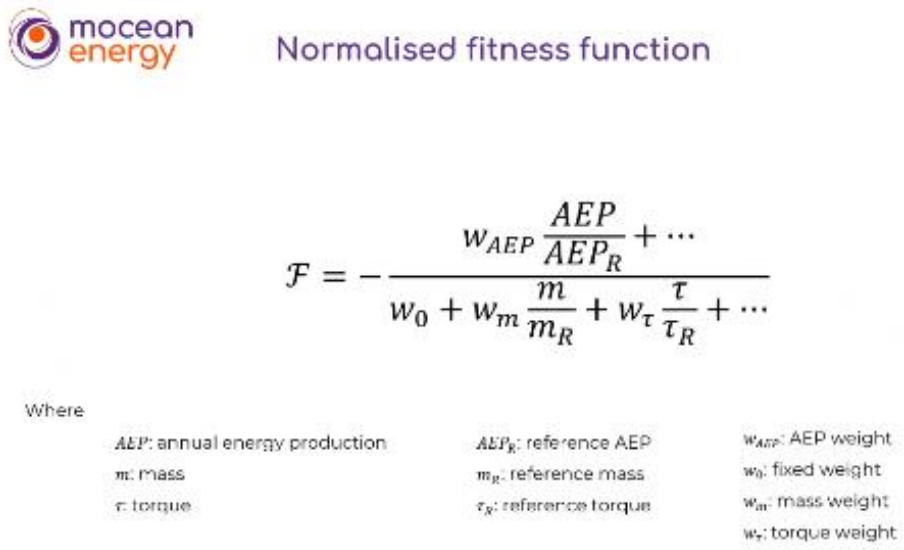

Figure 189 - Illustration of normalised fitness function. Courtesy: Mocean Energy.

  - Everything is non-dimensionalised, weighting are also non-dimensional
  - It is 'extensible' – can add other elements of performance at the top or cost at the bottom
    - E.g. battery cost at bottom if looking at min continuously available power.
  - Can set the same object for multiple objectives – e.g. can set w_m to zero and then you're just optimising for a torque cost.
  - The 'R' terms act as target values, which can be changed depending on the device or site targeted
  - The weightings can be assigned as percentages of the total cost of the Blue X prototype, for example, as that is the hard data we have available (though for a FOAK device).
  - Avoids the need for specific values that obfuscate the process somewhat
  - Can run sensitivity analyses specifically on each weighting
  - Fitness function is device agnostic – can simply change target parameters and everything is non-dimensionalised
- [2020-10-13]
  - At the moment, can only drop torque limit in order to regulate cost (that is the only PTO related mod that the optimisation can make) (nacelle diameter is fixed)
- The plate thickness is now 12mm and CZ says ok but decision to change to 15mm effective
- Gabriel mentions efficiency of 0.8 being used. Q: at what point was this introduced? What was it before?

D.6.2 Optimisation parameters

Some inputs are constant, some are variable parameters that feed into the optimisation. Two PTO parameters only in the numerical model underlying optimisation: torque limit and PTO damping.

Number	Parameter	LowerBound	UpperBound	Units	Description
1	NacIsFwd	1.99	1.99	bool	Nacelle hull is forward
2	NacDiam	4	4	m	Nacelle diameter
3	NacBeam	7	7		Nacelle beam
4	Zloc	-1.9	0.5	m	Location of hinge below SWL
5	TLim	1	2	MNm	Torque limit
6	dpto	1	55	MNms/rad	Power take off damping range
7	FwdChanWSlope	30	30	deg	Angle of channel wall with vertical
8	FwdChanBSlope	55	90	deg	Angle of channel base plate with vertical
9	FwdChanBLength	2	7	m	Length of wave channel base plate
10	FwdChanWLength	5	7	m	Length of wave channel top wall
11	FwdChanWBeam	4.5	15	m	Beam width of wave channel wall section
12	FwdChanBBeam	4.5	15	m	Beam width of wave channel end section
13	AftChanWSlope	30	30	deg	Angle of channel wall with vertical
14	AftChanBSlope	55	90	deg	Angle of channel base plate with vertical
15	AftChanBLength	2	7	m	Length of wave channel base plate
16	AftChanWLength	5	7	m	Length of wave channel top wall
17	AftChanWBeam	4.5	15	m	Beam width of wave channel wall section
18	AftChanBBeam	4.5	15	m	Beam width of wave channel end section
19	FwdD1	4.5	4.5	m	Main tube diameter start
20	FwdD2	4.5	4.5	m	Main tube diameter end
21	FwdB1	4.5	4.5	m	Main tube start beam
22	FwdB2	4.5	4.5	m	Main tube end beam
23	FwdL1	5	25	m	Main tube length
24	FwdL2	1	3	m	Main tube end to wave channel wall
25	AftD1	4.5	4.5	m	Main tube diameter start
26	AftD2	4.5	4.5	m	Main tube diameter end
27	AftB1	4.5	4.5	m	Main tube start beam
28	AftB2	4.5	4.5	m	Main tube end beam
29	AftL1	5	25	m	Main tube length
30	AftL2	1	3	m	Main tube end to wave channel wall

Figure 190 - Showing 30 possible parameters as input to geometry optimisation. Courtesy of: Mocean Energy.

D.6.3 Numerical modelling of PTO

This section discusses how the torque limit and Dpto are taken into account/modelled.

As previously seen, WAMIT is the step that performs the hydrodynamic computation, and takes the most amount of time in the optimisation. Thus, a range of different Dpto values are ‘trialled’ subsequently to the WAMIT computation.

These are specified as a central input Dpto value, and an exponential range going from 0.1 to 10 times this central value (i.e. the optimisation can pick from 9 different Dtpo values). A different Dpto value can be chosen (from the 9 possible) according to the value that maximises each particular cell of the Power Matrix.

A single Dpto value is then chosen corresponding to the value that gives the maximum Energy Matrix cell entry. This is then linearised according to the set torque limit. The RAO curve is plotted using this single linearised PTO damping value that gives the maximum energy captured cell. The physical model damping should aim to match this linearised Dpto value, which is outputted by the optimisation. Each damping value would give a different RAO shape with a shifted peak.

Tuning of the Dpto value depending on the particular sea state encountered is what a control system would then try to execute. This is not carried out in the optimisation. Therefore, the resulting AEP value can be considered conservative, since it relies on a non-controllable Dpto, which ideally would actually vary (e.g. as a function of sea state). The PTO damping value is only set for the ‘flex’ DoF, and is set to zero for all other DoFs, since the WEC is only extracting power in flex.

D.7 Previous testing programmes

D.7.1 Wave Energy Scotland NWEC1

Tests performed during the first stage of the NWEC programme primarily focused on concept selection and validation. Four 50th scale active models were built and tested in Edinburgh University’s Curved Tank. Once a candidate was chosen, a larger 20th scale model with a motorised and instrumented hinge was tested in FloWave focusing on further validation and performance tests. The goal of the latter was to extend the validation and understanding of WEC hydrodynamics. A comparison of plates vs hulls was made and the aim was to be able to apply a damping of 120MNms/rad equivalent full-scale.

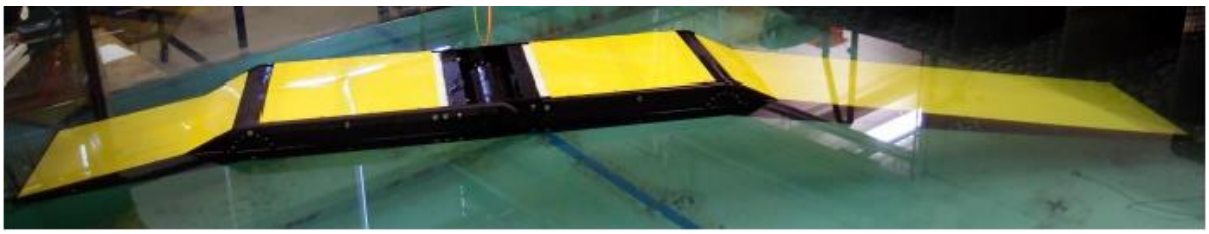

Figure 191 - 20th scale model being ballasted at the Edinburgh University Curved Tank (Image courtesy of Mocean Energy).

The following metrics were used to compare 1/50 scale concepts:

1. (linearised) Annual Energy Production (AEP)
2. (linearised) Non-dimensional annual average climate capture width (ACCW)

ACCW is defined as the ratio of AEP to the average incident energy flux density (E_f) multiplied by the number of hours in a year:

$$ACCW = \frac{AEP}{8760 \times E_f},$$

This is then normalised by characteristic length, r0, defined as the radius of a sphere with equivalent displacement as the WEC:

$$r_0 = \sqrt[3]{3V_s/2\pi}$$

V_s is the submerged volume of the WEC.

Given the mismatch between (over)predicted and measured performance, “real power factors” are defined for each tested 50th scale geometry to adjust AEP and ACCW metrics. These are defined as the interval [mean, std] of:

- ratio of power curve peaks
- ratio of power curve integrals (areas under curve)

Broadly speaking, the more nonlinear a response of the physical model, the smaller the values of the “real power factors” become – i.e. the more the numerical prediction tends to overestimate power capture.

Numerical model notes:

- 2D features only modelled by numerical geometry 'generator'. Now Blue Insight can generate 3D features, albeit with some time/debugging/etc. costs and limitations.

- Tests were a good example of how relatively low-fidelity models (in this case, linearised FD) may likely work better if doing concept studies where you're comparing performance to pick a or some best candidates, and less well if you're trying to be accurate about performance achieved.

Lessons learned:

- Nonlinear effects need to better understood and characterised - points to need for higher order numerical models
    - "Understanding of nonlinear effects would benefit from controlled experiments, which would likely be faster to carry out than to set up and run a high-order numerical model"
- Results point to the fact that reducing nonlinear effects will improve machine performance

D.7.2 Wave Energy Scotland NWEC2

Three physical models were tested during this development phase. The first was a (formally) 1/53[97] scale model primarily conceived for validation (Figure 192) and tested in the Curved Tank. Two further models were designed and tested for a combination of performance and validation purposes, at 1/40th and 1/20th scales. The latter two models were optimised with an upgraded numerical model that included wave channel damping plates. The geometry is therefore different (see Figure 193 and Figure 194). These two models were tested in FloWave.

[97] Scale was chosen according to the minimum width and diameter of the hinge to accommodate the motor and torque sensors. Cannot compare this to the 20th scale model because although full-scale width is the same, hull height, mass and drafts differ. This is considered acceptable because the primary use for it is validation and not performance comparison at different scales. The chosen full-scale equivalent dimensions can be manually entered into the numerical model.

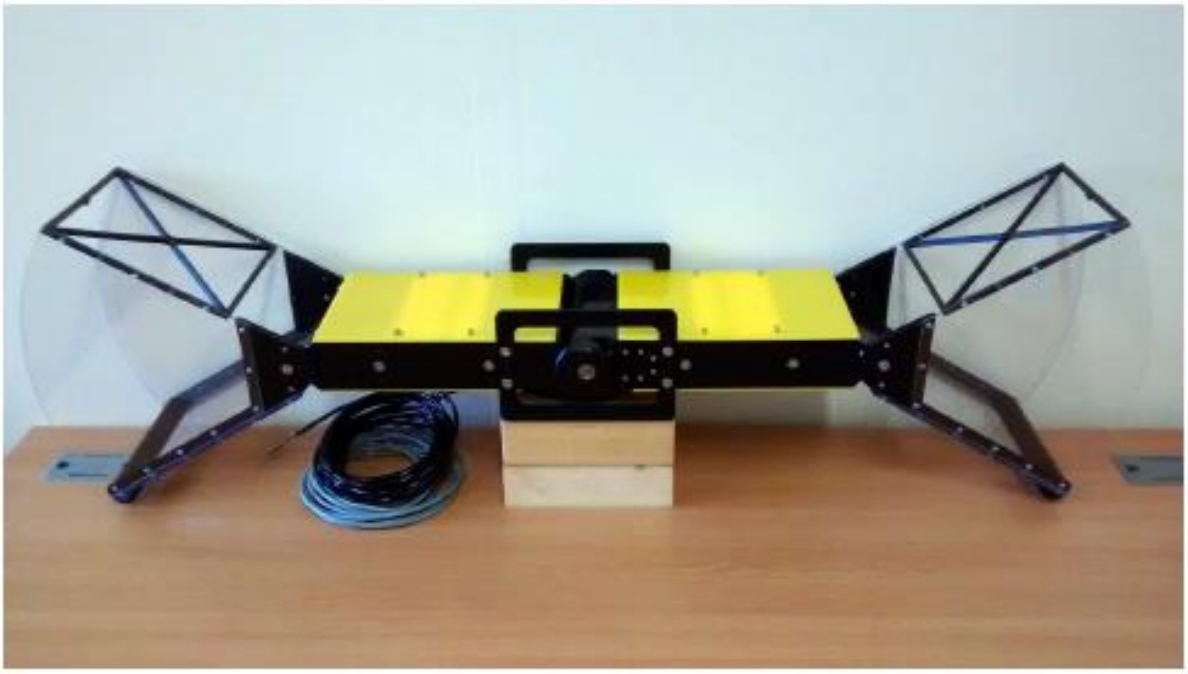

Figure 192 - Validation model used in NWEC2.

Figure 192 shows the 1/53 scale model with the hinge supported by raised wooden blocks. A cross brace can be seen around the hinge, which is used to fix the hulls together in a particular validation configuration. Inclined plates extend downwards at the end of each hull and have a foil section at the lowest incident wave edge to mitigate vortex shedding. The angle of inclination of these plates can be varied. Transparent side guards limit lateral flow, and a brace at the top helps with structural stability. Two cables are also visible, corresponding to motor and torque sensors.

Figure 193 - 40th scale model as-built - 3D printed ABS plastic.

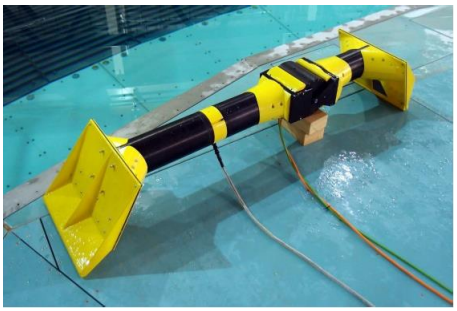

Figure 194 - 20th scale model as-built- anodised aluminium (black) and 3D printed ABS plastic (yellow).

Figure 193 and Figure 194 show geometrically equivalent models based on later optimisations carried out during NWEC2. It can be seen that the WEC is relatively narrower, which means it can no longer accommodate a torque sensor, nor a gearbox, in line with the motor within the hinge nacelle. In some respects this can be viewed as a feature, as opposed to a bug. A simpler drive train – particularly one that excludes gearboxes – reduces backlash and wind up in the drivetrain, improving the quality of data. On the other hand, the lack of torque sensor means that friction impacts on the measured power have to be estimated instead of directly measured. It is therefore a compromise.

The scale of the 20th model was chosen such that it could include a motor with the appropriate torque requirement to avoid the need for a gearbox (Kollmorgen AKM43E with continuous/peak torque capacity of 4.7/15.9Nm, corresponding to 0.8/2.4MNm full scale).

Two phases of tests were carried out with the validation model. Phase ‘a’ explored the effect of geometry changes and PTO control, to further validate the numerical model. The second, Phase ‘b’, aimed to validate a more complex and higher fidelity numerical model, while testing configurations that limited the introduction of uncertainty due to the influence of the hinge. The aim was to improve the fidelity while maintaining simplicity (speed) of the model for its use as part of optimisation routine.

The 40th model was primarily tested to verify survival mode behaviour, without any hinge damping, and towing behaviour. The 20th model involved a thorough testing campaign that included validation and performance. It provides a comparison with the NWEC1 20th scale model power performance.

Appendix E – Chapter 5

E.1 System block diagram

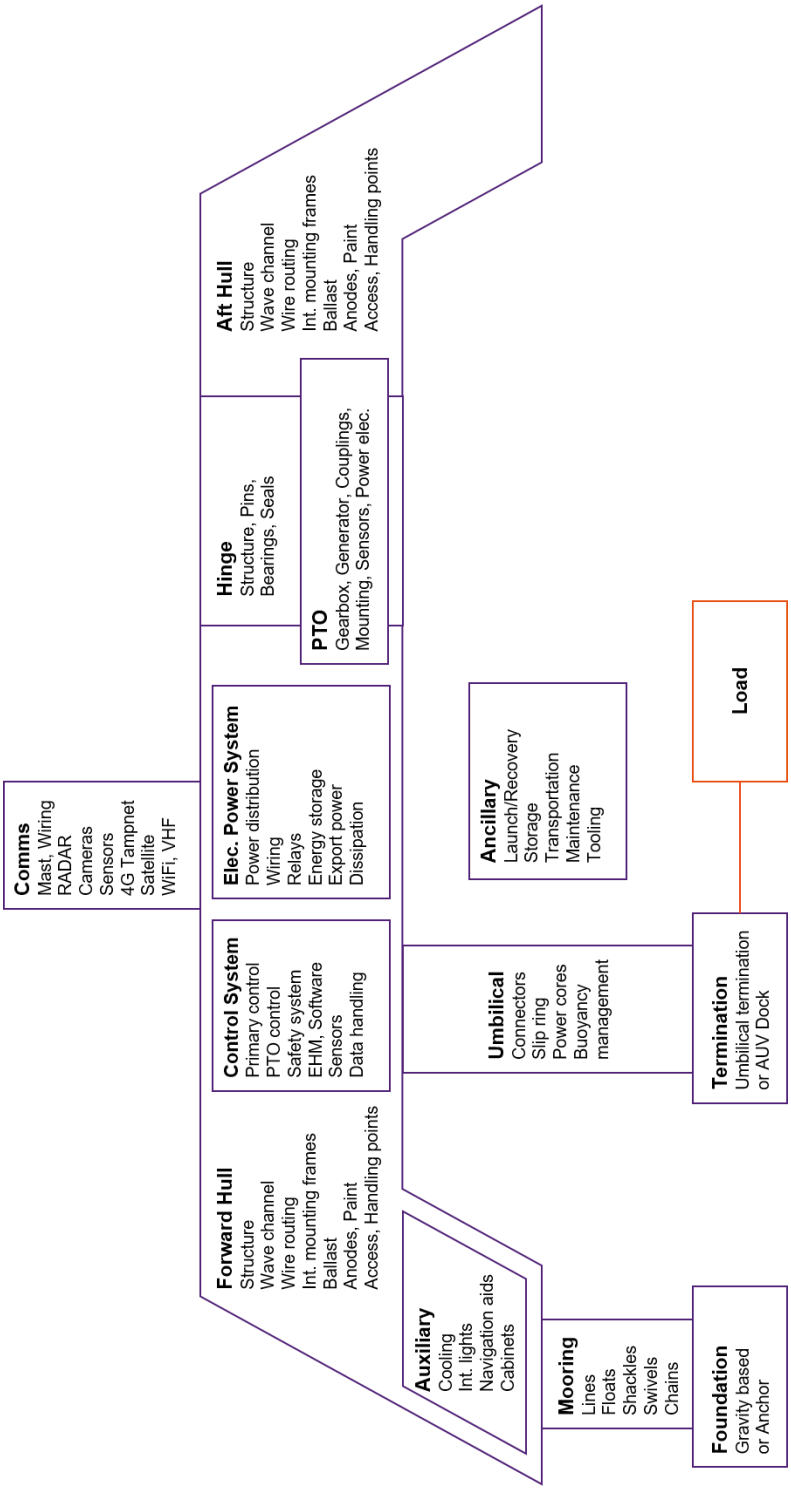

Figure 195 - Blue Star WEC system block diagram.

E.2 Dimensionality of metrics

Different metrics scaled according to Froude law are shown below:

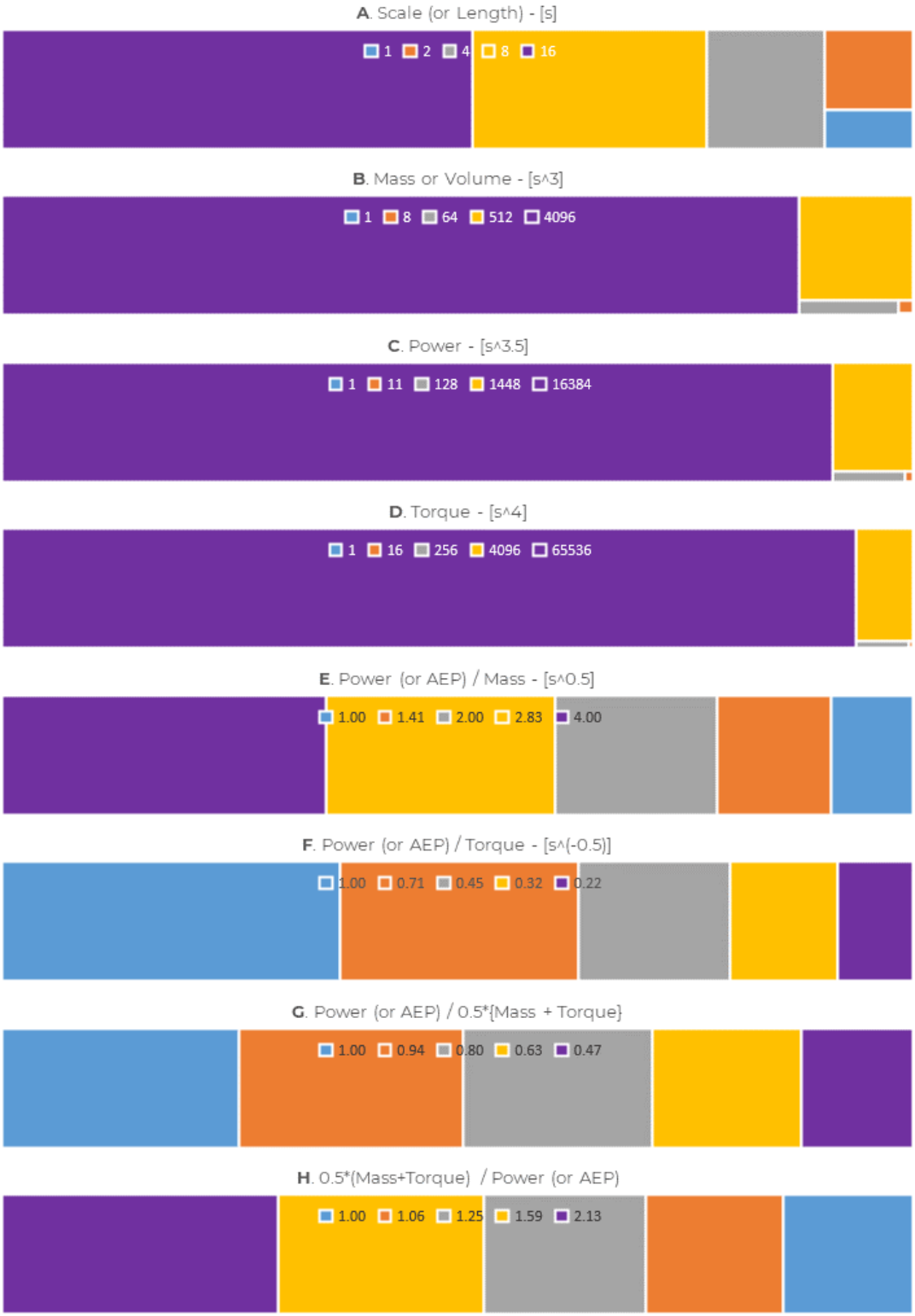

Figure 196 - Showing areas proportional to the Froude scaling factor associated with different metrics.

Appendix F

This Appendix provides additional context and details to support the theoretical underpinning highlighted in Chapter 6.

F.1 Model build

Figure 197 - 3D printed physical realisation of non-instrumented FWD (left) and AFT (right) sections. (Visible topside holes are designed to fit optical tracking system targets during testing.

F.1.1 Wave channel fins

Figure 198 - 3d printed AFT and FWD fins.

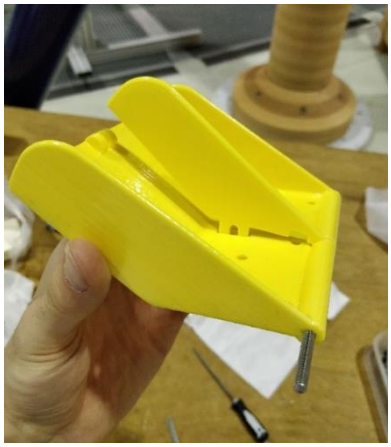

Figure 199 - Showing locating rod and pivoting AFT fin.

Figure 200 - Showing wave channel underside with screw slot location.

The model is set up to have removable ‘fins’ at the FWD and AFT wave channels, so that it can be tested in multiple configurations; the numerical model seems to suggest that these have a non-negligible effect on resulting AEP. To facilitate assembly, each fin is held by a threaded rod that runs across the wave channel sections – allowing them to pivot – and secured by a nut-and-screw

arrangement on the underside of the wave channels Figure 200. Figure 199 and Figure 200 illustrate this at the AFT wave channel.

F.1.2 Permitted angular flex range

The flex motion is not shown but is equal to the aft pitch motion minus the forward pitch motion; hinge hogging angles are positive. Throughout testing, it is necessary to avoid bottoming out of the AFT hull with respect to the Nacelle. Based on previous M100 scaled testing at 40th scale (most representative compared to the chosen scale of BST-baseline model), the maximum flex angle occurs in hogging and approaches 90° in extreme waves. Thus, to allow for potential survivability testing a positive flex angle up to 110° is permitted, at which the flanges bottom out on the nacelle (see Figure 201). Similarly, a negative flex angle up to 90° is permitted, illustrated in Figure 202.

Figure 201 - Maximum hogging angle of AFT hull w.r.t. nacelle (110 degrees).

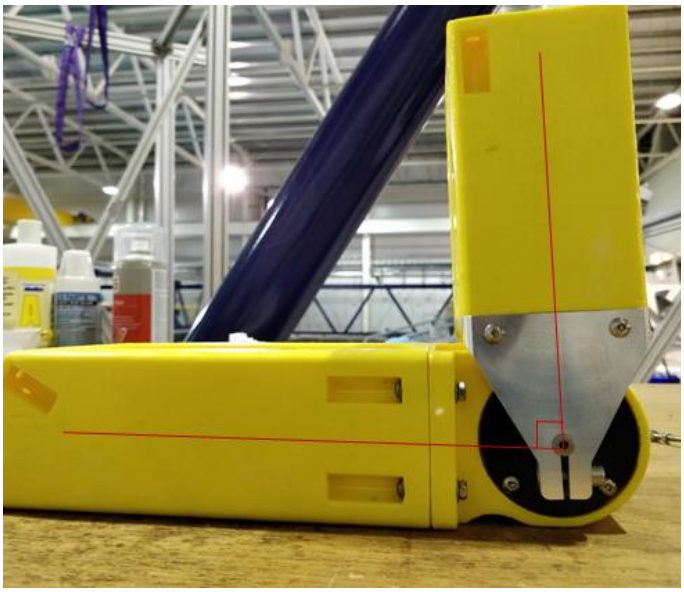

Figure 202 - Maximum negative flex angle of AFT hull w.r.t. nacelle (90 degrees).

F.1.3 Concept sketches

Figure 203 illustrates a manual sketch of the rotary sensor-activator interface, with its associated recommended mounting arrangement. Of particular noteworthiness is the recommended 0.5-2.0mm spacing between activator and sensor faces.

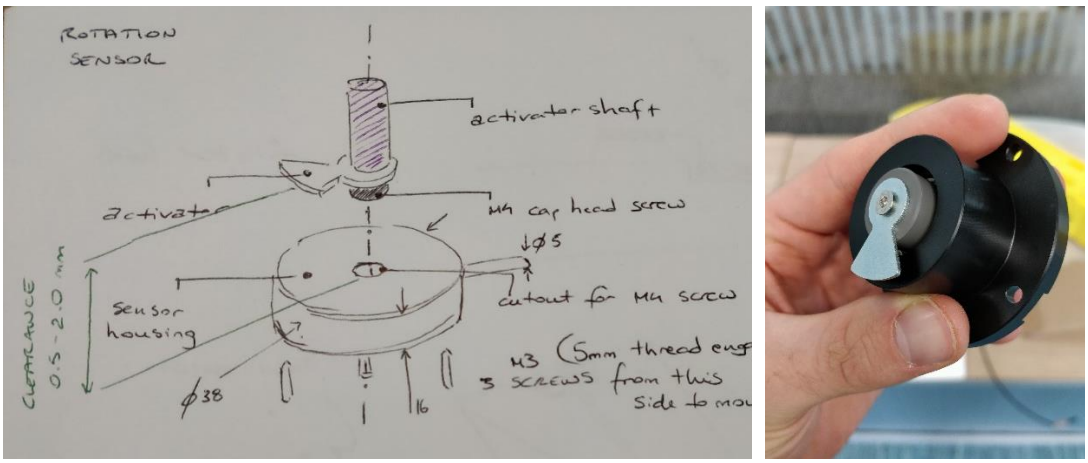

Figure 203 - Rotary sensor mounting arrangement (left) and activator location on shaft spacer (right).

Figure 204 illustrates a preliminary tolerance analysis of the rotary sensor-activator mounting arrangement, in order to ensure a 0.5-2.0mm spacing to be achieved.

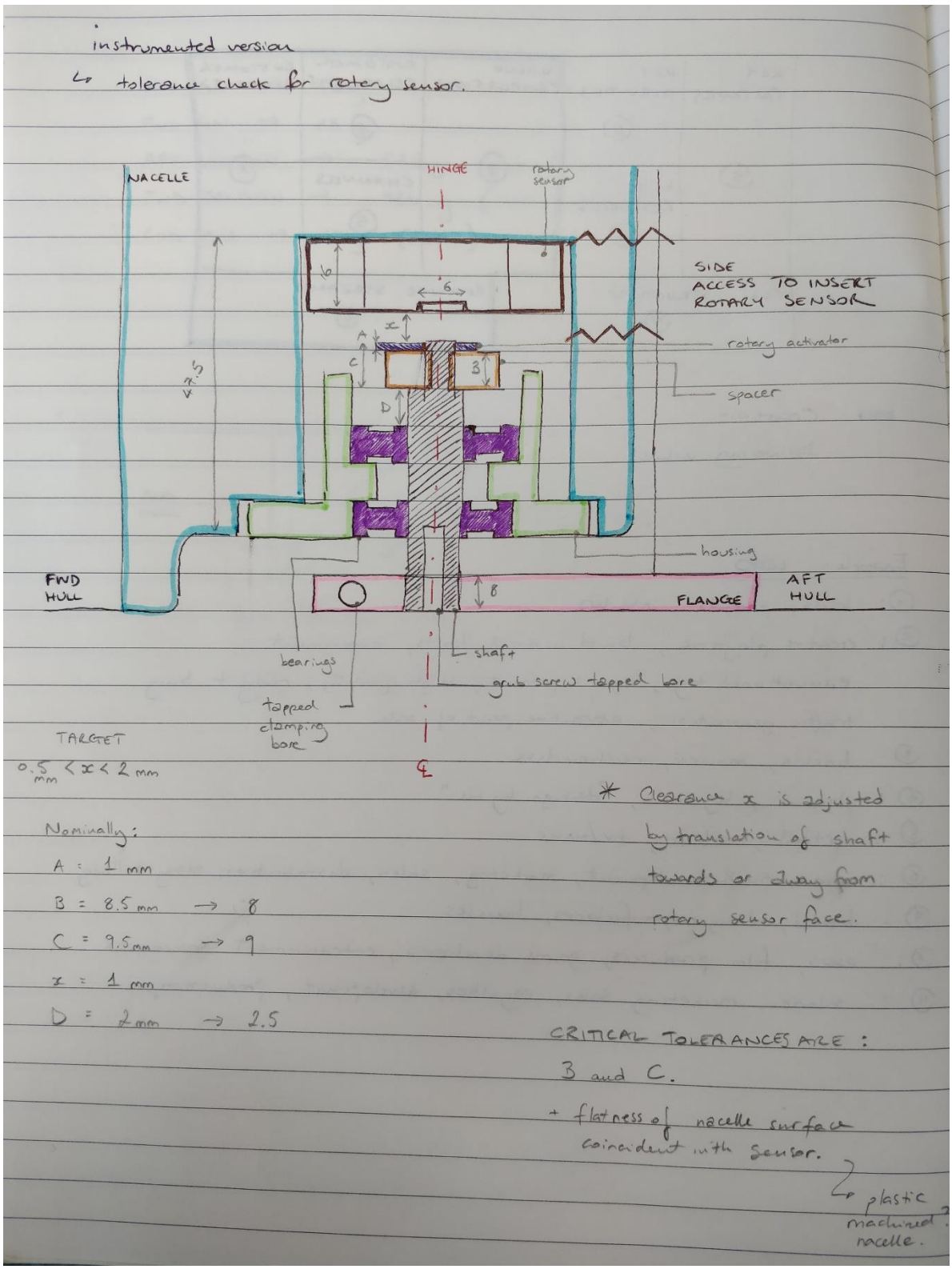

Figure 204 - Preliminary tolerance analysis of rotary activator position with respect to sensor interface.

F.2 Flange clamping forces

The hinge arrangement involves side flanges – attached to the AFT hull via side screws – that grip two shafts (one either side of the nacelle), each sliding within a bearing pair. M5 cap head screws are used to produce the clamping force, F, between the clamp and rotating shaft at a perpendicular distance, d = 12mm, from the shaft axis (see *Figure 205*).

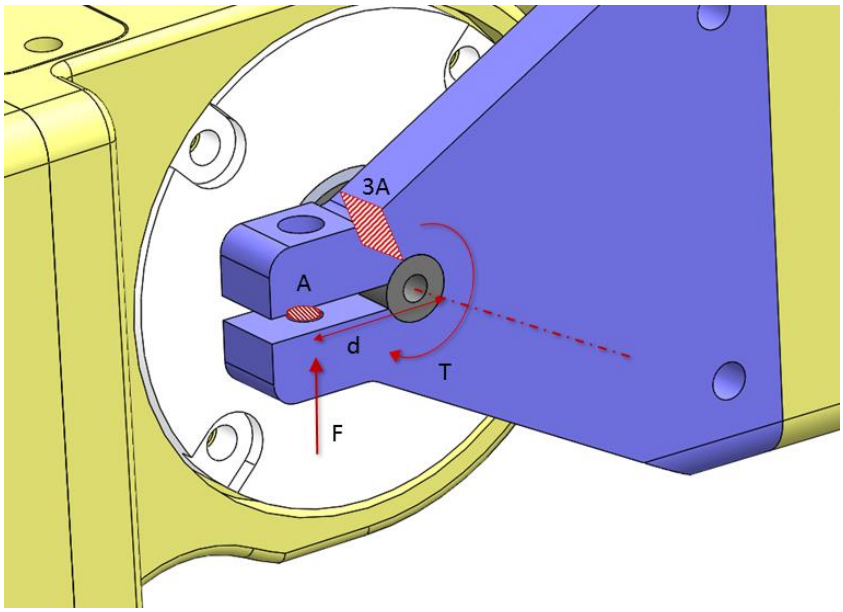

Figure 205 - Diagram showing clamping force variables at rotary sensor side of nacelle.

For structural integrity, the minimum flange material cross-section around the shaft should be at least 3 times greater than the screw's cross-section (A). An M5 screw has a diameter of about 4.2mm, and a cross-section A = π(2.1)^2 = 13.85mm². Thus, in the specific case, 3A = 41.56mm² > 8*7.37 = 58.96mm².

The relation between slipping torque and clamping force is given by:

$$T = F \times d \times C_f \times 1/SF$$

where F is the load from the screw, C_f is the static coefficient of friction and SF is the safety factor. C_f is material dependent and in the range of 0.1-1. We would like to select a clamping force, and distance that allows us to achieve the minimum torque requires to overcome slipping during operation.

For an Aluminium-to-Stainless Steel interface, [Roymech][98] gives a dry sliding coefficient of 0.47, while another source[99] gives the following:

Interface	Clean	Lubricated
Al – Al	1.35	0.3
Al – Stainless Steel	0.61	0.1*

Table 38 - Friction coefficient table (value is interpolated).*

We conservatively estimate 0.1 as the C_f value in water, interpolating as 0.61*(0.3/1.35) = 0.14 and rounding down.

The slipping torque is calculated by considering the maximum torque the hinge will be subject to. By assuming a rotational velocity of 60rpm – occurring at the tank's central frequency of 1Hz (i.e. 1 rps) – and combining this with the PTO damping value of 0.3144 Nms/rad = 3.3 Ncm.rpm; the slipping torque, T_{min}= 3.3 * 60 = 240 Ncm = 2.4 Nm.

The maximum torque is achieved at the maximum clamping load of the screw, F_max, equal to 0.75 times the screw's proof load. M5 screws have a proof load of 5.4kN [Roymech][100], based on property class 5.8] and in accordance with BS-EN-IOS-898-1: 1999. Thus,

$$T_{max} = F_{max} \times d \times C_f \times SF$$

$$T_{max} = 0.75 \times 5.4x10^{3} \times 12x10^{-3} \times 0.1 \times \frac{1}{3} = 2.835\ Nm$$

On the opposite side of the nacelle the shaft diameter is 5mm as opposed to 8mm, thus the same geometry and M5 screw can be applied.

Note that flanges are bored out in order to reduce mass around the hinge location.

[98] https://www.roymech.co.uk/Useful_Tables/Tribology/co_of_frict.htm#coef

[99] www.carbidedepot.com

[100] https://www.roymech.co.uk/Useful_Tables/Screws/Screw_loads.htm

F.2.1 PTO damper inclusion

A torque damper with a quasi-linear torque-angular velocity curve was sought, having a scaled damping value of 3.3Ncm/rpm. The closest off-the-shelf components found was the FRT-K2-103 damper from manufacturer ACE-Fabreeka, having the following characteristic curve:

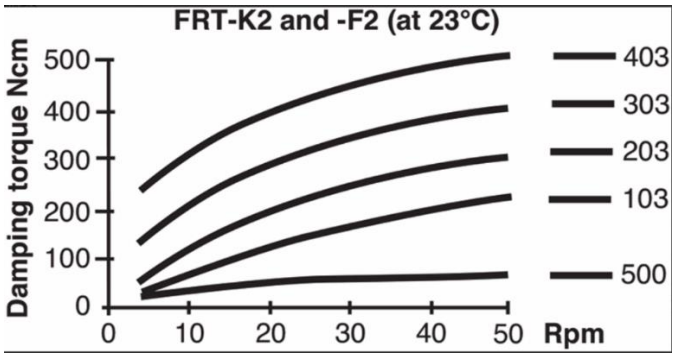

Figure 206 - Characteristic curves of different torque dampers from ACE-Fabreeka (Source: https://www.ondrive.com/frtk2502).

We can take a reference frequency of 1Hz, which corresponds to the central frequency of the tank. By specifying a typical angular amplitude, say, A = +/- 15°, the velocity amplitude can be calculated as:

$$v = \omega A = 2\pi f A = 2\,\pi * 1 * \left(\frac{15}{360}\right) = 0.262 rev\, s^{-1} = 15.7 rpm$$

At this angular velocity we would like our torque damper slope to match the numerical model, with a PTO damping of 0.22495 MNms/rad full scale.

To convert the above to model scale, the following equation is used:

$$D_{pto,model} = \frac{D_{pto}}{20^{4.5}} = \frac{0.22495 * 10^6}{20^{4.5}} 0.3144 Nms/rad$$

This is equivalent to:

$$D_{pto,model} = \frac{0.3144 Nms/rad}{1 rad/s} = \frac{0.3144/9.55 Nm}{1 rpm} = \frac{0.033 Nm}{rpm} = 3.3 Ncm/rpm$$

Observing Figure 206, choosing the most linear looking plot and interpolating linearly from the origin to point (50,240), suggests a slope of 240/50 = 4.8Ncm/rpm. We note that the slope decreases as the angular velocity increases and is likely to be further from the target value at 15.7rpm.

The numerical model also includes a torque limit of 0.05MNm, based on representative generator torque that could be fit, such as C-GEN. At model scale this equates to 0.3125Nm or 31.25Ncm. Unfortunately, the damper has an operating torque range an order of magnitude above this (up to 300Ncm) so the damper will not be included in the tests at this stage, though it may be useful in later iterations.

F.3 Model trimming

F.3.1 Ballasting

Once both FWD and AFT sections were fully assembled, they were joined via the freely rotating hinge and placed in a trimming tank for a rough assessment of baseline trim levels. As observed from Figure 207, the hinge sat above the water line, but significantly lower down than the wave channels.

Each section was subsequently independently trimmed, with the outcome shown in Figure 208 and Figure 209. Lead cut-outs were weighed and sequentially applied to different model locations, as detailed in Table 39.

Note that this process was carried out without moorings being attached and without Qualisys targets in place, so it likely to slightly evolve once the model is fully set-up in the test basin.

Section	**Lead cut-outs (#; orientation)**	**Location**	**Total mass (g)**
FWD	1; flat	Underneath FWD wave channel	120
FWD	3; vertical	Nacelle slot – damper side	22
AFT	4; vertical	Hull slot – wave channel end	60

Table 39 - Summary of added Lead ballast, mass and location.

A total mass of 202g was therefore preliminarily added. The lead sheets used had a nominal thickness of an estimated density of $0.0156/t$ g/mm^3, where t is thickness.

The model appeared remarkably stable to roll.

F.3.2 Trimming images

Figure 207 shows the model being initially assessed for trim. No rotary sensor or activator are present, and the model is evaluated joined at the hinge (free-hinge). Blue lines indicate the target trim level.

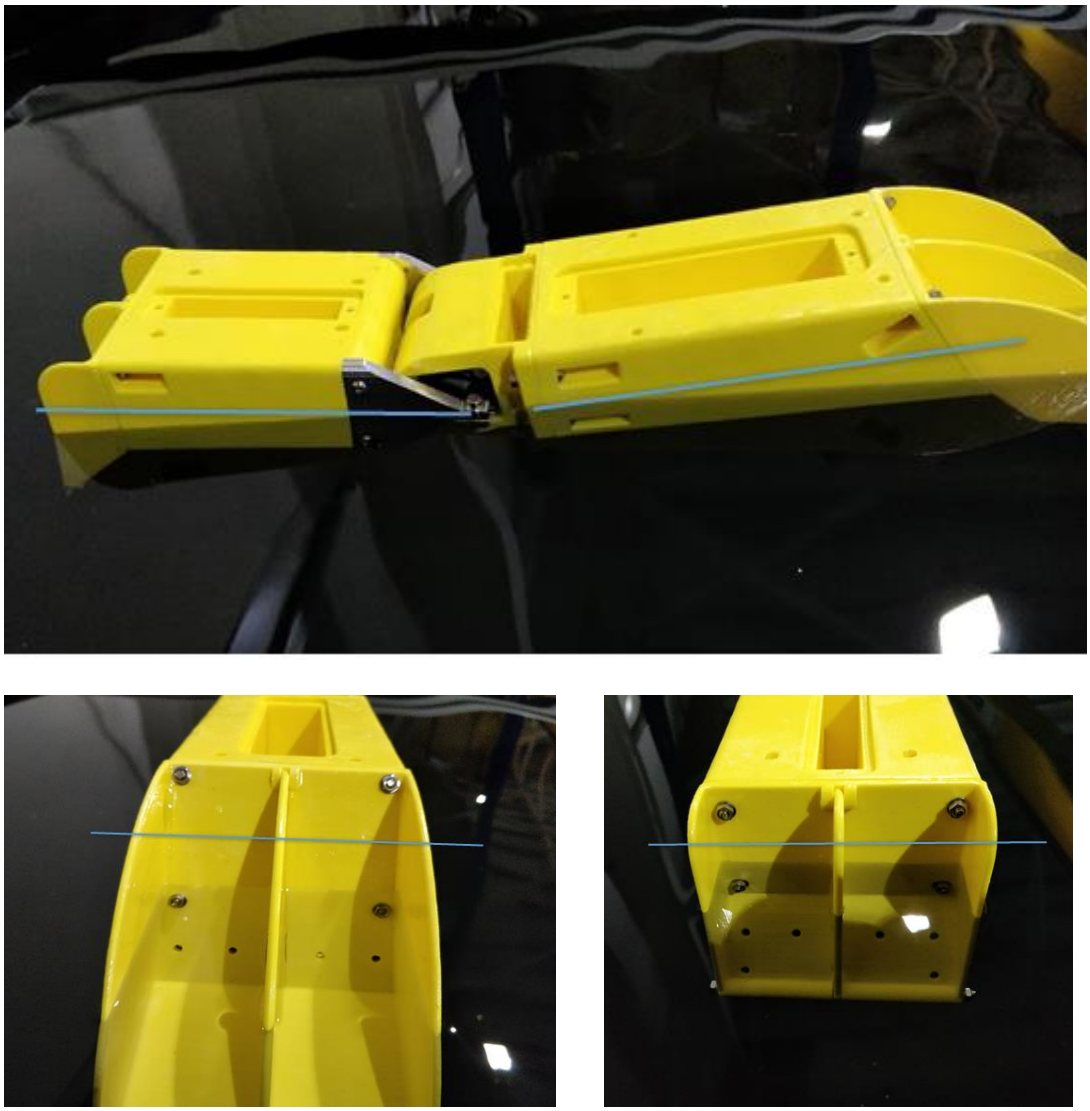

Figure 207 - Showing initial trim line evaluation (no rotary sensor present).

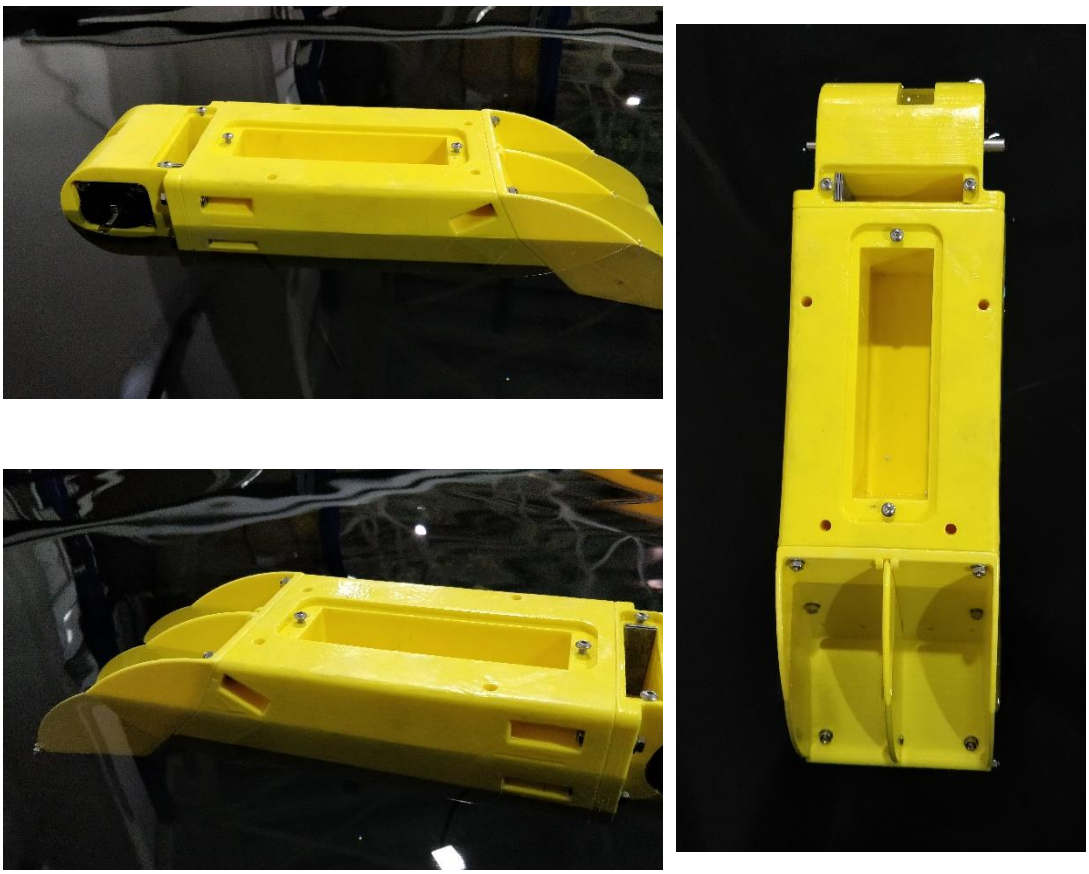

Figure 208 - Showing independently trimmed FWD section.

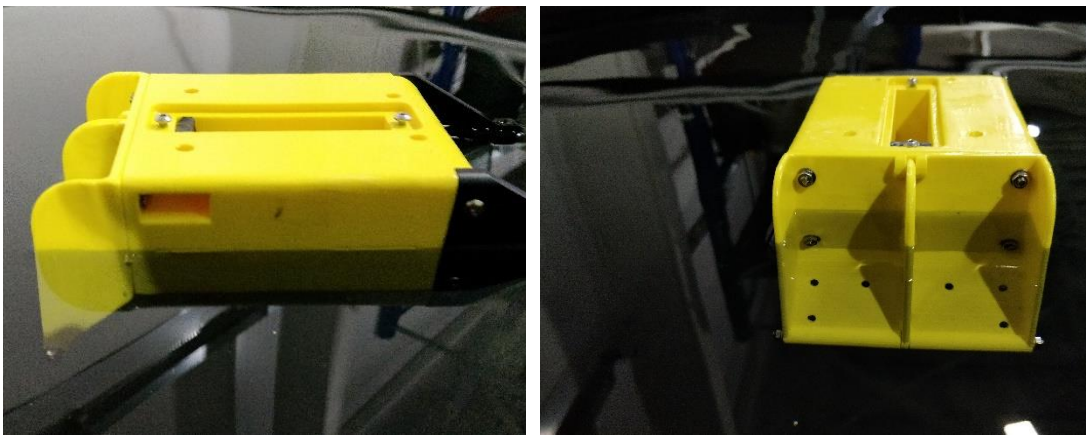

Figure 209 - Showing independently trimmed AFT section.

F.4 Curved Tank operational envelope

The Curve Tank (CT) document provided by the University of Edinburgh specifies three performance points:

- 0.220m H @ 1.0 Hz
- 0.075m H @ 0.5Hz
- 0.060m H @ 2.0 Hz

These are just three points on the typical wave height (H) – Frequency (Hz) plots, which show a performance curve delineated by wave steepness limits on the one hand, and stroke limit of the tank wavemakers on the other. In addition, the data may be obsolete following the replacement of wavemakers which changed the operating water depth from 1.20m to 1.15m, and thus unrepresentative of true tank characteristics.

The wave steepness limits (H/λ) are dictated by physical characteristics of the waves themselves, whereas stroke limits depend on the design, construction and control of the wavemakers. Steepness limits and stroke limits are investigated in turn to determine the upper bound of the CT performance envelope. Other factors, such as wave reflections within the basin, are likely to further reduce performance in practice.

F.4.1 Steepness Limit

Wave steepness limits are dictated by physics. Wave steepness depends on the height of the waves and their period (or frequency). For deep water conditions, wave period is related to wavelength by the dispersion relation:

$$\lambda = \frac{g}{2\pi} T^2$$

Thus, wave steepness can be specified as follows:

$$\frac{H}{\lambda} = \frac{2\pi}{g}\frac{H}{T^2} = 0.64\frac{H}{T^2}$$

For a set wavelength, waves begin to “break“ beyond a certain wave height, thus breaking down linear wave theory assumptions. The waves get progressively less linear (sinusoidal) as wave steepness increases.

The absolute steepness limit is typically given by: H/lambda = 0.14

F.4.2 Stroke Limit

The stroke limit depends on the wavemaker characteristics and is determined experimentally.

Obtain amplitude (A) limit from wave synthesis Njoror software for a given frequency (i.e. ‘demand amplitude limit’). Each wave series is run as a regular wave with gain starting at 50% and then manually adjusted until one of either: max wavemaker deflection (wavemaker #17) approached 15deg, wave break, or tank cuts out. Then identified limit wave is re-run (i.e. nominal amplitude = ‘resultant amplitude’) for 64s repeat period for data analysis purposes.

Wave gauges were calibrated at the start of the day following 2 minutes of water mixing. The calibration errors are given as: 1.15%, 1.04%, 1.06%.

Nominal frequency (Hz)	**0.5**	**0.6**	**0.7**	**0.8**	**0.9**	**1.0**
Frequency (Hz)	0.5	0.59375	0.703125	0.796875	0.90625	1.0
Demand amplitude limit (mm)	45.0	60.0	83.0	103.0	125.0	141.0
Gain achieved (%)	100	100	95	95	60	75
Resultant amplitude (mm)	45.0	60.0	78.9	97.9	75.0	105.8
Measured incident amplitude (mm)	**46.5**	**64.8**	**82.0**	**92.8**	**103.3***	**97.3****
Observed max |angle| of paddle 17 (deg)	13.5	14.2	14.0	14.3	12	11.6

Table 40. Summary table.

* WGs almost maxing out

** Waves break, WGs almost maxing out

NB: the above ‘Measured incident amplitude’ values result from reflection analysis via the Suryanto method.

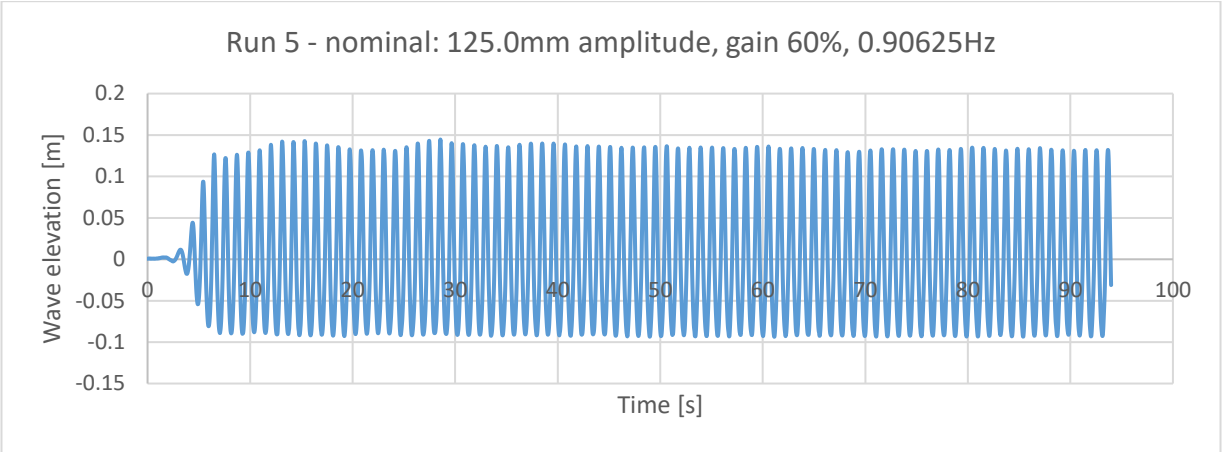

Figure 210 - Raw wave gauge data at 0.9Hz nominal frequency.

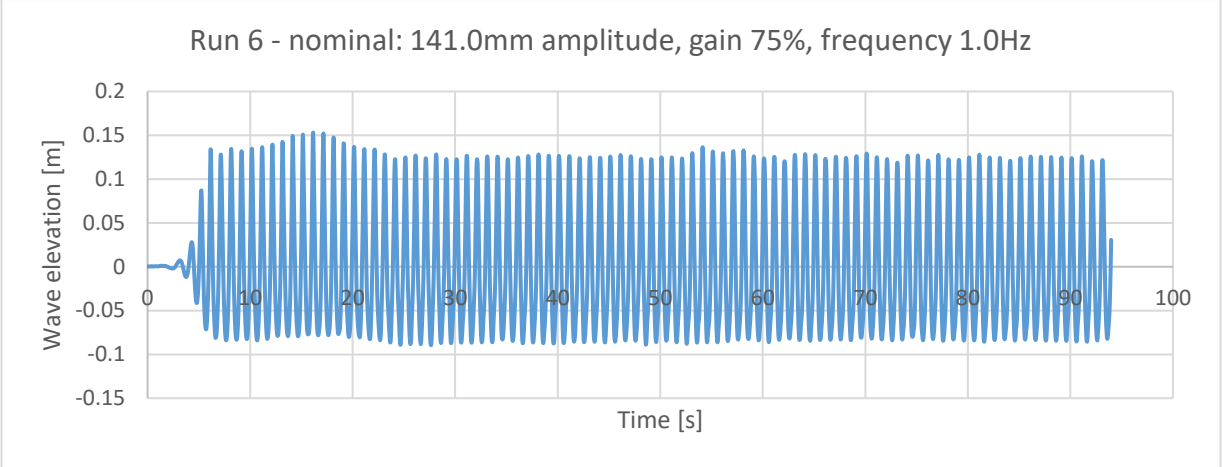

Figure 211 - Raw wave gauge data at 1.0Hz nominal frequency.

The plots above show two features:

- WGs are not ‘maxing out’ at these highest demand amplitude conditions.
- The peaks are higher than the troughs, demonstrating nonlinear behaviour as the demand wave height increases.

F.4.3 Operating Envelope

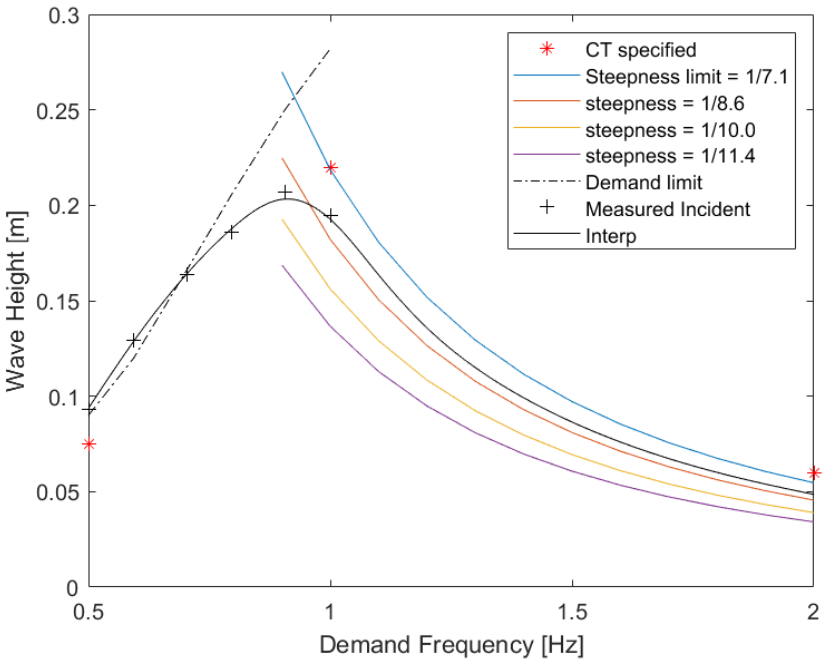

Figure 212 - Summary plot showing the estimated tank performance envelope.

Figure 212 shows the estimated tank performance envelope (black continuous line), i.e. the combinations of wave height and frequency it can achieve. The left hand side of the boundary is determined by the stroke limit of the tank paddles; the right hand side by the physical steepness limit of the waves before they break. The points in red are those stated in the CT manual. For the purposes of choosing sea states for these tests, the solid black line is considered as the effective tank operating envelope.

It is noted that for regular waves, exceeding 4-5% (1/25-1/20) steepness is undesirable. Although 1/7 steepness is the theoretical absolute breaking limit for waves, waves will degrade in “quality” well before this threshold. As the threshold is approached, waves will start to break off the wavemaker, so that energy will be dissipated before the waves arrive at the model location. There are different kinds of breakers. For example, in the case of spilling breakers, the wave crest starts to fall, resulting in a non-canonical wave that is dissipating energy in its crest. Non-canonical waves reduce the applicability of linear wave theory.

For irregular waves, we would like to plot an equivalent curve of Hs-Te.

It is assumed that the average period, Tz = 1/f, and can then relate it to Te = 1.206Tz (assuming fully developed seas). Hs = sqrt(2)*H. (Hs = 4sqrt(mo) = 4*std(elevation) = 4* (sqrt(2)/2)*Amplitude

In addition, it is noted from 15 year EMEC wave buoy data, that the steepness limit for irregular seas is Hs = (Te^2)/13. We can plot this, relate it scale relative to the regular steepness limit, and apply the same scale to the stroke limit side of the plot to complete the envelope.

Using Table 40 as a starting point, equivalent Hs-Te limits for the stroke limited part of the envelope can be estimated. To calculate Hs, 2x measured incident amplitude is considered as H.

Frequency (Hz)	0.5	0.59375	0.703125	0.796875	0.90625	1.0
Resultant amplitude (mm)	45.0	60.0	78.9	97.9	75.0	105.8
Measured incident amplitude (mm)	46.5	64.8	82.0	92.8	103.3*	97.3**
Wave height (mm)	93.0	129.6	164.0	185.6	206.6	194.6
Te (s) = 1.2/f	**2.4**	**2.02**	**1.71**	**1.51**	**1.32**	**1.20**
Hs, FW (mm) = 0.725*H	**67.4**	**94.0**	**118.9**	**134.6**	**149.8**	**141.1**
Hs, Cons (mm) = (2/3)*H	**62.0**	**86.4**	**109.3**	**123.7**	**137.7**	**129.7**
Te [FS] (s)	**10.73**	**9.03**	**7.65**	**6.75**	**5.90**	**5.37**
Hs, FW [FS] (m)	**1.35**	**1.88**	**2.38**	**2.69**	**3.00**	**2.82**
Hs, Cons [FS] (m)	**1.24**	**1.73**	**2.19**	**2.47**	**2.75**	**2.59**

Table 41 - Estimated irregular wave parameters. [FS = full scale]

Table 41 shows estimates of Te and Hs at tank scale and at full scale [FS], by multiplying tank scale values respectively by a factor of sqrt(20) and 20.

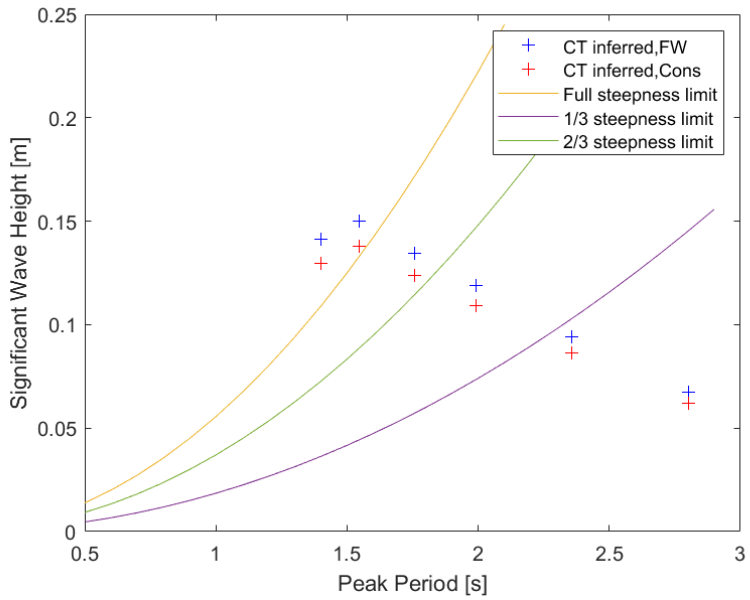

Figure 213 - Curved Tank operating envelope (irregular seas).

Figure 213 represents a mirrored version of (horizontal axis is now period as opposed to frequency) of Figure 212, though adapted to irregular wave parameters. Note that North Atlantic steepness limit is used here (Hs = Te^2/13), as opposed to a literature informed steepness limit of S = 0.14 (for deep water waves, this is equivalent to Hs = Te^2/6.6, approximately double that observed in N Atlantic).

It may be that the CT allows greater steepness waves to be produced – certainly it would appear so if the stroke limited part of the plot is extrapolated to lower period values. This should be checked by running the basin ahead of the tests. For the purposes of the test plan, the stroke limit indicates that wave runs at full steepness cannot go above Tp = 1.6s; those at 2/3 limiting steepness can be run up to Tp = 1.8s; and those with 1/3 limiting steepness can be run up to Tp=2.3s.

Comparing these with Section 2.3, and in particular with the energy matrix, we note that the peak contribution to AEP occurs at full scale Hs = 2.25m, T02 = 5.4s; 20th scale Hs = 0.113m, T02=Tz = 1.2s; Tp = (1.2*5.4/0.875)/(sqrt(20)) = 1.66s (Te = 1.2Tz = 11.45s; Tp = Te/0.875 = 13.09s).

We can therefore assume that sufficient “operational seas” (those considered representative, and corresponding to the main AEP contributing seas), including that of AEP peak contribution, will be reproducible in the tank.

We replot Figure 213, superimposing equivalent Hs-Tp value combinations from the Froude scaled energy matrix. The size of each circle corresponds to the amount of energy contribution.

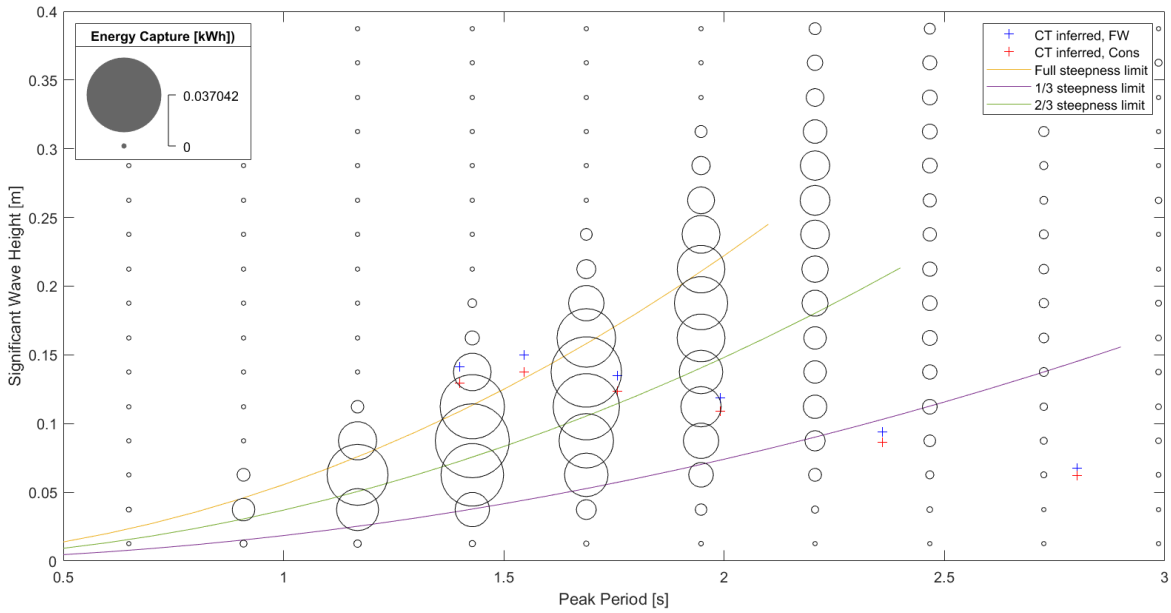

Figure 214 - CT irregular seas performance envelope, with scaled energy matrix overlap.

Figure 214 shows that, while the CT's stroke limit excludes some 'energy capture-able' seas, the largest bubbles lie within the tank's bounds, and the salient part of the WEC's performance area of interest is not significantly affected. A larger version of this plot is shown in Appendix B.

We pick out some of the coordinate centres of bubbles closest to the tank envelope bounds:

Tp = 1.43; Hs = 0.113; P = 0.0275

Tp = 1.69; Hs = 0.138; P = 0.0334

Tp = 1.95; Hs = 0.113; P = 0.00985

Tp = 2.21; Hs = 0.0875; P = 0.00194

It is clear that the higher Hs-Tp combinations will not be reproducible in the CT. This is particularly relevant in the region Tp range 1.5-2.0s and Hs range 0.15-0.25m.

F.5 Tank snapshot

Figure 215 - Showing Blue Star baseline model as set up in the Curved Tank.

F.6 Measured wave signals

For frequency sweep data, only steepness 1/60 plots are presented as examples. NB: In all plots, f = 2.1875Hz should be replaced with f=2.000Hz.

F.6.1 Amplitude spectra from Rotary Sensor data

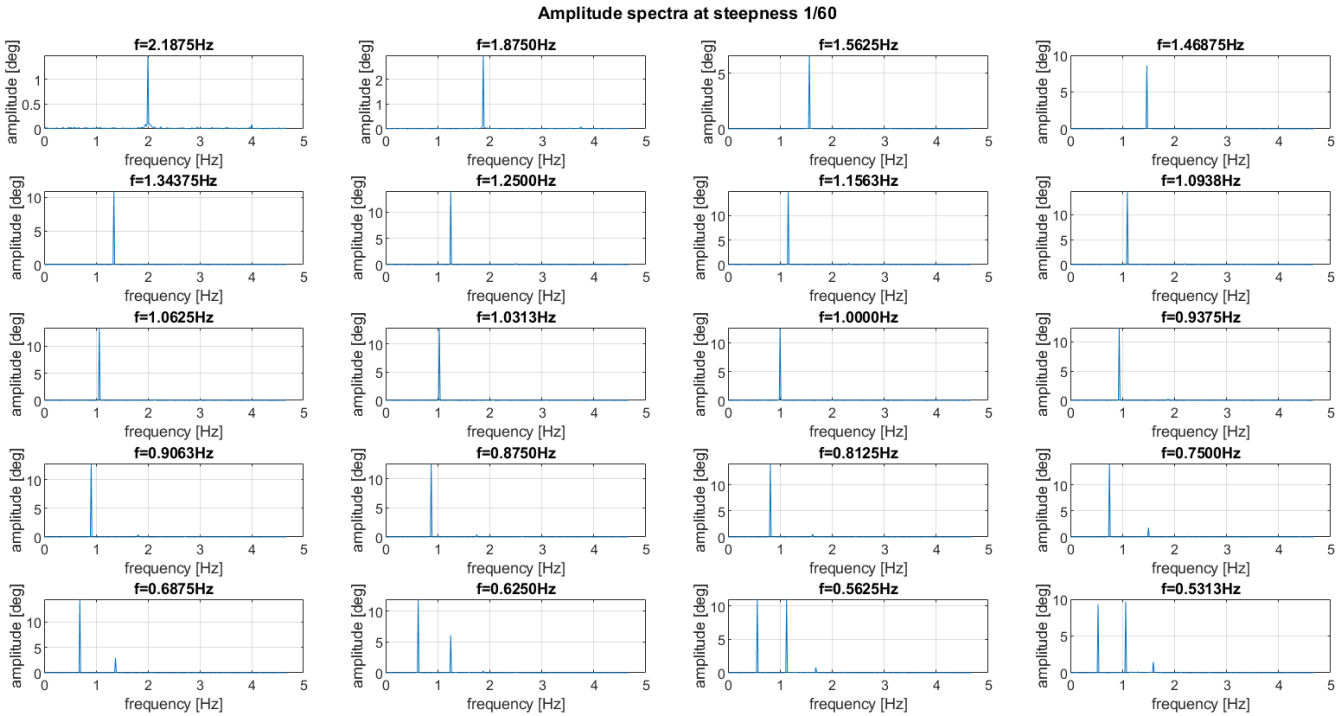

Figure 216 - Showing amplitude spectra for frequency sweep at steepness 1/60; rotary sensor analysis.

F.6.2 Cropped time series from Rotary Sensor data

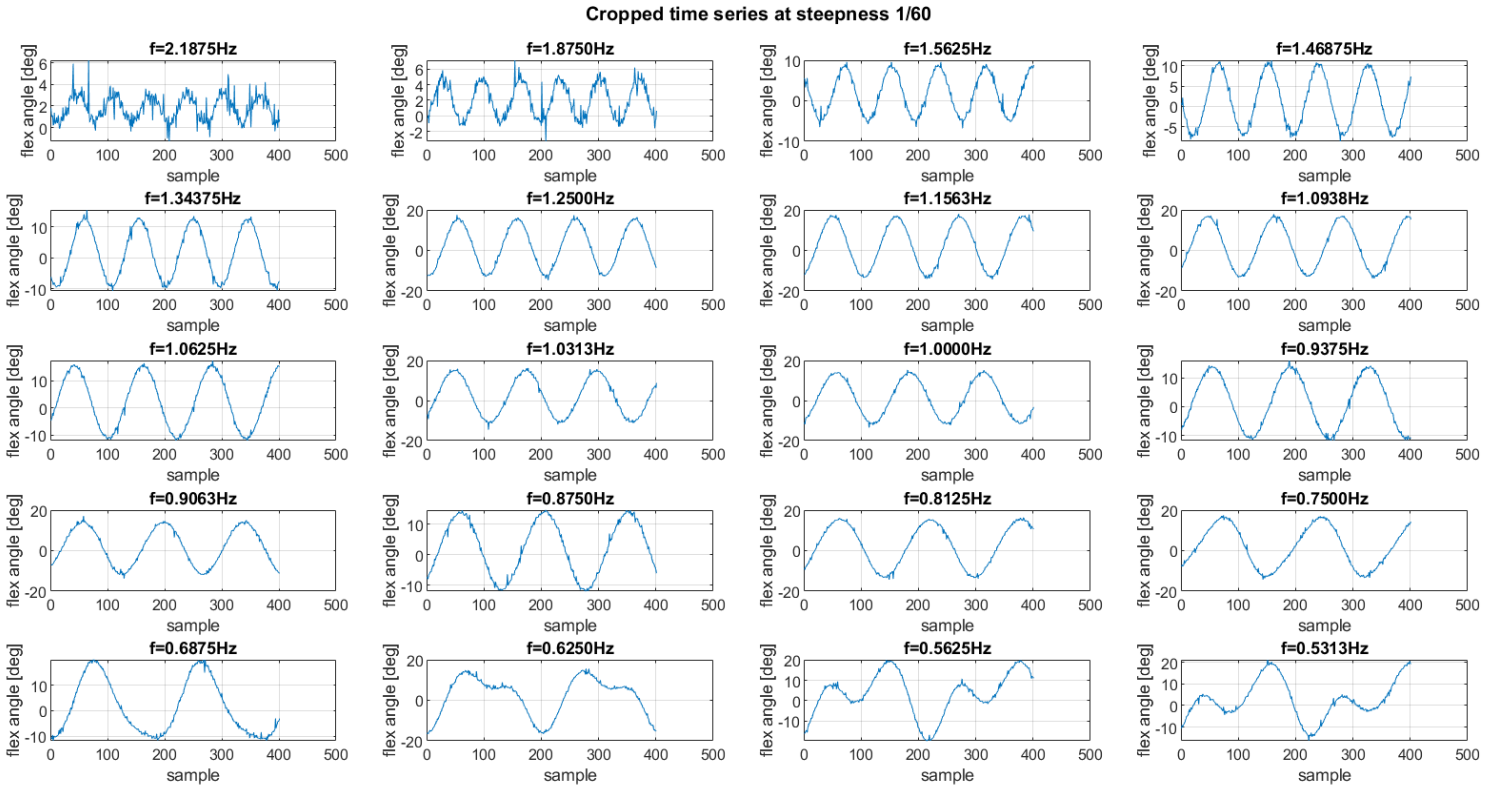

Figure 217 - Showing cropped time series of hinge flex angle signals for frequency sweep at steepness 1/60; rotary sensor data.

F.6.3 Amplitude spectra from Qualisys analysis

Only given for steepness 1/60 seas.

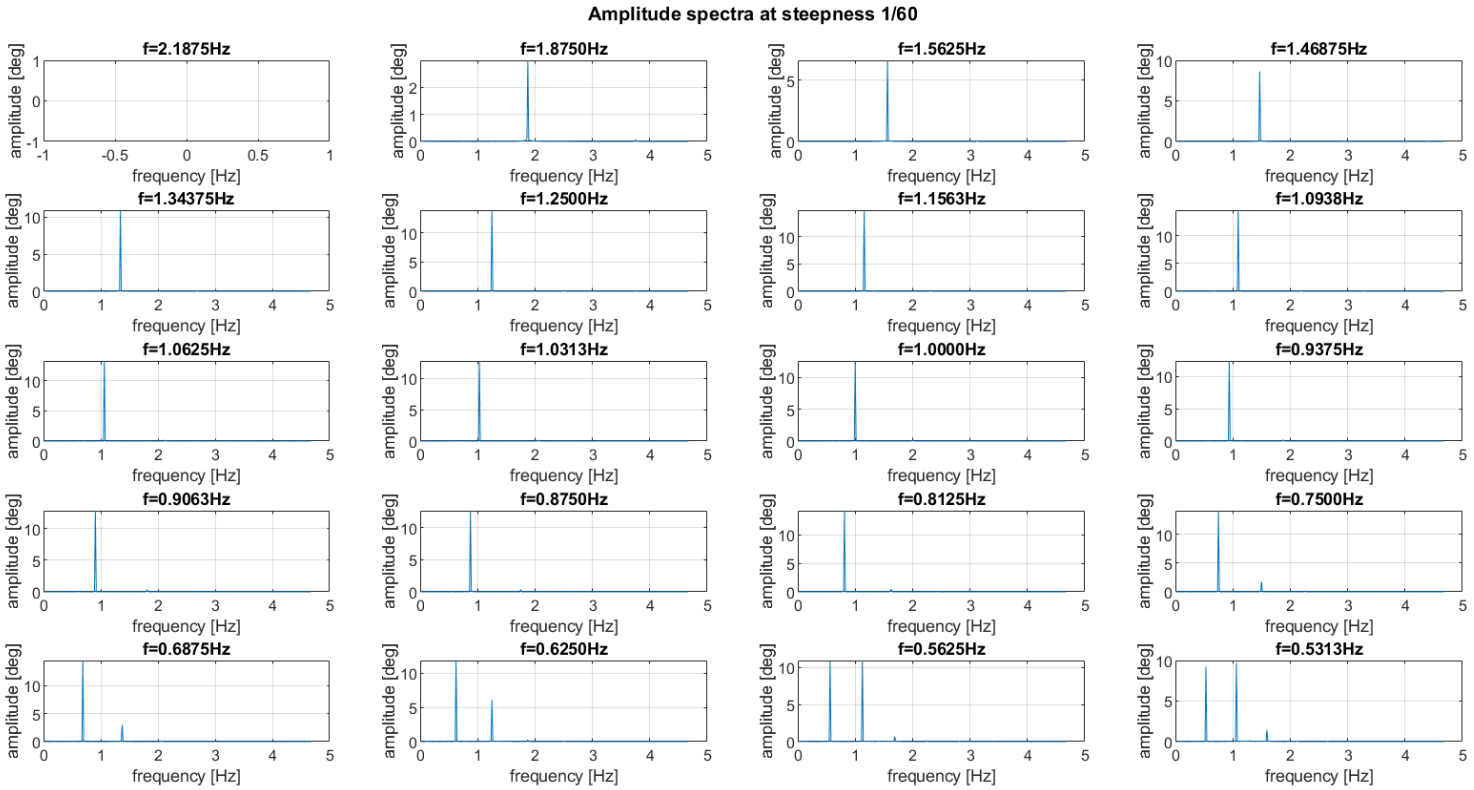

Figure 218 - Showing amplitude spectra for frequency sweep at steepness 1/60; Qualisys analysis.

F.6.4 Cropped time series from Qualisys analysis

Only given for steepness 1/60 seas.

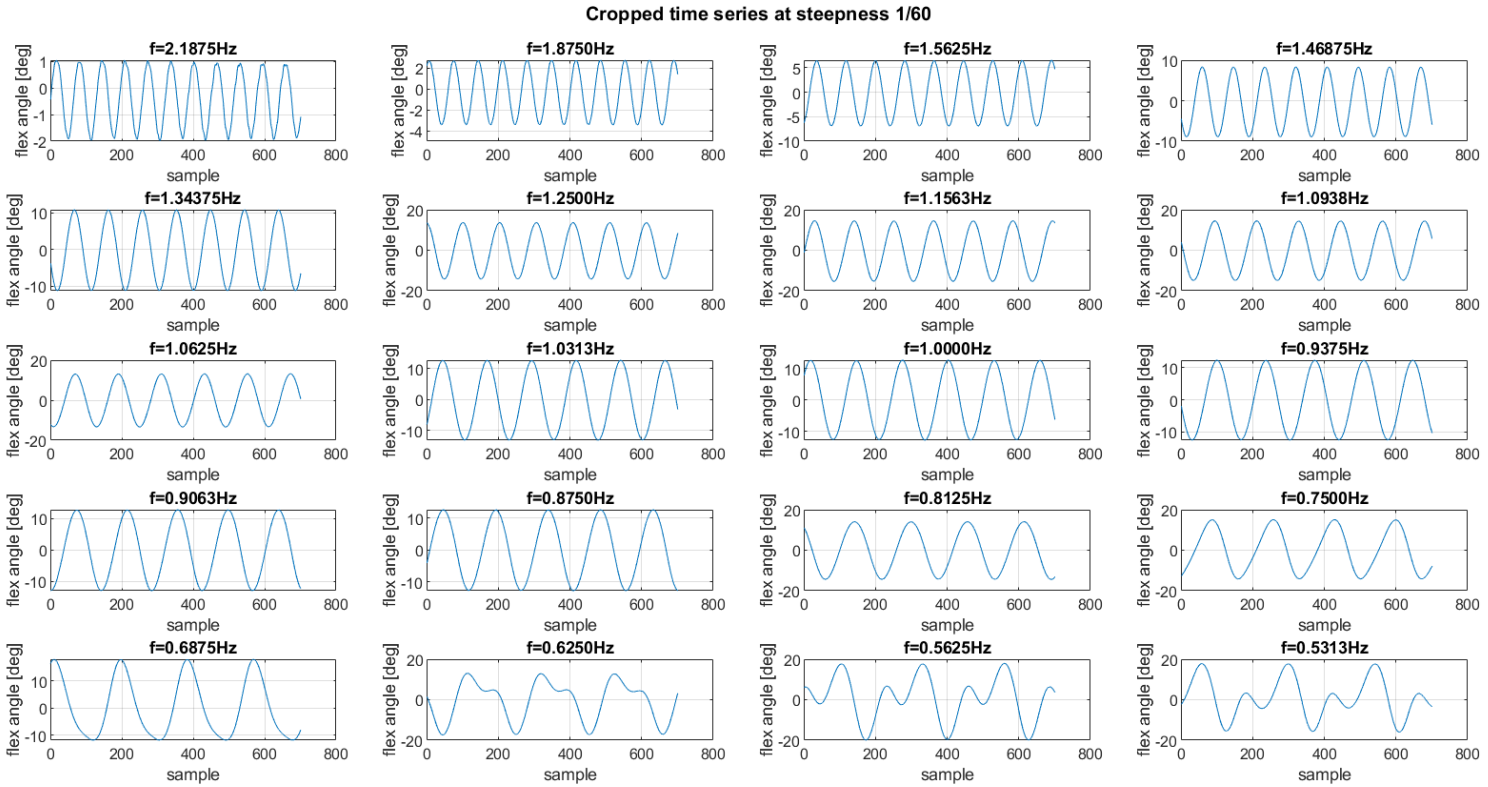

Figure 219 - Showing cropped time series of flex angles for frequency sweep at steepness 1/60; Qualisys analysis.

F.6.5 Amplitude sweep spectra from Rotary Sensor data

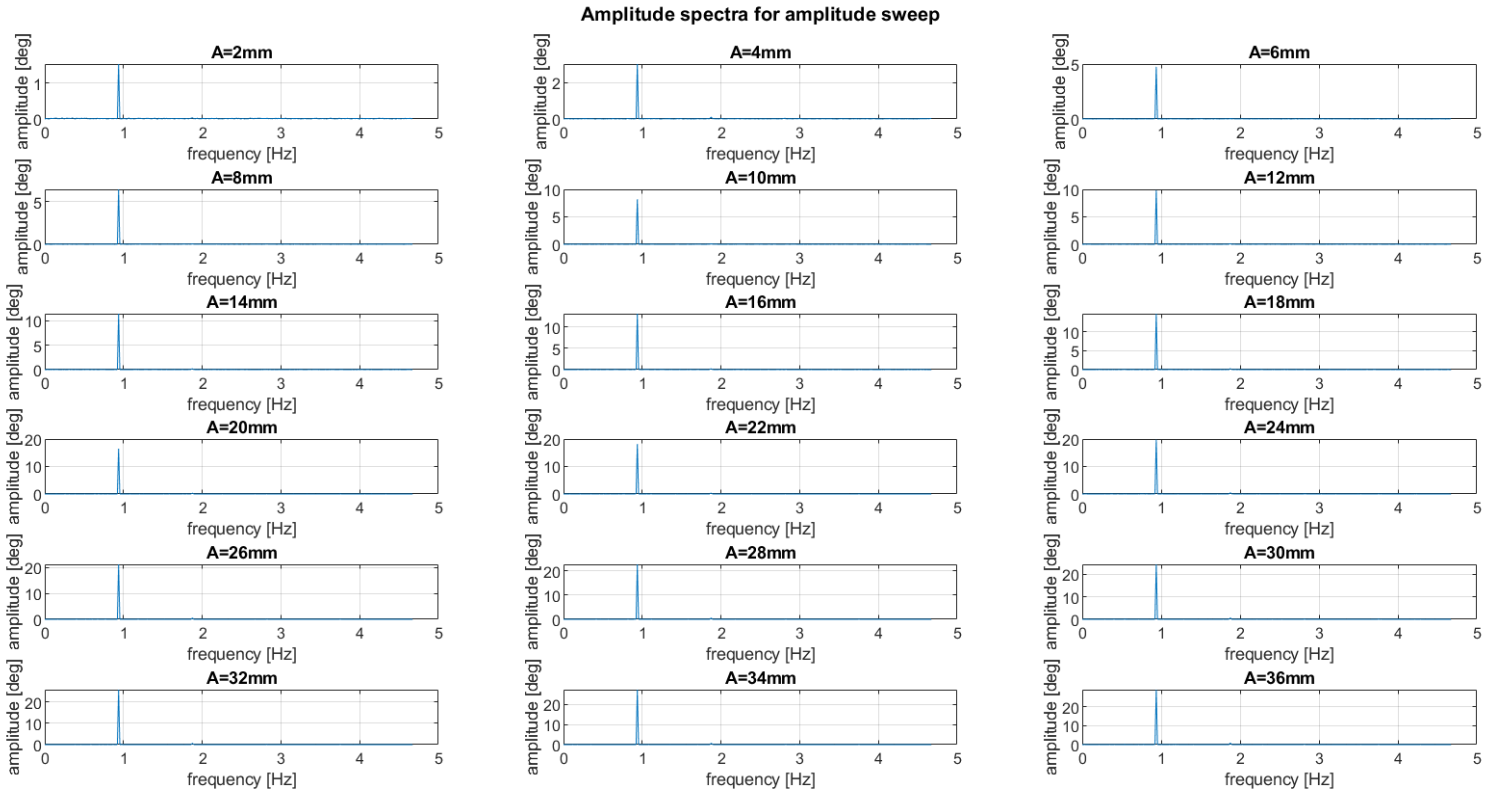

Figure 220 - Showing spectra from amplitude sweep at steepness; rotary sensor data.

F.6.6 Cropped time series from amplitude sweep Rotary Sensor data

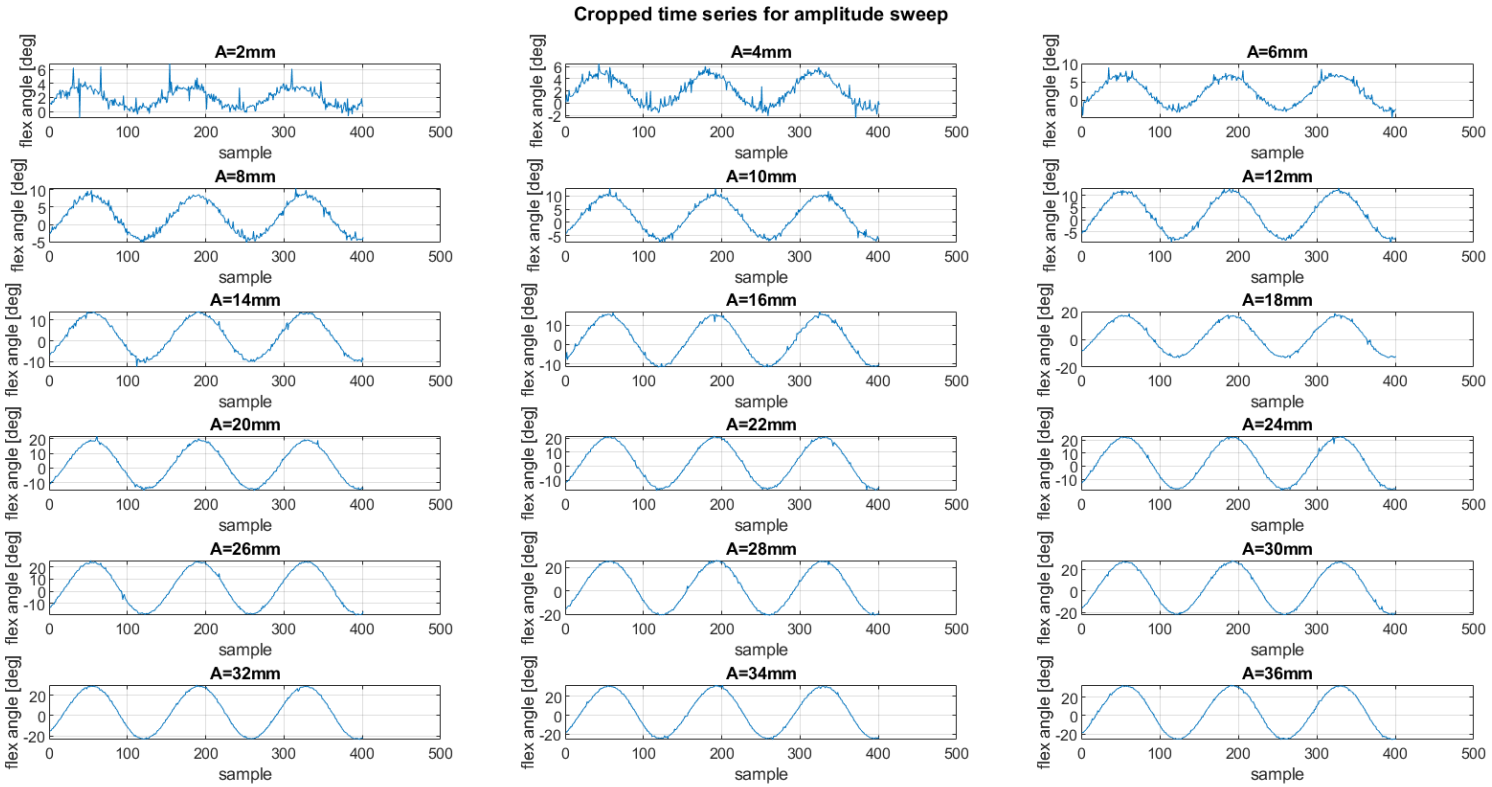

Figure 221 - Showing cropped time series of flex angle during amplitude sweep; rotary sensor data.

Appendix G

G.1 Calibration set-up

G.1.1 Equations

First, key parameters are defined:
P_effective = P_absorbed + P_lost
i.e. [overall power removed from waves] = [power absorbed by model PTO] + [power lost to friction]

Equivalently:
T_effective = T_motor + T_friction
i.e. [torque experienced by hinge] = [torque applied by motor] + [torque needed to overcome friction]

In the dry bench-tests, one can measure T_effective and T_motor to derive T_friction
In the wet tests, one can estimate T_effective by assuming T_friction and measuring T_motor

Once can also write:
D_effective = D_motor + D_friction
where D_motor depends on the gain (G) and D_friction is independent of G

One can therefore define: D_motor = G*D_normalised
Where G has no units and D_normalised is in units of [Nms/rad per unit gain]

In the dry bench-tests, want to check that D_normalised is constant with G, to give confidence that the desired level of damping can be set via the controller.

Overall,
P_effective = T_effective * v
where v is in units of [rad/s]

This is the step that shows how friction can be taken into account in the computation of T_effective, but its feedback effects on v (i.e. model dynamics) cannot be accounted for. Hence the emphasis of minimising friction effects.

Expanding the above,
P_effective = (T_motor + T_friction) * v
= {(D_motor*v + k_motor*Θ) + (D_friction*v + C_friction*sign(v))} *v
= {(G*D_normalised*v + G*k_normalised* Θ) + (D_friction*v + C_friction*sign(v))} *v

In dry-bench tests for the 10th scale model, k_motor contributes 8% of total torque at the max gain setting used, and will have a lower contribution at lower gains.

k_normalised was found to be equal to 0.034 Nm/rad
D_normalised was found to be equal to 0.1058 Nms/rad
D_friction was found to be equal to 0.0389 Nms/rad
C_friction was found to be equal to 0.0419 Nm

Neglecting k_normalised, and D_friction, the above can be rewritten as:

P_effective = {G*D_normalised*v + C_friction*sign(v)} * v

The equations relate to the computation of P_effective, with k_normalised and D_friction terms neglected. Thus:

P = D*V.*V + C*V.*sign(V)
P = G*0.1058*V.*V + 0.0419*V.*sign(V)

where D is D_effective, which equals G*D_normalised as D_friction is neglected; C is C_friction

G.1.2 Set-up

Some bench set-up images are provided below:

Figure 222 - Showing nacelle subassembly clamped to bench with rigid coupling (black), torque sensor (blue), and clamped lever arm at the top.

Figure 223 - Showing nacelle clamped to bench, power (orange), feedback (green), and sensor (grey) cables.

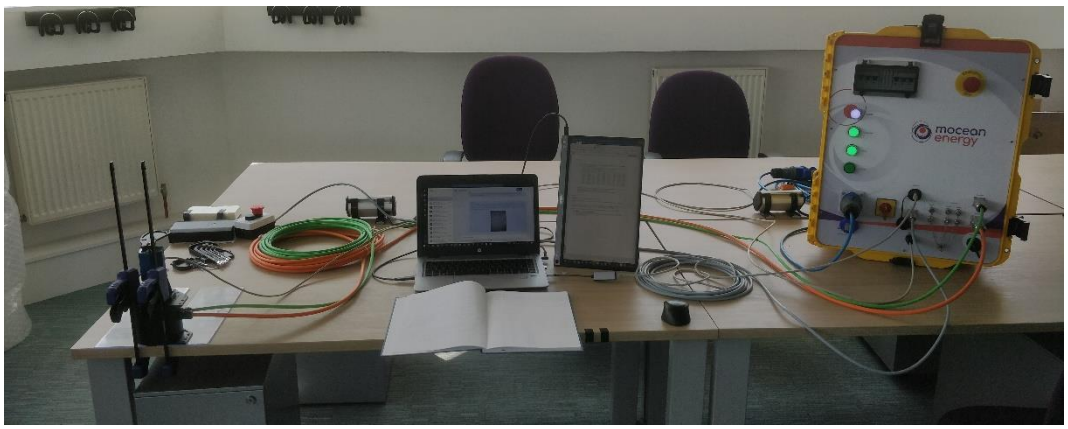

Figure 224 - Showing overall set-up, including motor controller box on the far right.

It can be seen that the Nacelle subassembly is characterised in a vertical configuration. This is because:

- Can achieve more rigid mounting of the nacelle subassembly to the bench, utilising the large flat faces of its two end plates
- Gravity acting in line with the motor shaft axis, which reduces the mass of the lever arm and the rigid coupling themselves affecting the recorded torque readings

G.1.3 Torque sensor

The available torque sensor is a 2Nm rated Interface Force Measurements Ltd. contactless torque transducer, model T8-2Nm, Serial No 132662, Output +/-5V. Nominally, it has a +/-0.05% non-repeatability error and a +/-0.25% combined error, as specified on its datasheet. The analogue to digital converter in the controller (ADC) has a sensitivity of 335microV/division (where 1 division is 1 bit). A 5V output equates to 2Nm of torque.

Figure 225. Utilised torque sensor.

A 0.25% error translates to a 0.005Nm error, i.e. 1.3% of the peak demand torque of 0.375Nm.

G.2 Calibration

G.2.1 Static calibration

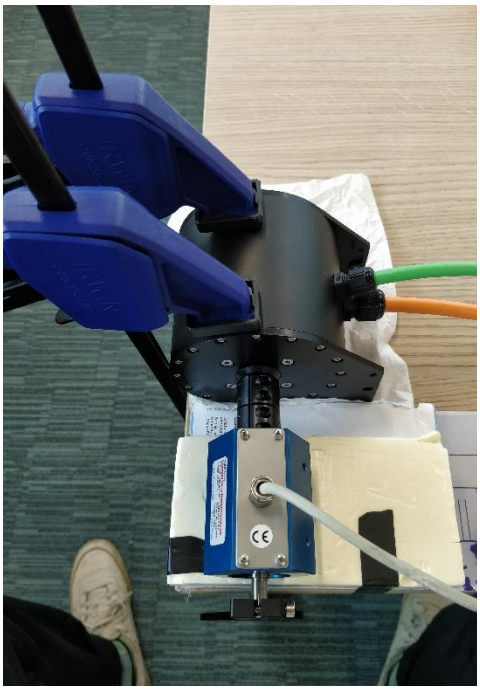

Figure 226. Showing horizontal PTO 'train' set-up.

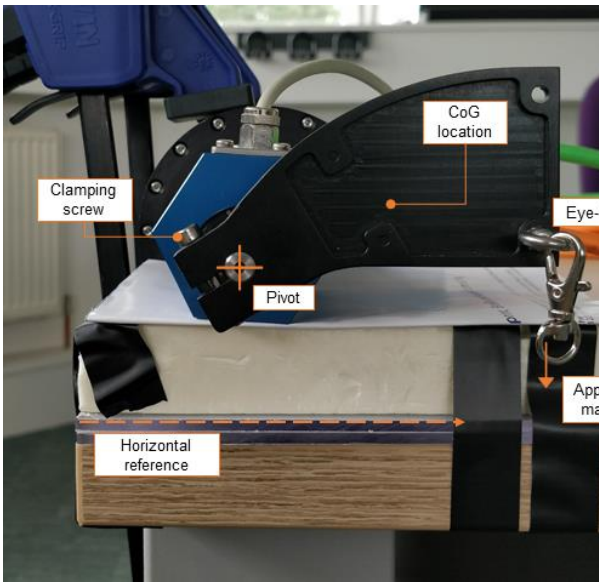

Figure 227. Showing horizontal lever arm, clamping screw, eye-bolt, and key clip to apply known mass.

Initial static calibration is as follows:

- Mass of lever arm: 34.42g; CoG distance from axis = 29.66mm
- Applied torque = 34.42/101.97 * 29.66/1000 = 0.010001174Nm ([101])
- Measured torque = 0.010428 Nm (averaged over time) → error = 0.010428-0.010001174/0.010001174 * 100 = +4.27%

If an additional 3.04g is hung from arm at ~75mm from the axis:

- Delta torque = (3.04/101.97* 75/1000) = 0.00223595 Nm
- Measured delta torque = 0.012485 – 0.010428 = 0.002057 Nm → error = -8.00%, albeit we are measuring extremely small values

The above is repeated with a heavier weight:

- Reference Tx value of lever arm and string[102] (0.40g) = 0.01317Nm

[101] Note that the clamping screw is not being taken into account here; the theoretical applied torque is actually 0.009766Nm.

[102] Later on, the string was replaced with an eye-bolt to facilitate clamping of the additional weights.

- Add 10.58g at 75mm distance; nominal delta torque = 10.58/101.92 * 75/1000 = 0.007786Nm
- Measured torque = 0.021029 Nm
    - Measured delta torque = 0.021029-0.01317 = 0.007859Nm
    - Error = 0.007859-0.007786/0.007786 * 100 = +0.94%

We also check the zero value of the sensor for its offset average and range.

In a horizontal axis position, over a time of 70s this is:

- Average = -0.00013 Nm
- Min = 0.000805 Nm
- Max = -0.001070 Nm
- Range = 0.001879 Nm

If the lever arm is lightly rotated and then let go of, in both directions sequentially, the trace looks like:

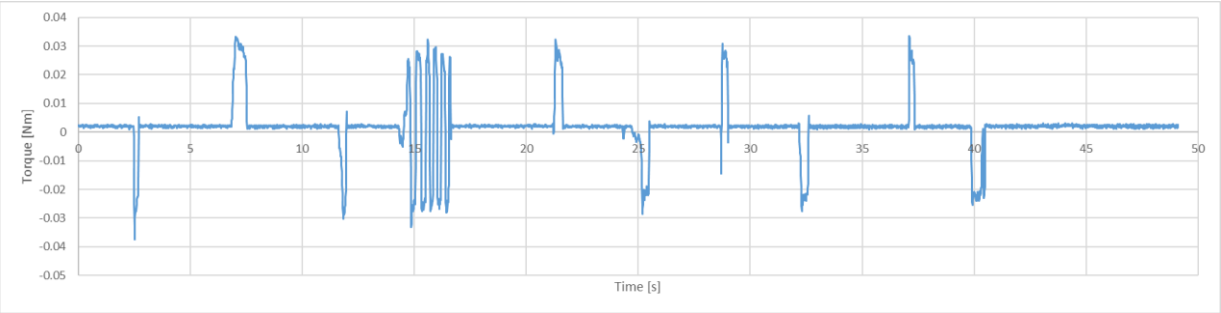

Figure 228 - Exciting the torque arm in different directions to overcome static friction.

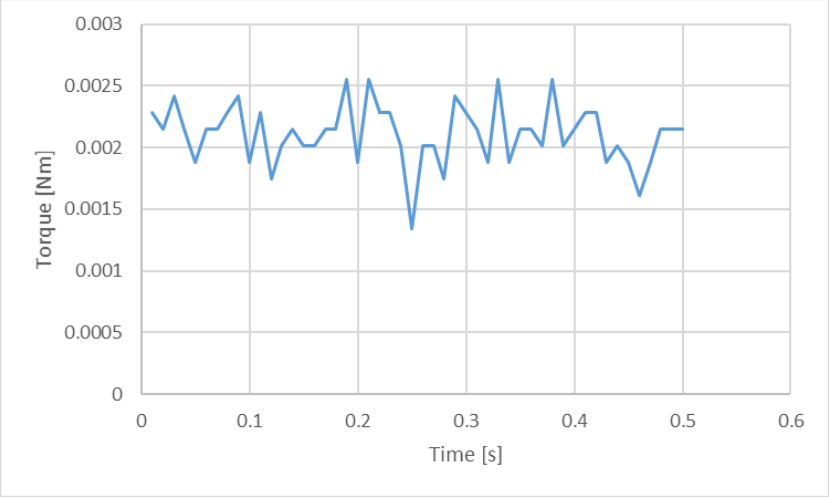

Figure 229 - Showing baseline signal noise.

Choosing the first segments where the lever arm is stationary, the average torque readings are:

- 0.002023, 0.002005, 0.001956, 0.001988, 0.002063 Nm

The range observed purely due to noise during the first 0.5s of signal:

- 0.002551-0.001342 = 0.001209 Nm

When another 2.60g is added at 75mm, the lever arm starts moving etremely slowly, suggesting that the static friction is just at the point of being overcome.

- Total added mass at 75mm from shaft axis: 0.40+2.60+10.58g = 13.58g
- Total nominal moment: 0.0099931Nm + 0.010001174Nm = 0.0199943 Nm; measured torque is 0.02215 Nm
- Add another 2.68g, lever arm moves very slowly (total nominal Tx = 0.02197 Nm
- Add another 2.59g, lever arm visibly moves *{offsetarm_2021_07_15_15_52_42.csv}* – see plots below.

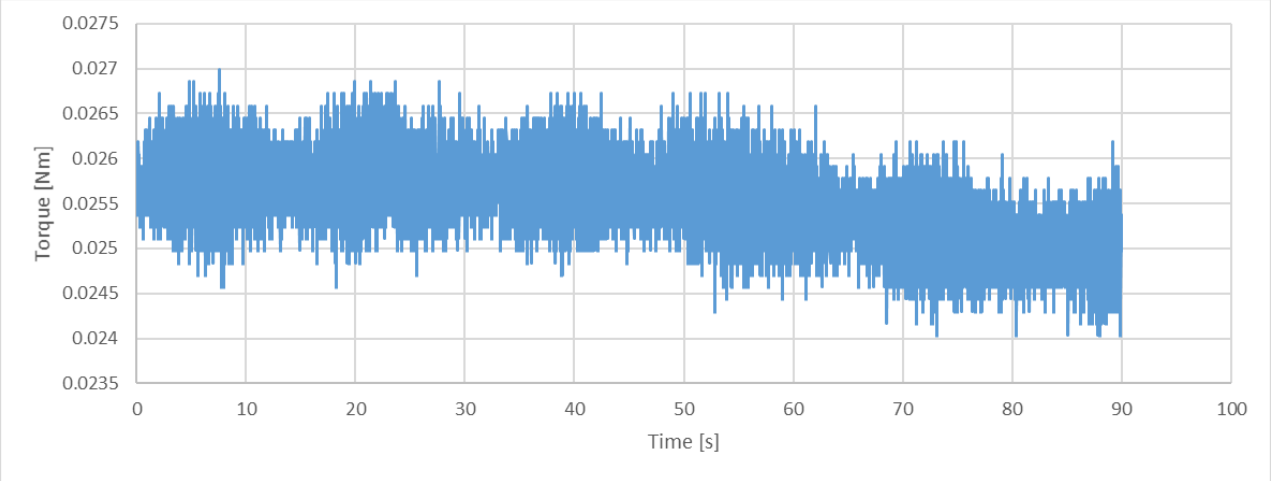

Figure 230 - Plot showing torque versus time at the point where static friction is being overcome.

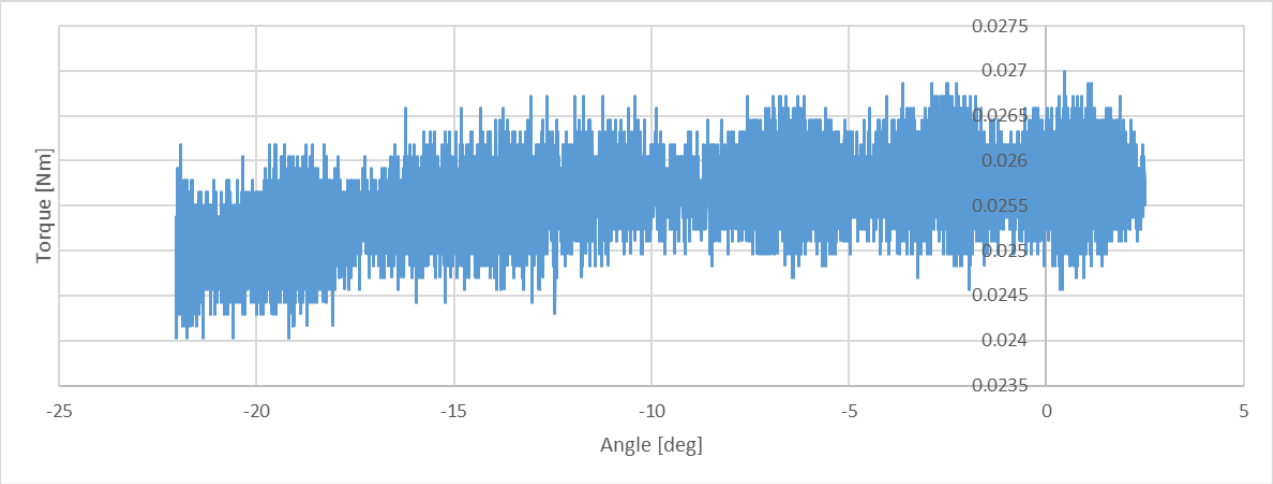

Figure 231 - Plot showing torque versus angle at the point where static friction is being overcome.

The two plots are mirrors of one another. The lever is let go of just above horizontal, and roughly reaches max torque around the angle = 0 point, as

expected. Max value of torque measured is 0.02699 Nm, which should be close to the static friction value. The torque then decreases as the lever rotates past the horizontal position, where –ve angles are clockwise angles. Note that there is some inherent error in defining 'horizontal' since we are approximating this by eye. The CoG point is not quite aligned with the flat side of the lever arm (see Figure 71), so it makes sense that the max torque is detected once the lever has rotated past the horizontal point.

Again, we can clearly see the noise oscillations of approx. +/-0.001 Nm around the average signal value.

The static calibration was repeated after 5 days (on the 21st July) of characterisation testing, using an eyebolt instead of a string attached to the lower bore of the lever arm (see Figure 71).

The combined CoG of lever arm and clamping screw is at 26.74mm from the pivot, and the combined mass is 37.24g. Thus, the actual applied moment is 0.009766Nm.

- Nothing is placed on the sensor shaft
    - Average Tx reading: -0.00254 Nm
- The lever arm is attached with the clamping screw, and visually located horizontally, as per Figure 71
    - Average Tx reading: 0.007525 Nm
    - Delta = 0.007525+0.00254 = 0.010065 Nm; Applied = 0.009766Nm
    - Error = 0.010065-0.009766/0.009766 = +3.1%
- Then add eyebolt+nut (3.15g) and clip (2.63g) at 75mm from pivot
    - Moving very slowly, max Tx: 0.012756Nm
    - Delta applied = 0.0042513Nm
    - Delta measured = 0.005231 Nm
- Add another clip (2.69g) at 75mm
    - Slow movement, max Tx = 0.016113 Nm
    - Delta applied = 0.001979 Nm
    - Delta measured = 0.003357 Nm
- Add another 2.64g at 75mm
    - Faster but consistent movement, Max Tx = 0.01853 Nm
    - Delta applied = 0.0019417Nm
    - Delta measured = 0.002417Nm
- Add another 5.32g at 75mm
    - Consistent movement, Max Tx = 0.023633Nm
    - Delta applied = 0.0039129Nm

    - Delta measured = 0.003894Nm
- Add another 5.28g at 75mm
    - Consistent movement then slips all of a sudden at max Tx: 0.025379Nm (see Figure 232)

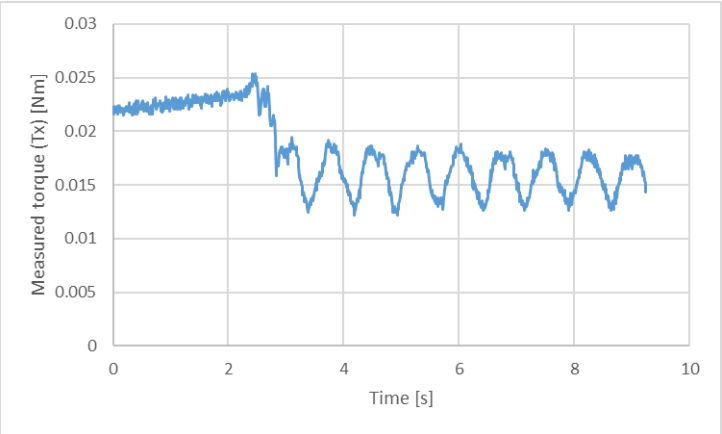

Figure 232 - Showing torque versus time at the static friction threshold.

    - The torque slowly increases as the lever arm slowly rotates clockwise after it is let go of
    - After the lever arm slips, the torque drops and then oscillates due to the various clips (masses) swinging on the eye bolt; the lever arm itself is stationary.
- Remove all masses so that just lever arm & clamping screw are left
    - Average Tx reading: 0.009174Nm
- Remove everything from shaft
    - Average Tx reading: -0.000284 Nm
    - Therefore, some drift (-0.000284-(-0.00254)=0.002256 Nm) has taken place[103]; the differences between applied and measured all lie within the drift value.

If the two 'zero offset' values of measured torque with nothing clamped on the shaft are taken into account, the following two estimates of static friction threshold from the static calibration are obtained:

0.025379-(-0.00254) = 0.027919 Nm; 0.025379-(-0.000284) = 0.025663 Nm

[103] Drift is not necessarily linear and can occur in either positive or negative directions, so it is possible that it accounts for any non-consistent differences in delta torque values at each applied mass step.

The overall applied torque is 21.71g at 75mm plus the moment of the combined lever and screw: 0.015976+0.009766 = 0.025742 Nm, which is very close to the measured value.

Finally, we plot a time series where the lever arm is slightly tapped in each direction, with a pause in between, to verify that peak torques measured. The max and min torques are 0.028201 and -0.026182 Nm respectively.[104]

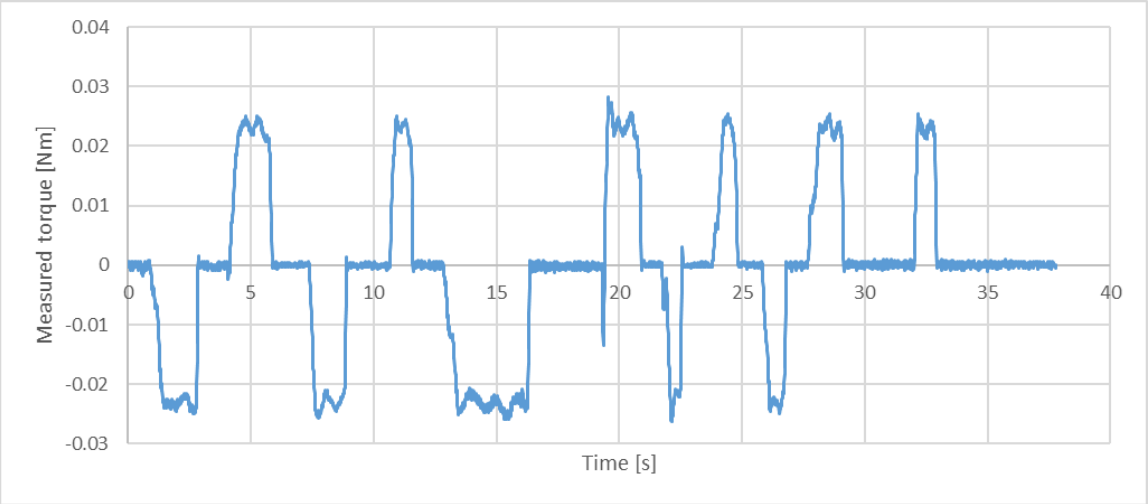

Figure 233 – Showing torque versus time series while lever arm is lightly tapped to stimulate motion in either rotational direction.

[104] This slight difference in magnitude depending on sign is confirmed in the dynamic calibration.

G.2.2 Dynamic calibration

A initial fine resolution calibration sweep for gains between 2-52 is carried out and relevant plots ore hereby shown. Low-pass filter @20Hz, gain steps of 2 between 2-42; low-pass filter @10Hz, gain steps of 2 between 44-52. Gains increase left to right, bottom to top.

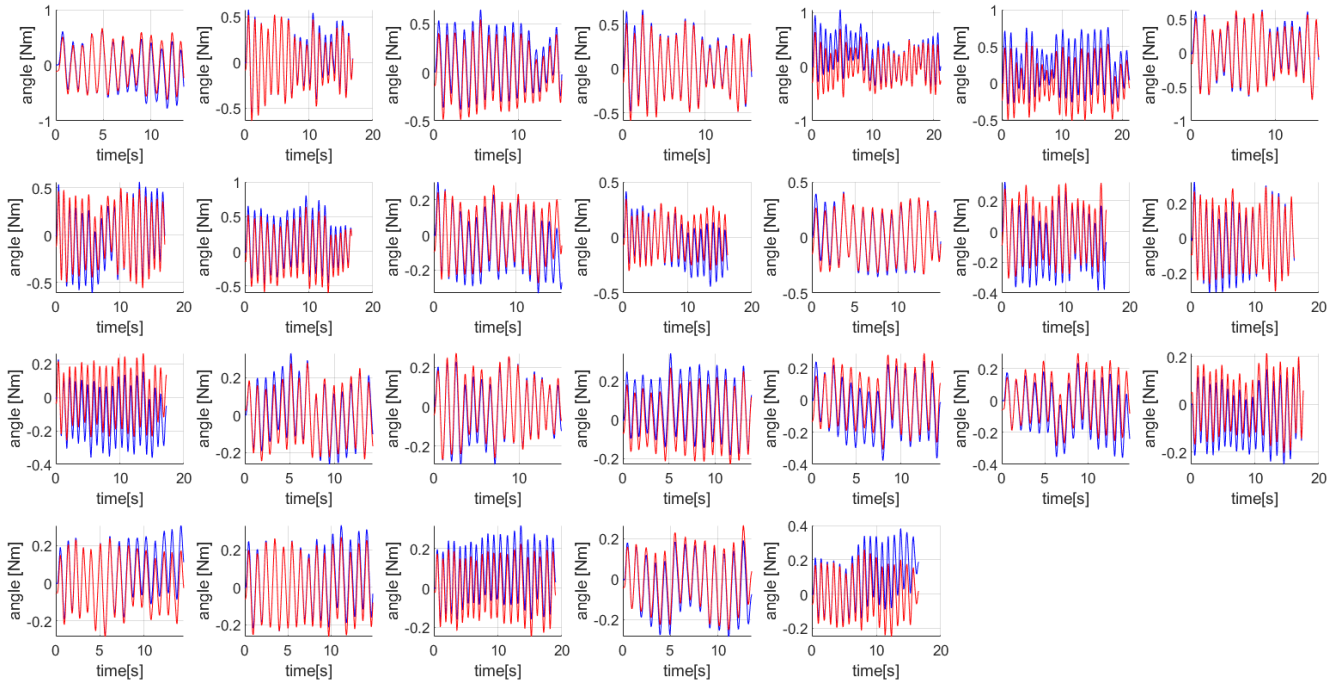

Figure 234 - Input position of lever arm (blue), and associated de-trended positions (red).

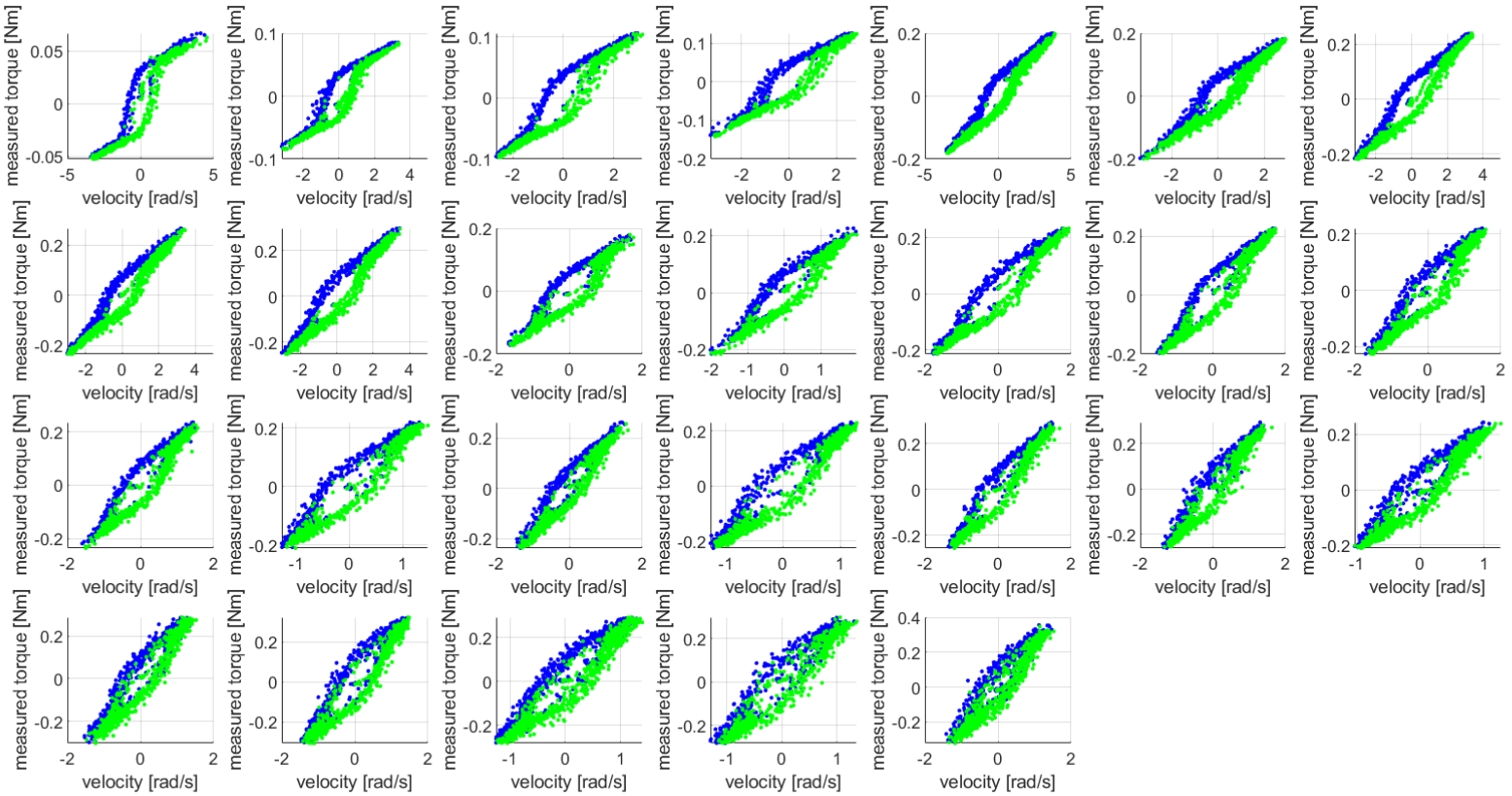

Figure 235 - Measured torque versus angular velocity; negative accelerations in blue, positive accelerations in green.

The corrected torque – that excludes friction – is based on:

- (-ve vel) T_motor = T_measured -0.0276
- (+ve vel) T_motor = T_measured +0.0276

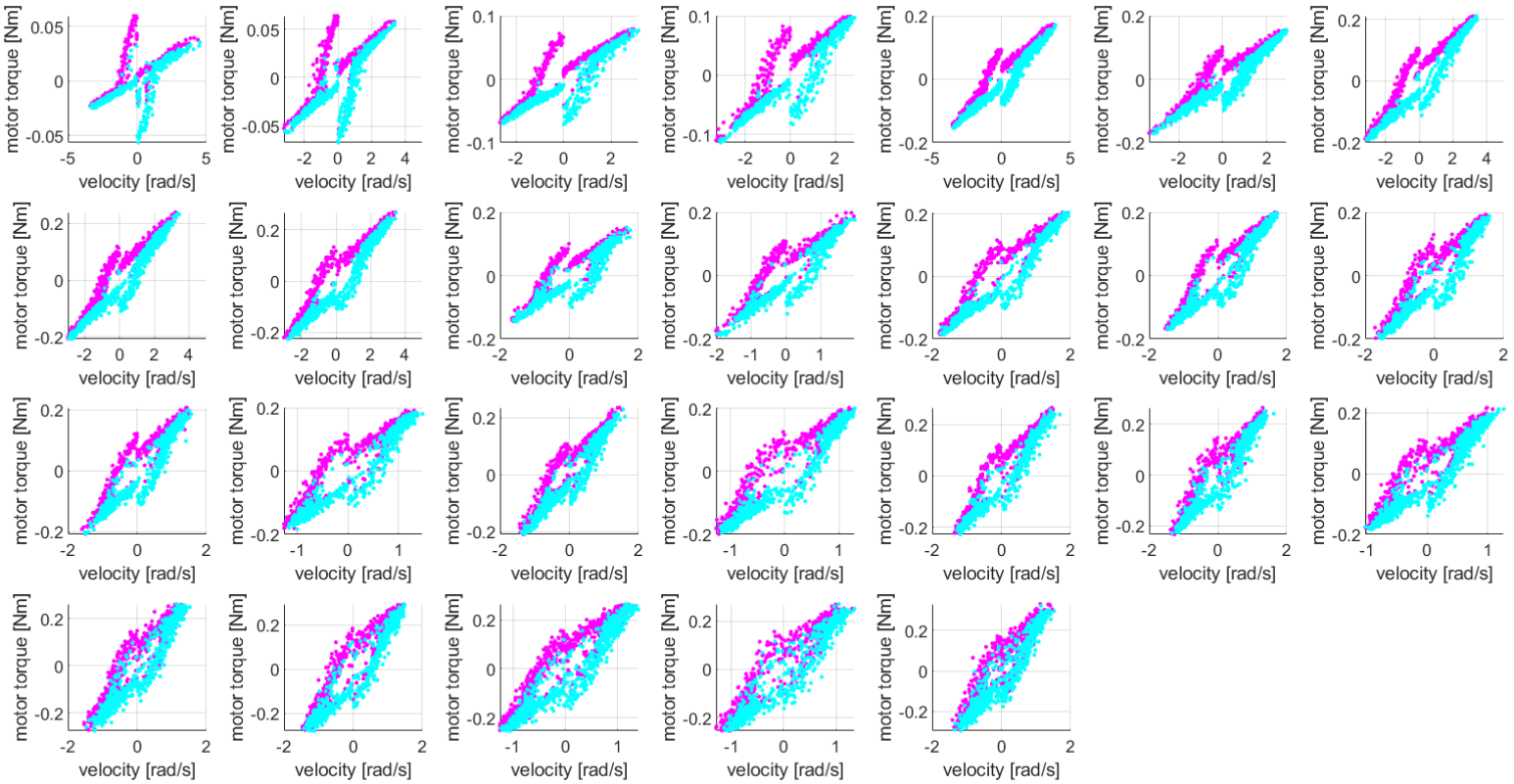

Figure 236 - Motor torque versus angular velocity, negative accelerations in purple, positive accelerations in cyan.

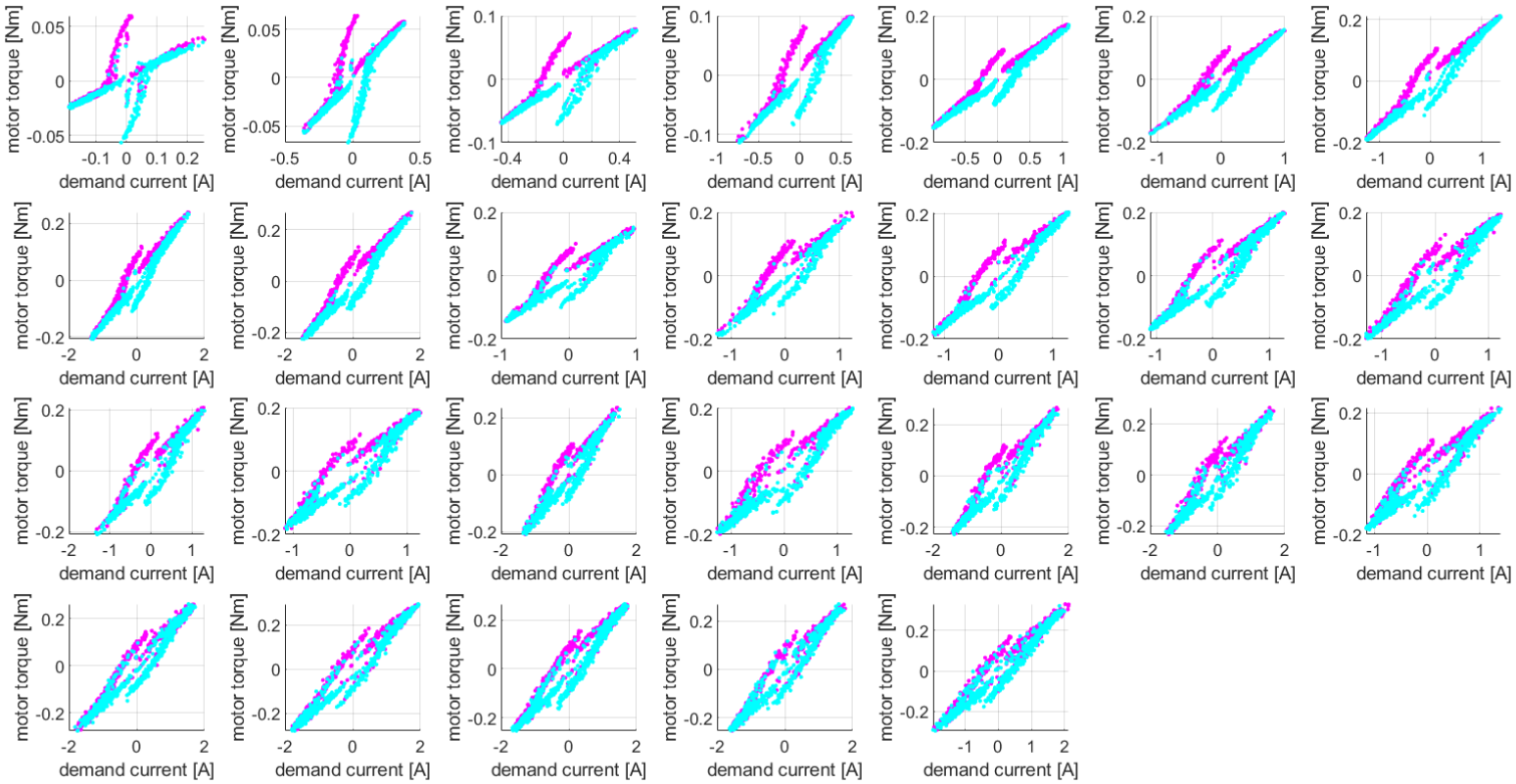

Figure 237 - Motor torque versus demand current; negative acceleration in purple, positive acceleration in cyan.

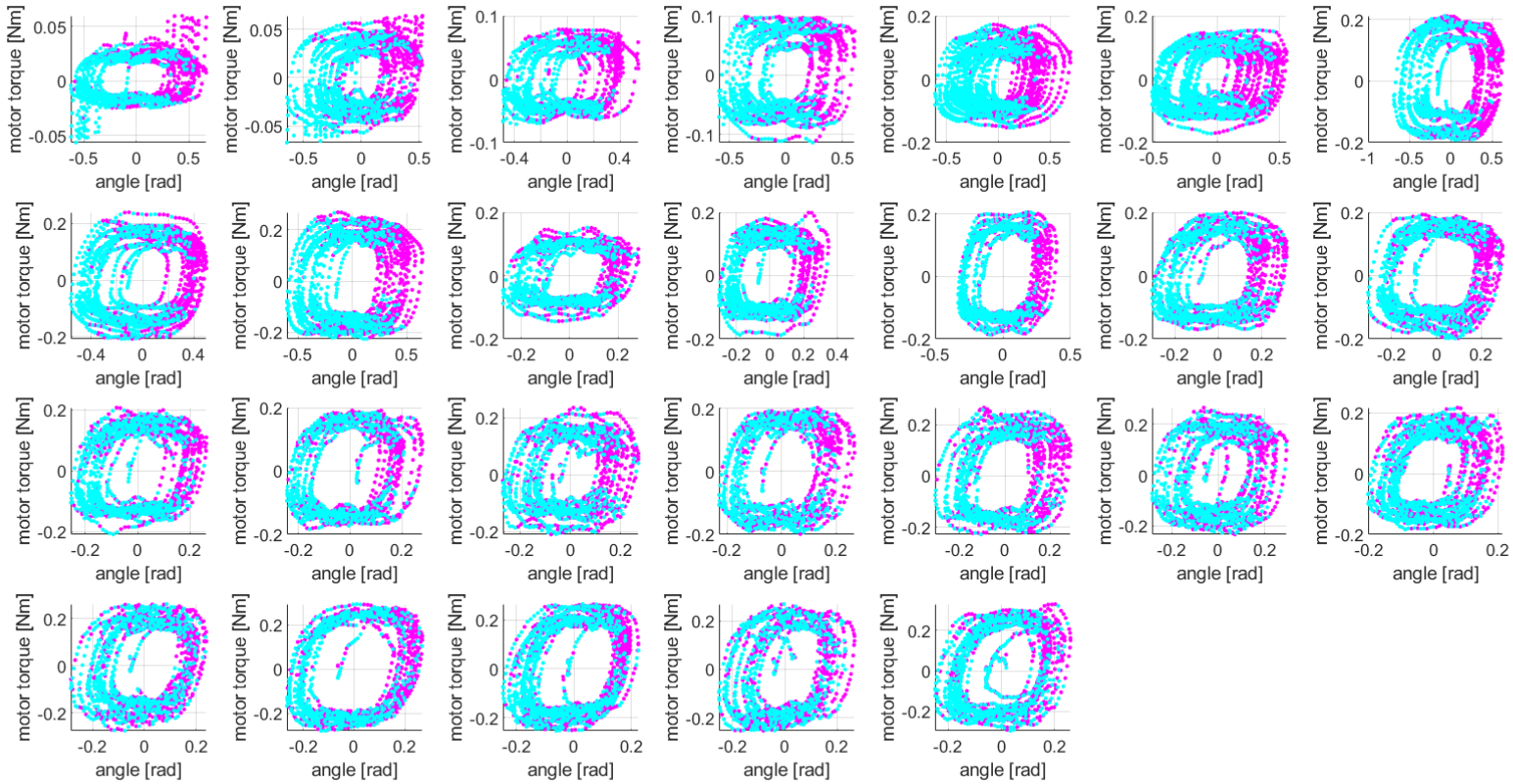

Figure 238 - Motor torques versus de-trended angle; negative acceleration in purple, positive acceleration in cyan.

G.2.3 Calibration sweep data

G.2.3.1 Initial

Baseline gain = 0 run:

- *offset_2021_07_16_11_17_26.csv* -> 0.001768 Nm
- *gain0_2021_07_16_11_18_15.csv* -> 0.9596s mean period

Cal	Gain	LP filter freq. [Hz]	Filename gainXX_2021_07_16_...	Offset [Nm]	Mean period [105] [s]	Dpto norm [Nms/rad]	Tconst [Nm/A]	Kpto norm [Nm/rad]
01	2	20	_11_23_38.csv	0.001465	1.02	0.00388116	0.13973204	0.00991936
02	4	“	_11_59_34	0.001106	0.98	0.00414517	0.14869082	0.00982378
03	6	…	_11_29_20	0.000900	0.92	0.00415251	0.14870376	0.00799091
04	8		_12_01_22	0.001083	0.99	0.00428314	0.15285898	0.00616547
05	10		_11_45_19	0.001276	1.00	0.00426620	0.15190714	0.0067472
06	12		_11_47_27	0.001176	1.07	0.00429483	0.15261575	0.00533609
07	14		_11_50_23	0.001393	0.94	0.00433795	0.15349046	0.00493423
08	16		_11_55_13	0.001196	0.97	0.00434459	0.15408462	0.00536759
09	18		_12_03_30	0.001112	0.95	0.00435323	0.15433589	0.00503618
10	20		_12_05_46	0.000997	0.95	0.00425311	0.15291837	0.00724307
11	22		_12_08_04	0.001085	0.95	0.00431963	0.15430115	0.00680983

[105] NB: these mean periods were recorded before de-trending the angle signal (via time_domain_stats6.m function), and may therefore deviate (albeit only slightly) from de-trended values.

12	24		_12_10_53	0.001056	1.06	0.00436762	0.15489043	0.0051942
13	26		_12_15_25	0.001028	0.99	0.00435033	0.15463307	0.0059580 6
14	28		_12_17_58	0.000962	1.01	0.00432393	0.15429372	0.0060622 6
15	30		_12_24_07	0.000993	0.93	0.00433828	0.15472794	0.0069435 1
16	32		_12_26_17	0.000975	0.96	0.00430576	0.15389655	0.0067443 4
17	34		_12_28_43	0.000978	1.00	0.00430051	0.15381992	0.0059916 2
18	36		_12_31_56	0.000919	0.97	0.00429826	0.15389816	0.0067190 6
19	38		_12_36_19	0.000837	1.00	0.00433619	0.15472413	0.0055415
20	40		_12_38_34	0.000810	1.03	0.00430620	0.15424482	0.0054908 3
21	42		_12_41_15	0.000869	0.99	0.00426412	0.15309228	0.0068491 9
22	44	10	_14_26_49	0.001215	0.99	0.00413832	0.15136538	0.0071459 9
23	46	“	_14_29_39	0.001177	0.98	0.00416997	0.15209121	0.0068948 7
24	48	…	_14_31_08	0.001177	0.96	0.00414926	0.15122438	0.0078278 8
25	50		_14_36_02	0.001058	1.01	0.00416429	0.15244655	0.0065038 1
26	52		_14_39_02	0.001011	1.03	0.00414792	0.15170484	0.0074029 4

Table 42. Fine calibration sweep

Cal	Gain	LP filter freq. [Hz]	Filename gainXX_2021_07_16_...	Offset [Nm]	Mean period [s]	Dpto norm [Nms/rad]	Tconst [Nm/A]	Kpto norm [Nm/rad]
01	10	20	_11_45_19.csv	0.001276	1.00	0.0042643	0.1517986	0.0067363 5
02	20	20	_12_05_46	0.000997	0.95	0.0042568 3	0.1528938 5	0.0072436 7
03	30	20	_12_24_07	0.000993	0.93	0.0043332 8	0.1545389 3	0.0066581 5
04	40	20	_12_38_34	0.000810	1.03	0.0042992	0.1540156 5	0.0056710 7
05	50	10	_14_36_02	0.001058	1.01	0.0041729 3	0.1525057 9	0.0066547 7
06	60	10	_14_56_48	0.000938	0.99	0.0038519 7	0.1468020 8	-0.0089884
07	70	10	_14_51_27	0.000895	0.98	0.0038184 9	0.1453022 7	0.0099538 1

Table 43. Coarse calibration sweep

Note that gains 10-50 are the same data sets as for the fine sweep above.

G.2.3.2 Calibration Repeats to check calibration parameter effects

De-trending with power 3, using MATLAB *detrend* function and *GainCal.m* script.

Comparison of LP filtering frequency:

Cal	Gain	LP filter freq. [Hz]	Filename (.csv)	Offset [Nm]	Mean period [s]	Dpto norm [Nms/rad]	Tconst [Nm/A]	Kpto norm [Nm/rad]
01	40	20	gain40_2021_07_16_12_38_34	0.000869	0.99	0.004306	0.15417	0.005483
02	40	10	filter10gain40_2021_07_19_10_47_10	0.000065	1.09	0.004125	0.14996	0.006829
03	20	20	gain20_2021_07_19_11_41_44	-0.00152	0.98	0.004229	0.14993	0.005090
04	20	10	gain20_2021_07_20_18_01_56	0.001426	1.03	0.004188	0.15088	0.005274

05	30	20	gain30_2021_07_16_12_24_07	0.000993	0.96	0.004338	0.15470	0.006937
06	30	10	gain30_2021_07_20_18_16_28	0.001162	0.96	0.004166	0.15078	0.006878

Comparing mean period at gain = 0:

Cal	Gain	LP filter freq. [Hz]	Filename (.csv)	Offset [Nm]	Mean period [s]	Max |static fr|[Nm]	Max |static fr|[Nm]	Mean |static fr|[Nm]
01	0	-	gain0_2021_07_16_11_18_15	0.001768	0.96	0.03044	0.02482	0.0276
02	0	-	gain0_2021_07_19_11_01_45	-0.00116	0.56	-	-	-
03	0	-	gain0_2021_07_19_10_56_55	-0.00074	2.02	-	-	-
04	0	-	gain0_2021_07_21_16_11_15*	0.00273	0.92	0.02106	0.02359	0.0223
05	0	-	gain0_2021_07_21_16_14_30*	0.001128	1.05	0.02181	0.02533	0.0236

*static friction has slightly dropped as a result of wear?

**what is the effect of a change in 0.0025Nm on calibration variables?

Comparing mean period at non-zero gains:

Cal	Gain	LP filter freq. [Hz]	Filename (.csv)	Offset [Nm]	Mean period [s]	Dpto norm [Nms/rad]	Tconst [Nm/A]	Kpto norm [Nm/rad]
01	20	20	gain20_2021_07_19_11_41_44	-0.00152	0.98	0.004229	0.14993	0.005090
02	20	20	gain20_2021_07_19_11_08_16	0.000952	0.51	0.004081	0.14770	0.013620
03	20	20	gain20_2021_07_19_11_10_44	0.001017	2.03	0.004003	0.14168	0.001660
04	20	20	gain20_2021_07_20_18_45_55	0.000895	0.67	0.004155	0.14896	0.010366
05	20	20	gain20_2021_07_20_18_29_42	0.000865	2.24	0.004044	0.14348	0.002029
06	20	20	gain20_2021_07_20_18_53_53	0.000702	0.56	0.004173	0.14972	0.011634
07	20	20	gain20_2021_07_20_18_39_20	0.000874	1.86	0.003988	0.14192	0.002666

Comparing repeatability at same nominal conditions:

Cal	Gain	LP filter freq. [Hz]	Filename (.csv)	Offset [Nm]	Mean period [s]	Dpto norm [Nms/rad]	Tconst [Nm/A]	Kpto norm [Nm/rad]
01	20	20	gain20_2021_07_16_12_05_46	0.000997	0.95	0.004253	0.15290	0.007243
02	20	20	gain20_2021_07_19_11_41_44	-0.00152	0.98	0.004229	0.14993	0.005090
03	20	20	gain20_2021_07_19_12_51_07	0.001798	0.97	0.004274	0.15132	0.004733
04	20	20	gain20_2021_07_19_12_54_53	0.001056	1.08	0.004246	0.15027	0.004282
05	20	20	gain20_2021_07_19_12_58_30	0.000763	1.15	0.004250	0.15041	0.004350
06	20	20	gain20_2021_07_19_13_01_53	0.000794	1.04	0.004250	0.15053	0.004717

…and same nominal conditions at higher gains:

Cal	Gain	LP filter freq. [Hz]	Filename (.csv)	Offset [Nm]	Mean period [s]	Dpto norm [Nms/rad]	Tconst [Nm/A]	Kpto norm [Nm/rad]
01	50	10	gain50_2021_07_16_14_36_02	0.001058	1.01	0.004164	0.15246	0.006497
02	50	10	gain50_2021_07_20_19_12_32	0.000221	1.12	0.004155	0.14997	0.005057
03	60	10	gain60_2021_07_16_14_56_48	0.000938	0.99	0.003816	0.14689	0.009025
04	60	10	gain60_2021_07_20_19_15_45	0.000483	0.92	0.004021	0.14861	0.007613

(perhaps more variation here because higher gain tests tended to be shorter?)G.2.3.3

Alternative friction correction

Correcting using the hysteretic slope as well as static friction.

Cal	Gain	LP filter freq. [Hz]	Filename gainXX_2021_07_16_...	Offset [Nm]	Mean period [106] [s]	Dpto norm [Nms/rad]	Tcosnt [Nm/A]	Kpto norm [Nm/rad]
01	2	20	_11_23_38.csv	0.001465	1.02	0.0040637	0.14342	0.003510
02	4	“	_11_59_34	0.001106	0.98	0.00437568	0.15469	0.004726
03	6	…	_11_29_20	0.000900	0.92	0.00426826	0.15122	0.004997
04	8		_12_01_22	0.001083	0.99	0.00434811	0.15420	0.004517
05	10		_11_45_19	0.001276	1.00	0.00430714	0.15264	0.005282
06	12		_11_47_27	0.001176	1.07	0.00435916	0.15415	0.003896
07	14		_11_50_23	0.001393	0.94	0.00435644	0.15378	0.004222
08	16		_11_55_13	0.001196	0.97	0.004375	0.15471	0.004423
09	18		_12_03_30	0.001112	0.95	0.00436901	0.15455	0.004451
10	20		_12_05_46	0.000997	0.95	0.00465829	0.16560	0.005289
11	22		_12_08_04	0.001085	0.95	0.00452605	0.16051	0.005162
12	24		_12_10_53	0.001056	1.06	0.00448775	0.15844	0.003869
13	26		_12_15_25	0.001028	0.99	0.00455967	0.16104	0.004444
14	28		_12_17_58	0.000962	1.01	0.00455141	0.16136	0.004877
15	30		_12_24_07	0.000993	0.93	0.00462095	0.16353	0.005369
16	32		_12_26_17	0.000975	0.96	0.00460354	0.16323	0.005426
17	34		_12_28_43	0.000978	1.00	0.00463158	0.16423	0.004778
18	36		_12_31_56	0.000919	0.97	0.00460985	0.16371	0.005357
19	38		_12_36_19	0.000837	1.00	0.00456583	0.16187	0.004303
20	40		_12_38_34	0.000810	1.03	0.00455115	0.16182	0.004435

[106] NB: these mean periods were recorded before de-trending the angle signal (via *time_domain_stats6.m* function), and may therefore deviate (albeit only slightly) from de-trended values.

21	42		_12_41_15	0.000869	0.99	0.00474016	0.16826	0.005266
22	44	10	_14_26_49	0.001215	0.99	0.00437585	0.15837	0.006210
23	46	“	_14_29_39	0.001177	0.98	0.00430504	0.15584	0.005942
24	48	…	_14_31_08	0.001177	0.96	0.00440197	0.15868	0.006532
25	50		_14_36_02	0.001058	1.01	0.00442534	0.16021	0.005648
26	52		_14_39_02	0.001011	1.03	0.00434647	0.15751	0.006413

This is ultimately not pursued as it would be a “blind” and more complex correction, since the correction would be a function of the mean excitation period. Having run it for the fine calibration sweep as a trial, it was also found that the accuracy of calibration variables does not improve.

G.3 Motor comparison

Some notes on constraints/requirements:

- The maximum torque needed for the motor should be as close as possible to the PTO torque limit of 65kNm (full-scale) → 40.6 Ncm (20^{th} scale) = 0.406 Nm
- The WEC model nacelle – which will house the motor – has a diameter of 100mm and a width of 120mm

Gaps indicate missing information.

Manufacturer	Kollmorgen	Moog	Aerotech	Aeroflex Laboratories
Model	AKM11	DB-1500-L-1ES	SM35 NEMA17	TQ 34
Mass (g)	350	153	500	454
Diameter (mm)	46	38.1	42.2	47
Length (mm) [excluding shaft]	79	19.05	115	17.8
Inertia (kg cm²)	0.017	0.019	0.102	0.644
Friction (Nm)	0.0011 static friction from motor itself	0.0078 friction torque	n/a	None
Max stall torque, Tps (Nm)	0.62	0.45	0.78	0.28
Cont. torque at stall, Tcs (Nm)	0.19	n/a	n/a	n/a
Pros	No need for separate rotary sensor/encoder to track angular position	Smaller than Kollmorgen but higher friction	Zero cogging	Submersible No friction

	Has accompanying plug-and-play servo drive Have used this motor type before in NWEC2 test programme	Includes hall effect sensors for commutation	Includes hall effect sensors for commutation Encoder feedback available as an option	
Cons	Static friction + additional friction from shaft seals may be too high	Frameless – mounting unclear Requires switching mode electronics?		Limited to +/-25deg rotation (50deg overall) (lower torque rating model has 120deg overall limit Torque provision decreases with increasing angular rotation
Other	3D CAD model available online It likely that the torque figures include a 10% safety margin so there is probably extra torque headroom (can probably run with T>Tcs before running into power limitation issues	Brushless DC Torque motor 3D model available Can request particular mounting/flanges options	"Custom integration can be engineered to requirement with minimal lead time"	

Link	https://www.kollmorgen.com/en-us/products/catalogs/kollmorgen-akm-servomotor-selection-guide/	https://www.moog.com/products/motors-servomotors/brushless-motors/high-performance-direct-drive-brushless-dc-motors/db-1500-matrix-series.html	https://www.aerotech.co.uk/product-catalog/motors/rotary-motors/sm-series.aspx	https://archive.org/details/TNM_Brushless_DC_Torque_Motors_-_Aeroflex_Laborat_20171024_0014/page/n1/mode/2up
Cost	Cost of motor and drive ~ £1k			
Lead time	6-8 weeks			
Voltage (V)	75-320 dc			
Figures	Figure 239		Figure 240	Figure 241

Table 44 - Motor comparison table.

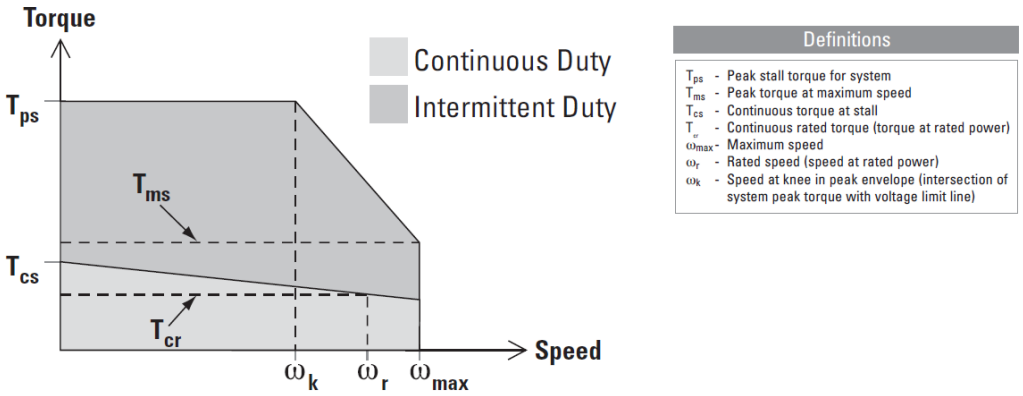

Figure 239 – Operating envelope of Kollmorgen motors. [Source: Kollmorgen AKM Manual].

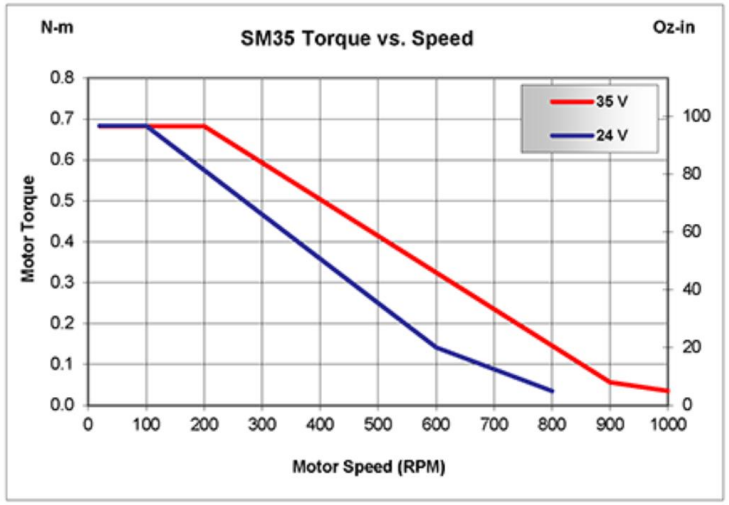

Figure 240 - Operating envelope of Aerotech motor. [Source: Aerotech Manual]

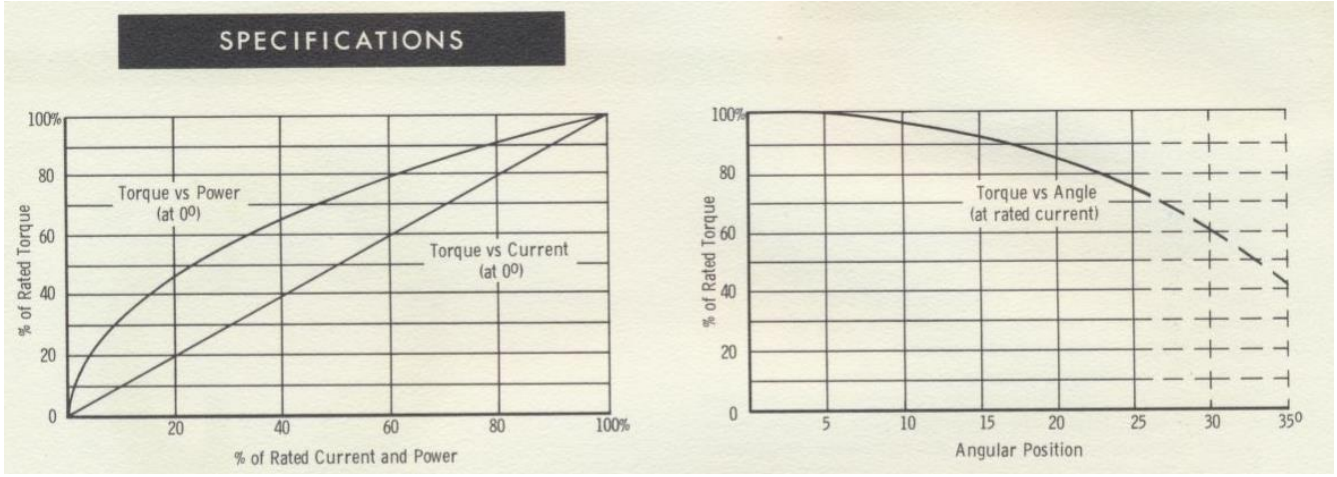

Figure 241 - Operating envelope of Aeroflex motors. [Source: Aeroflex Manual]

G.4 Additional supporting images

G.4.1 Nacelle build

From top left, going across and down, the images show:

- an axial view of the nacelle tube, showing the cable entries via glands on the right hand side, and the tight space for the various components and wires in the main cavity;
- the 3D printed custom PET-G part that holds the two Molex connector pairs;
- the overall hinge assembly, with visible cables, glands, and motor shaft on the right hand side;
- the star connection of the earthing wires on the motor mounting plate;
- a meniscus of water around the motor shaft that suggests the rotary seal is water tight, which remains even when the shaft is exercised;
- silicone sealant applied in the counter-bores of each of the four motor mounting screws. The same was also applied to the tapped hole at the nacelle tube used for earthing.

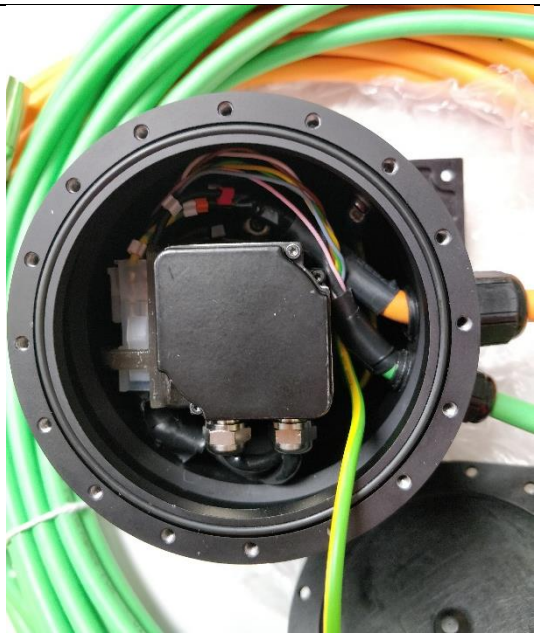	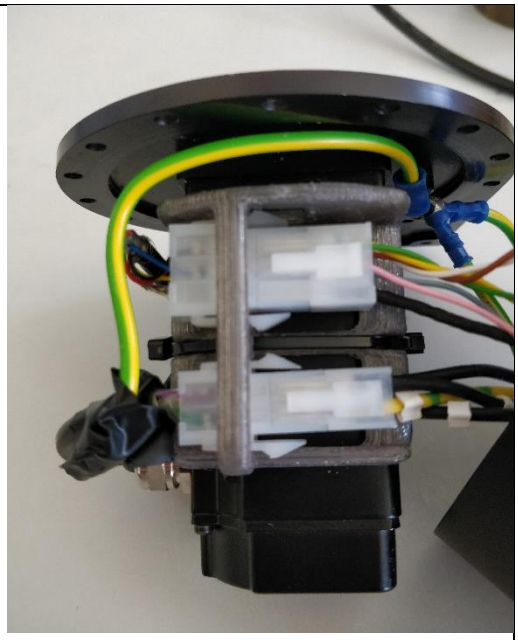
a	b

	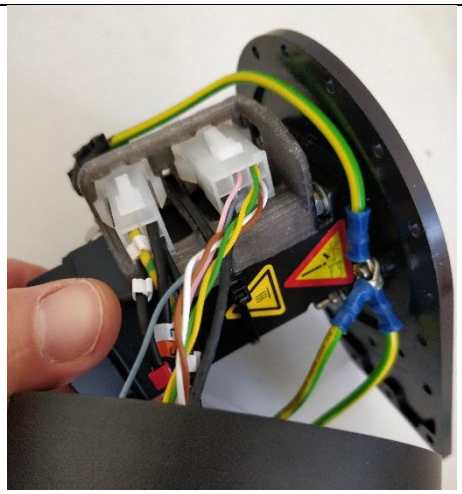
c	d
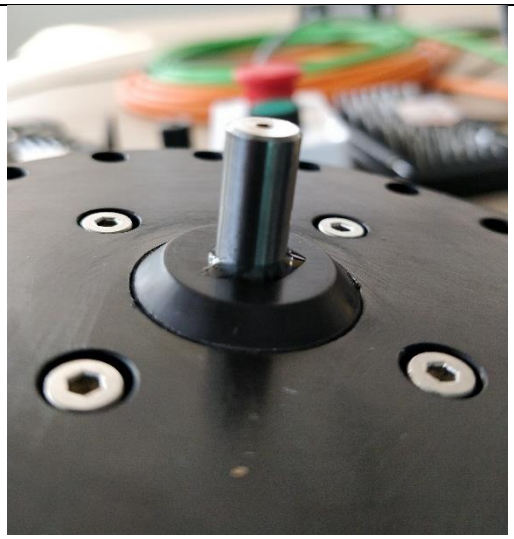	
e	f

Table 45 - Showing images of motorised nacelle build.

G.4.2 Weighing the nacelle

The mass of the nacelle was measured, without lever arm, but with all the screws, cable glands, sealant, and dessicant bag inside. The cables were resting on the desk beside it. The DYMO scale was calibrated with a known 100g mass, and displayed 100g everywhere apart from right in the middle of the scale where it displayed 98g. In practice, the measured mass is only a rough estimate as the cable stiffness and mass affects the reading considerably.

Figure 242 - Image of nacelle weighing ahead of water submersion period. (NB: mass shown is not precise due to cable presence).

Appendix H

H.1 BST-folding optimisation output

A view of the Blue Star folding (BST-folding) 20th scale physical model is shown in Figure 243. This version is the passive one, having an angle sensor in the nacelle, with its cable shown extending from the underside of the fwd hull, which is folded into the aft hull in the figure.

Figure 243 - Second view of the passive model in folded configuration (from aft wave channel).

The associated matrices from the numerical optimisation are shown below, and relate to Central North Sea site conditions, 12-year hindcast data.

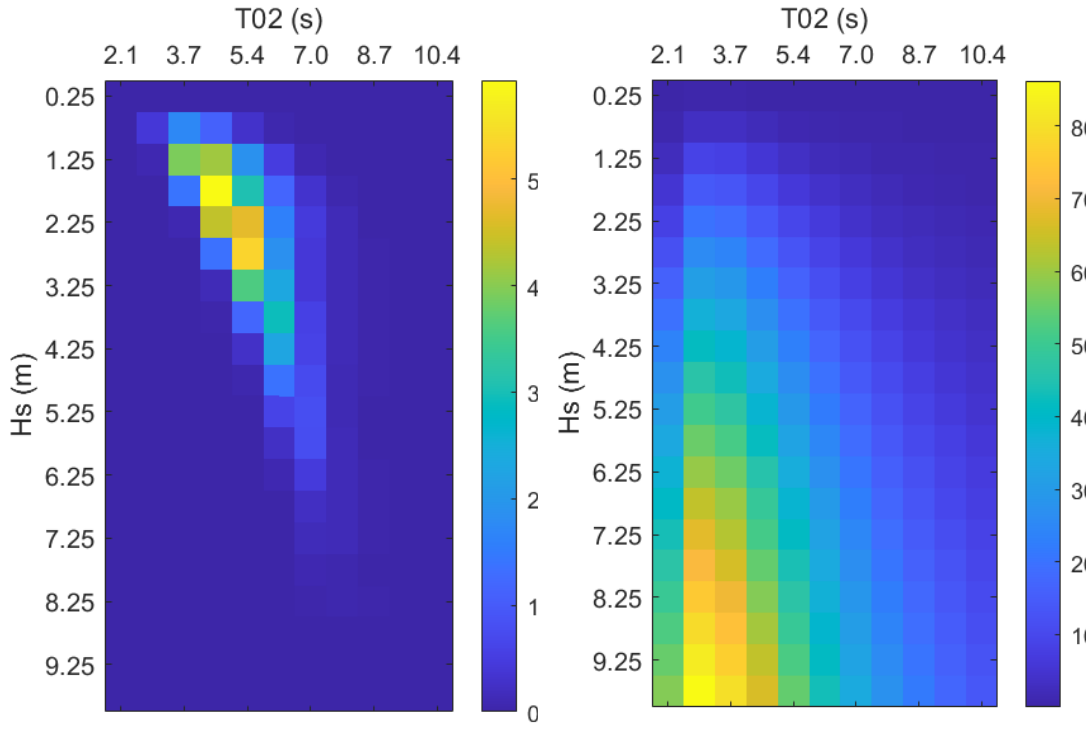

Figure 244 - Numerically predicted energy matrix (left) and power matrix (right) at full-scale.

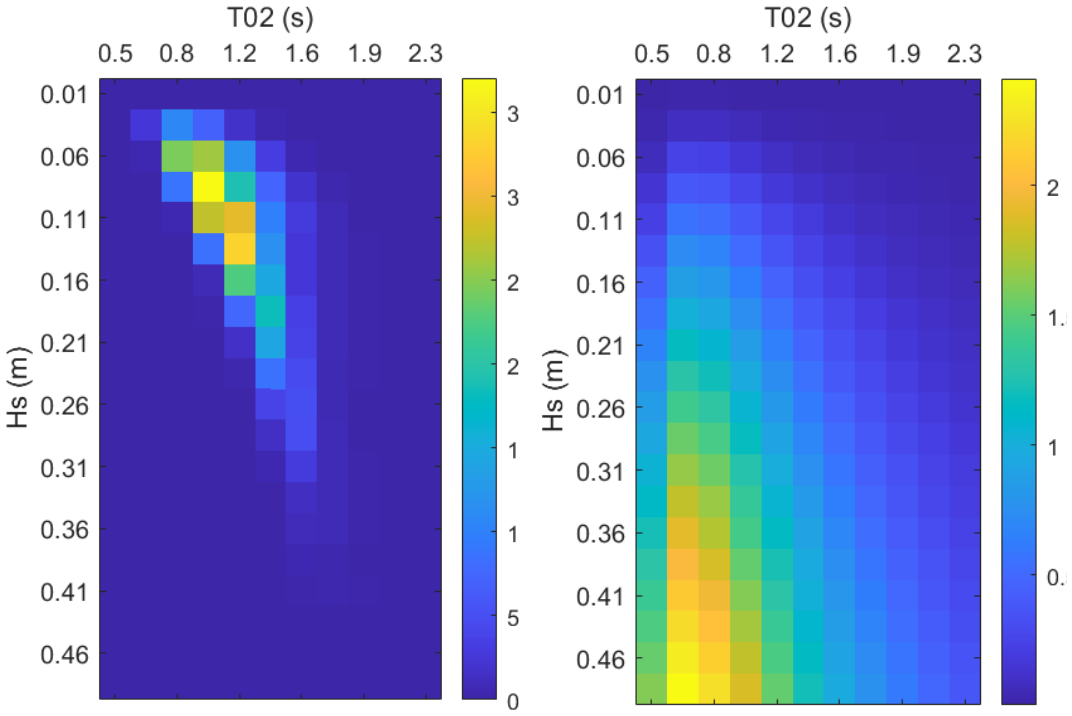

Figure 245 - Numerically predicted energy matrix (left) and power matrix (right) at 1:20 scale.

H.2 Guidance and applicability of IEC TS 62600-103 Standards

This set of tests spans elements of Stage 1 (Concept model) and Stage 2 (Design model) as defined in the latest IEC test guidance, which is considered to be the state-of-the-art best practice (IEC TS 62600-103, 2018). It involves performance verification in realistic seaways and a power take-off, but includes only limited component and control monitoring. In addition, the scale of this model theoretically places it in the 'Design model' category (1:20).

The guidance recognises that iterations will be needed within each stage, particularly Stages 1 and 2. Nevertheless, it is reminded that if more subsystems can be included in Stage 1, and the more representative these can be made, the more the model evolution can be streamlined, while likely reducing involved costs.

H.2.1 Stage 1 criteria

The specified Stage 1 assessment criteria is as follows:

A. Proof-of-concept (PoC): verify that device design operates under wave excitation as predicted and described
B. Optimisation of design: evolve the most favourable device configuration(s) in regular and irregular waves
C. Device performance: obtain a first indication of power performance in five sea states for the optimised PTO setting of the device

Criteria A is addressed via appropriate RAO data collection. Criteria B is addressed via numerical optimisation prior to testing, and then by adjusting torque limit and PTO damping values during tests, as well as via inclusion of hull filler to check "no gap" geometry version performance. Criteria C is addressed by measuring torque and velocity and selecting appropriate sea state runs.

Stage 1 tests additionally envisage a PTO that "*can be represented by a simplified, accurate, mechanism. The selected PTO mechanism shall provide a damping that can be characterised across an appropriate range of settings*." This is indeed the case; the damping can be varied by controlling the current demand to the motor, which is being used as a representative PTO.

Furthermore, "a *generic station keeping system can be used if the mooring behaviour is not an integral part of the device hydrodynamic motion and energy conversion scheme*". This is also the case. Two mooring configurations will be used: a slack mooring that isolates device motions from mooring behaviour, and a generic semi-representative taut system that allows mooring loads to be measured and mooring line angles to be adjusted.

Appraisals in each category are to be based on:

Energy absorption	**Seakeeping**	**Mooring (if implemented)**
- Set of power response transfer function (RAO, for similar wave heights) - Power capture prospects estimated on a minimum of five selected sea states	- RAO for the dominant or relevant degrees of freedom (i.e. *flex*)	- Time series and associated analysis (e.g. RAOs) of the mooring line loads

Table 46 - Stage 1 testing appraisal categories and criteria. (NB: Stage 2 appraisal categories are the same).

H.2.2 Stage 2 criteria

For Stage 2, the assessment criteria is by nature the same as for Stage 1 (see Table 46), but results from more thorough testing.

A. Stage 1 validation: validate tech conclusions drawn from previous test programme and identify potential scaling issues between the two stages.
B. Mooring function check: verify the proposed full-scale mooring and anchorage system design and assess realistic mooring response.
C. Verify energy conversion performance.
D. Device dynamics and kinematics.
E. Survivability check: introducing storm conditions to observe device response in survival conditions, and to discover device-specific failure modes.

The following recommendations are also made:

i. Use largest feasible scale for available facilities to reduce influence of scale effects
ii. If practical the flexible umbilical electrical cable should be incorporated in selected tests
iii. Inclusion of advance PTO simulation to evaluate different control strategies
iv. As far as possible, model and tests should be comparable to Stage 1

Criteria A is not being satisfied fully as we are, to an extent, merging Stages 1 and 2 together. It could be argued that some of the Stage 1 iterative optimisation has occurred numerically or from previous Blue X/WES experimental modelling. An attempt at evaluating/estimating scaling issues is made by testing a passive 40th scale model.

Criteria B is not satisfied as the implemented mooring system does not match the exact envisaged full-scale system, although the 3-line taut system is somewhat representative[107]. This is because the device geometry has changed since this physical model was designed and built, and the full-scale mooring system is still being finalised at the time of performing this test programme.

Criteria C and D are satisfied as we can calculate power conversion and kinematics from PTO pre-calibration (inferring torque from current) and measure device dynamics and kinematics via Qualisys motion tracking of the model.

Criteria E is not satisfied as the Curved Tank facility does not allow sufficiently 'extreme' sea states to be run with a 20th scale physical model.

All recommendations are implemented. Although the control strategy will consist in linear damping control only, this is actually representative of the implemented control strategy in the full-scale WEC, as per development progress at the time of testing. A sophisticated control strategy is not envisaged in the full-scale device, since its power capture envelope is already predicted to be very broad and detailed control investigations are yet to be performed numerically. However, more advanced control strategies can be potentially implemented via the controller and PTO set up used in these tests.

H.2.3 Additional notes on scaling

(IEC TS 62600-103, 2018) states, in relation to hydrodynamic scaling, that the model should be made as large as possible to mitigate Fr and Re scaling

[107] Current BST Feed mooring design involves catenaries and submerged buoys to allow more compliance to the WEC device motions, while guaranteeing more constrained mooring circle.

mismatches, since they cannot be simultaneously met. Re number, in particular, relates to viscous forces.

As outlined in Chapter 3-4, drag forces can be broken down into three components: *viscous*, *form*, and *induced*. The former is typically scale-dependent while the latter two are not (Palm *et al.*, 2018). Nevertheless, minimisation of vortex shedding (a type of induced drag) is still desirable – because (i) WAMIT cannot explicitly take into account vortex shedding in its computation (or viscous drag); (ii) the drag coefficient that is tuned is an equivalent (lumped) drag coefficient, which is calibrated using a TD model and then linearly applied to the FD model (see Chapter 4). Thus, minimising vortex shedding renders FD and experimental models more like-for-like, while also helping to isolate other drag effects (such as viscous drag, which does scale with model scale) in the TD model. Vortex shedding can be significant at small scale but can be mitigated by minimising some of its causes such as sharp edges and narrow fluid gaps. This has been attempted to the greatest possible degree in the model, but some sharp edges (e.g. around the carbon fibre sheets) and narrow fluid gaps (around the nacelle and perhaps also the aft hull gap) remain.

A side note in relation to viscous losses. Previously, Mocean had conducted tests for Blue X at 10th and 20th scales as part of the WES NWEC2 phase of development. The models were close to geometrically identical but overlapping test conditions to enable comparison were not run. However, during towing tests, so-called ‘fishtailing’ behaviour was observed as a consequence of unsteady forces arising from vortex shedding. If a body is sufficiently streamlined, it will shed few or no vortices in its wake. However, the 20th scale model was observed to oscillate in yaw when under tow, with its motion increasing in amplitude and frequency as flow speed increased. A coupling of roll and yaw responses was also observed. This was thought to be a serious limiting factor to the towing speed of the full-scale device. Nevertheless, stable towing speeds were achieved at full-scale at roughly twice the speeds tested in FloWave. This suggested that for the particular model and geometry, hydrodynamic losses may have been more significant at model scale compared to full-scale. In other words, viscous forces are proportionally greater at smaller

scale, where the relative viscosity of the water increases. This seems to be particularly the case in the context of towing, but a lesser effect is likely to occur during normal WEC dynamics, where Froude scaling should remain relatively more applicable.

With regards to the PTO inclusion, (IEC TS 62600-103, 2018) warns that representational PTOs that can be included in Stages 1 and 2 can introduce frictional effects, like stiction, or non-physical hysteretic effects. It therefore recommends careful consideration of the power conversion chain (PCC), and a frictional analysis being carried out to determine performance differences arising from an inability to scale frictional losses. The PCC in this particular physical model is composed of the prime mover, shaft bearings, motor shaft rotary seal, and the motor itself, all of which have associated efficiencies. These are estimated via nacelle dry bench tests ahead of testing in the tank [see Chapter 7]. In particular, we need to be confident that we can infer torque from current measurements to a sufficiently high level of accuracy, since it cannot be measured directly due to lack of space in the nacelle that prevents a torque sensor being incorporated.

H.2.4 Reporting

Notes on reporting in reference to the IEC guidance are given in relevant subsections of Chapter 8. Relevant general guidelines are:

- Provide peak distributions and spectral shapes for irregular wave tests
- Provide RAO error bars governed by STD of performance indicator and STD of wave amplitude (relating to uncertainty analysis)
- For capture width (CW) and capture width ratio (CWR) – both forms of RAOs – it is best to report these at model scale or as non-dimensional parameters

H.3 Model build

Detailed information regarding 20th and 40th physical model builds is outlined in this subsection.

H.3.1 20th scale model

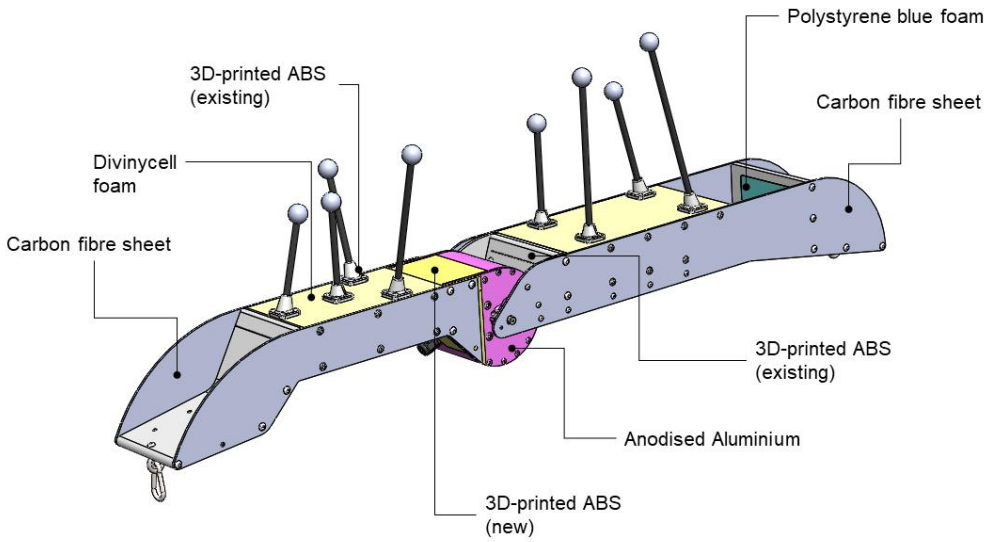

Figure 246 - Indicating material selection for different components.

In Figure 246, the materials selected for this model are indicated. Dark grey components are 2.5mm thick laser cut carbon fibre sheets, which give the model torsional stiffness and strength. The light colour grey components (central part of the wave channels, and the aft clevis) are 3D-printed ABS components re-utilised from the previous passive model. The light colour yellow components forming the central section of each hull are made of stiff, lightweight, closed cell, Divinycell foam (machined). The darker yellow component that interfaces between nacelle and the FWD hull Divinycell block is a new 3D-printed ABS component. It has a cavity (hidden in the figure) that is filled with closed-cell polystyrene blue foam blocks. These are extremely lightweight and help to reduce the mass in non-load-bearing areas. The rear side of the AFT wave channel is also filled with polystyrene blue foam to reduce its mass.

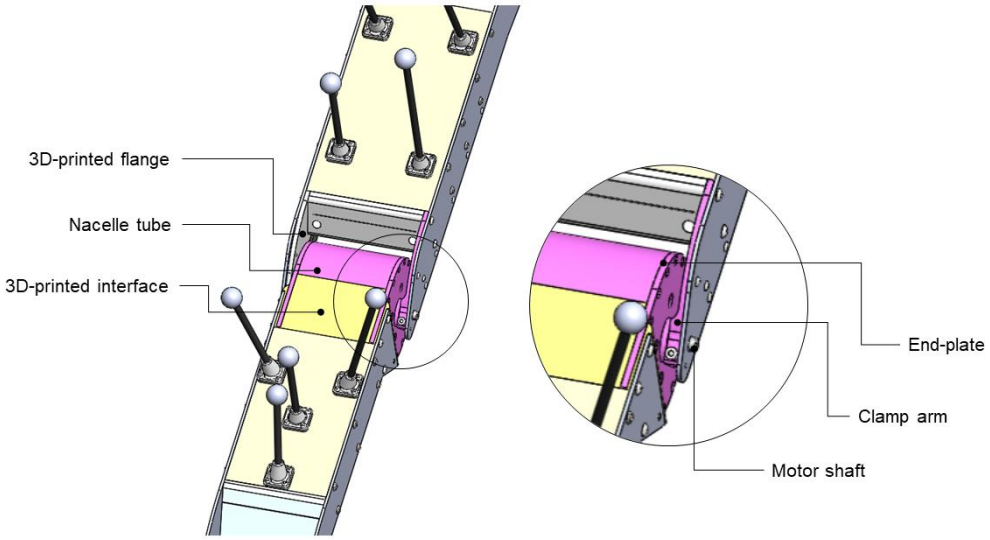

Figure 247 - Top view of the nacelle and clamp arm.

The purple components (forming the nacelle tube and end-caps) are made of anodised machined aluminium. A clamp arm that attaches to the motor shaft is also made of aluminium but not visible in the figure, as it lies behind part of the CF sheet near the nacelle (port side). Finally, the Qualisys rod bases that screw into the main hull Divinycell blocks are also made from 3D-printed ABS. Stainless steel screws are used throughout. In the original passive BST-folding model, the nacelle was composed primarily of 3D-printed ABS, with some machined ABS parts forming the subassembly that housed the non-contact angular sensor. Careful design was undertaken such that the old nacelle could be straight swapped with a new one, containing the model PTO. The various assembly steps also had to be considered with great care, to ensure assembly and disassembly was possible and practicable.

H.3.2 40th scale model

The 40th scale model is a much simpler design, primarily made from two single-build 3D-printed ABS parts, separate flanges around the nacelle, nylon screws, nuts, and bolts, and a stainless steel eye-bolt for the mooring attachment. Two types of Qualisys target are utilised: very small wet-proof balls at the lower vertical locations, and larger (yet still lightweight) targets in raised locations, where targets are less likely to be splashed during tank testing. Stainless steel

screws and small bearings are only utilised at the hinge, at the side flanges, and to hold the lead strips in place at the underside. Buoyancy and trim are managed similarly to the 20th scale model, via polystyrene blue blocks within the main hull sections (underneath the two cover components) as well as at the underside of the model (see Figure 250). Figure 249 shows the version without hull gap. This is identical, safe for 2 additional components: a 3D-printed ABS frame, and another polystyrene blue block within it. The part is self-trimmed, so no additional trimming adjustments are required when swapping it in and out.

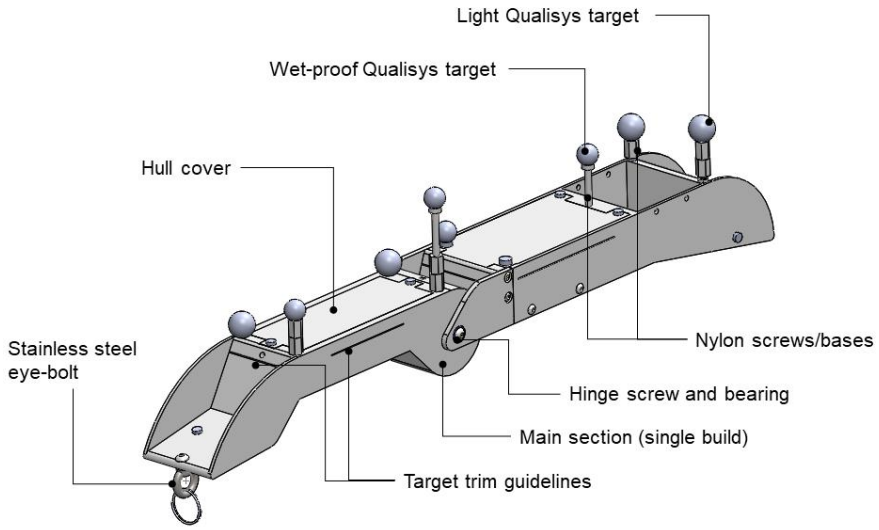

Figure 248 - 40th scale model, showing salient features.

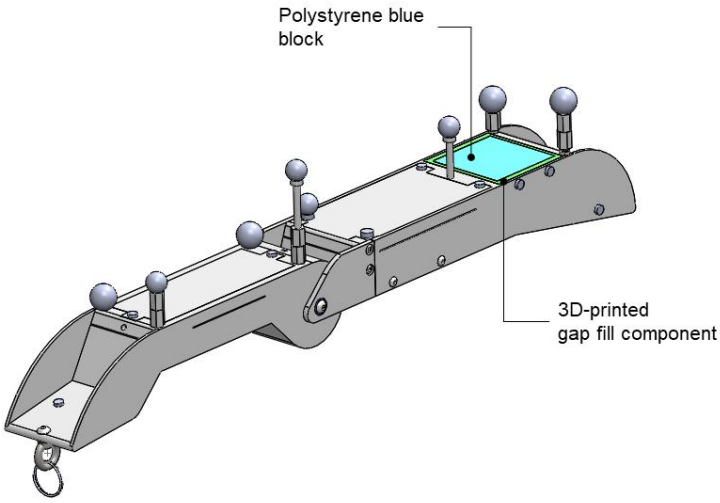

Figure 249 - 40th scale model - version without hull gap.

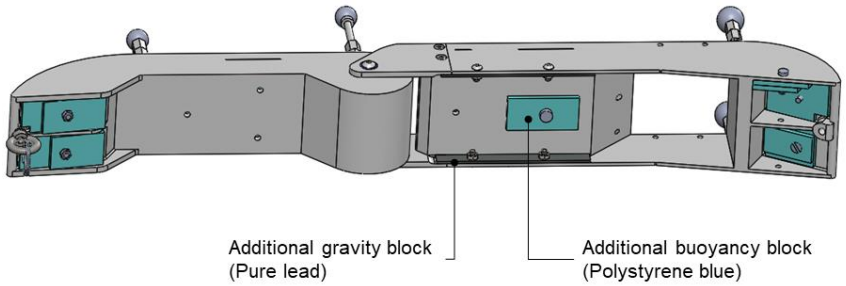

Figure 250 – Underside of 40th scale model, showing parts introduced for additional trimming adjustments.

Trimming analysis is shown in Appendix N.

H.4 Mooring set up

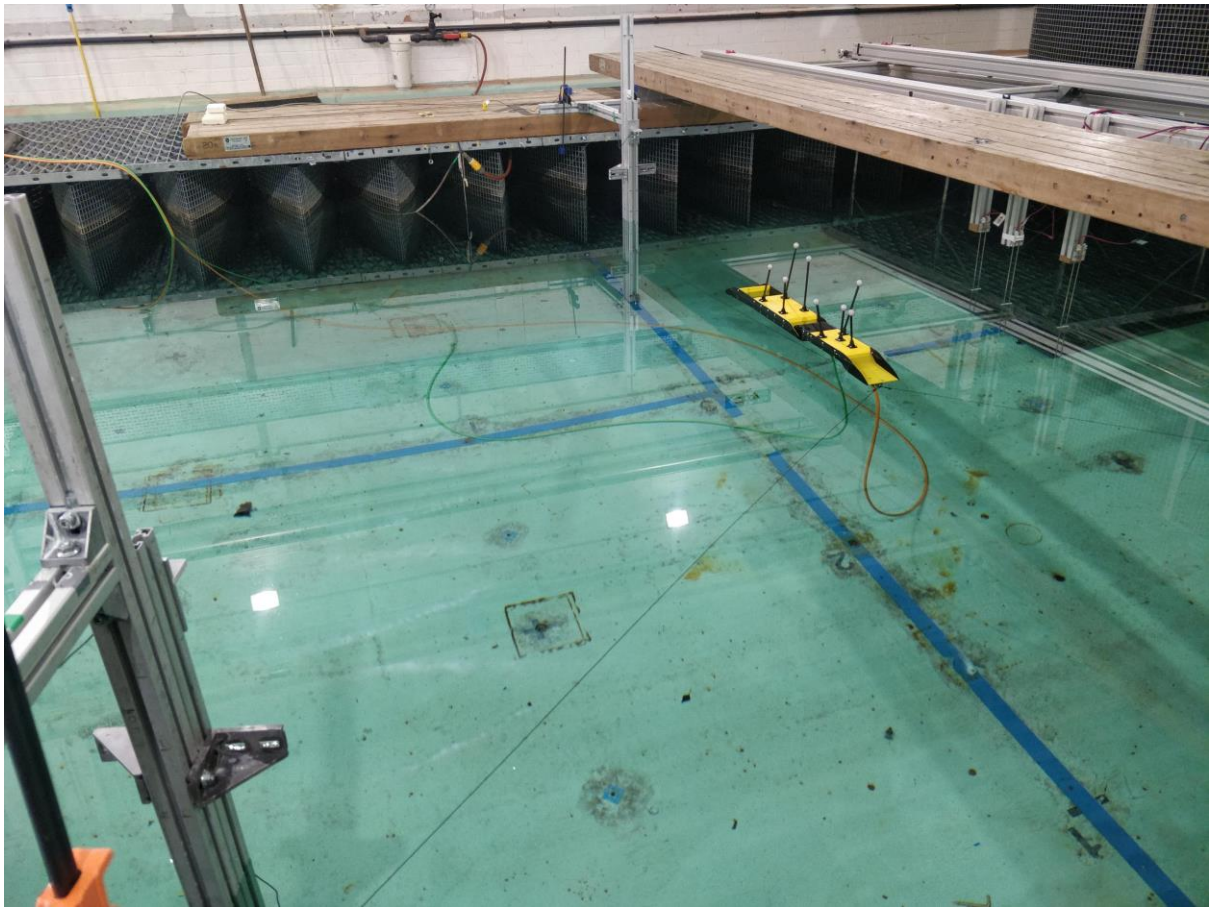

Figure 251 - Showing BST-folding in its taut moored set up with two of the three mooring poles visible.

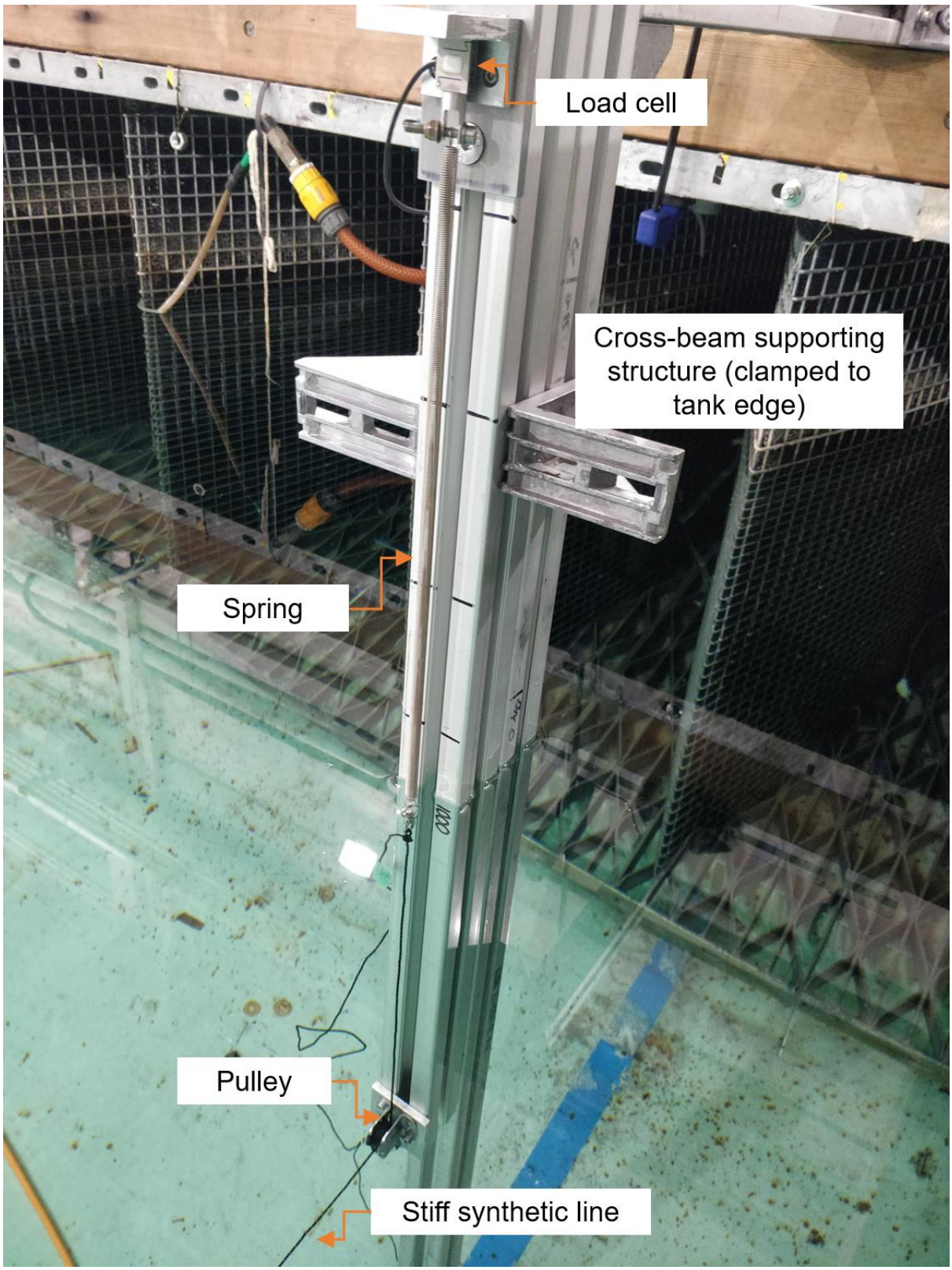

Figure 252 - Annotated image of one of the three mooring poles for taut mooring set up.

H.5 Prescribed seas

(IEC TS 62600-103, 2018) does not specify specific wave conditions for RAO measurement, aside from a minimum number of waves for a sea state to be considered representative. However, it does suggest conditions for power capture estimations.

- Stage 1: power capture prospects estimated on a minimum of 5 selected sea states.
- Stage 2: power capture for a minimum of 15 standard sea states (power matrix).

The IEC also prescribes the following minimum test conditions for Stage 2:

- Regular waves: 10 periods per configuration[108] of the model for **50 waves duration each**. For selected device configurations, the testing should be repeated with at least two other wave amplitudes.
- Irregular long-crested: 15 operational sea states (for each tested spectral shape) of **250 waves duration each**.
- Irregular short-crested: 3 directional sea states for **1500 waves duration each**.

Note that for regular wave sweeps, the number of waves or cycles N = f*T_R, where T_R is the repeat time (set to 64s). The number of samples (N) should be a power of 2 in order to avoid spilling[109] effects. Each test run is then 94s, taking into account an additional 30s for: (i) the sea state to become fully developed; and (ii) for the waves to reach the model. It is accepted that with this value of repeat time, less than 50 waves will be run for regular seas at the lower frequencies.

For irregular waves, we assume that each cycle takes approximately 1s, which is approximately the peak period at model scale. Previously, the repeat time had been set to 512s (a power of 2) which equates to ~37mins at full scale, noting

[108] Unclear as to whether this assumes that different geometries or model versions are being used, or whether it also refers to tuning parameters such as PTO damping value or Torque limit value.

[109] i.e. amplitude of true frequency component not spread over nearest direct Fourier transform (DFT) components. Resolution frequency of the DFT is 1/T_R.

that a wave buoy record of 30mins is considered sufficient to characterise a sea state. However, due to the greater number of irregular wave sweeps envisaged, and the increased probability of the motor's thermal limit being reached as the tests get longer in duration, the repeat time is set to 256s for long-crested seas, with the relevant additional 30s buffer as regular waves. For short-crested seas, the ideal run time should be 2048s to satisfy the 1500 minimum cycle, but may need to be reduced to 1024s or even 512s to satisfy the motor's thermal limit. Ultimately, short-crested seas are also run with 512s repeat period.

H.6 Proposed seas

Regular, irregular (long and short crested), IR0. [Refer to table above and to relevant Appendices).] Additional notes on focused and 40th scale seas are given below.

H.6.1 Focused waves

It is decided not to run focused waves for the following reason. In focused waves, all the energy is concentrated at a single point at a single time; a focused wave is essentially a large wave that rolls by the machine. From prior Mocean testing experience, this actually doesn't produce particularly 'bad' angles; about half as 'bad' as when testing with irregular waves. Since this large wave comes out of nowhere, the machine is 'ready for it', since it is at steady state with hinge angle at zero when the focused wave arrives. The WEC gets excited as a one-off, but this is not as bad as the condition where hinge can be at some unfortunate angle and then the WEC gets excited by another unfavourable wave. In other words, phasing is more of an issue in causing extreme angles in the hinge.

H.6.2 40th scale waves

At 40th scale, there are two important considerations to make. Firstly, it is desirable to ensure that at least some of the waves are as 'linear' as possible, in order to isolate *model* – as opposed to *wave* – nonlinearities. In this campaign, the 1/100 steepness waves used at 20th scale are used again at 40th scale, being equivalent to 1/50 at this reduced scale. This was done to save time on wave characterisation.

H.6.3 Tuning of the PTO

This section outlines the PTO-related parameters to be considered during wave runs, namely: PTO damping, torque limit, thermal limit. It also touches on short-crested seas considerations.

H.6.3.1 PTO damping

The effect of changing PTO damping is investigated by running a regular wave series and changing the PTO damping value during the run. This is carried out with a number of seas at steepness 1/100, and ideally also at a different steepness (1/50). Figure 253 shows the mean power versus time during a previous Mocean testing campaign that followed this method; the damping was changed by setting the gain to seven levels of 30, 50, 70, 90, 110 and 130 – the top level is chosen to equal the gain used in most of the model tests. The gain is briefly returned to zero between each gain setting so that the transitions are clear. This method is consistent with guidance provided by IEA Annex II (Nielsen, 2003).

These runs are performed at the beginning of the test programme, and the subsequent frequency sweeps are performed at the gain value corresponding to max average power capture suggested by the plots. Three values of damping are chosen for the regular wave frequency sweep so that they can be plotted against one another. One is the value as indicated by the equivalent of Figure 253; a value and below this are also chosen. It is also desirable to run the irregular waves with at least two different PTO damping values.

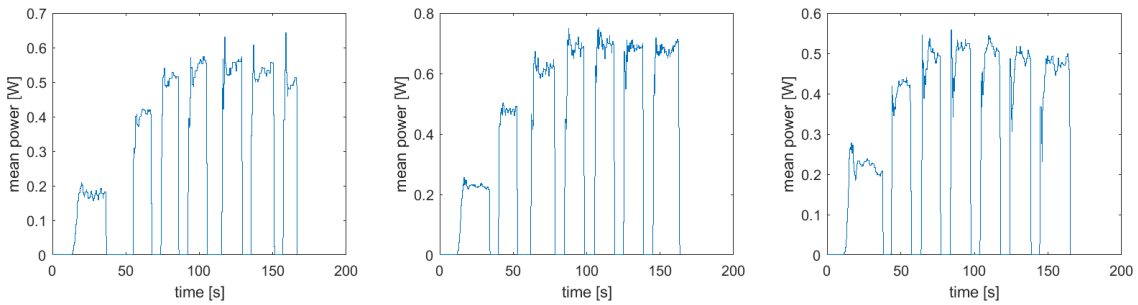

Figure 253 - Example of damping tests in 3 regular waves – 5.96s, 6.81s, 7.95s (left to right). Each bin shows the mean power for a gain of 30, 50, 70, 90, 110 and 130 respectively [Courtesy of Mocean Energy, NWEC2 tests].

Once the above has been carried out, one can identify what looks like the Dpto value that maximises the overall power response. This value, and two others either side, are then used to generate RAOs of power [kW/m2] vs period [s].

H.6.3.2 Torque limit

PTO cost scales with torque limit. It is noted that the highest levels of torque occur rarely (i.e. in the lower occurrence, larger seas), so there are diminishing energy captured/cost returns in trying to convert energy from these seas via a higher and higher torque limit. This consideration is especially true if the WEC is used for a minimum continuous power delivery application, and thus limited by (northern hemisphere) summer wave climates where seas tend to be smaller (particularly July).

During the NWEC2 campaign, NWEC1 data was used to assess the above trade-off. Specifically:

> *"Torque records from the NWEC1 model in irregular waves were clipped to a limit before multiplying by the velocity record; it was recognised that this would conservatively estimate the power because it did not and could not take account of the increase in velocity that would result from the torque clip. Nonetheless, this simple exercise revealed that large torque and cost savings were possible. Later numerical studies in a representative wave climate were used to set a range of torque limits to determine the profitable trade-off between the reduction in annual energy production (AEP) and the PTO cost. The present torque limit of 1MNm was decided from this study."*[110]

The torque limit for BST-folding is set to 60kNm. In the experimental tests, it is limited by setting a maximum current limit for the motor.

To check the torque limit indicated by the numerical study, the PTO damping is to be set on its optimal setting to yield highest average power, and three different torque limits are explored in a given irregular sea. It makes sense for this sea to be as close as possible to conditions of the peak occurrence matrix. This is in accordance with the approach undertaken during NWEC2, whose

[110] Extract from a previous Mocean testing campaign report.

results are shown below. The damping was set to 80 (to give highest average power), and the utilised sea was [Te 6.6s, Hs 1.5m][111].

Full scale torque limit	0.5MNm	1.0MNm	1.5MNm
Mean power [kW]	28.3	34.1	33.7
% torque over limit	30.1	3.0	0.1

Table 47. Effect of torque limit on power output in WES IR01, model damping gain 80 [Mocean Energy, NWEC2]

The next step is to plot the numerically obtained curve of power (or fraction of max power) vs torque limit with the experimentally obtained results from whatever chosen sea state. Note that AEP depends on all the weighted sea states, but it is nonetheless possible to obtain some reassurance as to the economic choice of torque limit from this plot – see Figure 254 (i.e. the plotted lines more or less follow one another with the same shape and inflection point). In this case, an 'economic' torque value of 60kNm has been selected, being less than 5% AEP drop from the optimal value of 70kNm.

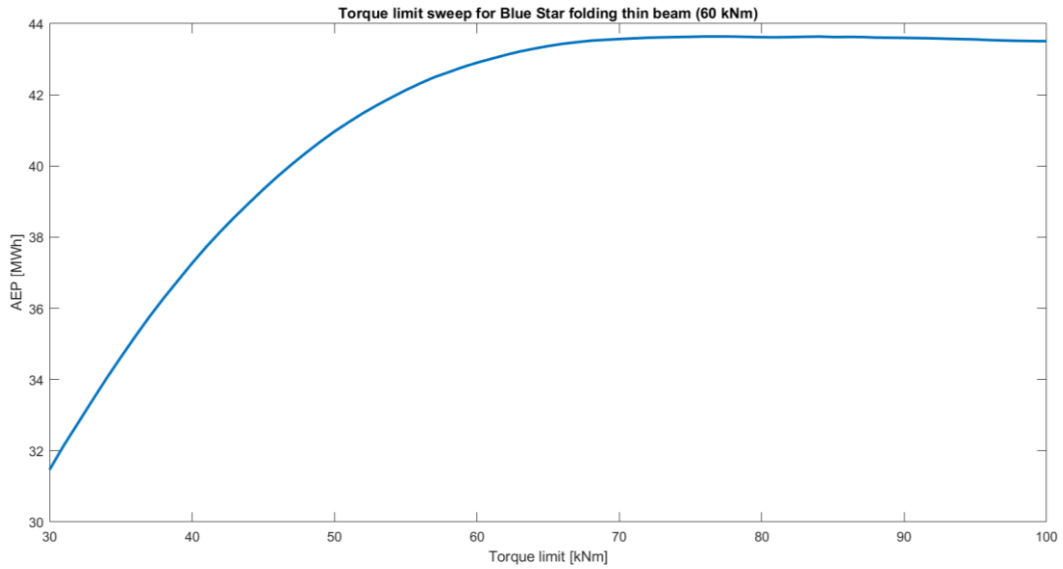

Figure 254 - Variation of predicted AEP with torque limit.

[111] Ideally one would do this in more than one irregular sea.

H.6.3.3 Thermal limits

Consideration needs to be paid to the duration of each irregular test if higher torque limits are utilised. This is because the motor risks cutting out (by manufacturer design) if it reaches its thermal limit during these tests. This is a mechanism commonly employed to protect motors from overheat damage.

For example, in NWEC2 short-crested seas: “The length of the tests meant that the model PTO could not be run at the usual 1MNm limit because the PTO motor exceeds its thermal limit after around 12 minutes in these seas. The torque limit was therefore reduced to 0.75MNm.“[112]

In this set of tests, the desired torque limit is 0.06MNm full scale (0.375Nm at 20th scale), while the continuous motor torque limit is 0.029MNm equivalent, i.e. about 50% of that nominally required. The peak motor torque limit is 0.0974MNm at full scale.

H.6.3.4 Comparing power in short-crested seas

If torque limit is reduced to circumvent thermal limits of the motor (as is likely to be the case), we will need to adjust power prediction in short-crested seas to enable comparison with long-crested seas. We can do so by applying the relationship obtained in Section H.6.3.2. Thus, it is preferable to choose same Te and Hs combinations for short-crested seas as some of the previously run long-crested seas. In practice, the torque limit was not often reached in the seas that were run.

H.7 Moonpooling effects

A few observations are given with respect to fluid interaction at the aft hull gap.

- From RR09 sea onwards, water comes out of hull gap and over the AFT WC
- AR05 – spray through AF hull gap, from the underside of the angles face nearer to the hinge

[112] Ibid. Note that the nominal continuous torque limit for the motor was 0.75MNm equivalent. Peak torque limit was 2.5MNm.

- Similar for AR06, 07 (more spray)
- AR08 – some noticeable overtopping at the FWD WC

Photos of AR07 sea, PTO gain 0, taken on 2021-10-11:

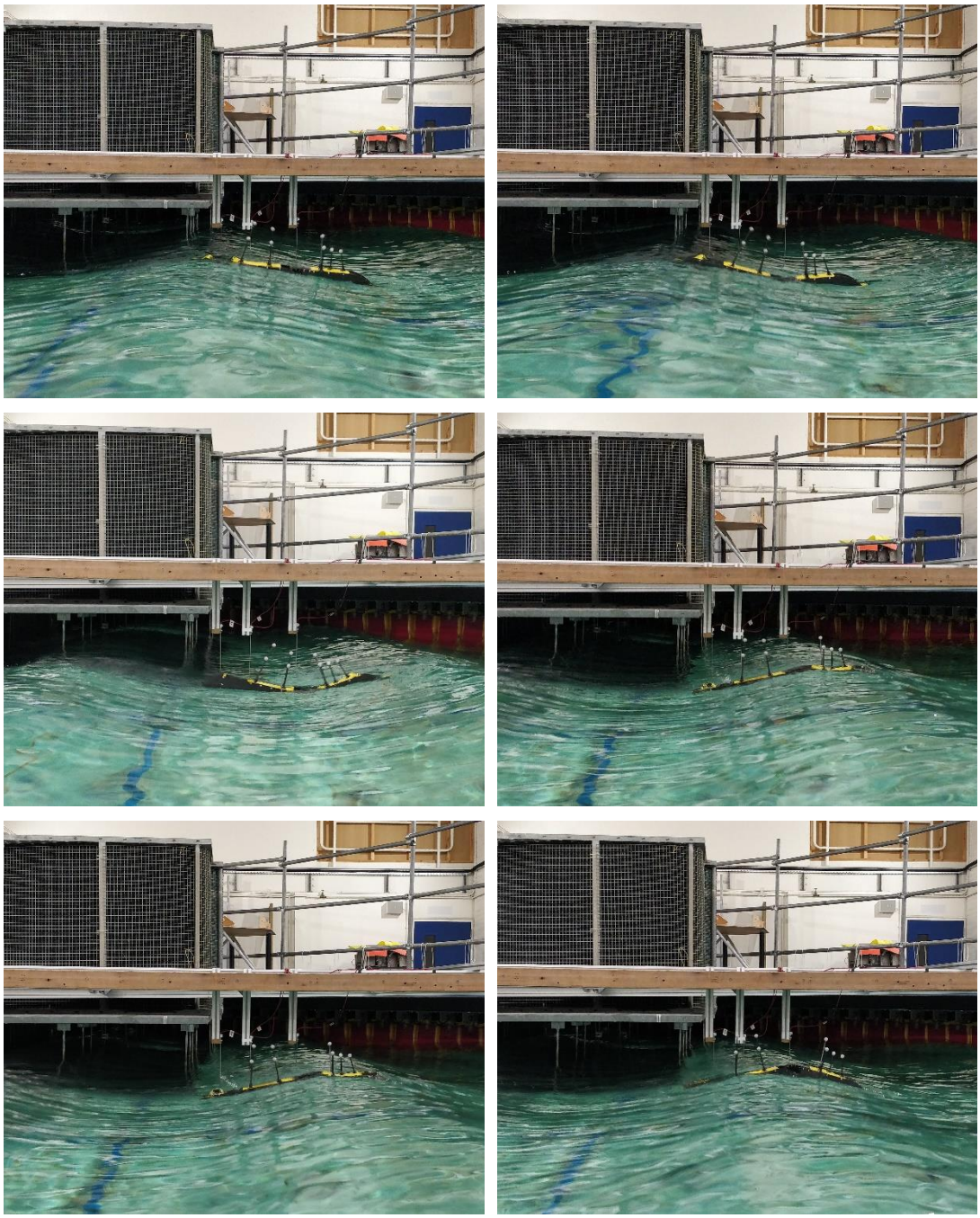

Figure 255 - Screenshot sequences of BST-folding, showing salient aft hull gap behaviour.

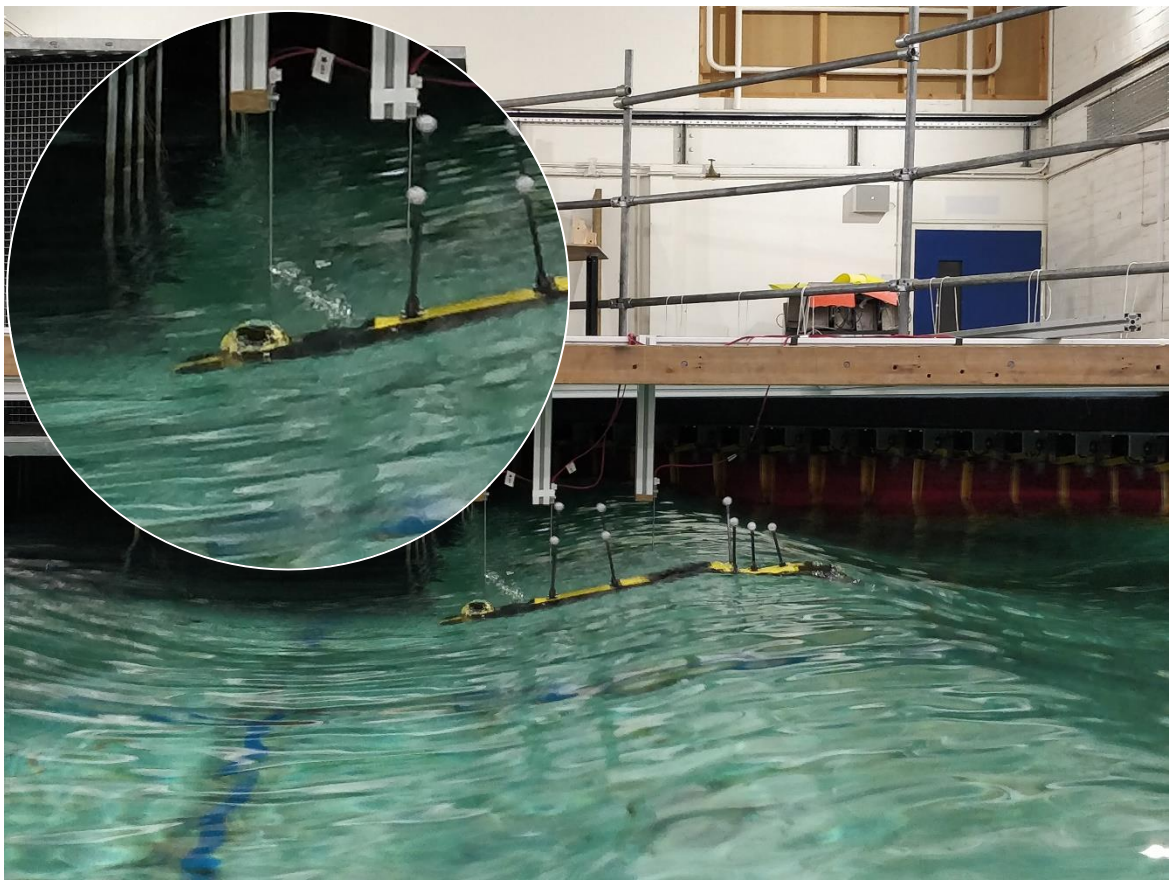

Figure 256 - Showing fluid projectile effects and spray at the gap in aft hull.

H.8 Signal checks

Signal checks are initially carried out to check the consistency between motor controller (AKM) and Qualisys (QTM) obtained measurements.

Figure 257 shows a very close match between AKM controller angular position measurement and QTM Qualisys equivalent. In order to obtain angular velocity signals, the QTM measurement is differentiated, while the AKM controller outputs velocity directly. Figure 258 shows a difference of 0.03 to 0.05deg in peak angular positions measured (QTM measuring greater angles), which can be considered negligible.

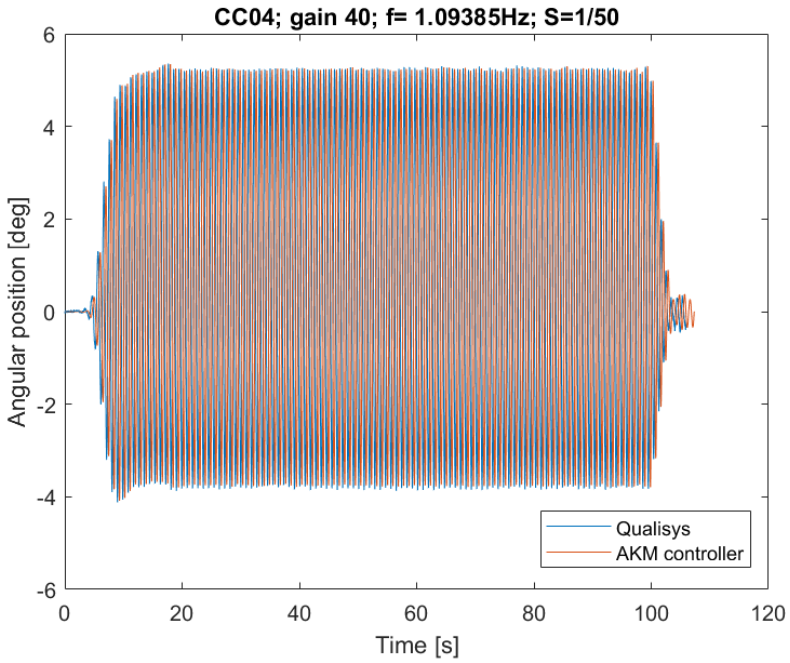

Figure 257 - AKM vs QTM position measurement signal check.

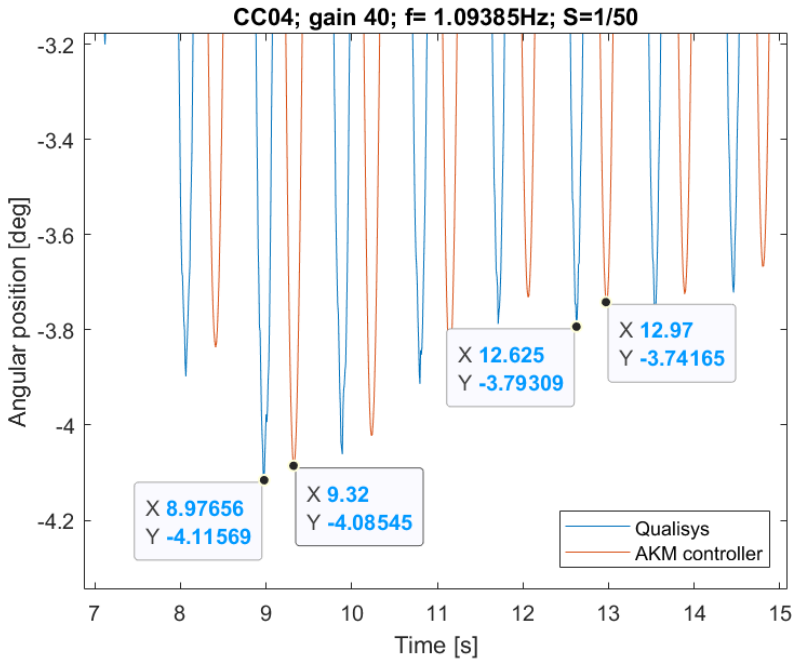

Figure 258 - Showing discrepancy between QTM ad AKM position readings.

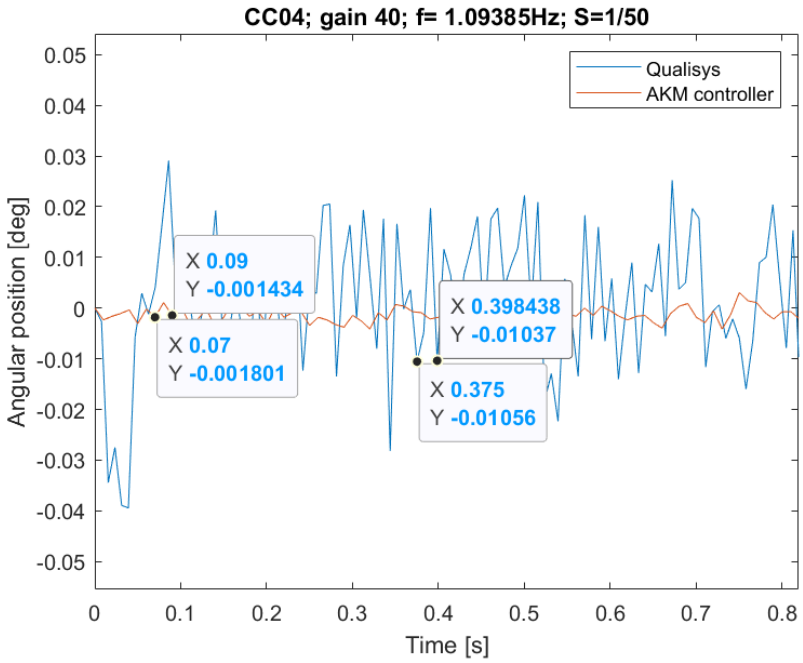

Figure 259 - Showing noise in the QTM signal.

It can also be seen from Figure 259 that the QTM signal is noisier than the AKM signal; this noise can be magnified when differentiated to calculate QTM derived hinge velocity. The noise is at ~42Hz. The AKM position signal has lower magnitude noise at 50Hz. The position signal from QTM is LP filtered at 10Hz before differentiating; the effects are shown in Figure 111, showing a much closer match with the AKM velocity signal than its unfiltered counterpart. It should be noted that the velocity signals from the motor controller are LP filtered at 20Hz before being fed to the feedback loop in the controller that determines the application of the resisting motor torque. As such, a 20Hz LP filtering is also applied to the QTM position signal before computing velocity, resulting in the traces shown in Figure 261.

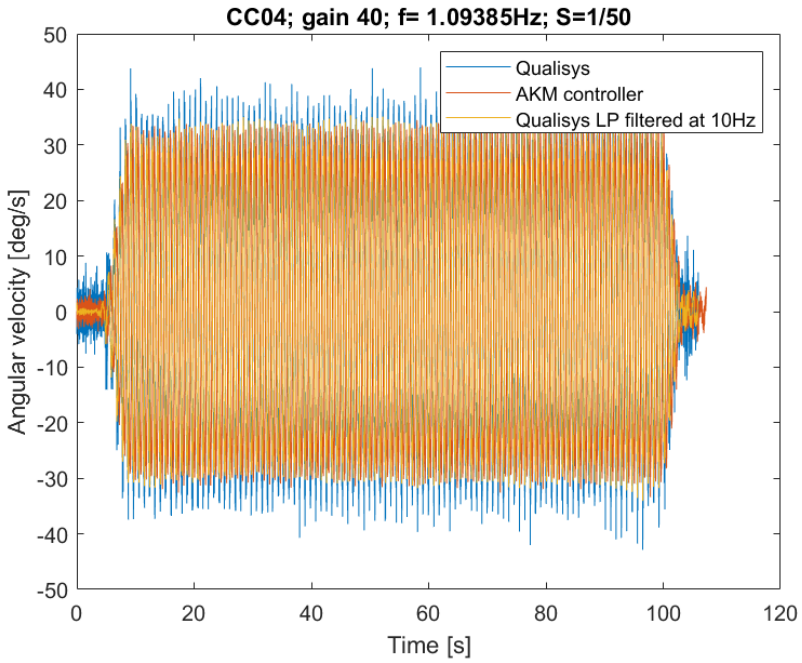

Figure 260 - AKM vs QTM velocity time series check; QTM is LP filtered at 10Hz.

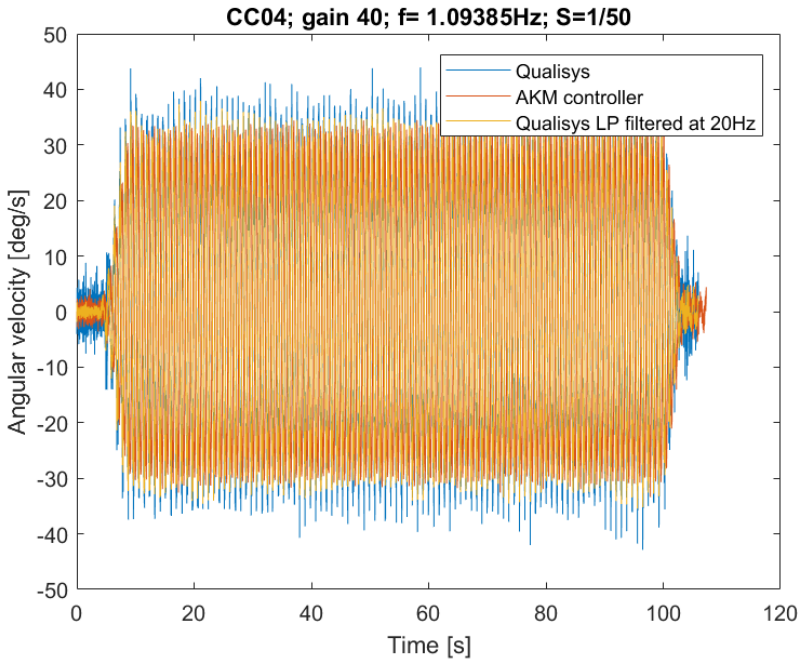

Figure 261 - AKM vs QTM velocity time series check; QTM is LP filtered at 20Hz.

As a final sanity check, the AKM position signal is differentiated to check that the resulting hinge velocity matches that computed by the AKM controller directly (raw). Figure 262 shows excellent agreement. The raw velocity is also integrated to provide an angular position check (top-right).

Based on this preliminary analysis, it is decided to use AKM signals for hinge velocity related calculations, while it is deemed inconsequential to use QTM or AKM signals for position related calculations such as DoF RAOs.

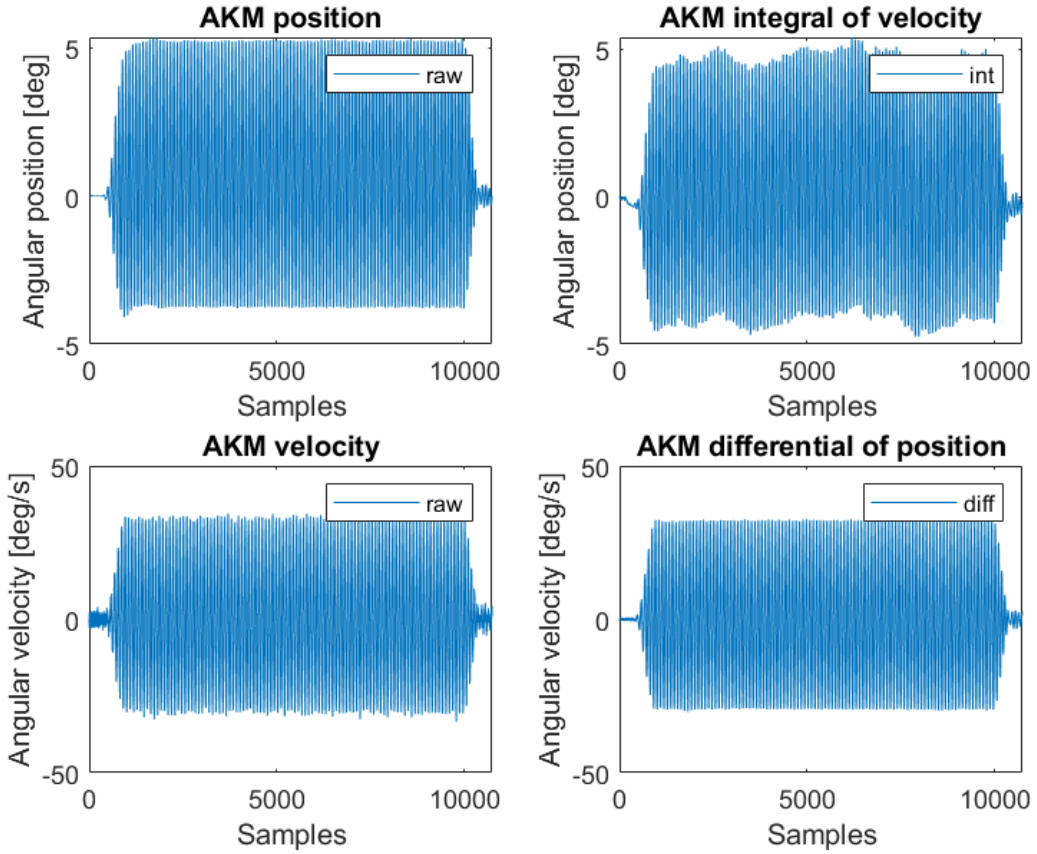

Figure 262 - Manual check of hinge velocity from AKM controller.

H.8.1 Regular waves

The following figures show cropped time series of the hinge flex, for regular wave frequency sweeps at 1/50 and 1/100 steepness. Associated fundamental frequencies extracted via FFTs are also shown. The second order responses at longer periods are visible in flex responses and the multiple fundamental frequency components.

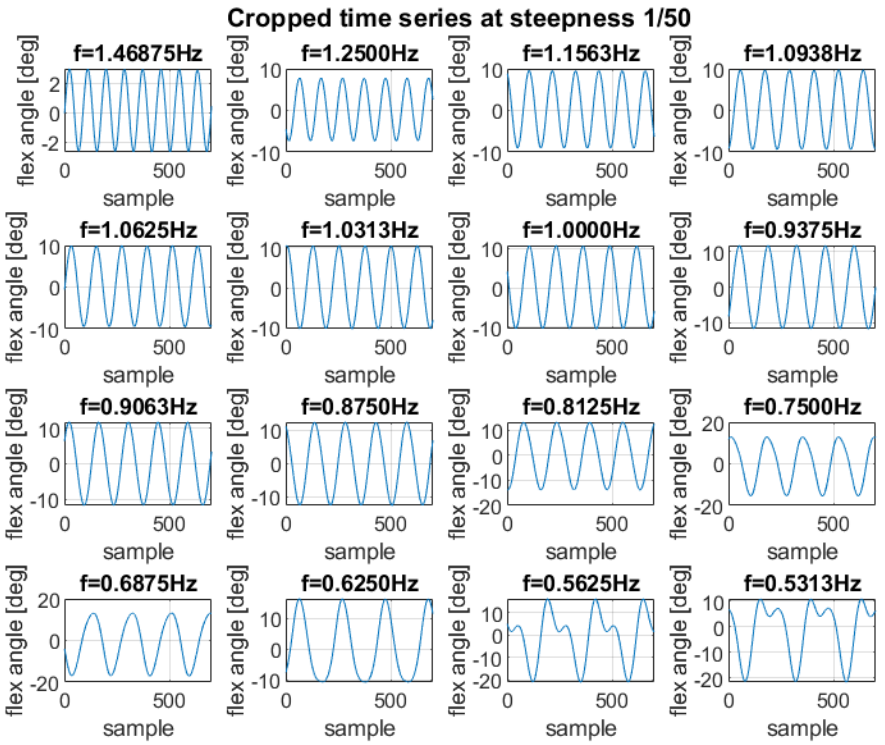

Figure 263 - Cropped time series of hinge flex at regular waves of steepness 1/50.

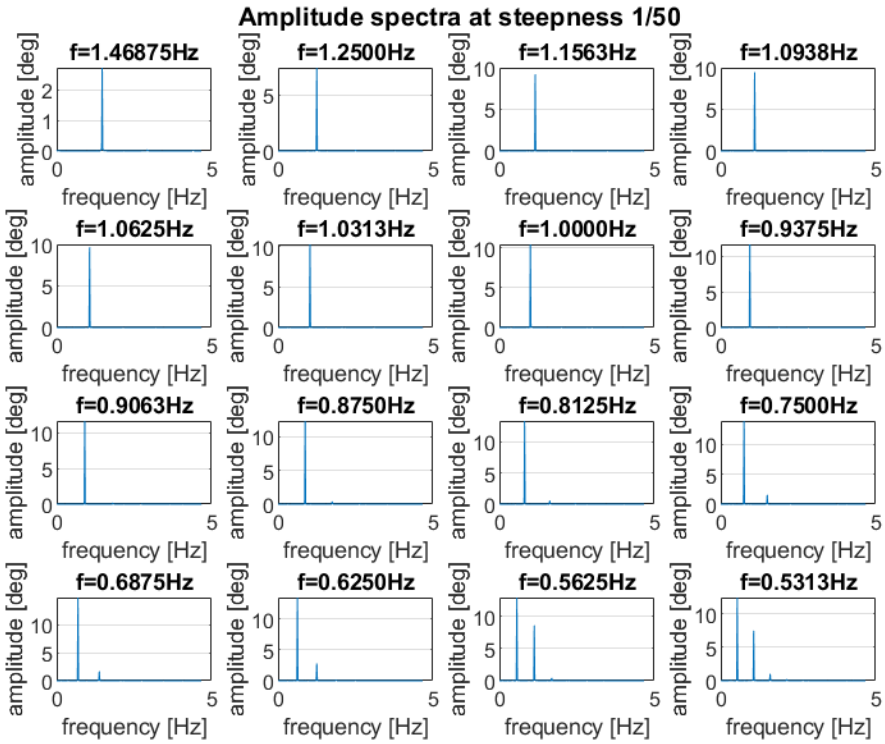

Figure 264 - Fundamental frequencies of hinge flex responses under regular waves of steepness 1/50.

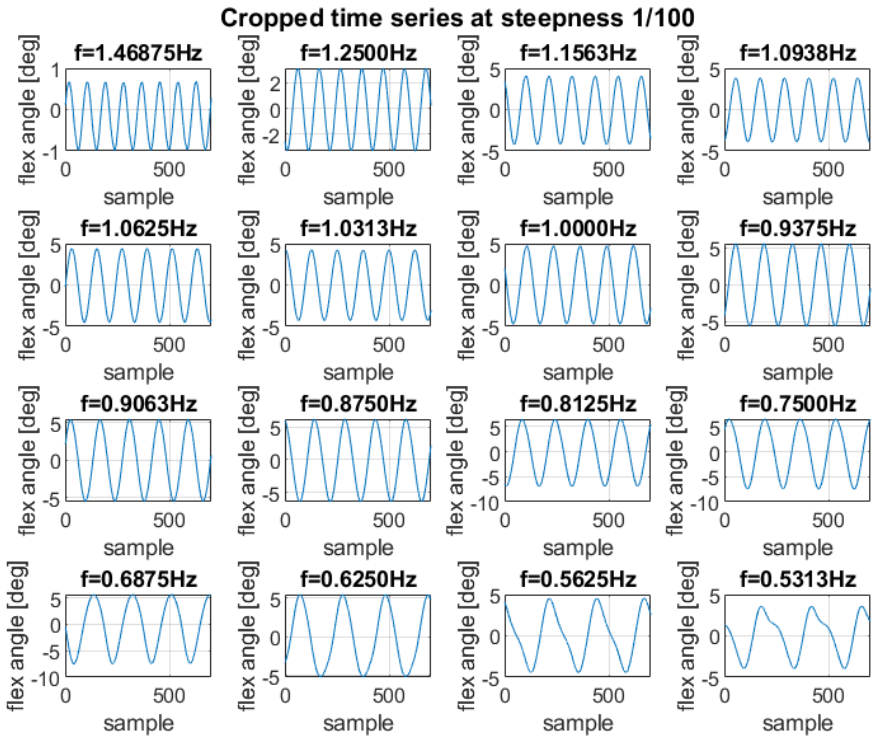

Figure 265 - Cropped time series of hinge flex at regular waves of steepness 1/100.

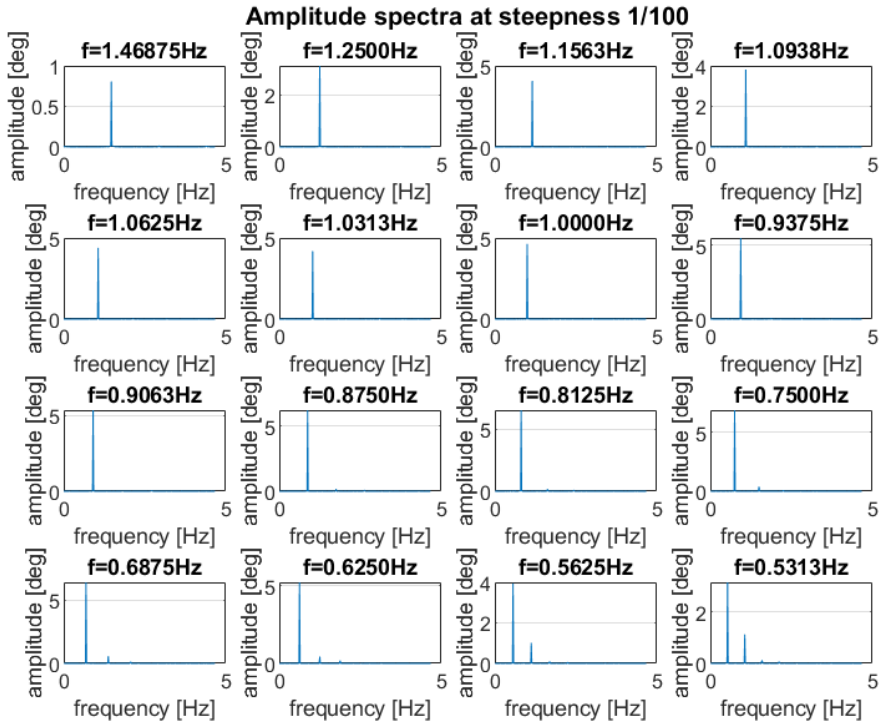

Figure 266 - Fundamental frequencies of hinge flex responses under regular waves of steepness 1/100.

H.9 Optimal PTO damping

Figure 267 shows instantaneous measured power at different PTO damping gain for slack (blue) and taut (red) mooring configurations, at - and either side of - the peak response frequency.

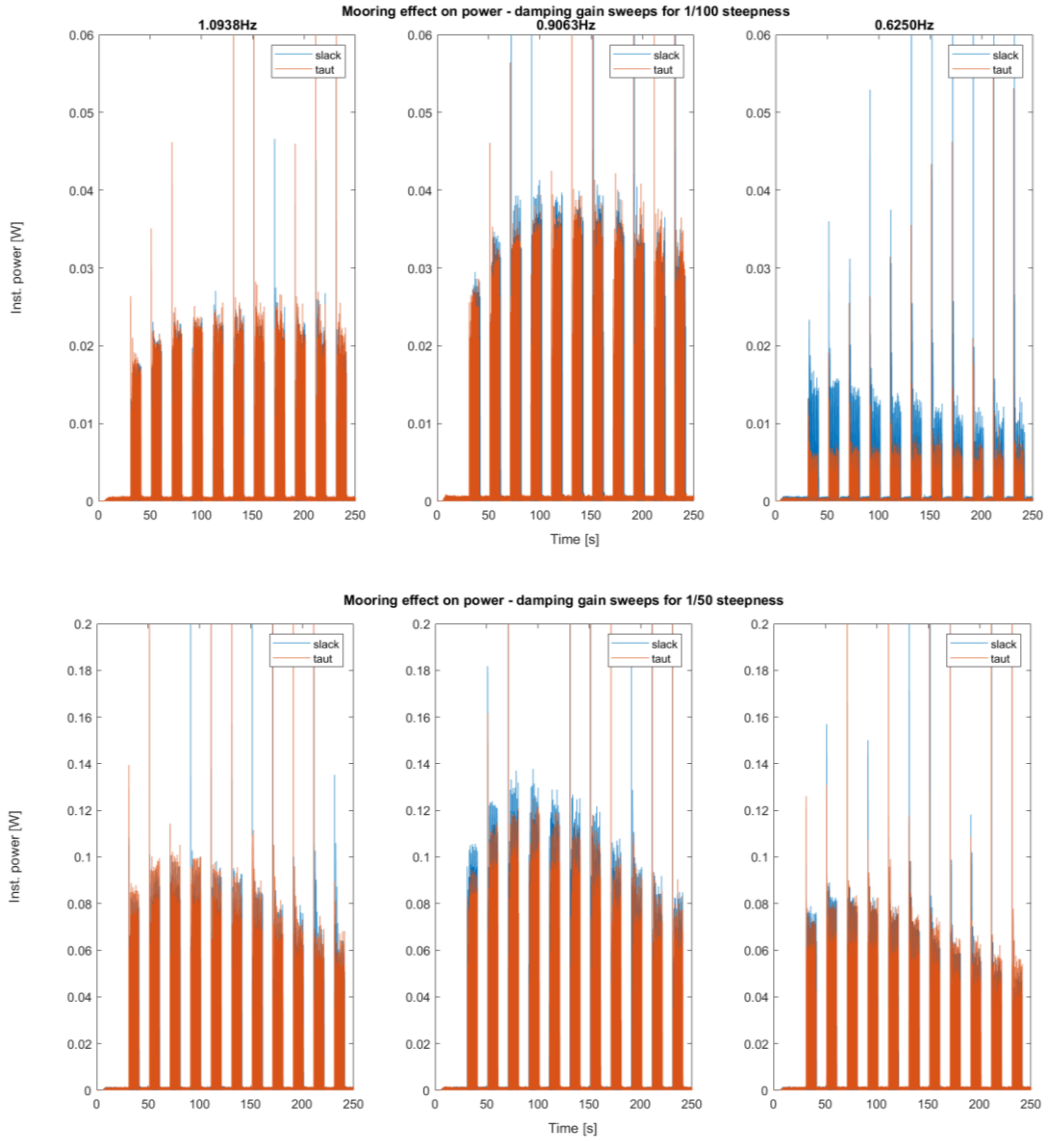

Figure 267 – PTO damping sweeps showing instantaneous demand power for slack and taut moorings (both steepnesses).

Observing Figure 268, no reading is available for RR09 slack. The top row is obtained with 1/100 steepness, while the others with 1/50 wave steepness, hence the higher mean power values.

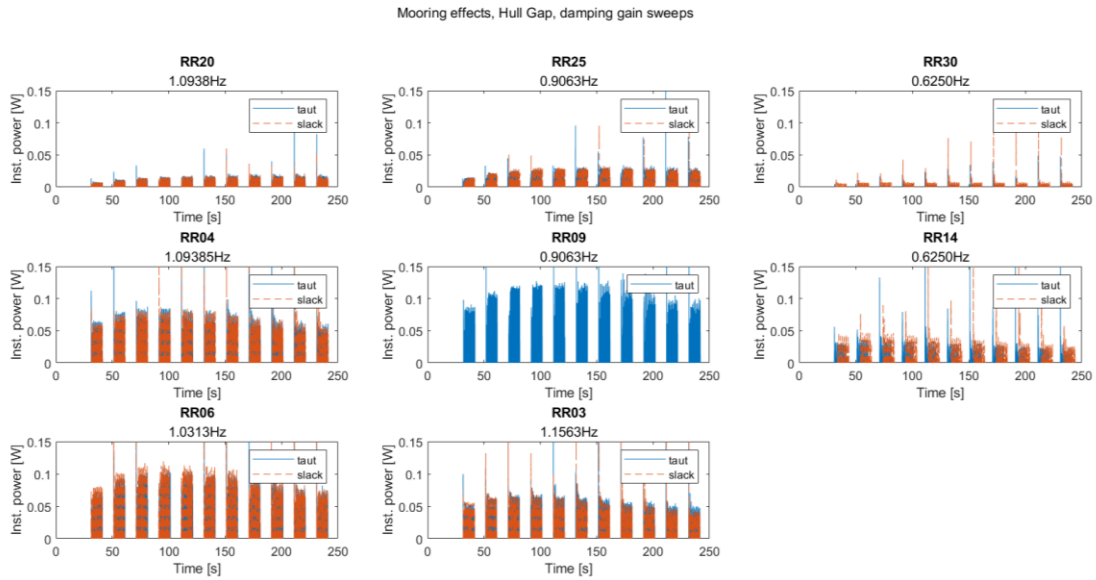

Figure 268 - Mooring effect on instantaneous mechanical power.

Demand torque for each PTO damping gain sweep is plotted in Figure 269, showing that the scaled limit on the demand torque signal (0.375Nm) is never reached, even for the 1/50 steepness waves.

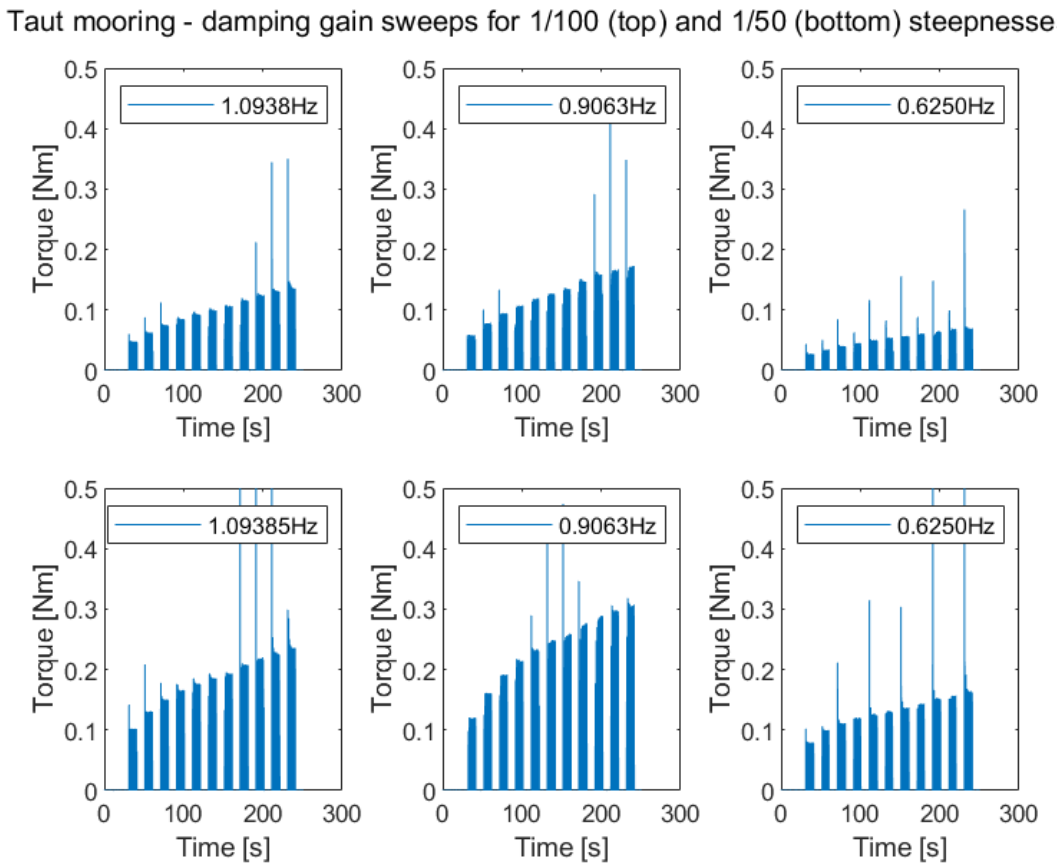

Figure 269 - Demand torques for PTO gain sweeps with taut mooring.

H.10 Capture Width

For the calculation of capture width (CW) and capture width ratio (CWR), we utilise the following approach, as per the method outlined in (Ohana *et al.*, 2021):

$$CW = \frac{P_{mean,absorbed}}{P_{wave}}$$

The mean mechanical power captured by the WEC is defined as:

$$P_{mean,absorbed} = \frac{1}{T_{analysis}} \int_0^{T_{analysis}} \tau \dot{\theta}\, dt$$

Where T_{period} is the analysis period. The power per unit crest length of a regular wave is given by:

$$P_{wave} = \frac{1}{2}\rho g a^2 * \frac{1}{2}\frac{\omega}{k}\left(1 + \frac{2kh}{\sinh 2kh}\right)$$

Capture width ratio (CWR), the non-dimensional equivalent, is defined as CW/r_0, where r_0 is the radius of a hemisphere with same volume as the WEC's wetted volume, V_s.

$$r_0 = \sqrt[3]{\frac{V_s}{\frac{2}{3}\pi}}$$

In accordance with Mocean's historical practice, CWR is plotted against non-dimensional wavelength, which is defined as:

$$ND\ l = \frac{2\pi}{kr_0}$$

H.11 Power capture checks

Power response comparisons are given below as reference.

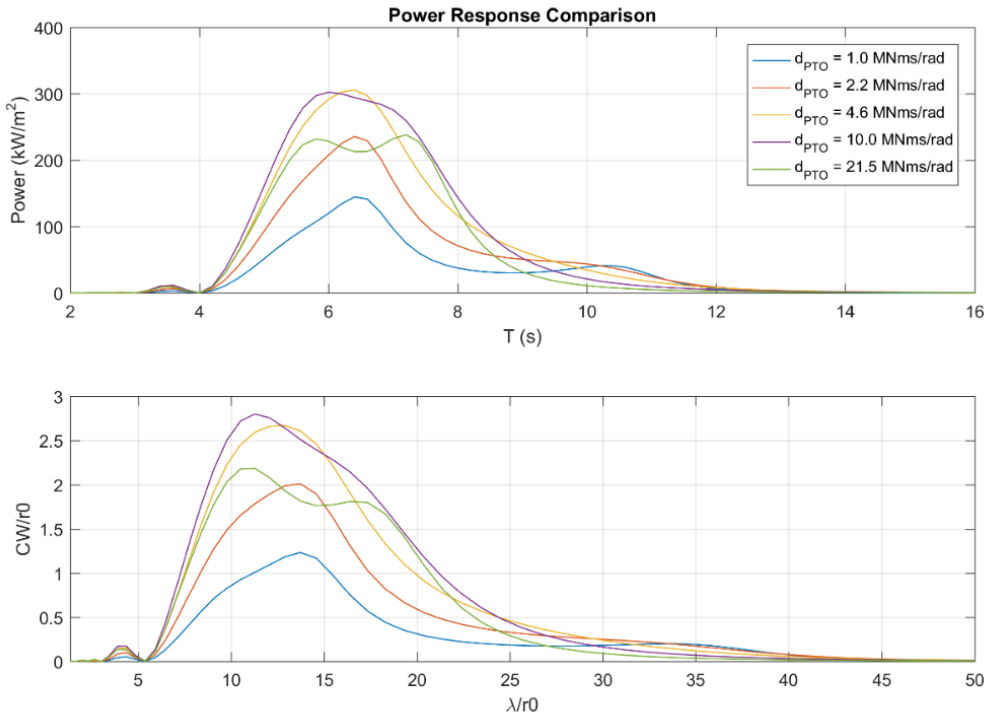

Figure 270 - NWEC2 numerically predicted CWR plot at different PTO gain values.

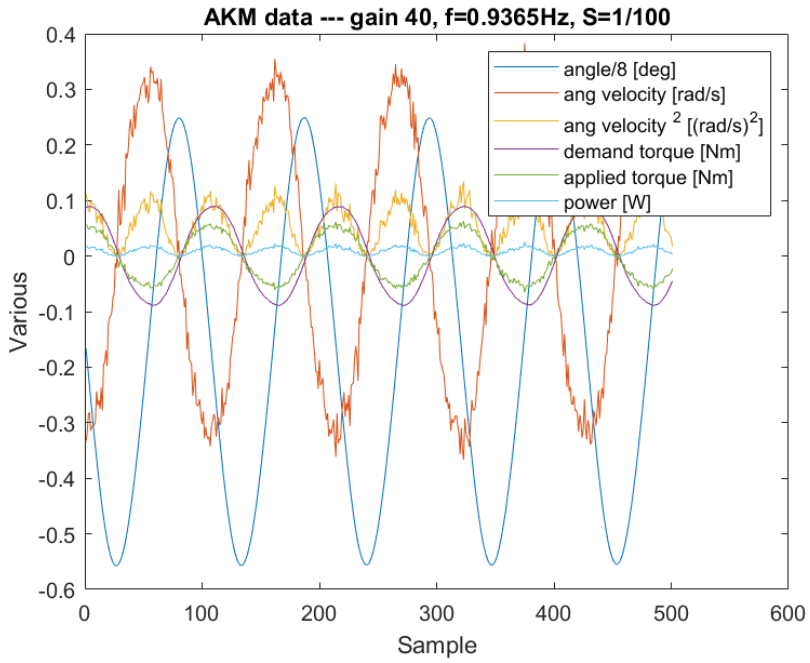

Figure 271 - Checking phase of various signals.

Figure 271 shows sensible phasing of signals. Power check is the calculated one with the calibrated torque constant and the current, and should be equal to the demand power, as it does.

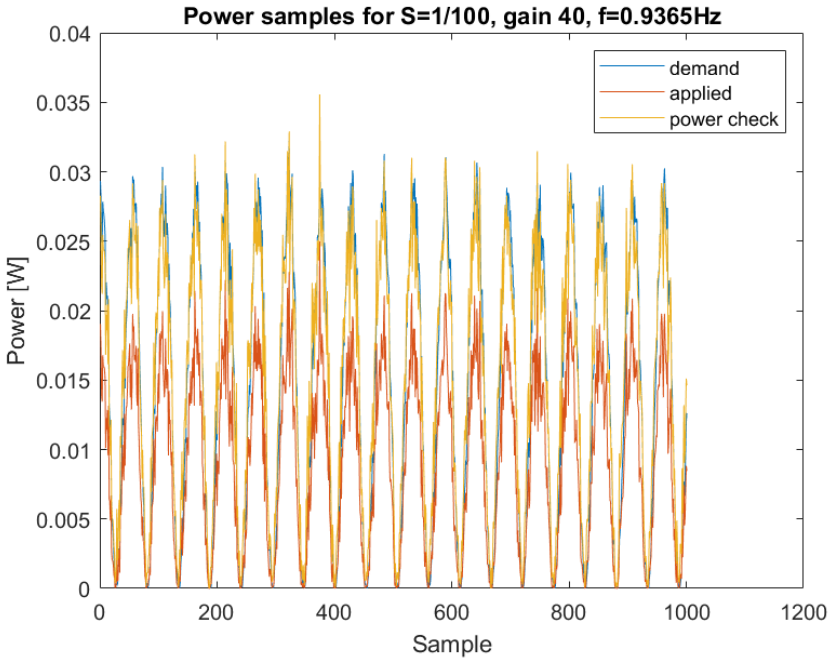

Figure 272 - Power check for demand and applied torque signals.

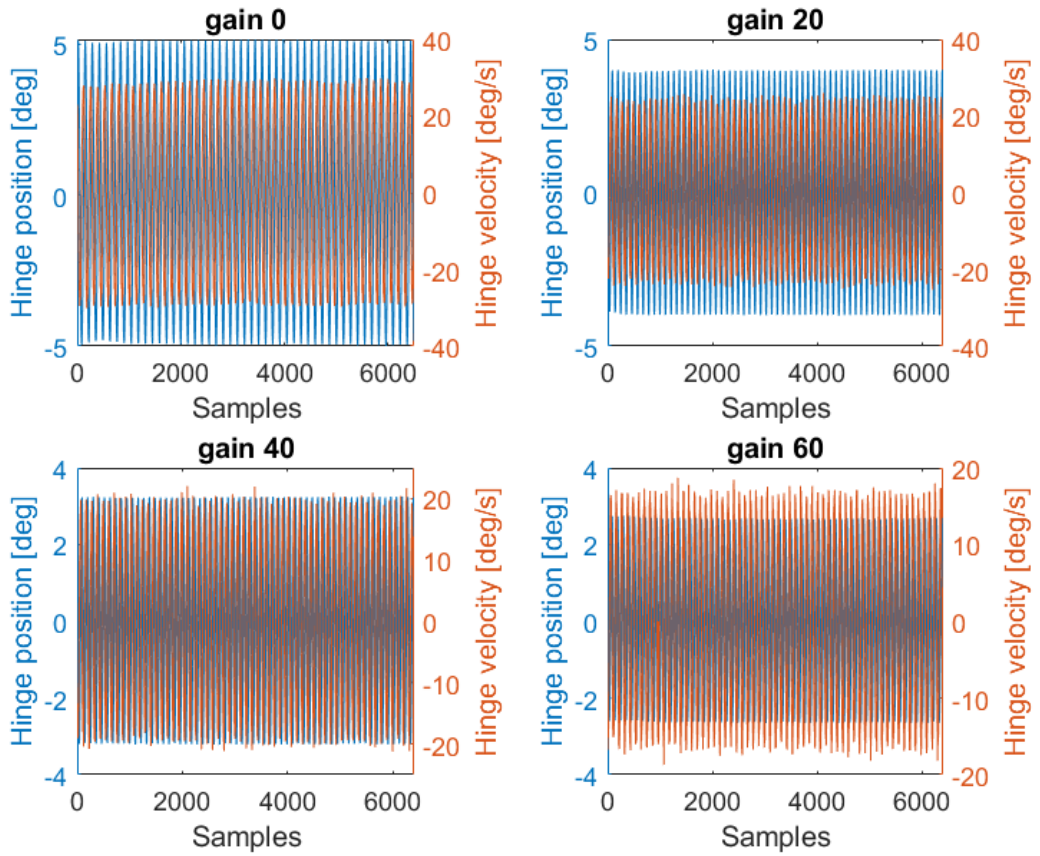

Figure 273 – Experimental hinge position and velocity time series, for S=1/100, f=0.9375Hz.

Next, the numerically predicted hinge angular position and velocity signals are compared, with and without accounting for static friction effects. Frequency is 0.9375Hz (model scale) and S=1/100.

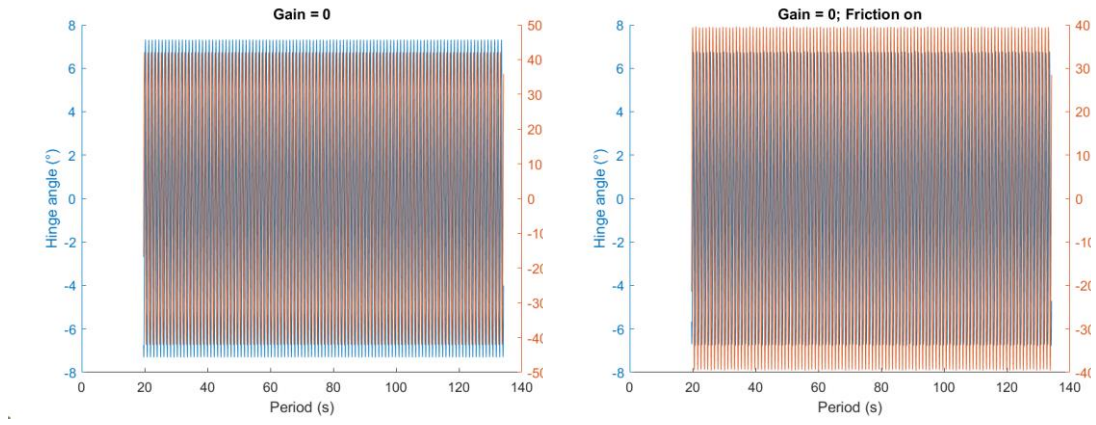

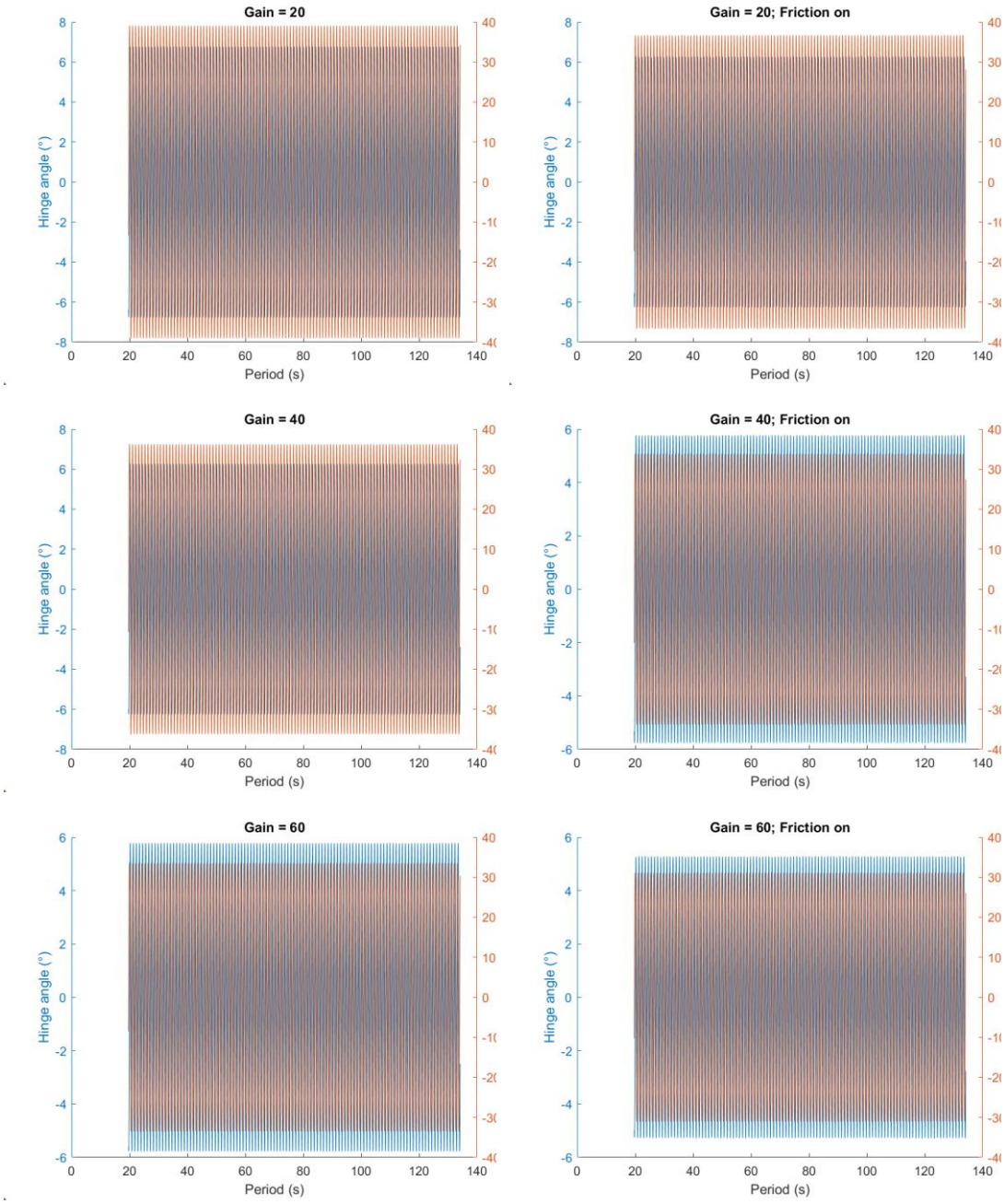

Figure 274 - Matrix showing numerical predictions of hinge angular position and velocity without (left) and with (right) static friction accounted for.

Several more plots are provided for reference purposes.

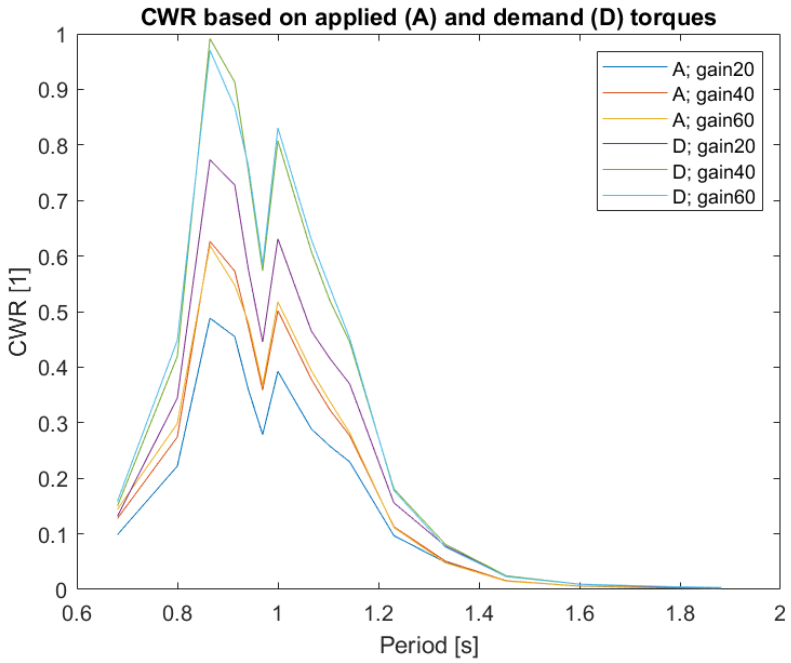

Figure 275 - Comparing CWR plots obtained via demand and applied torques.

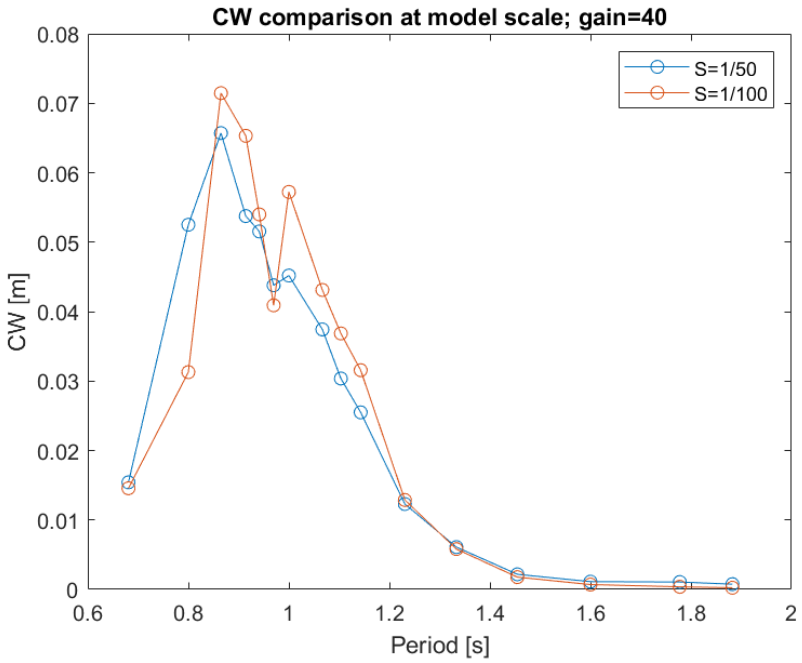

Figure 276 - Comparing CW at model scale, for different wave steepness values.

H.12 Gap vs No Gap

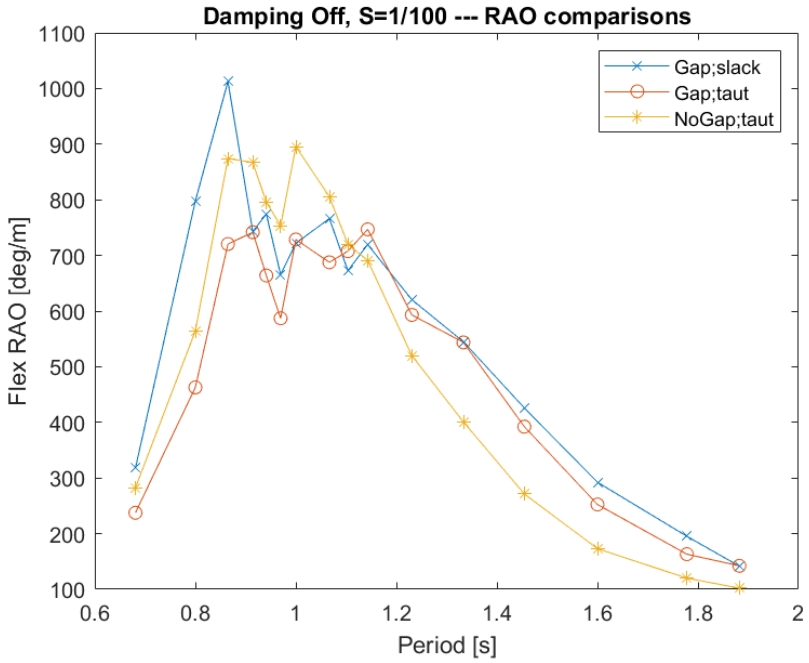

Figure 277 - Gap and NoGap flex RAO responses obtained with slack and taut mooring set-ups, regular wave frequency sweep at constant demand steepness 1/100.

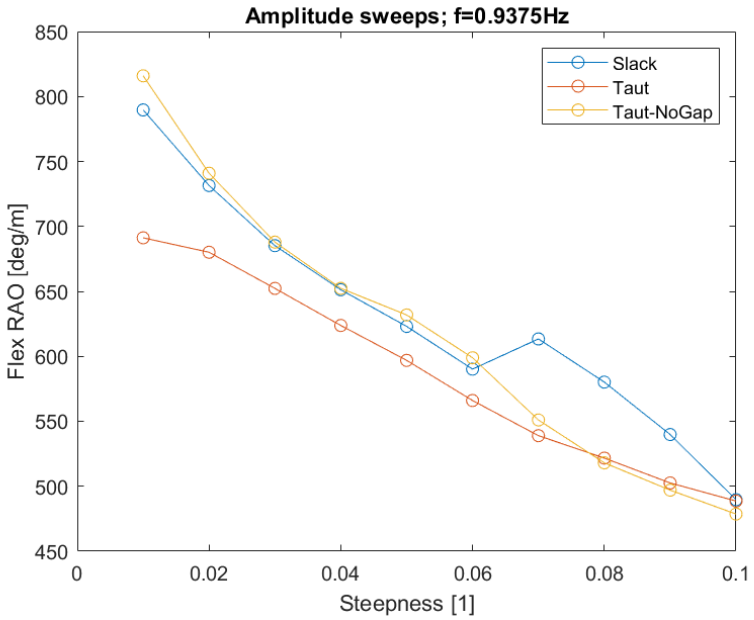

Figure 278 - Gap and NoGap flex RAO responses for regular wave amplitude sweep.

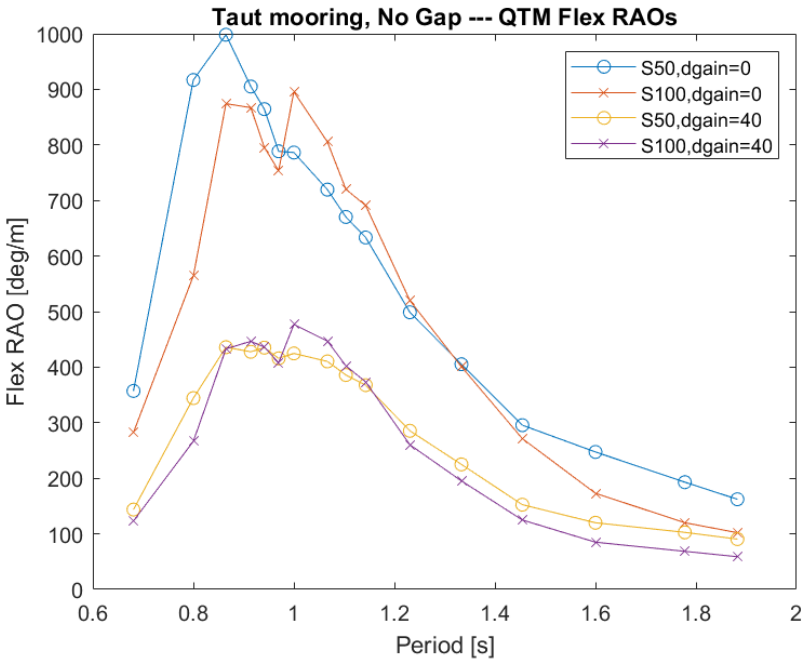

Figure 279 - NoGap flex RAOs at different steepness and PTO gain.

H.13 Effect of torque limit on power capture

First, plots to check whether torque limit boundaries for regular wave frequency sweeps have been surpassed or not; PTO gains 20, 40, 60. NB: applied signal = demand torque – static friction torque losses. The torque limit would affect the demand torque. This limit is only just surpassed around the peak response frequency with gain 40 and wave steepness 1/50. It is likely that it would be reached at the same instances with PTO gain = 60.

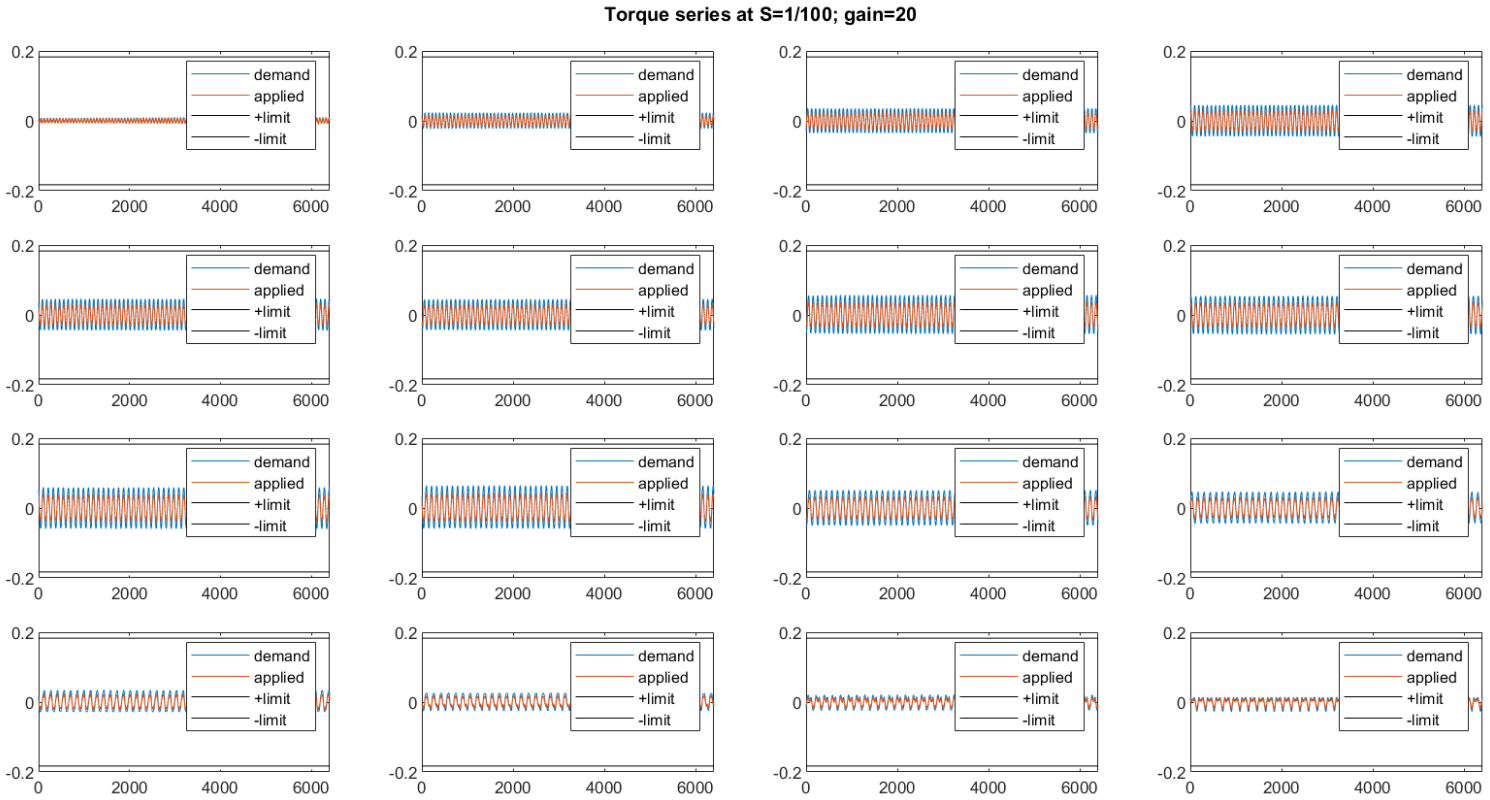

Figure 280 - Demand and applied torques, S=1/100, PTO gain=20 (regular wave frequency sweep).

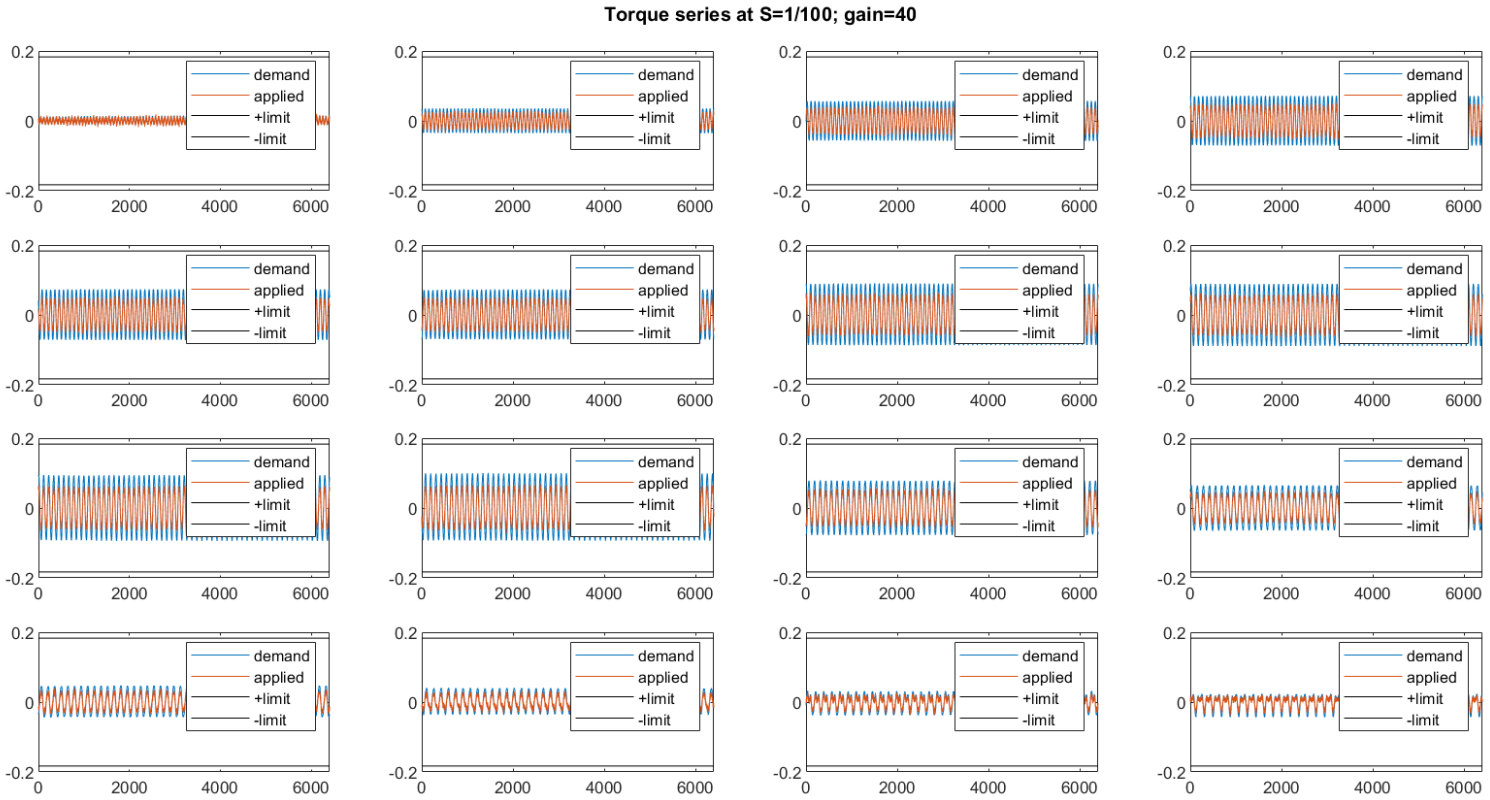

Figure 281 - Demand and applied torques, S=1/100, PTO gain=40 (regular wave frequency sweep).

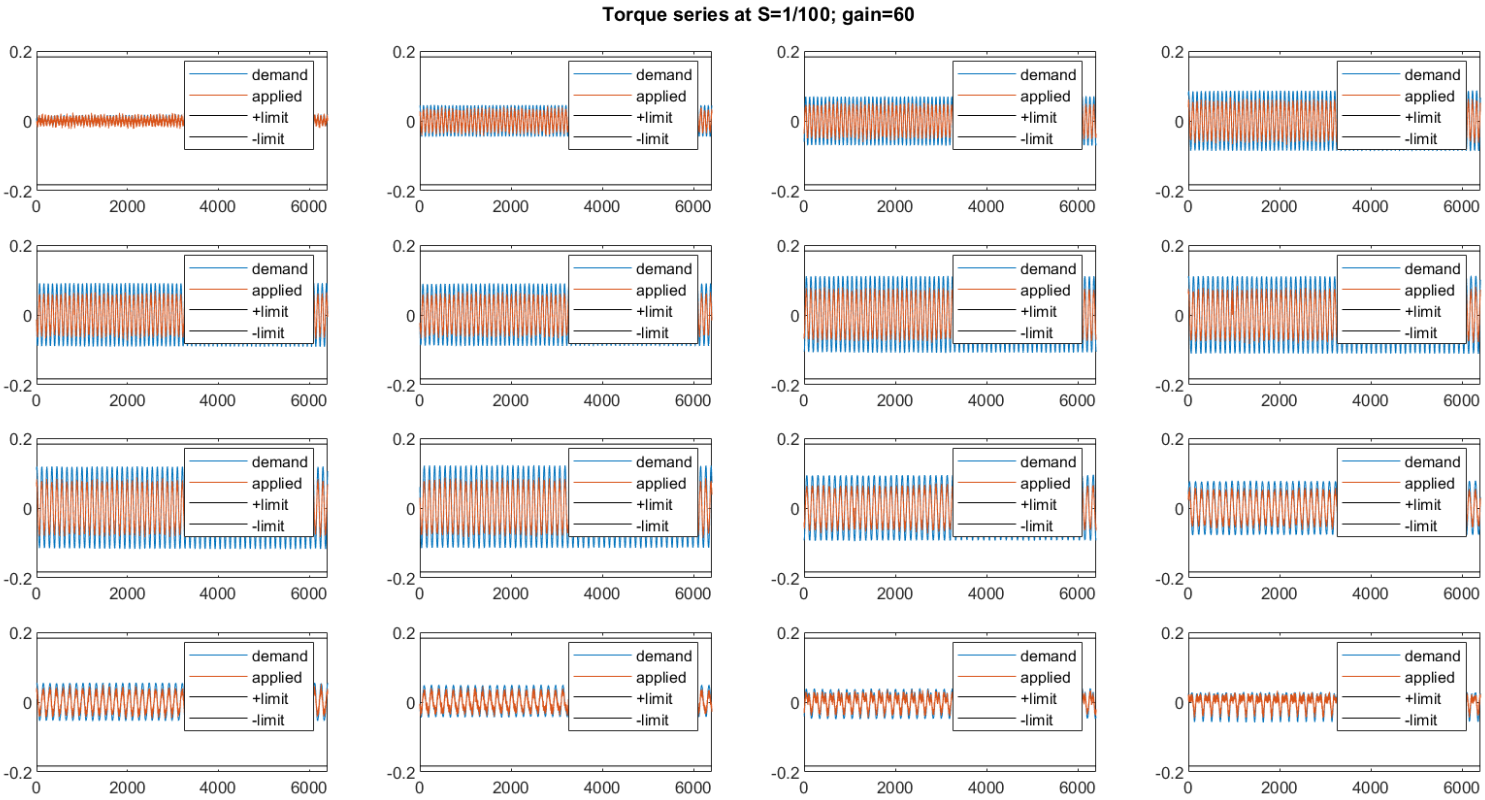

Figure 282 - Demand and applied torques, S=1/100, PTO gain=60 (regular wave frequency sweep).

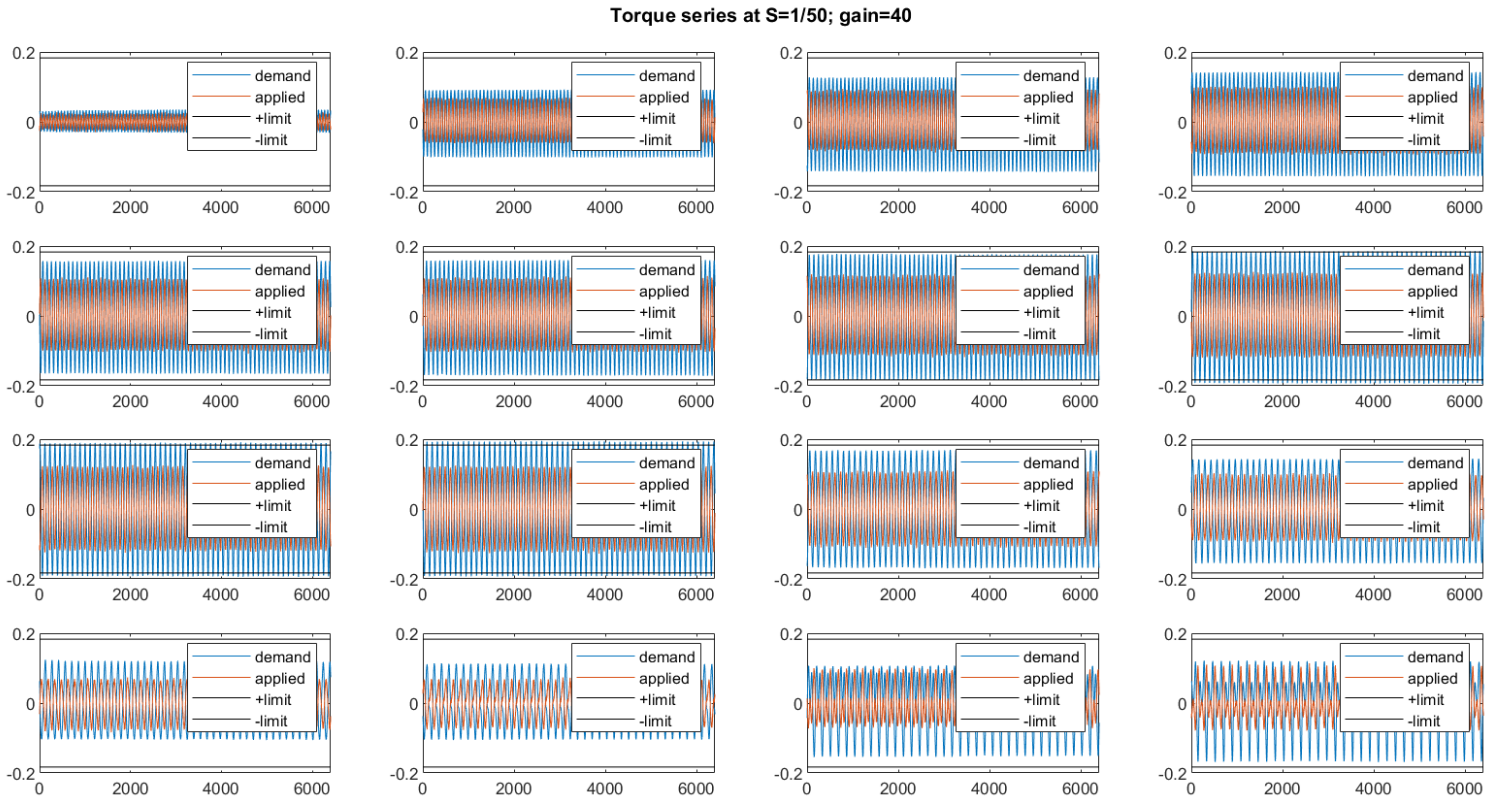

Figure 283 - Demand and applied torques, S=1/50, PTO gain=40 (regular wave frequency sweep).

Next, the effect of torque limit on mean power capture is investigated from irregular wave runs. A PTO gain of 40 is used unless otherwise specified.

IRX01 sea is the most frequently occurring sea in the occurrence matrix, while IRX03 sea is close to ‘hot spot’ of the energy matrix.

The data is actually not very representative of AEP dropping with Tlim as predicted numerically, because the higher end seas were not executable with Curved Tank and this model scale.

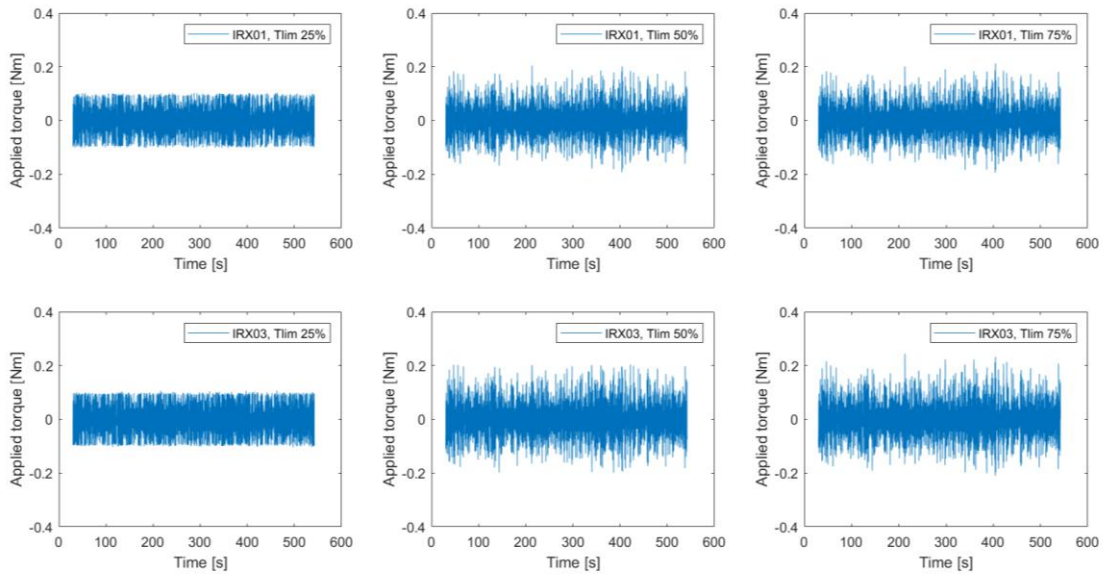

Figure 284 - IRLx runs with varying torque limits applied.

Figure 284 and Figure 285 are obtained with a taut mooring setup. For IRX01 power drops by roughly 0.022-0.0195/0.022 = 11.4%; this is less than predicted numerically for the AEP, but not a like-for-like comparison because this is only one sea.

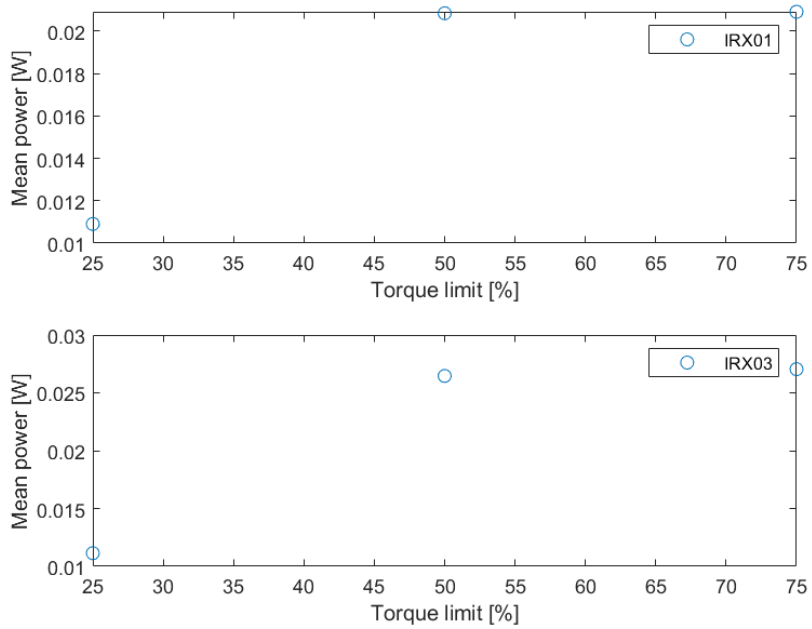

Figure 285 - Effect of torque limit on mean power measured in IRX01 and iRX03 seas.

A similar plot for IRX01 with slack mooring and a gain of 60 is shown in Figure 286. This time torque limits of 100% torque, 75% and 50% are explored. Note, 100% means nominal torque limit is applied; 50% means that a lower torque limit is applied.

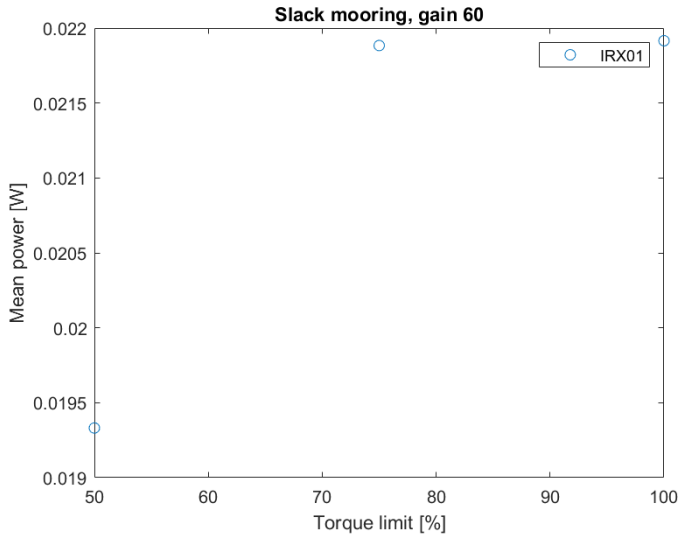

Figure 286 - Torque limit effects on mean power with PTO gain 60 (slack mooring).

H.13 40th scale model

The following plots show data collected from Qualisys measurements of the 40th scale passive model of BST-folding, as support the related plots shown in the body of Chapter 8.

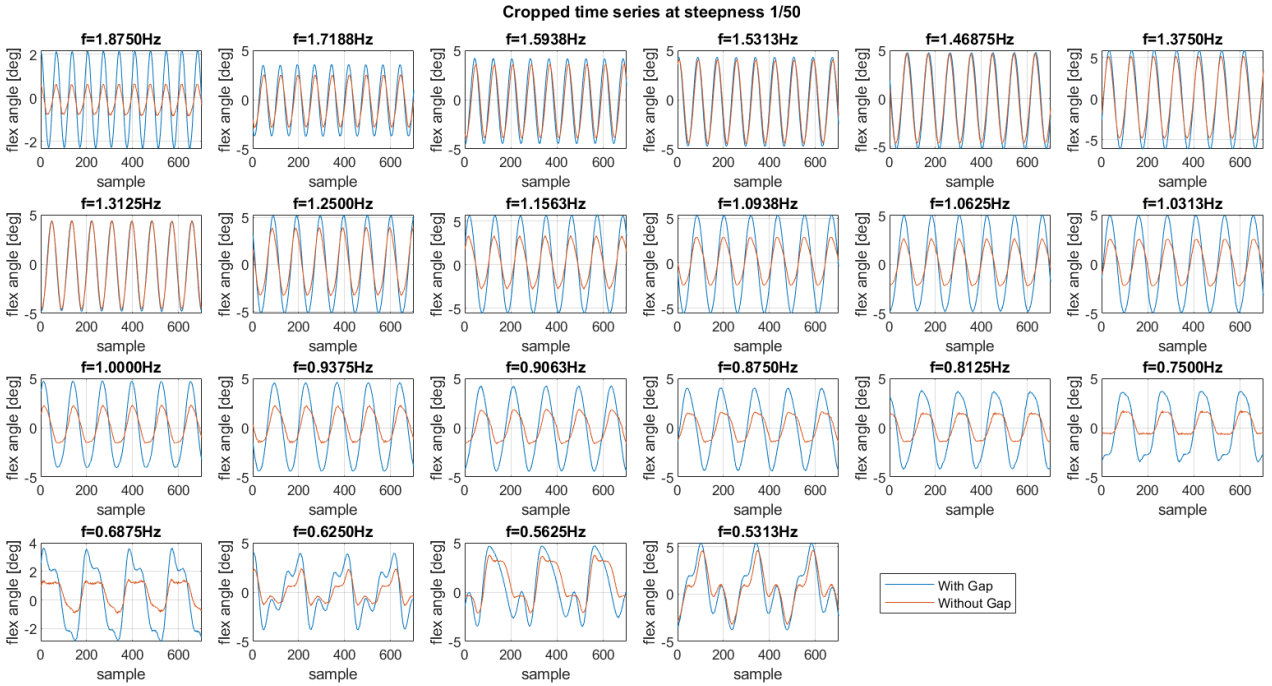

Figure 287 - Cropped time series of 40th scale flex for regular wave sweep at 1/50 steepness.

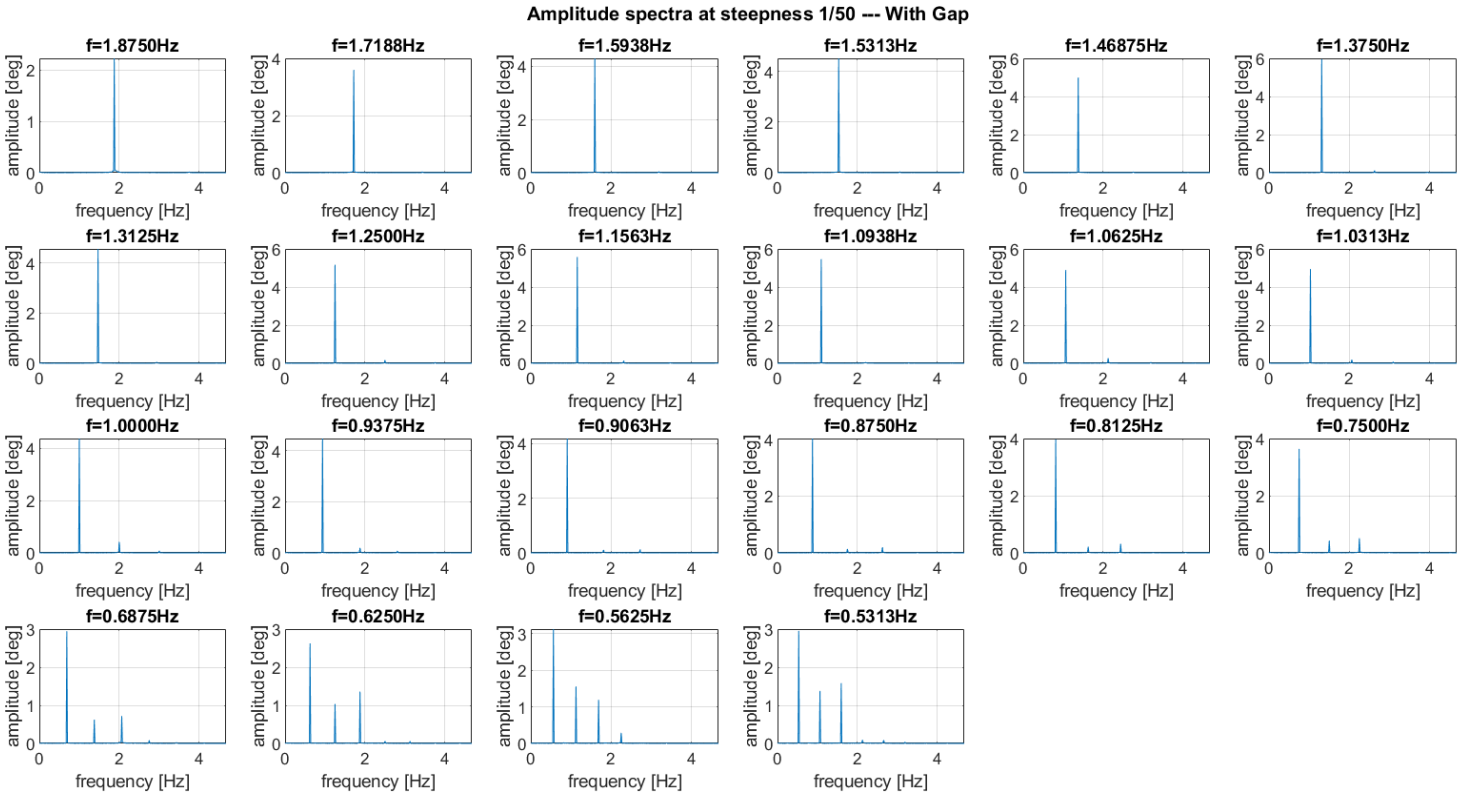

Figure 288 - Fundamental frequency components for regular wave frequency sweep at 1/50 steepness (Gap).

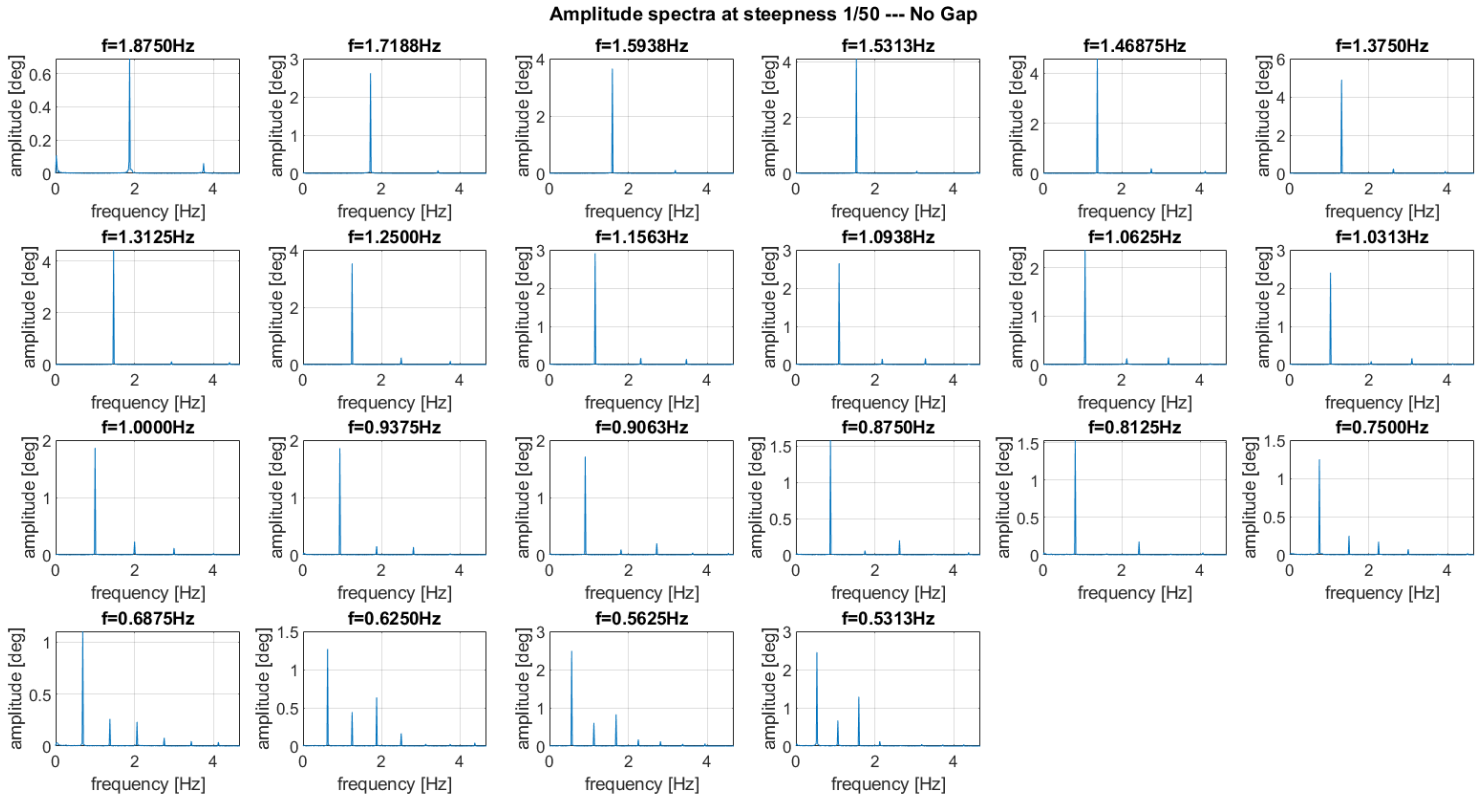

Figure 289 - Fundamental frequency components for regular wave frequency sweep at 1/50 steepness (NoGap).

Appendix I – Chapter 9

I.1 Metrics plots

The below plots support the device comparison metrics outlined in Chapter 9.

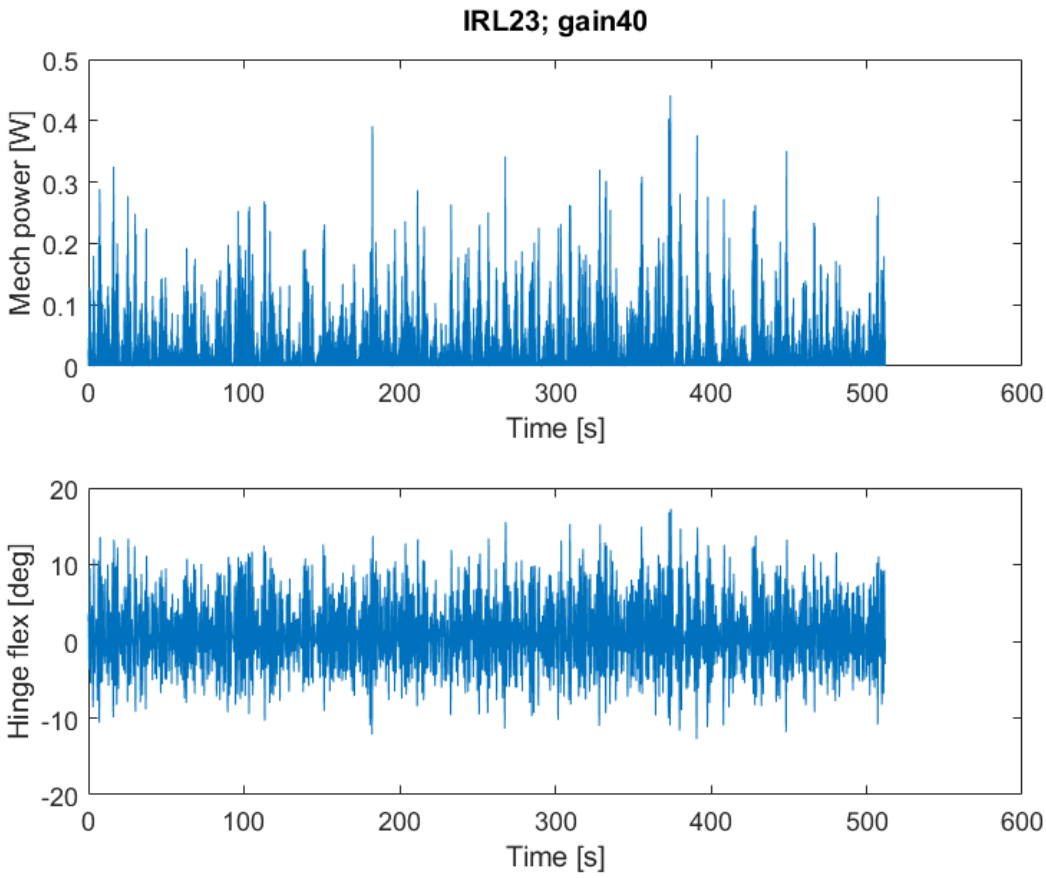

Figure 290 - Showing mechanical power at hinge and hinge flex at model scale for IRL23 run.

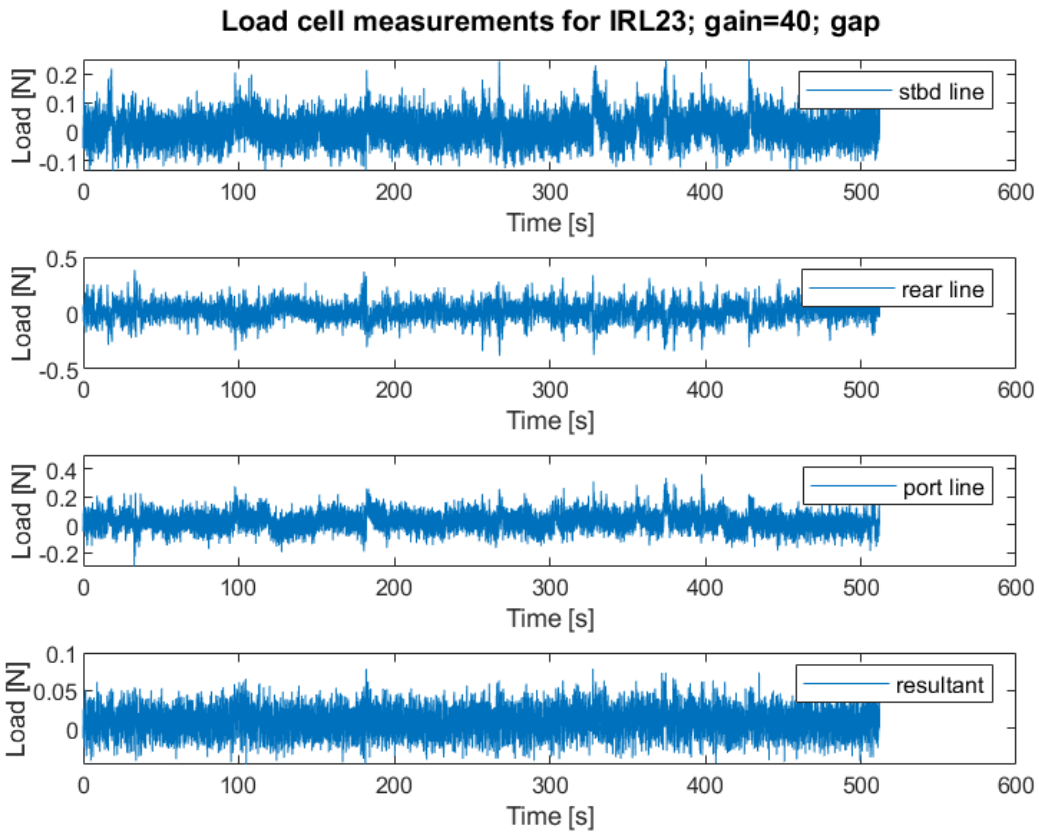

Figure 291 - Showing mooring line tensions (starboard, rear, portside, resultant) during IRL23 run.

I.2 Survival tests Plymouth

In particular, tests involved a ‘Lazy-S’ single mooring line arrangement that combined umbilical and mooring in one subsystem. Snatch loads were simulated, which occurred when the mooring line became taut. The model was the passive version of BST-folding, in accordance with the PTO-off survival strategy.

Figure 292 - BST-folding active, at COAST Lab.

Figure 293 - Screenshot of underwater video showing 'lazy S' mooring.

I.2.1 Lazy ‘S’ mooring

A ‘lazy-S’ shape mooring line was made up using scaled properties from a design provided by a mooring subcontractor, Leask Marine. The synthetic line is shrouded with a transparent section of Silicone tube, which represents the additional bend stiffness of the upper cable synthetic bend stiffener to protect the umbilical.

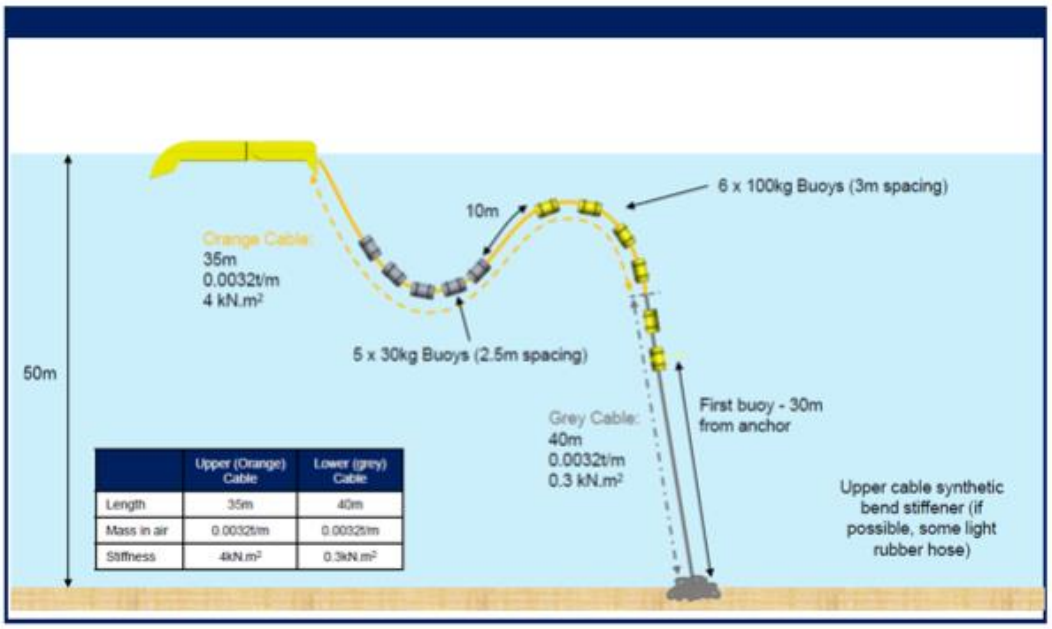

Figure 294 - Design basis for single line mooring set-up (waves travelling right to left).

Tube samples were approximated to behave like a built-in beam subject to a mid-point load, in order to estimate bending stiffness (EI) values.

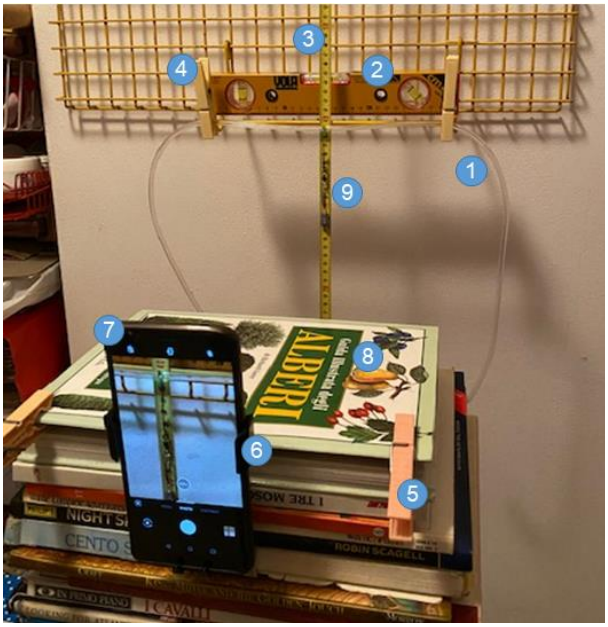

Key:

1. Tube sample
2. Level gauge
3. Tape measure
4. Clip to secure tube end(s)
5. Clip to adjust phone angle
6. Phone support
7. Phone for image capture
8. Make-shift tripod
9. Loading hook subassembly to apply deflection

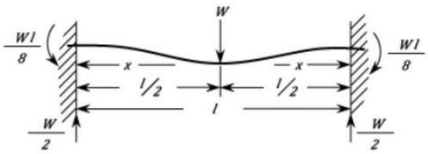

Figure 295 - Showing test set-up.

A selection of different plastic tubings was tested for bend stiffness in order to select the most appropriate type. The measured average bend stiffness across the load range of the tubing used was estimated as 0.00365 Nm^2, with a dry mass/length of 15.21 g/m.

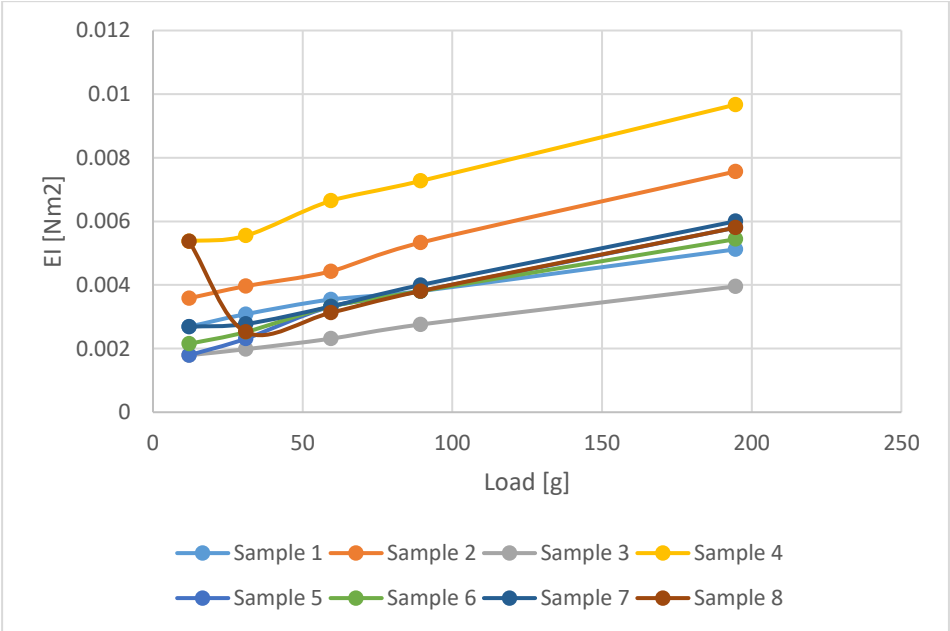

Figure 296 - Showing estimated measured EI values across loading range, assuming built-in ends case.

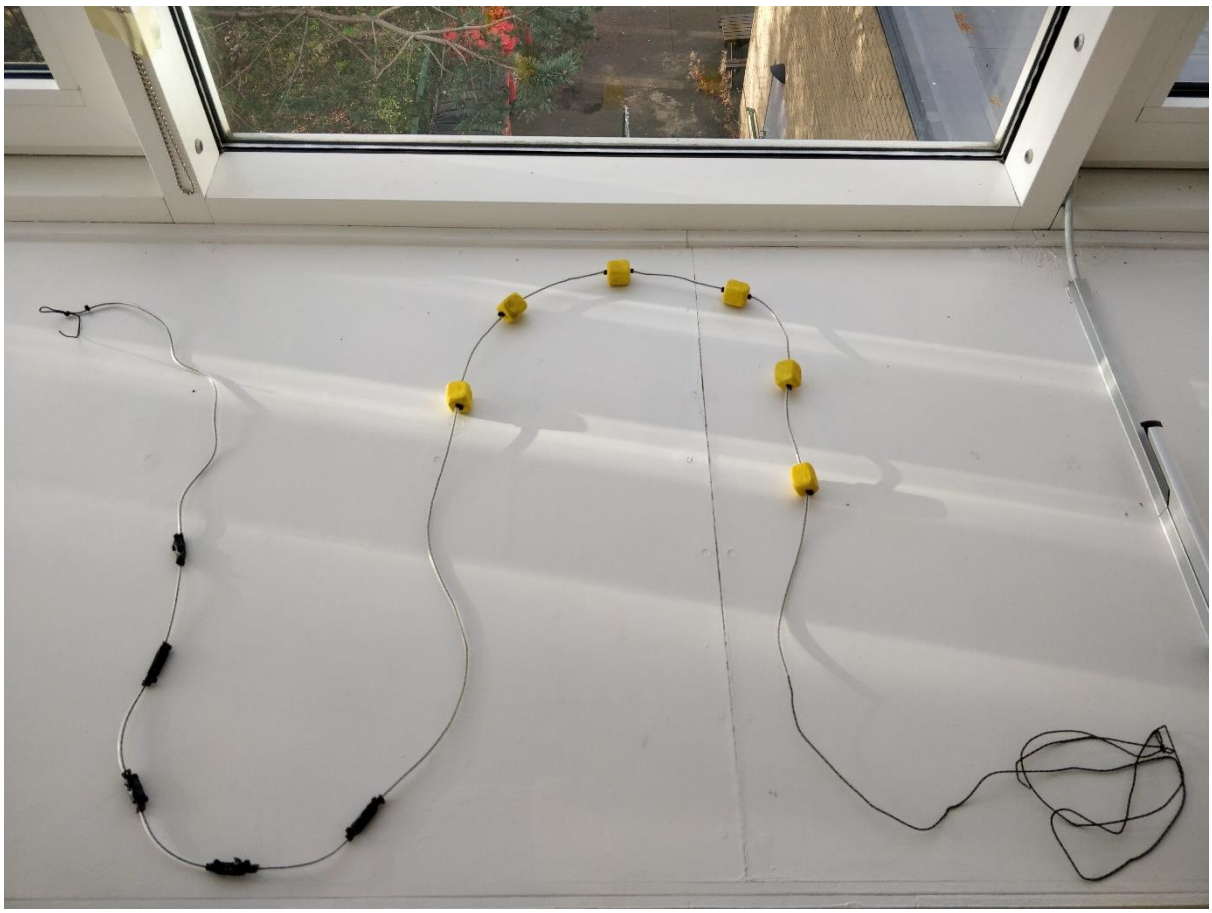

Figure 297 - showing overall lazy-S single line mooring with floats, clump masses, and tube to providing bending stiffness.

Figure 298 - Clump mass arrangement.

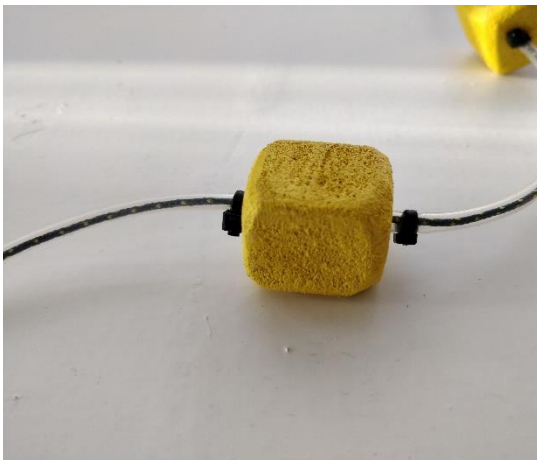

Figure 299 - Float arrangement

Finally, still images taken from a video supplied by the COAST Lab at Plymouth University are shown in Figure 300. In the figure, time increases from left to right.

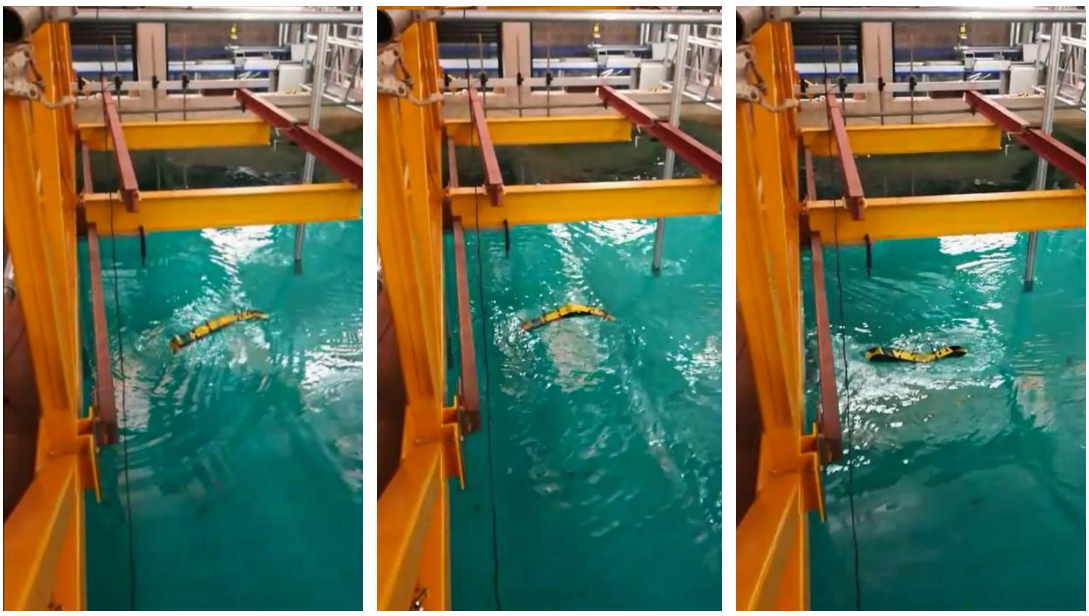

Figure 300 - Successive stills of the passive BST-folding model tested at the COAST Lab.

Appendix J – Blue Star – baseline seas calibration

J.1 Reflection analysis

Reflection analysis is performed in order to evaluate the extent to which the Curved Tank ‘suffers from’ reflected waves, and to quantify the effect that reflections may have on the obtained RAOs.

Three regular wave frequency sweeps between 0.5313-2.1875Hz were carried out with constant demand steepnesses of: 1/80 (0.0125), 1/60 (0.0167), 1/120 (0.0083).

Additionally, an amplitude sweep at constant f = 0.9375Hz (the predicted model scale peak response frequency) was carried out between 2mm and 36m demand amplitude, in steps of 2mm amplitude.

J.1.1 Suryanto method

Suryanto method (Suryanto, 2006) carried out using 3 wave gauges (WGs) aligned with the wave propagation direction and with distances referenced from the WG that first sees waves:

x_{12} = 0.268m
x_{13} = 0.445m

Figure 301 compares the incident wave amplitude with the demand amplitude for each frequency sweep. Generally speaking, the largest discrepancies occur at 0.625Hz, 0.725Hz, 0.8125Hz, 1.0Hz, 1.031H, 1.063Hz, 1.344Hz, and 2.000Hz. The frequency sweep for 1/120 steepness exhibits greater average discrepancies.

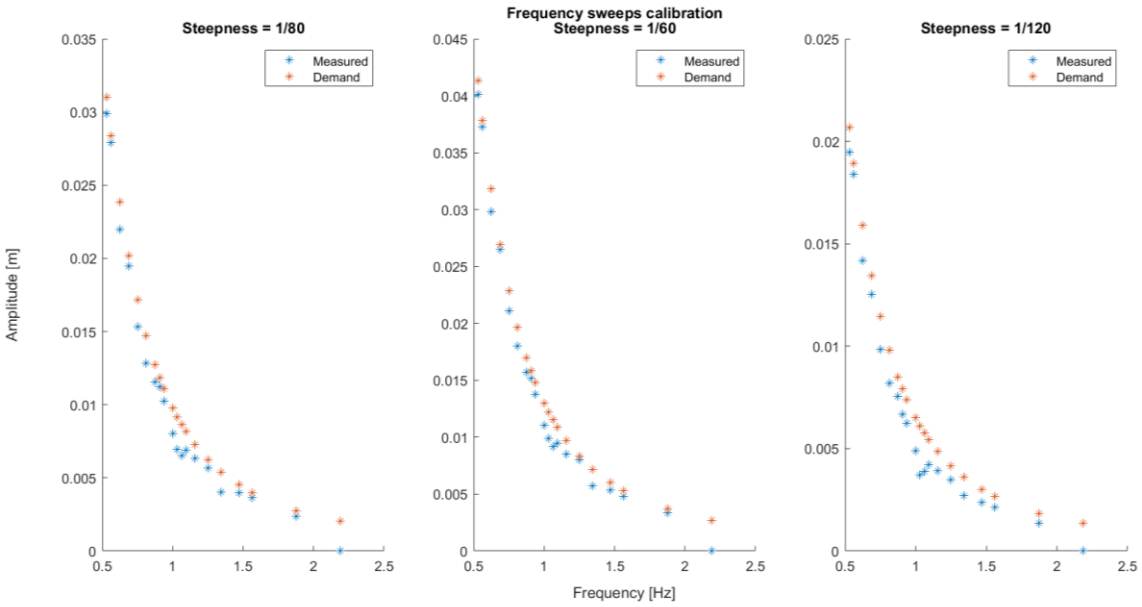

Figure 301 - Incident wave amplitude comparison for frequency sweeps.

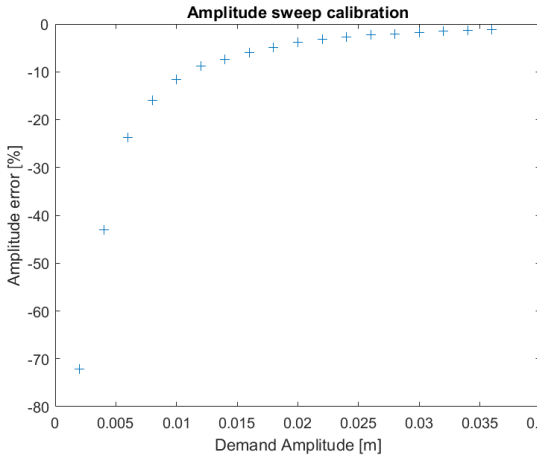

Figure 302 - Amplitude error vs Demand amplitude.

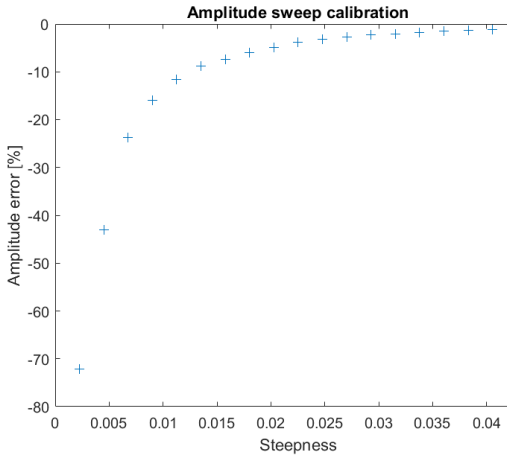

Figure 303 - Amplitude error vs demand steepness.

Figure 302 and Figure 303 are obtained by running a constant frequency sweep while varying the demand amplitude. A few comments can be made by observing the plots:

- Both plots display a clear reduction in amplitude error as the demand amplitude increases (see Figure 302).
- Incident amplitudes are significantly below demand values at the smaller amplitude end of the range, with the error lying within -10% above amplitudes of 12mm.

- Figure 303 also shows that the error is within -10% at steepnesses above 0.0135 (i.e. 1/74).

A reflection coefficient (R) is defined as the reflected/incident amplitude. Ideally, R values would be as close to 0 as possible, and in any case remain below 10% (0.1). R values extracted from the WG signals using the Suryanto method are plotted in Figure 304. It can be seen that:

- Higher R values correspond to the frequencies highlighted above from Figure 301, with particularly high values of R (in one case exceeding 1!) at the highest frequency (i.e. lowest amplitude) values for each constant steepness sweep. These correspond to the very lowest amplitudes and therefore seem to confirm observations arising from Figure 302.
- However, we note that, taking the plot for 1/80 steepness below, R = 0.89 @ f = 2.000Hz, A = 2.039mm, but R = 0.12 @ f = 1.875Hz, A = 2.776mm, thus demand amplitude is not the explanation for these significant outliers.
- Similarly, if we observe the plot for 1/120 steepness, R = 0.18 @ f = 1.875Hz, A = 1.850mm.
- R values for the 1/120 steepness sweep are on average higher than for the higher steepnesses.
- All plots show multiple R values above the 0.1 desired threshold.

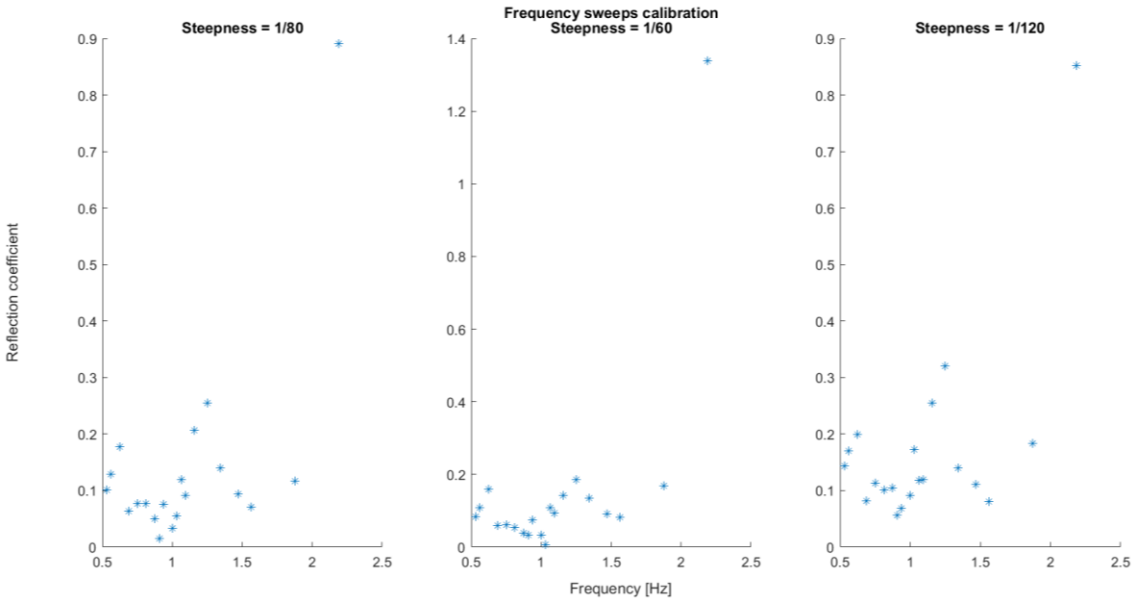

Figure 304 - Suryanto reflection coefficients for each frequency sweep.

J.1.2 Comparison with raw WG signals

It is decided that individual WG signals should be analysed in order to check whether any obvious WG errors might be causing the above-expected R values. Assuming each wave gauge detects a sinusoidal wave elevation signal, the measured amplitudes are estimated as: sqrt(2)*std(wave elevation time series).

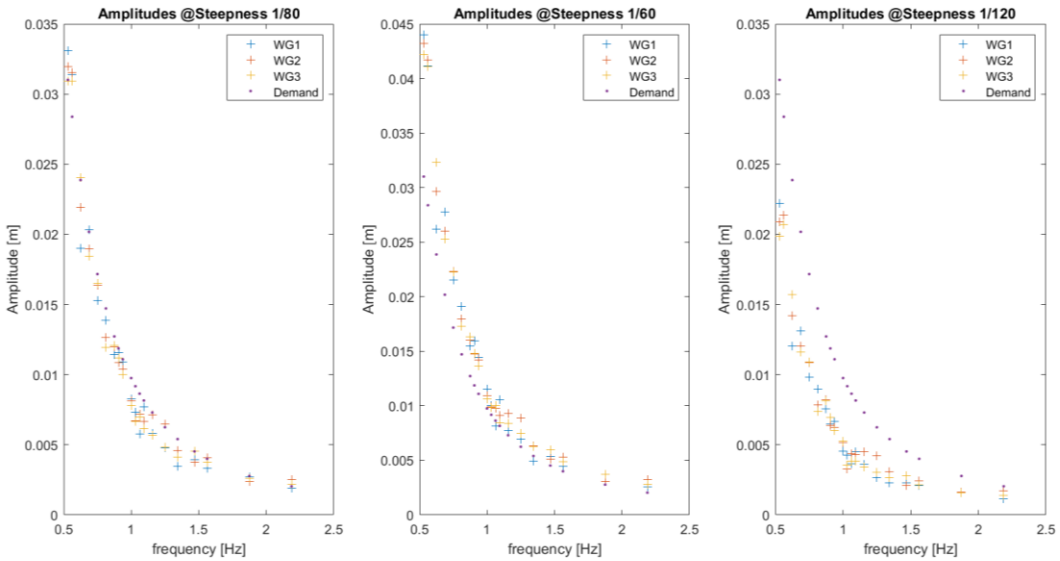

Figure 305 - Comparison of demand amplitude with raw WG signal amplitudes.

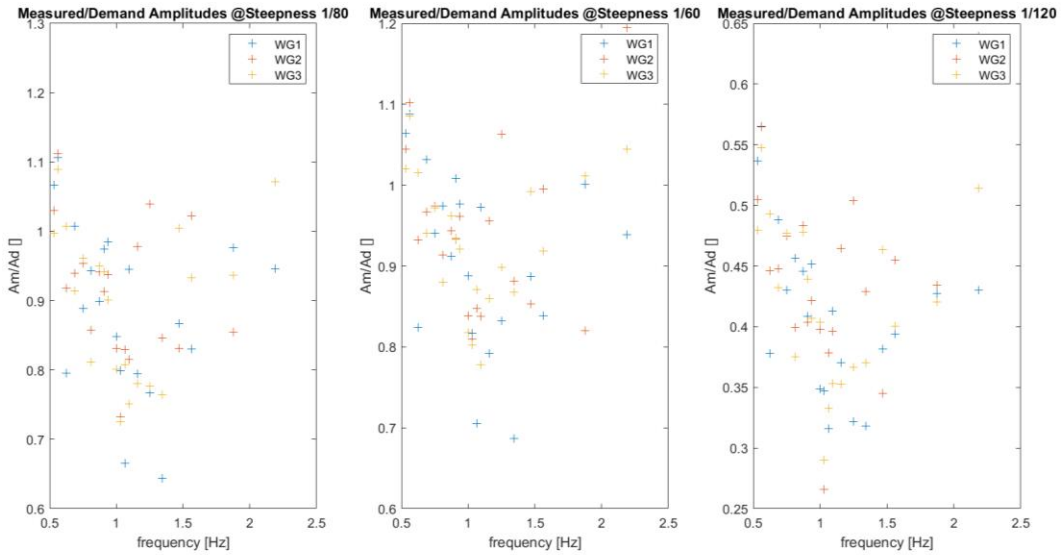

Figure 306 - Raw WG amplitudes normalised by demand amplitude.

Figure 305 shows an over-estimate of raw WG amplitude in the 1/60 steepness case and an under-estimation from the 1/120 case. Significant discrepancies occur at the lowest frequency.

J.1.3 Comparison with WaveLab analysis

A reflection analysis is carried out in WaveLab3 for comparative purposes, in order to ‘sanity check’ incident amplitudes, reflected amplitudes, and associated reflection coefficient values. This should either give greater confidence in the analysis performed via Suryanto method, or, if the analyses offer different results, give an additional error bound estimate. The analysis used the method of (Mansard and Funke, 1980) and is performed using the following input parameters:

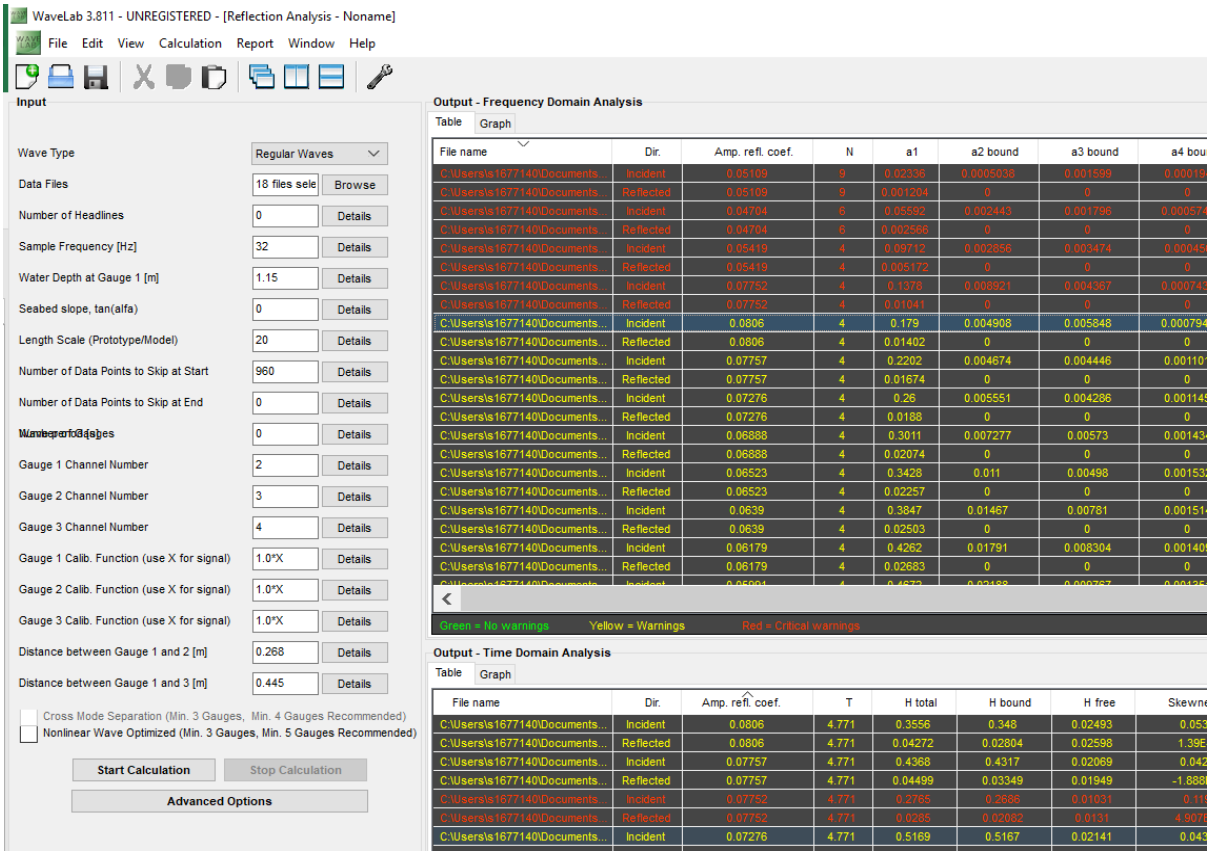

Figure 307 - Screenshot showing WaveLab analysis window.

Figure 308 shows that, in all cases, demand values exceed measured incident amplitude values. This difference appears to increase as steepness drops, with the greatest difference at the lowest steepness sweep of 1/120. Both trends are in agreement with those shown in Figure 301.

Figure 309 shows a plot of R values for each constant steepness frequency sweep. The following observations can be made:

- The average R value decreases as wave steepness increases, as per Figure 304 (if the outlier values at maximum frequency are ignored).
- The extremely large values of R at the highest frequency are not replicated in the WaveLab analysis.

Steepness	Mean R (Wave Lab)	Mean R (Suryanto) [without outlier]
1/80	0.1004	0.1420 [0.1026]
1/60	0.0918	0.1528 [0.0904]
1/120	0.1313	0.1742 [0.1384]
Amplitude sweep	0.0628	0.0635

Table 48 - Comparison of mean R values.

Table 48 shows good agreement (both in absolute values and trend) between mean R values obtained via the two methods, when the Suryanto outliers are discarded.

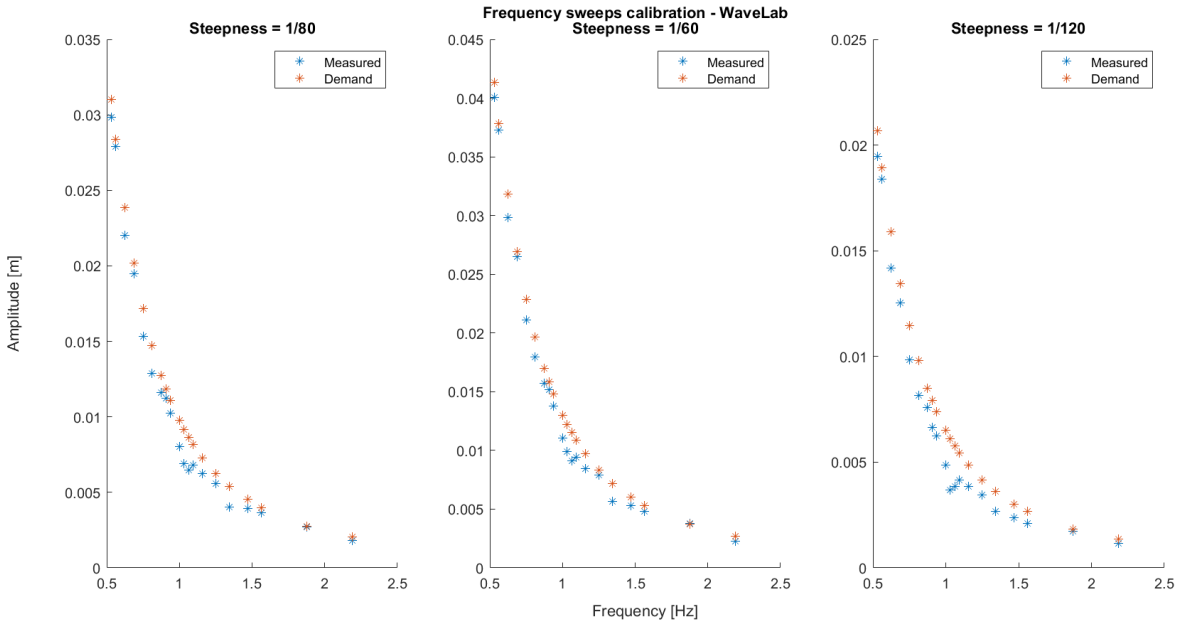

Figure 308 - Measured incident amplitudes compared with demand amplitudes for each frequency sweep at constant steepness.

Observing Figure 309 and comparing it with Figure 304, we can observe whether the higher R values occur at the same frequencies.

- From Figure 309, highest R values in all plots occur at f: 0.625Hz, 1.156Hz, 1.250Hz, 2.000Hz. The fifth highest are f = 1.344Hz for 1/80 and 1/60, and f = 1.031Hz for 1/120.
- From Figure 304, highest R values occur at f: 0.625Hz, 1.156Hz, 1.250Hz, 2.000Hz for 1/80 steepness; 0.625Hz, 1.250Hz, 1.875Hz, 2.188Hz for 1/60; 0.625Hz, 1.156Hz, 1.250Hz, 2.000Hz for 1/120.

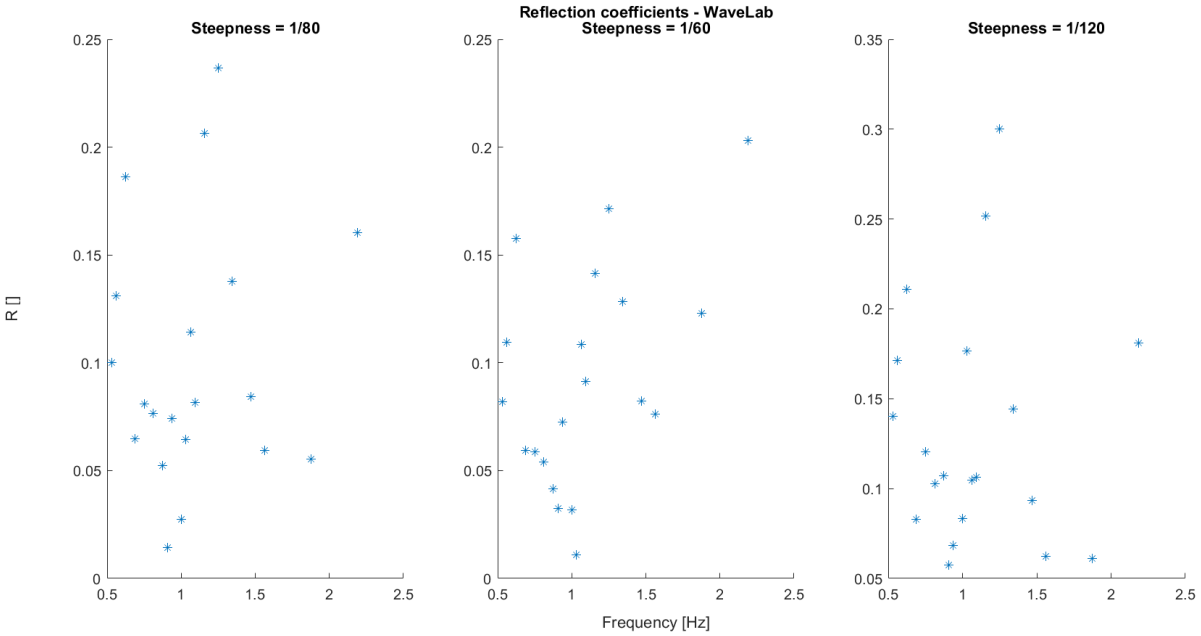

Figure 309 - Reflection coefficients from WaveLab analysis.

Incident amplitudes as well as demand amplitudes are compared in Figure 310. Figure 311 shows associated amplitude errors. Apart from the lowest demand amplitude, the amplitude error drops as demand amplitude increases, in agreement with Figure 303. The difference is that in the case of WaveLab, the errors are positive since the incident amplitude is less than the demand value.

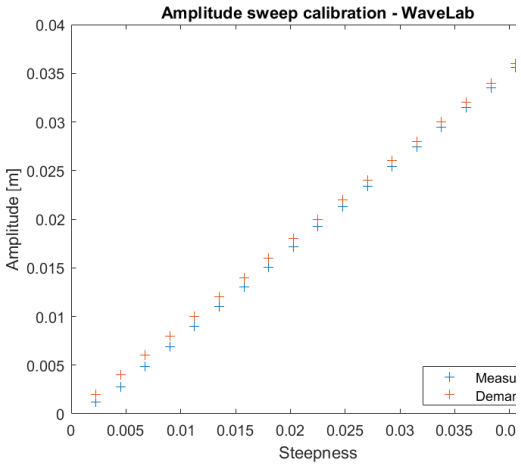

Figure 310 - Showing incident (measured) and demand amplitude values at constant f.

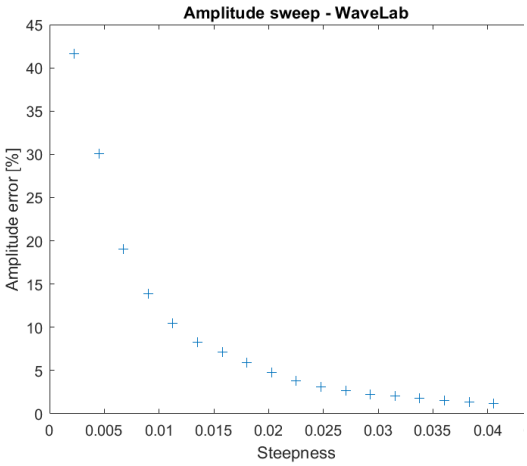

Figure 311 - Showing amplitude error as a function of wave steepness.

J.1.4 Quantification of reflection error

Both analyses show good agreement in both mean reflection coefficient (R) values, and in terms of the frequencies at which higher R values occur. Thus, error bars corresponding to % R values are extracted from the Suryanto method, to be then added to the obtained RAO plots.

The table below summarises these, where R_{mean} is 0.5*($R_{suryanto}$+$R_{wavelab}$):

Frequency [Hz]	**Steepness 1/80**			**Steepness 1/60**			**Steepness 1/120**		
	$R_{suryanto}$	**$R_{wavelab}$**	**R_{mean}**	**$R_{suryanto}$**	**$R_{wavelab}$**	**R_{mean}**	**$R_{suryanto}$**	**$R_{wavelab}$**	**R_{mean}**
2.0000	0.1602	0.8908	0.1602*	0.2031	1.3386	0.2031*	0.1810	0.8527	0.1810*
1.8750	0.0553	0.1174	0.0863	0.1230	0.1686	0.1458	0.0610	0.1841	0.1225
1.5625	0.0594	0.0707	0.0651	0.0761	0.0815	0.0788	0.0622	0.0807	0.0715
1.4688	0.0843	0.0944	0.0893	0.0823	0.0922	0.0872	0.0933	0.1111	0.1022
1.3438	0.1377	0.1402	0.1389	0.1284	0.1346	0.1315	0.1441	0.1400	0.1421
1.2500	0.2368	0.2547	0.2457	0.1713	0.1860	0.1787	0.3002	0.3204	0.3103
1.1563	0.2065	0.2063	0.2064	0.1415	0.1421	0.1418	0.2515	0.2555	0.2535
1.0938	0.0817	0.0910	0.0863	0.0914	0.0931	0.0923	0.1065	0.1192	0.1128
1.0625	0.1142	0.1196	0.1169	0.1086	0.1087	0.1086	0.1047	0.1184	0.1115
1.0313	0.0644	0.0552	0.0598	0.0109	0.0072	0.0090	0.1766	0.1723	0.1744
1.0000	0.0276	0.0329	0.0303	0.0317	0.0327	0.0322	0.0831	0.0909	0.0870
0.9375	0.0740	0.0754	0.0747	0.0725	0.0745	0.0735	0.0684	0.0681	0.0683
0.9063	0.0142	0.0150	0.0146	0.0324	0.0335	0.0329	0.0573	0.0567	0.0570
0.8750	0.0524	0.0508	0.0516	0.0415	0.0391	0.0403	0.1073	0.1043	0.1058
0.8125	0.0764	0.0767	0.0766	0.0541	0.0537	0.0539	0.1025	0.1015	0.1020
0.7500	0.0810	0.0774	0.0792	0.0588	0.0609	0.0599	0.1204	0.1136	0.1170
0.6875	0.0649	0.0642	0.0645	0.0593	0.0590	0.0592	0.0830	0.0814	0.0822
0.6250	0.1861	0.1774	0.1818	0.1578	0.1594	0.1586	0.2107	0.1996	0.2051
0.5625	0.1309	0.1295	0.1302	0.1096	0.1080	0.1088	0.1715	0.1698	0.1706
0.5313	0.1000	0.1008	0.1004	0.0818	0.0829	0.0824	0.1403	0.1430	0.1416

Table 49. R value comparison summary table.

**indicates that value is obtained directly from $R_{wavelab}$ term due to $R_{suryanto}$ likely being an outlier.*

J.2 Rotary Sensor Calibration

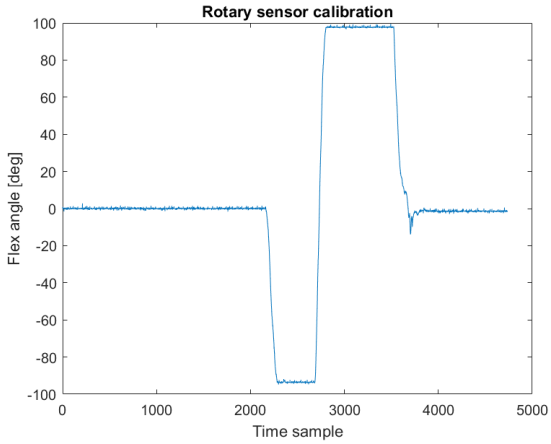

Figure 312 – Rotary sensor full flex range (degrees).

A rotary position sensor from Gill Sensors & Controls (Part 1498) is housed within the model nacelle to record angular flex. The sensor outputs a voltage, which, together with inclinometer readings, can be used to plot the full flex range of the WEC model (see Figure 312).

Hogging angles are positive and sagging angles are negative. The gain is calculated as 38.42 deg/V, with an offset of 2.83 V, giving a calibration function:

$$\theta = (V - Offset) * Gain$$

It is noted that the presence of Qualisys rods extending above the model's hulls restricts the maximum sagging angle, as shown in Figure 313. The calibration curve parameters are shown in the table below:

Parameter	**Measured voltage [V]**	**Measured angle [deg]**
Horizontal reference	2.83	-0.2
Max hogging	0.40	-93.2
Max sagging	5.38	98.1
Max permissible sagging	1.00	-70.2
Nominal fluctuation error	0.01	0.38

Table 50. Summary of rotary sensor calibration parameters.

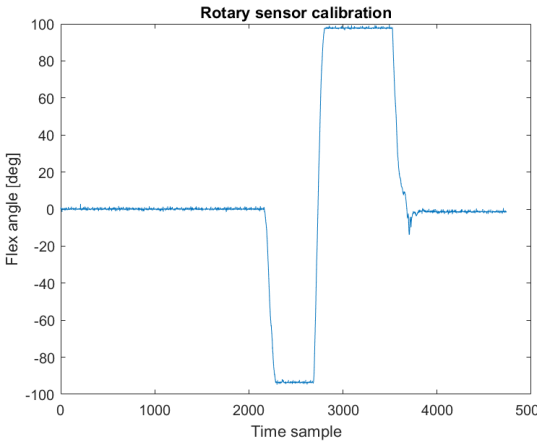

Figure 313 - Rotary sensor full flex range (degrees).

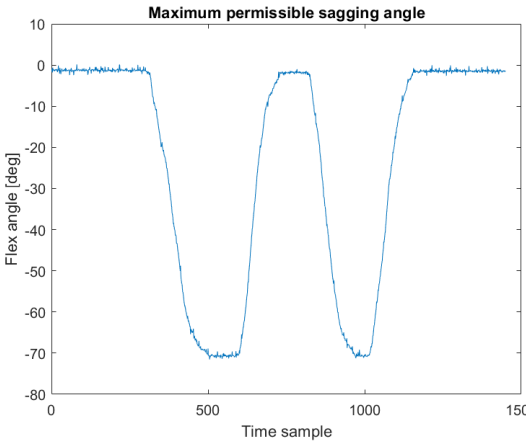

Figure 314 - Max permissible flex in sag due to Qualisys targets interference.

Appendix K – Irregular seas

This Appendix gives supporting data for irregular seas run during BST-folding 20th scale testing campaign in the Curved Tank.

K.1 Flex RAOs

Plots shown in this section are shown after low-pass filtering at 1Hz to smooth out signals, apart from Figure 316. For sea sweep and individual sea terminology, please refer to the summary table in the test plan shown in Chapter 8. All plots in this Appendix show flex RAO at model scale on the vertical axis. Horizontal axis values are also given at model scale.

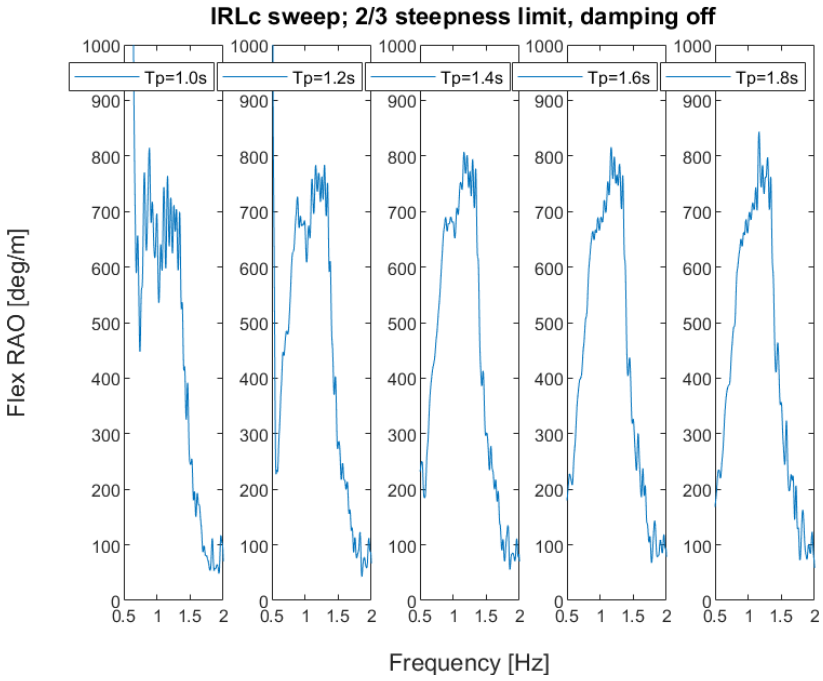

Figure 315 - Free hinge long-crested sea sweep at 2/3 limiting steepness.

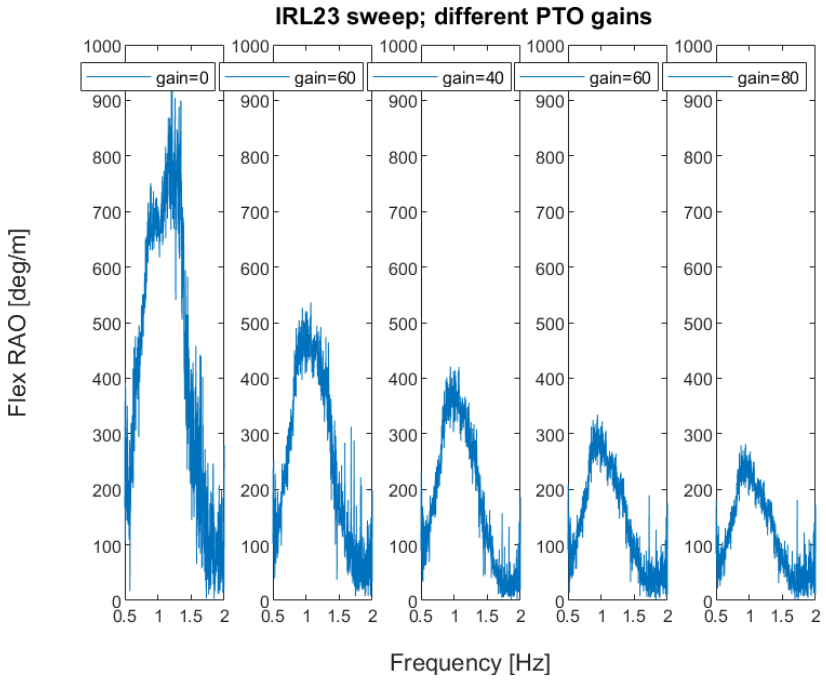

Figure 316 - Showing a PTO damping gain sweep from 0-80 for IRL23 sea.

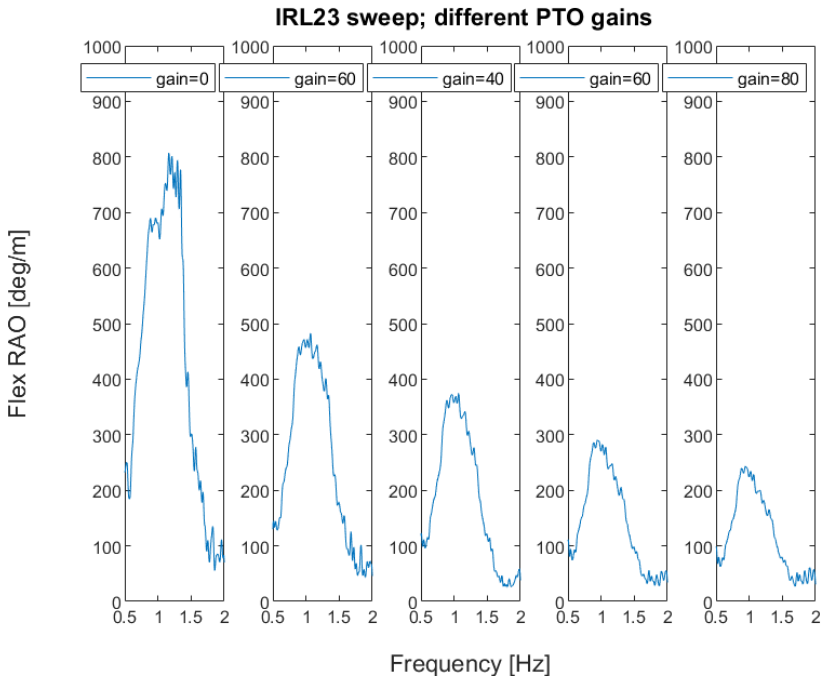

Figure 317 - Showing PTO gain sweep for individual IRL23 sea.

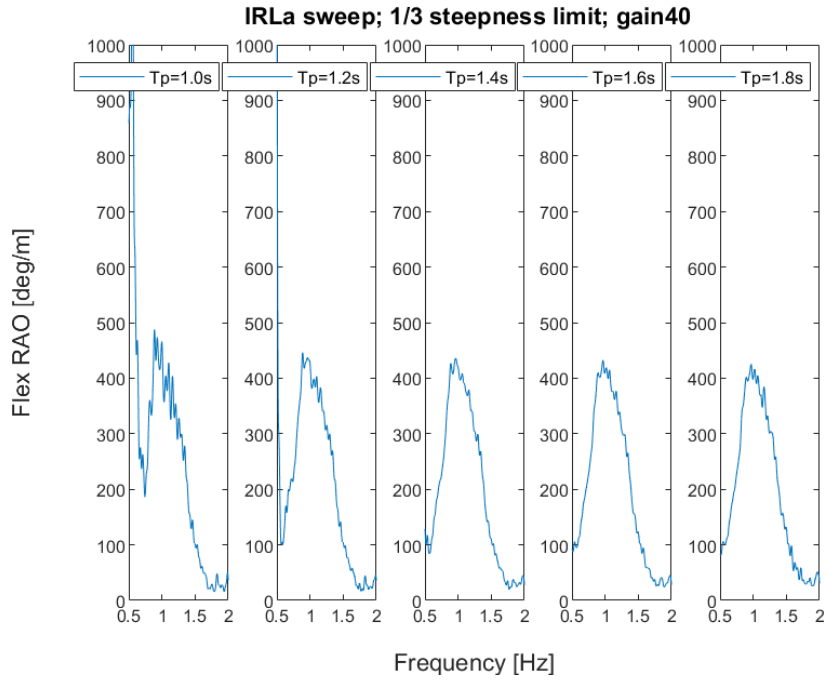

Figure 318 - Showing sweep at PTO gain 40, 1/3 limiting steepness.

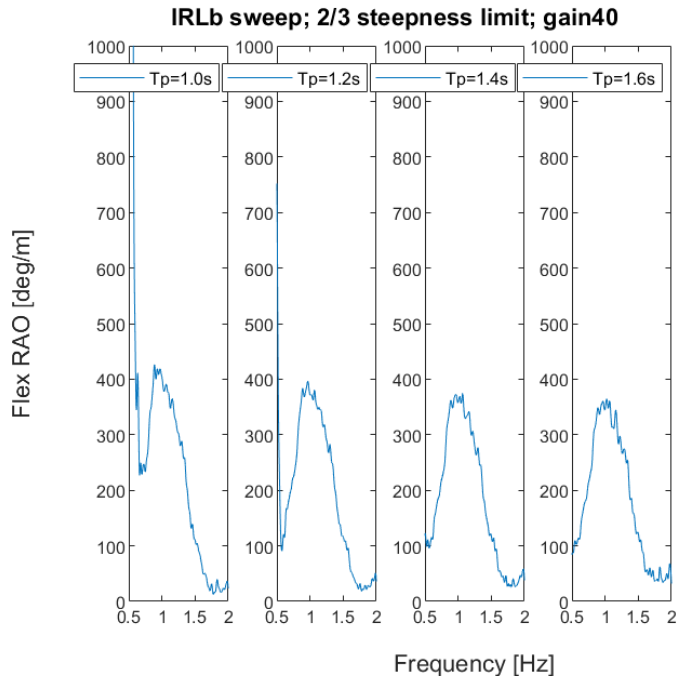

Figure 319 - Showing sweep at PTO gain 40, 2/3 limiting steepness.

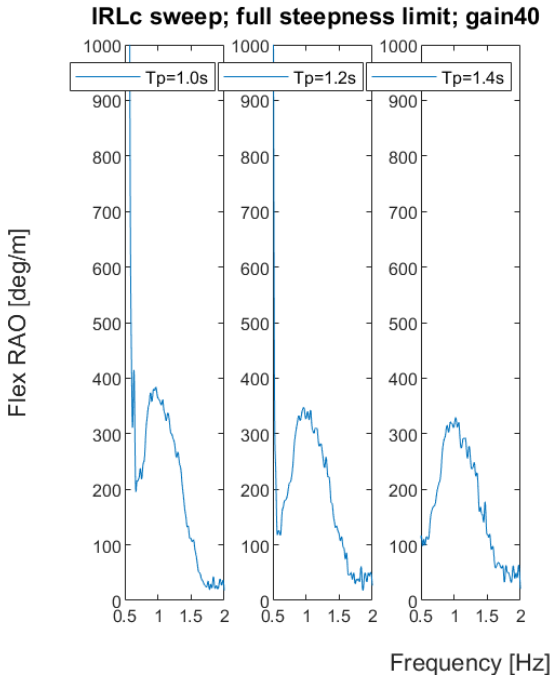

Figure 320 - Showing sweep for PTO gain 40, full limiting steepness.

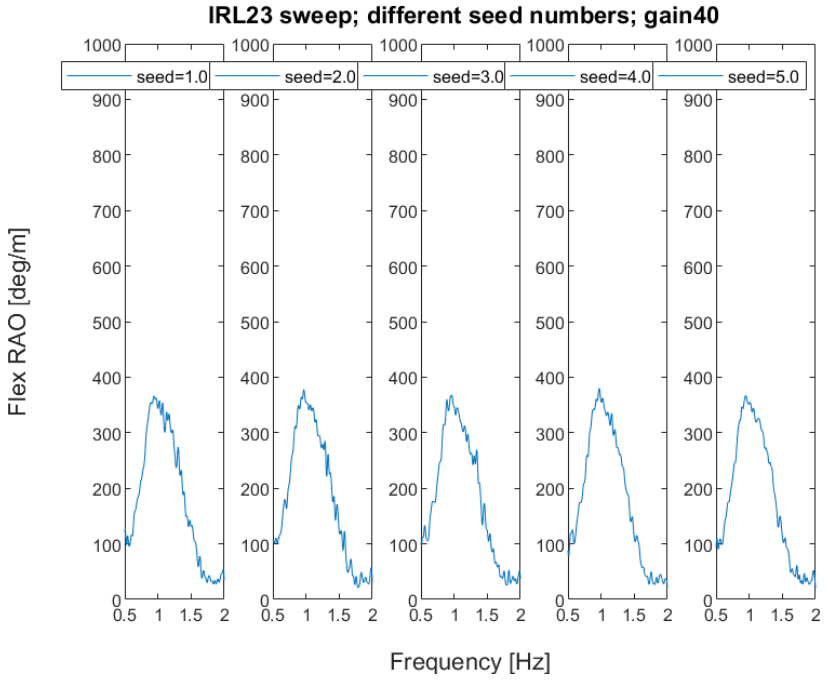

Figure 321 - Showing seed number sweep for IRL23 sea, PTO gain 40.

Appendix L – Ir0 seas calibration

This Appendix gives supporting data for Ir0 seas run during BST-folding 20th scale testing campaign in the Curved Tank. Unless stated otherwise, plot axes show data at model scale.

L.1 Initial set up

In (Pascal *et al.*, 2021), the authors apply the following principles:

- An amplitude spectrum is defined so as to be in the middle of the "scatter diagram" or occurrence table, and giving higher amplitude to more 'important' components – i.e. those with higher AEP contributions
    - Ir0 sea defined with 25 components and a 256s repeat period
    - Spectrum "shape" set up to have more energy in the middle period, but still enough range.
    - Target [Hs, Te] combination is [2.1m, 10.0s]
- Three calibration runs are performed in the absence of the model in the basin – all of these are run with the same random phases in each repeat run. (Ideally, the phases of components would also be varied to verify if/what the effects are).
- Check whether the amplitude spectrum peaks are sharp or whether too much spilling occurs
- Repeat time of 256s + ramp up time of 60s for device to reach steady state. The latter can be ~30s in our case since the Curved Tank is shorter than the one used by the authors (Aalborg University test basin).

In order to calculate the equivalent [Hs, Te] values of a particular Ir0 sea, the authors utilise the moment of the spectrum, defined as:

$$m_n = \int_0^\infty f^n \, S(f) \, df$$

The significant wave height and energy period values can then be calculated from the 0th and -1th moments, as follows:

$$H_{m0} = 4\sqrt{m_0}$$

$$T_{mm10} = \frac{m_{-1}}{m_0}$$

For the discrete spectrum, the following approximation is used:

$$S(f) = a^2/2df$$

in units of [m^2/Hz], where df = 1/repeat time.

In the paper, the authors note a target combination of [2.1m, 10.0s], the calculation to check this yields a 2.68m and 10.0s. The overall energy of the sea can be calculated as:

$$E_{tot} = \frac{1}{16}\rho g H_s^2$$

And the power per metre crest length as (W/m):

$$P_{tot} = \rho g^2 H_s^2 T_e/64\pi$$

The target versus achieved energy is 2.70e3 versus 4.41e3, and the power per metre crest length is 2.11e4 kW/m versus 3.44e4 kW/m. They do not exactly match due to different Hs values and rounding errors. The process of specifying the frequency of the components, their number, and their amplitudes is fairly trial and error in terms of achieving the desired [Hs, Te] combination – this is accepted by the authors. Note that adjusting the gain of the sweep affects Hs only, provided the component amplitude ratios and their frequencies remain constant.

L.2 Proposed IR0 seas

All Ir0 seas are run three times in an empty basin first, to measure reflections and to check amplitudes of each fundamental frequency component that are achieved. It is also ensured that the [Hs, Te] combinations match some of the irregular seas in the long-crested sweeps to enable meaningful comparisons. For reference, in the case of the Central North Sea wave climate, the most commonly occurring [Hs, Te] sea in the occurrence matrix is [1.75m, 6.5s], followed by [0.75m, 4.5s] and [2.25m, 7.5s].

Three sets of *Ir0* seas are hereby defined (all have a repeat time of 256s and a ramp up of 32s; thus 288s total run time):

1. Ir0 ‘steepness’ seas – based on constant steepness frequency components (to isolate wave from WEC non-linearities)[113] – each of these will have a different level of overall energy (higher steepness, higher energy).
    a. A target for 25 components is set – this then had to be reduced to 22 due to significant (more than 50%) power clipping predicted by the tank wavemaker software.
    b. Set the components so that 16 of them exactly overlap with the regular wave run components, which are already set to avoid spilling effects.
    c. Ideally, set steepness values of 1/50, 1/75, 1/100
        i. It is found that values of steepness above 1/100 result in significant peak and power clipping for wavemakers. Even a 1/100 steepness set with 22 components gives 0.3% power clipping and 0.7% peak clipping. Nevertheless, it is important to have at least one set with steepness matching one of the regular wave frequency sweeps.
        ii. Thus, a baseline Ir0 set is defined based on 1/50 steepness and 22 component. Two gains are then applied: 0.333 (resulting in 1/150 steepness) and 0.5 (1/100 steepness)
    d. Ensure no component has amplitude below 5mm; if it does, change to 5mm
        i. This was followed for the Ir0 ‘energy’ seas where min. amplitudes were set to 5mm, but not for the other types of Ir0 seas. The latter is because it was realised that with this minimum amplitude constraint, overall seas would become

[113] For the waves, constant steepness maintains geometrical similarity and non-linearity content so it is a good metric to use. However, for the WEC non-linearity, it is the relative motion of the WEC to the water that is of more practical importance, and the load shedding, namely the relative reduction of power and thus stress to the WEC and PTO as wave size increases. For power, load shedding is probably more important at the WEC resonant period; for survival, it is the WEC response (and shedding) at the long high waves. Thus, choosing 3x Ir0 sets and running each over a range of steepness up to the maximum seems a valid and valuable approach.

too large and strain the tank, which struggled to produce them. Since we did not want to sacrifice on frequency resolution, the minima were kept as they were computed. It was thought that this would actually not be too much of an issue given that all components combine to form the overall spectrum.

e. Ideally, repeat these with different PTO damping values (choose 5)
    i. Each damping value is considered as a ‘configuration’

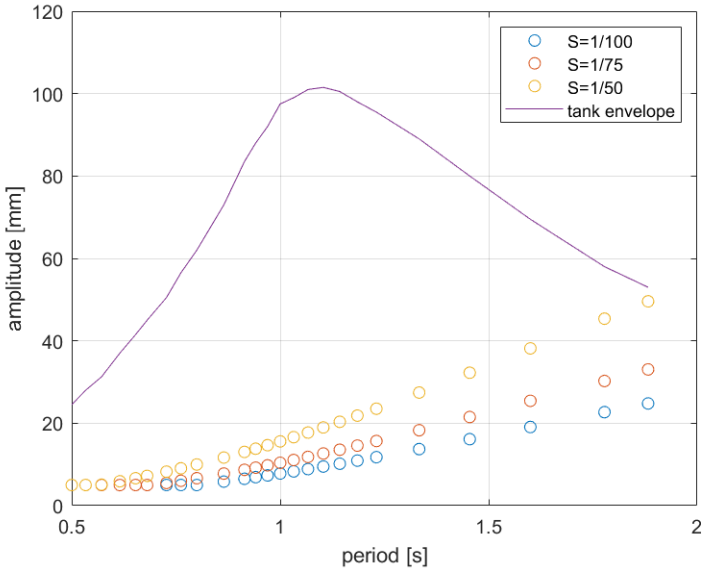

Figure 322 - Ir0 seas with constant steepness plotted against the derived Curved Tank envelope: {IROa}

Equivalent [Hs, Te] combinations: [3.10m, 6.46s], [4.08m, 6.56s], [6.09m, 6.61s].

2. Ir0 ‘envelope’ seas – based on wave tank envelope limits
    a. Here the shape of the spectrum follows the shape of the tank envelope
    b. Set 3 different wavemaker gains (i.e. scaling the amplitudes by a particular scalar gain value) so that the largest of these sets is at - or near to - the tank envelope
        i. Try gains of 0.25, 0.5, 0.9
        ii. [Hs, Te] = [5.5, 5.27], [11.0 5.27], [19.8 5.27]
        iii. Equivalent to steepnesses (Se) of: 0.127, 0.254, 0.457

iv. The latter two are extremely large seas with unphysical equivalent steepness values -> thus need to reduce the gain scalars.

c. The [Hs, Te] combinations above are very different to any that would be encountered in real seas.

i. Thus, gains of 0.05 and 0.1 used.

Equivalent [Hs, Te] combinations of the actual runs in the set that have gains of 0.05 and 0.1: [2.19m, 5.27s], [4.39m, 5.27s].

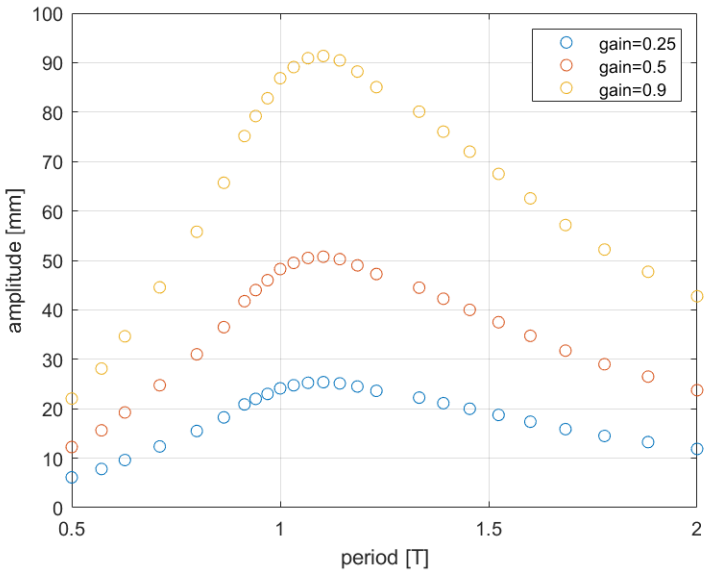

Figure 323 - Ir0 seas defined based on alignment with the shape of the tank performance envelope: {IRObj}

3. Ir0 'energy' seas – based on a target [Hs, Te] combination

a. Based on middle hot spot of the wave resource occurrence matrix

b. In order to have sufficient amplitude values, and to hit the [Hs, Te] target, may either have to reduce the number of components or increase the repeat time

c. With a 256s repeat time and 25 components, can get the [1.75m, 5.5s] (corresponds to between IRL23 and IRL33) sea with amplitudes between 5mm and 7mm.

d. There is a risk that these will be too low and overly affected by noise – this will be verified from post-processing of empty basin runs

e. Alternatively, one could increase the repeat period – e.g. to 512s, but this was not done because it would compromise the accelerated testing benefit offered by Ir0 in the first place

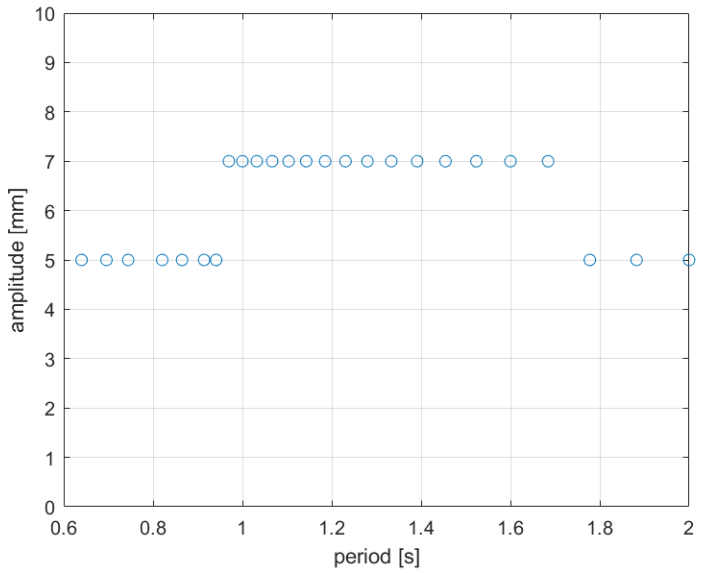

Figure 324 - Ir0 sea based on a target Hs, Te combination: {IROc}

In addition, three repeat seas of IR0c are defined but with different seed numbers in order to introduce different component phasing. IR0c has a seed number of 1.0, while the three seas in IR0d experiment have seed numbers 4.0, 9.0 and 14.0.

Once the target Ir0 seas, as listed above, were input to the CT wavemaker software, overall gains generally had to be lowered in order to comply with wave generation capabilities of the tank with respect to the resultant sea. Hence lower gain values can be seen in summary table (Table 51).

Some trial and error adjustment of the random phase for each Ir0 set was also carried out in order to avoid power clipping from the tank generation software. As a result, IROa sets had a random seed number of 14.0, IROb of 7.0, and IROc (baseline) of 1.0. IROd series was then a copy of IROc but with altered seed numbers of 4.0, 9.0, and 14.0.

Demand and measured Ir0 conditions are given in the following section.

L.3 Demand seas

Table 51 summarises the properties of the various Ir0 seas, as demanded. The seed number series {IROd} was run based on the lower gain {IROc} sea.

Ir0 sea type (& name)	**Gain**	**Equivalent Steepness**	**Hs [m]**	**Te [s]**
Steepness	0.50	1/17.2	2.18	6.13
Steepness	1.00	1/13.5	3.10	6.46
Envelope	0.05	1/12.7	2.19	5.27
Envelope	0.10	1/6.33	4.39	5.27
Energy	1.00	1/17.3	1.75	5.51
Energy	1.25	1/13.7	2.22	5.51

Table 51 – Summary demand properties of Ir0 seas run. Hs and Te are given at full-scale.

It can be seen from the equivalent steepness values in the above table that the resultant Ir0 conditions are relatively high steepness seas. In the case of *Envelope* with 0.10 gain, they verge on the physically unfeasible boundary of ~1/7.

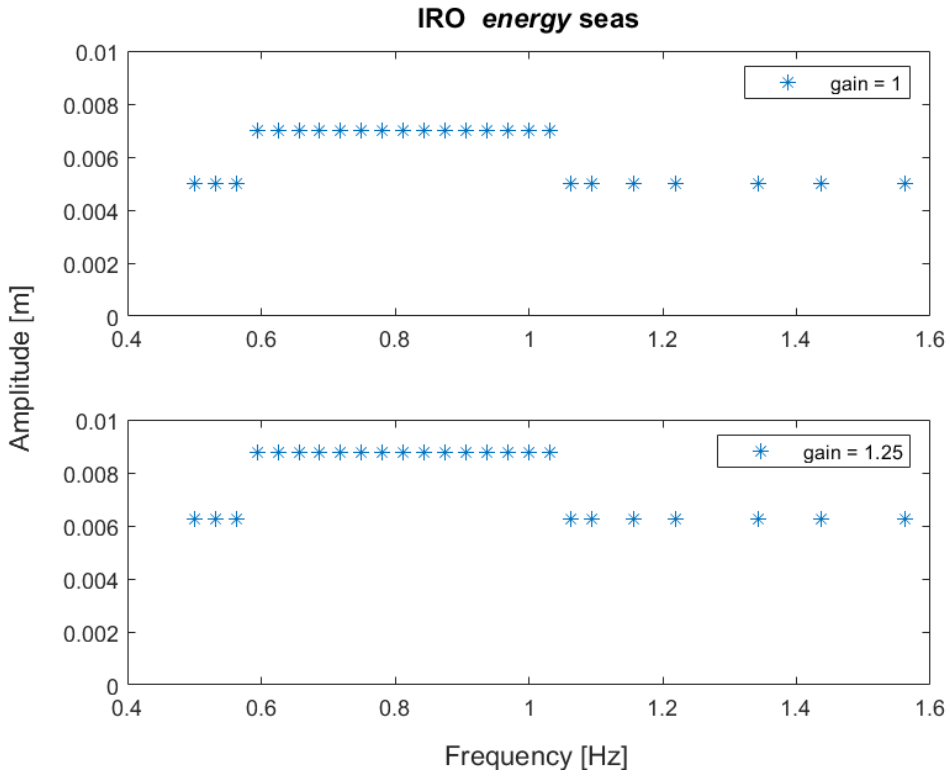

Figure 325 - Definition of Ir0 energy seas {IROc}.

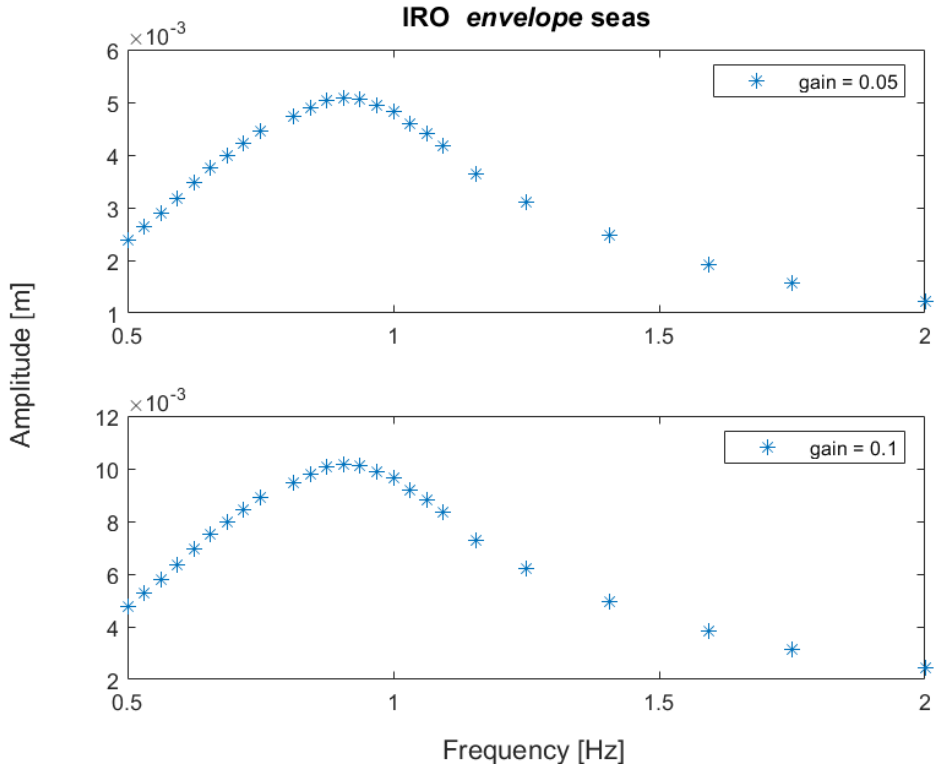

Figure 326 - Definition of Ir0 envelope seas {IROb}.

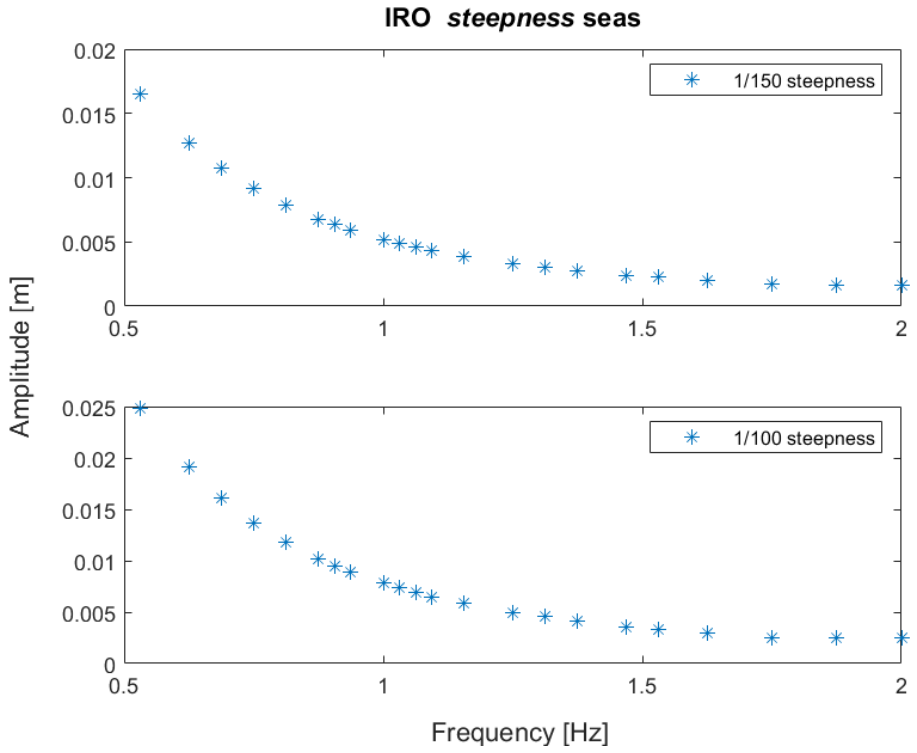

Figure 327 - Definition of Ir0 steepness seas {IROa}.

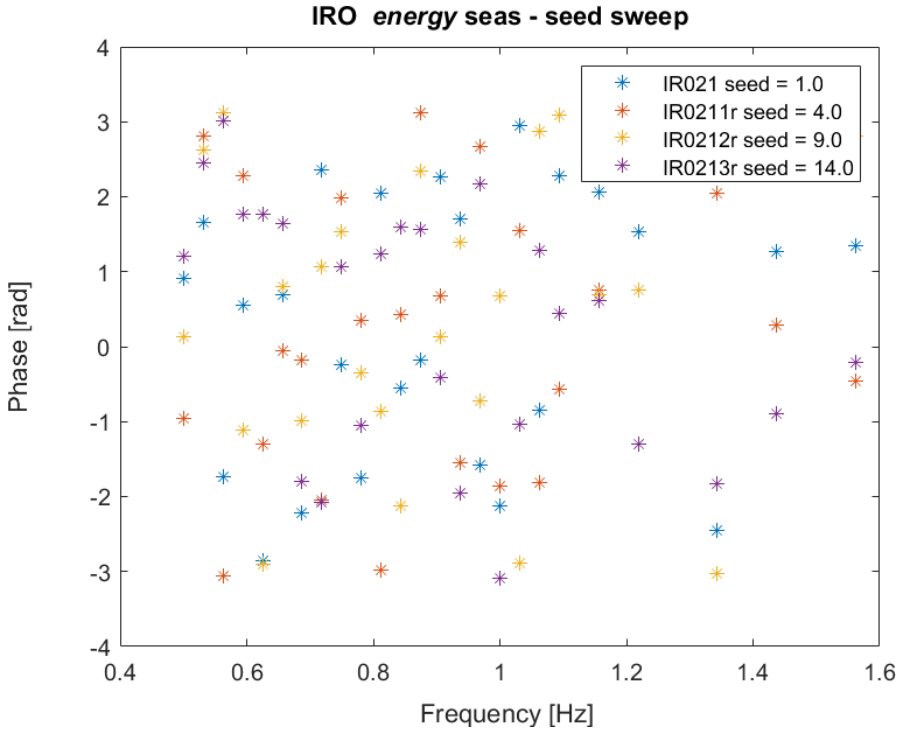

Figure 328 - Phase differences in frequency components within seed sweep of Ir0 energy seas.

L.3.1 Summary tables

In the following tables, parameter ‘k’ represents the number of waves; [ref] corresponds to a wavemaker gain of 1; ‘f’ is frequency; ‘S’ is wave steepness; ‘G’ is gain; {Rcoeff} is the reflection coefficient given as a %.

Ir0 steepness sweeps {IROa}:

k (64s repeat time)	k (256s repeat time)	f [Hz]	Amp [mm] Depth-corrected, S=1/50 [ref]	S=1/150 (G=0.333) {Rcoeff}	S=1/100 (G=0.5) {Rcoeff}	T, full scale [s]
128	512	2	5	1.7 {112}	2.5 {150}	2.2361
120	480	1.875	5	1.7 {10.7}	2.5 {10.0}	2.3851
112	448	1.75	5.1	1.7 {4.3}	2.6 {18.1}	2.5555
104	416	1.625	5.9	2.0 {18.4}	3.0 {24.6}	2.7521
98	392	1.5313	6.7	2.2 {11.4}	3.4 {29.0}	2.9206
94	376	1.4688	7.2	2.4 {19.4}	3.6 {27.1}	3.0449
88	352	1.375	8.2	2.7 {5.3}	4.1 {8.8}	3.2525
84	336	1.3125	9.1	3.0 {1.4}	4.6 {2.5}	3.4073
80	320	1.25	10.0	3.3 {7.1}	5.0 {5.8}	3.5777

74	296	1.1563	11.7	3.9 {6.5}	5.8 {7.5}	3.8678
70	280	1.0938	13.0	4.3 {6.2}	6.5 {4.4}	4.0888
68	272	1.0625	13.8	4.6 {5.0}	6.9 {6.6}	4.2091
66	264	1.0313	14.7	4.9 {4.0}	7.3 {5.5}	4.3366
64	256	1	15.6	5.2 {7.6}	7.8 {9.1}	4.4721
60	240	0.9375	17.7	5.9 {0.8}	8.9 {4.0}	4.7703
58	232	0.9063	19.0	6.3 {3.2}	9.5 {2.8}	4.9348
56	224	0.8750	20.3	6.8 {3.5}	10.2 {2.4}	5.1110
52	208	0.8125	23.5	7.8 {4.7}	11.8 {5.9}	5.5042
48	192	0.75	27.4	9.1 {6.0}	13.7 {6.6}	5.9628
44	176	0.6875	32.3	10.8 {8.1}	16.1 {8.0}	6.5049
40	160	0.625	38.2	12.7 {10.8}	19.1 {7.4}	7.1554
~~36~~	~~144~~	~~0.5625~~	~~45.4~~	~~15.1~~	~~22.7~~	~~7.9505~~
34	136	0.5313	49.6	16.5 {4.1}	24.8 {4.1}	8.4181

Table 52 - Definition of Ir0 'steepness' seas {IROa: IRO01, IRO02}

NB: Blue highlights are additional components to ‘standard’ regular wave sweeps; strikethrough rows are the components that were removed in order to avoid wavemaker power clipping. For IROb and IROc tables, full-scale periods are not given as they largely overlap IROa values in Table 52.

- IRO01 random seed: 13.0; [Hs, Te] = [2.18m, 6.13s]
  IRO02 random seed: 13.0; [Hs, Te] = [3.10m, 6.46s]

Ir0 envelope sweeps:

k (64s repeat time)	k (256s repeat time)	f [Hz]	Amp [mm] Depth-corrected [ref]	G=0.05 {Rcoeff}	G=0.1 {Rcoeff}
128	512	2	24.5	1.2 {173}	2.5 {366}
112	448	1.75	31.3	1.6 {4.7}	3.1 {8.8}
102	408	1.5938	38.5	1.9 {6.9}	3.9 {14.6}
90	360	1.4063	49.5	2.5 {9.5}	5.0 {6.8}
80	320	1.25	62.0	3.1 {8.8}	6.2 {8.4}
74	296	1.1563	73.0	3.7 {1.2}	7.3 {3.3}
70	280	1.0938	83.5	4.2 {4.9}	8.4 {4.2}
68	272	1.0625	88.0	4.4 {3.6}	8.8 {4.1}
66	264	1.0313	92.0	4.6 {3.9}	9.2 {4.6}

64	256	1	96.5	4.8 {4.7}	9.7 {6.9}
62	248	0.9688	99.0	5.0 {4.5}	9.9 {5.5}
60	240	0.9375	101.0	5.1 {3.9}	10.1 {1.8}
58	232	0.9063	101.5	5.1 {2.1}	10.2 {2.5}
56	224	0.875	100.5	5.0 {4.1}	10.1 {1.5}
54	216	0.8438	98.0	4.9 {2.6}	9.8 {3.7}
52	208	0.8125	94.5	4.7 {5.8}	9.5 {6.5}
48	192	0.75	89.0	4.5 {6.6}	8.9 {6.6}
46	184	0.7188	84.5	4.2 {8.2}	8.5 {7.9}
44	176	0.6875	80.0	4.0 {11.1}	8.0 {7.1}
42	168	0.6563	75.0	3.8 {13.3}	7.5 {11.4}
40	160	0.625	69.5	3.5 {18.7}	7.0 {12.9}
38	152	0.5938	63.5	3.2 {20.6}	6.4 {13.4}
36	144	0.5625	58.0	2.9 {19.8}	5.8 {11.6}
34	136	0.5313	53.0	2.7 {11.3}	5.3 {7.8}
32	128	0.5	47.5	2.4 {16.7}	4.8 {7.1}

Table 53 - Definition of Ir0 'envelope' seas {IRObs: IRO11 and IRO12}

- IRO11 random seed: 7.0; [Hs, Te] = [2.19m, 5.27s]
- IRO12 random seed: 7.0; [Hs, Te] = [4.39m, 5.27s]

Ir0 energy sweeps:

k (64s repeat time)	k (256s repeat time)	f [Hz]	Amp [mm] Depth-corrected [ref] {Rcoeff}	Amp [mm] G=1.25 {Rcoeff}
100	400	1.5625	5 {11.2}	6.25 {15.3}
92	368	1.4275	5 {8.6}	6.25 {9.0}
86	344	1.3438	5 {6.6}	6.25 {7.4}
78	312	1.2188	5 {2.0}	6.25 {2.4}
74	296	1.1563	5 {2.2}	6.25 {3.0}
70	280	1.0938	5 {5.4}	6.25 {6.0}
68	272	1.0625	5 {3.6}	6.25 {3.8}
66	264	1.0313	7 {3.8}	8.75 {4.9}
64	256	1	7 {5.3}	8.75 {5.9}
62	248	0.9688	7 {4.7}	8.75 {4.5}
60	240	0.9375	7 {1.3}	8.75 {0.8}
58	232	0.9063	7 {1.4}	8.75 {2.2}
56	224	0.875	7 {5.7}	8.75 {5.5}

54	216	0.8438	7 {2.4}	8.75 {1.2}
52	208	0.8125	7 {7.3}	8.75 {6.9}
50	200	0.7813	7 {8.8}	8.75 {9.7}
48	192	0.75	7 {6.7}	8.75 {6.6}
46	184	0.7188	7 {7.9}	8.75 {7.7}
44	176	0.6875	7 {8.2}	8.75 {8.3}
42	168	0.6563	7 {7.2}	8.75 {6.5}
40	160	0.6250	7 {13.8}	8.75 {12.3}
38	152	0.5938	7 {15.0}	8.75 {13.6}
36	144	0.5625	5 {16.3}	6.25 {14.5}
34	136	0.5313	5 {10.3}	6.25 {7.9}
32	128	0.5	5 {9.6}	6.25 {7.8}

Table 54 - Definition of Ir0 'energy' seas {IROc: IRO21, IRO22}.

NB: the second run was set to a gain of 1.5 originally, but then was changed to 1.25 to avoid overly large seas with visible breaking.

- IRO21 random seed: 1.0
- IRO22 random seed: 1.0
- IRO211 random seed: 4.0
- IRO212 random seed: 9.0
- IRO213 random seed: 14.0

{IROc} gain=1: [1.75m, 5.51s]; gain=1.5: [2.65, 5.51s]; gain=1.25: [2.22m, 5.51s]

An anomalous error is observed at f=1.25Hz for the IRO12 sea, which is the frequency at which the different between demand and measured is greatest (~73 %). This also occurs for IROa, and is visible in the IRO02 plot, and to a lesser extent for IRO01. Other relatively high errors are observed around peak at 0.90625Hz, in both IRO11 and IRO12 seas. Measured IRO11 peak amplitude is 88% of demand, same for IRO12. The reflection coefficient value at f=2Hz is much higher than the rest and is therefore omitted. For example, for IROa, the reflection coefficient at f=2Hz is approximately 6x the next highest.

IROc (and IROd) perhaps exhibit the worst properties in terms of demand and measured relationships – there is relatively high spilling, especially at higher frequencies.

- Largest amplitude drops are at f=0.90625Hz, and f=1.4375Hz, which do not seem R related
- Largest R in IRO21 is 16%, and largest R in IRO22 is 14%, most below 10% in both runs
- From IROc analysis repeats: is the tank consistent? Yes
- IROd analysis shows that the method is relatively 'resilient' to different seed numbers (Figure 329). Note that the vertical axis starts at 3mm.

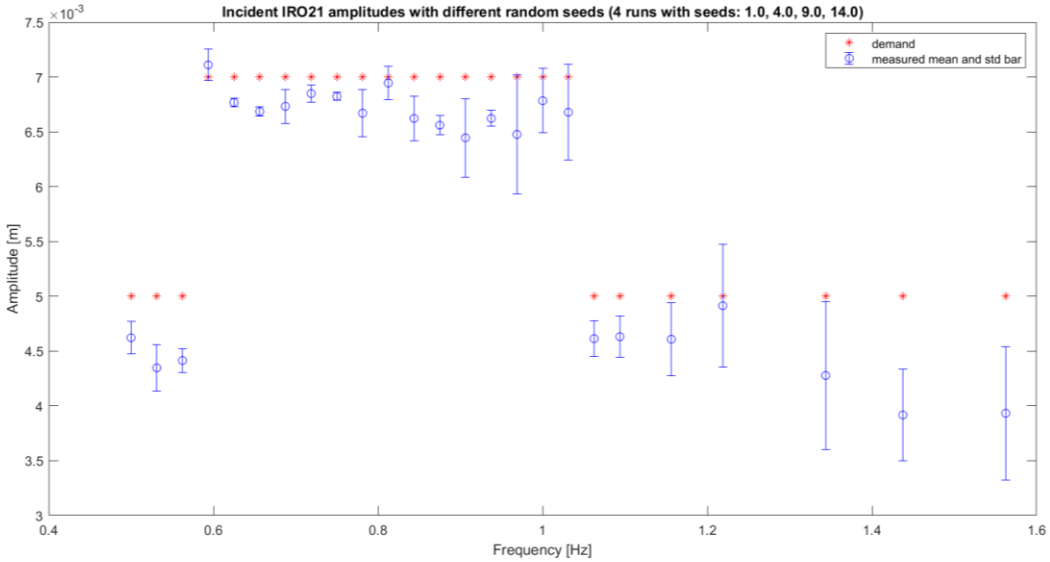

Figure 329 - Showing measured amplitude components across seed sweep IRO21 sea.

The largest standard deviation occurs at f=1.34375Hz, corresponding to +/- 0.7mm. In general, higher frequencies have higher bars perhaps due to higher reflection coefficients.

Ir0 envelope, **seed sweep**:

f [Hz]	Rcoeff, % seed 1.0	Rcoeff, % seed 4.0	Rcoeff, % seed 9.0	Rcoeff, % seed 14.0	Rcoeff, % mean	Rcoeff, % std
1.5625	11.2	1.1	2.2	2.2	4.2	4.7
1.4275	8.6	5.9	5.1	5.1	6.2	1.7
1.3438	6.6	9.2	5.4	5.4	6.6	1.8
1.2188	2.0	1.9	1.3	1.3	1.6	0.4
1.1563	2.2	3.0	2.9	2.9	2.7	0.4
1.0938	5.4	4.8	5.3	5.3	5.2	0.3
1.0625	3.6	3.5	2.4	2.4	3.0	0.7

1.0313	3.8	3.9	5.2	5.2	4.5	0.8
1	5.3	4.5	5.6	5.6	5.3	0.5
0.9688	4.7	4.2	6.9	6.9	5.7	1.4
0.9375	1.3	2.1	0.8	0.8	1.3	0.6
0.9063	1.4	0.9	2.6	2.6	1.9	0.8
0.875	5.7	5.6	2.7	2.7	4.2	1.7
0.8438	2.4	1.3	1.4	1.4	1.6	0.5
0.8125	7.3	6.0	7.3	7.3	6.9	0.6
0.7813	8.8	3.4	6.9	6.9	6.5	2.2
0.75	6.7	5.6	5.4	5.4	5.7	0.6
0.7188	7.9	6.6	5.1	5.1	6.2	1.3
0.6875	8.2	7.2	8.8	8.8	8.3	0.8
0.6563	7.2	11.2	9.3	9.3	9.2	1.6
0.6250	13.8	13.5	12.2	12.2	12.9	0.8
0.5938	15.0	14.0	15.8	15.8	15.1	0.8
0.5625	16.3	11.6	18.6	18.6	16.3	3.3
0.5313	10.3	8.8	10.4	10.4	10.0	0.8
0.5	9.6	8.4	2.9	2.9	6.0	3.6

Table 55 - Summary table for reflection coefficients across IRO21 seed sweeps.

L.3.1.1 Qualitative observations of ‘open tank’ Ir0 seas

- IROa: large sea with fairly steep waves.
- IRObb: no obvious wave breaking observed.
- IROc: for IRO22 sea, no white capping or obvious wave breaking observed, though some waves appear on the limit of what the paddles can produce and appear as though they begin to disperse. Note that IRO22 sea has a max wavemaker gain limited to 148.427 by the tank, as opposed to usual 150.
- IROd: as per IROc.

L.4 Empty basin calibration runs

L.4.1 IROa (steepness seas)

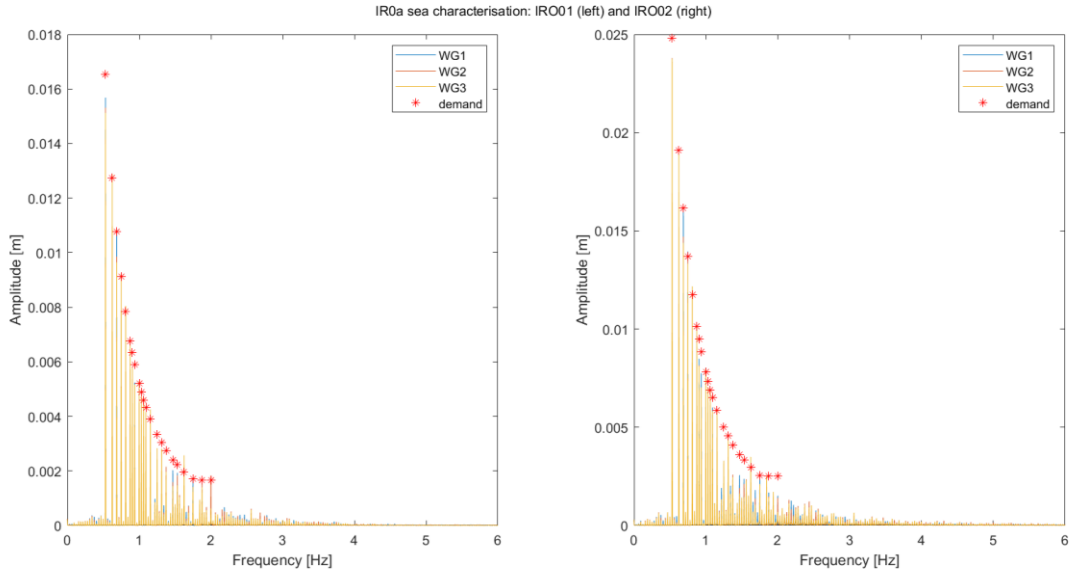

Figure 330 - Wave gauge (WG) measured amplitudes versus demand {IROa}.

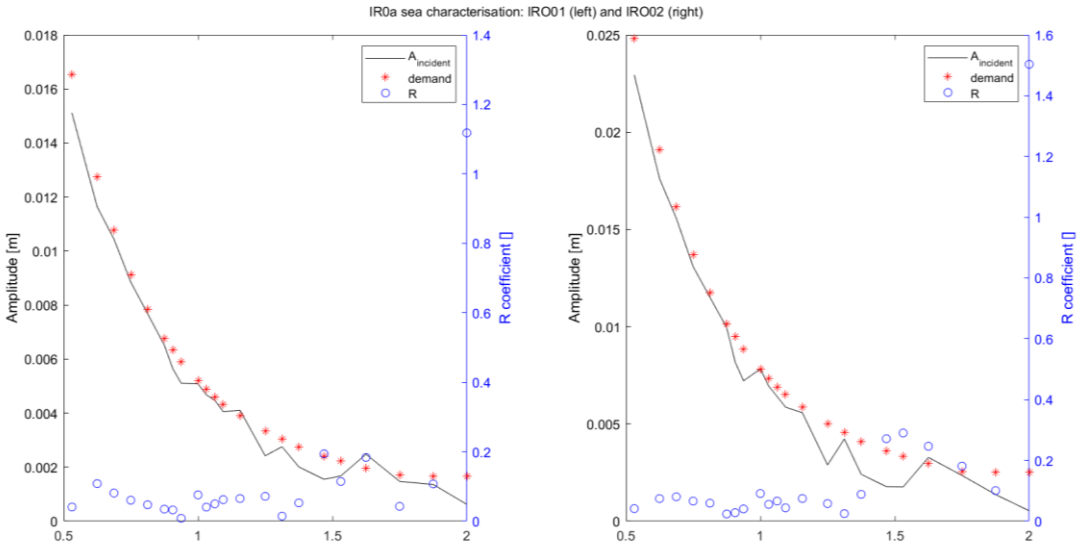

Figure 331 - Demand, incident amplitudes, and associated reflection coefficients {IROa}.

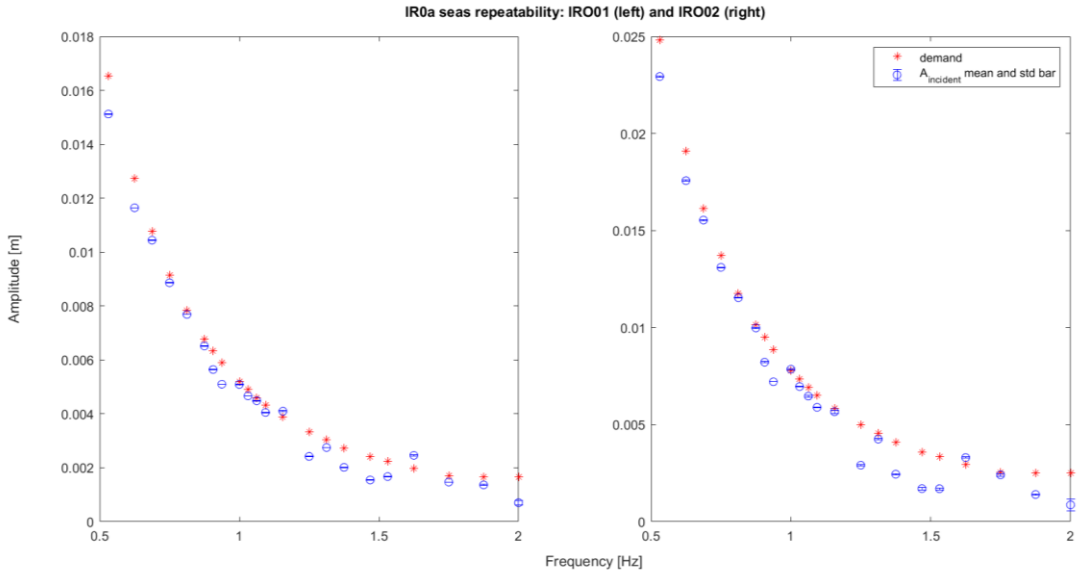

Figure 332 - Repeatability of IROa seas.

L.4.2 IRObb (envelope seas)

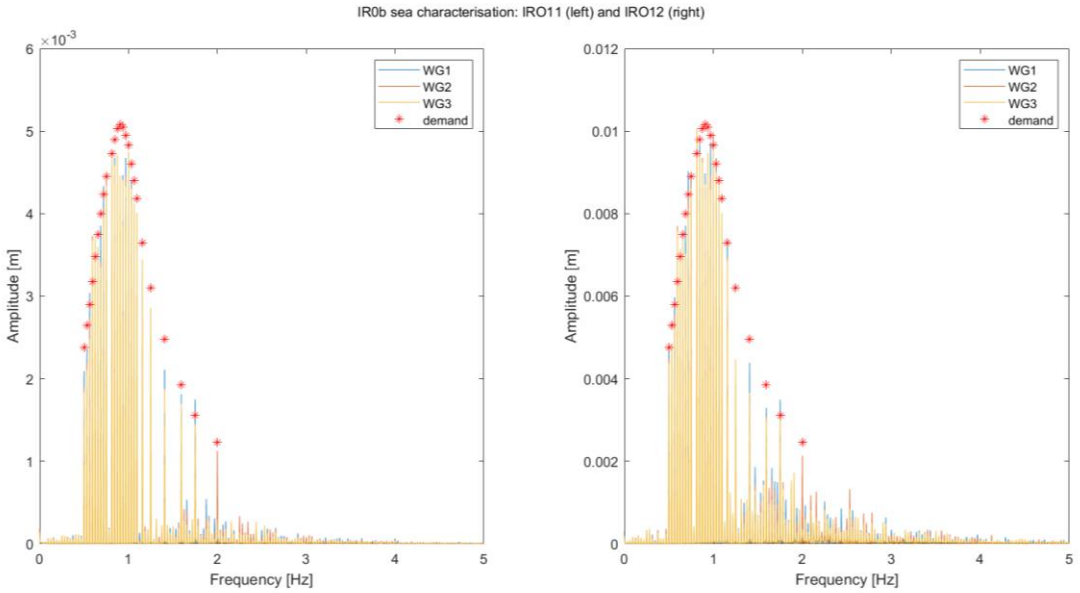

Figure 333 - Wave gauge (WG) measured amplitudes versus demand {IRObb}.

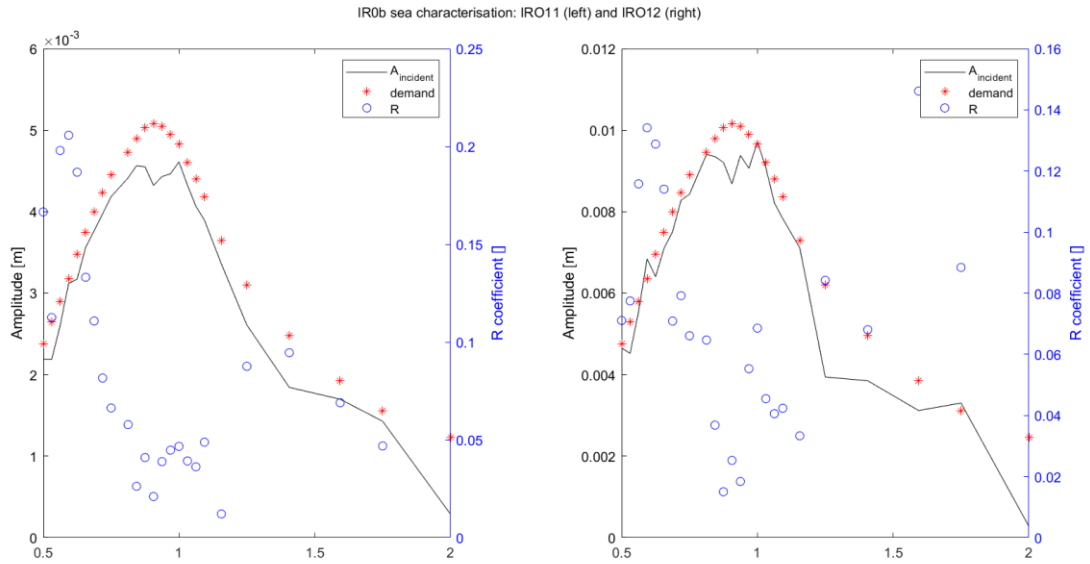

Figure 334 - Demand, incident amplitudes, and associated reflection coefficients {IROb}.

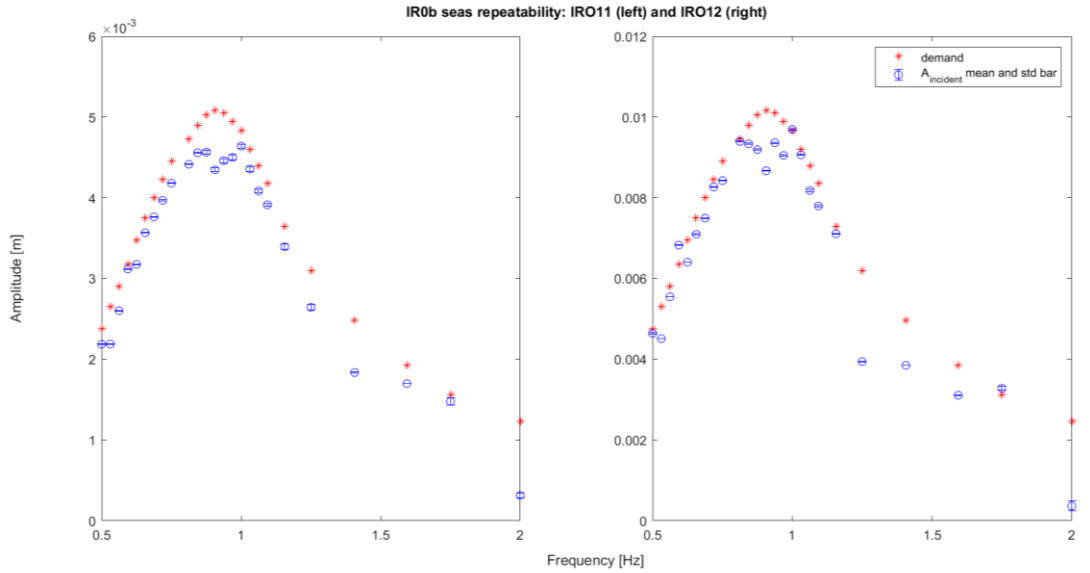

Figure 335 - Repeatability of IROb seas

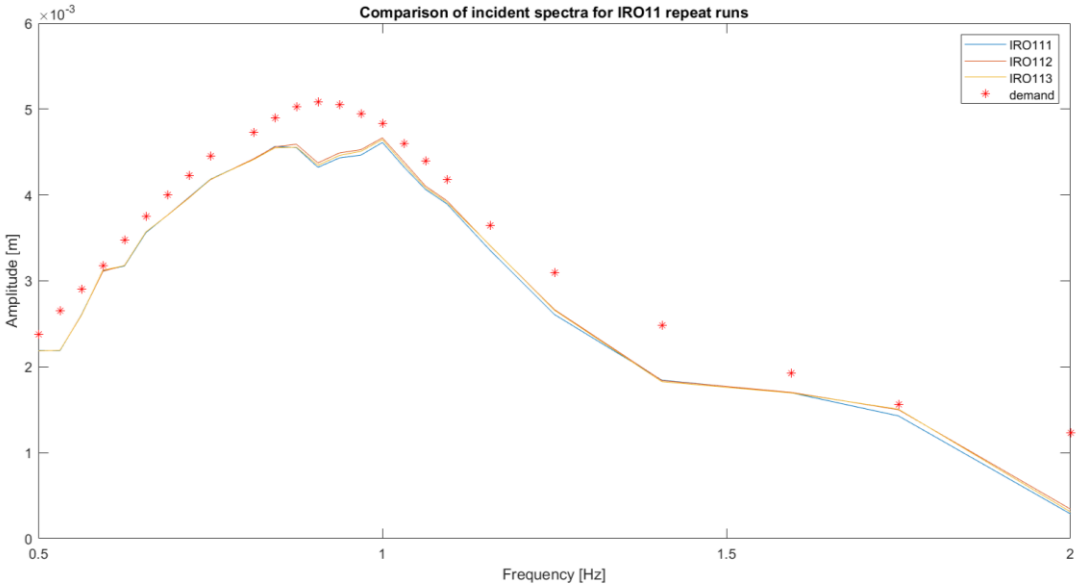

Figure 336 - Repeatability of IRO11 sea.

L.4.3 IROc (energy seas)

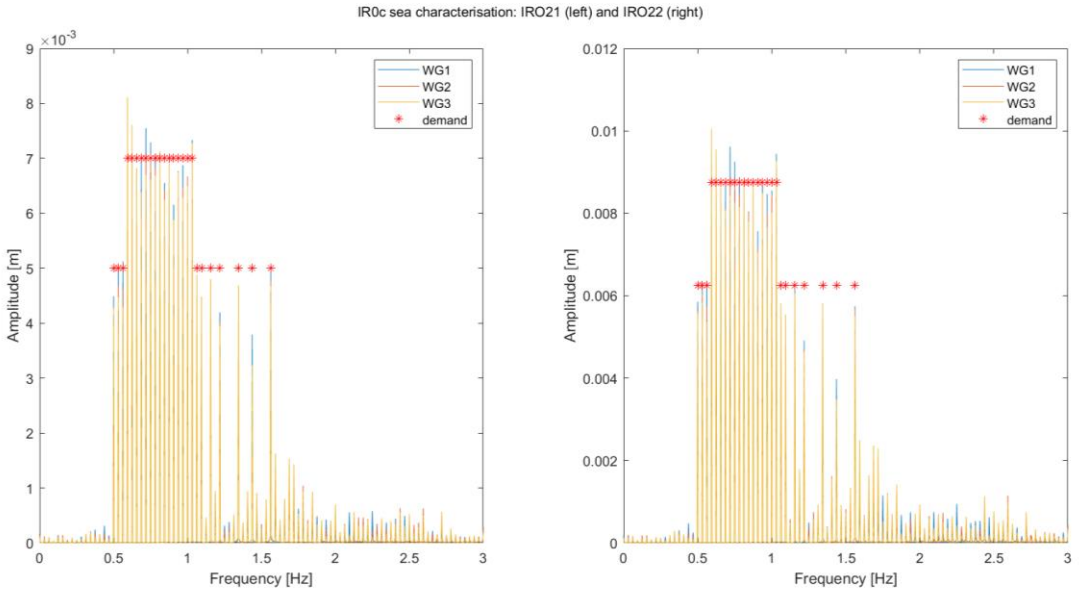

Figure 337 - Wave gauge (WG) measured amplitudes versus demand {IROc}.

Relatively more spilling is visible for IROc runs compared to IROa and IROb.

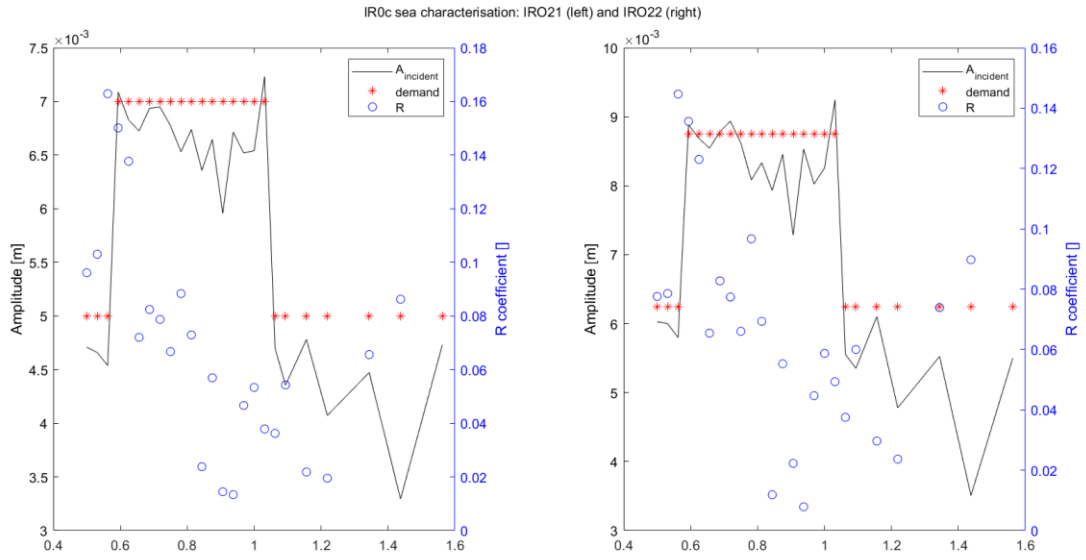

Figure 338 - Demand, incident amplitudes, and associated reflection coefficients {IROc}.

Incident wave amplitudes display greater differences to demand values in IROc runs.

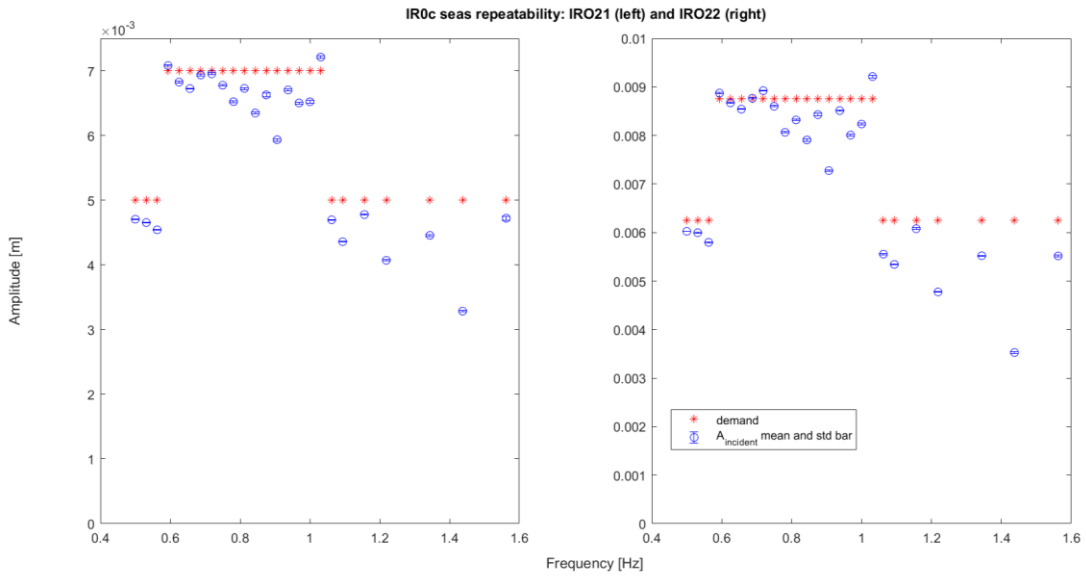

Figure 339 - Repeatability of IROc seas.

Consistency is still maintained for a particular seed number.

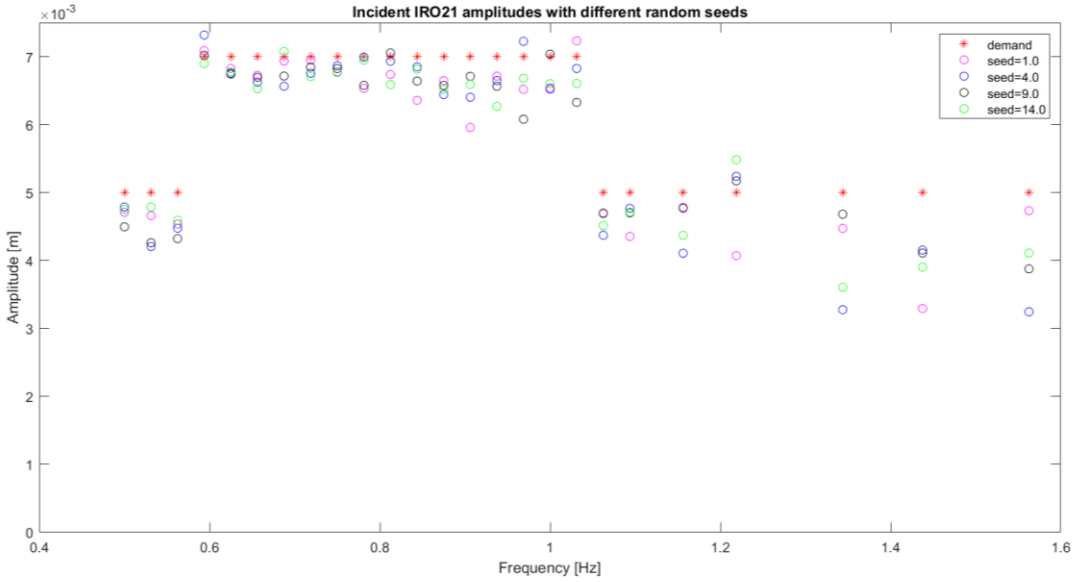

Figure 340 - Repeatability of IROd seas, showing each sea's amplitude components.

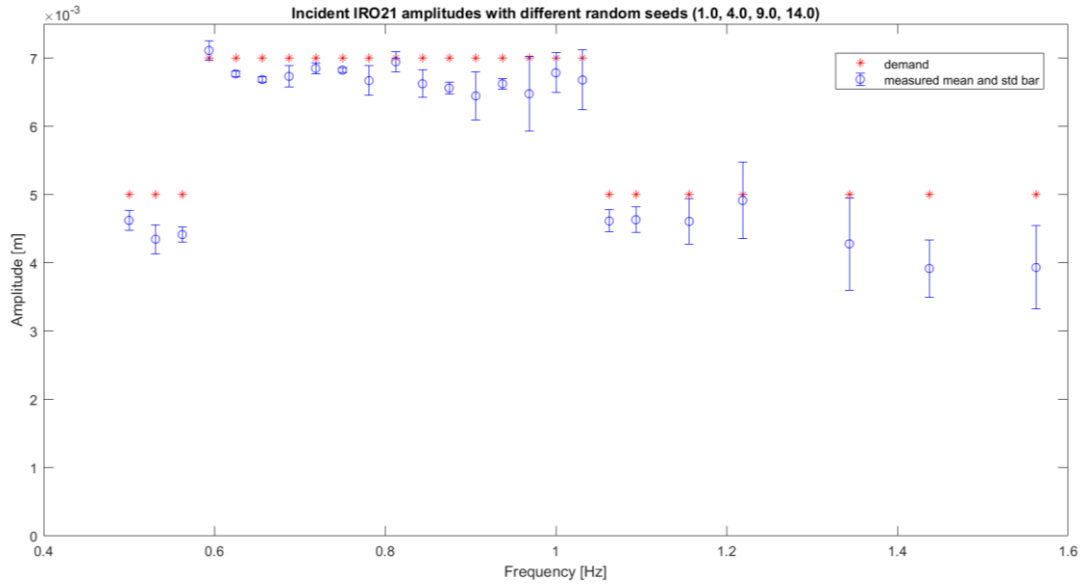

Figure 341 - Repeatability of IROd seas.

Variability with random seeds varies from 3.7131e-05 to 6.7554e-04 std across the individual frequency components.

L.5 Segmenting of individual Ir0 seas

The first run of both IRO01 and IRO02 is segmented in 8 parts, as per shortest repeat period possible of 32s within the overall repeat period of 256s.

Sea	Repeat	Segment	P_{mean}	P_{max}	$Flex_{mean}$	$\lvert Flex_{max} \rvert$	$\lvert Flex_{min} \rvert$
			W	*W*	*deg*	*deg*	*deg*
IRO01	1	1	0.0384	0.3454	4.065	13.792	11.508
	1	2	0.0386	0.3522	4.086	13.805	11.539
	1	3	0.0387	0.3484	4.095	13.868	11.566
	1	4	0.0387	0.3624	4.098	13.838	11.607
	1	5	0.0386	0.3561	4.091	13.847	11.638
	1	6	0.0385	0.3750	4.090	13.872	11.592
	1	7	0.0386	0.3585	4.089	13.914	11.579
	1	8	0.0386	0.3585	4.093	13.958	11.510
	1	TOT	0.0386	0.3750	4.088	13.958	11.638
	2	TOT	0.0388	0.3733	4.046	13.545	12.058
	3	TOT	0.0388	0.3678	4.044	13.524	12.020
IRO02	1	1	0.0679	0.5257	5.490	16.576	14.981
	1	2	0.0688	0.5572	5.507	16.460	15.139
	1	3	0.0703	0.6456	5.568	15.607	15.659
	1	4	0.0713	0.6624	5.603	16.828	15.794
	1	5	0.0714	0.6782	5.608	16.938	16.100
	1	6	0.0715	0.6322	5.616	16.963	16.000
	1	7	0.0717	0.6487	5.625	16.964	15.836
	1	8	0.0712	0.6393	5.611	16.905	15.961
	1	TOT	0.0706	0.6782	5.579	16.964	16.100
	2	TOT	0.0702	0.6550	5.570	17.010	15.935
	3	TOT	0.0701	0.6623	5.552	16.827	16.005

Table 56 – Segmented max and mean values of IROa seas.

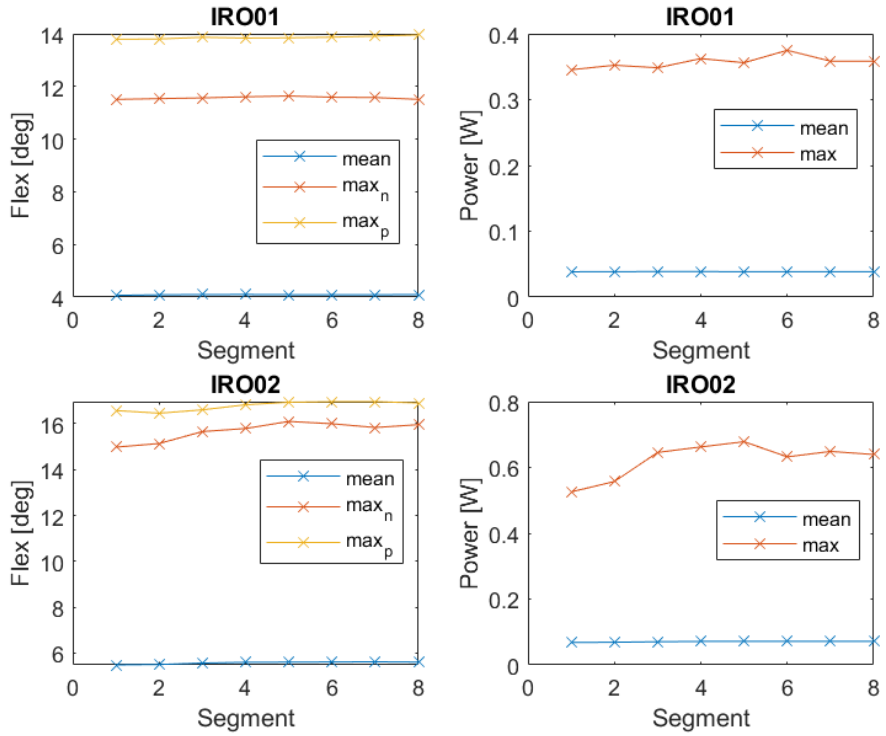

Figure 342 – Showing max positive (p) and negative (n) flex in degrees for different segments.

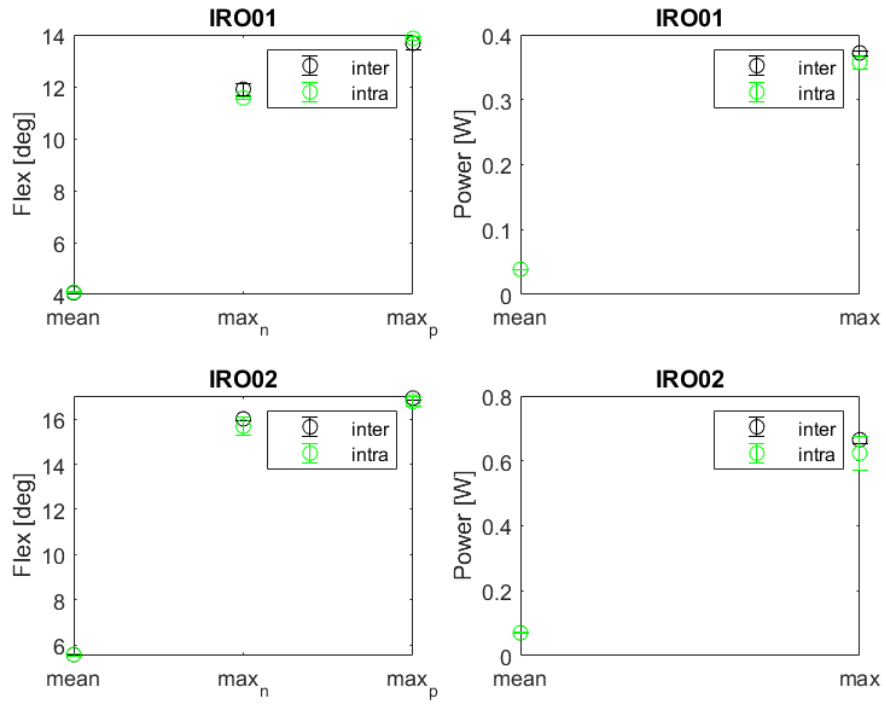

Figure 343 – Showing consistency of max flex angles within an Ir0 sea (intra) and between different repeats of the overall sea (inter).

Flex [deg], std	mean	max_n	max_p
IRO01 full	0.0250	0.2320	0.2448
IRO02 full	0.0135	0.0828	0.0953
IRO01 segments	0.0099	0.0462	0.0547
IRO02 segments	0.0524	0.4100	0.2017

Table 57 - Summary table for IROa intra and inter variability.

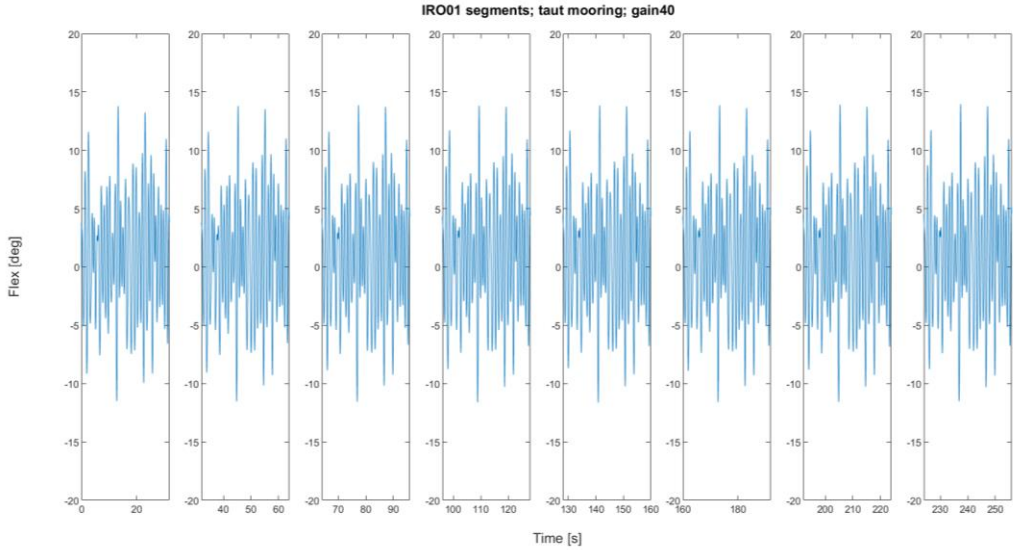

Figure 344 – Showing flex angles for individual segments in IRO01 sea; PTO gain 40.

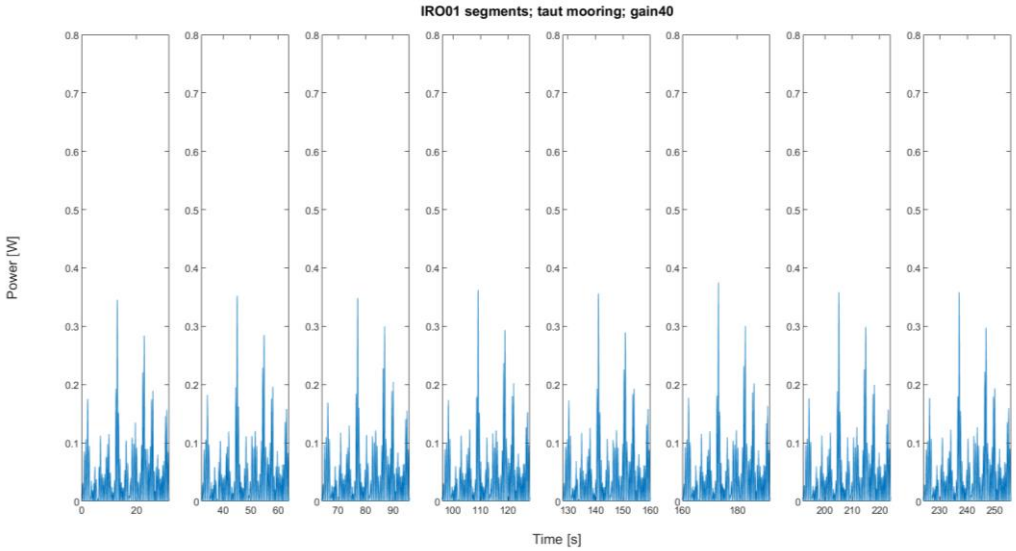

Figure 345 – Showing power signal for individual segments in IRO01 sea; PTO gain 40.

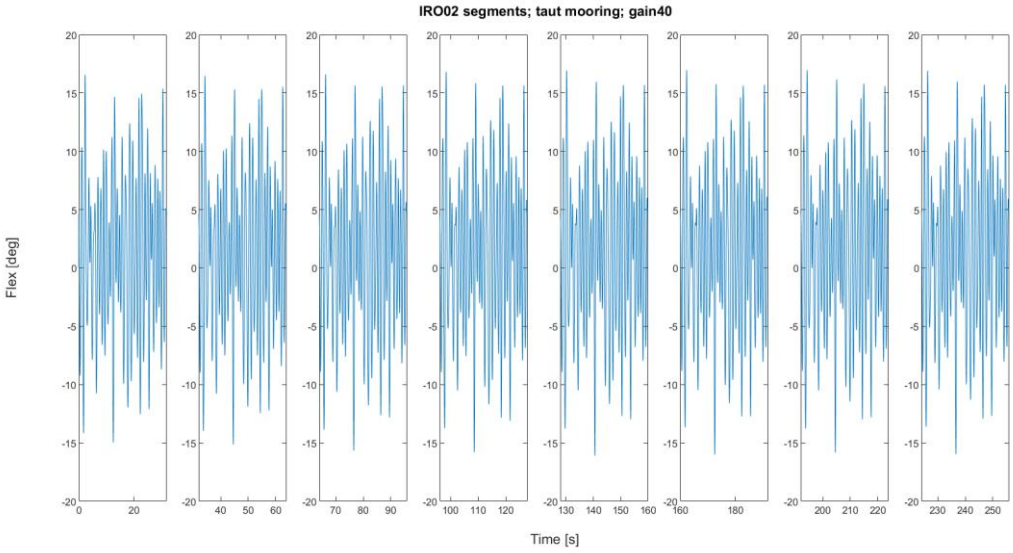

Figure 346 – Showing flex angles for individual segments in IRO02 sea; PTO gain 40

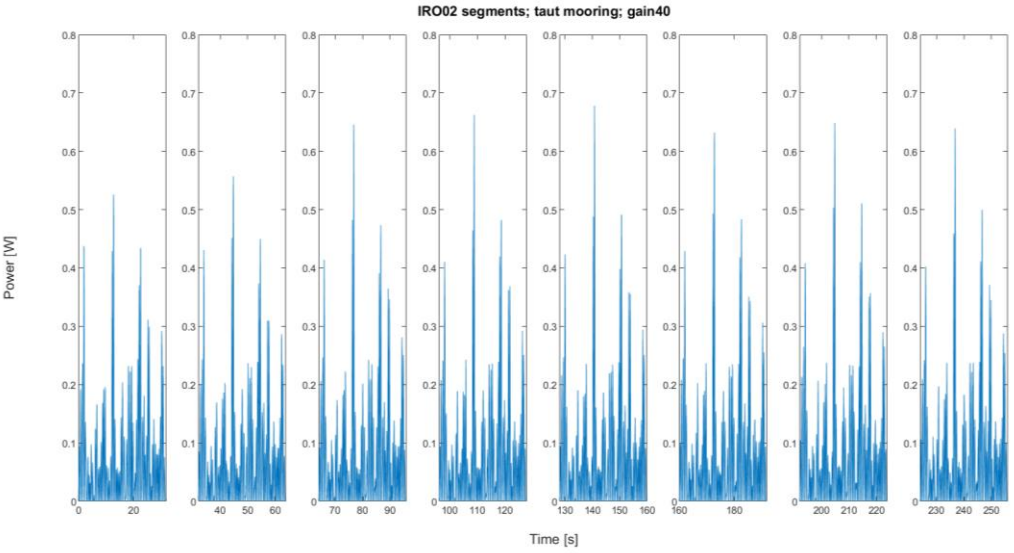

Figure 347 – Showing power signal for individual segments in IRO02 sea; PTO gain 40.

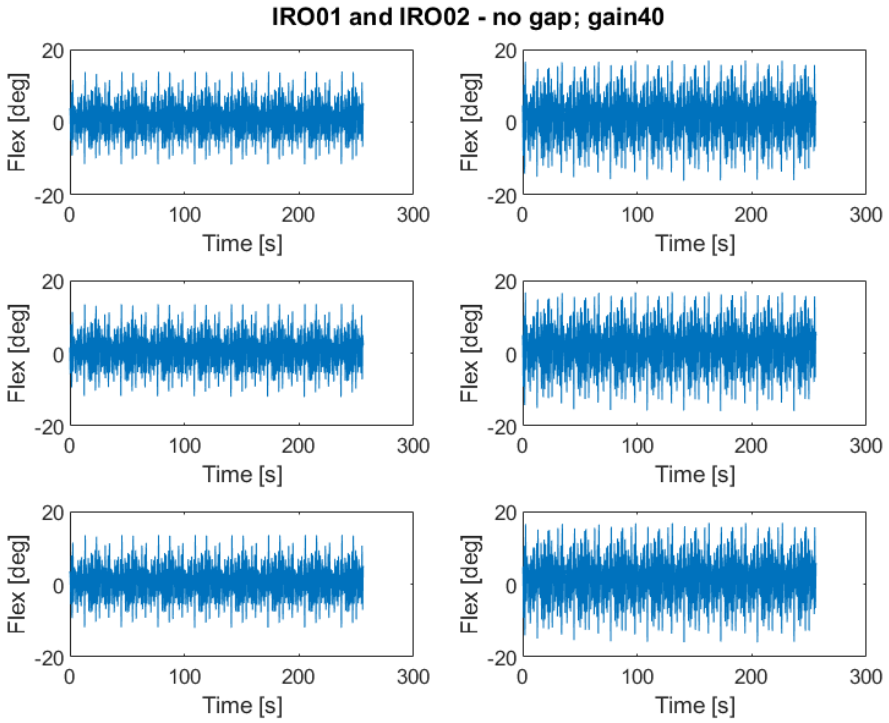

Figure 348 - Showing repeatability of IRO01 (left) and IRO02 (right) full run seas; flex.

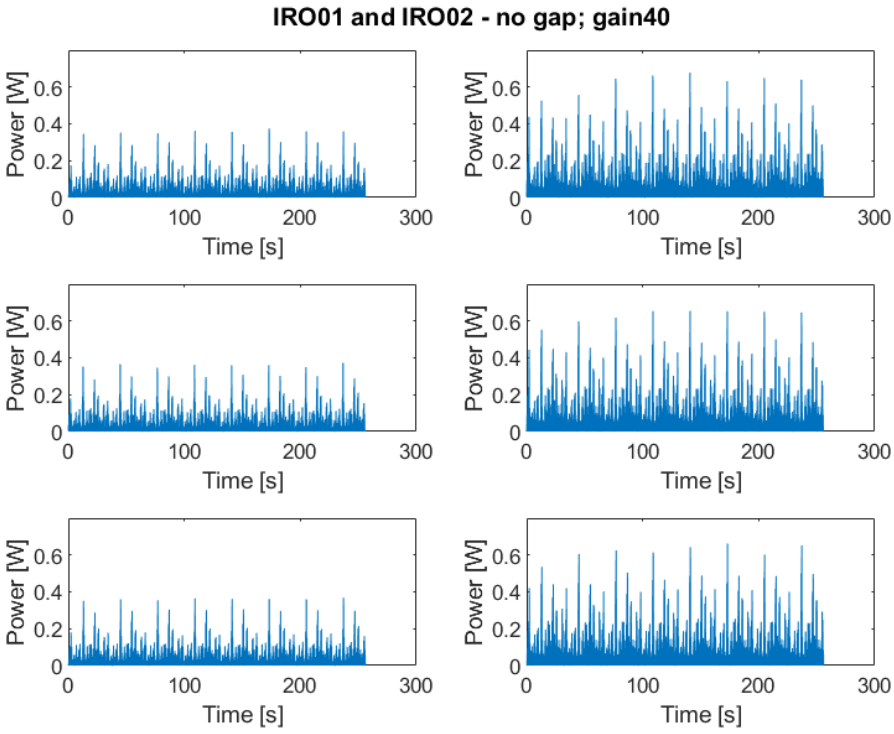

Figure 349 - Showing repeatability of IRO01 (left) and IRO02 (right) full run seas; power.

Appendix M – Mass properties

This Appendix gives supporting data for BST-folding 20th and 40th scale physical model mass matrices derived from CAD analysis. Mass matrices relate to ‘as-tested’, ‘gap’ and ‘no gap’ versions at each scale.

M.1 20th scale

20th scale	Gap			No Gap		
Dimensions [mm]	Length	Width	Height	Length	Width	Height
Overall	926.5	120	100	926.5	120	100
Trim line [mm above hinge axis]	36.0			35.0		
Mass [g]						
Fwd section	1,729.33			1,729.33		
Aft section	1,379.70			2,002.41		
Overall	3,109.03			3,731.74		
Centre of mass [mm]	x	y	z	x	y	Z
Fwd section	0.64	-61.69	114.01	0.64	-61.69	114.01
Aft section	-0.13	6.44	-238.20	-0.09	4.53	-275.55
Overall	0.30	-31.45	-42.29	0.25	-26.16	-95.02
Moments of inertia~ [g mm^2]						
Fwd section	x	y	z	x	y	Z
x	141506244	55338	-125898	141506244	55338	-125898
y	55338	57940155	-31913625	55338	57940155	-31913625
z	-125898	-31913625	86843289	-125898	-31913625	86843289
Aft section	x	y	z	x	y	z
X	114169543	103465	136253	194777113	103465	136255
Y	103465	115888026	-217979	103465	196926276	-250357
z	136253	-217979	5241542	136255	-250357	5829085
Overall	x	y	z	x	y	z
X	255675787	158803	10355	336283357	158803	10357
y	158803	173828181	-32131605	158803	254866431	-32163982
z	10355	-32131605	92084830	10357	-32163982	92672374

Table 58 - Summary properties of 20th scale models with and without gap (model scale).

M.2 40th scale

40th scale	Gap			No Gap		
Dimensions [mm]	Length	Width	Height	Length	Width	Height
Overall	463.25	60	50	463.25	60	50
Trim line [mm above hinge axis]	16.5			16.5		
Mass [g]						
Fwd section	204.84			204.84		
Aft section	164.33			245.75		
Overall	369.18			450.60		
Centre of mass [mm]	x	y	z	x	y	z
Fwd section	0.06	-0.42	59.68	0.06	-0.42	59.68
Aft section	0.09	5.60	-117.44	0.06	5.86	-135.53
Overall	0.07	2.26	-19.16	0.06	3.00	-46.79
Moments of inertia~ [g mm^2]						
Fwd section	x	y	z	x	y	Z
x	183226	963	-58	1832261	963	-58
y	963	1812121	-95859	963	1812121	-95859
z	697	-100997	122949	697	-100997	122949
Aft section	x	y	z	x	y	z
X	3201247	670	-4431	5654535	670	-4431
Y	670	3256032	-97574	670	5724971	-184485
z	-4431	-97574	116065	-4431	-184485	147360
Overall	x	y	z	x	y	z
X	5033509	1633	-3734	7486796	1633	-3734
y	1633	5068153	-198570	1633	7537092	-285482
z	-3734	-198570	239014	-3734	-285482	270309

Table 59 - Summary of properties of 40th scale model with and without gap (model scale).

Appendix N – Trimming

This Appendix presents supporting data used for the trimming of BST-folding 20th and 40th scale models. This includes both mass distributions and images. An analogous approach was utilised to trim the BST-baseline 20th scale model.

N.1 Trimming analysis

Each model is initially trimmed via CAD software based on a target mean water line (MWL) level. Before assembly, all components are weighed and CAD mass inputs updated to provide a more accurate representation of mass distribution. Appropriate masses/volumes and locations of any additional required ballast and/or buoyancy modules are then updated. This iterative process is ultimately validated by trimming the physical model in a trimming tank. It is considered robust if the real components and observations match those predicted by CAD, as was largely the case.

The aim is to have the centre of buoyancy vertically above the centre of gravity, in order to obtain level trim and roll stability. In addition, it is desirable to be able to trim each forward (FWD) and rear (AFT) section of the model independently. This was also successfully achieved. Detailed buoyancy and ballast component masses, dimensions, and locations are not included here. Note that when a ‘default’ configuration is referred to, this is the model version with all the various different materials included and is used to calculate centre of gravity and associated gravitational mass properties. The configuration ‘buoyancy’ is used to refer to the portion of the model below the MWL, with all components having the density of water, in order to calculate associated centre of buoyancy and related buoyancy mass properties. Note also that in all models, the origin is at the hinge axis midpoint.

N.1.1 20th model

MWL for 20th model with hull gap found at 36.0mm above hinge axis, and 35.0mm above hinge axis for configuration without hull gap.

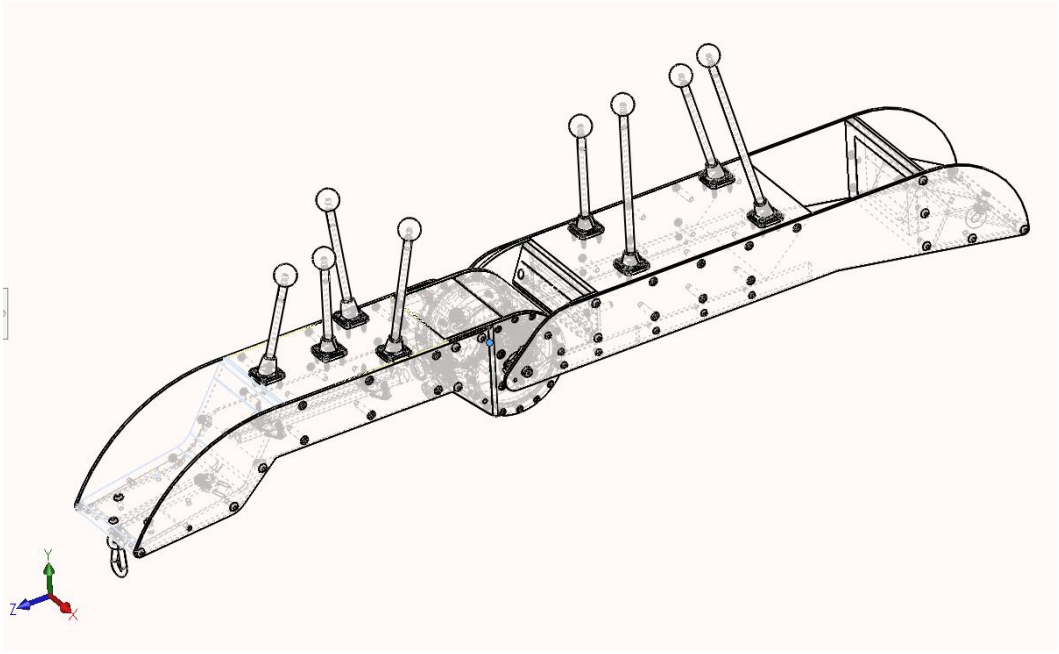

Figure 350 - Transparent assembly of 20th scale model, and global coordinate system.

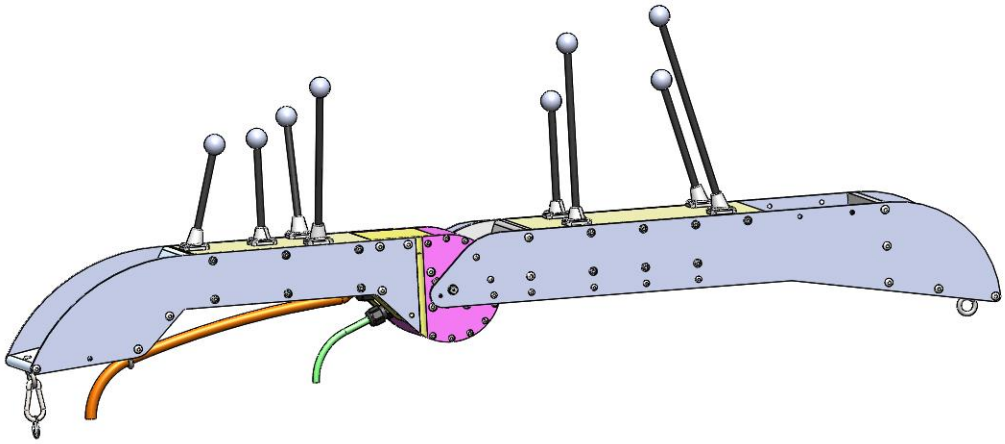

Figure 351 - Different view of 20th scale model, including part of the motor cables.

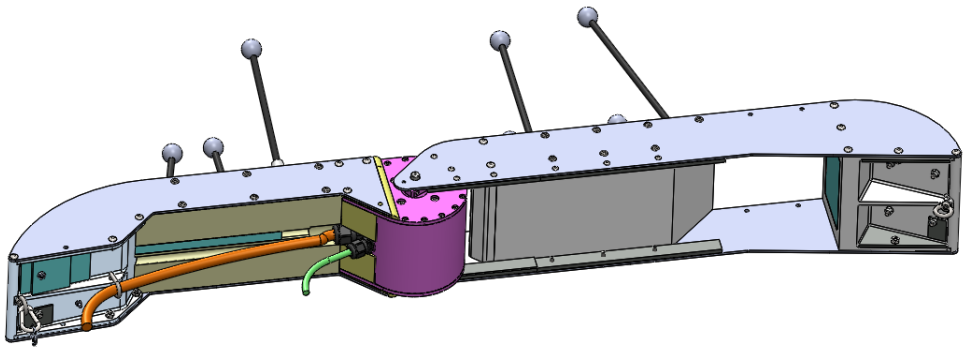

Figure 352 - Underside view, showing some buoyancy and ballast additions.

Compared to Figure 352, including the net mass of the power and feedback cables of the motor, and extending these all the way to the tank floor, was found to be required in order to account for the trimming requirements observed in practice also into the CAD model.

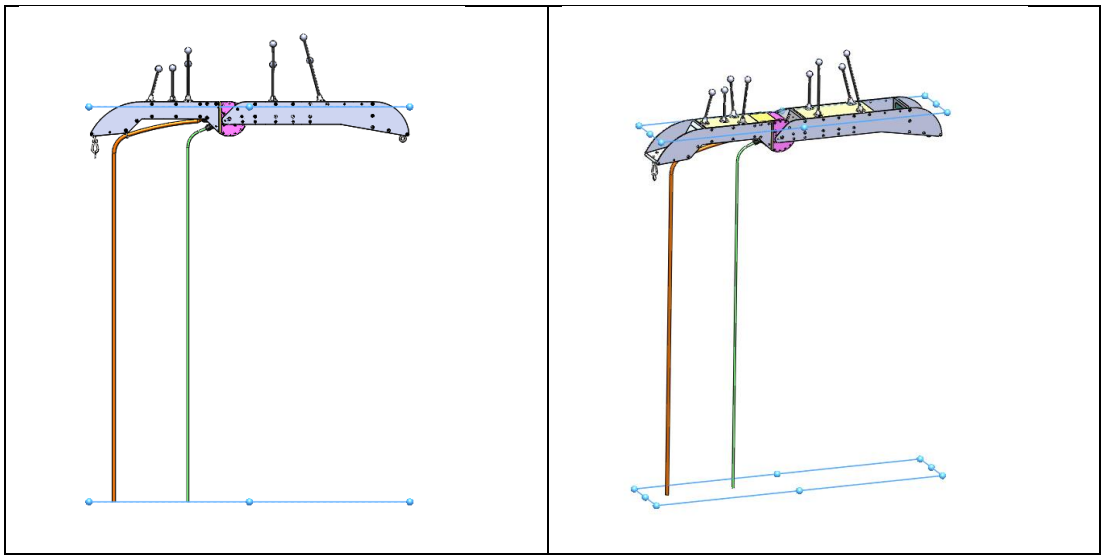

Table 60 - Images showing extended cables down to tank floor plane (blue rectangle).

The resulting individual section and overall model properties are given in the tables that follow.

FWD section properties:

Default	Buoyancy
Mass = 1729.33 grams Volume = 1749190.28 cubic millimeters Surface area = 567232.87 square millimeters Center of mass: (millimeters) X = 0.64 Y = -61.69 Z = 114.01 Principal axes of inertia and principal moments of inertia: (grams * square millimeters Taken at the center of mass. Ix = (0.00, 0.94, -0.35) Px = 27995391.68 Iy = (-0.01, 0.35, 0.94) Py = 87723615.90 Iz = (1.00, 0.00, 0.01) Pz = 112447222.14 Moments of inertia: (grams * square millimeters) Taken at the center of mass and aligned with the output coordinate system. Lxx = 112445227.41 Lxy = 123800.12 Lxz = -252431.46 Lyx = 123800.12 Lyy = 35459374.98 Lyz = -19750558.85 Lzx = -252431.46 Lzy = -19750558.85 Lzz = 80261627.33 Moments of inertia: (grams * square millimeters) Taken at the output coordinate system. Ixx = 141506244.28 Ixy = 55337.96 Ixz = -125898.05 Iyx = 55337.96 Iyy = 57940155.12 Iyz = -31913625.05 Izx = -125898.05 Izy = -31913625.05 Izz = 86843288.50	Mass = 1747.10 grams Volume = 1747098.43 cubic millimeters Surface area = 461797.73 square millimeters Center of mass: (millimeters) X = 0.18 Y = -33.68 Z = 117.57 Principal axes of inertia and principal moments of inertia: (grams * square millimeters Taken at the center of mass. Ix = (0.00, 0.93, -0.36) Px = 22056351.90 Iy = (0.00, 0.36, 0.93) Py = 53753294.45 Iz = (1.00, 0.00, 0.00) Pz = 73105830.73 Moments of inertia: (grams * square millimeters) Taken at the center of mass and aligned with the output coordinate system. Lxx = 73105636.84 Lxy = 464.72 Lxz = 63824.04 Lyx = 464.72 Lyy = 26241896.33 Lyz = -10730827.98 Lzx = 63824.04 Lzy = -10730827.98 Lzz = 49567943.91 Moments of inertia: (grams * square millimeters) Taken at the output coordinate system. Ixx = 99238351.28 Ixy = -10002.45 Ixz = 100358.34 Iyx = -10002.45 Iyy = 50392316.81 Iyz = -17649965.05 Izx = 100358.34 Izy = -17649965.05 Izz = 51550348.40

Table 61 - Summary of trimming properties for 20th scale FWD section.

Appendix N

AFT section properties:

Default	Buoyancy
Mass = 1379.70 grams Volume = 1827575.09 cubic millimeters Surface area = 457043.32 square millimeters Center of mass: (millimeters) X = -0.13 Y = 6.44 Z = -238.20 Principal axes of inertia and principal moments of inertia: (grams * square millimete Taken at the center of mass. Ix = (0.00, 0.06, 1.00) Px = 5072909.96 Iy = (1.00, 0.05, -0.01) Py = 35825342.22 Iz = (-0.05, 1.00, -0.06) Pz = 37722129.79 Moments of inertia: (grams * square millimeters) Taken at the center of mass and aligned with the output coordinate system. Lxx = 35830202.01 Lxy = 104623.44 Lxz = 93444.75 Lyx = 104623.44 Lyy = 37605971.11 Lyz = 1900107.83 Lzx = 93444.75 Lzy = 1900107.83 Lzz = 5184208.84 Moments of inertia: (grams * square millimeters) Taken at the output coordinate system. Ixx = 114169542.82 Ixy = 103465.17 Ixz = 136253.18 Iyx = 103465.17 Iyy = 115888025.96 Iyz = -217979.51 Izx = 136253.18 Izy = -217979.51 Izz = 5241541.62	Mass = 1360.63 grams Volume = 1360626.63 cubic millimeters Surface area = 365758.90 square millimeters Center of mass: (millimeters) X = -0.05 Y = 10.97 Z = -232.15 Principal axes of inertia and principal moments of inertia: (grams * square millimeters Taken at the center of mass. Ix = (0.00, 0.06, 1.00) Px = 2334538.74 Iy = (1.00, 0.00, 0.00) Py = 24974775.95 Iz = (0.00, 1.00, -0.06) Pz = 26664223.87 Moments of inertia: (grams * square millimeters) Taken at the center of mass and aligned with the output coordinate system. Lxx = 24974777.28 Lxy = 2795.67 Lxz = 6530.33 Lyx = 2795.67 Lyy = 26561522.05 Lyz = 1577363.31 Lzx = 6530.33 Lzy = 1577363.31 Lzz = 2437239.24 Moments of inertia: (grams * square millimeters) Taken at the output coordinate system. Ixx = 98468602.15 Ixy = 2106.93 Ixz = 21102.06 Iyx = 2106.93 Iyy = 99891528.48 Iyz = -1888616.76 Izx = 21102.06 Izy = -1888616.76 Izz = 2601063.45

Table 62 - Summary of trimming properties for 20th scale AFT section.

Overall model properties:

Default	Buoyancy
Mass = 3109.03 grams Volume = 3576765.37 cubic millimeters Surface area = 1024276.19 square millimeters Center of mass: (millimeters) X = 0.30 Y = -31.45 Z = -42.29 Principal axes of inertia and principal moments of inertia: (grams * square millimeters) Taken at the center of mass. Ix = (0.00, -0.36, 0.93) Px = 74918925.45 Iy = (0.00, -0.93, -0.36) Py = 182357521.72 Iz = (1.00, 0.00, 0.00) Pz = 247040940.22 Moments of inertia: (grams * square millimeters) Taken at the center of mass and aligned with the output coordinate system. Lxx = 247040359.89 Lxy = 188056.93 Lxz = 49686.21 Lyx = 188056.93 Lyy = 168268186.83 Lyz = -36266828.96 Lzx = 49686.21 Lzy = -36266828.96 Lzz = 89008840.68 Moments of inertia: (grams * square millimeters) Taken at the output coordinate system. Ixx = 255675787.11 Ixy = 158803.12 Ixz = 10355.12 Iyx = 158803.12 Iyy = 173828181.08 Iyz = -32131604.56 Izx = 10355.12 Izy = -32131604.56 Izz = 92084830.12	Mass = 3107.73 grams Volume = 3107725.06 cubic millimeters Surface area = 827556.63 square millimeters Center of mass: (millimeters) X = 0.08 Y = -14.13 Z = -35.54 Principal axes of inertia and principal moments of inertia: (grams * square millimeters) Taken at the center of mass. Ix = (0.00, -0.21, 0.98) Px = 48959642.73 Iy = (0.00, -0.98, -0.21) Py = 150928441.98 Iz = (1.00, 0.00, 0.00) Pz = 193160074.38 Moments of inertia: (grams * square millimeters) Taken at the center of mass and aligned with the output coordinate system. Lxx = 193159947.47 Lxy = -4391.00 Lxz = 130274.40 Lyx = -4391.00 Lyy = 146357533.81 Lyz = -21099704.87 Lzx = 130274.40 Lzy = -21099704.87 Lzz = 53530677.81 Moments of inertia: (grams * square millimeters) Taken at the output coordinate system. Ixx = 197706953.42 Ixy = -7895.51 Ixz = 121460.40 Iyx = -7895.51 Iyy = 150283845.29 Iyz = -19538581.80 Izx = 121460.40 Izy = -19538581.80 Izz = 54151411.85

Table 63 - Summary of trimming properties for 20th scale overall model.

N.1.1.1 20th model without hull gap

For this configuration, the hull gap is ‘plugged’, or filled in, with a dedicated subassembly made of Divinycell, 3D print ABS, and Lead sheets – see Table 64.

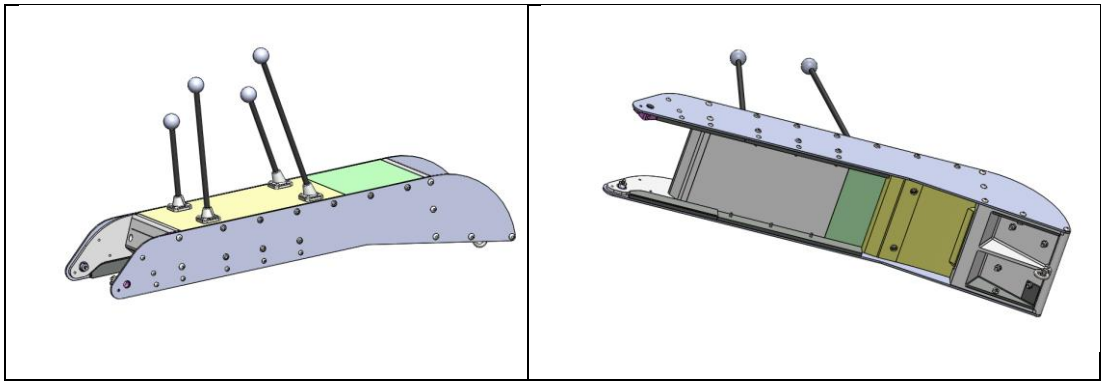

Table 64 - Showing two views of the AFT section including the hull 'filler' subassembly (green and yellow on underside).

Updated mass matrix and trimming properties for this configuration are given in the tables that follow.

Updated FWD section:

Default	Buoyancy
Mass = 1729.33 grams Volume = 1749190.28 cubic millimeters Surface area = 567232.87 square millimeters Center of mass: (millimeters) X = 0.64 Y = -61.69 Z = 114.01 Principal axes of inertia and principal moments of inertia: (grams * square millimeters Taken at the center of mass. Ix = (0.00, 0.94, -0.35) Px = 27995391.68 Iy = (-0.01, 0.35, 0.94) Py = 87723615.90 Iz = (1.00, 0.00, 0.01) Pz = 112447222.14 Moments of inertia: (grams * square millimeters) Taken at the center of mass and aligned with the output coordinate system. Lxx = 112445227.41 Lxy = 123800.12 Lxz = -252431.46 Lyx = 123800.12 Lyy = 35459374.98 Lyz = -19750558.85 Lzx = -252431.46 Lzy = -19750558.85 Lzz = 80261627.33 Moments of inertia: (grams * square millimeters) Taken at the output coordinate system. Ixx = 141506244.28 Ixy = 55337.96 Ixz = -125898.05 Iyx = 55337.96 Iyy = 57940155.12 Iyz = -31913625.05 Izx = -125898.05 Izy = -31913625.05 Izz = 86843288.50	Mass = 1718.22 grams Volume = 1718223.08 cubic millimeters Surface area = 457334.00 square millimeters Center of mass: (millimeters) X = 0.18 Y = -34.85 Z = 117.62 Principal axes of inertia and principal moments of inertia: (grams * square millimeters Taken at the center of mass. Ix = (0.00, 0.93, -0.36) Px = 21837012.44 Iy = (0.00, 0.36, 0.93) Py = 53576151.78 Iz = (1.00, 0.00, 0.00) Pz = 72756913.36 Moments of inertia: (grams * square millimeters) Taken at the center of mass and aligned with the output coordinate system. Lxx = 72756717.30 Lxy = 826.34 Lxz = 63808.65 Lyx = 826.34 Lyy = 26009732.93 Lyz = -10725085.87 Lzx = 63808.65 Lzy = -10725085.87 Lzz = 49403627.35 Moments of inertia: (grams * square millimeters) Taken at the output coordinate system. Ixx = 98613628.20 Ixy = -10002.29 Ixz = 100358.34 Iyx = -10002.29 Iyy = 49780206.57 Iyz = -17767586.89 Izx = 100358.34 Izy = -17767586.89 Izz = 51490177.01

Table 65 - Summary of trimming properties for 20th scale FWD section without hull gap.

Updated AFT section:

Default	Buoyancy
Mass = 2000.01 grams Volume = 2698158.57 cubic millimeters Surface area = 560085.38 square millimeters Center of mass: (millimeters) X = -0.09 Y = 4.52 Z = -275.39 Principal axes of inertia and principal moments of inertia: (grams * square millimeter Taken at the center of mass. Ix = (0.00, 0.06, 1.00) Px = 5656487.95 Iy = (1.00, 0.04, 0.00) Py = 42642660.28 Iz = (-0.04, 1.00, -0.06) Pz = 44969500.78 Moments of inertia: (grams * square millimeters) Taken at the center of mass and aligned with the output coordinate system. Lxx = 42646659.73 Lxy = 104277.52 Lxz = 86761.97 Lyx = 104277.52 Lyy = 44836178.20 Lyz = 2248939.54 Lzx = 86761.97 Lzy = 2248939.54 Lzz = 5785811.08 Moments of inertia: (grams * square millimeters) Taken at the output coordinate system. Ixx = 194363310.48 Ixy = 103465.23 Ixz = 136254.70 Iyx = 103465.23 Iyy = 196511989.16 Iyz = -240408.95 Izx = 136254.70 Izy = -240408.95 Izz = 5826683.16	Mass = 2002.95 grams Volume = 2002954.82 cubic millimeters Surface area = 457973.35 square millimeters Center of mass: (millimeters) X = -0.03 Y = 11.37 Z = -270.02 Principal axes of inertia and principal moments of inertia: (grams * square millimeter Taken at the center of mass. Ix = (0.00, 0.05, 1.00) Px = 3155726.51 Iy = (1.00, 0.00, 0.00) Py = 31285984.60 Iz = (0.00, 1.00, -0.05) Pz = 33555908.24 Moments of inertia: (grams * square millimeters) Taken at the center of mass and aligned with the output coordinate system. Lxx = 31285986.98 Lxy = 2821.57 Lxz = 4160.69 Lyx = 2821.57 Lyy = 33488879.69 Lyz = 1425866.49 Lzx = 4160.69 Lzy = 1425866.49 Lzz = 3222752.68 Moments of inertia: (grams * square millimeters) Taken at the output coordinate system. Ixx = 177577647.20 Ixy = 2108.04 Ixz = 21102.14 Iyx = 2108.04 Iyy = 179521495.44 Iyz = -4724680.53 Izx = 21102.14 Izy = -4724680.53 Izz = 3481801.09

Table 66 - trimming properties for 20th scale AFT section without hull gap.

Updated Overall:

Default	Buoyancy
Mass = 3729.34 grams Volume = 4447348.85 cubic millimeters Surface area = 1127318.25 square millimeters Center of mass: (millimeters) X = 0.25 Y = -26.18 Z = -94.82 Principal axes of inertia and principal moments of inertia: (grams * square millimeter Taken at the center of mass. Ix = (0.00, -0.28, 0.96) Px = 78105367.26 Iy = (0.00, -0.96, -0.28) Py = 232931143.39 Iz = (1.00, 0.00, 0.00) Pz = 299785667.65 Moments of inertia: (grams * square millimeters) Taken at the center of mass and aligned with the output coordinate system. Lxx = 299785040.51 Lxy = 183154.26 Lxz = 98544.49 Lyx = 183154.26 Lyy = 220923793.35 Lyz = -41412064.31 Lzx = 98544.49 Lzy = -41412064.31 Lzz = 90113344.43 Moments of inertia: (grams * square millimeters) Taken at the output coordinate system. Ixx = 335869554.76 Ixy = 158803.18 Ixz = 10356.65 Iyx = 158803.18 Iyy = 254452144.28 Iyz = -32154034.00 Izx = 10356.65 Izy = -32154034.00 Izz = 92669971.67	Mass = 3721.18 grams Volume = 3721177.90 cubic millimeters Surface area = 915307.35 square millimeters Center of mass: (millimeters) X = 0.07 Y = -9.97 Z = -91.03 Principal axes of inertia and principal moments of inertia: (grams * square millimeters Taken at the center of mass. Ix = (0.00, -0.17, 0.99) Px = 50091765.27 Iy = (0.00, -0.99, -0.17) Py = 202977527.04 Iz = (1.00, 0.00, 0.00) Pz = 244987147.93 Moments of inertia: (grams * square millimeters) Taken at the center of mass and aligned with the output coordinate system. Lxx = 244987034.30 Lxy = -5421.88 Lxz = 144035.86 Lyx = -5421.88 Lyy = 198467268.52 Lyz = -25869146.41 Lzx = 144035.86 Lzy = -25869146.41 Lzz = 54602137.43 Moments of inertia: (grams * square millimeters) Taken at the output coordinate system. Ixx = 276191275.40 Ixy = -7894.25 Ixz = 121460.48 Iyx = -7894.25 Iyy = 229301702.01 Iyz = -22492267.42 Izx = 121460.48 Izy = -22492267.42 Izz = 54971978.10

Table 67 - Summary of trimming properties for 20th scale overall model without hull gap.

N.1.2 40th model

The 40th model is successfully trimmed at a target MWL of 16.5mm above the hinge axis, in both ‘gap’ and ‘no gap’ configurations.

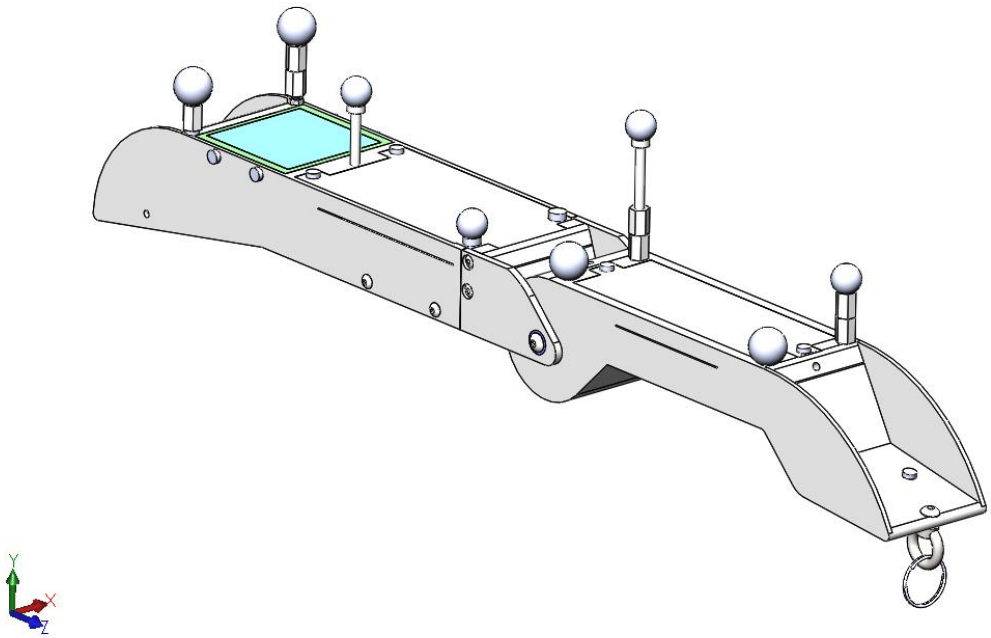

Figure 353 – Showing 40th scale model with the aft hull gap filled in (green and blue components).

For the FWD section:

Default	Buoyancy
Mass = 204.84 grams Volume = 277498.21 cubic millimeters Surface area = 92344.37 square millimeters Center of mass: (millimeters) X = 0.06 Y = -0.42 Z = 59.68 Principal axes of inertia and principal moments of inertia: (grams * square millimet Taken at the center of mass. Ix = (0.00, -0.10, 1.00) Px = 113429.41 Iy = (-0.09, -0.99, -0.10) Py = 1091899.41 Iz = (1.00, -0.09, -0.01) Pz = 1102693.13 Moments of inertia: (grams * square millimeters) Taken at the center of mass and aligned with the output coordinate system. Lxx = 1102607.45 Lxy = 968.10 Lxz = -57.69 Lyx = 968.10 Lyy = 1082502.80 Lyz = -95859.30 Lzx = -57.69 Lzy = -95859.30 Lzz = 122911.69 Moments of inertia: (grams * square millimeters) Taken at the output coordinate system. Ixx = 1832261.21 Ixy = 962.79 Ixz = 696.85 Iyx = 962.79 Iyy = 1812121.17 Iyz = -100996.54 Izx = 696.85 Izy = -100996.54 Izz = 122948.65	Mass = 209.10 grams Volume = 209104.07 cubic millimeters Surface area = 68511.68 square millimeters Center of mass: (millimeters) X = 0.02 Y = 0.85 Z = 56.45 Principal axes of inertia and principal moments of inertia: (grams * square millimet Taken at the center of mass. Ix = (0.00, -0.02, 1.00) Px = 72662.68 Iy = (1.00, 0.00, 0.00) Py = 798562.10 Iz = (0.00, 1.00, 0.02) Pz = 818062.34 Moments of inertia: (grams * square millimeters) Taken at the center of mass and aligned with the output coordinate system. Lxx = 798562.13 Lxy = -87.60 Lxz = 466.64 Lyx = -87.60 Lyy = 817860.01 Lyz = -12269.01 Lzx = 466.64 Lzy = -12269.01 Lzz = 72864.98 Moments of inertia: (grams * square millimeters) Taken at the output coordinate system. Ixx = 1465012.78 Ixy = -84.43 Ixz = 678.18 Iyx = -84.43 Iyy = 1484160.68 Iyz = -2270.03 Izx = 678.18 Izy = -2270.03 Izz = 73015.10

Table 68 - Summary of trimming properties for 40th scale FWD section.

For the AFT section:

Default	Buoyancy
Mass = 164.33 grams Volume = 242333.38 cubic millimeters Surface area = 119884.88 square millimeters Center of mass: (millimeters) X = 0.09 Y = 5.60 Z = -117.44 Principal axes of inertia and principal moments of inertia: (grams * square millimet Taken at the center of mass. Ix = (0.00, 0.01, 1.00) Px = 110773.59 Iy = (1.00, 0.01, 0.00) Py = 929415.06 Iz = (-0.01, 1.00, -0.01) Pz = 989483.47 Moments of inertia: (grams * square millimeters) Taken at the center of mass and aligned with the output coordinate system. Lxx = 929412.79 Lxy = 585.85 Lxz = -2664.53 Lyx = 585.85 Lyy = 989351.00 Lyz = 10525.93 Lzx = -2664.53 Lzy = 10525.93 Lzz = 110908.32 Moments of inertia: (grams * square millimeters) Taken at the output coordinate system. Ixx = 3201247.43 Ixy = 670.08 Ixz = -4430.71 Iyx = 670.08 Iyy = 3256031.67 Iyz = -97573.74 Izx = -4430.71 Izy = -97573.74 Izz = 116065.05	Mass = 169.72 grams Volume = 169603.95 cubic millimeters Surface area = 87203.21 square millimeters Center of mass: (millimeters) X = 0.22 Y = 4.13 Z = -122.48 Principal axes of inertia and principal moments of inertia: (grams * square millimet Taken at the center of mass. Ix = (-0.01, 0.07, 1.00) Px = 72482.09 Iy = (1.00, -0.01, 0.01) Py = 842849.10 Iz = (0.01, 1.00, -0.07) Pz = 896243.43 Moments of inertia: (grams * square millimeters) Taken at the center of mass and aligned with the output coordinate system. Lxx = 842833.41 Lxy = -837.43 Lxz = -4034.73 Lyx = -837.43 Lyy = 892482.72 Lyz = 55487.24 Lzx = -4034.73 Lzy = 55487.24 Lzz = 76258.49 Moments of inertia: (grams * square millimeters) Taken at the output coordinate system. Ixx = 3391905.79 Ixy = -684.42 Ixz = -8575.53 Iyx = -684.42 Iyy = 3438671.97 Iyz = -30312.37 Izx = -8575.53 Izy = -30312.37 Izz = 79157.81

Table 69 – Summary of trimming properties for 40th scale AFT section.

For the Overall model:

Default	Buoyancy
Mass = 369.18 grams Volume = 519831.59 cubic millimeters Surface area = 212229.25 square millimeters Center of mass: (millimeters) X = 0.07 Y = 2.26 Z = -19.16 Principal axes of inertia and principal moments of inertia: (grams * square millime Taken at the center of mass. Ix = (0.00, -0.04, 1.00) Px = 230034.76 Iy = (1.00, 0.03, 0.00) Py = 4895996.25 Iz = (-0.03, 1.00, 0.04) Pz = 4939706.30 Moments of inertia: (grams * square millimeters) Taken at the center of mass and aligned with the output coordinate system. Lxx = 4896041.78 Lxy = 1570.31 Lxz = -3203.38 Lyx = 1570.31 Lyy = 4932569.59 Lyz = -182580.77 Lzx = -3203.38 Lzy = -182580.77 Lzz = 237125.93 Moments of inertia: (grams * square millimeters) Taken at the output coordinate system. Ixx = 5033508.64 Ixy = 1632.87 Ixz = -3733.86 Iyx = 1632.87 Iyy = 5068152.84 Iyz = -198570.27 Izx = -3733.86 Izy = -198570.27 Izz = 239013.70	Mass = 378.83 grams Volume = 378708.02 cubic millimeters Surface area = 155714.88 square millimeters Center of mass: (millimeters) X = 0.11 Y = 2.32 Z = -23.72 Principal axes of inertia and principal moments of inertia: (grams * square millime Taken at the center of mass. Ix = (0.00, 0.00, 1.00) Px = 150094.21 Iy = (1.00, -0.01, 0.00) Py = 4641802.04 Iz = (0.01, 1.00, 0.00) Pz = 4709787.52 Moments of inertia: (grams * square millimeters) Taken at the center of mass and aligned with the output coordinate system. Lxx = 4641802.78 Lxy = -863.42 Lxz = -6929.23 Lyx = -863.42 Lyy = 4709745.72 Lyz = -11767.72 Lzx = -6929.23 Lzy = -11767.72 Lzz = 150135.26 Moments of inertia: (grams * square millimeters) Taken at the output coordinate system. Ixx = 4856918.57 Ixy = -768.85 Ixz = -7897.35 Iyx = -768.85 Iyy = 4922832.66 Iyz = -32582.40 Izx = -7897.35 Izy = -32582.40 Izz = 152172.92

Table 70 - Summary of trimming properties for overall 40th scale model with hull gap.

N.1.2.1 40th model without hull gap

The additional subassembly to fill in the AFT hull gap is now added, and updated mass properties are summarised in the below tables. The achieved trimming line does not vary.

Updated AFT section:

Default	Buoyancy
Mass = 245.75 grams Volume = 350762.76 cubic millimeters Surface area = 145579.33 square millimeters Center of mass: (millimeters) X = 0.06 Y = 5.86 Z = -135.53 Principal axes of inertia and principal moments of inertia: (grams * square millimet Taken at the center of mass. Ix = (0.00, 0.01, 1.00) Px = 138808.14 Iy = (1.00, 0.01, 0.00) Py = 1132129.58 Iz = (-0.01, 1.00, -0.01) Pz = 1211114.03 Moments of inertia: (grams * square millimeters) Taken at the center of mass and aligned with the output coordinate system. Lxx = 1132128.49 Lxy = 581.96 Lxz = -2392.56 Lyx = 581.96 Lyy = 1211002.82 Lyz = 10689.18 Lzx = -2392.56 Lzy = 10689.18 Lzz = 138920.44 Moments of inertia: (grams * square millimeters) Taken at the output coordinate system. Ixx = 5654534.90 Ixy = 670.08 Ixz = -4430.71 Iyx = 670.08 Iyy = 5724971.20 Iyz = -184485.49 Izx = -4430.71 Izy = -184485.49 Izz = 147360.31	Mass = 250.27 grams Volume = 250150.31 cubic millimeters Surface area = 107118.89 square millimeters Center of mass: (millimeters) X = 0.15 Y = 4.65 Z = -138.72 Principal axes of inertia and principal moments of inertia: (grams * square millimet Taken at the center of mass. Ix = (0.00, 0.05, 1.00) Px = 97753.59 Iy = (1.00, -0.01, 0.00) Py = 1018718.89 Iz = (0.01, 1.00, -0.05) Pz = 1088963.87 Moments of inertia: (grams * square millimeters) Taken at the center of mass and aligned with the output coordinate system. Lxx = 1018712.21 Lxy = -856.75 Lxz = -3432.90 Lyx = -856.75 Lyy = 1086128.62 Lyz = 52876.17 Lzx = -3432.90 Lzy = 52876.17 Lzz = 100595.51 Moments of inertia: (grams * square millimeters) Taken at the output coordinate system. Ixx = 5839825.73 Ixy = -684.42 Ixz = -8575.53 Iyx = -684.42 Iyy = 5901840.01 Iyz = -108497.73 Izx = -8575.53 Izy = -108497.73 Izz = 106008.62

Table 71 - Summary of trimming properties for the 40th scale AFT section without hull gap.

Updated Overall:

Default	Buoyancy
Mass = 450.60 grams Volume = 628260.96 cubic millimeters Surface area = 237923.70 square millimeters Center of mass: (millimeters) X = 0.06 Y = 3.00 Z = -46.79 Principal axes of inertia and principal moments of inertia: (grams * square millimet Taken at the center of mass. Ix = (0.00, -0.04, 1.00) Px = 258395.73 Iy = (1.00, 0.02, 0.00) Py = 6496408.91 Iz = (-0.02, 1.00, 0.04) Pz = 6558681.76 Moments of inertia: (grams * square millimeters) Taken at the center of mass and aligned with the output coordinate system. Lxx = 6496442.29 Lxy = 1549.69 Lxz = -2438.78 Lyx = 1549.69 Lyy = 6550805.65 Lyz = -222133.87 Lzx = -2438.78 Lzy = -222133.87 Lzz = 266238.46 Moments of inertia: (grams * square millimeters) Taken at the output coordinate system. Ixx = 7486796.10 Ixy = 1632.87 Ixz = -3733.86 Iyx = 1632.87 Iyy = 7537092.37 Iyz = -285482.03 Izx = -3733.86 Izy = -285482.03 Izz = 270308.96	Mass = 459.37 grams Volume = 459254.38 cubic millimeters Surface area = 175630.57 square millimeters Center of mass: (millimeters) X = 0.09 Y = 2.92 Z = -49.88 Principal axes of inertia and principal moments of inertia: (grams * square millime Taken at the center of mass. Ix = (0.00, -0.01, 1.00) Px = 174785.10 Iy = (1.00, -0.01, 0.00) Py = 6158076.62 Iz = (0.01, 1.00, 0.01) Pz = 6243478.99 Moments of inertia: (grams * square millimeters) Taken at the center of mass and aligned with the output coordinate system. Lxx = 6158081.03 Lxy = -887.96 Lxz = -5861.30 Lyx = -887.96 Lyy = 6243151.16 Lyz = -43907.19 Lzx = -5861.30 Lzy = -43907.19 Lzz = 175108.52 Moments of inertia: (grams * square millimeters) Taken at the output coordinate system. Ixx = 7304838.51 Ixy = -768.85 Ixz = -7897.35 Iyx = -768.85 Iyy = 7386000.69 Iyz = -110767.76 Izx = -7897.35 Izy = -110767.76 Izz = 179023.72

Table 72 - Summary of trimming properties for the 40th scale overall model without hull gap.

N.2 Trimming images

20th model ‘gap’ version in Curved Tank:

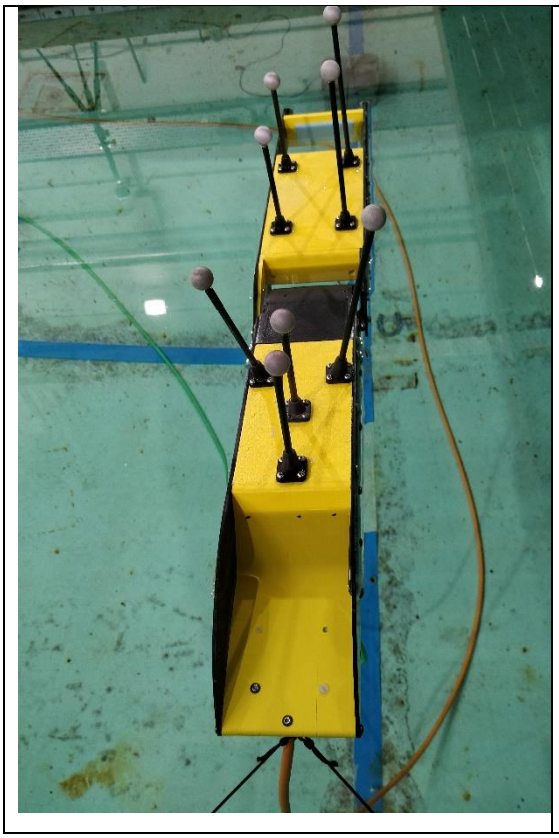	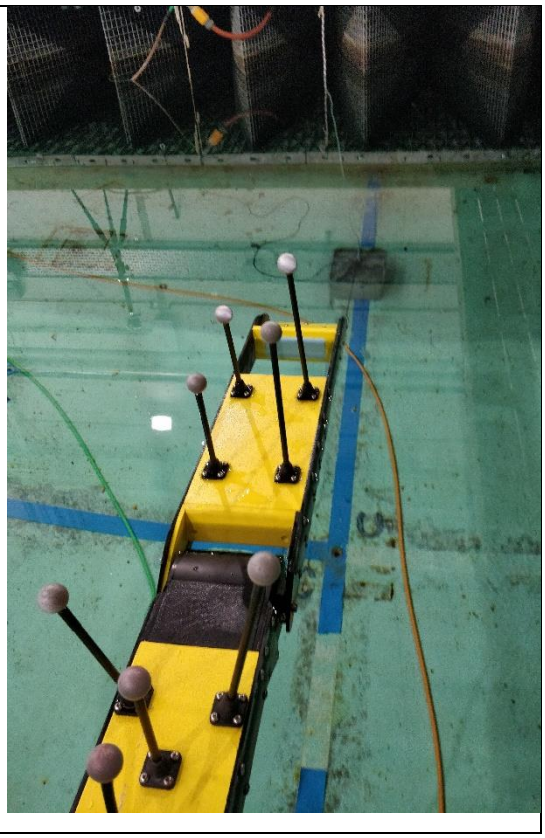

Table 73 - Images of 20th model with the gap in AFT hull in the Curved Tank at even trim.

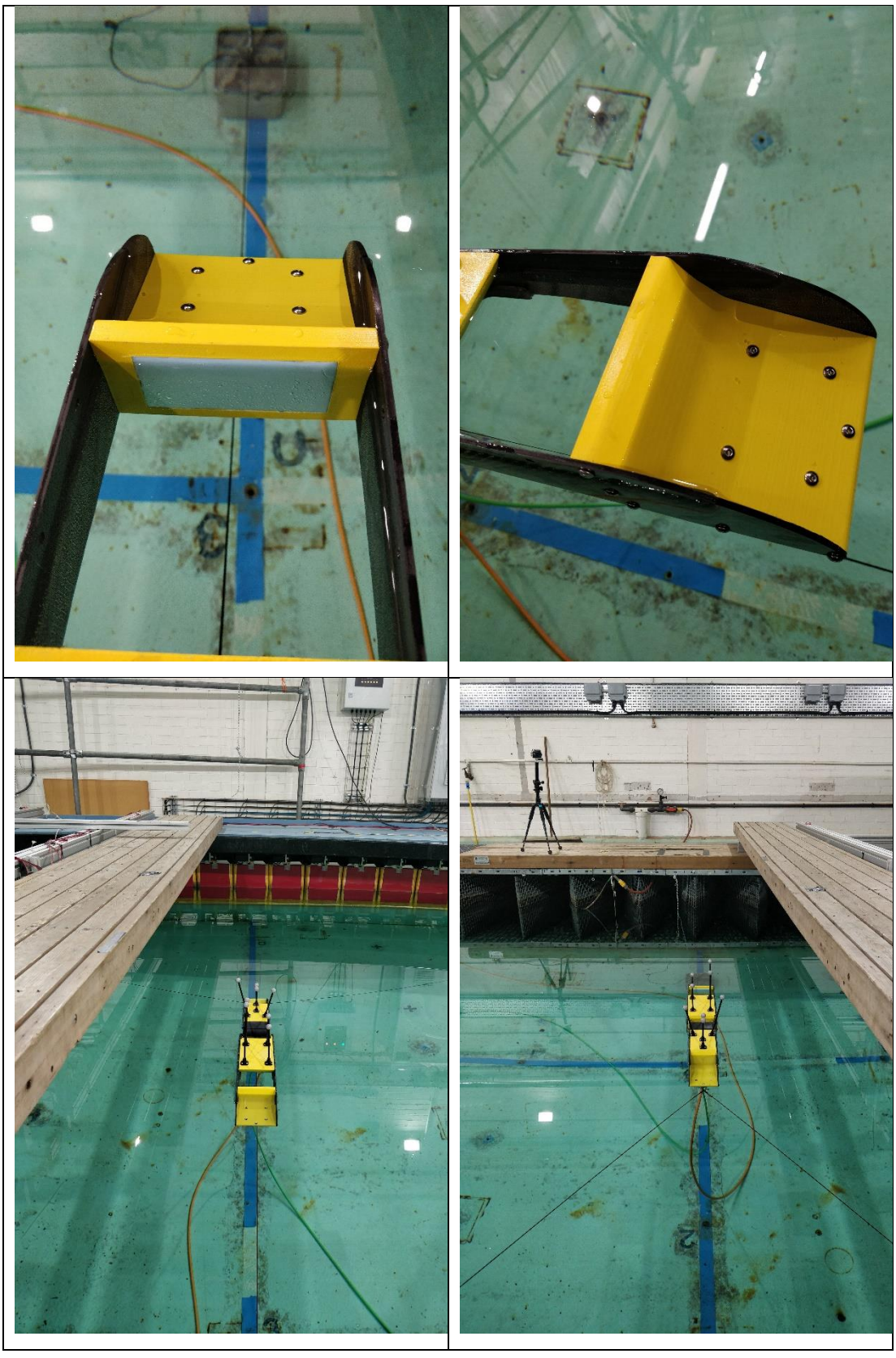

Table 74 - More images of 20th model with the gap in AFT hull in the Curved Tank at uniform even trim.

20th model ‘no gap’ version trimmed in Curved Tank:

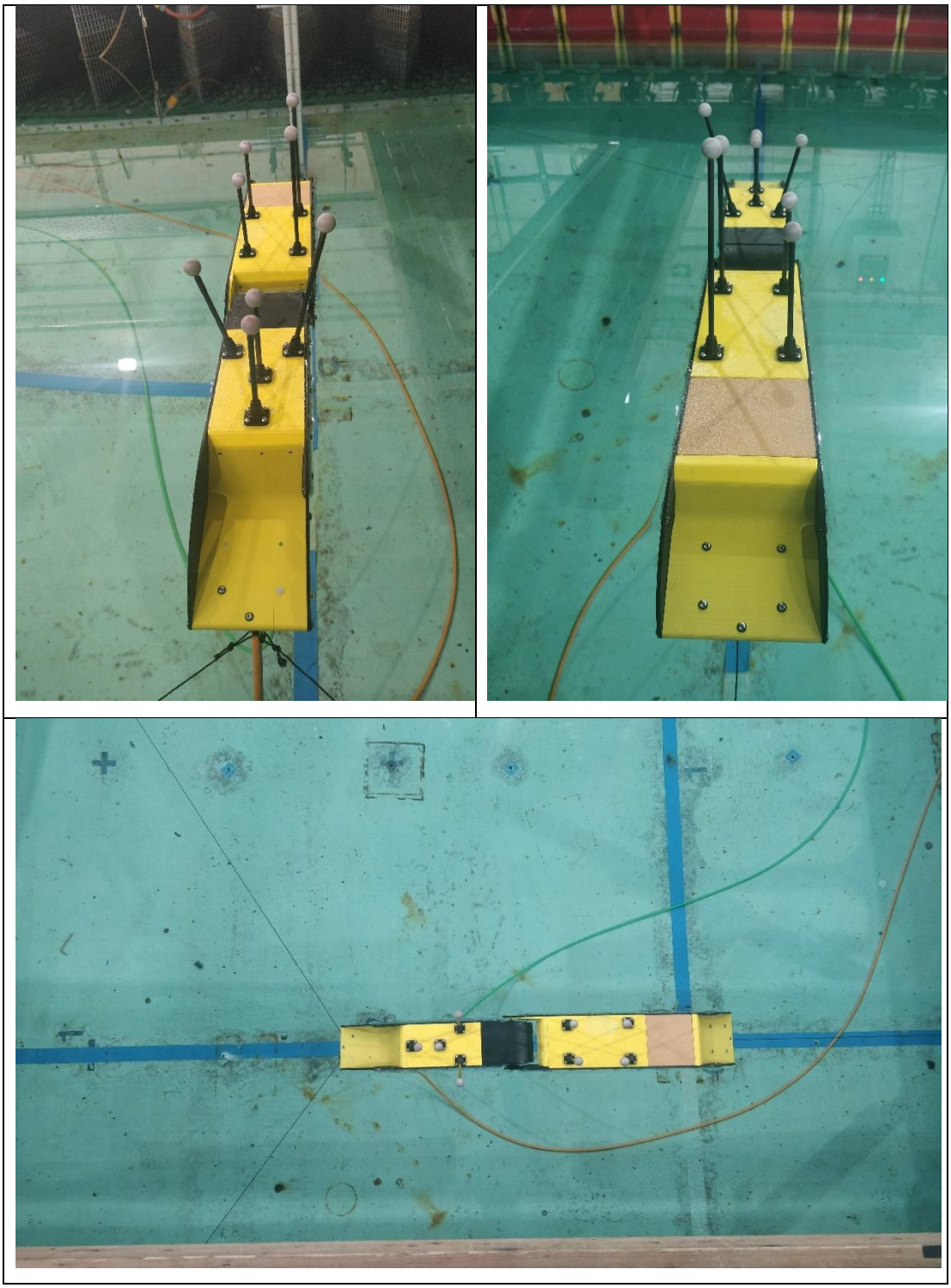

Table 75 - Images of trimmed model in its 'no gap' configuration in the Curved Tank at even trim.

Appendix O – Uncertainties

This section provides supporting material to its analogous section in Chapter 8. It explores several sources of error and uncertainty, among which: mean water line (MWL) and trim line effects, Morison's damping coefficient (Cd), friction effects, and seed effects on both irregular long-crested and Ir0 seas.

O.1 Effects of MWL and trim line

A full-scale Blue X numerical study was carried out in the time-domain by Dr Alfred Cotton, where the MWL was moved from its target of 0.15m above the hinge axis, to 0.05m (i.e. device sitting higher by 0.10m) and to 0.30m (i.e. device sitting lower by 0.15m). The analysis assumes wetted geometry changes but mass and inertia properties remaining constant.

- For the 0.30m case, the shape of the power RAO is the same, but with a slight change in peak of approximately 118/108 kW/m2 → i.e. -8.5%
- For the 0.05m case, the shape of the RAO is the same, but with a change in peak that is approximately between the 0.15m and 0.30m case, i.e. -4%

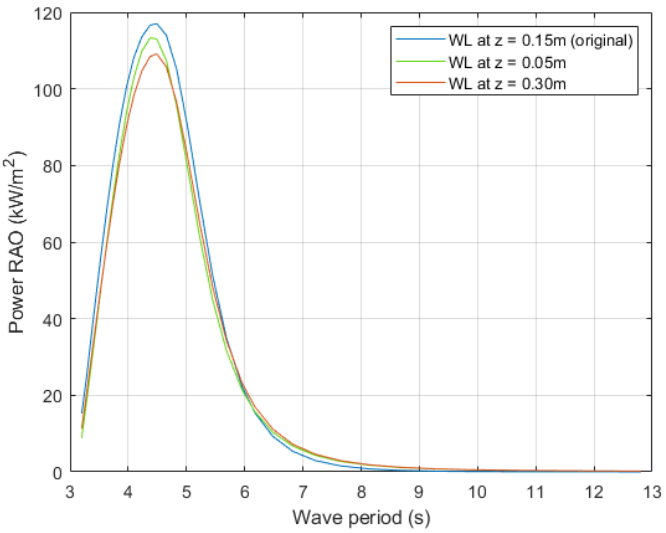

Figure 354 - MWL numerical study (Courtesy of Alfred Cotten).

- For a difference of 0.35m (device lower in water), there is a small increase in power at higher wave periods, but the change in power is within +/-5% for the most commonly occurring waves.

It was found from CAD (matched with real physical tank observations) that the 40th model sits approximately 1.0mm higher than the intended MWL plane in both Aft Hull configurations → 0.04m difference. On the other hand, the 20th model sits 1mm lower (0.02m full-scale) in its Hull Gap configuration and at the correct level in the No Hull Gap configuration.

- On the basis of the above, MWL changes in BST-folding 20th of around 2mm model scale equate to 0.04m full-scale. By linear interpolation, this suggests a peak RAO delta of around -8.5*(0.04/0.15)= -2.3%
- For the 40th scale model, sitting higher by 1mm means 0.04m higher at full-scale, roughly -2% difference in power RAO peak

Next an attempt to estimate MWL difference during individual test days is made. The analysis looks at individual days and calculates difference in Z (vertical) values between the start and end of day readings. The model is typically not removed or re-deployed during the course of a day, but only at the end and start of each day – thus inaccuracies associated are mitigated for. This analysis represents a worst case scenario because the Z value can also be affected by: tank water depth moving down as water slowly evaporates; cable movement; water sitting on top of the model if the seas run during the day are large enough.

NB: A positive delta Z means a relative sinking of the model

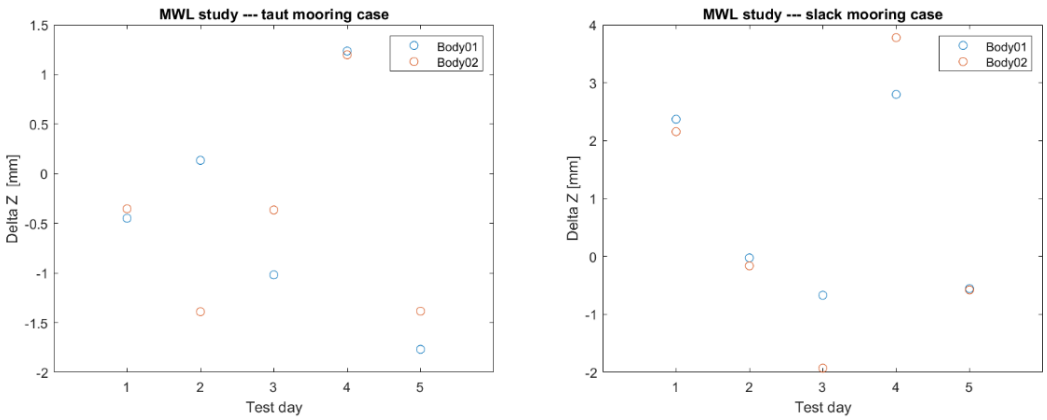

Figure 355 - MWL experimental study.

From Figure 355:

- Largest difference is a ~4mm change for the Aft hull in day 4, slack mooring configuration.
- In general, Body01 and Body02 move together; large differences imply some rotation between the hulls (Z is read as an average across that body's Q_targets by Qualisys)
- Plots suggest that slack mooring has more variation than taut (makes sense, because less controlled)

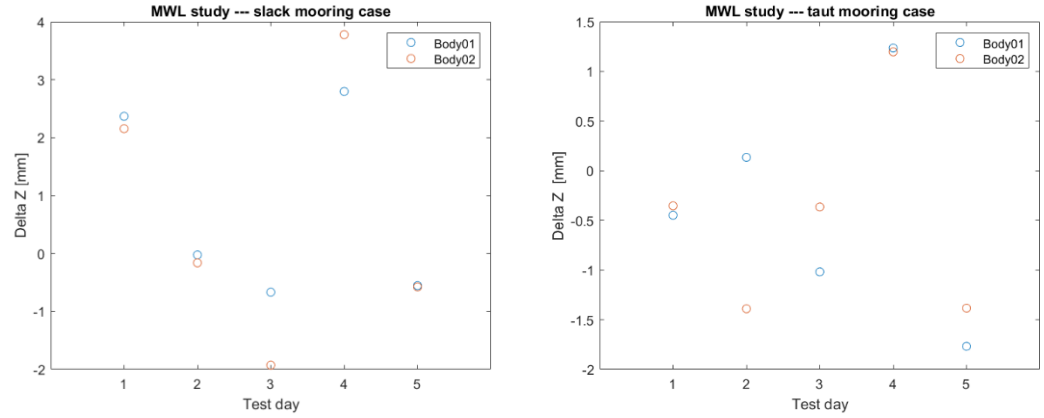

Figure 356 - MWL study showing change in equilibeium Z position over different test days; for slack (left) and taut (right) mooring configurations.

The plots here show daily variations (start of day to end of day) in the Z position of the model, where Body01 is the Fwd hull, and Body02 is the Aft hull.

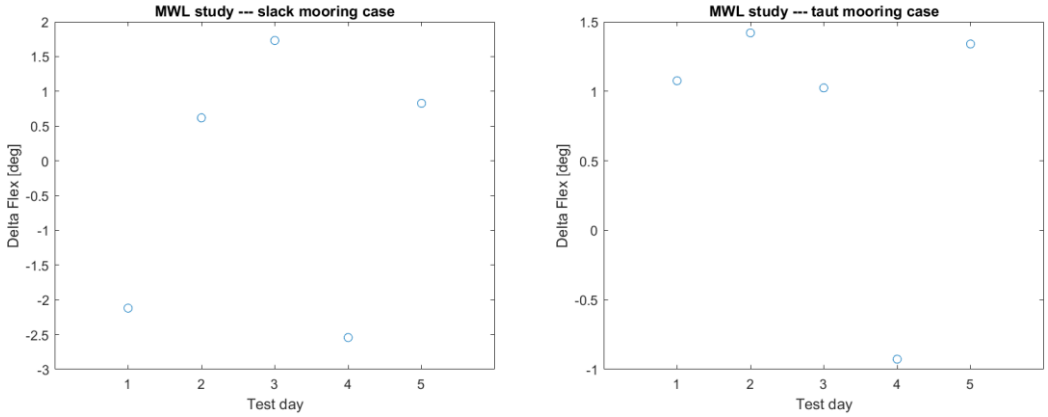

Figure 357 - MWL study showing change in equilibrium Flex position over different test days; for slack (left) and taut (right) mooring configurations.

O.2 Morison's damping

Flex responses sensitivity to Morison damping coefficient (Cd) values in both frequency-domain (FD) and time-domain (TD) numerical domains is shown in Figure 358 and Figure 359. It makes sense for TD model to be less sensitive to Cd variation as it is inherently taking more nonlinearities into account.

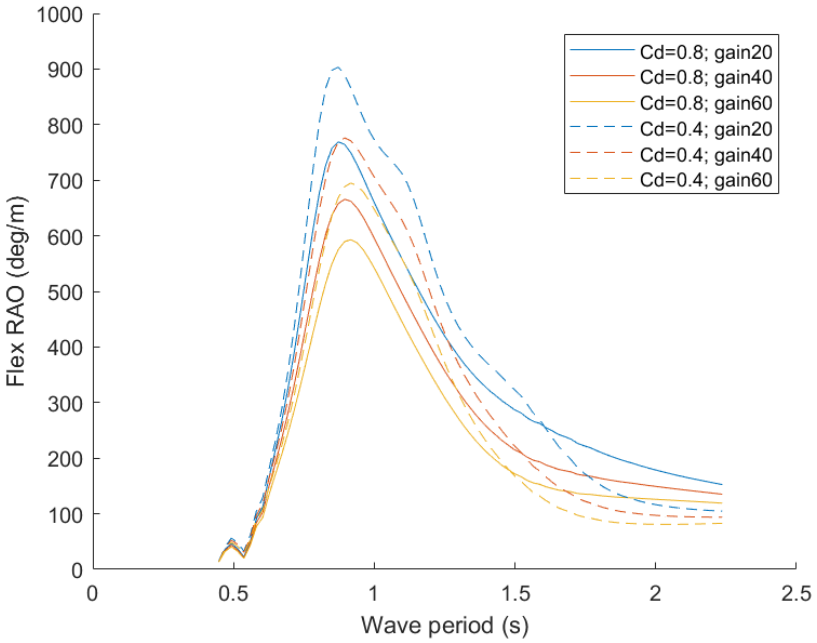

Figure 358 - FD response sensitivity to Cd.

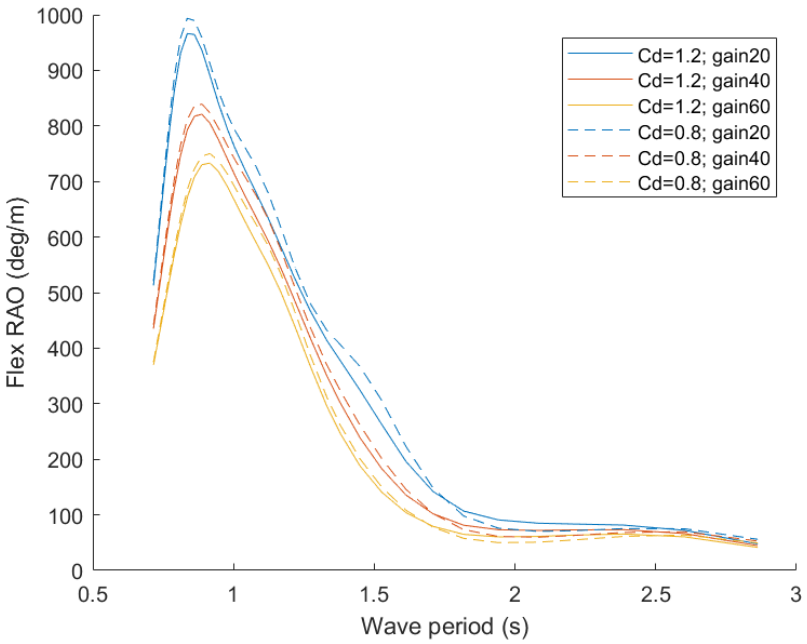

Figure 359 - TD response sensitivity to Cd.

O.3 Friction effects

This section shown results from numerical TD model run by Alfred Cotten, where the static friction value measured in Chapter 7 can be represented.

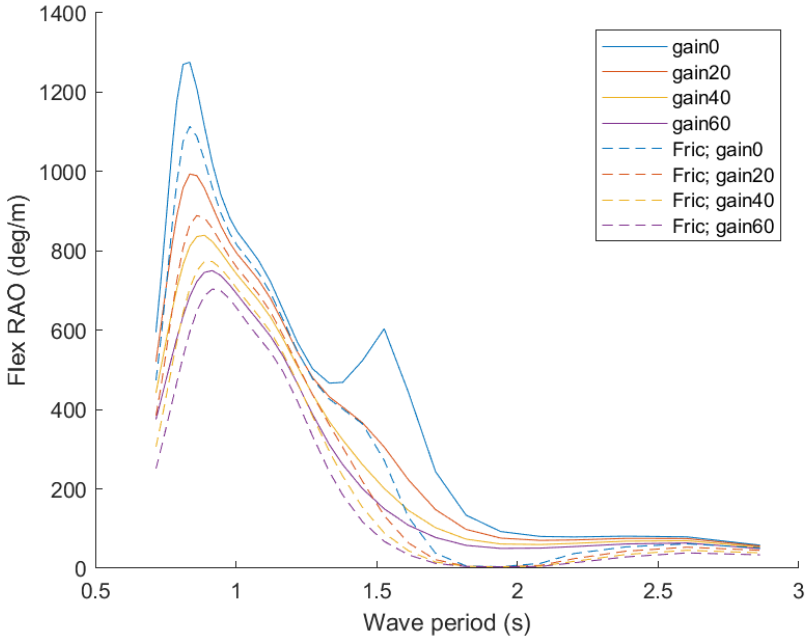

Figure 360 - Predicted effect of friction on flex RAOs.

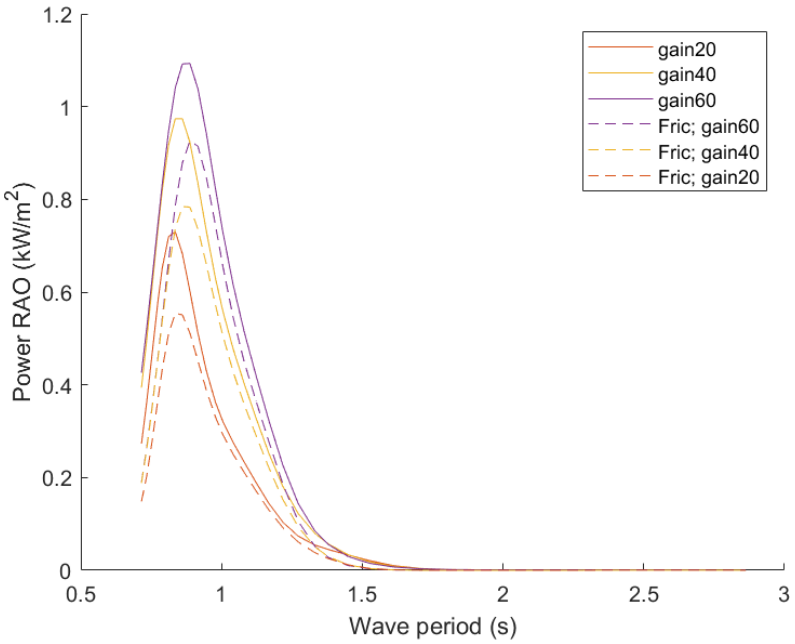

Figure 361 - Predicted effect of friction on power RAOs.

O.4 Irregular waves

Seed number effects on flex RAOs and mean power measurements are shown in Figure 362 and Figure 363. These do not seem significant for this length of runs and this particular sea state (IRL23 and a PTO gain 40).

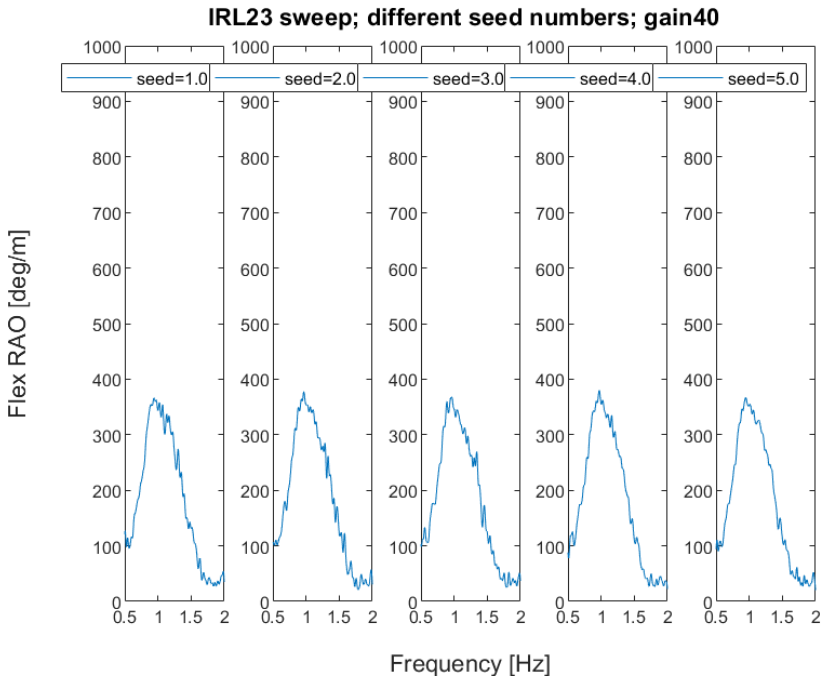

Figure 362 - Flex RAO variation with seed number; IRL23 sea with PTO gain 40.

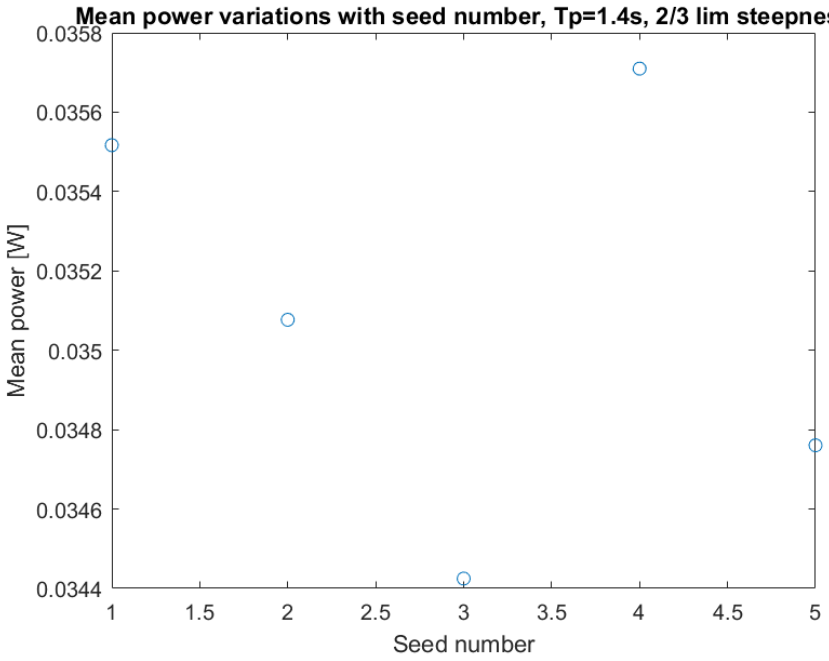

Figure 363 - Mean power variation with seed number, Tp=1.4s {IRL23}.

O.5 Seed number effects

Four different seed numbers were run for IRO21 sea: 1.0, 4.0, 9.0, 14.0.

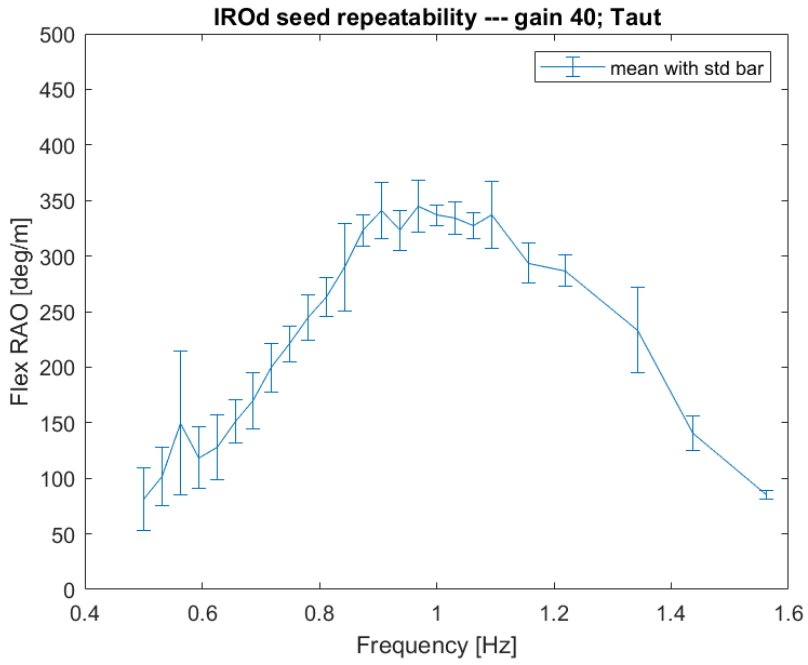

Figure 364 - Seed variation effects on RAO repeatability for IRO21 sea; PTO gain 40.

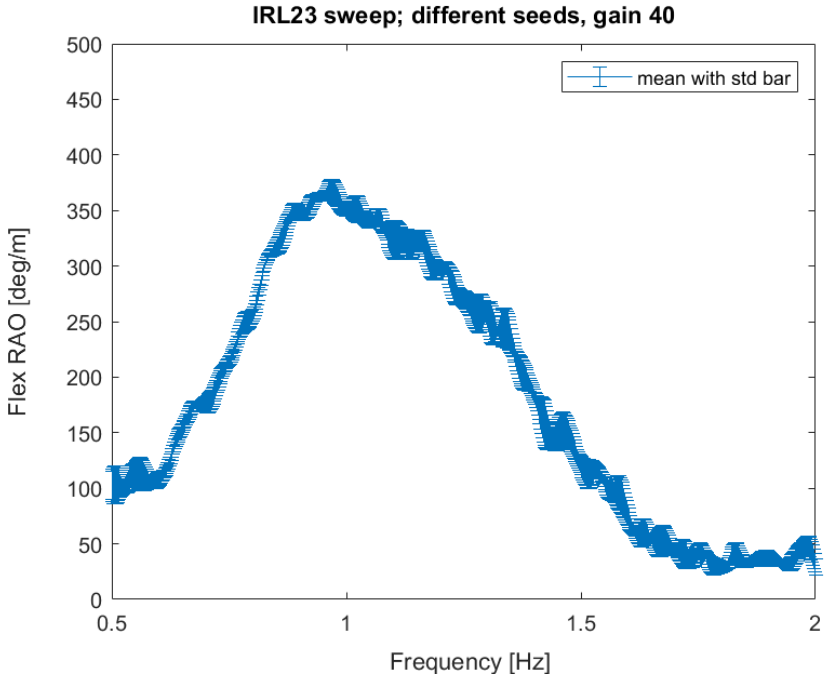

Figure 365 - IRL23 seed sweep, PTO gain 40.

NB: irregular plots are not presented net of reflections so tricky to compare. However, shapes are very similar, which gives confidence to utilisation of Ir0 for RAO measurement more representative of real sea.

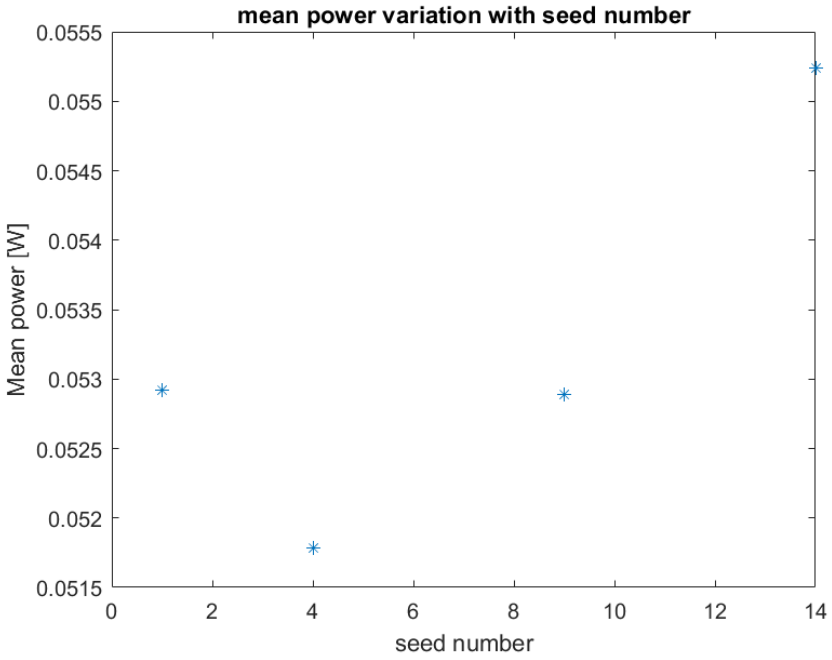

Figure 366 - Seed variation effects on mean power repeatability for IRO21 sea; gain 40.

Sea	Mean power [W]	Std [W]	Number of runs
IRL23 (seeds)	0.0351	0.000529	5
IRO21 (seeds)	0.0532	0.001500	4
IRO01	0.0387	0.000084	3
IRO02	0.0703	0.000243	3
IRO11	0.0315	0.000359	2
IRO12	0.1077	0.003100	2

Table 76 - Repeatability summary of IRO and IRL seas with PTO gain 40.

Bibliography

Addison, V. (2018) *Offshore oil companies dip into ocean wave energy to power up*, *EP Mag*. Available at: https://www.hartenergy.com/exclusives/offshore-oil-companies-dip-ocean-wave-energy-power-30934 (Accessed: 1 March 2019).

Aderinto, T. and Li, H. (2019) 'Review on power performance and efficiency of wave energy converters', *Energies*, 12(22), pp. 1–24. doi: 10.3390/en12224329.

Alves, M. (2016) 'Frequency-Domain Models', in Folley, M. (ed.) *Numerical Modelling of Wave Energy Converters*. Elsevier Inc., pp. 11–30. doi: 10.1016/b978-0-12-803210-7.00002-5.

de Andres, A. *et al.* (2016) 'Techno-economic related metrics for a wave energy converters feasibility assessment', *Sustainability*, 8(11). doi: 10.3390/su8111109.

de Andres, A. *et al.* (2017) 'Beyond LCOE: A study of ocean energy technology development and deployment attractiveness', *Sustainable Energy Technologies and Assessments*. Elsevier Ltd, 19, pp. 1–16. doi: 10.1016/j.seta.2016.11.001.

Astariz, S. and Iglesias, G. (2015) 'The economics of wave energy: A review', *Renewable and Sustainable Energy Reviews*, 45, pp. 397–408. doi: 10.1016/j.rser.2015.01.061.

Babarit, A. *et al.* (2012) 'Numerical benchmarking study of a selection of wave energy converters', *Renewable Energy*. Elsevier Ltd, 41, pp. 44–63. doi: 10.1016/j.renene.2011.10.002.

Babarit, A. *et al.* (2017) 'Stakeholder requirements for commercially successful wave energy converter farms', *Renewable Energy*, 113, pp. 742–755. doi: 10.1016/j.renene.2017.06.040.

Bacic, M., Neild, S. and Gawthrop, P. (2009) 'Introduction to the special issue

on hardware-in-the-loop simulation', *Mechatronics*. Elsevier Ltd, 19(7), pp. 1041–1042. doi: 10.1016/j.mechatronics.2009.09.005.

Bascom, W. (1959) 'Ocean Waves', *Scientific American*, 201(2), pp. 74–88. Available at: http://www.jstor.com/stable/24940361.

Beckman, J. (2022) *Wave energy converter offers lower-cost subsea power option*, *Offshore Magazine*. Available at: https://www.offshore-mag.com/renewable-energy/article/14223853/wave-energy-converter-offers-lowercost-subsea-power-option (Accessed: 9 March 2022).

BEIS (2021) *Methodology used to set Administrative Strike Prices for CfD Allocation Round 4*. Available at: https://assets.publishing.service.gov.uk/government/uploads/system/uploads/attachment_data/file/1016681/cfd-ar4-asp.pdf.

Berque, J. (Tecnalia) *et al.* (2019) *Deliverable D5.3 - Uncertainty in Wave Energy Converter Power Performance Assessment*.

Berriel, R. O. *et al.* (2021) 'Hardware-in-the-loop development of a heaving point absorber wave energy converter using inertia emulation', *Electrical Engineering*. Springer Berlin Heidelberg, 103(6), pp. 2675–2684. doi: 10.1007/s00202-021-01244-2.

Blažauskas, N., Pašilis, A. and Knolis, A. (2015) 'Potential applications for small scale wave energy installations', *Renewable and Sustainable Energy Reviews*, 49(2015), pp. 297–305. doi: 10.1016/j.rser.2015.04.122.

Bracco, G. *et al.* (2015) 'Hardware-In-the-Loop test rig for the ISWEC wave energy system', *Mechatronics*. Elsevier Ltd, 25, pp. 11–17. doi: 10.1016/j.mechatronics.2014.10.007.

Budar, K. and Falnes, J. (1975) 'A resonant point absorber of ocean-wave power', *Nature*, 256, pp. 478–479. doi: https://doi.org/10.1038/256478a0.

Bull, D. *et al.* (2015) 'Scoring the Technology Performance Level (TPL) Assessment', in *Proceedings of the 11th European Wave and Tidal Energy Conference*. Nantes, pp. 1–9.

Bull, D. *et al.* (2017) *Technology Performance Level Assessment Methodology*.

Caio, A., Davey, T. and McNatt, C. (2019) 'Tackling the wave energy paradox – stepping towards commercial deployment', *Proceedings of the International Offshore and Polar Engineering Conference*, 1, pp. 246–252.

Caio, A., Davey, T. and McNatt, J. C. (2021) 'Preliminary hydrodynamic assessment of Mocean Energy's blue star WEC via fast-turnaround physical model testing', in *Proceedings of the 14th European Wave and Tidal Energy Conference*. Plymouth, pp. 1951-1-1951–9.

Caio, A. and Miller, J. (2021) *POSTnote on Sustainable Cooling*. London, UK. Available at: https://post.parliament.uk/research-briefings/post-pn-0642/.

Cameron McNatt, J. and Retzler, C. H. (2019) 'The performance of the Mocean M100 wave energy converter described through numerical and physical modelling', in EWTEC (ed.) *Proceedings of the 13th European Wave and Tidal Energy Conference*. Napoli, pp. 11–19. doi: 10.36688/imej.3.11-19.

Choupin, O., Henriksen, M. and Tomlinson, R. (2022) 'Interrelationship between variables for wave direction-dependent WEEC/site-configuration pairs using the CapEx method', *Energy*. Elsevier Ltd, (110), p. 131932. doi: 10.1016/j.jcms.2021.11.008.

Clément, A. *et al.* (2002) 'Wave energy in Europe: Current status and perspectives', *Renewable and Sustainable Energy Reviews*, 6(5), pp. 405–431. doi: 10.1016/S1364-0321(02)00009-6.

Clemente, D. *et al.* (2020) 'Proof-of-concept study on a wave energy converter based on the roll oscillations of multipurpose offshore floating platforms', *Energy Conversion and Management*. Elsevier Ltd, 224(August), p. 113363. doi: 10.1016/j.enconman.2020.113363.

Clemente, D. *et al.* (2021) 'Experimental study combining a triboelectric nanogenerator solution with the e-motions wave energy converter under irregular waves', in *Proceedings of the European Wave and Tidal Energy*

Conference. Plymouth, pp. 2294-1-2294–8.

Clemente, D., Rosa-Santos, P. and Taveira-Pinto, F. (2021) 'On the potential synergies and applications of wave energy converters: A review', *Renewable and Sustainable Energy Reviews*. Elsevier Ltd, 135(July 2020), p. 110162. doi: 10.1016/j.rser.2020.110162.

CorPower Ocean (2022) *Wave energy - Plugging the wind and solar void*. Available at: https://www.corpowerocean.com/wave-energy-plugging-the-wind-and-solar-void/ (Accessed: 22 February 2022).

Costello, R. *et al.* (2019) 'WaveSPARC : Evaluation of Innovation Techniques for Wave Energy', in *13th Euopean Wave and Tidal Energy Conference*. Naples.

Cruz Atcheson and ARUP (2016) *Structural Forces and Stresses for Wave Energy Devices - Final Report*.

Cruz, J. (2008) *Ocean Wave Energy*. Springer.

Cruz, J., Pascal, R. and Taylor, J. (2006) 'Characterisation of the wave profile in the Edinburgh Curved Tank', in *25th International Conference on Offshore Mechanics and Arctic Engineering*. Hamburg, Germany: OMAE 2006, pp. 1–10.

Cummins, W. E. (1962) 'The impulse response function and ship motions', *Schiffstechnik 9*, pp. 101–109.

Dai, S. *et al.* (2019) 'Investigation on the hydrodynamic scaling effect of an OWC type wave energy device using experiment and CFD simulation', *Renewable Energy*. Elsevier Ltd, 142, pp. 184–194. doi: 10.1016/j.renene.2019.04.066.

Dallman, A. *et al.* (2018) 'Evaluation of performance metrics for the Wave Energy Prize converters tested at 1/20th scale', *Renewable and Sustainable Energy Reviews*. Elsevier Ltd, 98(September), pp. 79–91. doi: 10.1016/j.rser.2018.09.002.

Dalton, G. and Ó Gallachóir, B. P. (2010) ‘Building a wave energy policy focusing on innovation, manufacturing and deployment’, *Renewable and Sustainable Energy Reviews*, 14(8), pp. 2339–2358. doi: 10.1016/j.rser.2010.04.007.

Davey, T. *et al.* (2021) ‘Round robin testing: Exploring experimental uncertainties through a multifacility comparison of a hinged raft wave energy converter’, *Journal of Marine Science and Engineering*, 9(9), pp. 1–24. doi: 10.3390/jmse9090946.

Day, A. H. *et al.* (2015) ‘Hydrodynamic modelling of marine renewable energy devices: A state of the art review’, *Ocean Engineering*, 108, pp. 46–69. doi: 10.1016/j.oceaneng.2015.05.036.

DeBord Jr, F. *et al.* (2003) ‘Design optimization for the International America’s Cup Class’, in *Transactions - Society of Naval Architects and Marine Engineers*, pp. 52–53.

DNV GL (2018) *DNVGL-SE-0160: Technology qualification management and verification*.

Drew, B., Plummer, A. R. and Sahinkaya, M. N. (2009) ‘A review of wave energy converter technology’, *Proceedings of the Institution of Mechanical Engineers, Part A: Journal of Power and Energy*, 223(8), pp. 887–902. doi: 10.1243/09576509JPE782.

Driscoll, F. *et al.* (2018) *Methodology to Calculate the ACE and HPQ Metrics Used in the Wave Energy Prize*. Available at: https://www.osti.gov/biblio/1426063%0Ahttps://www.osti.gov/servlets/purl/1426063.

Driscoll, F., Mauer, E. and Rieks, J. (2018) *2017 Marine Hydrokinetic Instrumentation Workshop Report*. Golden, CO. Available at: https://www.nrel.gov/docs/fy18osti/70591.

EMEC (2020) *Press release: WES awards £1.4 million for wave energy connection systems*. Available at: www.emec.org.uk/press-release-wes-

awards-for-wave-energy-connection-systems/. (Accessed: 18 March 2021).

EMEC (no date) *Pelamis Wave Power*, *The European Marine Energy Centre*. Available at: https://www.emec.org.uk/about-us/wave-clients/pelamis-wave-power/ (Accessed: 3 June 2022).

Ersdal, S. and Moe, A. M. (2013) 'Model test of the Aker wave energy converter concept', in ASME (ed.) *32nd International Conference on Ocean, Offshore and Arctic Engineering*. Nantes, pp. 1–8. Available at: https://watermark.silverchair.com/v008t09a030-omae2013-10537.pdf?token=AQECAHi208BE49Ooan9kkhW_Ercy7Dm3ZL_9Cf3qfKAc485ysgAABDswggQ3BgkqhkiG9w0BBwagggQoMIIEJAIBADCCBB0GCSqGSIb3DQEHATAeBglghkgBZQMEAS4wEQQMSBTo3xkXkQpxuva1AgEQgIID7pRDQ7fwc4QDUSo8I4IAReEwmy5t.

ETIP Ocean (2016) *An Integrated Framework of Ocean Energy Sector Challenges*. Brussels.

European Commission (2020) *An EU Strategy to harness the potential of offshore renewable energy for a climate neutral future*. Brussels.

European Commission Joint Research Centre (2019) *LCEO Ocean Energy Technology Development Report*. EUR 299907. Edited by D. Magagna and M. Soede. Luxembourg: Office of the European Union. doi: 10.2760/158132.

EuropeWave (2022) *Mocean Energy's Blue Horizon wave energy machine undergoes testing at FloWave*, *EuropeWave*. Available at: https://www.europewave.eu/news/phase1-mocean-bluehorizon250 (Accessed: 20 September 2022).

EuropeWave (no date) *Five wave energy projects to continue to next phase of EuropeWave*, *EuropeWave*. Available at: https://www.europewave.eu/news/europewave-phase2-announcement (Accessed: 22 September 2022).

Falcao, A. F. (2009) 'The Development of Wave Energy Utilisation', in Brito-Melo, A. and Bhuyan, G. (eds) *Annual Report 2008*. IEA-OES.

Falcão, A. F. d. O. (2010) ‘Wave energy utilization: A review of the technologies’, *Renewable and Sustainable Energy Reviews*, 14(3), pp. 899–918. doi: 10.1016/j.rser.2009.11.003.

De Falcão, A. F. O. *et al.* (2010) ‘Hydrodynamic simulation of a floating wave energy converter by a U-tube rig for power take-off testing’, *Ocean Engineering*, 37(14–15), pp. 1253–1260. doi: 10.1016/j.oceaneng.2010.05.007.

Falnes, J. (2002) *Ocean Waves and Oscillating Systems*. Cambridge: CUP.

Fitzgerald, J. and Bergdahl, L. (2009) ‘Rigid moorings in shallow water: A wave power application. Part I: Experimental verification of methods’, *Marine Structures*. Elsevier Ltd, 22(4), pp. 809–835. doi: 10.1016/j.marstruc.2009.09.002.

Folley, Matt (2016) *Numerical Modelling of Wave Energy Converters*. Edited by R. Zanol and A. C. Abad Garcia. Elsevier Inc. Available at: http://dx.doi.org/10.1016/B978-0-12-803210-7.00002-5.

Folley, M (2016) ‘Spectral-Domain Models’, in Folley, Matt (ed.) *Numerical Modelling of Wave Energy Converters*. Elsevier Ltd., pp. 67–80. doi: 10.1016/b978-0-12-803210-7.00002-5.

Folley, M. and Whittaker, T. (2010) ‘Spectral modelling of wave energy converters’, *Coastal Engineering*. Elsevier B.V., 57(10), pp. 892–897. doi: 10.1016/j.coastaleng.2010.05.007.

Folley, M. and Whittaker, T. (2013) ‘Validating a spectral-domain model of an OWC using physical model data’, *International Journal of Marine Energy*. Elsevier Ltd, 2, pp. 1–11. doi: 10.1016/j.ijome.2013.05.003.

Fong, T. (2019) *Robotics and autonomous systems in O&M - removing the barriers to BVLOS operations*. Available at: https://ore.catapult.org.uk/app/uploads/2019/02/Autonomous-Systems-in-OM-Removing-the-Barriers-to-BVLOS-Operations-Tony-Fong-AP0019.pdf.

Foteinis, S. and Tsoutsos, T. (2017) ‘Strategies to improve sustainability and

offset the initial high capital expenditure of wave energy converters (WECs)', *Renewable and Sustainable Energy Reviews*. Elsevier Ltd, 70(February 2016), pp. 775–785. doi: 10.1016/j.rser.2016.11.258.

Garanovic, A. (2021a) *Energy companies invest £1.6M in wave-powered demo for subsea projects*, *Offshore Energy*. Available at: https://www.offshore-energy.biz/energy-companies-invest-1-6m-in-wave-powered-demo-for-subsea-projects/ (Accessed: 17 September 2022).

Garanovic, A. (2021b) *Finnish wave energy company enters green hydrogen market*, *Offshore Energy*. Available at: https://www.offshore-energy.biz/finnish-wave-energy-company-enters-green-hydrogen-market/ (Accessed: 9 April 2022).

Garanovic, A. (2022) *Mocean Energy lands funds to build wave energy device for oil and gas sector*, *Offshore Energy*. Available at: https://www.offshore-energy.biz/mocean-energy-lands-funds-to-build-wave-energy-device-for-oil-and-gas-sector/ (Accessed: 17 September 2022).

Gemmrich, J. and Cicon, L. (2022) 'Generation mechanism and prediction of an observed extreme rogue wave', *Nature Scientific Reports*. Nature Publishing Group UK, 12(1), pp. 1–10. doi: 10.1038/s41598-022-05671-4.

Giorgi, G. and Ringwood, J. V. (2017) 'Consistency of viscous drag identification tests for wave energy applications', in EWTEC 2017 (ed.) *12th European Wave and Tidal Energy Conference*. Cork, pp. 1–8.

Giorgi, S. *et al.* (2018) 'Hydraulic PTO model emulator for WEC tank tests', in *SPEEDAM 2018 - Proceedings: International Symposium on Power Electronics, Electrical Drives, Automation and Motion*, pp. 1257–1262. doi: 10.1109/SPEEDAM.2018.8445383.

Girard, P. et fils (1799) 'Brevet d'invention de quinze ans pour divers moyens d'employer les vagues de la mer'. France.

Governo Italiano. Presidenza del Consiglio dei Ministri (2021) *Piano Nazionale di Ripresa e Resilienza*. Available at:

https://www.governo.it/sites/governo.it/files/PNRR.pdf.

Green, R. *et al.* (2019) *Enabling Power at Sea : Opportunities for Expanded Ocean Observations through Marine Renewable Energy Integration Preprint Enabling Power at Sea : Opportunities for Expanded Ocean Observations through Marine Renewable Energy Integration Preprint*. Boulder, USA.

Gyongy, I. *et al.* (2014) 'Validation of a hydrodynamic model for a curved, multi-paddle wave tank', *Applied Ocean Research*. Elsevier Ltd., 44, pp. 39–52. doi: 10.1016/j.apor.2013.11.002.

Henry, A. *et al.* (2021) 'Wave Farm Design: Simulation of Marine Operations for Improved Cost of Energy', in *14th European Wave and Tidal Energy Conference*. Plymouth: EWTEC.

Hodges, J. *et al.* (2021) *An International Evaluation and Guidance Framework for Ocean Energy Technology*.

Hodges, J. and Colby, J. (2022) *Supporting ocean energy technology developent and commercialisation: current application of guidance, standards and certification*. Available at: https://www.ocean-energy-systems.org/publications/oes-documents/guidelines/document/supporting-ocean-energy-technology-development-and-commercialisation/.

Hodson, H. (2018) 'Blue-sea thinking', *The Economist*, March. Available at: https://www.economist.com/sites/default/files/tq_march_2018.pdf.

Hughes, S. A. (1993) *Physical models and laboratory techniques in coastal engineering*. Advanced S. World Scientific. doi: https://doi.org/10.1142/2154.

IEA-OES (2015) *International Levelised Cost of Energy for ocean energy technologies*.

IEA-OES (2020) *Blue Economy and its Promising Markets for Ocean Energy*.

IEA-OES (2021) *Strategic Plan 2022-2026*.

IEC TS 62600-103 (2018) *Marine energy — Wave , tidal and other water current converters — Part 103: Guidelines for the Early Stage Development*

of Wave Energy Converters: Best Pratices and Recommended Procedures for the Testing of Pre-Prototype Scale Devices. Geneva.

Ingram, D. *et al.* (2011) *Protocols for the Equitable Assessment of Marine Energy Converters*. Edinburgh.

Intergovernmental Oceanographic Commission (2017) *Global ocean science report: the current status of ocean science around the world; executive summary*, *UNESCO Digital Library*. Available at: https://unesdoc.unesco.org/ark:/48223/pf0000249373 (Accessed: 1 March 2019).

IPCC (2018) 'Summary for policymakers.', in Masson-Delmotte, V. et al. (eds) *Global warming of 1.5C. An IPCC special report.*

ITTC (2017) *ITTC Quality System Manual: Recommended Procedures and Guidelines - Uncertainty Analysis for a Wave Energy Converter*.

Jin, S. and Greaves, D. (2021) 'Wave energy in the UK: Status review and future perspectives', *Renewable and Sustainable Energy Reviews*. Elsevier Ltd, 143(February), p. 110932. doi: 10.1016/j.rser.2021.110932.

Jin, S., Zheng, S. and Greaves, D. (2022) 'On the scalability of wave energy converters', *Ocean Engineering*. Elsevier Ltd, 243(August 2021), p. 110212. doi: 10.1016/j.oceaneng.2021.110212.

Jones, D. O. B. *et al.* (2019) 'Autonomous marine environmental monitoring: Application in decommissioned oil fields', *Science of the Total Environment*. The Authors, 668, pp. 835–853. doi: 10.1016/j.scitotenv.2019.02.310.

Joslin, J. *et al.* (2019) 'The wave-powered adaptable monitoring package: hardware design, installation, and deployment', in *Proceedings of EWTEC 2019*. Naples: EWTEC, pp. 1–9.

Judge, F. (University C. C.-M. *et al.* (2021) *MaRINET2 Deliverable 2.8: Ocean Energy Technology Guidance Report*. doi: 10.13140/RG.2.2.12146.22729.

Keiner, D. *et al.* (2022) ‘Powering an island energy system by offshore floating technologies towards 100% renewables: A case for the Maldives’, *Applied Energy*. Elsevier Ltd, 308, p. 118360. doi: 10.1016/j.apenergy.2021.118360.

Kerr, P., Noble, D. R. and Hodges, J. (2021) ‘Implementing radical innovation in renewable energy experience curves’, *Energies*, 14(2364), pp. 1–28.

Kramer, M. B. *et al.* (2021) ‘Highly accurate experimental heave decay tests with a floating sphere: A public benchmark dataset for model validation of fluid–structure interaction’, *Energies*, 14(2). doi: 10.3390/en14020269.

Lamont-Kane, P., Folley, M. and Whittaker, T. (2013) ‘Investigating Uncertainties in Physical Testing of Wave Energy Converter Arrays’, in *Proceedings of 10th European Wave and Tidal Energy Conference*. Aalborg.

Li, X. *et al.* (2017) ‘Design, fabrication and testing of wave energy converters(WECs) using different power take-off mechanism with mechanical motion rectifier’, in EWTEC 2017 (ed.) *Proceedings of the 12th European Wave and Tidal Energy Conference. Cork, Ireland*. Cork.

Liang, C., Ai, J. and Zuo, L. (2017) ‘Design, fabrication, simulation and testing of an ocean wave energy converter with mechanical motion rectifier’, *Ocean Engineering*. Elsevier Ltd, 136(December 2015), pp. 190–200. doi: 10.1016/j.oceaneng.2017.03.024.

Liu, Z. *et al.* (2019) ‘Overall performance evaluation of a model-scale OWC wave energy converter’, *Renewable Energy*, 149, pp. 1325–1338. doi: 10.1016/j.renene.2019.10.126.

Lopes de Almeida, J. P. P. G., Mujtaba, B. and Oliveira Fernandes, A. M. (2018) ‘Preliminary laboratorial determination of the REEFS novel wave energy converter power output’, *Renewable Energy*. Elsevier Ltd, 122, pp. 654–664. doi: 10.1016/j.renene.2018.01.030.

Lucas, J. *et al.* (2008) ‘Update on the design of a 1:33 scale model of a moified Edinburgh Duck WEC’, in *27th International Conference on Offshore*

Mechanics and Arctic Engineering. Estoril, Portugal: OMAE 2008.

MacGillivray, A. *et al.* (2014) 'Innovation and cost reduction for marine renewable energy: A learning investment sensitivity analysis', *Technological Forecasting and Social Change*. Elsevier Inc., 87, pp. 108–124. doi: 10.1016/j.techfore.2013.11.005.

Magagna, D. and Uihlein, A. (2015) 'Ocean energy development in Europe: Current status and future perspectives', *International Journal of Marine Energy*. Elsevier Ltd, 11, pp. 84–104. doi: 10.1016/j.ijome.2015.05.001.

Mansard, E. P. D. and Funke, E. R. (1980) 'The measurement of incident and reflected spectra using a least squares method', *in: Proc. Seventeenth Coastal Engng. Conf., (Sydney, Australia: Mar. 23-28, 1980)*, 1, New Yo, pp. 154–172. doi: 10.1061/9780872622647.008.

Martin, D. *et al.* (2020) 'Numerical analysis and wave tank validation on the optimal design of a two-body wave energy converter', *Renewable Energy*. Elsevier Ltd, 145, pp. 632–641. doi: 10.1016/j.renene.2019.05.109.

Masuda, Y. (1971) 'Wave-activated generator', in *Proceedings of the International Colloquium on the Exposition of Oceans*. Bordeaux, France.

McCombes, T. *et al.* (2010) *Deliverable 3.3 - Assessment of current practice for tank testing of small marine energy devices*. Available at: https://www.equimar.org/equimar-project-deliverables.html.

McCormick, M. (1981) *Ocean Wave Energy Conversion*. New York: Wiley.

McMaster, A. (2014) *Froude Scaling Laws*, *BEng (Hons) Mechanical Engineering with Renewable Energy Final Year Project*. Available at: https://adammcmaster.wordpress.com/wave-tank-testing/froude-scaling-laws/.

McShane, B. (2017) *Marine and hydrokinetic distributed and alternate applications*. Available at: https://www.energy.gov/sites/prod/files/2017/11/f46/MHK Forum Backgrounder Information.pdf.

Mendoza, N. *et al.* (2021) ‘Developing technology performance level assessments for early-stage wave energy converter technologies’, in *Proceedings of the 14th European Wave and Tidal Energy Conference*. Plymouth.

Morison, J. R., Johnson, J. W. and Schaaf, S. A. (1950) ‘The Force Exerted by Surface Waves on Piles’, *Journal of Petroleum Technology*, 2(05), pp. 149–154. doi: 10.2118/950149-g.

Muller, J. Z. (2018) *The Tyranny of Metrics*. Princeton: Princeton University Press.

Newman, J. N. (1979) ‘The Theory of Ship Motions’, in Yih, C.-S. (ed.) *Advances in Applied Mechanics*. Michigan: Academic Press, pp. 221–283. doi: 10.1016/S0065-2156(08)70268-0.

Nielsen, K. (Ramboll) (2003) *IEA | Ocean Energy Systems - Annex II Report*, *Implementing Agreement on Ocean Energy Systems*.

Noble, D. R. (2017) *Combined wave-current scale model testing at FloWave*, *IDCORE Thesis*. University of Edinburgh, IDCORE. Available at: http://hdl.handle.net/1842/31170.

Noble, D. R. *et al.* (2017) ‘Design diagrams for wavelength discrepancy in tank testing with inconsistently scaled intermediate water depth’, *International Journal of Marine Energy*. The Authors, 18, pp. 109–113. doi: 10.1016/j.ijome.2017.04.001.

Noble, D. R. *et al.* (2018) *D2.1 Test recommendations and gap analysis report*, *MaRINET2 Report*. Edinburgh.

Noble, D. R. *et al.* (2021) ‘Standardising marine renewable energy testing: Gap analysis and recommendations for development of standards’, *Journal of Marine Science and Engineering*, 9(9). doi: 10.3390/jmse9090971.

O’Boyle, L. *et al.* (2015) ‘The Value of Full Scale Prototype Data - Testing Oyster 800 at EMEC , Orkney’, *Proceedings of the 11th European Wave and Tidal Energy Conference*, (September), pp. 1–10.

Ocean Energy Forum (2016) *Building ocean energy for Europe*, *Ocean Energy Strategic Roadmap 2016*.

Ocean Energy Systems (2021) *Wave Energy Developments Highlights*.

OCEANERA-NET (2017) *Deliverable 2.6: Annual study of EU-OE sector development and opportunities – Updated report : 2017*.

OES (2008) *Annual Report 2008*.

OES (2019) *Annual Report: An Overview of Ocean Energy Activities in 2019*, *IEA-OES*. Available at: https://www.rtda.gov.rw/fileadmin/templates/documents/Annual_Report_2017_2018_FINAL.pdf;

Office of Energy Efficiency and Renewable Energy (EERE) (2019) *Exploring Opportunities for Marine Renewable Energy in Maritime Markets*, *U.S. Department of Energy*. Available at: https://www.ocean-energy-systems.org/about-oes/what-is-ocean-energy/.

Offshore staff (2022) *Mocean gets further funds for wave energy development*, *Offshore Magazine*. Available at: https://www.offshore-mag.com/renewable-energy/article/14234954/mocean-gets-further-funds-for-wave-energy-development (Accessed: 15 September 2022).

Ohana, J. *et al.* (2021) 'Round robin tests on a hinged raft wave energy converter', *Proceedings of the 14th European Wave and Tidal Energy Conference*, (December), pp. 2312-1-2312–10.

Otaola, E. *et al.* (2019) 'A Comparative Analysis of Self-Rectifying Turbines for the Mutriku Oscillating Water Column Energy Plant', *Complexity*. Hindawi, 2019. doi: 10.1155/2019/6396904.

Otter, A. *et al.* (2021) 'A review of modelling techniques for floating offshore wind turbines', *Wind Energy*, (November), pp. 1–27. doi: 10.1002/we.2701.

Oxford Creativty (no date) *What is TRIZ?* Available at: www.triz.co.uk/what (Accessed: 1 March 2019).

Palm, J. *et al.* (2018) ‘Assessment of scale effects, viscous forces and induced drag on a point-absorbing wave energy converter by CFD simulations’, *Journal of Marine Science and Engineering*, 6(4), pp. 11–13. doi: 10.3390/jmse6040124.

Pascal, R. *et al.* (2009) ‘Assessing and improving the Edinburgh curved wave tank’, in *Proceedings of the 19th International Offshore and Polar Engineering Conference*. Osaka, pp. 269–275.

Pascal, R. C. R. *et al.* (2018) ‘The right size for a WEC : a study on the consequences of the most basic design choice .’, in *Proceedings of the 7th International Conference on Ocean Energy*.

Pascal, R. C. R. *et al.* (2021) ‘An innovative tank testing method to efficiently characterise wave energy converters’, in *Proceedings of the European Wave and Tidal Energy Conference*, pp. 1943-1-1943–10.

Passas, G. (2016) *Experimental characterisation of a magnetic particle brake to simulate the power take-off system of a marine energy converter*. The University of Edinburgh.

Payne, G. (2008) *Guidance for the experimental tank testing of wave energy converters*. Edinburgh.

Pearson, J. *et al.* (2002) ‘Violent wave overtopping - measurements at large and small scale’, *Coastal Engineering*. Available at: https://doi.org/10.1142/9789812791306_0187.

Pecher, A. and Kofoed, J. P. (2017) *Handbook of Ocean Wave Energy*. Ocean Engi. Edited by M. R. Dhanak and N. I. Xiros. Springer Open. doi: 10.1007/978-3-319-39889-1_11.

Pecher, A., Kofoed, J. P. and Larsen, T. (2012) ‘Experimental study of the WEPTOS wave energy converter’, in *OMAE 2012*. Rio de Janeiro, Brazil: ASME, pp. 1–10. doi: OMAE2012-83751.

Pennock, S. *et al.* (2022) ‘Temporal complementarity of marine renewables with wind and solar generation: Implications for GB system benefits’, *Applied*

Energy. Elsevier Ltd, 319(November 2021), p. 119276. doi: 10.1016/j.apenergy.2022.119276.

Pitt, E. (2009) *Assessment of Performance of Wave Energy Conversion Systems*, *Marine Renewable Energy Guides*. Orkney, Scotland. Available at: www.emec.org.uk/standards/assessment-of-performance-of-wave-energy-conversion-systems/.

PLOCAN (2021) *The Government sets out the Offshore Wind and Renewable Energy Roadmap for Spain*, *Plataforma Océanica de Canarias*. Available at: https://www.plocan.eu/en/el-gobierno-fija-la-hoja-de-ruta-de-la-eolica-marina-y-las-energias-del-mar-para-espana-2/ (Accessed: 4 May 2022).

Portillo, J. C. C. *et al.* (2020) 'Wave energy converter physical model design and testing: The case of floating oscillating-water-columns', *Applied Energy*. Elsevier Ltd, 278(February), p. 115638. doi: 10.1016/j.apenergy.2020.115638.

Rahmati, M. T. and Aggidis, G. A. (2016) 'Numerical and experimental analysis of the power output of a point absorber wave energy converter in irregular waves', *Ocean Engineering*. Elsevier, 111, pp. 483–492. doi: 10.1016/j.oceaneng.2015.11.011.

Resource (no date) *Online Etymology Dictionary*. Available at: https://www.etymonline.com/word/resource (Accessed: 3 June 2022).

Ricci, P. (2016) 'Time-Domain Models', in Folley, M. (ed.) *Numerical Modelling of Wave Energy Converters*. Elsevier Ltd., pp. 31–66. doi: 10.1016/b978-0-12-803210-7.00002-5.

Roberts, O. *et al.* (2021) 'Bringing Structure to the Wave Energy Innovation Process with the Development of a Techno-Economic Tool', *Energies*, 14, p. 8201. doi: https://doi.org/10.3390/en14248201.

Robertson, A. N. (2017) 'Uncertainty analysis of OC5-DeepCwind floating semisubmersible offshore wind test campaign', in *Proceedings of the*

International Offshore and Polar Engineering Conference. San Francisco, California, pp. 482–489.

Robertson, A. N. *et al.* (2018) 'Assessment of experimental uncertainty for a floating wind semisubmersible under hydrodynamic loading', in *Proceedings of the International Conference on Offshore Mechanics and Arctic Engineering - OMAE*. Madrid, Spain. doi: 10.1115/OMAE2018-77703.

Rodrigues, C. *et al.* (2020) 'Emerging triboelectric nanogenerators for ocean wave energy harvesting: State of the art and future perspectives', *Energy and Environmental Science*. Royal Society of Chemistry, 13(9), pp. 2657–2683. doi: 10.1039/d0ee01258k.

Rodríguez, C. A., Rosa-Santos, P. and Taveira-Pinto, F. (2018) 'Assessment of the power conversion of wave energy converters based on experimental tests', *Energy Conversion and Management*. Elsevier, 173(68), pp. 692–703. doi: 10.1016/j.enconman.2018.08.009.

De Rose, A., Olivieri, N. and Strazza, C. (2017) *Technology readiness level: guidance principles for renewable energy technologies - annexes*. Available at: https://data.europa.eu/doi/10.2777/863818.

Ross, D. (1981) *Power from the Waves*. 2d edn. Elsevier. doi: https://doi.org/10.1016/C2009-0-10993-5.

Ruiz-Minguela, P., Nava, V. and Blanco, J. M. (2022) *Technical Report: External forces influencing the development of wave energy technologies for power markets*.

Ruiz-Minguela, P., Nava, V. and Hodges, J. (2020) 'Review of Systems Engineering (SE) Methods and Their Application to Wave Energy Technology Development', *Marine Science and Engineering*, 8.

Salter, S. (2005) 'A Personal View of Renewable Marine Energy', in *Wave and Tidal Technologies Symposium*. Aberdeen, pp. 1–8.

Salter, S. (2008) 'Chapter 2. Looking back', in Cruz, J. (ed.) *Ocean Wave Energy: Current Status and Future Perspectives*. Berlin: Springer. doi:

10.1007/978-3-540-74895-3.

Salter, S. (2016) ‘Wave energy: Nostalgic Ramblings, future hopes and heretical suggestions’, *Journal of Ocean Engineering and Marine Energy*. Springer International Publishing, 2(4), pp. 399–428. doi: 10.1007/s40722-016-0057-3.

Salter, S. H. (1974) ‘A proposal to the Science Research Council’. Edinburgh. Available at: https://era.ed.ac.uk/bitstream/handle/1842/23669/1974 A proposal to the Science Research Council.pdf?sequence=1&isAllowed=y.

Salter, S. H. (2003) *Research requirements for fourth generation wave energy devices*. Available at: http://scholar.google.com/scholar?hl=en&btnG=Search&q=intitle:Research+Requirements+for+4+th+Generation+Wave+Energy+Devices#1.

Sandberg, A. B. *et al.* (2016) ‘Critical Factors Influencing Viability of Wave Energy Converters in Off-Grid Luxury Resorts and Small Utilities’, *Sustainability*, 8, pp. 1–22. doi: 10.3390/su8121274.

Schmitt, P. and Elsäßer, B. (2017) ‘The application of Froude scaling to model tests of Oscillating Wave Surge Converters’, *Ocean Engineering*. Elsevier Ltd, 141(June), pp. 108–115. doi: 10.1016/j.oceaneng.2017.06.003.

Shahroozi, Z. *et al.* (2020) ‘Design and evaluation of linear and rotational generator scale models for wave tank testing’, in *Developments in Renewable Energies Offshore - Proceedings the 4th International Conference on Renewable Energies Offshore, RENEW 2020*. 1st edn. CRC Press, pp. 132–139. doi: 10.1201/9781003134572-17.

Shahroozi, Z., Göteman, M. and Engström, J. (2021) ‘Experimental results of force measurements from a scaled point absorbing wave energy converter subjected to extreme waves’, in EWTEC (ed.) *Proceedings of the European Wave and Tidal Energy Conference*. Plymouth, pp. 1881-1-1881–10.

Sheng, W. (2019) ‘Wave energy conversion and hydrodynamics modelling technologies: A review’, *Renewable and Sustainable Energy Reviews*.

Elsevier Ltd, 109(April), pp. 482–498. doi: 10.1016/j.rser.2019.04.030.

Sheng, W., Alcorn, R. and Lewis, T. (2014) ‘Physical modelling of wave energy converters’, *Ocean Engineering*. Elsevier, 84, pp. 29–36. doi: 10.1016/j.oceaneng.2014.03.019.

Signorelli, C. D., Villegas, C. and Ringwood, J. V. (2011) ‘Hardware-In-The-Loop Simulation of a Heaving Wave Energy Converter’, in *Proceedings of the 9th European Wave and Tidal Energy Conference*. Southampton, pp. 1–10.

Skyner, D. J. (1987) *Solo Duck Linear Analysis*. Edinburgh. Available at: http://hdl.handle.net/1842/23535.

Smith, G. and Taylor, J. (2007) *Preliminary Wave Energy Performance Protocol*.

Spencer, B. (2022) ‘An offshore wind revolution has begun - can it meet the UK’s power needs?’, *The Sunday Times*, 28 August. Available at: https://www.thetimes.co.uk/article/an-offshore-wind-revolution-has-begun-can-it-meet-the-uks-power-needs-ph6w5bt09?gclid=EAIaIQobChMIvIm4raW9-wIVR-ztCh2P3QXUEAAYASAAEgJuVvD_BwE.

Stansby, P., Carpiteno Moreno, E. and Stallard, T. (2015) ‘Capture width of the three-float multi-mode multi-resonance broadband wave energy line absorber M4 from laboratory studies with irregular waves of different spectral shape and directional spread’, *Ocean Engineering and Marine Energy*, 1, pp. 287–298.

Stephen Salter: pioneer of wave power (2007) *The Engineer*. Available at: https://www.theengineer.co.uk/stephen-salter-pioneer-of-wave-power/ (Accessed: 7 February 2022).

Suryanto, A. (2006) ‘Estimation of incident and reflected waves in irregular wave experiments’, *Indonesian Mathematical Society*, 12(2), pp. 141–153. Available at: https://www.researchgate.net/publication/265152596_ESTIMATION_OF_INC

IDENT_AND_REFLECTED_WAVES_IN_IRREGULAR_WAVE_EXPERIMENTS.

Taylor, J. R. M., Rea, M. and Rogers, D. J. (2003) ‘The Edinburgh curved tank’, in *5th European Wave Energy Conference*. Cork, pp. 307–314.

Teillant, B. *et al.* (2012) ‘Productivity and economic assessment of wave energy projects through operational simulations’, *Renewable Energy*. Elsevier Ltd, 48, pp. 220–230. doi: 10.1016/j.renene.2012.05.001.

Tetu, A. *et al.* (2013) *D2.5EC Report on Instrumentation Best Practice*.

The Executive Committee of Ocean Energy Systems (2017) *Annual Report: An Overview of Ocean Energy Activities in 2017*, *IEA-OES*. Available at: https://report2018.ocean-energy-systems.org/.

The Executive Committee of Ocean Energy Systems (2018) *Annual Report: An Overview of Ocean Energy Activities in 2018*, *IEA-OES*. doi: 10.3934/Math.2019.1.166.

Thiébaut, F., Sutton, G. and Johnstone, C. (2015) *D 2.28 Model Construction Methods*.

Thomas, A. (2022) *Mocean, Verlume and Baker Hughes announce subsea wave energy link-up*, *Energy Voice*. Available at: https://www.energyvoice.com/renewables-energy-transition/wave-tidal/uk-wave-tidal/445840/mocean-verlume-and-baker-hughes-announce-subsea-wave-energy-link-up/.

Thurman, H. V. (1993) *Essentials of Oceanography*. 4th edn. Prentice Hall.

Torre-Enciso, Y. *et al.* (2009) ‘Mutriku Wave Power Plant: from the thinking out to the reality’, in EWTEC 2009 (ed.) *8th European Wave and Tidal Energy Conference*. Uppsala, Sweden, pp. 319–328. Available at: http://tethys.pnnl.gov/sites/default/files/publications/Torre-Enciso_et_al_2009.pdf.

Tosdevin, T. *et al.* (2021) ‘Extreme responses of a hinged raft type wave

energy converter', in *14th European Wave and Tidal Energy Conference*. Plymouth, UK.

Trueworthy, A. and Dupont, B. (2020) 'The wave energy converter design process: Methods applied in industry and shortcomings of current practices', *Journal of Marine Science and Engineering*, 8(11), pp. 1–49. doi: 10.3390/jmse8110932.

Trueworthy, A. M. *et al.* (2021) 'Supporting the transition from grid-scale to emerging market wave energy converter design and assessment', in *Proceedings of the European Wave and Tidal Energy Conference*, pp. 2101-1-2101–10.

Tunga, I. *et al.* (2021) 'Addressing European ocean energy challenge: The dtoceanplus structured innovation tool for concept creation and selection', *Energies*, 14(18). doi: 10.3390/en14185988.

UNDP (no date) *Goal 14: Life below water*, *Sustainable Development Goals*. Available at: https://www1.undp.org/content/oslo-governance-centre/en/home/sustainable-development-goals/goal-14-life-below-water.html (Accessed: 1 March 2019).

University of Edinburgh (2017) 'IDCORE Handbook'.

University of Edinburgh (2018) *C-GEN Technology*. Available at: https://www.cgen.eng.ed.ac.uk/c-gen-technology (Accessed: 18 March 2022).

Ursell, F. (1951) 'Trapping modes in the theory of surface waves', *Mathematical Proceedings of the Cambridge Philosophical Society*, 47(2), pp. 347–358. doi: 10.1017/S0305004100026700.

US Department of Energy (2016) *How does the Wave Energy Prize calculate ACE?*, *Wave Energy Prize Blog*. Available at: https://waveenergyprize.wordpress.com/2016/08/18/how-does-the-wave-energy-prize-calculate-ace/ (Accessed: 25 January 2022).

Vanegas-Cantarero, M. M. *et al.* (2022) 'Beyond LCOE: A multi-criteria

evaluation framework for offshore renewable energy projects', *Renewable and Sustainable Energy Reviews*. Elsevier Ltd, 161(December 2021). doi: 10.1016/j.rser.2022.112307.

VGA *et al.* (2021) *Introducing IMPACT*, *IMPACT*. Available at: https://www.impact-h2020.eu/about/ (Accessed: 25 November 2022).

Villate, J. *et al.* (2020) *Strategic Research and Innovation Agenda for Ocean Energy*.

Wave Energy Scotland (no date) *Stage Gate Metrics*, *WES*. Available at: https://www.waveenergyscotland.co.uk/strategic-activity/strategic-activity-2/technology-development/stage-gate-metrics-an-internationally-accepted-approach-to-evaluation-of-wave-energy-technologies-1/ (Accessed: 26 November 2022).

Weber, J. (2012) 'WEC Technology Readiness and Performance Matrix – finding the best research technology development trajectory', in *International Conference on Ocean Energy, ICOE*, pp. 1--10.

Weber, J. *et al.* (2019) 'Requirements for Realistic and Effective Wave Energy Technology Performance Assessment Criteria and Metrics', in *Proceedings of the 13th European Wave and Tidal Energy Conference*. Naples. Available at: https://www.osti.gov/biblio/1641817.

Weber, J., Costello, R. and Ringwood, J. (2013) 'WEC Technology Performance Levels (TPLs) - Metric for Successful Development of Economic WEC Technology', in *EWTEC 2013 Proceedings*.

Weber, J. and Laird, D. (2015) 'Structured innovation of high performance Wave Energy Converter technology', in *Proceedings of the 11th European Wave and Tidal Conference*, pp. 1–7.

Wendt, F. *et al.* (2019) 'Ocean Energy Systems Wave Energy Modelling Task: Modelling, Verification and Validation of Wave Energy Converters', *Marine Science and Engineering Article*, 11(379). doi: https://doi.org/10.3390/jmse7110379.

Wilkinson, L. *et al.* (2015) ‘Assessing the performance of a modular flap-type wave energy converter’, *Proceedings of the 11th European Wave and Tidal Energy Conference*, (November), pp. 1–10.

Wilkinson, L. *et al.* (2017) ‘The power-capture of a nearshore, modular, flap-type wave energy converter in regular waves’, *Ocean Engineering*. Elsevier Ltd, 137(April), pp. 394–403. doi: 10.1016/j.oceaneng.2017.04.016.

Wilkinson, L. F. (2018) *An assessment of a nearshore modular flap-type wave energy converter*. The University of Edinburgh, The University of Strathclyde, The University of Exeter, Industiral Doctoral Centre for Offshore Renewable Energy (IDCORE).

Yemm, R. *et al.* (2012) ‘Pelamis : experience from concept to connection’, *Philosophical Transactions of the Royal Society*, (370), pp. 365–380. doi: 10.1098/rsta.2011.0312.

Zanuttigh, B., Angelelli, E. and Kofoed, J. P. (2013) ‘Effects of mooring systems on the performance of a wave activated body energy converter’, *Renewable Energy*. Elsevier Ltd, 57, pp. 422–431. doi: 10.1016/j.renene.2013.02.006.

Zhang, D. (2022) *Wave energy pt 2: the wild world of wave energy converters*, *etechmonkey*. Available at: https://etechmonkey.com/index.php/2022/11/04/wave-energy-pt-2-the-wild-world-of-wave-energy-converters/ (Accessed: 20 November 2022).